CHLOROPLAST BIOTECHNOLOGY FOR CROP IMPROVEMENT

EDITED BY: Clelia De-la-Peña, Thomas D. Sharkey and Patricia León

PUBLISHED IN: Frontiers in Plant Science

frontiers Research Topics

ISSN 1664-8714
ISBN 978-2-88974-564-7
DOI 10.3389/978-2-88974-564-7

About Frontiers

Frontiers is more than just an open-access publisher of scholarly articles: it is a pioneering approach to the world of academia, radically improving the way scholarly research is managed. The grand vision of Frontiers is a world where all people have an equal opportunity to seek, share and generate knowledge. Frontiers provides immediate and permanent online open access to all its publications, but this alone is not enough to realize our grand goals.

Frontiers Journal Series

The Frontiers Journal Series is a multi-tier and interdisciplinary set of open-access, online journals, promising a paradigm shift from the current review, selection and dissemination processes in academic publishing. All Frontiers journals are driven by researchers for researchers; therefore, they constitute a service to the scholarly community. At the same time, the Frontiers Journal Series operates on a revolutionary invention, the tiered publishing system, initially addressing specific communities of scholars, and gradually climbing up to broader public understanding, thus serving the interests of the lay society, too.

Dedication to Quality

Each Frontiers article is a landmark of the highest quality, thanks to genuinely collaborative interactions between authors and review editors, who include some of the world's best academicians. Research must be certified by peers before entering a stream of knowledge that may eventually reach the public - and shape society; therefore, Frontiers only applies the most rigorous and unbiased reviews.
Frontiers revolutionizes research publishing by freely delivering the most outstanding research, evaluated with no bias from both the academic and social point of view. By applying the most advanced information technologies, Frontiers is catapulting scholarly publishing into a new generation.

What are Frontiers Research Topics?

Frontiers Research Topics are very popular trademarks of the Frontiers Journals Series: they are collections of at least ten articles, all centered on a particular subject. With their unique mix of varied contributions from Original Research to Review Articles, Frontiers Research Topics unify the most influential researchers, the latest key findings and historical advances in a hot research area! Find out more on how to host your own Frontiers Research Topic or contribute to one as an author by contacting the Frontiers Editorial Office: frontiersin.org/about/contact

CHLOROPLAST BIOTECHNOLOGY FOR CROP IMPROVEMENT

Topic Editors:
Clelia De-la-Peña, Scientific Research Center of Yucatán (CICY), Mexico
Thomas D. Sharkey, Michigan State University, United States
Patricia León, National Autonomous University of Mexico, Mexico

Citation: De-la-Peña, C., Sharkey, T. D., León, P., eds. (2022). Chloroplast Biotechnology for Crop Improvement. Lausanne: Frontiers Media SA.
doi: 10.3389/978-2-88974-564-7

Table of Contents

frontiers in Plant Science

EDITORIAL
published: 01 February 2022
doi: 10.3389/fpls.2022.848034

Editorial: Chloroplast Biotechnology for Crop Improvement

Clelia De-la-Peña[1]*, *Patricia León*[2] *and Thomas D. Sharkey*[3,4,5]

[1] Unidad de Biotecnología, Centro de Investigación Científica de Yucatán, Mérida, Mexico, [2] Instituto de Biotecnología Universidad Nacional Autónoma de Mexico, Cuernavaca, Mexico, [3] MSU-DOE Plant Research Laboratory, Michigan State University, East Lansing, MI, United States, [4] Department of Biochemistry and Molecular Biology, Michigan State University, East Lansing, MI, United States, [5] Plant Resilience Institute, Michigan State University, East Lansing, MI, United States

Keywords: chloroplast, crops, biotechnology, editorial, photosynthesis

Editorial on the Research Topic

Chloroplast Biotechnology for Crop Improvement

Ever since the first photosynthetic eukaryote organisms appeared, chloroplasts have been an enigmatic cellular compartment where complex biochemical and molecular processes essential for the plant take place. As a result, substantial efforts in plant biotechnology have been linked to improve photosynthetic efficiency and also the production of a diversity of important compounds synthesized in this organelle that are of biological, medical and industrial importance.

Chloroplast biotechnology may open new frontiers of crop development (Maliga and Bock, 2011) having broad impacts on medicine, fuel, food, bioplastics, and chemicals and also may help mitigate deleterious effects of global warming on plant function and productivity. Therefore, it is of central importance to study and investigate the molecular mechanisms that chloroplasts use and that can be exploited by crop biotechnology in the future. Understanding how chloroplasts work will open opportunities for modifications and improvement that would benefit our modern society.

This Research Topic includes an excellent combination of Reviews and Original Research Articles focused on *Chloroplast Biotechnology for Crop Improvement*, and provides up-to-date information on chloroplast genome sequencing, photosynthesis improvement, chloroplast metabolic engineering, and plastid-related metabolite production, using new approaches and novel technologies.

One of the biotechnological tools for crop improvement has been the use of high-throughput technologies such as the newest-generation sequencing to obtain genome sequence information, the use of nanotechnology for plastid transformation, and genetic engineering. For instance, in their Original Research article Yu et al. reported the complete chloroplast genome of an important medicinal plant *Erigeron breviscapus* identifying regulatory elements and providing a foundation for the establishment of the subsequent chloroplast genetic transformation system for genetic improvement. On the other hand, specific topics on the role of nanotechnology are discussed by Newkirk et al. providing interesting new insights and up to date status into this field. In their Review, they highlight recent discoveries on the interactions between chloroplasts and nanomaterials, nanomaterial uses for crop performance monitoring and improvement and nanotechnological applications for plastid synthetic biology that enable chloroplast uses for manufacturing. These tools may allow increased plant productivity and make sustainable technologies widely available.

It is known the potential risk of contaminating genetically modified (GM)-free cropland with GM pollen or seed can be increased if GM plants are cultivated in areas where there are wildtype relatives of the respective GM plant present. Alternatively, the integration into the plastid genome of the genes of interest can avoid the risk of GM pollen spread and sterility

Edited and reviewed by:
Soren K. Rasmussen, University of Copenhagen, Denmark

***Correspondence:**
Clelia De-la-Peña
clelia@cicy.mx
orcid.org/0000-002-9093-9489

Specialty section:
This article was submitted to Plant Biotechnology, a section of the journal Frontiers in Plant Science

Received: *03 January 2022*
Accepted: *10 January 2022*
Published: *01 February 2022*

Citation:
De-la-Peña C, León P and Sharkey TD (2022) Editorial: Chloroplast Biotechnology for Crop Improvement. Front. Plant Sci. 13:848034. doi: 10.3389/fpls.2022.848034

technologies may prevent the genetic exchange altogether (Clark and Maselko, 2020). Since chloroplast transformation has many advantages over the classic genomic transformation such as high expression and transgene safety, identification of high efficiency regulatory elements is central for developing and improving efficient chloroplast transformation in diverse species. In their Research Topic Shahinnia et al. offer a convincing case for engineering the photosynthetic electron transport chain with heterologous proteins, aimed to increase barley productivity. Furthermore, Moreno et al. found that the manipulation of carotenoid metabolism results in higher biomass production under normal cultivar conditions, with improved stress tolerance bearing no negative impact on the overall plant growth. In their Research Topic Moreno et al. take advantage of a multi-OMICs (transcriptomics, proteomics, metabolomics, and lipidomics) approaches to deeply characterize the phenotype of transgenic tobacco plants overexpressing the carrot lycopene β-cyclase 1 (*LCYB1*) gene. This study will certainly help in the future identification of transcription factors associated with stress responses.

Photosynthetic carbon assimilation has two major problems: stomatal density and CO_2 levels, and different authors address these challenges in crop productivity. Sakoda et al., using different *Arabidopsis* genotypes that differ in stomatal density, find that most of the effects of stomatal density are on photosynthesis, CO_2 assimilation rate, and biomass production. The authors also demonstrated that a short-term effect on photosynthesis rate measured per unit leaf area can well translate to significant whole-plant growth effects. Also, the effect of CO_2-concentrating mechanisms was highlighted in the Review of Rottet et al., who give an overview of the major candidate proteins to be considered for engineering carbon concentrating mechanisms into C_3 chloroplasts and highlight the complexities associated with the heterologous expression and generation of functional HCO_3^- transport systems in C_3 chloroplasts for increased Rubisco carboxylation rate and thereby for higher photosynthetic rates.

Understanding the control mechanisms underlying carbon partitioning is critical for engineering starch content and metabolic flux in plants (Santelia and Zeeman, 2011; Kölling et al., 2015). In the Research Topic of Preiser et al., kinetic properties of plastidic and cytosolic isoforms of phosphoglucoisomerase in the presence and absence of different regulatory factors was characterized. This is an important question for exploring plant carbon partitioning dynamics, which vary with growth, environmental conditions, metabolic state, and the circadian clock.

High-value nutritional compounds and therapeutic proteins have been obtained from chloroplasts. Jackson et al. review current knowledge on *Chlamydomonas* chloroplast system as a potential tool for testing synthetic biology strategies, which could be further translated in higher plants. In their Review, Jackson et al. describe some of the radical synthetic biology (SynBio) ideas and Design-Build-Test-Learn (DBTL) strategies highlighting the speed and versatility of *Chlamydomonas* chloroplast genetic engineering for improving photosynthesis, carbon fixation, nitrogen fixation, and production of novel metabolites. Arias et al. investigate the effect of the direct expression of transgenes phytoene synthase (*DcPSY2*) and lycopene cyclase (*DcLCB1*) from *Daucus carota* and carotene desaturase (*XdCrtI*) from yeast *Xanthophyllomyces dendrorhous* in tomato and apple fruits. They find a clear increase in the β-carotene and carotenoid levels demonstrating the potential use of these genes for biotechnological applications. This kind of Research Topic will certainly help to increase the nutritional value in fruits.

On the other hand, in their Research Topic, Hung et al. show that a long-lived albino mutant can be used as a model for analyzing the function of chloroplast-development genes and facilitate the purification of therapeutic proteins without chlorophyll interference. Vaccine production is one of most intensively studied fields in molecular farming. The production of proteins in chloroplasts can considerably reduce the costs of producing proteins focused on the pharmaceutical area. Whereas, many scientists have developed different systems to produce large amounts of vaccines, Nakahira et al. reported in their Research Topic, chloroplast transformation to optimize a high production of recombinant protein in transgenic plants without the risk of gene transfer through pollen distribution, i.e., *via* maternal inheritance. They reported the production of virus-like particles (VLPs) of red-spotted grouper nervous necrosis virus (RGNNV) in tobacco plants using chloroplast transformation techniques.

The Research Topic presented here is significant because it is expected to increase and strengthen the information needed to develop, in the near future, novel approaches to manipulate and selectively activate chloroplast development to increase crop productivity. New approaches of the type presented here, and the advancement of new technologies will certainly increase our knowledge of currently known photosynthetic organisms and will facilitate the understanding of their roles as sources of sustainable foods, novel biopharmaceuticals, and next-generation biomaterials essential for modern society.

AUTHOR CONTRIBUTIONS

CD-l-P, PL, and TS provided the idea of the work and critically reviewed the manuscripts. CD-l-P wrote the paper. All authors read and approved the final manuscript and contributed to the article and approved the submitted version.

FUNDING

This work was supported by CONACYT grants CB-2016 # 285898 and # 286368 to CD-l-P. DGAPA-UNAM IN207320 for PL. TS was supported by the Division of Chemical Sciences, Geosciences and Biosciences, Office of Basic Energy Sciences of the United States Department of Energy Grant DE-FG02-91ER20021 and receives partial salary support from MSU AgBioResearch.

REFERENCES

Clark, M., and Maselko, M. (2020). Transgene biocontainment strategies for molecular farming. *Front. Plant Sci.* 11:210. doi: 10.3389/fpls.2020.00210

Kölling, K., Thalmann, M., Müller, A., Jenny, C., and Zeeman, S. C. (2015). Carbon partitioning in *Arabidopsis thaliana* is a dynamic process controlled by the plants metabolic status and its circadian clock. *Plant Cell Environ.* 38, 1965–1979. doi: 10.1111/pce.12512

Maliga, P., and Bock, R. (2011). Plastid biotechnology: food, fuel, and medicine for the 21st century. *Plant Physiol.* 155, 1501–1510. doi: 10.1104/pp.110.170969

Santelia, D., and Zeeman, S. C. (2011). Progress in Arabidopsis starch research and potential biotechnological applications. *Curr. Opin. Biotechnol.* 22, 271–280. doi: 10.1016/j.copbio.2010.11.014

Conflict of Interest: The authors declare that the research was conducted in the absence of any commercial or financial relationships that could be construed as a potential conflict of interest.

frontiers in Plant Science

ORIGINAL RESEARCH
published: 21 October 2020
doi: 10.3389/fpls.2020.589603

Higher Stomatal Density Improves Photosynthetic Induction and Biomass Production in Arabidopsis Under Fluctuating Light

Kazuma Sakoda[1,2], Wataru Yamori[1], Tomoo Shimada[3], Shigeo S. Sugano[4], Ikuko Hara-Nishimura[5] and Yu Tanaka[6,7]*

[1] Graduate School of Agricultural and Life Sciences, The University of Tokyo, Nishitokyo, Japan, [2] Japan Society for the Promotion of Science, Tokyo, Japan, [3] Graduate School of Science, Kyoto University, Kyoto, Japan, [4] National Institute of Advanced Industrial Science and Technology (AIST), Tsukuba, Japan, [5] Faculty of Science and Engineering, Konan University, Kobe, Japan, [6] Graduate School of Agriculture, Kyoto University, Kyoto, Japan, [7] JST, PRESTO, Kyoto, Japan

OPEN ACCESS

Edited by:
Thomas D. Sharkey, Michigan State University, United States

Reviewed by:
Elias Kaiser, Wageningen University & Research, Netherlands
Ningyi Zhang, Wageningen University & Research, Netherlands

***Correspondence:**
Kazuma Sakoda
sakoda@g.ecc.u-tokyo.ac.jp

Specialty section:
This article was submitted to Plant Biotechnology, a section of the journal Frontiers in Plant Science

Received: *31 July 2020*
Accepted: *29 September 2020*
Published: *21 October 2020*

Citation:
Sakoda K, Yamori W, Shimada T, Sugano SS, Hara-Nishimura I and Tanaka Y (2020) Higher Stomatal Density Improves Photosynthetic Induction and Biomass Production in Arabidopsis Under Fluctuating Light. Front. Plant Sci. 11:589603. doi: 10.3389/fpls.2020.589603

Stomatal density (*SD*) is closely associated with photosynthetic and growth characteristics in plants. In the field, light intensity can fluctuate drastically within a day. The objective of the present study is to examine how higher *SD* affects stomatal conductance (g_s) and CO_2 assimilation rate (A) dynamics, biomass production and water use under fluctuating light. Here, we compared the photosynthetic and growth characteristics under constant and fluctuating light among three lines of *Arabidopsis thaliana* (L.): the wild type (WT), *STOMAGEN/EPFL9*-overexpressing line (ST-OX), and *EPIDERMAL PATTERNING FACTOR 1* knockout line (*epf1*). ST-OX and *epf1* showed 268.1 and 46.5% higher *SD* than WT ($p < 0.05$). Guard cell length of ST-OX was 10.0% lower than that of WT ($p < 0.01$). There were no significant variations in gas exchange parameters at steady state between WT and ST-OX or *epf1*, although these parameters tended to be higher in ST-OX and *epf1* than WT. On the other hand, ST-OX and *epf1* showed faster A induction than WT after step increase in light owing to the higher g_s under initial dark condition. In addition, ST-OX and *epf1* showed initially faster g_s induction and, at the later phase, slower g_s induction. Cumulative CO_2 assimilation in ST-OX and *epf1* was 57.6 and 78.8% higher than WT attributable to faster A induction with reduction of water use efficiency (*WUE*). *epf1* yielded 25.6% higher biomass than WT under fluctuating light ($p < 0.01$). In the present study, higher *SD* resulted in faster photosynthetic induction owing to the higher initial g_s. *epf1*, with a moderate increase in *SD*, achieved greater biomass production than WT under fluctuating light. These results suggest that higher *SD* can be beneficial to improve biomass production in plants under fluctuating light conditions.

Keywords: leaf photosynthesis, fluctuating light, photosynthetic induction, stomata, stomatal density and conductance, water use efficiency

INTRODUCTION

Enhancing leaf photosynthesis has been attempted to drive further increases in biomass production in crop plants (von Caemmerer and Evans, 2010; Yamori et al., 2016; Sakoda et al., 2018). Gas diffusional resistance from the atmosphere to the chloroplast is one of the limiting factors for leaf photosynthetic capacity (Farquhar and Sharkey, 1982). Stomata, pores on the epidermis of plant leaves, function to maintain the balance between CO_2 uptake for photosynthesis and water loss for transpiration (Mcadam and Brodribb, 2012). It has been highlighted that the conductance to gas diffusion via stomata (g_s) can be a major determinant of CO_2 assimilation rate (A) (Wong et al., 1979). The potential of g_s is mainly determined by the size, depth, and opening of single stoma, and their density (Franks and Beerling, 2009). It has been controversial how the change in the stomatal density (*SD*), defined as the stomata number per unit leaf area, affects photosynthetic and growth characteristics in plants (Lawson and Blatt, 2014). Doheny-Adams et al. (2012) reported that lower *SD* yielded higher growth rate and biomass production in Arabidopsis under constant light owing to the favorable water condition and temperature for metabolism and low metabolic cost for stomatal development (Doheny-Adams et al., 2012). Contrastingly, lower *SD* resulted in the depression of g_s and/or A in Arabidopsis and poplar plants (Büssis et al., 2006; Yoo et al., 2010; Wang et al., 2016). An *SDD1* knockout line of Arabidopsis with higher *SD* showed higher g_s and A than a wild-type line, depending on light condition (Schlüter et al., 2003). Previously, we reported that higher *SD* by overexpressing *STOMAGEN/EPFL9* resulted in the enhancement of g_s and A in Arabidopsis under constant and high light conditions (Tanaka et al., 2013). Therefore, *SD* manipulation could have the potential to enhance photosynthetic and growth characteristics in plants, even though that effect can depend on the species or environmental conditions.

In the field, light intensity can fluctuate at different scales, from less seconds to minutes, over the course of a day owing to changes in the solar radiation, cloud cover, or self-shading in the plant canopy (Kaiser et al., 2018). The gradual increase in A can be shown after the transition from low to high light intensity, and this phenomenon is called "photosynthetic induction." A simulation analysis demonstrated that the potential loss of the cumulative amount of CO_2 assimilation caused by photosynthetic induction can reach at least 21% in wheat (*Triticum aestivum* L.) and soybean (*Glycine max* (L.) Merr.) (Taylor and Long, 2017; Tanaka et al., 2019). In rice (*Oryza sativa* L.) and soybean, there is genotypic variation in the speed of photosynthetic induction, which causes significant differences in the cumulative carbon gain under fluctuating light (Soleh et al., 2016, 2017; Adachi et al., 2019). Consequently, speeding up photosynthetic induction can yield more efficient carbon gain, which will open a new pathway to improve biomass production in plants under field conditions.

Photosynthetic induction is typically limited by three phases of the biochemical and diffusional processes: (1) activation of electron transport, (2) activation of the enzymes in the Calvin-Benson cycle, and (3) stomatal opening (Pearcy, 1990; Yamori, 2016; Yamori et al., 2020). Especially, the activation of Rubisco (5–10 min for full induction) and stomatal opening (20–30 min for full induction) constitute a major limitation to photosynthetic induction (Yamori et al., 2012; Carmo-Silva and Salvucci, 2013). The overexpression of *PATROL1*, controlling the translocation of a major H^+-ATPase (AHA1) to the plasma membrane, resulted in faster g_s induction to fluctuating light in Arabidopsis without the change in *SD* (Hashimoto-Sugimoto et al., 2013). Arabidopsis knockout mutants of ABA transporter, which plays pivotal roles in stomatal closure, improved stomatal response to fluctuating light and photosynthesis (Shimadzu et al., 2019). Furthermore, the rapid stomatal response is important for plants to achieve high water use efficiency (*WUE*) (Qu et al., 2016). Notably, the faster stomatal opening improved the photosynthetic induction and thus biomass production in Arabidopsis under the fluctuating light (Papanatsiou et al., 2019; Kimura et al., 2020). These facts evidence that rapid stomatal response can be beneficial for the effective carbon gain and water use under fluctuating light conditions. However, how *SD* changes affect g_s and A dynamics, biomass production, and water use under these conditions has been understudied (Drake et al., 2013; Papanatsiou et al., 2016; Schuler et al., 2017; Vialet-Chabrand et al., 2017).

It is hypothesized that higher *SD* results in higher initial g_s (Tanaka et al., 2013), which can contribute to faster photosynthetic induction due to the lower stomatal limitation under the fluctuating light. The objective of this study was to examine how higher *SD* affects the photosynthetic and growth characteristics in plants under fluctuating light conditions. Here, we investigated the induction response of g_s, A, transpiration rate (E) and water use efficiency (*WUE*) after step increase in light by gas exchange measurements, and biomass production under fluctuating light conditions in the three Arabidopsis lines differing in *SD*.

MATERIALS AND METHODS

Plant Materials and Growth Conditions

The peptide signals in a family of EPIDERMAL PATTERNING FACTOR (EPF) were identified to function in the stomatal development of Arabidopsis (*Arabidopsis thaliana* (L.) Heynh) (Hara et al., 2007). It has been demonstrated that EPF1 and EPF2 combine with the receptor-like protein, TOO MANY MOUTHS (TMM) and ERECTA family leucine-rich repeat-receptor-like kinases and, consequently, restrain a specific process in stomatal development. Contrastingly, STOMAGEN/EPFL9 combines with TMM competitively to EPF1 and EPF2, and promote stomatal development (Sugano et al., 2010; Lee et al., 2015). In the present study, Columbia-0 (CS60000) of *Arabidopsis thaliana* (L.) Heynh, was used as a wild-type line (WT). In addition, we used *STOMAGEN/EPFL9* overexpressing line (ST-OX10-3; ST-OX) which was used in Tanaka et al. (2013), and an *EPF1* knockout line (SALK_137549) (*epf1-1*; *epf1*) which was used in Sugano et al. (2010).

For analyzing photosynthetic and stomatal traits, six plants per line were sown and grown in the soil in the growth chamber at

an air humidity of 60%, CO_2 concentration of 400 μmol mol^{-1} and a photosynthetic photon flux density (PPFD) of 100 μmol photon m^{-2} s^{-1} for the gas exchange analysis. The day/night period was set to 8/16 h with a constant air temperature of 22°C. We randomly changed plant arrangement every 3–4 days during their growth period to avoid the spacing effects. For the biomass analysis, plants were sown and grown in the soil at an air temperature of 22°C and a PPFD of 120 μmol photon m^{-2} s^{-1} for 24 days after sowing with the day/night period of 8/16 h. Subsequently, four plants per line were subjected to constant and fluctuating light conditions, for 20 days with a day/night cycle of 12/12 h. During daytime, the light intensity in the constant light condition was changed from a PPFD of 60 μmol photon m^{-2} s^{-1} for 4 h to 500 μmol photon m^{-2} s^{-1} for 4 h, followed by 60 μmol photon m^{-2} s^{-1} for 4 h, while a PPFD of 60 μmol photon m^{-2} s^{-1} for 10 min after 500 μmol photon m^{-2} s^{-1} for 5 min was repeated for 12 h in the fluctuating light condition as described in Kimura et al. (2020). Plants were exposed to the same total amount of light intensity per day under both light conditions. We randomly changed plant arrangement every 3–4 days during their growth period to avoid the spacing effects. Dry weight of above ground biomass grown under each light condition was evaluated at 44 days after sowing.

Evaluation of Stomatal Density, Size, and Clustering

The stomatal density (*SD*), size (L_g), and clustering were evaluated in the leaves of the six plants per line at the same growth stage as the gas exchange measurements were conducted. We used the six leaves of the three plants in which gas exchange measurements were conducted and the other three plants. A section of the leaf (5 × 5 mm) was excised and immediately fixed in the solution (Ethanol : acetic acid = 9:1, v/v) overnight. The fixed tissues were cleared in chloral hydrate solution (chloral hydrate : glycerol : water = 8:1:2, w/v/v) overnight. The cleared tissues were stained with safranin-O solution (200 μg ml^{-1}) for 30 min to 1 h. The abaxial side of the leaves was observed at a 200 × magnification using an optical microscope and six digital images (0.072 mm^2) were obtained per leaf (CX31 and DP21, Olympus, Tokyo, Japan). We used imaging analysis software, ImageJ (NIH, Bethesda, MD, United States) to assess the stomatal number and guard cell length from the images. *SD* was calculated from the stomatal number per unit leaf area. L_g, defined as guard cell length, of all the stomata (2–86 stomata) was measured in each image. Each clustering category (2–5 er) means the number of clustered stomata. The percentage of clustered stomata to total number was measured for each clustering category from 2 to 5 as described in Hara et al. (2007). The mean values of each trait were calculated in six images obtained from each leaf. Subsequently, the average value of each trait for six leaves was calculated for each line.

Gas Exchange Measurements

Gas exchange measurements were conducted using a portable gas-exchange system LI-6400 (*LI-COR*, Lincoln, NE, United States). All plants were kept in the dark (a PPFD of 0 μmol photon m^{-2} s^{-1}) overnight before and during the measurements. In the leaf chamber, we set flow rate at 300 μmol s^{-1}, CO_2 concentration at 400 μmol mol^{-1}, and air temperature at 25°C. After the leaf was clamped in the chamber, light intensity was kept at a PPFD of 0 μmol photon m^{-2} s^{-1} for the initial 10 min and, subsequently, under a PPFD of 500 μmol photon m^{-2} s^{-1} for 120 min. A, g_s, intercellular CO_2 concentration (C_i), and E were recorded every 10 s during the measurements. *WUE* was calculated as the ratio of A to E. Gas exchange measurements were conducted with three plants per line during 68 to 73 days after sowing.

Data Processing

To evaluate the induction speeds of A and g_s, we calculated $A_{induction}$ and $g_{sinduction}$ defined as the following equations:

$$g_{sinduction} = \frac{g_{st} - g_{si}}{g_{sf} - g_{si}} \quad (1)$$

$$A_{induction} = \frac{A_t - A_i}{A_f - A_i} \quad (2)$$

where A_i and g_{si} represent steady-state values under a PPFD of 0 μmol photon m^{-2} s^{-1}, steady-state A and g_s, A_f and g_{sf}, represent the maximum values which were reached in 120 min under a PPFD of 500 μmol photon m^{-2} s^{-1}, and A_t and g_{st} represent values at a given time under illumination. We evaluated the differences in the time when $A_{induction}$ and $g_{sinduction}$ reached the closest values of 5, 10, 20, 40, 60, and 80% of those maximum values after step change in light from 0 to 500 μmol photon m^{-2} s^{-1} (t_{5-80gs} and t_{5-80A}) between WT and ST-OX or *epf1*.

The cumulative CO_2 assimilation (*CCA*) and transpiration (*CE*) under fluctuating light were calculated by summing A and E in first 10 min under illumination after the initial dark period. An integrated *WUE* (WUE_i) was calculated as the ratio of *CCA* to *CE*. Assuming the absence of induction response of A to the step increase in light, a theoretically maximum *CCA* (CCA_t) was defined by the following equation:

$$CCA_t = A_f \cdot T_{500} \quad (3)$$

where T_{500} is the seconds for which the light intensity was maintained at 500 μmol photon m^{-2} s^{-1} for 10 min. The potential loss rate of *CCA* caused by photosynthetic induction was defined by the following equation:

$$Loss\ rate = \left(1 - \frac{CCA}{CCA_t}\right) \times 100 \quad (4)$$

Statistical Analysis

The variation in stomatal size and all the parameters of photosynthetic and growth characteristics were compared between WT and ST-OX or *epf1* by a Dunnett's test. Steel test was applied to evaluate *SD* variation between WT and ST-OX or *epf1* because the distribution of values was extremely different among the lines. Statistical analysis was conducted using R software version 3. 6. 1 (R Foundation for Statistical Computing, Vienna, Austria).

RESULTS

Stomatal Density, Size, and Clustering

We evaluated stomatal density (*SD*), size (L_g) and clustering in the three Arabidopsis lines. ST-OX and *epf1* showed 268.1 and 46.5% higher *SD* than WT ($p < 0.05$) (**Figure 1A**). L_g of ST-OX was 10.0% lower than that of WT ($p < 0.01$) (**Figure 1B**). Stomatal clustering was scarcely observed in WT, while two to five stomata were clustered in ST-OX and *epf1* (**Figure 1C**). The ratio of stomata in each clustering category was higher in ST-OX than that in *epf1*.

Photosynthesis and Stomatal Conductance After Step Increase in Light

To examine how higher *SD* affects the photosynthetic characteristics under the fluctuating light, we conducted gas exchange measurements. ST-OX and *epf1* maintained higher g_s, C_i, *A*, and *E* than WT under the non-steady state at high light intensity (500 μmol photon m^{-2} s^{-1}) (**Figures 2A–D**), while they showed lower *WUE* (**Figure 2E**). Under the steady state, there was no significant difference in g_s and *A* between WT and ST-OX or *epf1*, although these parameters of ST-OX and *epf1* tended to be higher than those of WT (**Supplementary Figure S1**).

Subsequently, we evaluated the induction speed of g_s and *A* to the step increase in light in the three Arabidopsis lines. After the change from darkness (0 μmol photon m^{-2} s^{-1}) to high light, g_s induction was initially faster in ST-OX and *epf1* than WT during photosynthetic induction, while it was slower in ST-OX and *epf1* than WT at the later phase (**Figure 3A**). g_s in WT and *epf1* was fully induced at 80 min after step increase in light, while that of ST-OX slightly but continuously increased in 120 min (**Figure 2A**). t_{5gs} in ST-OX and *epf1* was significantly shorter than that in WT ($p < 0.05$) (**Figure 3B**). On the other hand, t_{60gs} in ST-OX and t_{80gs} in ST-OX and *epf1* were significantly larger than that in WT ($p < 0.05$). *A* induction was faster in ST-OX and *epf1* than WT after the step increase in light (**Figure 3C**). t_{60A} in ST-OX and *epf1* and t_{80A} in *epf1*were significantly shorter than that in WT ($p < 0.05$) (**Figure 3D**). In the steady state under darkness, g_{si} in ST-OX and *epf1* were 264.5% ($p < 0.01$) and 160.6% higher (not significant), respectively, than that in WT (**Figure 3E**). t_{60A} decreased with the increase in g_{si} when $g_{si} < 0.074$, and it was constantly independent of g_{si} for $g_{si} > 0.074$ (**Figure 3F**).

CO_2 Assimilation and Biomass Production Under Fluctuating Light

Cumulative CO_2 assimilation and transpiration were evaluated to compare the efficiency of carbon gain and water use during photosynthetic induction in the three Arabidopsis lines. *CCA* in ST-OX and *epf1* was 57.6 and 78.8% higher ($p < 0.05$), respectively, than that in WT, while Loss rate in ST-OX and *epf1* was 27.7% and 36.5% lower ($p < 0.05$) (**Figures 4A,C**). *CE* in

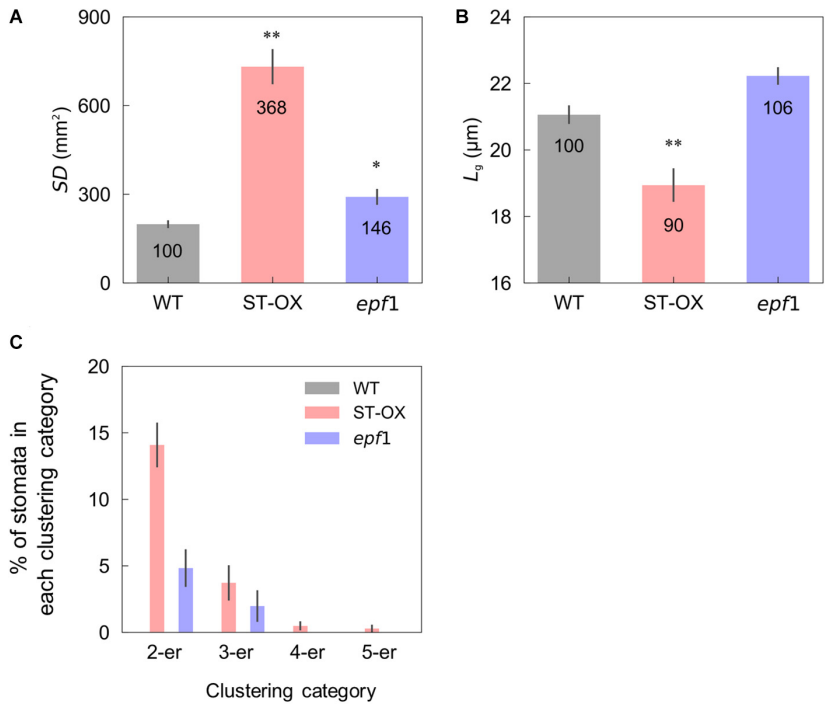

FIGURE 1 | Stomatal density, size, and clustering. **(A)** The stomatal density (*SD*), **(B)** guard cell length (L_g) and **(C)** the rate of stomata in 2–5 clustering categories were evaluated on fully expanded leaves in the wild-type line (WT), a *STOMAGEN/EPFL9* overexpressing line (ST-OX), and an *EPF1* knockout line (*epf1*) of *Arabidopsis thaliana*. The vertical bars indicate the standard error ($n = 6$). * and ** indicate the significant variation in each parameter between WT and each transgenic line at $p < 0.05$, and 0.01, respectively, according to the Steel test in **(A)** or Dunnett's test in **(B)**. The value in each column represents the relative value of each line to WT.

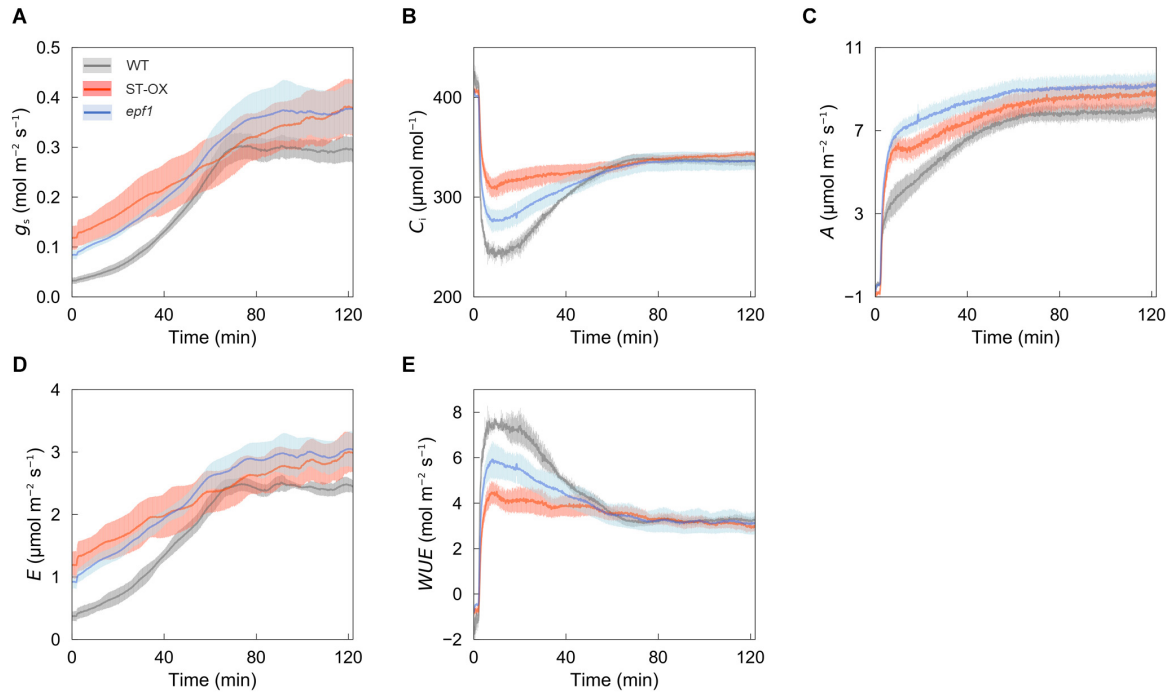

FIGURE 2 | Photosynthetic dynamics after step increase in light. **(A)** A stomatal conductance (g_s), **(B)** intercellular CO_2 concentration (C_i), **(C)** CO_2 assimilation rate (A), **(D)** transpiration rate (E), and **(E)** water use efficiency (WUE) were measured on fully expanded leaves in the three lines of Arabidopsis. The gas exchange measurements were conducted at a CO_2 concentration of 400 ppm, air temperature of 25°C and dark condition for the initial 10 min and, subsequently, under a PPFD of 500 µmol photon m^{-2} s^{-1} for 120 min. Vertical bars indicate the standard error (n = 3).

ST-OX and *epf1* were 193.7% and 138.7% higher ($p < 0.05$), respectively, than that in WT (**Figure 4B**). There was no significant variation in WUE_i between WT and *epf1*, while WUE_i in ST-OX was 44.9% lower than WT ($p < 0.05$) (**Figure 4D**). Finally, we evaluated the biomass production under the constant (**Figure 5A**) and fluctuating light (**Figure 5B**) in the three Arabidopsis lines to examine how higher *SD* affects growth characteristics. Compared with WT, dry weight of the above ground biomass under constant light ($DW_{constant}$) in *epf1* was similar, while that under fluctuating light ($DW_{fluctuating}$) in *epf1* was 25.6% higher than that of WT ($p < 0.01$) (**Figures 5C,D**). There was no significant variation in $DW_{constant}$ and $DW_{fluctuating}$ between ST-OX and WT.

DISCUSSION

Stomata play a significant role in the regulation of gas exchange between the outside and inside of the leaf. However, how the *SD* change affects photosynthetic and growth characteristics in plants has been controversial, and the effect of *SD* change on photosynthesis and growth can vary depending on the plant species or environmental conditions. Previously, we reported that higher *SD* resulted in the enhancement of g_s and A in Arabidopsis under constant and saturated light conditions (Tanaka et al., 2013). Lawson and Blatt (2014) suggested that with higher *SD*, it would be instructive to determine biomass productivity under fluctuating light, although only a few studies investigated the relationship between *SD* and photosynthetic or growth characteristics under that condition (Drake et al., 2013; Papanatsiou et al., 2016; Schuler et al., 2017; Vialet-Chabrand et al., 2017). Here, we attempted to examine how higher *SD* affects g_s and A dynamics, biomass production, and water use in Arabidopsis under fluctuating light.

Stomatal Density Affects the Induction of Stomatal Opening

We revealed that the three Arabidopsis lines differing in *SD* showed significant differences in the dynamics of g_s in the non-steady state. *SD* differences had significant (Vialet-Chabrand et al., 2017) or non-significant (Papanatsiou et al., 2016; Schuler et al., 2017) effect on g_s induction to light transients from low to high in previous studies. In the present study, ST-OX and *epf1* showed initially faster g_s induction than WT, while those lines showed slower g_s induction in the later phase after step increase in light from a PPFD of 0 to 500 µmol photon m^{-2} s^{-1} (**Figures 3A,B**). The different responses of g_s could be attributable to the difference in the size, density, and patterning of stomata. Drake et al. (2013) reported that smaller stomata respond the fluctuating light faster than larger stomata among several species of the genus *Banksia*. On the contrary, smaller stomata resulted in the slower response of g_s to fluctuating light in the genus *Oryza* (Zhang et al., 2019). In the present study, the variation in the speed of g_s induction did not correspond to that in L_g (**Figures 1**, **3**), indicating that the stomatal size

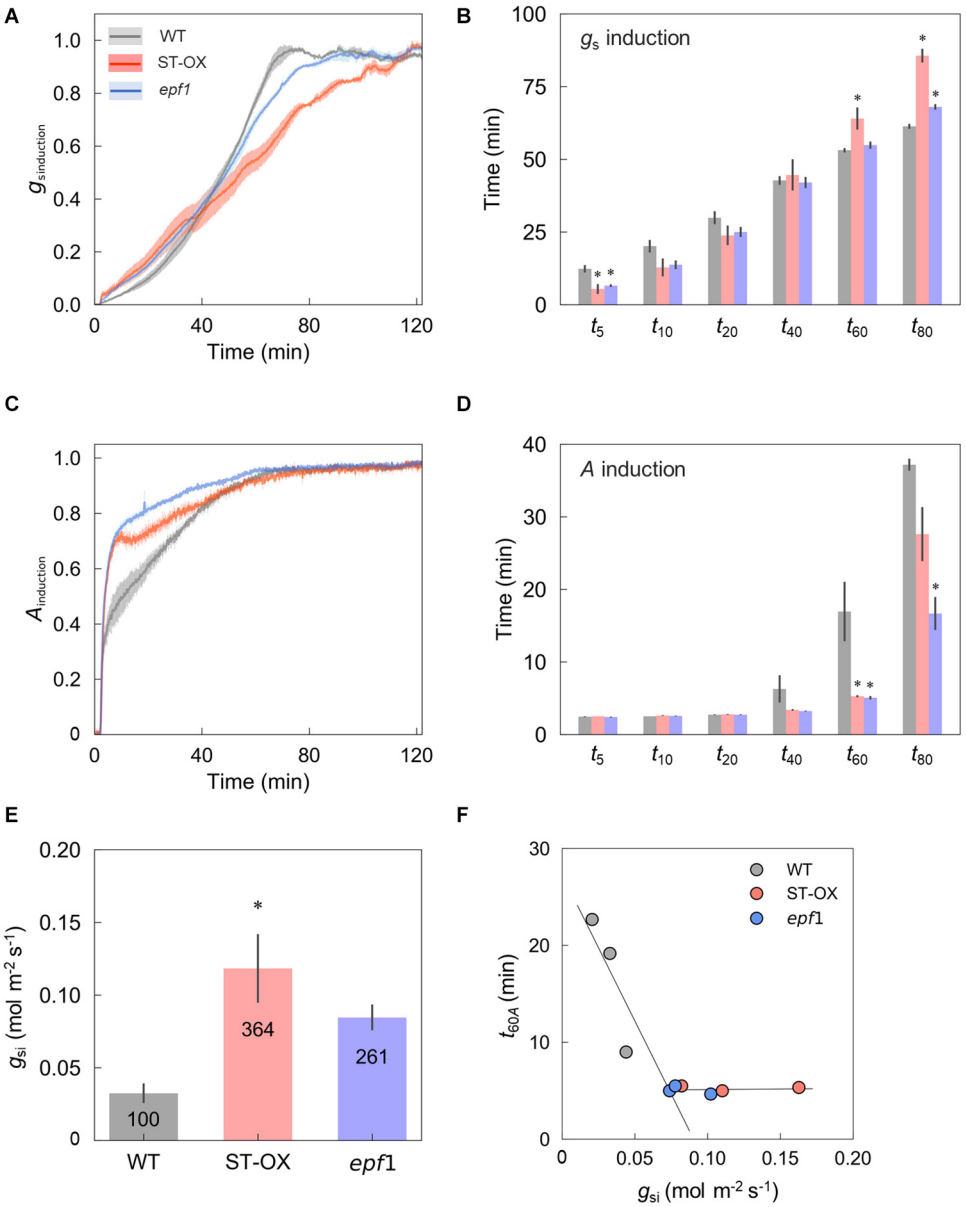

FIGURE 3 | The induction speed of stomatal conductance and CO_2 assimilation rate after step increase in light. The induction state of **(A)** stomatal conductance (g_s) and **(C)** CO_2 assimilation rate (A) were evaluated in the three lines of Arabidopsis based on $g_{sinduction}$ and $A_{induction}$ defined as Eqs. 1 and 2, respectively, under a PPFD of 500 μmol photon m^{-2} s^{-1} for 120 min after the dark period for 10 min. The time when **(B)** $g_{sinduction}$ and **(D)** $A_{induction}$ reached 5, 10, 20, 40, 60, and 80% (t_{5-80gs} and t_{5-80A}) of those maximum values was compared between WT and each transgenic line. **(E)** The steady-state value of g_s under the dark condition (g_{si}) was compared between WT and each transgenic line. **(F)** The relationship was investigated between g_{si} and t_{60A}. Vertical bars indicate the standard error ($n = 3$). *indicates significant differences in each parameter between WT and each transgenic line at $p < 0.05$, according to Dunnett's test. The values in each column represent the relative value of each line to WT.

would have a minor effect on g_s induction in Arabidopsis under fluctuating light.

The stomatal opening is regulated by at least three key components, blue-light receptor phototropin, plasma membrane H^+-ATPase, and plasma membrane inward rectifying K^+ channels in the guard cell (Inoue and Kinoshita, 2017). The activation of H^+-ATPase induced by blue light as the initial signal facilitates K^+ uptake through the inward rectifying K^+ channel to increase the turgor pressure of guard cells, resulting in the stomatal opening. In addition, stomatal opening dynamics depend on the water status in the plant (Lawson and Blatt, 2014). With more stomata, higher metabolic cost and water uptake would be required for stomatal movement. The gas-exchange and theoretical-modeling analysis indicated that the stomatal clustering decreased the maximum value of g_s and A under the steady state because of the misplacement of stomatal pores over

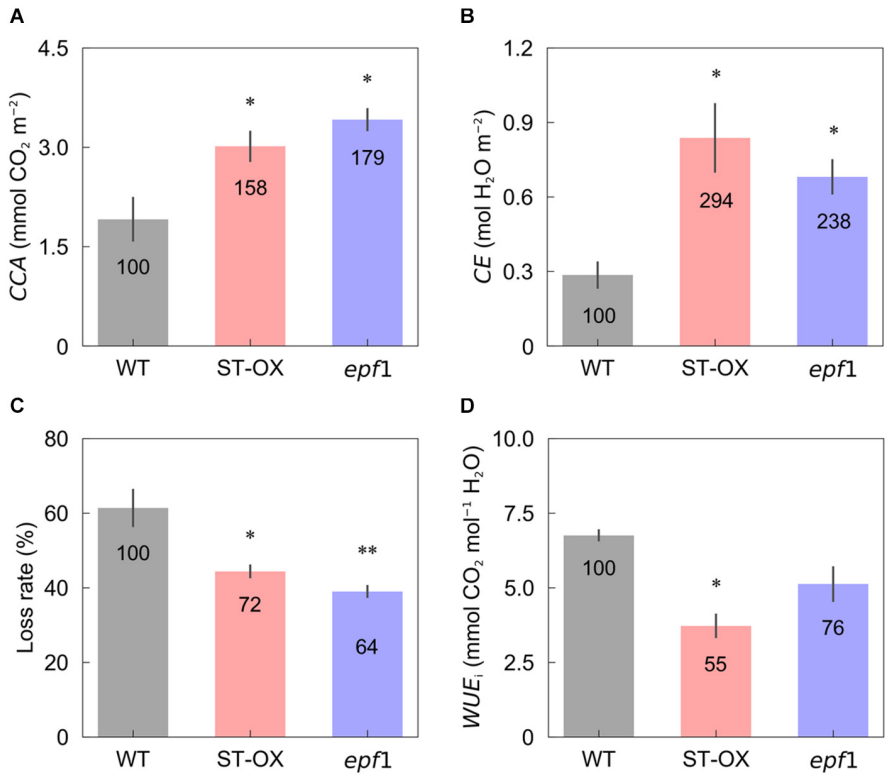

FIGURE 4 | Cumulative carbon gain and water use after step increase in light. **(A)** Cumulative CO_2 assimilation (*CCA*) and **(B)** transpiration (*CE*) were measured in the first 10 min under illumination after initial darkness in the three lines of Arabidopsis under the fluctuating light. **(C)** The loss rate of CO_2 assimilation caused by the induction response was calculated based on Eq. 3. **(D)** Integrated water use efficiency (WUE_i) was calculated as the ratio of *CCA* to *CE*. Vertical bars indicate the standard error ($n = 3$). * and ** indicate significant differences in each parameter between WT and each transgenic line at $p < 0.05$ and 0.01, respectively, according to Dunnett's test. The value in each column represents the relative value of each line to WT.

mesophyll cells (Dow and Bergmann, 2014; Lehmann and Or, 2015). It was also shown that clustering suppressed stomatal movement owing to the decreased capacity of the K^+ flux and K^+ accumulation in the guard cells (Papanatsiou et al., 2016). Additionally, g_s induction to fluctuating light in *Begonia* species with clustered stomata was slower than that in those without clustered stomata (Papanatsiou et al., 2017). In this study, ST-OX and *epf1* with higher *SD* and clustering rate showed initially faster g_s induction and, at the later phase, slower induction than WT (**Figures 1**, **3**). These results suggest that the changes in stomatal density and patterning can affect g_s induction to fluctuating light owing to the change in water uptake for stomatal opening and the opening speed of single stomata.

Stomatal Density Affects the Dynamics of CO_2 Assimilation

In ST-OX and *epf1*, *A* induction to step change from darkness to high light was faster than that of WT (**Figures 3C,D**). Photosynthetic induction is typically limited by three phases of the biochemical or diffusional processes; (1) activation of electron transport, (2) activation of the enzymes of the Calvin-Benson cycle, and (3) stomatal opening (Pearcy, 1990; Yamori et al., 2016). The significance of stomatal limitation to photosynthetic induction depends on the initial value of g_s as well as photosynthetic capacity and the induction state of biochemical processes (Kirschbaum and Pearcy, 1988). Activation speed of the electron transport and enzymes of the Calvin-Benson cycle after step increase in light intensity can be largely affected by CO_2 concentration (Jackson et al., 1991; Urban et al., 2008; Kaiser et al., 2017). The variation of g_s under dark or low light conditions corresponded to that in the speed of photosynthetic induction in several plant species (Kaiser et al., 2016; Soleh et al., 2017). In this study, t_{60A} correlated with g_{si} if $g_{si} < 0.074$ mol m^{-2} s^{-1}, and it was constant regardless of g_{si} if $g_{si} > 0.074$ mol m^{-2} s^{-1} (**Figure 3F**). g_{si} of WT, ST-OX, and *epf1* were 0.032, 0.118, and 0.085 mol m^{-2} s^{-1}, respectively (**Figure 3E**), suggesting that the variation in g_{si} would cause the response difference of *A*. Therefore, higher *SD* resulted in higher initial value of g_s and then higher C_i, which would contribute to the rapid activation of RuBP regeneration and carboxylation in the Calvin-Benson cycle.

The transition from a short period of low to high light is frequently observed in the crop canopy throughout the day (Tanaka et al., 2019). The present study confirmed that higher *SD* resulted in faster *A* induction after step increase in light from darkness, which can be observed at the limited part of the day in field. It is not clear how *SD* affects g_s and *A* induction after the adaptation to low light for short period. It has been

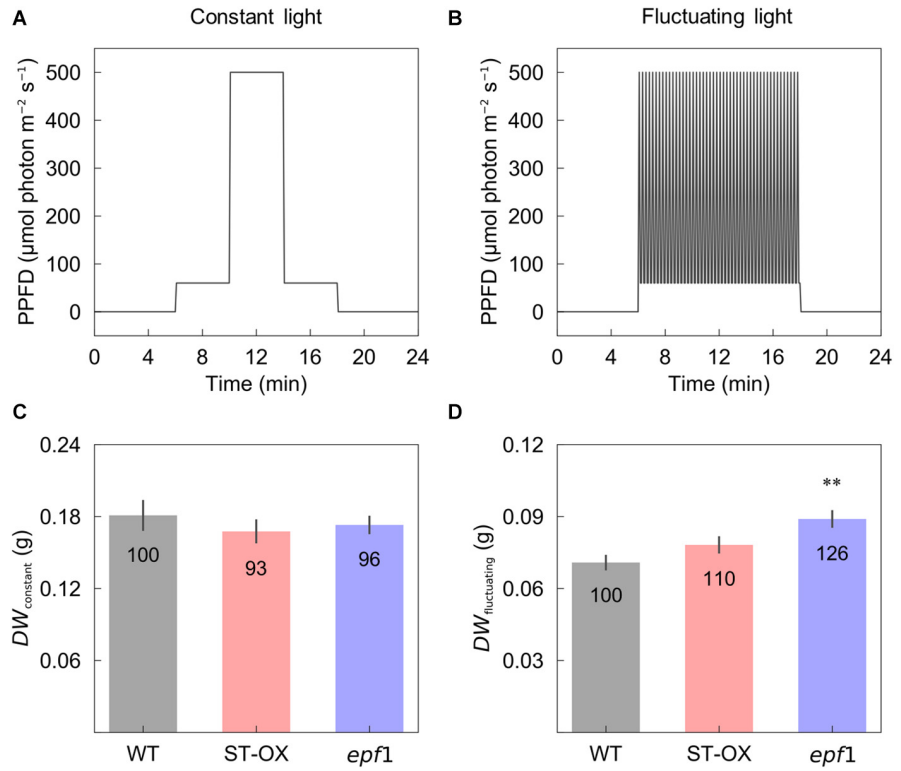

FIGURE 5 | Biomass production under the constant and fluctuating light conditions. Dry weight of the above ground biomass was evaluated in the three lines of Arabidopsis under **(C)** the constant ($DW_{constant}$) and **(D)** fluctuating ($DW_{fluctuating}$) light conditions as described in **(A)** and **(B)**. Vertical bars indicate the standard error ($n = 4$). ** indicates significant differences in each parameter between WT and each transgenic line at $p < 0.01$, according to Dunnett's test. The values in each column represent the relative value of each line to WT.

considered that stomatal opening and Rubisco activation would not be a major limitation to *A* under such light conditions since these would not change rapidly (MuAusland et al., 2016). A rapid change in the RuBP regeneration was reported to limit photosynthetic induction under high light after a short period of low light or darkness (Kobza and Edwards, 1987; Sassenrath-Cole and Pearcy, 1994). On the other hand, the significant stomatal limitation to photosynthesis has been shown in Arabidopsis (Kimura et al., 2020) and rice (Yamori et al., 2020) under natural light conditions where the light fluctuations are highly variable. Future study is required to elucidate that higher *SD* would be beneficial for carbon gain under more rapid and frequent fluctuation of light.

Stomatal Density Affects Biomass Production Under the Fluctuating Light

Manipulating CO_2 diffusion via stomata has been attempted to enhance photosynthetic capacity and induction in plants. Under constant light conditions, overexpression of H^+-ATPase (AHA2) in guard cells resulted in higher g_s as well as *A*, leading to greater biomass production in Arabidopsis (Wang et al., 2014). In addition, Arabidopsis plants with stay-opening or fast-moving stomata have been shown to achieve greater carbon gain and biomass production under fluctuating light conditions (Papanatsiou et al., 2019; Kimura et al., 2020). These studies confirmed the significant limitation of photosynthesis imposed by stomata, and the potential of g_s to improve biomass production of plants under field. On the other hand, higher g_s generally results in lower *WUE*, which can depress the benefit of greater photosynthetic performance for biomass production (Tanaka et al., 2013; Kimura et al., 2020). Under drought condition, transgenic plants with lower *SD* and g_s exhibited improved growth performance owing to high *WUE* in several species (Yoo et al., 2010; Wang et al., 2016; Caine et al., 2018). It is, therefore, import to optimize a balance between carbon gain and water loss via stomata for plant growth depending on water conditions (Lawson and Blatt, 2014; MuAusland et al., 2016).

$DW_{fluctuating}$ was much lower than $DW_{constant}$ in three Arabidopsis lines, although the total amount of light intensity exposed to the plants was equal between both light conditions (**Figure 5**). This difference would be caused by the loss of carbon gain owing to photosynthetic induction under fluctuating light condition. $DW_{constant}$ in ST-OX was slightly lower than that in WT, although steady-state *A* was significantly or slightly higher in Tanaka et al. (2013) and this study, respectively (**Figures 2**, **5**). The increase in water loss would have a negative effect on biomass production in ST-OX under constant light (Tanaka et al., 2013). ST-OX showed significantly lower *WUE* during photosynthetic induction in the present study (**Figures 2**, **4**). Despite of these

penalties resulting from the drastic increase in *SD*, $DW_{fluctuating}$ in ST-OX was 10.5% higher than that in WT with no significance. Moreover, biomass production in *epf1*, with moderate increase in *SD*, was significantly higher than that in WT under fluctuating light, while there was no difference between these two lines under constant light (**Figure 5**). It is possible that a moderate increase in *SD* could achieve more efficient carbon gain attributable to the faster response of *A* in Arabidopsis under fluctuating light, while it would cause small penalties on water loss for stomatal movement. Overall, higher *SD* can be beneficial to improve biomass production in plants under fluctuating light conditions under favorable water conditions.

CONCLUSION

Under fluctuating light, there was a significant variation in the photosynthetic and growth characteristics among Arabidopsis lines differing in the stomatal density (*SD*). Higher *SD* resulted in faster CO_2 assimilation rate (*A*) induction to fluctuating light owing to the higher initial value of the stomatal conductance (g_s) and faster g_s induction in the early phase of photosynthetic induction. On the other hand, higher *SD* resulted in slower g_s induction in the later phase of photosynthetic induction. *epf1*, with a moderate increase in *SD*, achieved more efficient carbon gain with small penalty on water use efficiency attributable to the faster *A* induction, which would contribute to higher biomass production than that in WT under fluctuating light. This study suggests that higher *SD* can be beneficial to improve biomass production in plants under fluctuating light.

DATA AVAILABILITY STATEMENT

The original contributions presented in the study are included in the article/**Supplementary Material**, further inquiries can be directed to the corresponding author.

AUTHOR CONTRIBUTIONS

KS conceived and designed this project, performed all the gas exchange experiments, wrote the manuscript with inputs from co-authors. WY conducted the biomass analysis. All authors contributed to the article and approved the submitted version.

FUNDING

This work was supported by a Grant-in-Aid for Scientific Research to IH-N (Grant Nos. 22000014 and 15H05776), to KS (Grant No. 20J00594), to WY (Grant Nos. 16H06552, 18H02185, 18KK0170, and 20H05687), and to YT (Grant No. 20H02968) from Japan Society for the Promotion of Science (JSPS), and PRESTO to YT (Grant No. JPMJPR16Q5) from Japan Science and Technology Agencys.

ACKNOWLEDGMENTS

We are grateful to Mr. S. Shimadzu for help in the biomass analysis. This manuscript has been released as a pre-print at *bioRxiv*, Sakoda et al. (2020).

SUPPLEMENTARY MATERIAL

The Supplementary Material for this article can be found online at: https://www.frontiersin.org/articles/10.3389/fpls.2020.589603/full#supplementary-material

Supplementary Figure 1 | Stomatal conductance and CO2 assimilation rate under steady state. **(A)** A stomatal conductance (g_{sf}) and **(B)** CO_2 assimilation rate (A_f) under steady state were measured on fully expanded leaves in the three lines of Arabidopsis. The gas exchange measurements were conducted at a CO_2 concentration of 400 ppm, air temperature of 25°C and dark condition for the initial 10 min and, subsequently, under a PPFD of 500 μmol photon m^{-2} s^{-1} for 120 min. Vertical bars indicate the standard error (n = 3). The values in each column represent the relative value of each line to WT.

REFERENCES

Adachi, S., Tanaka, Y., Miyagi, A., Kashima, M., Tezuka, A., Toya, Y., et al. (2019). High-yielding rice Takanari has superior photosynthetic response under fluctuating light to a commercial rice *Koshihikari*. *J. Exp. Bot.* 70, 5287–5297. doi: 10.1093/jxb/erz304

Büssis, D., Von Groll, U., Fisahn, J., and Altmann, T. (2006). Stomatal aperture can compensate altered stomatal density in *Arabidopsis thaliana* at growth light conditions. *Funct. Plant Biol.* 33, 1037–1043. doi: 10.1071/FP06078

Caine, R., Yin, X., Sloan, J., Harrison, E. L., Mohammed, U., Fulton, T., et al. (2018). Rice with reduced stomatal density conserves water and has improved drought tolerance under future climate conditions. *New Phytol.* 221, 371–384. doi: 10.1111/nph.15344

Carmo-Silva, A. E., and Salvucci, M. E. (2013). The regulatory properties of rubisco activase differ among species and affect photosynthetic induction during light transitions. *Plant Physiol.* 161, 1645–1655. doi: 10.1104/pp.112.213348

Doheny-Adams, T., Hunt, L., Franks, P. J., Beerling, D. J., and Gray, J. E. (2012). Genetic manipulation of stomatal density influences stomatal size, plant growth and tolerance to restricted water supply across a growth carbon dioxide gradient. *Philos. Trans. R. Soc. B Biol. Sci.* 367, 547–555. doi: 10.1098/rstb.2011.0272

Dow, G. J., and Bergmann, D. C. (2014). Patterning and processes: how stomatal development defines physiological potential. *Curr. Opin. Plant Biol.* 21, 67–74. doi: 10.1016/j.pbi.2014.06.007

Drake, P. L., Froend, R. H., and Franks, P. J. (2013). Smaller, faster stomata: Scaling of stomatal size, rate of response, and stomatal conductance. *J. Exp. Bot.* 64, 495–505. doi: 10.1093/jxb/ers347

Farquhar, G. D., and Sharkey, T. D. (1982). Stomatal conductance and photosynthesis. *Annu. Rev. Plant Physiol.* 33, 317–345. doi: 10.1146/annurev.pp.33.060182.001533

Franks, P. J., and Beerling, D. J. (2009). CO2-forced evolution of plant gas exchange capacity and water-use efficiency over the phanerozoic. *Geobiology* 7, 227–236. doi: 10.1111/j.1472-4669.2009.00193.x

Hara, K., Kajita, R., Torii, K. U., Bergmann, D. C., and Kakimoto, T. (2007). The secretory peptide gene EPF1. *Genes Dev.* 7, 1720–1725. doi: 10.1101/gad.1550707.metric

Hashimoto-Sugimoto, M., Higaki, T., Yaeno, T., Nagami, A., Irie, M., Fujimi, M., et al. (2013). A Munc13-like protein in Arabidopsis mediates H+-ATPase translocation that is essential for stomatal responses. *Nat. Commun.* 4:3215. doi: 10.1038/ncomms3215

Inoue, S., and Kinoshita, T. (2017). Blue light regulation of stomatal opening and the plasma membrane H^+-ATPase. *Plant Physiol.* 174, 531–538. doi: 10.1104/pp.17.00166

Jackson, R. B., Woodrow, I. E., and Mott, K. A. (1991). Nonsteady-state photosynthesis following an increase in photon flux density (PFD). *Plant Physiol.* 95, 498–503. doi: 10.1104/pp.95.2.498

Kaiser, E., Kromdijk, J., Harbinson, J., Heuvelink, E., and Marcelis, L. F. M. (2017). Photosynthetic induction and its diffusional, carboxylation and electron transport processes as affected by CO_2 partial pressure, temperature, air humidity and blue irradiance. *Ann. Bot.* 119, 191–205. doi: 10.1093/aob/mcw226

Kaiser, E., Morales, A., and Harbinson, J. (2018). Fluctuating light takes crop photosynthesis on a rollercoaster ride. *Plant Physiol.* 176, 977–989. doi: 10.1104/pp.17.01250

Kaiser, E., Morales, A., Harbinson, J., Heuvelink, E., Prinzenberg, A. E., and Marcelis, L. F. M. (2016). Metabolic and diffusional limitations of photosynthesis in fluctuating irradiance in Arabidopsis thaliana. *Sci. Rep.* 6, 1–13. doi: 10.1038/srep31252

Kimura, H., Hashimoto-Sugimoto, M., Iba, K., Terashima, I., and Yamori, W. (2020). Improved stomatal opening enhances photosynthetic rate and biomass production in fluctuating light. *J. Exp. Bot.* 71, 2339–2350. doi: 10.1093/jxb/eraa090

Kirschbaum, M. U. F., and Pearcy, R. W. (1988). Gas exchange analysis of the fast phase of photosynthetic induction in *Alocasia macrorrhiza*. *Plant Physiol.* 87, 818–821. doi: 10.1104/pp.87.4.818

Kobza, J., and Edwards, G. E. (1987). The photosynthetic induction response in wheat leaves: net CO_2 uptake, enzyme activation, and leaf metabolites. *Planta* 171, 549–559. doi: 10.1007/BF00392305

Lawson, T., and Blatt, M. R. (2014). Stomatal size, speed, and responsiveness impact on photosynthesis and water use efficiency. *Plant Physiol.* 164, 1556–1570. doi: 10.1104/pp.114.237107

Lee, J. S., Hnilova, M., Maes, M., Lin, Y. C. L., Putarjunan, A., Han, S. K., et al. (2015). Competitive binding of antagonistic peptides fine-tunes stomatal patterning. *Nature* 522, 439–443. doi: 10.1038/nature14561

Lehmann, P., and Or, D. (2015). Effects of stomatal clustering on leaf gas exchange. *New Phytol.* 15, 1015–1025. doi: 10.1111/nph.13442

Mcadam, S. A. M., and Brodribb, T. J. (2012). Stomatal innovation and the rise of seed plants. *Ecol. Lett.* 15, 1–8. doi: 10.1111/j.1461-0248.2011.01700.x

MuAusland, L., Vialet-Chanbrand, S., Davey, P., Baker, N. R., Brendel, O., and Lawson, T. (2016). Effects of kinetics of light-induced stomatal responses on photosynthesis and water-use efficiency. *New Phytol.* 211, 1209–1220. doi: 10.1111/nph.14000

Papanatsiou, M., Amtmann, A., and Blatt, M. R. (2016). Stomatal spacing safeguards stomatal dynamics by facilitating guard cell ion transport independent of the epidermal solute reservoir. *Plant Physiol.* 172, 254–263. doi: 10.1104/pp.16.00850

Papanatsiou, M., Amtmann, A., and Blatt, M. R. (2017). Stomatal clustering in Begonia associates with the kinetics of leaf gaseous exchange and influences water use efficiency. *J. Exp. Bot.* 68, 2309–2315. doi: 10.1093/jxb/erx072

Papanatsiou, M., Petersen, J., Henderson, L., Wang, Y., Christie, J. M., and Blatt, M. R. (2019). Optogenetic manipulation of stomatal kinetics improves carbon assimilation, water use, and growth. *Science* 363, 1456–1459. doi: 10.1126/science.aaw0046

Pearcy, R. W. (1990). Sunflecks and photosynthesis in plant canopies. *Ann. Rev. Plant Biol.* 41, 421–453. doi: 10.1146/annurev.pp.41.060190.002225

Qu, M., Hamdani, S., Li, W., Wang, S., Tang, J., Chen, Z., et al. (2016). Rapid stomatal response to fluctuating light: an under-explored mechanism to improve drought tolerance in rice. *Funct. Plant Biol.* 43:727. doi: 10.1071/fp15348

Sakoda, K., Kaga, K., Tanaka, Y., Suzuki, S., Fujii, K., Ishimoto, M., et al. (2018). Two novel quantitative trait loci affecting the variation in leaf photosynthetic capacity among soybeans. *Plant Sci.* 291:110300. doi: 10.1016/j.plantsci.2019.110300

Sakoda, K., Yamori, W., Shimada, T., Sugano, S. S., Hara-Nishimura, I., and Tanaka, Y. (2020). Stomatal density affects gas diffusion and CO_2 assimilation dynamics in *Arabidopsis* under fluctuating light. *bioRxiv* [Preprint]. doi: 10.1101/2020.02.20.958603

Sassenrath-Cole, G. F., and Pearcy, R. W. (1994). Regulation of photosynthetic induction state by the magnitude and duration of low light exposure. *Plant Physiol.* 105, 1115–1123. doi: 10.1016/j.biopsych.2016.03.2100

Schlüter, U., Muschak, M., Berger, D., and Altmann, T. (2003). Photosynthetic performance of an *Arabidopsis* mutant with elevated stomatal density (sdd1-1) under different light regimes. *J. Exp. Bot.* 54, 867–874. doi: 10.1093/jxb/erg087

Schuler, M. L., Sedelnikova, O. V., Walker, B. J., Westhoff, P., and Langdale, J. A. (2017). SHORTROOT-mediated increase in stomatal density has no impact on photosynthetic efficiency. *Plant Physiol.* 176, 752–772. doi: 10.1104/pp.17.01005

Shimadzu, S., Seo, M., Terashima, I., and Yamori, W. (2019). Whole irradiated plant leaves showed faster photosynthetic induction than individually irradiated leaves via improved stomatal opening. *Front. Plant Sci.* 10:1512. doi: 10.3389/fpls.2019.01512

Soleh, M. A., Tanaka, Y., Kim, S. Y., Huber, S. C., Sakoda, K., and Shiraiwa, T. (2017). Identification of large variation in the photosynthetic induction response among 37 soybean [Glycine max (L.) Merr.] genotypes that is not correlated with steady-state photosynthetic capacity. *Photosynth. Res.* 131, 305–315. doi: 10.1007/s11120-016-0323-1

Soleh, M. A., Tanaka, Y., Nomoto, Y., Iwahashi, Y., Nakashima, K., Fukuda, Y., et al. (2016). Factors underlying genotypic differences in the induction of photosynthesis in soybean [Glycine max (L.) Merr.]. *Plant Cell Environ.* 39, 685–693. doi: 10.1111/pce.12674

Sugano, S. S., Shimada, T., Imai, Y., Okawa, K., Tamai, A., Mori, M., et al. (2010). Stomagen positively regulates stomatal density in *Arabidopsis*. *Nature* 463, 241–244. doi: 10.1038/nature08682

Tanaka, Y., Adachi, S., and Yamori, W. (2019). Natural genetic variation of the photosynthetic induction response to fluctuating light environment. *Curr. Opin. Plant Biol.* 49, 52–59. doi: 10.1016/j.pbi.2019.04.010

Tanaka, Y., Sugano, S. S., Shimada, T., and Hara-Nishimura, I. (2013). Enhancement of leaf photosynthetic capacity through increased stomatal density in *Arabidopsis*. *New Phytol.* 198, 757–764. doi: 10.1111/nph.12186

Taylor, S. H., and Long, S. P. (2017). Slow induction of photosynthesis on shade to sun transitions in wheat may cost at least 21% of productivity. *Philos. Trans. R. Soc. B Biol. Sci.* 17:372. doi: 10.1098/rstb.2016.0543

Urban, O., Šprtová, M., Košvancová, M., Tomášková, I., Lichtenthaler, H. K., and Marek, M. V. (2008). Comparison of photosynthetic induction and transient limitations during the induction phase in young and mature leaves from three poplar clones. *Tree Physiol.* 28, 1189–1197. doi: 10.1093/treephys/28.8.1189

Vialet-Chabrand, S. R. M., Matthews, J. S. A., McAusland, L., Blatt, M. R., Griffiths, H., and Lawson, T. (2017). Temporal dynamics of stomatal behavior: modeling and implications for photosynthesis and water use. *Plant Physiol.* 174, 603–613. doi: 10.1104/pp.17.00125

von Caemmerer, S., and Evans, J. R. (2010). Enhancing C3 photosynthesis. *Plant Physiol.* 154, 589–592. doi: 10.1104/pp.110.160952

Wang, C., Liu, S., Dong, Y., Zhao, Y., Geng, A., Xia, X., et al. (2016). PdEPF1 regulates water-use efficiency and drought tolerance by modulating stomatal density in poplar. *Plant Biotechnol. J.* 14, 849–860. doi: 10.1111/pbi.12434

Wang, Y., Noguchi, K., Ono, N., Inoue, S., Terashima, I., and Kinoshita, T. (2014). Overexpression of plasma membrane H^+-ATPase in guard cells promotes light-induced stomatal opening and enhances plant growth. *Proc. Natl. Acad. Sci. U.S.A.* 111, 533–538. doi: 10.1073/pnas.1305438111

Wong, S. C., Cowan, I. R., and Farquhar, G. D. (1979). Stomatal conductance correlates with photosynthetic capacity. *Nature* 282, 424–426. doi: 10.1038/282424a0

Yamori, W. (2016). Photosynthetic response to fluctuating environments and photoprotective strategies under abiotic stress. *J. Plant Res.* 129, 379–395. doi: 10.1007/s10265-016-0816-1

Yamori, W., Kondo, E., Sugiura, D., Terashima, I., Suzuki, Y., and Makino, A. (2016). Enhanced leaf photosynthesis as a target to increase grain yield: Insights from transgenic rice lines with variable Rieske FeS protein content in the

cytochrome b6/f complex. *Plant Cell Environ.* 39, 80–87. doi: 10.1111/pce.12594

Yamori, W., Kusumi, K., Iba, K., and Terashima, I. (2020). Increased stomatal conductance induces rapid changes to photosynthetic rate in response to naturally fluctuating light conditions in rice. *Plant. Cell Environ.* 43, 1230–1240. doi: 10.1111/pce.13725

Yamori, W., Masumoto, C., Fukayama, H., and Makino, A. (2012). Rubisco activase is a key regulator of non-steady-state photosynthesis at any leaf temperature and, to a lesser extent, of steady-state photosynthesis at high temperature. *Plant J.* 71, 871–880. doi: 10.1111/j.1365-313X.2012.05041.x

Yoo, C. Y., Pence, H. E., Jin, J. B., Miura, K., Gosney, M. J., Hasegawa, P. M., et al. (2010). The Arabidopsis GTL1 transcription factor regulates water use efficiency and drought tolerance by modulating stomatal density via transrepression of SDD1. *Plant Cell* 22, 4128–4141. doi: 10.1105/tpc.110.078691

Zhang, Q., Peng, S., and Li, Y. (2019). Increase rate of light-induced stomatal conductance is related to stomatal size in the genus Oryza. *J. Exp. Bot.* 70, 5259–5269. doi: 10.1093/jxb/erz267

Conflict of Interest: The authors declare that the research was conducted in the absence of any commercial or financial relationships that could be construed as a potential conflict of interest.

frontiers in Plant Science

ORIGINAL RESEARCH
published: 10 December 2020
doi: 10.3389/fpls.2020.580726

Phosphoglucoisomerase Is an Important Regulatory Enzyme in Partitioning Carbon out of the Calvin-Benson Cycle

*Alyssa L. Preiser[1,2], Aparajita Banerjee[2], Sean E. Weise[1], Luciana Renna[1], Federica Brandizzi[1,3] and Thomas D. Sharkey[1,2,4]**

[1] MSU-DOE Plant Research Laboratory, Michigan State University, East Lansing, MI, United States, [2] Department of Biochemistry and Molecular Biology, Michigan State University, East Lansing, MI, United States, [3] Department of Plant Biology, Michigan State University, East Lansing, MI, United States, [4] Plant Resilience Institute, Michigan State University, East Lansing, MI, United States

OPEN ACCESS

Edited by:
James Lloyd,
Stellenbosch University, South Africa

Reviewed by:
Je Hyeong Jung,
Natural Product Research Center, Korea Institute of Science and Technology, South Korea
Francesca Sparla,
University of Bologna, Italy

***Correspondence:**
Thomas D. Sharkey
tsharkey@msu.edu

Specialty section:
This article was submitted to Plant Metabolism and Chemodiversity, a section of the journal Frontiers in Plant Science

Received: 06 July 2020
Accepted: 18 November 2020
Published: 10 December 2020

Citation:
Preiser AL, Banerjee A, Weise SE, Renna L, Brandizzi F and Sharkey TD (2020) Phosphoglucoisomerase Is an Important Regulatory Enzyme in Partitioning Carbon out of the Calvin-Benson Cycle. Front. Plant Sci. 11:580726. doi: 10.3389/fpls.2020.580726

Phosphoglucoisomerase (PGI) isomerizes fructose 6-phosphate (F6P) and glucose 6-phosphate (G6P) in starch and sucrose biosynthesis. Both plastidic and cytosolic isoforms are found in plant leaves. Using recombinant enzymes and isolated chloroplasts, we have characterized the plastidic and cytosolic isoforms of PGI. We have found that the *Arabidopsis* plastidic PGI K_m for G6P is three-fold greater compared to that for F6P and that erythrose 4-phosphate is a key regulator of PGI activity. Additionally, the K_m of spinach plastidic PGI can be dynamically regulated in the dark compared to the light and increases by 200% in the dark. We also found that targeting *Arabidopsis* cytosolic PGI into plastids of *Nicotiana tabacum* disrupts starch accumulation and degradation. Our results, in combination with the observation that plastidic PGI is not in equilibrium, indicates that PGI is an important regulatory enzyme that restricts flow and acts as a one-way valve preventing backflow of G6P into the Calvin-Benson cycle. We propose the PGI may be manipulated to improve flow of carbon to desired targets of biotechnology.

Keywords: phosphoglucoisomerase, starch, Calvin-Benson cycle, carbon partitioning, erythrose 4-phosphate

INTRODUCTION

Partitioning of carbon out of central metabolism toward desired end-products is a key feature of biotechnological efforts in plants. This may be directed toward increased yields of starch, carotenoids, novel compounds, or other products (see Botella-Pavía and Rodríguez-Conceptión, 2006; Ausich, 2009; Santelia and Zeeman, 2011; and Abiri et al., 2016 for examples). In normal plant physiology, plants partition carbon out of the Calvin-Benson cycle to starch synthesis. This must be a regulated process as carbon must be carefully partitioned out of the Calvin-Benson cycle in order to not deplete metabolite pools needed for continuation of the Calvin-Benson cycle while still accumulating adequate amounts of starch to survive the night (Sulpice et al., 2014). Study of the regulation of carbon partitioning to starch synthesis can provide insight how plastid metabolism is regulated to control how much carbon stays in the Calvin-Benson cycle. This is essential for

future biotechnological applications in order to maintain photosynthetic metabolite pools to support carbon assimilation and to redirect carbon to desired end products.

While starch synthesis has been well-studied for decades, our knowledge of the regulation of the entire pathway remains incomplete. The primary pathway for carbon conversion to starch is by action of the plastid phosphoglucoisomerase (PGI) converting fructose 6-phosphate (F6P) of the Calvin-Benson cycle to glucose 6-phosphate (G6P), forming a branch point out of the Calvin-Benson cycle and initiating starch synthesis. Phosphoglucomutase then converts G6P to glucose 1-phosphate and ADP glucose pyrophosphorylase uses the glucose 1-phosphate to make ADPglucose, the substrate for starch synthases. The regulation of PGI, the enzyme that partitions carbon out of the Calvin-Benson cycle, is not clearly understood (Bahaji et al., 2015). This reaction is reversible but is displaced from equilibrium (Schnarrenberger and Oeser, 1974; Gerhardt et al., 1987; Sharkey and Vassey, 1989; Backhausen et al., 1997; Szecowka et al., 2013) indicating that it is kinetically limited. What is more, a similar degree of disequilibrium is found at different rates of photosynthesis indicating that it is regulated (Schleucher et al., 1999). Additionally, it has been shown that plastidic PGI has a higher K_m for G6P than for F6P (Schnarrenberger and Oeser, 1974). The cytosolic isoform, which is involved in sucrose synthesis, has neither of these characteristics. It is unknown why the plastidic PGI is displaced from equilibrium and appears to be regulated, despite catalyzing an easily reversible reaction. We explore the regulation of PGI using recombinant enzymes and reexamine some previously held assumptions about PGI regulation. We confirm erythrose 4-phosphate (E4P) as a key regulator, show that the K_m of PGI is dynamically regulated in the dark and light, and demonstrate that manipulating the regulation of PGI can change the accumulation of starch.

MATERIALS AND METHODS

Overexpression and Purification of Recombinant Enzymes

N-terminal His-tagged *Arabidopsis thaliana* plastidic (with targeting peptide removed) and cytosolic PGI cDNA sequences were commercially synthesized by GenScript[1]. Both constructs were placed in separate pET11a bacterial expression vectors (Millipore-Sigma, Burlington, MA, United States) and were overexpressed in *Escherichia coli* strain BL21. Cells were grown at 37°C to an OD_{600} of 0.6 to 1.0 and induced with 0.5 mM isopropyl β-D-1 thiogalactopyranoside (IPTG) at room temperature overnight. Cells were centrifuged and resuspended in lysis buffer (5 mL lysis buffer/g of pellet; 50 mM sodium phosphate, pH 8.0, 300 mM NaCl) containing 1 mg mL^{-1} lysozyme, 1 μg mL^{-1} of DNAseI, and 1x protease inhibitor cocktail (Sigma Aldrich)[2]. Cells were then lysed by sonication (Branson Sonifier 250)[3]. The sonicator was set at 50% duty cycle and an output level of 1. The cells were sonicated using five steps where each step consisted of a 15 s pulse followed by 15 s on ice. The lysate was centrifuged and supernatant collected. Ni-NTA resin (0.25 volume of lysate; Qiagen)[4] was added to the crude lysate with gentle stirring for 1 h. The mixture was loaded into a column and allowed to settle, then washed with wash buffer (50 mM sodium phosphate, pH 8.0, 300 mM NaCl, 10 mM imidazole) until the OD_{280} of the effluent was less than 0.05. Protein was eluted with six volumes of elution buffer (50 mM sodium phosphate pH 8.0, 300 mM NaCl, 250 mM imidazole) containing 1x protease inhibitor cocktail [Sigma Aldrich (see text footnote 2)]. The Ni-NTA column purification was performed in a cold room at 4°C. For all purified proteins, protein concentration was determined using a Pierce 660 nm protein assay reagent kit (Thermo Fisher Scientific)[5] using a bovine serum albumin standard. Fractions containing >95% of the protein of interest were combined and concentrated using Amicon Ultra 0.5 ml centrifugal filters (molecular weight cut off of 3 kDa). Glycerol was added to the concentrated protein to obtain a final protein solution with 15% glycerol. The glycerol stock of the proteins was aliquoted into small volumes, frozen in liquid nitrogen, and stored at −80°C. Final preparations of purified protein were run on a 12% SDS-polyacrylamide gel and stained with Coomassie Blue to check the purity of the enzymes and concentration was determined as described above. Molecular weights were estimated from the protein construct using Vector NTI [Thermo Fisher Scientific (see text footnote 5)].

Coupled Spectrophotometric Assay for PGI (F6P to G6P Reaction)

The activity of the purified plastidic and cytosolic PGI was studied using coupled spectrophotometric assays. Concentrations of G6P and F6P were measured spectrophotometrically using NADPH-linked assays (Lowry and Passonneau, 1972). All assays were validated by demonstrating linear product formation, proportional to the time of the assay and amount of enzyme added. All coupling enzymes (glucose-6-phosphate dehydrogenase (G6PDH) for the F6P to G6P direction and phosphofructokinase for the G6P to F6P direction) were added in excess so that no change in product formation was seen when varying the coupling enzyme. PGI assays were done in 50 mM bicine buffer pH 7.8, containing 4.8 mM DTT, 0.6 mM $NADP^+$, 2 U glucose-6-phosphate dehydrogenase (G6PDH) (from *Leuconostoc mesenteroides* Sigma-Aldrich catalog number G8529), varying concentrations of F6P as indicated below, and 1.31 ng plastidic or cytosolic PGI. The reaction was:

$$\mathrm{F6P} \rightleftarrows \mathrm{G6P} + \mathrm{NADP^+} \rightarrow 6-\mathrm{phosphogluconate} + \mathrm{NADPH} + \mathrm{H^+}$$

The concentrations used to study the K_m of PGI for F6P were 0-4.8 mM. Under these conditions, less than 5% of the

[1]https://www.genscript.com

[2]http://www.sigmaaldrich.com

[3]us.vwr.com

[4]https://www.qiagen.com

[5]http://www.thermofisher.com

non-limiting substrate was consumed over the duration of the assay. The assay mixtures were prepared by adding all the components except the enzyme. Activity was recorded with a dual wavelength filter photometer (Sigma ZFP2) as the increase in absorbance at 334 nm minus absorbance at 405 nm caused by $NADP^+$ reduction to NADPH using an extinction coefficient of 6190 M^{-1} cm^{-1}. These wavelengths were used because they correspond to emission wavelengths of the lamp used in the filter photometer.

Mass Spectrometry Assay for PGI (G6P to F6P Reaction)

The activity of the purified plastidic and cytosolic PGI in the G6P to F6P direction was studied using a coupled mass spectrometer assay. The assay mixture contained 50 mM Tris pH 7.8, 2.5 mM $MgCl_2$, 1 mM ATP, 5 mM DTT, 0.15 U phosphofructokinase (from *Bacillus stearothermophilus* from Sigma Aldrich catalog number F0137), varying concentrations of G6P from 0 to 3.6 mM, and 1.6 ng of plastidic or cytosolic PGI.

The reaction was:

$$\text{G6P} \rightleftarrows \text{F6P} \rightarrow \text{FBP}$$

The assay mixtures were prepared by adding all the components except the enzyme. The reaction was initiated upon addition of the enzyme. After 5 min, the reaction was quenched with four volumes of 100% ice-cold methanol. The concentration of fructose-1,6-bisphosphate (FBP) produced was shown to be linear for up to 10 min. Five nmol of D-[UL-$^{13}C_6$] FBP was added as an internal standard for quantification, and the sample was heated for 5 min at 95°C. Six volumes of 10 mM tributylamine, pH 5.0, was added and the sample was filtered through a Mini-UniPrep 0.2 μm Syringeless Filter Device (GE Healthcare Life Sciences, Whatman). LC/MS-MS was carried out on a Waters Quattro Premier XE system and was operated in electrospray negative ion mode with multiple reaction monitoring (**Table 1**). The capillary voltage was 2.75 kV; the cone voltage, 50 V; the extractor voltage, 5 V. The source temperature was 120°C and the desolvation temperature was 350°C. Gas flow for the desolvation and cone was set to 800 and 50 L h^{-1}, respectively. MassLynx software and the Acquity UPLC Console were used to control the instrument. Samples were passed through an Acquity UPLC BEH Column (Waters) with a multi-step gradient with eluent A (10 mM tributylamine with 5% methanol, adjusted to pH 6 with 500 mM acetic acid) and eluent B (methanol): 0–1 min, 95–85% A; 1–3 min, 85–65% A; 3–3.5 min, 65–40% A; 3.5–4 min, 40–0% A; 4–8.50 min, 0% A; 8.5–10 min, 100% A. The flow rate was 0.3 mL min^{-1}. FBP peaks were integrated using QuanLynx software and the concentration of the metabolites was quantified by comparing the peak response to an external calibration curve.

TABLE 1 | Parameters used for detection of fructose bisphosphate (FBP) and the internal standard with LC/MS/MS.

Metabolite	Cone (V)	Collision (V)	+0 Parent (m/z)	Daughter (m/z)
FBP	26	18	339	97
D-[UL-$^{13}C_6$] FBP	26	18	345	97

Parameters were optimized using 10 μM standards before analyzing samples.

Kinetic Characterization

Enzymes were assayed at varying concentrations of substrate as described above. The K_m values for plastidic and cytosolic PGI were determined by fitting the data with non-linear regression using the Hill function in OriginPro 8.0 (OriginLab Corporation).

Inhibition Studies

Different metabolites of the Calvin-Benson cycle were tested for their effect on PGI activity. All the metabolites were purchased from Sigma Aldrich [Sigma Aldrich (see text footnote 2)]. In metabolite screening assays, metabolites were assayed at a 1:1 molar ratio with the substrate. To determine the K_i of PGI for different metabolites, the assay was carried out in presence of various concentrations of F6P or G6P and the inhibitory metabolite. Assay mixtures were prepared as described above. In inhibition assays, 0–0.98 mM F6P or 0–1.5 mM G6P was used. The concentration range used to study the K_i of PGI for E4P was 0–0.05 mM and that for 6PG was 0–1.5 mM. The mechanism of inhibition was determined from Hanes–Woolf plots. The K_i was determined from the non-linear least squares fitting of the activity vs. concentration plot using Solver in Excel using the standard equation for competitive inhibition as described below:

$$v = \frac{V^*_{max} S}{K_m \left(1 + \frac{I}{K_i}\right) + S} \quad (1)$$

where $V_{\max}$ is the maximum velocity, S is the substrate concentration, K_m is the Michaelis constant, and K_{i} is the inhibition constant. For non-competitive inhibition, the equation below was used.

$$v = \frac{V^*_{max} S / \left(1 + \frac{I}{K_i}\right)}{\left(K_m \left(1 + \frac{I}{K_i}\right) / \left(1 + \frac{I}{K_i}\right) + S\right)} \quad (2)$$

Plant Material

Fresh *Spinacia oleracea* (So) was purchased at a local market for use that day. Spinach was either dark or light treated for 1.5 h before beginning isolation and petioles were kept in water to prevent wilting.

Arabidopsis thaliana (At) Col-0 was grown in SureMix soil (Michigan Grower Products, Inc., Galesburg, MI, United States) in a growth chamber at a 12 h light at 120 μmol m^{-2} s^{-1}, 23°C and 12 h dark at 21°C. Plants were harvested either midday for light samples or midnight for dark samples.

Nicotiana tabacum seeds were planted in SureMix soil. The plants were grown in the greenhouse, starting in October 2019 with an average daytime temperature of 27°C and nighttime temperature of 20°C. Plants were fertilized twice per week with commercially available Peters 20-20-20 fertilizer (ICL Specialty

Fertilizers)[6] at 100 ppm. Experiments were done when plants were 5–12 weeks old on the fifth to seventh fully expanded leaves.

Chloroplast Isolation

Chloroplasts were isolated using a Percoll gradient (Weise et al., 2004). Leaves were placed in a chilled blender with grinding buffer (330 mM mannitol, 50 mM Hepes, pH 7.6, 5 mM $MgCl_2$, 1 mM $MnCl_2$, 1 mM EDTA, 5 mM ascorbic acid, 0.25% BSA), blended, and then filtered through four layers of cheese cloth. Filtered liquid was centrifuged, and the pellet was resuspended in resuspension buffer (330 mM mannitol, 50 mM Hepes, pH 7.6, 5 mM $MgCl_2$, 1 mM $MnCl_2$, 1 mM EDTA, 0.25% BSA). The resuspended pellet was layered on top of a 20–80% Percoll gradient which was centrifuged at 1,200 × *g* for 7 min. The bottom band in the gradient containing the intact chloroplasts was collected. One volume of resuspension buffer was added to the collected chloroplasts and centrifuged at 1,200 × *g* for 2 min. The pellet was resuspended in 50 μL of water and vortexed to lyse the chloroplasts. One volume of 2x buffer (100 mM Hepes, pH 7.6, 10 mM $MgCl_2$, 2 mM $MnCl_2$, 2 mM EDTA, 2 mM EGTA, 60% glycerol, 0.2% Triton X-100, 0.2% PVPP) was added. Samples were stored at −80°C until used for further analysis. Chlorophyll was quantified by lysing 50 μL of purified chloroplasts by sonication and adding supernatant to 1 mL of 95% ethanol. OD_{654} was used to calculate the chlorophyll concentration (Wintermans and DeMots, 1965):

$$\text{mg Chl} = OD^{*}0.0398^{*}0.050\ \mu\text{L} \quad (3)$$

Assays that used isolated chloroplasts were normalized by amount of chlorophyll added to the assay mixture.

Transient Expression of PGI in *N. tabacum*

A fusion gene was generated using the transit peptide of the *Arabidopsis* chloroplast *PGI1* (*At4g24620*). This was determined by ChloroP[7] to be the first 144 bp starting at the ATG codon. The transit peptide was placed in front of the *Arabidopsis* cytosol *PGI2* (At5g42740) cDNA with the ATG from the *PGI2* sequence omitted, for a total length of 1824 bp. A second fusion gene was made by placing a YFP gene sequence at the end of the gene directly before the TGA stop codon. A third fusion gene was made by placing the YFP gene sequence at the N-terminus between the transit peptide and the *PGI2* cDNA sequence. These constructs were synthesized by Bio Basic Inc (Markham, ON, Canada) and placed in the pUC57 plasmid vector. The construct was then transferred to the pEAQ-HT-DEST1 destination vector containing the P19 suppressor of silencing (Sainsbury et al., 2009). The pEAQ-HT-DEST1 vector constructs were transformed into *Agrobacterium* strain GV3101 by electroporation. All constructs and transformed *E. coli* and *Agrobacterium* were confirmed with PCR.

Agrobacterium containing the desired construct was grown in LB media in a 5 mL culture tube at 28°C overnight. The next day cells were pelleted by centrifugation at 7,000 × *g* for 5 min at 20°C and washed twice with infiltration buffer (2 mM trisodium phosphate, 50 mM MES, 25 mM glucose, 200 mM acetosyringone). The OD_{600} was measured and used to calculate the necessary volume of *Agrobacterium* to dilute to an OD_{600} of 0.05, 0.025, or 0.01 for initial controls and 0.025 for all subsequent experiments. *N. tabacum* leaves were gently infiltrated using a 1 mL syringe without a needle according to Batoko et al. (2000). All experiments, except for initial controls, were done at 2 days post-infiltration.

Localization of Retargeted PGI

Protein transient expression was performed using 4-week-old *N. tabacum* plants and *Agrobacterium tumefaciens* (strain GV3101) with an OD_{600} of 0.05. Both N-terminal and C-terminal YFP fusion constructs were used.

Confocal images were acquired using an inverted laser scanning confocal microscope, Nikon A1RSi, on tobacco leaf epidermal cells, 2 days post-infiltration. Images were acquired using a 60X oil λS DIC N2 objective. YFP was excited by the 514 nm line of an argon ion laser and emission collected at 530–560 nm. Chlorophyll autofluorescence was excited with the 647 nm line and emission was collected at 680–750 nm (Mehrshahi et al., 2013).

Starch Time Course

Nicotiana tabacum leaves were infiltrated as described above. Starting 48 h post-infiltration, leaf punches were collected at 4:40 PM (+10:40 h after lights on), 10:00 PM (lights off), 12:40 PM (+ 2:40 h after lights off), 3:20 AM (+5:20 h after lights off), 6:00 AM (lights on), and 11:20 AM (+5:20 h after lights on). These times corresponded with lights on, lights off, and two points evenly spaced in between each change in light conditions. Samples were collected in 2 mL pre-weighed microcentrifuge tubes, frozen immediately in liquid nitrogen, and stored at −80°C. Fresh weight was determined before any further analysis.

Frozen plant material was ground using a ball mill (Retsch)[8] and was suspended in ice-cold 3.5% perchloric acid solution (50% w/v of plant tissue), homogenized, and incubated on ice for 5 min. Samples were then centrifuged at 28,000 × *g* for 10 min at 4°C. The pellet was washed twice with both 80% ethanol and deionized water and then dried in a Savant AES 1010 SpeedVac [Thermo Fisher Scientific (see text footnote 5)] for 15 min to remove any remaining ethanol. The dried pellet was resuspended in 500 μL of 0.2 M KOH and incubated at 95°C for 30 min to gelatinize the starch. Acetic acid was added to a final concentration of approximately 150 mM to bring the solution to a pH of 5. Fifty U of α-amylase and 0.2 U of amyloglucosidase were added to the sample. The starch solution was incubated for 2 days at room temperature on a shaker to convert the starch to glucose. Two hundred μL of an assay mixture of 110 mM HEPES, 500 nmol $NADP^+$, 500 nmol ATP, and 0.4 U G6PDH was added to wells in an assay plate. Twenty μL of the digested starch sample was added to each well and was measured at 340 nm

[6]https://www.icl-sf.com

[7]http://www.cbs.dtu.dk/services/ChloroP/

[8]https://www.retsch.com

on a FilterMax F5 Plate Reader (Molecular Devices)[9] until a stable baseline was obtained. A starting OD_{340} was measured. One U of hexokinase was added to each well, quickly shaken, and monitored at 340 nm until the reaction was completed. An endpoint OD_{340} was measured and starch (glucose equivalents) was determined using the ΔOD.

Significance of linearity for starch degradation at night was determined by linear regression statistics in OriginPro 8.0 (OriginLab Corporation).

RESULTS

Plastidic and Cytosolic PGI Have Different Kinetic Properties

Purified *Arabidopsis* plastid and cytosolic PGI, produced as described above, had specific activities of 787 μmol mg^{-1} protein min^{-1} for plastidic PGI and 1522 μmol mg^{-1} protein min^{-1} for cytosolic PGI. **Table 2** shows the K_m (for both F6P and G6P) of plastidic and cytosolic PGI (**Supplementary Figure 2**). For plastidic AtPGI, the K_m for G6P was ∼2.9-fold higher than that for F6P. The K_m's for F6P and G6P of the cytosolic enzyme were the same. We did not calculate the V_{max} value of G6P and F6P for both isoforms since initial results did not conform to the Haldane relation (Alberty, 1953):

$$K = \frac{k_{\text{cat F6P}\rightarrow\text{G6P}}}{k_{cat\ F6P\rightarrow G6P}} * \frac{k_{m\ G6P\rightarrow F6P}}{k_{m\ G6P\rightarrow F6P}} \quad (4)$$

Therefore, we concluded that the measured V_{max} was not reliable, either due to differences in methodology for measuring G6P or F6P kinetics or storage in the freezer. Using the determined K_{eq} of 3.70 (Dyson and Noltmann, 1968), we can calculate that the ratio of $k_{cat\ F6P\rightarrow G6P}/k_{cat\ G6P\rightarrow F6P}$ is 1.65 for the plastidic isoform and 4.75 for the cytosolic isoform. DTT did not significantly influence the specific activity of plastidic or cytosolic AtPGI (**Supplementary Figure 3**).

[9]https://moleculardevices.com

TABLE 2 | Kinetic constants and inhibition constants for plastidic and cytosolic AtPGI as determined by NADPH-linked spectrophotometric assays and LC-MS/MS assays.

	F6P G6P		G6P F6P	
	Plastidic PGI	**Cytosolic PGI**	**Plastidic PGI**	**Cytosolic PGI**
K_m (μM)	73 ± 80	203 ± 12	164 ± 43	158 ± 85
E4P K_i (μM)	2.3	1.5	6.0	3.7
6PG K_i (μM)	31	106	245	149

K_m and k_{cat} were determined by fitting the Michaelis-Menten equation. Data points used in model fitting were different preparations (n = 3). For inhibition constants, each number was determined from the fitted curves as described in the methods. Errors shown are SD, (n = 3). Sum of least-squares for inhibition parameters were determined using Solver in Excel.

Regulation of PGI Activity

Effects of different metabolites on the activity of PGI was similar for both plastidic and cytosolic AtPGI. Inhibition with erythrose 4-phosphate (E4P), 3-phosphoglyceric acid (PGA), dihydroxyacetone phosphate (DHAP), and 6-phosphogluconate (6PG) were screened (**Figure 1**). Only E4P and 6PG showed significant inhibition of PGI activity. **Figure 2** shows the activity of plastidic AtPGI over a range of 6PG and E4P concentrations. Activity of cytosolic AtPGI was analyzed in a similar manner as shown for plastidic AtPGI. The calculated K_i values of E4P and 6PG are shown in **Table 2**. The K_i values for 6PG were between 31 and 203 μM, depending on the isoform and substrate. E4P was shown to be more inhibitory with K_i's between 1.5 and 6 μM. Based on the Hanes-Woolf plots (**Supplementary Figure 4**), E4P was shown to be competitive, except above 0.04 mM, with G6P. 6PG was identified as competitive with F6P, except above 1.0 mM, and non-competitive with G6P.

Plastidic SoPGI activity from chloroplasts from dark-treated spinach leaves had a higher K_m for G6P compared to light-treated chloroplasts (**Figure 3**). The K_m of SoPGI for F6P did not change in the light or dark.

Retargeted Cytosolic AtPGI Localized in the Chloroplast

We transiently expressed retargeted cytosolic PGI. To confirm the intracellular location, we added YFP proteins on both the N-terminus and C-terminus. Tobacco leaf epidermes were observed by confocal microscopy. YFP fluorescence was seen

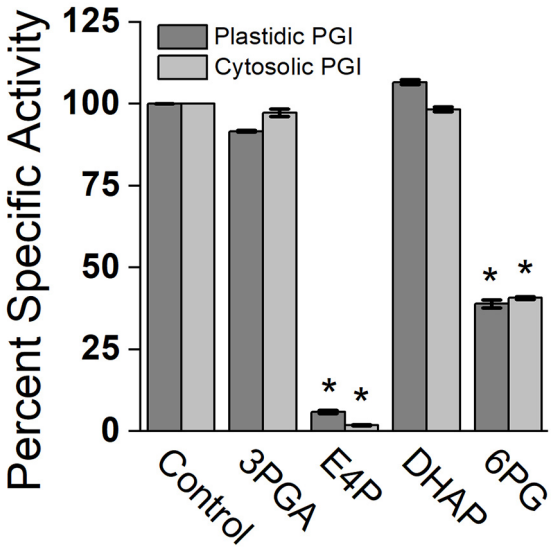

FIGURE 1 | Comparison of specific activity of plastidic and cytosolic AtPGI with various metabolites. Each bar represents mean and error bars represent SD, (n = 3). All metabolites were screened at 1:1 F6P substrate to metabolite. Data with an asterisk (*) are significantly different from the control as determined by Student's t-test ($P < 0.05$) (two tailed and assuming unequal variance). 3PGA, 3-phosphoglyceric acid; E4P, erythrose 4-phosphate; DHAP, dihydroxyacetone phosphate; 6PG, 6 phosphogluconate.

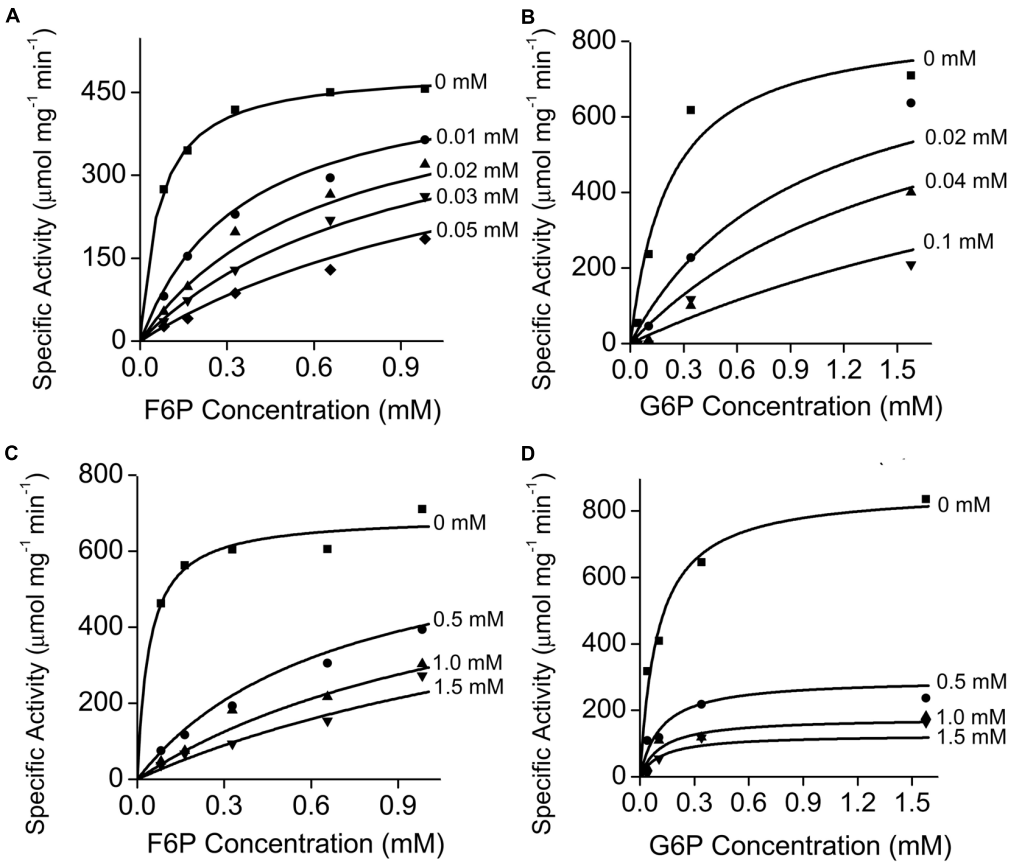

FIGURE 2 | Effect of erythrose 4-phosphate (E4P) and 6-phosphogluconate (6PG) on plastidic AtPGI. We measured the effect of E4P **(A,B)** and 6PG **(C,D)** on AtPGI. Different symbols represent different concentrations of inhibitor. PGI was more inhibited by E4P than by 6PG. Lines represent data fit to Eq. 2. F6P, fructose 6-phosphate; G6P, glucose 6-phosphate.

in the chloroplast for both the N-terminal and C-terminal constructs, confirming that our construct of cytosolic AtPGI targeted to the plastids was in the chloroplast (**Figure 4**).

After infiltrating *N. tabacum* with *Agrobacterium* transformed with the modified AtPGI construct without the YFP addition, we collected samples every 24 h for 3 days. Expression of the construct was highest on the second day after infiltration as determined by quantitative PCR (**Supplementary Figure 5A**). We also found that an *Agrobacterium* density of 0.025 OD_{600} resulted in the highest expression of the construct (**Supplementary Figure 5**). Photosynthetic assimilation was ∼50% of pre-infiltration values (**Supplementary Figure 5B**). After 2 days both expression and photosynthesis declined. Based on this, we used 2 days post-infiltration as the time point for all future experiments.

Time Course of Starch Accumulation in *N. tabacum* Transiently Expressing Retargeted AtPGI

Starting 48 h after infiltration, we measured starch content in *N. tabacum* that transiently expressed either the mislocalized PGI construct or an empty vector. We found that at the end of day and end of night, PGI plants had significantly more starch. End-of-day starch content was approximately 1.65-fold more than controls while end-of-night starch content was approximately 1.98-fold more than controls (**Figure 5A**). We found that PGI plants did not linearly breakdown starch at night (R^2 = 0.648), while empty vector plants did (R^2 = 0.998) (**Figure 5B**). The Prob(F) value (likelihood that the regression parameters are zero) for the linear regression of empty vector plants was 7.64×10^{-4} while Prob(F) for PGI plants was 0.20 indicating linearity for the empty vector plants but not plants expressing retargeted AtPGI. Daytime synthesis of starch did not increase consistently throughout the day and was not further analyzed. Plants were grown in greenhouse conditions and the experiment took place on a cloudy day. Lights came on in the greenhouse late in the day (5:00 pm) and caused an increase in light compared to daytime intensity for the last 5 h of the photoperiod. Therefore, we focused on end of day, end of night, and night degradation values.

DISCUSSION

Plastidic PGI partitions carbon out of the Calvin-Benson cycle to starch synthesis, however, it is often assumed that it does

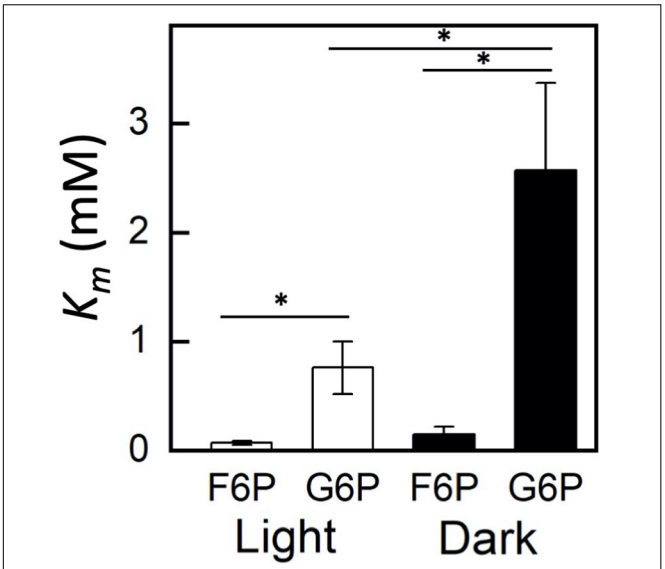

FIGURE 3 | Comparison of fructose 6-phosphate (F6P) and glucose 6-phosphate (G6P) K_m in plastidic phosphoglucoisomerase in dark and light-treated isolated spinach chloroplasts. Each bar represents mean and error bars represent SE, (n = 3 independent isolations of chloroplasts). The K_m for G6P increased in dark treated compared to light treated isolated chloroplasts. Bars with an asterisk (*) are significantly different from corresponding light treated samples as determined by Student's t-test ($P < 0.05$) (two tailed and assuming unequal variance).

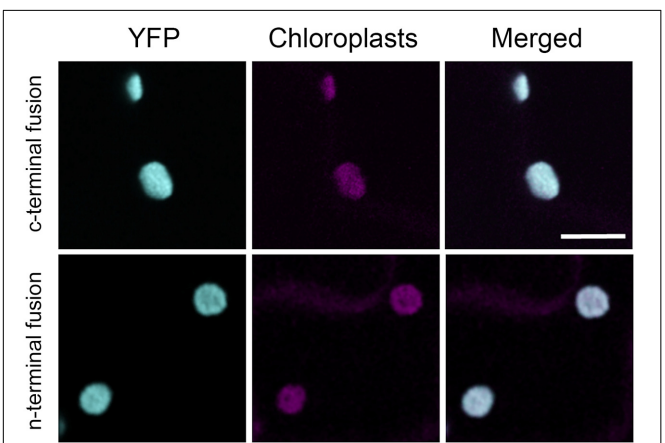

FIGURE 4 | Localization of modified plastid phosphoglucoisomerase (cPGI) to the chloroplast. Confocal images of *Nicotiana tabacum* epidermal cell transiently expressing N- or C-terminal tagged mislocalized PGI. Both fluorescent fusions localize at the chloroplasts (cyan) as the co-localization (merge channel) shows with the chloroplast autofluorescence (magenta). Scale bar 10 μm.

not exhibit control over pathway flux. It is thought that ADP-glucose pyrophosphorylase (AGPase) exhibits most, if not all, of regulatory control over the starch synthesis pathway (Preiss and Sivak, 1998; Tiessen et al., 2002; Ballicora et al., 2004). Discussion of key enzymes and regulation of starch synthesis and computational models of starch synthesis often leave out early steps of the starch synthetic pathway, i.e., PGI and PGM, focusing instead on formation of ADP-glucose (ADPG) by AGPase and donation of glucose from ADPG to the growing starch chain (Preiss and Sivak, 1998; Tetlow et al., 2004; Sonnewald and Kossmann, 2014; Wu et al., 2014). However, the calculated flux-control coefficient for PGI can be 0.35 (Neuhaus and Stitt, 1990). Additionally, it has been shown that a loss of 50% of plastidic PGI reduces starch synthesis by 50% while loss of 64% of cytosolic PGI has a negligible effect on sucrose synthesis, reinforcing the rate-limiting role of the plastidic isoform (Kruckeberg et al., 1989). Due to its key role in controlling flux out of the Calvin-Benson cycle, a more robust understanding of PGI is necessary in order to understand the regulation of partitioning carbon out of the cycle.

Three Levels of Regulation in Plastidic PGI

We have used recombinant enzymes to compare the plastidic isoform of PGI to the cytosolic. We have confirmed that the plastidic enzyme has a higher K_m for G6P than for F6P and that the cytosolic enzyme has similar K_m's for G6P and F6P. This makes it difficult for carbon to reenter the Calvin-Benson cycle as hexose phosphate. In addition to kinetic regulation, in the plastid the G6P/F6P ratio at equilibrium has been reported to be 3.70 at 25°C (Dyson and Noltmann, 1968). However, measurements from plastidic plant extracts show the ratio of G6P/F6P in the stroma to be close to 1 (Schnarrenberger and Oeser, 1974; Gerhardt et al., 1987; Sharkey and Vassey, 1989; Backhausen et al., 1997; Szecowka et al., 2013). In the cytosol, the G6P/F6P ratio is 2.4–4.7 (Gerhardt et al., 1987; Sharkey and Vassey, 1989; Szecowka et al., 2013). Kinetic isotope effects in starch, but not sucrose, also support the conclusion that plastidic PGI, but not cytosolic PGI, is unable to maintain equilibrium (Schleucher et al., 1999). Finally, our work suggests another mechanism of regulation. Using isolated chloroplasts to examine the *in vivo* kinetics of plastidic PGI, we have shown that the K_m of PGI can be dynamically regulated in the dark compared to the light. This may be due to post-translational modification or splice variants.

Changes in Plastidic PGI Regulation Can Manipulate Starch Accumulation and Degradation

We found that targeting cytosolic PGI to the plastid affects starch synthesis and degradation. During the day, disruption of the normal expression of PGI in the plastid causes a ∼60% reduction in starch. This confirms the importance of PGI as a rate-determining step to partition carbon out of the Calvin-Benson cycle and also provides new avenues of investigation in engineering increased yields in crops.

We confirmed that the K_m for G6P of the plastidic enzyme is higher than that for F6P. In some cases a chloroplast envelope G6P transporter can be expressed, including in CAM plants and in response to a sudden increase in light (Weise et al., 2019). The properties of PGI will direct G6P entering the stroma toward starch and does not provide an easy route for G6P entry into the Calvin-Benson cycle. In mutants where GPT2 is

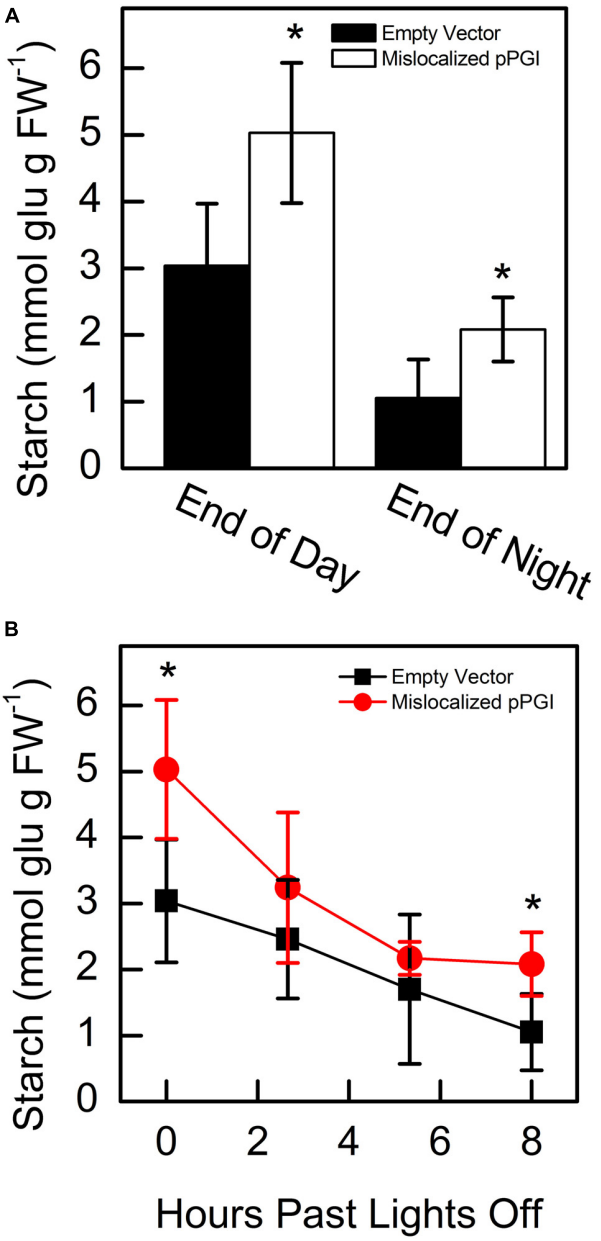

FIGURE 5 | Starch amounts at end of day and end of night **(A)** and degradation of starch **(B)** in *Nicotiana tabacum* expressing mislocalized plastid phosphoglucoisomerase (pPGI). Starch in plants with mislocalized pPGI was significantly higher than empty vector control plants. Starch breakdown in empty vector plants was linear through the night, however, starch breakdown was non-linear in mislocalized pPGI plants. Each bar or data point represents mean and error bars represent SE, (n = 5 biological replicates). Bars or data points with an asterisk (*) are significantly different from corresponding empty vector samples as determined by Student's t-test ($P < 0.05$) (two tailed and assuming unequal variance). Significance for linearity was determined by Prob(F) of the linear regressions.

expressed, G6P will enter the stroma but be unable to enter the Calvin-Benson cycle and will accumulate if starch synthesis cannot accommodate the influx of G6P. This can increase the activity of the plastidic G6PDH (Preiser et al., 2019) causing a G6P shunt that consumes ATP and, in some cases, requires cyclic electron flow, which compensates the ATP loss in the G6P shunt (Sharkey and Weise, 2016). This can explain the cyclic electron flow phenotype of many Calvin-Benson cycle mutants (Strand et al., 2017).

However, these results also demonstrate the need to consider other effects of manipulating flux out of the Calvin-Benson cycle. Targeting cytosolic PGI to chloroplasts, while increasing daytime starch accumulation, disrupted degradation of starch. Phosphorolytic starch breakdown results in the production of G1P and then G6P from starch and has been shown to be a significant contribution of carbon to the plastid (Weise et al., 2006). Mis-expressed PGI could increase degradation of starch by the phosphorolytic pathway by providing a pathway to enzymatic reactions that would not normally be available, in addition to the oxidative pentose phosphate pathway. This indicates that even at night PGI is an important regulatory point in starch metabolism and is a rate-limiting step that prevents early starch degradation through the night. The importance of nighttime activity of PGI was discussed relative to providing metabolites for the MEP pathway through the action of the oxidative pentose phosphate pathway, producing glyceraldehyde 3-phosphate (Bahaji et al., 2015). Many studies measure starch at end-of-day and end-of-night to assess effects on starch metabolism [see for example Scialdone et al. (2013)]. When manipulating partitioning from the Calvin-Benson cycle, future applications need to consider long-term consequences of early depletion of starch which may not be apparent in typical measurements.

E4P Is a Strong Inhibitor of PGI

We previously assumed that PGA is a strong inhibitor of PGI [e.g., Sharkey and Weise (2016)] based on the report by Dietz (1985). Surprisingly, we did not observe this to be the case. Examination of data from Dietz (1985) shows that in PGA inhibition assays, 6PG was also present in the reaction mixture at 50 μM. The G6P/F6P disequilibrium in chloroplasts was proportional to PGA (Dietz, 1985) but PGA was not tested alone for its effect on PGI. We found that the K_i of plastidic PGI for 6PG with limiting F6P was 31 μM or with limiting G6P was 203 μM. Based on our findings, we propose that PGI is not inhibited by PGA, and the previously reported inhibition can be explained by presence of 6PG or E4P. *In vivo* plastidic concentrations of 6PG are not known, therefore, the extent of inhibition of PGI *in vivo* by 6PG cannot be currently determined.

Phosphoglucoisomerase is inhibited by μM concentrations of E4P (Grazi et al., 1960; Salas et al., 1964; Backhausen et al., 1997). E4P may be inhibitory to both isoforms of PGI because it is a competitive inhibitor and the active sites of both isoforms may be similar (Backhausen et al., 1997). Presumably there is no E4P in the cytosol since the cytosol lacks crucial enzymes in the non-oxidative branch of the pentose phosphate pathway (Schnarrenberger et al., 1995). Measurements and estimations of plastidic E4P concentrations *in vivo* show E4P to be ∼17–20 μM (Bassham and Krause, 1969; Heldt et al., 1977; Backhausen et al., 1997). This is well above the K_i of E4P for plastidic PGI. Backhausen et al. (1997) propose that this regulation is necessary

in order to keep photosynthetic pool sizes stable during changes in light intensity.

In addition to stabilizing the Calvin-Benson cycle, we propose that inhibition of PGI by E4P can provide insight into the phenomenon of reverse sensitivity to CO_2 and O_2 of photosynthetic CO_2 assimilation rate. This somewhat common behavior in leaves in high light and high CO_2 can be explained in part by direct usage of glycine and serine from the photorespiratory pathway (Busch et al., 2018; Harley and Sharkey, 1991). However, in many cases the reverse sensitivity is greater than can be accounted for by this mechanism and is caused by a reduction in starch synthesis as reported by Sharkey and Vassey (1989). They proposed this was an effect of PGA inhibition of PGI, but because we did not find PGA to be inhibitory, we now suggest that the decrease in starch synthesis is due to an increase in E4P concentration (or possibly 6PG). On the other hand, Backhausen et al. (1997) found some inhibition of PGI by PGA but still they concluded that E4P was of particular interest in explaining control of PGI activity. It is possible that the degree of PGA inhibition of PGI is species-dependent but all available information clearly supports E4P as a powerful regulator of PGI.

Erythrose 4-phosphate inhibition of PGI may also explain some of the effects of sedoheptulose-1,7-bisphosphatase (SBPase) manipulation. SBPase is part of the Calvin-Benson cycle and converts sedoheptulose-1,7-bisphosphate to sedoheptulose 7-phosphate. It has been shown that overexpression of SBPase increases photosynthetic capacity and biomass (Miyagawa et al., 2001; Lefebvre et al., 2005; Rosenthal et al., 2011; Ogawa et al., 2015). Increased in SBPase activity would pull carbon forward in the Calvin-Benson cycle, reducing E4P levels. This would decrease PGI inhibition and partition more carbon toward starch synthesis. Conversely, reductions in SBPase decrease carbohydrates and total biomass (Harrison et al., 1998, 2001; Lawson et al., 2006). In this case, E4P may accumulate, decreasing PGI activity and the ability to partition carbon to starch. Decreased capability to synthesize starch has also been shown to decrease long-term triose phosphate usage capacity, reduce rubisco capacity, and limit RuBP regeneration (Yang et al., 2016).

CONCLUSION

Redirection of carbon flux in chloroplasts to cause accumulation of a desired product is a common biotechnology goal. We conclude that PGI is an important regulatory enzyme in partitioning carbon out of the Calvin-Benson cycle. Previous analyses of the starch pathways have overlooked this key role. Additionally, we have re-examined previous knowledge of PGI inhibition and have found that it was mistakenly thought that PGI is inhibited by PGA and is instead inhibited by E4P.

DATA AVAILABILITY STATEMENT

The original contributions presented in the study are included in the article/**Supplementary Material**, further inquiries can be directed to the corresponding author.

AUTHOR CONTRIBUTIONS

All authors listed have made a substantial, direct and intellectual contribution to the work, and approved it for publication.

FUNDING

This research was funded by the United States Department of Energy Award DE-FG02-91ER20021 and partial salary support for TS was provided by Michigan AgBioResearch. AP was partially supported by a fellowship from Michigan State University under the Training Program in Plant Biotechnology for Health and Sustainability (NIH-T32-GM110523).

ACKNOWLEDGMENTS

We thank Michigan State University Research Technology Support Facility Mass Spectrometry Core for providing the facility for the LC-MS/MS work and the Center for Advanced Microscopy for providing the facility for the confocal imaging. Sections of this article have appeared as part of a pre-print in *bioRxiv* https://www.bioRxiv.org/content/10.1101/442434v2.

SUPPLEMENTARY MATERIAL

The Supplementary Material for this article can be found online at: https://www.frontiersin.org/articles/10.3389/fpls.2020.580726/full#supplementary-material

REFERENCES

Abiri, R., Valdiani, A., Maziah, M., Azmi Shaharuddin, N., Sahebi, M., Norhana Balia Yusof, Z., et al. (2016). A critical review of the concept of transgenic plants: insights into pharmaceutical biotechnology and molecular farming. *Curr. Issues Mol. Biol.* 18, 21–42.

Alberty, R. A. (1953). The relationship between Michaelis constants, maximum velocities and the equilibrium constant for an enzyme-catalyzed reaction. *J. Am. Chem. Soc.* 75, 1928–1932. doi: 10.1021/ja01104a045

Ausich, R. L. (2009). Commercial opportunities for carotenoid production by biotechnology. *Pure Appl. Chem.*69, 2169–2173. doi: 10.1351/pac199769102169

Backhausen, J. E., Jöstingmeyer, P., and Scheibe, R. (1997). Competitive inhibition of spinach leaf phosphoglucose isomerase isoenzymes by erythrose 4-phosphate. *Plant Sci.* 130, 121–131. doi: 10.1016/s0168-9452(97)00208-202

Bahaji, A., Sánchez-López, ÁM., De Diego, N., Muñoz, F. J., Baroja-Fernández, E., Li, J., et al. (2015). Plastidic phosphoglucose isomerase is an important determinant of starch accumulation in mesophyll cells, growth, photosynthetic capacity, and biosynthesis of plastidic cytokinins in *Arabidopsis*. *PLoS One* 10:e0119641. doi: 10.1371/journal.pone.0119641

Ballicora, M. A., Iglesias, A. A., and Preiss, J. (2004). ADP-glucose pyrophosphorylase: a regulatory enzyme for plant starch synthesis. *Photosynth. Res.*79, 1–24. doi: 10.1023/b:pres.0000011916.67519.58

Bassham, J. A., and Krause, G. H. (1969). Free energy changes and metabolic regulation in steady-state photosynthetic carbon reduction. *Biochim. Biophys. Acta* 189, 207–221. doi: 10.1016/0005-2728(69)90048-6

Batoko, H., Zheng, H. Q., Hawes, C., and Moore, I. (2000). A rab1 GTPase is required for transport between the endoplasmic reticulum and golgi apparatus and for normal golgi movement in plants. *Plant Cell* 11, 2201–2218. doi: 10.2307/3871115

Botella-Pavía, P., and Rodríguez-Conceptión, M. (2006). Carotenoid biotechnology in plants for nutritionally improved foods. *Physiol. Plant.* 126, 369–381. doi: 10.1111/j.1399-3054.2006.00632.x

Busch, F. A., Sage, R. F., and Farquhar, G. D. (2018). Plants increase CO_2 uptake by assimilating nitrogen via the photorespiratory pathway. *Nat. Plants*. 4, 46–54. doi: 10.1038/s41477-017-0065-x

Dietz, K. J. (1985). A possible rate limiting function of chloroplast hexosemonophosphate isomerase in starch synthesis of leaves. *Biochim. Biophys. Acta* 839, 240–248. doi: 10.1016/0304-4165(85)90004-2

Dyson, J. E. D., and Noltmann, E. A. (1968). The effect of pH and temperature on the kinetic parameters of phosphoglucose isomerase. *J. Biol. Chem.* 243, 1401–1414.

Gerhardt, R., Stitt, M., and Heldt, H. W. (1987). Subcellular metabolite levels in spinach leaves. Regulation of sucrose synthesis during diurnal alterations in photosynthetic partitioning. *Plant Physiol.* 83, 399–407. doi: 10.1104/pp.83.2.399

Grazi, E., De Flora, A., and Pontremoli, S. (1960). The inhibition of phosphoglucose isomerase by D-erythrose 4-phosphate. *Biochem. Biophys. Res. Commun.* 2, 121–125. doi: 10.1016/s0168-9452(97)00208-2

Harley, P. C., and Sharkey, T. D. (1991). An improved model of C_3 photosynthesis at high CO_2: reversed O_2 sensitivity explained by lack of glycerate reentry into the chloroplast. *Photosyn Res.* 27, 169–178. doi: 10.1007/BF00035838

Harrison, E. P., Olcer, H., Lloyd, J. C., Long, S. P., and Raines, C. A. (2001). Small decreases in SBPase cause a linear decline in the apparent RuBP regeneration rate, but do not affect Rubisco carboxylation capacity. *J. Exp. Bot.* 52, 1779–1784. doi: 10.1093/jexbot/52.362.1779

Harrison, E. P., Willingham, N. M., Lloyd, J. C., and Raines, C. A. (1998). Reduced sedoheptulose-1,7-bisphosphatase levels in transgenic tobacco lead to decreased photosynthetic capacity and altered carbohydrate accumulation. *Planta* 204, 27–36. doi: 10.1007/s004250050226

Heldt, H. W., Chon, C. J., Maronde, D., Herold, A., Stankovic, Z. S., Walker, D. A., et al. (1977). Role of orthophosphate and other factors in the regulation of starch formation in leaves and isolated chloroplasts. *Plant Physiol.* 59, 1146–1155. doi: 10.1104/pp.59.6.1146

Kruckeberg, A. L., Neuhaus, H. E., Feil, R., Gottlieb, L. D., and Stitt, M. (1989). Decreased-activity mutants of phosphoglucose isomerase in the cytosol and chloroplast of *Clarkia xantiana*. Impact on mass-action ratios and fluxes to sucrose and starch, and estimation of flux control coefficients and elasticity coefficients. *Biochem. J.* 261, 457–467. doi: 10.1042/bj2610457

Lawson, T., Bryant, B., Lefebvre, S., Lloyd, J. C., and Raines, C. A. (2006). Decreased SBPase activity alters growth and development in transgenic tobacco plants. *Plant Cell Environ.* 29, 48–58. doi: 10.1111/j.1365-3040.2005.01399.x

Lefebvre, S., Lawson, T., Zakhleniuk, O. V., Lloyd, J. C., and Raines, C. A. (2005). Increased sedoheptulose-1,7-bisphosphatase activity in transgenic tobacco plants stimulates photosynthesis and growth from an early stage in development. *Plant Physiol.* 138, 451–460. doi: 10.1104/pp.104.055046

Lowry, O. H., and Passonneau, J. V. (1972). *A Flexible System of Enzymatic Analysis*. Orlando: Academic Press.

Mehrshahi, P., Stefano, G., Andaloro, J. M., Brandizzi, F., Froehlich, J. E., and DellaPenna, D. (2013). Transorganellar complementation redefines the biochemical continuity of endoplasmic reticulum and chloroplasts. *Proc. Nati. Acad. Sci.* 110, 12126–12131. doi: 10.1073/pnas.1306331110

Miyagawa, Y., Tamoi, M., and Shigeoka, S. (2001). Overexpression of a cyanobacterial fructose-1,6-/sedoheptulose-1,7-bisphosphatase in tobacco enhances photosynthesis and growth. *Nat. Biotechnol.* 19, 965–969. doi: 10.1038/nbt1001-965

Neuhaus, H. E., and Stitt, M. (1990). Control analysis of photosynthate partitioning. Impact of reduced activity of ADP-glucose pyrophosphorylase or plastid phosphoglucomutase on the fluxes to starch and sucrose in *Arabidopsis thaliana* (L.) Heynh. *Planta* 182, 445–454. doi: 10.1007/bf02411398

Ogawa, T., Tamoi, M., Kimura, A., Mine, A., Sakuyama, H., Yoshida, E., et al. (2015). Enhancement of photosynthetic capacity in *Euglena gracilis* by expression of cyanobacterial fructose-1,6-/sedoheptulose-1,7-bisphosphatase leads to increases in biomass and wax ester production. *Biotechnol. Biofuels* 8:80. doi: 10.1186/s13068-015-0264-5

Preiser, A. L., Fisher, N., Banerjee, A., and Sharkey, T. D. (2019). Plastidic glucose-6-phosphate dehydrogenases are regulated to maintain activity in the light. *Biochem. J.* 476, 1539–1551. doi: 10.1042/bcj20190234

Preiss, J., and Sivak, M. N. (1998). "Biochemistry, molecular biology and regulation of starch synthesis," in *Genetic Engineering*, Vol. 20, ed. J. K. Setlow (Boston, MA: Springer), 177–223. doi: 10.1007/978-1-4899-1739-3_10

Rosenthal, D. M., Locke, A. M., Khozaei, M., Raines, C. A., Long, S. P., and Ort, D. R. (2011). Over-expressing the C3 photosynthesis cycle enzyme sedoheptulose-1-7 bisphosphatase improves photosynthetic carbon gain and yield under fully open air CO_2 fumigation (FACE). *BMC Plant Biol.* 11:123. doi: 10.1186/1471-2229-11-123

Sainsbury, F., Thuenemann, E. C., and Lomonossoff, G. P. (2009). pEAQ: versatile expression vectors for easy and quick transient expression of heterologous proteins in plants. *Plant Biotechnol. J.* 7, 682–693. doi: 10.1111/j.1467-7652.2009.00434.x

Salas, M., Viñuela, E., and Sols, A. (1964). Spontaneous and enzymatically catalyzed anomerization of glucose 6-phosphate and anomeric specificity of related enzymes. *J. Biol. Chem.* 240, 561–568.

Santelia, D., and Zeeman, S. C. (2011). Progress in *Arabidopsis* starch research and potential biotechnological applications. *Curr. Opin. Biotechnol.* 22, 271–280. doi: 10.1016/j.copbio.2010.11.014

Schleucher, J., Vanderveer, P., Markley, J. L., and Sharkey, T. D. (1999). Intramolecular deuterium distributions reveal disequilibrium of chloroplast phosphoglucose isomerase. *Plant Cell Environ.* 22, 525–533. doi: 10.1046/j.1365-3040.1999.00440.x

Schnarrenberger, C., Flechner, A., and Martin, W. (1995). Enzymatic evidence for a complete oxidative pentose phosphate pathway in chloroplasts and an incomplete pathway in the cytosol of spinach leaves. *Plant Physiol.* 108, 609–614. doi: 10.1104/pp.108.2.609

Schnarrenberger, C., and Oeser, A. (1974). Two isoenzymes of glucosephosphate isomerase from spinach leaves and their intracellular compartmentation. *Eur. J. Biochem.* 45, 77–82. doi: 10.1111/j.1432-1033.1974.tb03531.x

Scialdone, A., Mugford, S. T., Feike, D., Skeffington, A., Borrill, P., Graf, A., et al. (2013). *Arabidopsis* plants perform arithmetic division to prevent starvation at night. *eLife* 2:e00669. doi: 10.7554/eLife.00669

Sharkey, T. D., and Vassey, T. L. (1989). Low oxygen inhibition of photosynthesis is caused by inhibition of starch synthesis. *Plant Physiol.* 90, 385–387. doi: 10.1104/pp.90.2.385

Sharkey, T. D., and Weise, S. E. (2016). The glucose 6-phosphate shunt around the Calvin-Benson Cycle. *J. Exp. Bot.* 67, 4067–4077. doi: 10.1093/jxb/erv484

Sonnewald, U., and Kossmann, J. (2014). Starches—from current models to genetic engineering. *Plant Biotechnol.* 11, 223–232. doi: 10.1111/pbi.12029

Strand, D. D., Livingston, A. K., Satoh-Cruz, M., Koepke, T., Enlow, H. M., Fisher, N., et al. (2017). Defects in the expression of chloroplast proteins leads to H2O2 accumulation and activation of cyclic electron flow around Photosystem I. *Front. Plant Sci.* 7:2073. doi: 10.3389/fpls.2016.02073

Sulpice, R., Flis, A., Ivakov, A. A., Apelt, F., Krohn, N., Encke, B., et al. (2014). *Arabidopsis* coordinates the diurnal regulation of carbon allocation and growth across a wide range of photoperiods. *Mol. Plant* 7, 137–155. doi: 10.1093/mp/sst127

Szecowka, M., Heise, R., Tohge, T., Nunes-Nesi, A., Vosloh, D., Huege, J., et al. (2013). Metabolic fluxes in an illuminated *Arabidopsis* rosette. *Plant Cell* 25, 694–714. doi: 10.1105/tpc.112.106989

Tetlow, I. J., Morell, M. K., and Emes, M. J. (2004). Recent developments in understanding the regulation of starch metabolism in higher plants. *J. Exp. Bot.* 55, 2131–2145. doi: 10.1093/jxb/erh248

Tiessen, A., Hendriks, J. H. M., Stitt, M., Branscheid, A., Gibon, Y., FarrÇ, E. M., et al. (2002). Starch synthesis in potato tubers is regulated by post-translational redox modification of ADP-glucose pyrophosphorylase: a novel regulatory mechanism linking starch synthesis to the sucrose supply. *Plant Cell* 14, 2191–2213. doi: 10.1105/tpc.003640

Weise, S. E., Liu, T., Childs, K. L., Preiser, A. L., Katulski, H. M., Perrin-Porzondek, C., et al. (2019). Transcriptional regulation of the glucose-6-phosphate/phosphate translocator 2 is related to carbon exchange across the chloroplast envelope. *Front. Plant Sci.* 10:827. doi: 10.3389/fpls.2019.00827

Weise, S. E., Schrader, S. M., Kleinbeck, K. R., and Sharkey, T. D. (2006). Carbon balance and circadian regulation of hydrolytic and phosphorolytic breakdown of transitory starch. *Plant Physiol.* 141, 879–886. doi: 10.1104/pp.106.081174

Weise, S. E., Weber, A., and Sharkey, T. D. (2004). Maltose is the major form of carbon exported from the chloroplast at night. *Planta* 218, 474–482. doi: 10.1007/s00425-003-1128-y

Wintermans, J. G. F. M., and DeMots, A. (1965). Spectrophotometric characteristics of chlorophylls a and b and their pheophytins in ethanol. *Biochim. Biophys. Acta* 109, 448–453.

Wu, A. C., Ral, J.-P., Morell, M. K., and Gilbert, R. G. (2014). New perspectives on the role of α- and β-amylases in transient starch synthesis. *PLoS One* 9:e100498. doi: 10.1371/journal.pone.0100498

Yang, J. T., Preiser, A. L., Li, Z., Weise, S. E., and Sharkey, T. D. (2016). Triose phosphate use limitation of photosynthesis: short-term and long-term effects. *Planta* 243, 687–698. doi: 10.1007/s00425-015-2436-8

Conflict of Interest: The authors declare that the research was conducted in the absence of any commercial or financial relationships that could be construed as a potential conflict of interest.

frontiers in Plant Science

ORIGINAL RESEARCH
published: 13 January 2021
doi: 10.3389/fpls.2020.613731

Plastid-Targeted Cyanobacterial Flavodiiron Proteins Maintain Carbohydrate Turnover and Enhance Drought Stress Tolerance in Barley

*Fahimeh Shahinnia[1], Suresh Tula[1], Goetz Hensel[1,2†], Narges Reiahisamani[1], Nasrin Nasr[1,3], Jochen Kumlehn[1], Rodrigo Gómez[4†], Anabella F. Lodeyro[4], Néstor Carrillo[4] and Mohammad R. Hajirezaei[1]**

[1] Department of Physiology and Cell Biology, Leibniz Institute of Plant Genetics and Crop Plant Research, Gatersleben, Germany, [2] Division of Molecular Biology, Centre of the Region Hana for Biotechnological and Agriculture Research, Faculty of Science, Palacký University, Olomouc, Czechia, [3] Department of Biology, Payame Noor University, Teheran, Iran, [4] Instituto de Biología Molecular y Celular de Rosario (IBR-UNR/CONICET), Facultad de Ciencias Bioquímicas y Farmacéuticas, Universidad Nacional de Rosario, Rosario, Argentina

OPEN ACCESS

Edited by:
Patricia León,
National Autonomous University of Mexico, Mexico

Reviewed by:
Ahmad Arzani,
Isfahan University of Technology, Iran
Diego H. Sanchez,
CONICET Instituto de Investigaciones Fisiológicas y Ecologicas Vinculadas a la Agricultura (IFEVA), Argentina

***Correspondence:**
Mohammad R. Hajirezaei
mohammad@ipk-gatersleben.de

†Present address:
Goetz Hensel,
Centre of Plant Genome Engineering, Institute of Plant Biochemistry, Heinrich-Heine-University, Duesseldorf, Germany
Rodrigo Gómez,
Dipartimento di Biotecnologie, Università di Verona, Verona, Italy

Specialty section:
This article was submitted to Plant Biotechnology, a section of the journal Frontiers in Plant Science

Received: 03 October 2020
Accepted: 18 December 2020
Published: 13 January 2021

Citation:
Shahinnia F, Tula S, Hensel G, Reiahisamani N, Nasr N, Kumlehn J, Gómez R, Lodeyro AF, Carrillo N and Hajirezaei MR (2021) Plastid-Targeted Cyanobacterial Flavodiiron Proteins Maintain Carbohydrate Turnover and Enhance Drought Stress Tolerance in Barley. Front. Plant Sci. 11:613731. doi: 10.3389/fpls.2020.613731

Chloroplasts, the sites of photosynthesis in higher plants, have evolved several means to tolerate short episodes of drought stress through biosynthesis of diverse metabolites essential for plant function, but these become ineffective when the duration of the stress is prolonged. Cyanobacteria are the closest bacterial homologs of plastids with two photosystems to perform photosynthesis and to evolve oxygen as a byproduct. The presence of *Flv* genes encoding flavodiiron proteins has been shown to enhance stress tolerance in cyanobacteria. In an attempt to support the growth of plants exposed to drought, the *Synechocystis* genes *Flv1* and *Flv3* were expressed in barley with their products being targeted to the chloroplasts. The heterologous expression of both *Flv1 and Flv3* accelerated days to heading, increased biomass, promoted the number of spikes and grains per plant, and improved the total grain weight per plant of transgenic lines exposed to drought. Improved growth correlated with enhanced availability of soluble sugars, a higher turnover of amino acids and the accumulation of lower levels of proline in the leaf. *Flv1* and *Flv3* maintained the energy status of the leaves in the stressed plants by converting sucrose to glucose and fructose, immediate precursors for energy production to support plant growth under drought. The results suggest that sugars and amino acids play a fundamental role in the maintenance of the energy status and metabolic activity to ensure growth and survival under stress conditions, that is, water limitation in this particular case. Engineering chloroplasts by *Flv* genes into the plant genome, therefore, has the potential to improve plant productivity wherever drought stress represents a significant production constraint.

Keywords: biomass, *Hordeum vulgare* L., metabolites, photosynthesis, plastid biotechnology, yield

INTRODUCTION

Drought poses a major constraint over crop productivity, both directly and through its aggravation of the impact of other stress factors (Wang et al., 2011; Gómez et al., 2019). Biochemical mechanisms of drought stress response have been presented to explain the carbon catabolite changes on primary metabolites utilization (Fàbregas and Fernie, 2019) and secondary metabolite

production (Hodaei et al., 2018). In general, plants respond to water restriction by closing their stomata, which in turn decreases the supply of the CO_2 needed for carbon assimilation via the Calvin-Benson cycle (CBC) and ultimately, starch synthesis (Lawlor and Tezara, 2009). A limitation in carbon assimilation results in down-regulation of carbohydrate metabolism, which serves as an immediate precursor for the production of e.g., amino acids and/or energy donors such as nucleotides. Thus, the balancing of biochemical processes, especially carbohydrate and nitrogen metabolisms and the concomitant pathways including glycolysis and the TCA cycle during stress is of great importance for plants to tolerate adverse conditions. Knowledge gained on the nature of plant stress responses allowed the development of various experimental strategies to improve drought tolerance (Pires et al., 2016; Fàbregas et al., 2018).

Limitations in the fixation of atmospheric CO_2, whether caused by internal or external factors, will result in over-reduction of the photosynthetic electron transport chain (PETC) in chloroplasts, leading to inhibition of both PSI and PSII activities (Haupt-Herting and Fock, 2002). Once the availability of terminal electron acceptors becomes limiting, the PETC begins to leak electrons, resulting in the reduction of oxygen to detrimental compounds such as peroxides, superoxide and hydroxyl radicals, commonly classified as reactive oxygen species (ROS; Takagi et al., 2016). The photorespiratory pathway of C3 plants represents a major sink for electrons under conditions of either limited CO_2 availability or drought stress (Cruz de Carvalho, 2008). Also, the plastid terminal oxidase (PTOX) can extract electrons from plastoquinone (PQ), which are used to reduce oxygen to water, thereby maintaining the oxidation status of PSII during stress episodes (Sun and Wen, 2011).

To overcome the restriction of photosynthesis and thus the limitation of carbohydrate and metabolite production for better growth, we have been pursuing an alternative strategy by expressing specific cyanobacterial electron shuttles in chloroplasts (Tognetti et al., 2006; Zurbriggen et al., 2009). This strategy has never been employed to the important crop plant barley so that the proof of concept is a straightforward step towards sustainable food security. Among alternative electron sinks, flavodiiron proteins (*Flvs*) represent a class of electron carriers able to reduce oxygen directly to water without ROS formation (Saraiva et al., 2004). Flavodiiron proteins have been found in many prokaryotic species (Wasserfallen et al., 1998) as well as in anaerobic protozoa, green algae, and most plant lineages, with the major exception being angiosperms (Zhang et al., 2009; Peltier et al., 2010; Allahverdiyeva et al., 2015b).

In photosynthetic organisms, *Flvs* protect against photoinhibition by reducing oxygen in the non-heme diiron active site of their metallolactamase-like domain. The flavin mononucleotide (FMN) present in the C-terminal flavodoxin-like domain acts as a co-factor for this reaction, enabling electron transfer to the Fe–Fe center (Silaghi-Dumitrescu et al., 2005). The genome of the cyanobacterium *Synechocystis* sp. PCC 6803 (hereafter *Synechocystis*) encodes four distinct *Flv*s, *Flv1* through *Flv4* (Allahverdiyeva et al., 2011). *Flv1* and *Flv3* may form part of a single operon or be interspersed with 1–5 open reading frames (ORFs), whereas *Flv2* and *Flv4* are organized as an *Flv4*-ORF-*Flv2* operon. *Flv1* and *Flv3* have been proposed to form a heterodimer able to protect PSI under fluctuating light conditions by preventing the accumulation of ROS at the level of PSI (Helman et al., 2003; Allahverdiyeva et al., 2013, 2015a; Sétif et al., 2020). *Flvs* can mediate Mehler-like reactions and therefore complement cyclic electron transfer pathways in relieving the excess of excitation energy on the PETC (Dang et al., 2014; Gerotto et al., 2016), a phenomenon recently also observed in *Arabidopsis thaliana* plants expressing the *Flv1*/*Flv3* orthologues from the moss *Physcomitrella patens* (Yamamoto et al., 2016). When Gómez et al. (2018) introduced the *Synechocystis Flv1/Flv3* genes into tobacco, the proton motive force of dark-adapted leaves was enhanced, while the chloroplasts' photosynthetic performance under steady-state illumination remained comparable to that of wild-type (WT) siblings. The heterologous expression of *P. patens Flv1* and *Flv3* in two rice mutants defective in cyclic electron transport was shown to restore biomass accumulation to WT levels (Wada et al., 2018). Recently, we demonstrated that the co-expression of *Synechocystis Flv1* and *Flv3* in *A. thaliana* enhanced the efficiency of light utilization, boosting the plant's capacity to accumulate biomass as the growth light intensity was raised (Tula et al., 2020).

Plants expressing Flv1 and Flv3 have been assayed for their photosynthetic performance and light responses (Yamamoto et al., 2016; Gómez et al., 2018; Wada et al., 2018; Tula et al., 2020), but the effects of this additional chloroplast electron sink on stress tolerance and yield were not reported. The present study, therefore, aimed to create for the first time an additional dissipating electron sink downstream of PSI in the chloroplasts of barley, achieved by co-expressing *Synechocystis Flv1* and *Flv3*, and to determine the benefits that the presence of such transgenes could bring to the plant response to drought stress with respect to the production of carbohydrates and accompanying intermediates. Barley is the fourth most important cereal as a source for food and fodder and considered a model crop to investigate the influence of *Flv1* and *Flv3* expression on productivity traits such as biomass and yield. The focus was to investigate whether metabolic activity through photosynthesis can improve drought stress tolerance, thereby supporting the growth of plants exposed to this commonly occurring constraint over crop productivity.

MATERIALS AND METHODS

Barley Transformation and Growth

The methods used to transform barley followed those reported by Marthe et al. (2015). Briefly, the *Synechocystis Flv1* and *Flv3* genes were PCR-amplified, integrated into the pUBI-AB-M plasmid and subsequently cloned via the *Sfi*I restriction sites into the binary vector p6i-2x35S-TE9 (**Figure 1A**), This generic vector harbors *hygromycin phosphotransferase* (*hpt*) as a

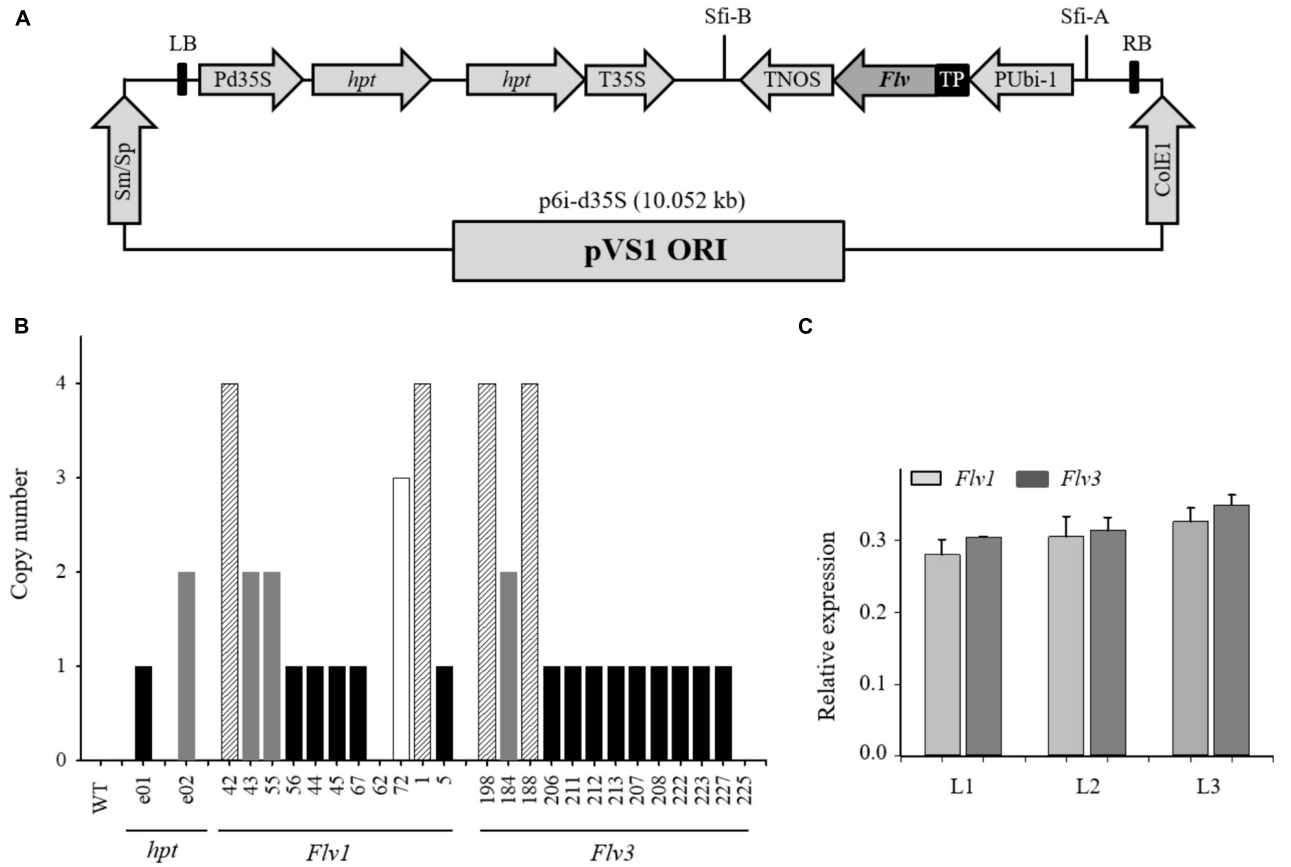

FIGURE 1 | Expression of cyanobacterial *Flv1-Flv3* genes in barley plants. **(A)** Schematic representation of the p6i-2x35S-TE9 binary vector used to clone *Flv1* and *Flv3* genes. The vector harbors the *hpt* plant selectable marker gene containing the potato LS1 intron and driven by a double-enhanced *CaMV 35S* promoter (Pd35S) and terminator (T35S) as well as the *Sm/Sp* bacterial selection marker gene. A sequence encoding the chloroplast-targeting FNR transit peptide (TP) was fused in-frame to the 5′-termini of *Flv1* and *Flv3* coding regions and placed under the control of the maize *Ubi-1* promoter with its 5′-untranslated regions and the first intron (PUbi-1) and the *nos* terminator (TNOS) between T-DNA borders (LB and RB) derived from the p6i plasmid. **(B)** Determination of the copy number of individual *Flv* genes harbored by transgenic barley plants, as estimated using quantitative real-time PCR. T_1 plants containing a single-locus of *Flv1* and *Flv3* (black bars) which could be identified by a 3:1 presence/absence were chosen as progenitors of the subsequently analyzed transgenic plants. WT barley represented the negative control and two plants (e01, e02) known to harbor one and two copies of the *hpt* gene, respectively, as positive controls. **(C)** Determination of *Flv* transcript levels in leaves from transgenic barley lines L1, L2, and L3 co-expressing *Flv1 and Flv3* genes. Data are shown in the form of means ± SE (n = 3). Single-locus T_2 homozygotes displaying similar expression levels were inter-crossed (44 × 211, 67 × 207, and 5 × 206) by two rounds of self-pollination to produce double-homozygous L1, L2, and L3 plants, respectively.

plant selectable marker gene containing the potato *LS1* intron and driven by a doubled-enhanced Cauliflower Mosaic Virus (*CaMV*) *35S* promoter, the *Sm/Sp* (Streptomycin/Spectinomycin) bacterial selection marker gene and T-DNA borders derived from the p6i plasmid (DNA-Cloning-Service, Hamburg, Germany). Each *Flv* gene was placed between the maize *Polyubiquitin-1* promoter including 5′-untranslated region and first intron and the *Agrobacterium tumefaciens nos* terminator, with its coding region being fused in-frame at its 5′-end to a DNA fragment encoding the pea ferredoxin-$NADP^+$ reductase (FNR) transit peptide for chloroplast targeting. The individual constructs harboring either *Flv1* or *Flv3* were transformed into the barley cultivar "Golden Promise" using *A. tumefaciens* AGL-1 (a hypervirulent succinamopine strain with C58 background) by electroporation. Putative transgenic calli were kept for 12 h at 24°C in the light (mean relative humidity 50%) and for additional 12 h at 18°C in the dark (mean relative humidity 80%) until the formation of plantlets following shoot and root development. Thereafter, plantlets were transferred to soil and maintained at 80% humidity for 7–10 days by covering with a plastic hood. Plants were grown in a greenhouse providing a 12-h photoperiod at 250 μmol photons m^{-2} s^{-1} and a day/night temperature of 16°C/12°C (ambient conditions) until maturity, and grains were harvested for further experiments.

T_1 generation grains were sown in 96-well trays containing substrate 2 (Klasmann-Deilmann GmbH, Geeste, Germany), compost and sand (2:2:1), held at 4°C for 14 days, then exposed to a 16-h photoperiod at a day/night temperature of 18°C/12°C. Seedlings at the four-leaf stage were potted into a 3:2:1 compost, vermiculite and sand mixture and grown to maturity in a greenhouse under ambient conditions.

Transgene Copy Number Determination

An estimate of the number of *Flv* transgene copies present in leaves of barley T_1 individuals was obtained using a quantitative real-time PCR assay as described by Song et al. (2002) and Kovalchuk et al. (2013). Briefly, DNA was extracted from the second leaf of each plant following the method of Saghai-Maroof et al. (1984) and was serially diluted in sterile deionized water to give solutions containing between 12.5 and 200 ng μL^{-1} DNA. For the calculation of transgene copy number from unknown DNA samples, a serial dilution (400, 200, 100, 50, and 25 ng) of genomic DNA extracted from an available plant known to contain 1-2 copies of the *hpt* gene was used as the target sequence. Primers and PCR conditions are listed in **Supplementary Table 1**. For template loading normalization, the PCR reactions included a dual-labeled sequence 5′-CAL fluor Gold 540-ATGGTGGAAGGGCGGCTGTGABHQ1 as a probe complementary to a portion of the barley orthologue of the wheat *Pin-b* gene (Kovalchuk et al., 2013). The PCR efficiency for each primer set was determined from an analysis of the Ct values obtained from the serial dilution. Transgene copy numbers were determined by applying the $2^{-\Delta\ \Delta\ CT}$ method (Li et al., 2004; **Figure 1B**). For each single-locus transgene construct harboring either *Flv1* or *Flv3*, 16 T_1 individuals were then self-pollinated. Homozygotes were selected by segregation analysis as determined by PCR amplification with primers *Flv1* F/R and *Flv3* F/R given in **Supplementary Table 1**. Only those behaving as having a single major gene (exhibiting a 3:1 segregation) in the T_2 generation were retained as illustrated in **Supplementary Figure 1**. Siblings lacking *Flv* fragments, confirmed by PCR amplification, were used as "azygous" control plants.

To produce double-homozygous plants harboring *Flv1/Flv3*, single-locus T_2 homozygotes (**Figure 1B**) with nearly the same expression level were then inter-crossed (44 × 211, 67 × 207 and 5 × 206) to render double-homozygous L1, L2, and L3 plants, respectively after two generations of self-pollination (**Supplementary Figure 2**).

Expression Analysis of the *Flv1*/*Flv3* Genes

To monitor the expression of the *Flv1/Flv3* genes in the three independent lines L1–L3 (**Figure 1C**), total RNA was extracted from young leaves according to Logemann et al. (1987). RNA was subjected to DNase treatment (Thermo Fischer Scientific, Dreieich, Germany) and converted to single-stranded cDNA using a RevertAid first-strand cDNA synthesis kit (Life Technologies, Darmstadt, Germany) with a template of 1 μg total RNA and oligo primer. The reaction was run at 42°C for 60 min. Quantitative reverse transcription-PCR (qRT-PCR) was performed in a CFX384 touch real-time system (Bio-Rad, United States) using the SYBR Green Master Mix Kit (Bio-Rad, Feldkirchen, Germany). Primers employed to amplify *Flv1* (Flv1-RT F/R) and *Flv3* (Flv3-RT F/R), along with those amplifying the reference sequence gene *ubiquitin-conjugating enzyme 2* (E2 F/R), that was stably expressed under the experimental conditions tested for barley, are listed in **Supplementary Table 1**. Relative transcript abundances were determined using the Schmittgen and Livak (2008) method. Each qRT-PCR result relied upon three biological replicates per line, each of which being represented by three technical replicates.

Quantifying the Barley Response to Drought Stress

A representative set of barley plants harboring *Flv1*/*Flv3* transgenes (L1–L3) were selected along with sibling azygous plants. A set of 24 plants of each of the *Flv1/Flv3* transgenic lines (F_3), non-transgenic barley cultivar "Golden Promise" (referred as WT) and azygous controls were grown for 28 days under a well-watered regime in a chamber providing ambient conditions. Twelve of the seedlings were then transferred into 5-cm pots with 50 g of soil (one seedling per pot) for the drought stress treatment at the vegetative stage and were allowed to recover for 3 days after being transferred. The other 12 seedlings were planted in larger pots (20-cm diameter and 200 g of soil, one seedling per pot) to assess the effect of stress at the reproductive stage. For the stress experiment at the seedling stage, six plants were kept under well-watered, ambient conditions, maintaining a soil moisture level of 65-70% of field capacity (FC; **Supplementary Figure 3A**). The remaining six plants were subjected to the drought treatment by withholding water for 3–4 days until the soil moisture level in the pots falls to 10–12% FC, and this state was maintained for five days (**Supplementary Figure 3B**). Subsequently, the 12 treated plants were transferred to the glasshouse and grown under well-watered conditions until maturity (∼90 days) to determine growth parameters such as days to heading.

For the reproductive stage stress experiment, plants were kept well-watered (65–70% FC) under ambient conditions until the emergence of the first spike in 90% of the plants. Drought stress treatment was imposed five days post-anthesis by withholding water until FC fell to 10–12% and leaf wilting was observed. Thereafter, each pot was given 200 mL water every fourth day to maintain the soil moisture level at 10–12% FC over 21 days. Control plants (n = 6) were kept fully watered throughout. Flag leaves were collected 10 days after stress had been initiated, and the fresh weight (FW) of each leaf was measured immediately before it was placed into a collection tube. The relative water content (RWC) was calculated using six individuals each of WT and transgenic plants applying the following equation: RWC (%) = [(FW - DW)/(TW - DW)] × 100, where FW is the fresh weight at harvest time, TW is the total weight at maximal turgor estimated after 24 h of imbibition, and DW is the dry weight after 48 h at 85°C (Marchetti Cintia et al., 2019).

Phenotypic Effects of Drought

The effect of drought stress on barley plants was assessed by measuring the following traits: days to heading, defined as the number of days from sowing to the time when 50% of the spikes had emerged from the flag leaf sheath, using Zadoks scale 55 (Zadoks et al., 1974); plant height (the height from

the soil surface to the tip of the longest spike, excluding awns); above-ground plant biomass at maturity measured after the plants had been oven-dried at 60°C for 72 h; the number of spikes produced per plant; the grain number per plant and the total grain weight per plant (g). The latter two traits were quantified using a Marvin-universal seed analyser (GTA Sensorik GmbH, Neubrandenburg, Germany).

Metabolite Measurements

Flag leaves of two spikes per plant (n = 6) with the same developmental stage (head emergence) were sampled when a completed leaf rolling as the primary visible symptom of drought stress occurred. The leaves were pooled, grinded and 50 mg of each sample were used for the measurement of the metabolites in WT, azygous and transgenic L1–L3 individuals. The contents of amino acids, including the stress marker proline, were quantified as described by Mayta et al. (2018), whereas extraction and analysis of soluble sugars were essentially performed according to Ahkami et al. (2013).

Adenine nucleotides were quantified employing a UPLC-based method developed from that described by Haink and Deussen (2003). Prior to the separation step, a 50-μL aliquot of the sample and a mixture of ATP, ADP, and AMP were derivatized by the addition of 25 μL of 10% (v/v) chloracetaldehyde and 425 μL of 62 mM sodium citrate/76 mM KH_2PO_4, pH 5.2, followed by a 40-min incubation at 80°C, cooling on ice, and centrifugation at 20,000 g for 1 min. The separation was achieved using an ultra-pressure reversed-phase chromatography system (AcQuity H-Class, Waters GmbH, Eschborn, Germany) consisting of a quaternary solvent manager, a sample manager-FTN, a column manager and a fluorescent detector (PDA eλ Detector). The gradient was established using eluents A (TBAS/KH_2PO_4: 5.7 mM tetrabutylammonium bisulfate/30.5 mM KH_2PO_4, pH 5.8) and B (a 2:1 mixture of acetonitrile and TBAS/KH_2PO_4); the Roti C Solv HPLC reagents were purchased from Roth (Karlsruhe, Germany). The 1.8-μm, 2.1 mm × 50 mm separation column was a Luna Omega C18, (Phenomenex, Aschaffenburg, Germany). The column was pre-equilibrated for at least 30 min in a 9:1 mixture of eluents A and B. During the first two min of the run, the column contained 9:1 A:B, changed thereafter to 2:3 A:B for 2 min followed by a change to 1:9 A:B for 1 min and set to initial values of 9:1 A:B for 2 min. The flow rate was 0.5 mL min^{-1} and the column temperature was maintained at 45°C. The excitation and emission wavelengths were 280 and 410 nm, respectively. Chromatograms were integrated using Empower Pro software (Waters, Eschborn, Germany). Energy charge was calculated from the expression ([ATP] + 0.5 [ADP])/([ATP] + [ADP] + [AMP]) (Atkinson and Walton, 1967).

Statistical Analyses

Descriptive statistics (means and SE) and data analysis were carried out using SigmaPlot (Systat Software, San Jose, CA, United States). The Student's t-test was applied for evaluating statistically significant differences between means of individual transgenic lines versus the wild-type.

RESULTS

Flv Expression Influences Plant Growth Under Drought Stress at the Seedling Stage

Homozygous plants containing a single copy of the transgenes and co-expressing high levels of *Flv1* and *Flv3* (L1–L3) were used to assess drought tolerance (**Figure 1**). When grown under ambient conditions, *Flv1/Flv3*-expressing plants were taller than their WT and azygous siblings (**Figure 2A** and **Supplementary Figure 3A**), without significant differences in aboveground biomass dry weight (**Figure 2B**). Height differences between WT and transgenic plants were maintained under drought stress applied at the seedling stage (**Figure 2A** and **Supplementary Figure 3B**). The treatment caused a major decrease (up to 40%) of total biomass in non-transformed and azygous plants, which was reduced to less than 10% in their transgenic siblings (**Figure 2B**). Compared to WT plants, up to 1.5-fold, more biomass was accumulated by *Flv1/Flv3*-expressing lines under drought (**Figure 2B**). In the absence of stress, *Flv1/Flv3* transgenic plants generally reached heading 2–3 days sooner than non-transformed and azygous counterparts, with these differences becoming more pronounced (5–7 days) under drought (**Figure 2C**).

Plants expressing both transgenes were the least compromised by drought stress with respect to the number of spikes produced (**Figure 2D**). Compared to WT and azygous plants, there was also significant preservation in the number of grains set per plant by drought-challenged Flv1/Flv3 transgenic lines. The stress treatment decreased grain number by as much as 4-fold in WT and azygous plants while the three transgenic lines displayed less than 20% reduction (**Figure 2E**), setting at least 3.7-fold more grain than their non-transgenic controls in drought-stressed conditions (**Figure 2E**). A similar trend was observed for the total grain weight per plant, which was reduced up to 3-fold in WT and azygous plants upon drought stress, but only up to 30% in the transformants (**Figure 2F**). Indeed, the total grain weight per plant of Flv1/Flv3 transgenic plants from lines L2 and L3 appeared not to be affected by the adverse condition. The total grain weight per plant was up to 3-fold higher in the Flv1/Flv3-expressing lines subjected to drought stress than that achieved by the non-transgenic plants (**Figure 2F**).

Flv Expression Influences Plant Performance Under Drought Stress at the Reproductive Stage

The increased height of the *Flv1/Flv3* transgenic plants under non-stressed conditions was maintained as plants entered the reproductive stage (**Figure 3A**). While the RWC measured at this stage decreased upon drought stress, it did not differ significantly between WT and transgenic plants grown under ambient conditions (about 78%) nor in plants exposed to drought stress (about 47%). The height increase driven by *Flv1/Flv3* presence was lost upon drought exposure at the reproductive stage (**Figure 3A**). In contrast, drought-dependent reduction in

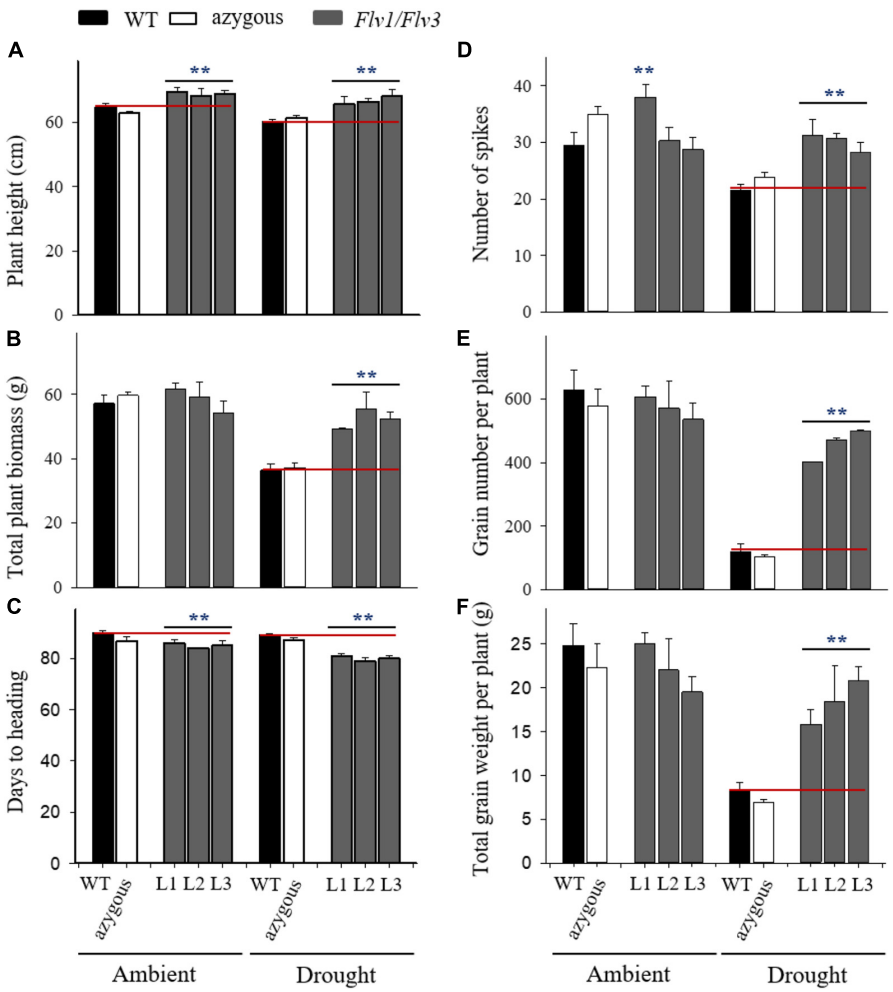

FIGURE 2 | Effect of heterologously expressing *Flv1/Flv3* genes on productivity-associated traits of barley plants grown either under ambient conditions or exposed to drought stress for 5 days at the seedling stage. Measurements were carried out at maturity (~90 days). Other experimental details are given in Materials and Methods. **(A)** Plant height, **(B)** total plant biomass, **(C)** days to heading, **(D)** the number of spikes per plant, **(E)** the total number of grains per plant, **(F)** the total grain weight per plant. Lines L1–L3 co-express *Flv1 and Flv3* genes. Data are shown as means ± SE (n = 6). **means differed significantly ($P \leq 0.01$) from those of non-transgenic plants.

aboveground biomass was similar to that observed upon stress application at the seedling stage and was equally protected by *Flv1/Flv3* (**Figure 3B**). The imposition of drought stress at the reproductive stage advanced heading only in line L3 of *Flv* transgenic plants by about three days (**Figure 3C**).

With respect to the number of spikes produced per plant, the *Flv1/Flv3* transgenic plants were notable for the protective effect exerted under drought, while there was no variation between lines in the absence of stress (**Figure 3D**). Drought also had a devastating effect on yield when applied at the reproductive stage, but *Flv1/Flv3* transgenic plants were able to set ~2- to 3-fold more grain per plant than their WT siblings (**Figure 3E**), and their total grain weight per plant was 8- to 9.5-fold greater (**Figure 3F**). Under these conditions, the total grain weight per plant of lines L2 and L3 were unaffected by the stress treatment. In summary, expression of *Flv1/Flv3* preserved major productivity traits such as the number of spikes, grain number and total grain weight per plant in transgenic barley plants exposed to drought treatments applied at either the seedling or the reproductive stages (**Figures 2**, **3**).

Flv Expression Influences Carbohydrate Contents and Amino Acid Levels Under Drought Stress

Under ambient conditions, flag leaf glucose and fructose were not detectable in control plants used for drought stress experiments applied at seedling stage or in a low amount at the reproductive stage, with no significant differences between WT, azygous and transgenic plants (**Figures 4A,B,D,E**). Sucrose also failed to display differences between lines, although their levels increased ~5-fold in plants challenged at the reproductive stage (**Figures 4C,F**).

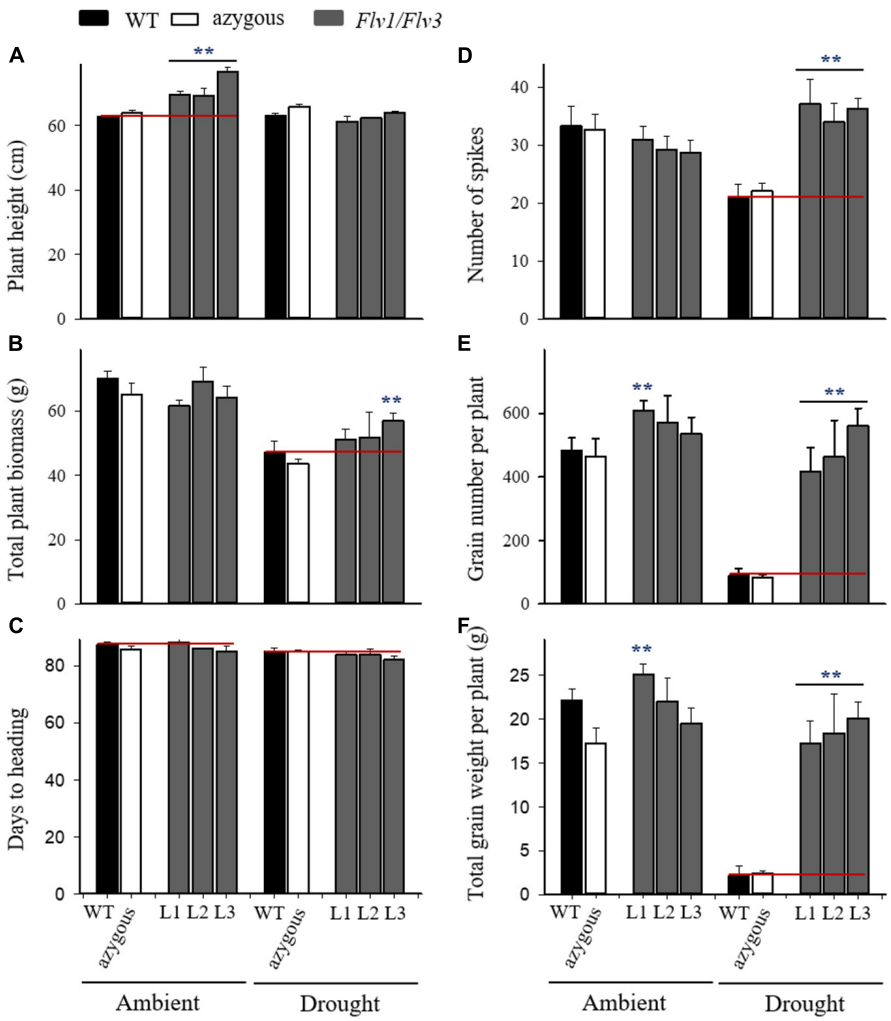

FIGURE 3 | Effect of heterologously expressing *Flv1/Flv3* genes on productivity-associated traits of barley plants grown either under ambient conditions or exposed to drought stress for 21 days at the reproductive stage. Measurements were carried out at the end of the 21-day drought treatment. Other experimental details are given in section "Materials and Methods." **(A)** Plant height, **(B)** total plant biomass, **(C)** days to heading, **(D)** the number of spikes per plant, **(E)** the total number of grains per plant, **(F)** the total grain weight per plant. Lines L1–L3 harbor both *Flv1 and Flv3* genes. Data are shown as means ± SE (n = 6). **means differed significantly ($P \leq 0.01$) from those of non-transgenic plants.

Application of the drought treatment at the seedling stage led to major increases in all soluble sugars, irrespective of the genotype (**Figures 4A–C**). Significant differences between lines became instead apparent when the stress treatment was assayed at the reproductive stage, with higher leaf glucose and fructose contents (**Figures 4D,E**) and lower sucrose levels in transgenic plants compared to their WT siblings (**Figure 4F**).

Flag leaf amino acid contents were not affected by *Flv1/Flv3* expression in plants grown under ambient conditions except for the case of glutamate, whose levels were up to 1.6-fold higher in the transformants relative to WT counterparts (**Figure 5A** and **Supplementary Table 2**). Drought treatment had little effect on the amounts of free amino acids in WT and azygous plants, but for significant increases in glycine and proline (**Figure 5**). In contrast, an increased pool of histidine, asparagine, serine, glutamine, glutamate, asparagine, threonine, and alanine was observed in *Flv1/Flv3* transgenics under stress conditions (**Figures 5A–E** and **Supplementary Table 2**). Leaf contents of proline increased strongly (up to 60-fold) in drought-exposed WT and azygous plants, which is in line with its recognized role as a stress marker. By contrast, proline levels increased significantly less in stress-treated *Flv* transformants, despite their higher proline levels under ambient conditions (**Figure 5F**, inset).

Under ambient conditions, the flag leaf contents of free amino acids increased significantly as the plants entered the reproductive stage (**Figure 6** and **Supplementary Table 3**), with no major differences between lines except for proline and glutamine, which accumulated to lower levels in *Flv*-expressing plants (**Figures 6B,F**). Drought exposure increased the amounts of several amino acids (most conspicuously proline) in WT

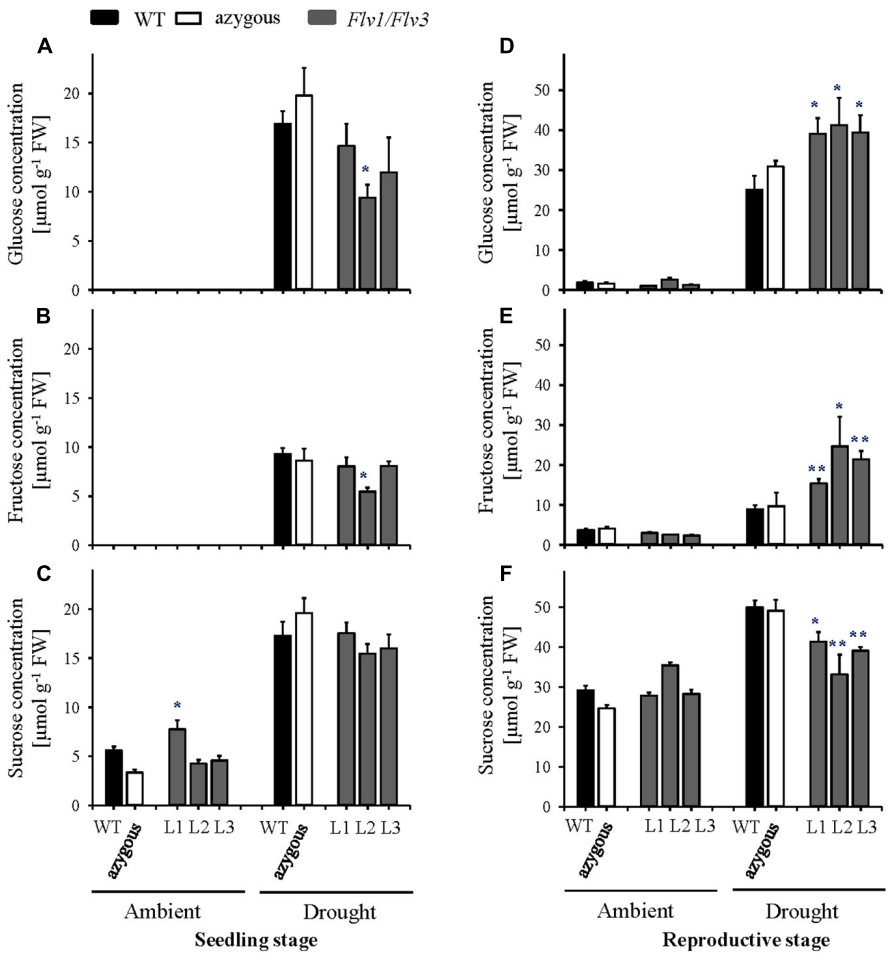

FIGURE 4 | Effect of heterologously expressing *Flv1/Flv3* genes on sugar contents in flag leaves of barley plants grown either under ambient conditions or exposed to drought stress at the seedling stage **(A–C)** and the reproductive stage **(D–F)**. Samples were collected at the leaf rolling stage. Other details are given in section "Materials and Methods." **(A,D)** Glucose, **(B,E)** fructose, **(C,F)** sucrose. Lines L1–L3 co-express *Flv1 and Flv3* genes. Data are shown as means ± SE (n = 6). **; *means differed significantly ($P \leq 0.01$ and $P \leq 0.05$, respectively) from those of non-transgenic plants. FW, fresh weight.

and azygous plants, (**Figure 6** and **Supplementary Table 3**). Noteworthy, the stress condition did not affect the amounts of specific amino acids derived from the glycolytic metabolism, such as glutamate, glutamine, asparagine, aspartate, and serine (**Figures 6A–E**), as well as glycine and threonine (**Supplementary Table 3**) in leaves of the *Flv* transformants. Proline levels were up-regulated by drought in *Flv1/Flv3* plants, but significantly less than in their WT and azygous counterparts (**Figure 6F**). No clear differences were observed for other amino acids following exposure to drought as compared to non-stressed plants (**Supplementary Table 3**).

Flv Expression Influences the Energy Status of Drought-Stressed Barley Plants

At the seedling stage, ATP and ADP contents were similar in leaves from WT, azygous and transgenic plants under ambient conditions while there was a decrease of AMP levels up to 1.7-fold in Flv-expressing lines compared to WT and azygous siblings (**Supplementary Figures 4A–C**). The contents of all adenylates strongly increased in drought-stressed WT and azygous plants and the transgenic line L1, whereas lines L2 and L3 maintained ATP and ADP at ambient levels (**Supplementary Figures 4A–C**).

Upon reaching the reproductive stage, adenylate contents increased 3- to 8-fold in WT and azygous plants under ambient conditions, but significantly less in the transformants (**Supplementary Figures 4D–F**). Accordingly, adenine nucleotide levels were as much as 3-fold (AMP), 1.8-fold (ADP), and 2.1-fold (ATP) lower in the leaves of Flv-expressing plants compared to WT and azygous counterparts (**Supplementary Figures 4D–F**). Drought stress, in turn, led to a moderate decline in adenylate contents (especially ADP and AMP) in WT and azygous plants but increased those of Flv transformants, resulting in similar levels for the three nucleotides in all lines (**Supplementary Figures 4D–F**).

As a consequence of these effects of Flv1/Flv3 expression on adenylate levels, the ATP/ADP ratio and the energy

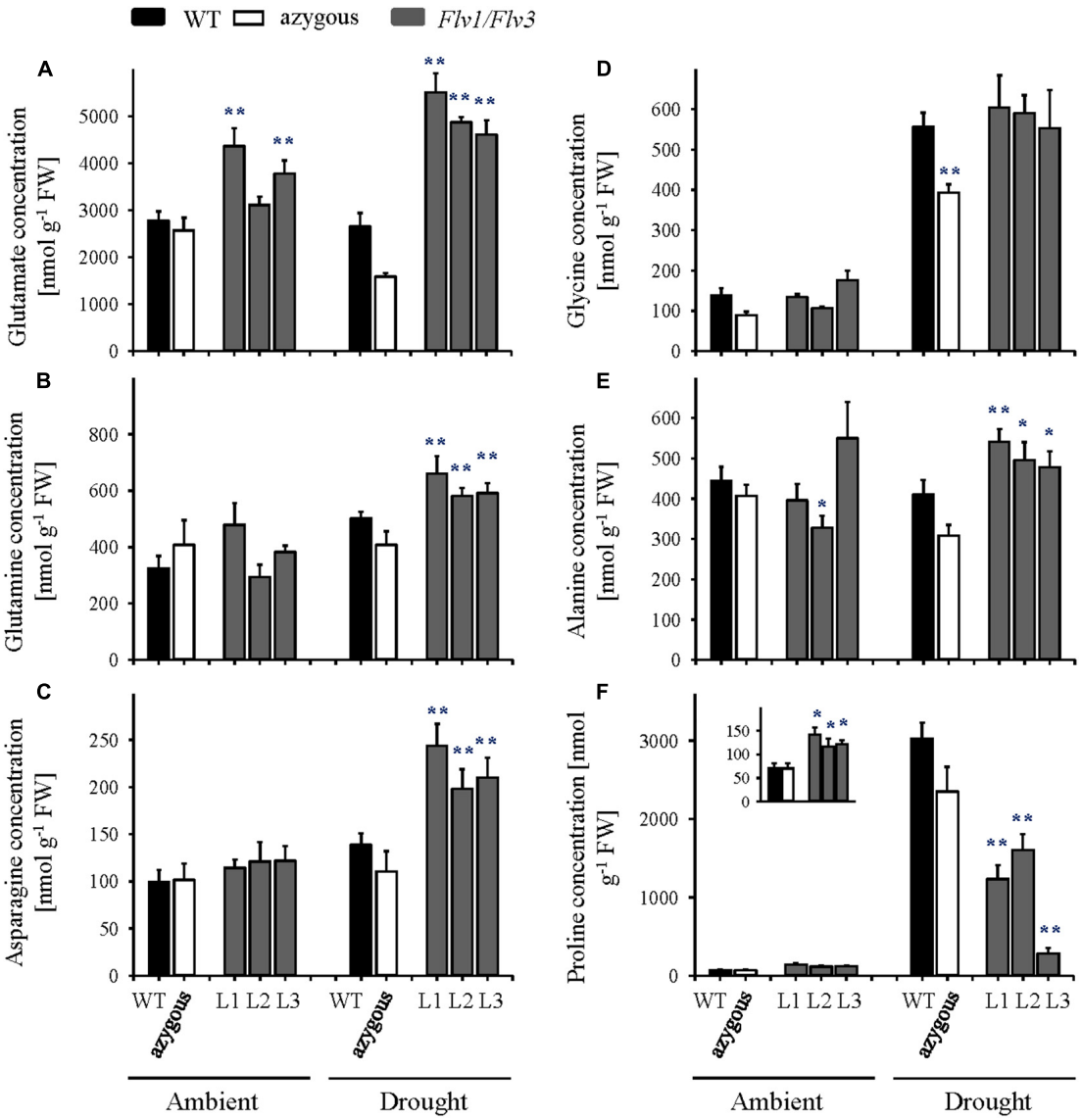

FIGURE 5 | Effect of heterologously expressing *Flv1/Flv3* genes on free amino acid contents in flag leaves of barley plants grown either under ambient conditions or exposed to drought stress at the seedling stage. Amino acid levels were measured in the same samples used for carbohydrate determinations. **(A)** Glutamate, **(B)** glutamine, **(C)** asparagine, **(D)** glycine, **(E)** alanine, and **(F)** proline. Lines L1–L3 harbor both *Flv1 and Flv3* genes. Data are shown as means ± SE (n = 5–7). **; *means differed significantly ($P \leq 0.01$ and $P \leq 0.05$, respectively) from those of non-transgenic plants. FW, fresh weight.

charge were largely similar between lines under both ambient and drought conditions applied at either the seedling or reproductive stages, with only a few exceptions illustrated in **Supplementary Figure 5**.

DISCUSSION

This is the first study to show that the introduction of the cyanobacterial *Flv1 and Flv3* gene products into the chloroplast improves the productivity of barley under drought through maintenance of metabolic activity and increasing carbohydrate and amino acid utilization.

The Heterologous Expression of Flv1/Flv3 in Barley Improves Plant Productivity Under Drought Stress

Crops frequently encounter drought as transient or terminal stress (Alegre, 2004) and indeed, terminal-drought stress is the most serious constraint to cereal production worldwide (Lonbani and Arzani, 2011). Plant survival under these unfavorable conditions depends on their duration and intensity. When exposed to moderate stress, plants survive by adaptation or acclimation strategies and by repair mechanisms. To cope with chronic drought conditions causing severe damage or death, they evolve resistance mechanisms further classified into drought

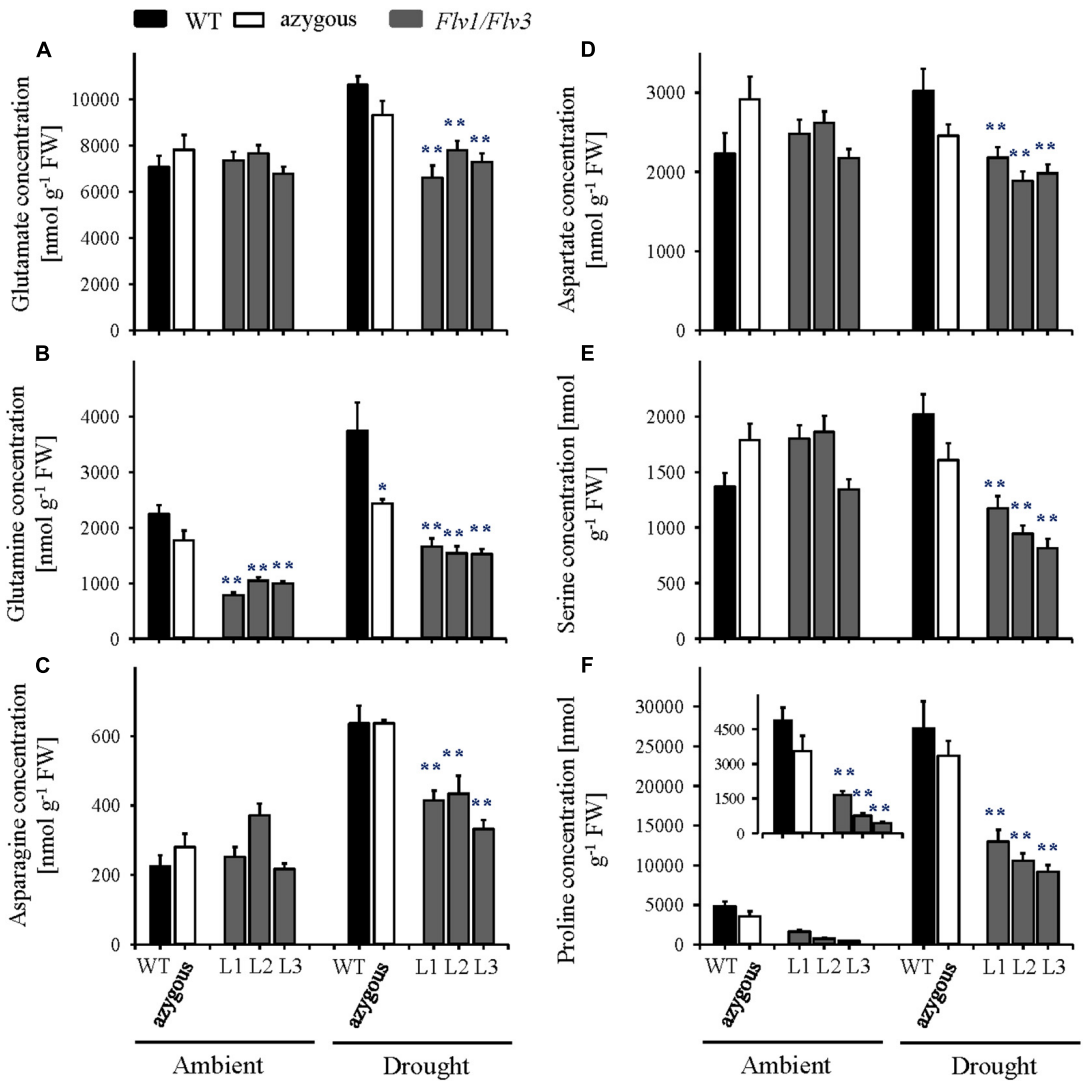

FIGURE 6 | Influence of heterologously expressing *Flv1/Flv3* genes on free amino acid contents in flag leaves of barley plants grown either under ambient conditions or exposed to drought stress at the reproductive stage. Amino acid levels were measured in the same samples used for carbohydrate determinations. **(A)** Glutamate, **(B)** glutamine, **(C)** asparagine, **(D)** aspartate, **(E)** serine, and **(F)** proline. Lines L1–L3 co-express *Flv1 and Flv3* genes. Data are shown as means ± SE (n = 6–7 for WT and azygous, and n = 8–14 for transgenic lines). **; *means differed significantly ($P \leq 0.01$ and $P \leq 0.05$, respectively) from those of non-transgenic plants. FW, fresh weight.

avoidance and drought tolerance (Price et al., 2002). A typical response of cereals such as barley to drought or high-temperature stress is to slow down their vegetative growth, followed by progressive leaf wilting if the adverse condition is prolonged. When these stresses occur around anthesis, the plant response may include premature leaf senescence, which results in a decline in photosynthesis and assimilates production as well as an acceleration of physiological maturation (Gan, 2003). Drought stress diminished grain yield by reducing the number of tillers, grains and spikes per plant and individual grain weight in barley (Farooq et al., 2009). Here, when barley plants were exposed to drought at the seedling stage, the heterologous expression of *Flv1/Flv3* resulted in the acceleration of heading time and flowering (**Figure 2C**). For such plants, one likely consequence is that they are less prone to experience terminal drought stress because they earlier reach maturity. The presence of the *Flv1/Flv3* transgenes was thus associated with the production of more spikes and a significantly higher grain number and yield under drought stress conditions applied at both the seedling and reproductive stages (**Figures 2**, **3**).

Under conditions of drought stress, the barley *Flv1/Flv3* transgenic plants out-performed their non-transgenic controls in the accumulation of aboveground biomass, the number of grains set and the total grain weight per plant (**Figures 2**, **3**). These observations suggest that heterodimeric Flvs are also functional in a monocotyledonous species, acting to maintain growth in a situation where surplus electrons are produced. Additional support for this contention is also provided by the

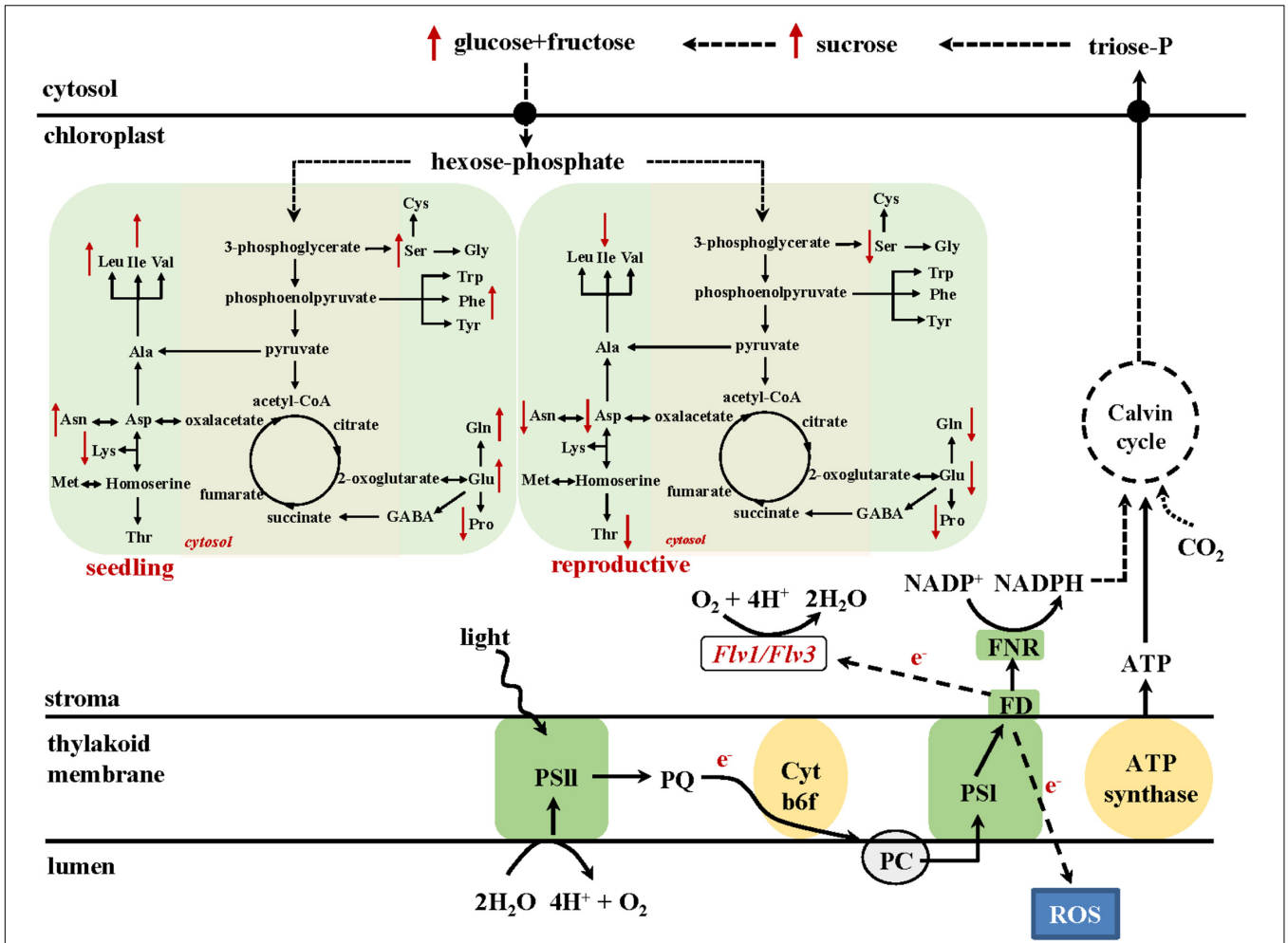

FIGURE 7 | A model describing the metabolic consequences of heterologously expressing *Flv1/Flv3* genes in the chloroplasts of barley plants exposed to drought stress at the seedling **(left)** and the reproductive stage **(right)**. The presence of *Flv* gene products generates an electron sink and balances the electron pressure generated under stress by delivering the surplus of reducing equivalents to oxygen, which is converted to water. Based on the results, we propose that this activity is acting as a valve to relieve the excess of electrons and does not affect NADPH production, allowing CO_2 assimilation through the Calvin-Benson cycle to form triose-phosphates. Sucrose produced from triose-phosphates is cleaved to soluble sugars glucose and fructose. The resulting hexose-phosphates are incorporated into amino acids, or used for energy production through glycolysis. As a consequence, these intermediates are preferentially employed to maintain the energy source necessary to support the growth of plants exposed to stress. PQ, plastoquinone; Cytb6/f, cytochrome b_6/f complex; PC, plastocyanin; FD, ferredoxin; FNR, ferredoxin-$NADP^+$ reductase.

reduced accumulation of proline (a marker of drought stress, see Szabados and Savouré, 2010) in leaves of the transgenic plants (**Figures 5**, **6**).

The Heterologous Expression of *Flv1/Flv3* Resulted in a Distinct Response of Carbohydrates, Amino Acids and Energy Status at Various Developmental Stages in Drought-Stressed Barley Plants

Drought stress suppresses the production of carbohydrates either by restricting CO_2 fixation following to stomatal closure (Quick et al., 1992; Brestic et al., 1995) or via limiting the supply of ATP as a result of inhibition of ATP synthase (Tezara et al., 1999). Sucrose synthesized during photosynthesis represents the major feedstock for starch production (Counce and Gravois, 2006), but in drought-stressed plants it also acts as an osmolyte, helping to maintain turgor pressure and to mitigate membrane damage (Couée et al., 2006).

The response of plants with respect to sugar accumulation under drought conditions depends on the species and even on the intraspecific lines within a given species, as reported for wheat by Guo et al. (2018). The comparison of drought-sensitive and -tolerant wheat varieties revealed that soluble sugars such as sucrose or fructose displayed opposite stress behavior, that is, they are reduced in the sensitive and increased in the tolerant plants under drought (Guo et al., 2018). In the present study, drought treatments applied at either the vegetative

or reproductive stages resulted in a strong accumulation of soluble sugars including glucose, fructose and sucrose in WT and transgenic plants (**Figure 4**). This indicates that these metabolites play important roles in the delivery of assimilates to sink organs for further growth (Fàbregas and Fernie, 2019, and references therein) or as osmoprotectants (Singh et al., 2015), and as such are highly sensitive markers of environmental adversities. Sugar accumulation is a general response to drought stress in different plant species, as demonstrated in the current study and several other reports (Singh et al., 2015; Das et al., 2017; Fàbregas et al., 2018; Fàbregas and Fernie, 2019). Remarkably, transgenic lines expressing *Flv1/Flv3* genes exhibited even higher glucose and fructose contents and a slightly lower sucrose content compared to WT and azygous plants under drought conditions (**Figure 5**), suggesting a higher activity of downstream pathways including glycolysis to keep pace with the environmental changes.

Improved metabolic activity exerted by chloroplast-expressed *Flv1/Flv3* is also reflected by the differential drought response of amino acid turnover. A schematic model describing metabolic fluxes in WT and Flv1/Flv3-transgenic plants is shown in **Figure 7**. At the vegetative stage, several amino acids such as Glu, Gln, Asp and Ala increased in the flag leaves of transgenic plants under drought with respect to those in WT siblings. By contrast, at the reproductive stage, most amino acids including Glu, Gln, Ser, Asp, and Asn decreased while being maintained at the levels found in the absence of stress (**Figure 5**, **6** and **Supplementary Tables 2**, **3**). This contrasting effect of drought on amino acid accumulation (**Figure 7**) might be because at the vegetative stage, barley plants invest available assimilates into defense mechanisms to resist the stress condition for better growth. Improved assimilate production in transgenic plants might result from a better performance of photosynthetic activity exerted by the presence of Flv1/Flv3 proteins as demonstrated in several studies (Yamamoto et al., 2016; Gómez et al., 2018; Wada et al., 2018).

At the reproductive stage, water limitation led to a strong increase in amino acid levels in WT flag leaves compared to non-stressed conditions (**Figures 5**, **7** and **Supplementary Table 2**). However, in the flag leaves of transgenic plants, the same amino acids were maintained at the levels found under non-stressed conditions or decreased in comparison to the contents of WT plants (**Figures 6**, **7** and **Supplementary Table 3**). At this stage, a stable metabolic activity is crucial for the maintenance of assimilates translocation from the flag leaves to the growing sink tissues, in this particular case the grains that are highly dependent on the delivery of the assimilates from the source organs. Thus, most likely WT plants use the produced sugars to synthesize amino acids such as Glu that serve as a key hub for the production of defense compounds such as proline, a sensitive marker of drought stress (Fàbregas and Fernie, 2019). However, due to a better performance of the metabolic activity, transgenic barley plants may compensate the loss of nitrogen-containing amino acids including a reduced production of proline (**Figures 5**, **6**). The saving of nitrogen-containing compounds such as glutamate, the immediate precursor of proline synthesis, might be used for further assimilation and translocation to sink organs (Rai and Sharma, 1991; Hildebrandt et al., 2015). This fact; however, does not refer to any specific role of proline in the stress tolerance displayed by *Flv1/Flv3* plants. Indeed, proline accumulation is a universal non-specific response to many sources of abiotic stress including drought and salt whose function is still a matter of debate. The contribution of proline in stress tolerance depends on various factors such as genetic background of the species, the intensity of abiotic stress, the physiological state of the plants and the environment, as outlined by Ebrahim et al. (2020). Proline is proposed to contribute to stabilization of sub-cellular structures, scavenging free radicals, and buffering cellular redox potential rather than to be used as energy source (Kaur and Asthir, 2015). Ebrahim et al. (2020) reported lower proline build-up in salt-tolerant barley cultivars compared to salt-sensitive varieties. This is basically the same phenomenon we observed with drought in our study: proline, unlike other amino acids, was down-regulated in our stress-tolerant *Flv* plants. A possible explanation for these observations is that proline accumulation is rendered less necessary in plants displaying other mechanisms of stress tolerance, such as expression of additional electron sinks.

Recent publications have demonstrated that high levels of energy and sugars improve plant development and tolerance to drought stress (Guo et al., 2018; Fàbregas and Fernie, 2019). This is also a fundamental basis for an active metabolism with increased pools of intermediates such as amino acids. Furthermore, amino acids have been reported to contribute to both membrane permeability and ion transport in the leaves of *Vicia faba* (Rai and Sharma, 1991). Indeed, *Flv*-expressing plants showed significant drought-associated increases in specific amino acids such as alanine, glutamate, serine and aspartate (**Figure 7**) which are derived from precursors of the glycolytic metabolism and serve as immediate primary substrates to build up nitrogen sources like glutamine and asparagine or antioxidative compounds like glutathione or polyamines. Thus, the metabolite profiling supports the idea that carbohydrates and amino acid metabolism help maintain the fitness of plants under drought stress, which is also in agreement with previously reported results of drought-tolerant varieties in other species (Guo et al., 2018).

Following exposure to drought, ATP levels were found to increase (relative to ambient conditions) in the leaves of *Flv* transgenic plants at both the seedling and reproductive stages (**Supplementary Figure 4**), indicating that *Flv1/Flv3* were able to maintain linear electron flow and thereby support ATP synthesis under the adverse condition. Sustaining cellular metabolism and ensuring growth and survival under stress rely heavily on a continuous supply of ATP (Sharkey and Badger, 1982). By improving the availability of electron acceptors at PSI, *Flv1/Flv3* can prevent ROS build-up (Rutherford et al., 2012), which may, in turn, inhibit both PSI and PSII activity and compromise the function of the ATP synthase complex (Lawlor, 1995).

CONCLUSION

Data presented here show how integrating additional electron sinks to the PETC can boost the level of drought tolerance in a monocotyledonous crop species, irrespective of whether the drought condition was applied at the seedling stage or

post-flowering. The heterologous expression of both *Flv1* and *Flv3* in barley had the effect of allowing efficient utilization of produced assimilates including sugars and amino acids, thereby supporting plant growth in the face of either early- or late-onset drought and ultimately supporting the conversion of assimilates into biomass and yield (**Figure 7**). Overall, the experiments have confirmed that adopting this genetic manipulation approach has substantial potential to enhance the level of stress tolerance exerted by crop plants.

DATA AVAILABILITY STATEMENT

The original contributions presented in the study are included in the article/**Supplementary Material**, further inquiries can be directed to the corresponding author.

AUTHOR CONTRIBUTIONS

FS and MH have made substantial contributions to conception and design, interpretation of the results, and preparation of the manuscript. FS conducted the experiments and analyzed the data. ST, GH, and JK supported producing of transgenic plants. NR and NN helped in the phenotypic evaluation of the plants. RG, AL, and NC have been involved in the interpretation of the data and editing the manuscript. NC reviewed the manuscript. All authors read and approved the final manuscript for publication.

FUNDING

This project was supported by funds of the Bundesministerium für Bildung und Forschung (BMBF), Germany, to FS, ST, and MH, by grant PICT 2015-3828 from the National Agency for the Promotion of Science and Technology (ANPCyT, Argentina) to NC, and by grants PICT 2017-3080 from ANPCyT, Argentina and IO 212-2017 from the Santa Fe Agency for Science, Technology and Innovation to AL.

ACKNOWLEDGMENTS

We wish to thank Melanie Ruff, Nicole Schäfer, Sabine Sommerfeld, Heike Büchner and Heike Nierig for their excellent technical assistances at the IPK. RG was a Fellow and AL and NC are Staff Researchers from CONICET, Argentina. AL and NC are Faculty members of the Facultad de Ciencias Bioquímicas y Farmacéuticas, Universidad Nacional de Rosario, Argentina. This manuscript has been released as a pre-print at bioRxiv 2020.09.29.318394 (Shahinnia et al., 2020).

SUPPLEMENTARY MATERIAL

The Supplementary Material for this article can be found online at: https://www.frontiersin.org/articles/10.3389/fpls.2020.613731/full#supplementary-material

Supplementary Figure 1 | A representative segregation analysis of the *Flv1* transgene in a set of barley T_2 individuals (lanes 1-16), as determined by PCR amplification. The selection of single-locus transgenic plants was made based on a monogenic (3:1) ratio for both *Flv1* and *Flv3*. M: 1 kbp DNA ladder, WT: wild-type, P: empty plasmid control, N: no-template negative control. The size of the target amplicon was 1.8 kbp. Plants lacking the *Flv1* amplicon (i.e., lanes 1, 3, 5, 9, 14) were used to produce azygous individuals.

Supplementary Figure 2 | A model describing the steps for producing double-homozygous plants harboring *Flv1/Flv3* to conduct drought experiments.

Supplementary Figure 3 | The appearance of typical barley plants heterologously expressing *Flv1/Flv3* genes at the seedling stage under ambient **(A)** and drought-stressed **(B)** conditions. Lines L1-L3 harbor both *Flv1* and *Flv3* genes. Images captured seven days after rewatering from a soil maintained at 10-12% FC for 5 days. Growth performance of WT, azygous and transgenic plants in ambient condition **(A)**. Seven days after re-watering, WT barley plants exposed to severe drought exhibited retarded growth and leaf wilting, while leaves of the three transgenic lines retained turgor (albeit turning slightly yellowish). Numerals on the left indicate height in cm.

Supplementary Figure 4 | Influence of heterologously expressing *Flv* genes on adenosine nucleotides in the flag leaves of barley plants grown either under ambient conditions or exposed to drought stress at the seedling stage **(A–C)** and the reproductive stage **(D–F)**. Adenine nucleotide levels were measured in the same samples used for carbohydrate determinations (**Figure 5**). **(A,D)** ATP, **(B,E)** ADP, **(C,F)** AMP. Lines L1-L3 harbor both *Flv1 and Flv3* genes. Data are shown as means ± SE (*n* = 5-6). **; *: means differed significantly ($P \leq 0.01$ or $P \leq 0.05$, respectively) from those of non-transgenic plants. FW, fresh weight.

Supplementary Figure 5 | Effect of heterologously expressing *Flv* genes on the energy status of flag leaves of barley plants grown either under ambient conditions or exposed to drought stress at the seedling stage **(A,B)** and the reproductive stage **(C,D)**. **(A,C)** ATP to ADP ratio, **(B,D)** energy charge. Lines L1-L3 co-express *Flv1 and Flv3* genes. Data are shown as means ± SE (*n* = 5-6). **; *: means differed significantly ($P \leq 0.01$ or $P \leq 0.05$, respectively) from the performance of non-transgenic plants.

Supplementary Table 1 | Sequence-specific forward (F) and reverse (R) primers, annealing temperature and extension time used for PCR and qRT-PCR analysis.

Supplementary Table 2 | Effect of heterologously expressing *Flv* genes on amino acid contents in flag leaves of barley plants grown either under ambient conditions or exposed to drought stress at the vegetative stage. Lines L1-L3 harbor both *Flv1* and *Flv3* genes. Data are shown in nmol g^{-1} FW and as means ± SE (*n* = 6-7 for WT and azygous and *n* = 8-14 for transgenic lines). Yellow and blue shading: means differed significantly ($P \leq 0.01$ and $P \leq 0.05$, respectively) from those of non-transgenic plants. FW, fresh weight.

Supplementary Table 3 | Effect of heterologously expressing *Flv* genes on amino acid contents in flag leaves of barley plants grown either under ambient conditions or exposed to drought stress at the reproductive stage. Lines L1-L3 harbor both *Flv1* and *Flv3* genes. Data are shown in nmol g^{-1} FW and as means ± SE (*n* = 6-7 for WT and azygous and n = 8-14 for transgenic lines). Yellow and blue shading: means differed significantly ($P \leq 0.01$ and $P \leq 0.05$, respectively) from those of non-transgenic plants. FW, fresh weight.

REFERENCES

Ahkami, A. H., Melzer, M., Ghaffari, M. R., Pollmann, S., Ghorbani Javid, M., Shahinnia, F., et al. (2013). Distribution of indole-3-acetic acid in Petunia hybrida shoot tip cuttings and relationship between auxin transport, carbohydrate metabolism and adventitious root formation. *Planta* 238, 499–517. doi: 10.1007/s00425-013-1907-z

Alegre, L. (2004). Review: Die and let live: leaf senescence contributes to plant survival under drought stress. *Funct. Plant Biol.* 31, 203–216. doi: 10.1071/fp03236

Allahverdiyeva, Y., Ermakova, M., Eisenhut, M., Zhang, P., Richaud, P., Hagemann, M., et al. (2011). Interplay between flavodiiron proteins and photorespiration in Synechocystis sp. PCC 6803. *J. Biol. Chem.* 286, 24007–24014. doi: 10.1074/jbc.M111.223289

Allahverdiyeva, Y., Isojärvi, J., Zhang, P., and Aro, E. M. (2015a). Cyanobacterial oxygenic photosynthesis is protected by flavodiiron proteins. *Life* 5, 716–743. doi: 10.3390/life5010716

Allahverdiyeva, Y., Mustila, H., Ermakova, M., Bersanini, L., Richaud, P., Ajlani, G., et al. (2013). Flavodiiron proteins Flv1 and Flv3 enable cyanobacterial growth and photosynthesis under fluctuating light. *Proc. Natl. Acad. Sci. U. S. A.* 110, 4111–4116. doi: 10.1073/pnas.1221194110

Allahverdiyeva, Y., Suorsa, M., Tikkanen, M., and Aro, E. M. (2015b). Photoprotection of photosystems in fluctuating light intensities. *J. Exp. Bot.* 66, 2427–2436. doi: 10.1093/jxb/eru463

Atkinson, D. E., and Walton, G. M. (1967). Adenosine triphosphate conservation in metabolic regulation. Rat liver citrate cleavage enzyme. *J. Biol. Chem.* 242, 3239–3241.

Brestic, M., Cornic, G., Fryer, M. J., and Baker, N. R. (1995). Does photorespiration protect the photosynthetic apparatus in French bean leaves from photoinhibition during drought stress? *Planta* 196, 450–457. doi: 10.1007/BF00203643

Couée, I., Sulmon, C., Gouesbet, G., and Amrani, A. E. I. (2006). Involvement of soluble sugars in reactive oxygen species balance and responses to oxidative stress in plants. *J. Expt. Bot.* 57, 449–459. doi: 10.1093/jxb/erj027

Counce, P. A., and Gravois, K. A. (2006). Sucrose synthase activity as a potential indicator of high rice grain yield. *Crop Sci.* 46, 1501–1507. doi: 10.2135/cropsci2005.0240

Cruz de Carvalho, M. H. (2008). Drought stress and reactive oxygen species: production, scavenging and signalling. *Plant Signal. Behav.* 3, 156–165. doi: 10.4161/psb.3.3.5536

Dang, K. V., Plet, J., Tolleter, D., Jokel, M., Cuiné, S., Carrier, P., et al. (2014). Combined increases in mitochondrial cooperation and oxygen photoreduction compensate for deficiency in cyclic electron flow in *Chlamydomonas reinhardtii*. *Plant Cell* 26, 3036–3035. doi: 10.1105/tpc.114.126375

Das, A., Rushton, P. J., and Rohila, J. S. (2017). Metabolomic profiling of soybeans (Glycine max L.) reveals the importance of sugar and nitrogen metabolism under drought and heat stress. *Plants* 6:21. doi: 10.3390/plants6020021

Ebrahim, F., Arzani, A., and Peng, J. (2020). Salinity tolerance of wild barley Hordeum vulgare ssp. *Spontaneum*. *Plant Breed.* 139, 304–316. doi: 10.1111/pbr.12770

Fàbregas, N., and Fernie, A. R. (2019). The metabolic response to drought. *J. Exp. Bot.* 70, 1077–1085. doi: 10.1093/jxb/ery437

Fàbregas, N., Lozano-Elena, F., and Blasco-Escámez, D. (2018). Overexpression of the vascular brassinosteroid receptor BRL3 confers drought resistance without penalizing plant growth. *Nat. Commun.* 9:4680. doi: 10.1038/s41467-018-06861-3

Farooq, M., Wahid, A., Kobayashi, N., Fujita, D., and Basra, S. (2009). Plant drought stress: effects, mechanisms and management. *Agron. Sust. Devel.* 29, 185–212. doi: 10.1051/agro:2008021

Gan, S. (2003). Mitotic and postmitotic senescence in plants. *Sci. Aging Knowl. Environ.* 24:RE7. doi: 10.1126/sageke.2003.38.re7

Gerotto, C., Alboresi, A., Meneghesso, A., Jokel, M., Suorsa, M., Aro, E. M., et al. (2016). Flavodiiron proteins act as safety valve for electrons in Physcomitrella patens. *Proc. Natl. Acad. Sci. U. S. A.* 113, 12322–12327. doi: 10.1073/pnas.1606685113

Gómez, R., Carrillo, N., Morelli, M. P., Tula, S., Shahinnia, F., Hajirezaei, M. R., et al. (2018). Faster photosynthetic induction in tobacco by expressing cyanobacterial flavodiiron proteins in chloroplasts. *Photosynth. Res.* 136, 129–138. doi: 10.1007/s11120-017-0449-9

Gómez, R., Vicino, P., Carrillo, N., and Lodeyro, A. F. (2019). Manipulation of oxidative stress responses as a strategy to generate stress–tolerant crops. From damage to signaling to tolerance. *Crit. Rev. Biotechnol.* 39, 693–708. doi: 10.1080/07388551.2019.1597829

Guo, R., Shi, L. X., Jiao, Y., Li, M. X., Zhong, X. L., Gu, F. X., et al. (2018). Metabolic responses to drought stress in the tissues of drought-tolerant and drought–sensitive wheat genotype seedlings. *AoB Plants* 10:ly016. doi: 10.1093/aobpla/ply016

Haink, G., and Deussen, A. (2003). Liquid chromatography method for the analysis of adenosine compounds. *J. Chromatogr.* 784, 189–193. doi: 10.1016/s1570-0232(02)00752-3

Haupt-Herting, S., and Fock, H. P. (2002). Oxygen exchange in relation to carbon assimilation in water-stressed leaves during photosynthesis. *Ann. Bot.* 89, 851–859. doi: 10.1093/aob/mcf023

Helman, Y., Tchernov, D., Reinhold, L., Shibata, M., Ogawa, T., Schwarz, R., et al. (2003). Genes encoding A-type flavoproteins are essential for photoreduction of O_2 in cyanobacteria. *Curr. Biol.* 13, 230–235. doi: 10.1016/S0960-9822(03)00046-0

Hildebrandt, T. M., Nunes Nesi, A., Araujo, W. L., and Braun, H. P. (2015). Amino acid catabolism in plants. *Mol. Plant.* 8, 1563–1579. doi: 10.1016/j.molp.2015.09.005

Hodaei, M., Rahimmalek, M., Arzani, A., and Talebi, M. (2018). The effect of water stress on phytochemical accumulation, bioactive compounds and expression of key genes involved in flavonoid biosynthesis in *Chrysanthemum morifolium* L. *Ind. Crops Prod.* 120, 295–304. doi: 10.1016/j.indcrop.2018.04.073

Kaur, G., and Asthir, B. (2015). Proline: a key player in plant abiotic stress tolerance. *Biol. Plant.* 59, 609–619. doi: 10.1007/s10535-015-0549-3

Kovalchuk, N., Jia, W., Eini, O., Morran, S., Pyvovarenko, T., Fletcher, S., et al. (2013). Optimization of TaDREB3 gene expression in transgenic barley using cold-inducible promoters. *Plant Biotechnol. J.* 11, 659–670. doi: 10.1111/pbi.12056

Lawlor, D. W. (1995). "Effects of water deficit on photosynthesis," in *Environment and Plant Metabolism: Flexibility and Acclimation*, ed. N. Smirnoff, (Oxford:BIOS Scientific Publishers Limited), 129–160.

Lawlor, D. W., and Tezara, W. (2009). Causes of decreased photosynthetic rate and metabolic capacity in water-deficient leaf cells: a critical evaluation of mechanisms and integration of processes. *Annals Bot.* 103, 561–579. doi: 10.1093/aob/mcn244

Li, Z., Hansen, J. L., Liu, Y., Zemetra, R. S., and Berger, P. H. (2004). Using real−time PCR to determine transgene copy number in wheat. *Plant Mol. Biol. Rep.* 22, 179–188. doi: 10.1007/BF02772725

Logemann, J., Schell, J., and Willmitzer, L. (1987). Improved method for the isolation of RNA from plant tissues. *Anal. Biochem.* 163, 16–20. doi: 10.1016/0003-2697(87)90086-8

Lonbani, M., and Arzani, A. (2011). Morpho-physiological traits associated with terminal droughtstress tolerance in triticale and wheat. *Agron. Res.* 9, 315–329.

Marchetti Cintia, F., Ugena, L., Humplík Jan, F., Polák, M., Ćavar Zeljković, S., Podlešáková, K., et al. (2019). A novel image-based screening method to study water-deficit response and recovery of barley populations using canopy dynamics phenotyping and simple metabolite profiling. *Front. Plant Sci.* 10:1252. doi: 10.3389/fpls.2019.01252

Marthe, C., Kumlehn, J., and Hensel, G. (2015). Barley (Hordeum vulgare L.) transformation using immature embryos. *Methods Mol. Biol.* 1223, 71–83. doi: 10.1007/978-1-4939-1695-5_6

Mayta, M. L., Lodeyro, A. F., Guiamet, J. J., Tognetti, V. B., Melzer, M., Hajirezaei, M. R., et al. (2018). Expression of a plastid-targeted flavodoxin decreases chloroplast reactive oxygen species accumulation and delays senescence in aging tobacco leaves. *Front. Plant Sci.* 9:1039. doi: 10.3389/fpls.2018.01039

Peltier, G., Tolleter, D., Billon, E., and Cournac, L. (2010). Auxiliary electron transport pathways in chloroplasts of microalgae. *Photosynth. Res.* 106, 19–31. doi: 10.1007/s11120-010-9575-3

Pires, M. V., Pereira Júnior, A. A., Medeiros, D. B., Daloso, D. M., Pham, P. A., and Barros, K. A. (2016). The influence of alternative pathways of respiration that utilize branched-chain amino acids following water shortage in *Arabidopsis*. *Plant Cell Environ.* 39, 1304–1319. doi: 10.1111/pce.12682

Price, A. H., Cairns, J. E., Horton, P., Jones, H. G., and Griffiths, H. (2002). Linking drought-resistance mechanisms to drought avoidance in upland rice using a QTL approach: progress and new opportunities to integrate stomatal and mesophyll responses. *J. Exp. Bot.* 53, 989–1004. doi: 10.1093/jexbot/53.371.989

Quick, W. P., Chaves, M. M., Wendler, R., David, M., Rodrigues, M. L., Passaharinho, J. A., et al. (1992). The effect of water stress on photosynthetic carbon metabolisms in four species grown under field conditions. *Plant Cell Environ.* 15, 25–35. doi: 10.1111/j.1365-3040.1992.tb01455.x

Rai, V. K., and Sharma, U. D. (1991). Amino acids can modulate ABA induced stomatal closure, stomatal resistance and K+ fluxes in Vicia faba leaves. *Beitr. Biol. Pflanz.* 66, 393–405. doi: 10.1016/S0015-3796(89)80057-5

Rutherford, A. W., Osyczka, A., and Rappaport, F. (2012). Back-reactions, short-circuits, leaks and other energy wasteful reactions in biological electron transfer: redox tuning to survive life in O_2. *FEBS Lett.* 586, 603–616. doi: 10.1016/j.febslet.2011.12.039

Saghai-Maroof, M. A., Soliman, K. M., Jorgensen, R. A., and Allard, R. W. (1984). Ribosomal DNA spacer-length polymorphisms in barley: Mendelian inheritance, chromosomal location and population dynamics. *Proc. Natl. Acad. Sci.* 81, 8014–8018. doi: 10.1073/pnas.81.24.8014

Saraiva, L. M., Vicente, J. B., and Teixeira, M. (2004). The role of the flavodiiron proteins in microbial nitric oxide detoxification. *Adv. Microb. Physiol.* 49, 77–129. doi: 10.1016/S0065-2911(04)49002-X

Schmittgen, T. D., and Livak, K. J. (2008). Analyzing real-time PCR data by the comparative C(T) method. *Nat. Protoc.* 3, 1101–1108. doi: 10.1038/nprot.2008.73

Sétif, P., Shimakawa, G., Krieger-Liszkay, A., and Miyake, C. (2020). Identification of the electron donor to flavodiiron proteins in *Synechocystis* sp. PCC6803 by *in vivo* spectroscopy. *Biochim. Biophys. Acta Bioenerg.* 1861:148256. doi: 10.1016/j.bbabio.2020.148256

Shahinnia, F., Tula, S., Hensel, G., Reiahisamani, N., Nasr, N., Kumlehn, J., et al. (2020). Integrating cyanobacterial flavodiiron proteins within the chloroplast photosynthetic electron transport chain maintains carbohydrate turnover and enhances drought stress tolerance in barley. *bioRxiv* doi: 10.1101/2020.09.29.318394

Sharkey, T. D., and Badger, M. R. (1982). Effects of water stress on photosynthetic electron transport, photophosphorylation and metabolite levels of Xanthium strumarium cells. *Planta* 156, 199–206. doi: 10.1007/BF00393725

Silaghi-Dumitrescu, R., Kurtz, D. M. Jr., Ljungdahl, L. G., and Lanzilotta, W. N. (2005). X-ray crystal structures of Moorella thermoacetica FprA. Novel diiron site structure and mechanistic insights into a scavenging nitric oxide reductase. *Biochemistry* 44, 6492–6501. doi: 10.1021/bi0473049

Singh, M., Kumar, J., Singh, S., Singh, V. P., and Prasad, S. M. (2015). Roles of osmoprotectants in improving salinity and drought tolerance in plants: a review. *Environ. Sci. Biotechnol.* 14, 407–426. doi: 10.1007/s11157-015-9372-8

Song, P., Cai, C. Q., Skokut, M., Kosegi, B., and Petolino, J. (2002). Quantitative real-time PCR as a screening tool for estimating transgene copy number in WHISKERSTM-derived transgenic maize. *Plant Cell Rep.* 20, 948–954. doi: 10.1007/s00299-001-0432-x

Sun, X., and Wen, T. (2011). Physiological roles of plastid terminal oxidase in plant stress responses. *J. Biosci.* 36, 951–956. doi: 10.1007/s12038-011-9161-7

Szabados, L., and Savouré, A. (2010). Proline: a multifunctional amino acid. *Trends Plant Sci.* 15, 89–97. doi: 10.1016/j.tplants.2009.11.009

Takagi, D., Takumi, S., Hashiguchi, M., Sejima, T., and Miyake, C. (2016). Superoxide and singlet oxygen produced within the thylakoid membranes both cause photosystem I photoinhibition. *Plant Physiol.* 171, 1626–1634. doi: 10.1104/pp.16.00246

Tezara, W., Mitchell, V. J., Driscoll, S. D., and Lawlor, D. W. (1999). Water stress inhibits plant photosynthesis by decreasing coupling factor and ATP. *Nature* 401, 914–917. doi: 10.1038/44842

Tognetti, V. B., Palatnik, J. F., Fillat, M. F., Melzer, M., Hajirezaei, M. R., Valle, E. M., et al. (2006). Functional replacement of ferredoxin by a cyanobacterial flavodoxin in tobacco confers broad-range stress tolerance. *Plant Cell* 18, 2035–2050. doi: 10.1105/tpc.106.042424

Tula, S., Shahinnia, F., Melzer, M., Rutten, T., Gómez, R., Lodeyro, A. F., et al. (2020). Providing an additional electron sink by the introduction of cyanobacterial flavodiirons enhances growth of *A. thaliana* under various light intensities. *Front. Plant Sci.* 11, 1–12. doi: 10.3389/fpls.2020.00902

Wada, S., Yamamoto, H., Suzuki, Y., Yamori, W., Shikanai, T., and Makino, A. (2018). Flavodiiron protein substitutes for cyclic electron flow without competing CO2 assimilation in rice. *Plant Physiol.* 176, 1509–1518. doi: 10.1104/pp.17.01335

Wang, X., Cai, J., Jiang, D., Liu, F., Dai, T., and Cao, W. (2011). Pre-anthesis high-temperature acclimation alleviates damage to the flag leaf caused by post-anthesis heat stress in wheat. *J. Plant Physiol.* 168, 585–593. doi: 10.1016/j.jplph.2010.09.016

Wasserfallen, A., Ragettli, S., Jouanneau, Y., and Leisinger, T. (1998). A family of flavoproteins in the domains Archaea and Bacteria. *Eur. J. Biochem.* 254, 325–332. doi: 10.1046/j.1432-1327.1998.2540325.x

Yamamoto, H., Takahashi, S., Badger, M. R., and Shikanai, T. (2016). Artificial remodelling of alternative electron flow by flavodiiron proteins in Arabidopsis. *Nat. Plants* 2:16012. doi: 10.1038/nplants.2016.12

Zadoks, J. C., Chang, T. T., and Konzak, C. F. (1974). A decimal code for the growth stages of cereals. *Weed Res.* 14, 415–421. doi: 10.1111/j.1365-3180.1974.tb01084.x

Zhang, P., Allahverdiyeva, Y., Eisenhut, M., and Aro, E. M. (2009). Flavodiiron proteins in oxygenic photosynthetic organisms: photoprotection of photosystem II by Flv2 and Flv4 in Synechocystis sp. PCC 6803. *PLoS One* 4:e5331. doi: 10.1371/journal.pone.0005331

Zurbriggen, M. D., Carrillo, N., Tognetti, V. B., Melzer, M., Peisker, M., Hause, B., et al. (2009). Chloroplast-generated reactive oxygen species play a major role in localized cell death during the non-host interaction between tobacco and Xanthomonas campestris pv. vesicatoria. *Plant J.* 60, 962–973. doi: 10.1111/j.1365-313X.2009.04010.x

Conflict of Interest: The authors declare that the research was conducted in the absence of any commercial or financial relationships that could be construed as a potential conflict of interest.

frontiers in Plant Science

ORIGINAL RESEARCH
published: 05 February 2021
doi: 10.3389/fpls.2021.624365

A Multi-OMICs Approach Sheds Light on the Higher Yield Phenotype and Enhanced Abiotic Stress Tolerance in Tobacco Lines Expressing the Carrot *lycopene β-cyclase1* Gene

Juan C. Moreno[1,2], Silvia Martinez-Jaime[1], Monika Kosmacz[1,2], Ewelina M. Sokolowska[1], Philipp Schulz[1], Axel Fischer[1], Urszula Luzarowska[1], Michel Havaux[3] and Aleksandra Skirycz[1,4]**

[1] Max Planck Institut für Molekulare Pflanzenphysiologie, Potsdam, Germany, [2] Biological and Environmental Science and Engineering Division, Center for Desert Agriculture, King Abdullah University of Science and Technology, Thuwal, Saudi Arabia, [3] Aix-Marseille Univ., CEA, CNRS UMR7265, BIAM, CEA/Cadarache, Saint-Paul-lez-Durance, France, [4] Boyce Thompson Institute, Cornell University, Ithaca, NY, United States

Recently, we published a set of tobacco lines expressing the *Daucus carota* (carrot) *DcLCYB1* gene with accelerated development, increased carotenoid content, photosynthetic efficiency, and yield. Because of this development, *DcLCYB1* expression might be of general interest in crop species as a strategy to accelerate development and increase biomass production under field conditions. However, to follow this path, a better understanding of the molecular basis of this phenotype is essential. Here, we combine OMICs (RNAseq, proteomics, and metabolomics) approaches to advance our understanding of the broader effect of *LCYB* expression on the tobacco transcriptome and metabolism. Upon *DcLCYB1* expression, the tobacco transcriptome (∼2,000 genes), proteome (∼700 proteins), and metabolome (26 metabolites) showed a high number of changes in the genes involved in metabolic processes related to cell wall, lipids, glycolysis, and secondary metabolism. Gene and protein networks revealed clusters of interacting genes and proteins mainly involved in ribosome and RNA metabolism and translation. In addition, abiotic stress-related genes and proteins were mainly upregulated in the transgenic lines. This was well in line with an enhanced stress (high light, salt, and H_2O_2) tolerance response in all the transgenic lines compared with the wild type. Altogether, our results show an extended and coordinated response beyond the chloroplast (nucleus and cytosol) at the transcriptome, proteome, and metabolome levels, supporting enhanced plant growth under normal and stress conditions. This final evidence completes the set of benefits conferred by the expression of the *DcLCYB1* gene, making it a very promising bioengineering tool to generate super crops.

Keywords: β-carotene, carotenoids, abiotic stress, lycopene β-cyclase, omics, ROS, *Nicotiana tabacum* cv Xanthi, transcription factors

OPEN ACCESS

Edited by:
Patricia León, National Autonomous University of Mexico, Mexico

Reviewed by:
Diego H. Sanchez, CONICET Instituto de Investigaciones Fisiológicas y Ecologicas Vinculadas a la Agricultura (IFEVA), Argentina
Maria Jesus Rodrigo, Institute of Agrochemistry and Food Technology (IATA), Spain

****Correspondence:***
Juan C. Moreno
juancamilo.morenobeltran@KAUST.edu.sa
Aleksandra Skirycz
skirycz@mpimp-golm.mpg.de

Specialty section:
This article was submitted to Plant Biotechnology, a section of the journal Frontiers in Plant Science

Received: *31 October 2020*
Accepted: *18 January 2021*
Published: *05 February 2021*

Citation:
Moreno JC, Martinez-Jaime S, Kosmacz M, Sokolowska EM, Schulz P, Fischer A, Luzarowska U, Havaux M and Skirycz A (2021) A Multi-OMICs Approach Sheds Light on the Higher Yield Phenotype and Enhanced Abiotic Stress Tolerance in Tobacco Lines Expressing the Carrot lycopene β-cyclase1 Gene. Front. Plant Sci. 12:624365. doi: 10.3389/fpls.2021.624365

INTRODUCTION

Carotenoids are C40 isoprenoid compounds synthesized in the plastids of photosynthetic and some nonphotosynthetic organisms (e.g., plants, algae, fungi, and bacteria) (Ruiz-Sola and Rodriguez-Concepcion, 2012). Carotenoid biosynthesis pathway is well-known and has been characterized in many plant species (Fraser et al., 1994; Moise et al., 2014; Nisar et al., 2015). Carotenoid synthesis is of great importance for plant physiology because of its important functions in photosynthesis and photoprotection (Niyogi et al., 1997; Holt et al., 2005), pollination (Bartley and Scolnik, 1995), scavenging of reactive oxygen species (ROS), and indirectly in hormone biosynthesis (serving as the precursors of abscisic acid/ABA and strigolactones/SLs) (Schwartz et al., 1997; Alder et al., 2012). In mammals, carotenoids (especially β-carotene) serve as a dietary precursor of vitamin A, which is required for the maintenance of normal vision, healthy immunity, and cell growth (Olson, 1996). In addition, carotenoids (e.g., β-carotene) have been shown to have antioxidant-promoting activities in humans (Fraser and Bramley, 2004; Rao and Rao, 2007). These properties make β-carotene a very valuable molecule for plant functioning, but also for improving food quality content in crops. Because of this, genetic engineering approaches have been used to increase the β-carotene content in several plant models by expressing the lycopene β-cyclase (*LCYB*) gene, which encodes for the enzyme (LCYB) involved in its production. For instance, (over)expression of the *LCYB* gene in Arabidopsis, tomato, and sweet potato leads to increased tolerance to abiotic stresses, such as salt and drought (D'Ambrosio et al., 2004; Chen et al., 2011; Kang et al., 2018). Moreover, increases in β-carotene, violaxanthin, zeaxanthin, and lutein have been reported to increase plant tolerance to high light, UV irradiation, and salt through scavenging ROS (Davison et al., 2002; Gotz et al., 2002; Han et al., 2008; Shi et al., 2015; Kang et al., 2018). Interestingly, in tobacco, carrot, and sweet potato *LCYB*-expressing lines, a carotenoid increase was accompanied by an induction in carotenoid genes such as phytoene synthase (*PSY*), phytoene desaturase (*PDS*), ζ-carotene desaturase (*ZDS*), zeaxanthin epoxidase (*ZEP*), violaxanthin de-epoxidase (*VDE*), and neoxanthin synthase (*NXS*) (Moreno et al., 2013; Shi et al., 2015; Kang et al., 2018); thus, this suggests the possibility that an additional signal coordinates the expression of carotenoid genes. Previous studies have shown that the coordinated expression of carotenogenic genes tightly regulates carotenoid metabolism (Liu et al., 2015; Yuan et al., 2015). However, knowledge of the transcriptional regulatory mechanisms controlling the expression of these genes is limited. Several studies have shown numerous transcription factors influencing carotenoid accumulation in plants. For instance, the MADS-box genes *AGAMOUS-like 1* and *FRUITFULL* regulate carotenoid accumulation during tomato fruit ripening (Vrebalov et al., 2009). Moreover, tomato ripening inhibitor (RIN) regulates carotenoid accumulation via binding to the promoter region of the *PSY* gene (Martel et al., 2011). Other transcription factors belonging to the AP2/ERF (Welsch et al., 2007; Chung et al., 2010; Lee et al., 2012), NAC (Ma et al., 2014; Zhu et al., 2014a,b), and MYB subgroups (Sagawa et al., 2016; Zhu et al., 2017) modulate fruit ripening and carotenoid accumulation in several plant models. Intriguingly, the WD40 and bZIP TF families have been reported to be involved in the control of multiple biological processes, including plant growth and development, fruit ripening, and stress responses (Smith et al., 1999; Jain and Pandey, 2018). Furthermore, a kiwi R2R3 MYB (*AdMYB7*) that binds to and activates the expression of *LCYB* (and chlorophyll biosynthetic genes) is responsible for chlorophyll and carotenoid accumulation in kiwi (Ampomah-Dwamena et al., 2019).

Recently, the expression of the *LCYB* gene from carrots (*DcLCYB1*) in tobacco resulted in an increase in pigment content (β-carotene and chlorophylls), gibberellin (GA_4), and plant biomass in T1 tobacco lines grown under controlled conditions (Moreno et al., 2016). This positive effect was confirmed to be stable through generations (T4–T5) and in plants grown under fully controlled (constant and fluctuating light regimes) and noncontrolled climate conditions. Moreover, an increased gibberellin (GA)/ABA ratio (along with increased carotenogenic gene expression and pigment accumulation) was associated with higher fitness, yield, and photosynthetic efficiency in these transgenic tobacco lines (Moreno et al., 2020). Intriguingly, we did not observe any trade-off or detrimental effect upon the *DcLCYB1* expression in our tobacco plants. However, we observed a general induction in the expression of key genes from several plastid pathways, such as GAs, chlorophyll, and carotenoids.

Over the past two decades, with the sequencing of entire genomes and the establishment of high-throughput methodologies for gene expression analysis, plant research has entered the genomic era (Leister, 2003). In recent years, with the peak of functional genomics (analysis of transcriptome, proteome, and metabolome), plant research has started to explore new gene, protein, and metabolite functions by the characterization of new pathways and new components of previously known pathways (Moreno, 2019). Here, we apply a multi-OMICs (RNAseq, proteomics, and metabolomics) approach and stress treatments to fully characterize the general plant response (beyond carotenogenesis and isoprenoid pathways) at molecular and physiological level in the tobacco *DcLCYB1* lines.

MATERIALS AND METHODS

Plant Material and Growth Conditions

Tobacco transgenic lines corresponding to the T4 generation of our previously published *DcLCYB1*-expressing lines were used in the current work (Moreno et al., 2016). Tobacco (*Nicotiana tabacum* cultivar Xanthi NN) wild type and transgenic lines were raised from seeds germinated in Petri dishes containing an MS medium supplemented with 30 g/L sucrose (Murashige and Skoog, 1962) and kanamycin (100 mg/mL). Radicle emergence and germination experiments were performed in Petri dishes supplemented with 3% sucrose ($n = 20$, experiment was repeated three times in three different Petri dishes). Leaf generations and internode length of 40-day-old tobacco wild type and transgenic

lines were measured. ImageJ software was used to quantify the leaf area ($n = 3$).

RNA Isolation

Total RNA was extracted from the frozen powder of tobacco leaves of 5-week-old T_3 plants (three biological replicates per lines, $n = 3$) using the Nucleo Spin RNA extraction kit (Macherey-Nagel, Germany). Genomic DNA traces were eliminated by a 15 min DNase I treatment.

RNA Sequencing (RNAseq) and Data Analysis

QuantSeq 3' mRNA-Seq services were performed for the wild type and transgenic *DcLCYB1* lines L14, L15, and L16 ($n = 3$ biological replicates per genotype) at Lexogen GmbH (Vienna, Austria). Here, 500 ng total RNA were used as input for generating sequencing-ready libraries using the QuantSeq FWD 3' mRNA-Seq library preparation kit (Lexogen, Vienna, Austria; SKU 015). The libraries were characterized by microcapillary electrophoresis and fluorometry prior to pooling and sequencing using the same methods on an Illumina NextSeq500. A sequencing yield of 572.9 M demultiplexed reads was obtained from a single run in SR75 HO mode. An integrated data analysis was performed by Lexogen (STAR aligner), where the reads were mapped against the NiTAB 4.5 reference genome, read-counts were determined, and differential expression was computed using DESeq2 in R (Love et al., 2014). In addition, NiTAB 4.5 identifiers were mapped in house (Max Planck Institute of Molecular Plant Physiology) to *Arabidopsis* genome, obtaining ∼25,000 mapped genes (out of 36951 NiTAB 4.5 identifiers). Lexogen GmbH (Vienna, Austria) provided the principal component analysis (PCA) analysis of the data and statistical tests. Localization analyses were performed using the SUBA3 database (Tanz et al., 2013). Venn diagrams were designed, including for all the genes that changed significantly (padjust < 0.05) in the transgenic lines. The N.A. values were removed from the data set, and only NiTABs properly mapped to AGIs were used. Because of the tetraploid origin of tobacco, several NiTABs could be mapped to the same AGI; therefore, for the Venn diagrams, those NiTABs were treated as one [e.g., L14 has only 2,138 unique AGIs (out of 2,624), L15 (2,428 out of 2,998), and L16 (3,792 out of 4,958)]. A fold enrichment analysis (Fisher's exact test with FDR correction $p < 0.05$) was performed using the PANTHER overrepresentation test (PANTHER13.1) with the GO ontology database released on 2018.02.02, here with the annotation data set GO biological process complete (Mi et al., 2017). The reference list corresponds to all annotated *Arabidopsis* genes, and our data set corresponds to the up- or downregulated genes in our analysis. A Fisher's exact test with FDR multiple test correction ($p < 0.05$) was used to select the up- and downregulated genes. Raw sequencing data were deposited at gene expression omnibus (GEO) from NCBI under project accession number GSE157541.

MapMan Analysis of the RNAseq Data

As input data for MapMan (Thimm et al., 2004), we selected genes changing significantly in at least two of the three transgenic lines (all overlaps between L14 and at least other transgenic line), and we chose the L14 (1,920 genes) expression data to visualize in the software. In this way, the majority of affected processes (comprising 1,542 genes) in all three lines are shown in the figure plus additional processes (comprising 382 genes) affected in at least 2 transgenic lines. We have selected line L14 because of its higher plant height (**Figure 1**) and biomass production (Moreno et al., 2020) but also to simplify the visualization of the data.

Protein Extraction, Trypsin Digestion, and Mass Spectrometric Analyses

Protein extraction (whole-leaf proteome) and further protein digestion were performed as described in Moreno et al. (2018) but only using 50 μg of the total protein for digestion. In brief, after total protein extraction, each sample ($n = 3$ biological replicates) was subjected to the filter-aid sample preparation (FASP) procedure (Wisniewski et al., 2009). Peptide purification was performed using SepPack columns (SPEC18 100 mg mL21; Teknokroma), and samples were dried in a SpeedVac for 5 h and kept frozen until use for mass spectrometry.

Liquid Chromatography-Mass Spectrometry

Prior to analysis peptides were resuspended in 50 μl of resuspension buffer [3% (v/v) acetonitrile, 2% (v/v) TFA]. Peptides were measured by the Q-Exactive HF (Thermo Scientific) high-resolution mass spectrometer coupled to ACQUITY UPLC M-Class system (Waters). Samples were separated by reverse-phase nano liquid chromatography in 120 min, gradient ramped from 3.2% ACN to 7.2% ACN over first 20 min then gradient increase to 24.8% ACN over next 70 min and to 35.2% ACN over 30 min, followed by a 5 min washout with 76% ACN. The MS was run using a data dependent top-N method that fragmented the top 15 most intense ions per full scan. Full scans were acquired at a resolution of 120,000 with an AGC target 3e6, maximum injection time 50 ms, scan range 300–1,600 m/z. Each dd-MS2 scan was recorded in profile mode at a resolution of 30,000 with an AGC target of 1e5, maximum injection time 100 ms, isolation window 1.2 m/z, normalized collision energy 27 and the dynamic exclusion set for 30 s.

Protein Identification and Label Free Quantitation

DDA raw MS/MS spectra was processed with MaxQuant (version 1.6) for protein identification and quantitation (Cox and Mann, 2008). Peptide identification by the Andromeda search engine was based on the in-house POTbaseMS database (Moreno et al., 2018). The following parameters were applied to the analysis: 10 ppm peptide mass tolerance; 0.8 Da MS/MS tolerance; Trypsin was specified as enzyme and a maximum of two missed cleavages were allowed; a decoy database search with a 1% FDR cutoff on the peptide and protein level; carbamidomethylation of cysteine was set as a fixed modification, while the oxidation of methionine was set as variable modification. The "label-free quantification" and "match between runs" settings were also highlighted in the software. Valid peptides were expected to have a minimum length of six amino acids. Peptide quantitation was performed for

FIGURE 1 | Plant phenotype of transgenic *DcLCYB1*-expressing lines. **(A,B)** Six- (left panel) and 16-week-old (right panel) wild type and transgenic *DcLCYB1* plants (L14, L15, and L16) grown under semicontrolled conditions in the greenhouse (light intensity: 144–1,000 μE m^{-2} s^{-1}; temperature: 20–28°C; R.H. 64%). Asterisks show the fourth leaf selected for each plant for further OMICs experiments. Scale bars: 10 cm. wt: wild type.

proteins identified with at least two peptides (a minimum of one unique and one razor) unmodified peptide. Peptides intensity was taken and further normalized by LFQ algorithm. Known contaminants and reversed hits were removed from the analysis.

Statistical Analysis and Data Processing of the Proteomics Data

Protein intensity was log2 transformed and the linear model for microarray analysis (limma) R package (Ritchie et al., 2015) was used for comparative analysis ($p \leq 0.05$). Limma offers robust differential analysis of data with missing values, common in DDA methods of label-free MS experiments (Lazar et al., 2016). PCA was implemented by using prcomp function and was visualized using ggbiplot R package. Arabidopsis ATG codes were mapped to the identified POTs, where each POT can comprise one or more Arabidopsis ATGs. A fold enrichment analysis (Fisher's exact test with FDR correction $p < 0.05$) was performed using PANTHER, as explained above. Arabidopsis ATG codes mapped to each POT were used for this analysis. The mass spectrometry proteomics data have been deposited to the ProteomeXchange Consortium via the PRIDE (Perez-Riverol et al., 2019) partner repository with the dataset identifier PXD023595.

Gene and Protein Network Analysis

Gene and protein network analyses were performed using the String database (Szklarczyk et al., 2017), and Cytoscape was used for a network visualization (Shannon et al., 2003). For gene networks, we selected the genes changing significantly in at least two of the three transgenic lines and used the String database for the gene–gene interaction analysis. The network edges represent the confidence of the data extracted from published experiments and databases. The highest interaction score was set at 0.900, which is the highest confidence parameter for the analysis. Disconnected nodes in the network were omitted. The interaction values were extracted and exported as an Excel table and then used as an input table for network visualization in Cytoscape. The obtained Cytoscape network was divided into clusters by using the ClusterOne app (set up with the standard parameters) in Cytoscape (51 clusters comprising 419 interacting genes). The same pipeline and parameters were used to build the protein–protein interaction network (410 proteins changing significantly in at least two lines) and to perform the cluster analysis (19 clusters). The cluster names were assigned by using the enrichment analysis provided by the String software (e.g., GO function, GO biological process, KEGG pathway).

Extraction and Phase Separation for LC-MS Analyses

A methyl *tert*-butyl ether (MTBE) extraction buffer was prepared, and the samples ($n = 6$ biological replicates) were subjected to the extraction method described in Salem et al. (2016).

Secondary Metabolite Measurements

The dried aqueous phase (300 μL), which contained the secondary metabolites, was measured using ultra-performance liquid chromatography coupled to an Exactive mass spectrometer (Thermo-Fisher Scientific) in positive and negative ionization modes, as described in Giavalisco et al. (2011). The LC-MS data were processed using Expressionist Refiner MS 11.0 (Genedata AG, Basel, Switzerland). The settings were as follows: chromatogram alignment (RT search interval 0.5 min), peak detection (summation window 0.09 min, minimum peak size 0.03 min, gap/peak ratio 50%, smoothing window five points, center computation by intensity-weighted method with threshold at 70%, boundary determination using inflection points), isotope clustering (RT tolerance at 0.015 min, m/z tolerance 5 ppm, allowed charges 1–5), filtering for a single peak not assigned to an isotope cluster, adduct detection, and clusters grouping (RT tolerance 0.05 min, m/z tolerance 5 ppm, maximum intensity of side adduct 100,000%). All metabolite clusters were matched to the in-house libraries of authentic reference compounds, allowing a 10 ppm mass and dynamic retention time deviation (maximum 0.2 min).

Targeted Lipid Profiling by LC-MS and Data Analysis

The measurement of the lipids from *N. tabacum* leaves was performed as described by Hummel et al. (2011). In brief, the dried organic phase was measured using a Waters Acquity ultra-performance liquid chromatography system (Waters, http://www.waters.com) coupled with Fourier transform mass spectrometry (UPLC-FT-MS) in positive and negative ionization

modes. The analysis and processing of the mass spectrometry data was performed with REFINER MS® 10.0 (Gene Data, http://www.genedata.com) and comprised peak detection, RT alignment, and chemical noise removal. The derived mass features, characterized by specific peak ID, m/z values, retention time, and intensity, were further processed using custom R scripts. Prior to annotation of the metabolic features using the in-house lipid database, isotopic peaks were removed from the MS data. Annotated lipids were confirmed by manual investigation of the chromatograms using Xcalibur (Version 3.0, Thermo-Fisher, Bremen, Germany). The database used in this project includes 279 lipid species. The peak intensities were day-normalized, sample median-normalized, and, subsequently, log-2 transformed. The resulting data matrices were used for further peak filtering and analysis in Excel (Microsoft, http://www.microsoft.com). Significant differences were determined using a nonpaired two-tailed student *t*-test ($p < 0.05$).

Photooxidative Stress

Leaf discz of a 1.2 cm diameter floating on water at 10°C were exposed for 18 h to a strong white light (PFD, 1,200 mmol photons m^{-2} s^{-1}) that was produced by an array of light-emitting diodes. Autoluminescence emission from the stressed leaf discz placed on wet filter paper was measured after 2 h of dark adaptation, as previously described (Birtic et al., 2011). The signal was imaged with a liquid nitrogen–cooled CCD camera (VersArray 1300B, Roper Scientific), with the sensor operating at a temperature of −110°C. The acquisition time was 20 min, and on-CCD binning of 2 × 2 was used, leading to a resolution of 650 × 670 pixels. As previously shown, the imaged signal principally emanates from the slow decomposition of lipid peroxides, which accumulated in the samples during the oxidative stress treatment (Birtic et al., 2011).

Oxidative and Salt Stress Experiments

Transgenic and wild type tobacco seeds (T4 generation) were sterilized and germinated on solid MS medium supplemented with 3% sucrose. After 12 days, seedlings were transferred to a 24-well plate, including six biological replicates of each genotype ($n = 6$). Seedlings were grown for seven days in liquid MS medium containing either mock (H_2O), H_2O_2 (50 mM) or catechin (0.175 mM), and kept on a horizontal orbital shaker (120 rpm), under constant light (80 μE m^{-2} s^{-1}, 22°C). Fresh weight was recorded after 7 days for each plant. For salt stress experiments tobacco seeds (T4 generation) were germinated on solid MS media (3% sucrose) supplemented with 0, 100, and 150 mM of NaCl. Fresh weight was recorded after 3 weeks ($n =$ 8–9; experiment was repeated twice).

RESULTS

RNAseq Revealed the Broader Impact of *DcLCYB1* Expression on the Transcriptome of Tobacco Plants With Increased Plant Yield

Our tobacco *DcLCYB1*-expressing lines showed a growth phenotype characterized by bigger leaves, long internode spaces, and early development (Moreno et al., 2020) (**Figure 1A**). Even at later stages of the tobacco life cycle (16-week-old plants), the transgenic lines L14, L15, and L16 showed higher plant height than the wild type (**Figure 1B**). Moreover, among the transgenic lines, L14 was the one that showed the best performance (**Figure 1B**). In our previous transcript analysis (qRT-PCR), most of the analyzed genes (e.g., carotenoid or carotenoid-related pathways and photosynthesis-related genes) were upregulated (Moreno et al., 2020). These genes were selected based on previous evidence of their carotenoid and/or carotenoid-related function (Moreno et al., 2020). However, we believe there has to be a reshaping and a "trade-off" of gene expression in the tobacco genome that supports a greater plant yield.

To obtain further insights into the additional genes or pathways that support growth in these tobacco lines, we performed RNAseq analysis and compared the transcriptome of the transgenic lines with the wild type (**Figure 2**). In our RNAseq experiment, the PCA showed how similar the replicates are between genotypes and also showed the differences between the wild type and the transgenic lines (**Figure 2A**). In addition, L14 and L15 were more similar than line L16. To better analyze and visualize our RNAseq results, the NiTAB identifiers (∼37,000) were annotated into *Arabidopsis* identifiers (e.g., At2g30390; see the Material and Methods section). Most of the proteins encoded by all the identified genes (∼25,000) that we could reliably annotate in *Arabidopsis* were localized across all cell compartments (SUBA3 database; **Supplementary Figure 1**; **Supplementary Table 1**). From those compartments, the nucleus, cytosol, and mitochondria showed the highest location frequency of genes in our data [excluding the not annotated (N.A.) group]. Interestingly, the highest localization frequency of differentially expressed genes (DEGs; upon *DcLCYB1* expression) was observed in the nucleus, cytosol, and chloroplast (**Supplementary Figure 1**) for lines L14 (2,624 genes), L15 (2,998 genes), and L16 (4,958 genes). Upregulated genes for lines L14 (1,278), L15 (1,557), and L16 (2,609) showed similar location frequency (in percentage) across the 11 cell compartments (**Supplementary Figure 1**). The same pattern was observed for downregulated genes in lines L14 (1,346), L15 (1,441), and L16 (2,349) across the same compartments (**Supplementary Figure 1**).

To narrow down our analysis, we built Venn diagrams with the DEGs in the transgenic lines (**Figures 2B,C**). In this case, we used only NiTAB identifiers with their mapped AGI code; the N.A. values were removed from our data set. In addition, because of the tetraploid origin of tobacco, several NiTAB identifiers could have been mapped to the same AGI code in Arabidopsis; therefore, those were treated as one for the Venn diagram analysis. Thus, the number of DEGs was reduced for L14 (2,138), L15 (2,428), and L16 (3,792). The Venn diagrams show an overlap of 793 and 749 upregulated and downregulated genes, respectively, for the three transgenic lines (**Figures 2B,C**). An enrichment analysis of processes (Fisher's exact test with FDR correction $p < 0.05$) were performed using the PANTHER overrepresentation test (PANTHER13.1) with the GO ontology database (Mi et al., 2017). The upregulated genes classified in processes such as glycogen metabolic process, positive regulation of defense responses to bacterium, and wax

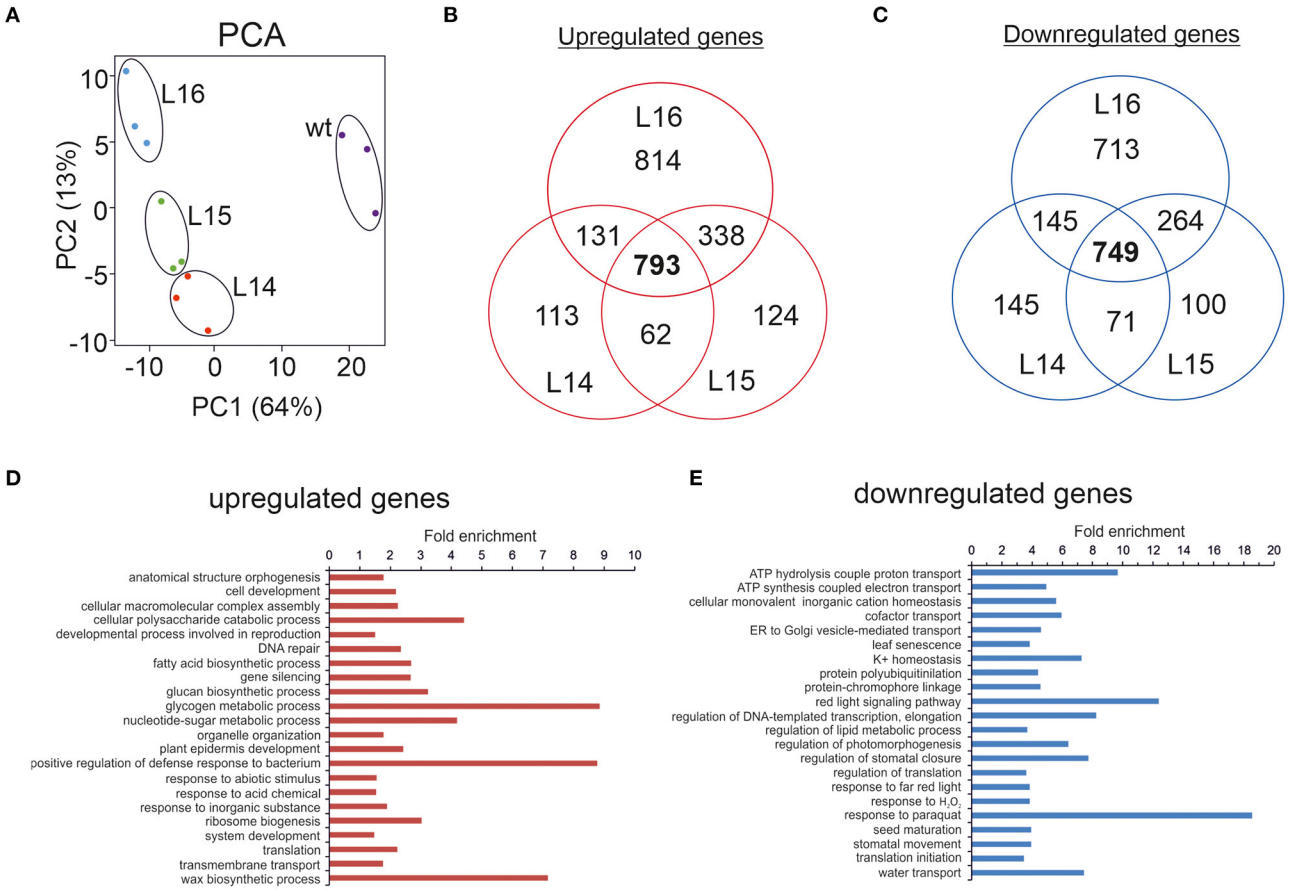

FIGURE 2 | RNA sequencing of transgenic *DcLCYB1* lines. **(A)** Principal component analysis (PCA). **(B,C)** Venn diagram of up- and downregulated genes in the L14, L15, and L16 transgenic lines. **(D,E)** Fold enrichment analysis of processes (GO terms) containing the up- and downregulated genes present in the *DcLCYB1* line L14. Three biological replicates for each genotype (wt, L14, L15, and L16) were used for RNAseq ($n = 3$).

biosynthetic process showed 7–9-fold enrichment, while the downregulated genes belonging to processes such as response to paraquat, red light signaling pathway, and ATP hydrolysis coupled to proton transport showed 9–18-fold enrichment (**Figures 2D,E**). Other processes with at least 2-fold enrichment are also shown (**Figures 2D,E**).

MapMan and Gene Network Analysis Reveal Enhanced Stress Response and Processes Related to Translation, Ribosome, and RNA Metabolism

To gain further insights into the pathways that might be affected by *DcLCYB1* expression in the transgenic lines, we used MapMan software for better visualization of our data set (see the Material and Methods section). To simplify the analysis, we decided to use the significant changes occurring in line L14 because of its higher fitness (**Figure 1**) and biomass production (Moreno et al., 2020). Because of the high number of DEGs analyzed in Thimm et al. (2004), they were classified across 34 out of 36 MapMan Bins (**Supplementary Table 2**). The top five bins are number 29 (Protein metabolism) with 314 genes, 27 (RNA metabolism) with 204 genes, 34 (transport) with 111 genes, 26 (miscellaneous) with 106 genes, and 30 (signaling) with 96 genes (**Supplementary Table 2**). In addition, there were about 12 bins with at least 20 or more significant genes. To perform a close up of our data and gain valuable information about the pathways and processes positively/negatively affected in our lines, we selected the metabolism overview option in MapMan to visualize metabolic perturbations (**Figure 3A**; **Supplementary Table 3**). On the one hand, the analysis revealed a general upregulation of genes involved in the processes related to secondary metabolism (e.g., waxes, terpenes, flavonoids, phenylpropanoids, and phenolics), cell wall, lipids, nucleotides, tetrapyrroles, and amino acids. On the other hand, downregulation was observed in processes such as electron transport in the mitochondria, light reactions of photosynthesis, ascorbate, and glutathione metabolism (**Figure 3A**). Moreover, the MapMan analysis identified 469 genes involved in biotic and abiotic stress responses (**Figure 3B**; **Supplementary Table 4**). Genes belonging to processes such as proteolysis, cell wall, abiotic stress, chaperones (HSP), secondary metabolites, heat shock proteins,

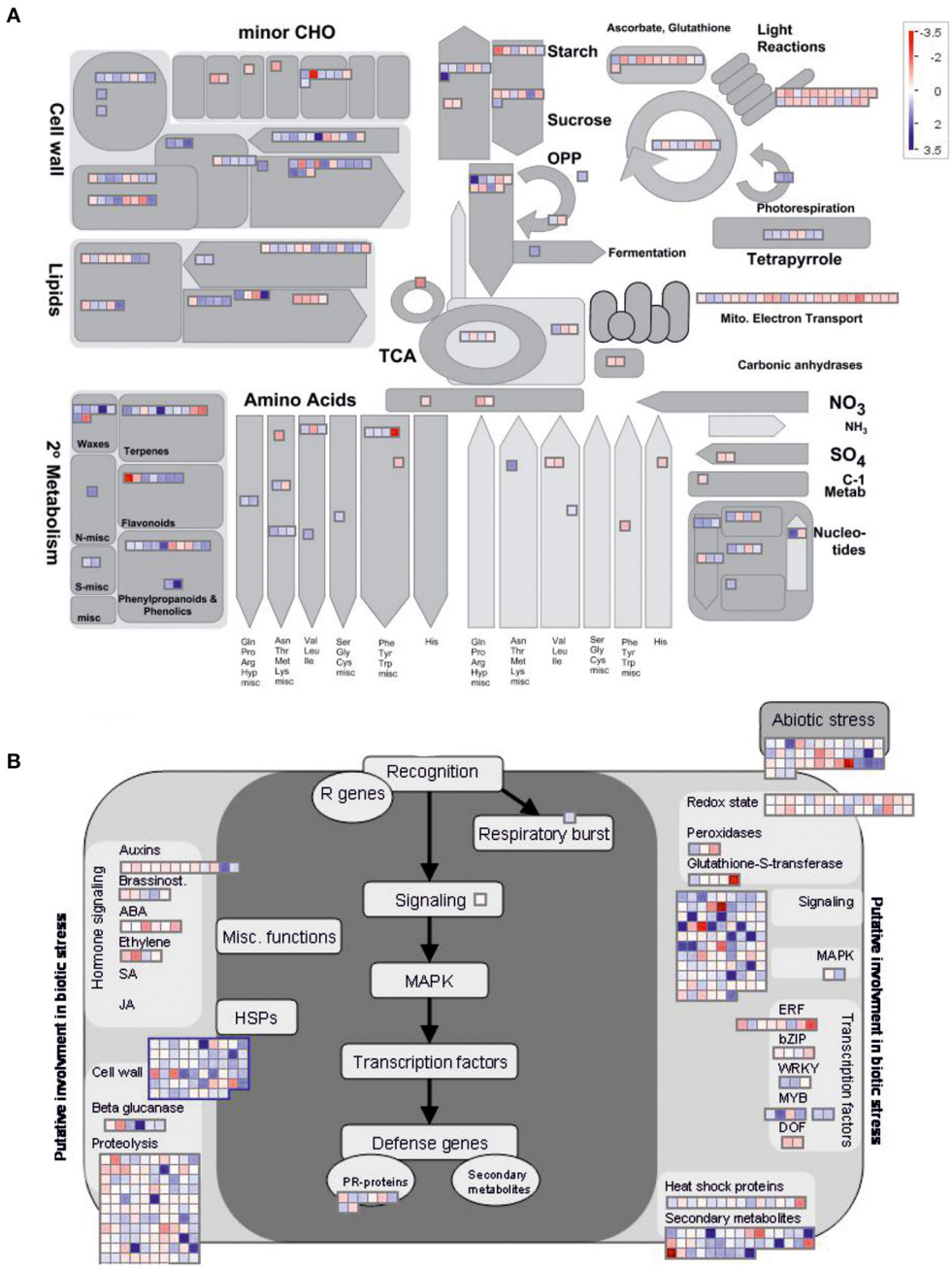

FIGURE 3 | MapMan representation of transcriptional perturbations in *DcLCYB1*-expressing plants. **(A)** Metabolism overview of the schematic representation generated in MapMan depicting metabolic perturbations. More than 300 genes (317) involved in different metabolic processes were significantly changed in the analysis. **(B)** Biotic stress schematic representation generated in MapMan depicting the changes in the genes involved in biotic and abiotic stress. More than 450 genes (469) involved in different metabolic processes were significantly changed in the analysis. Log2 fold change expression data were used.

and transcription factors were mainly upregulated, while genes belonging to processes such as hormone signaling and the redox state were mainly downregulated (**Figure 3B**). In addition, genes with regulatory functions were identified in processes such as transcription, protein modification and degradation, hormone network (IAA, ABA, BA, ethylene, cytokinin, and GA), and redox (**Supplementary Figure 2A**; **Supplementary Table 5**). Interestingly, most of the genes involved in biotic and abiotic stress (e.g., heat, cold, and drought/salt) responses were upregulated (**Supplementary Figure 2B**; **Supplementary Table 6**). Unexpectedly, 139 transcription factors, including auxin response factors (ARFs), bHLHs (basic

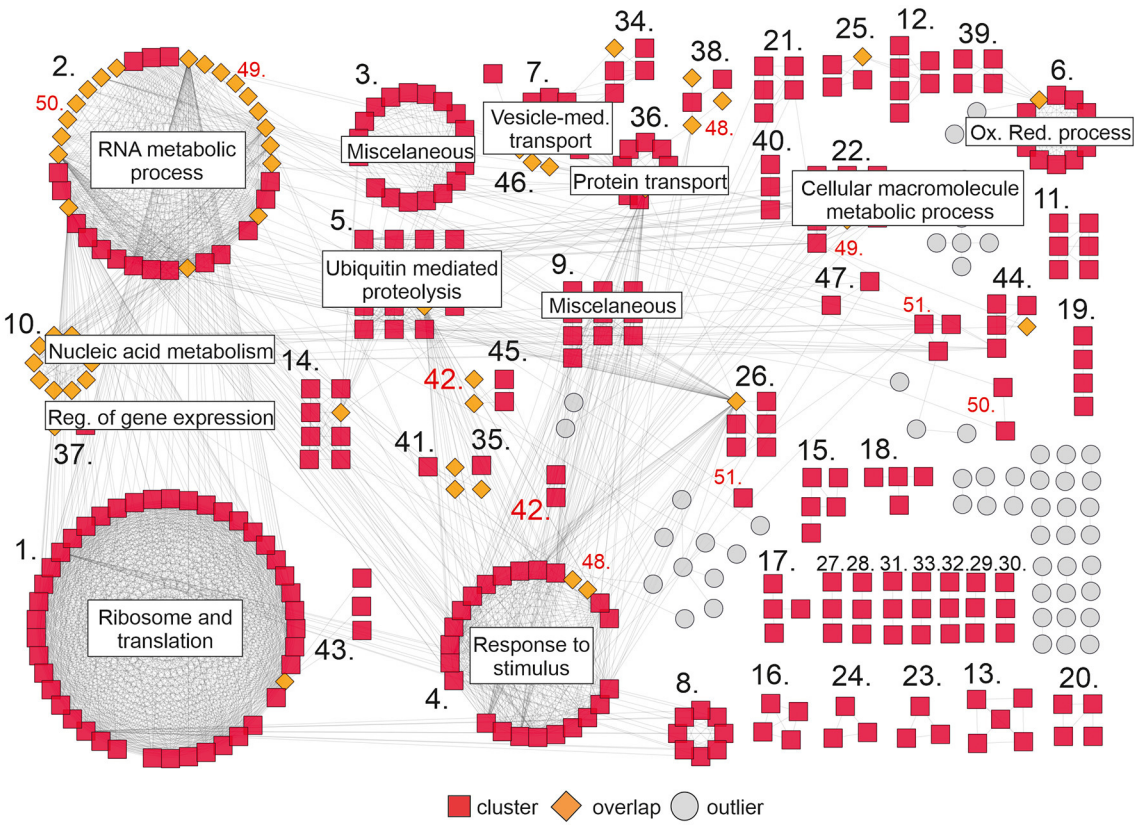

FIGURE 4 | Gene network of DEGs upon *DcLCYB1* expression in tobacco transgenic lines. Gene network representation of differentially expressed genes (up- and downregulated) in *DcLCYB1* transgenic lines. The network comprises 51 clusters (including 419 interacting genes). Only clusters with 10 or more members are provided with a name in the figure (detailed cluster composition can be found in **Supplementary Table 8**). A cluster number in red means there are genes grouped in different locations. Gene expression data from the RNAseq experiment were used to build the network.

helix-loop-helix), bZIPs (basic leucine zipper), ethylene response factors (ERFs), MYBs (oncogene from myeloblastosis virus), NACs [acronym derived from NAM (no apical meristem)], ATAF1/2, and CUC2 (cup-shaped cotyledon), which were the three initially discovered genes to contain a conserved NAC domain, and WRKYs (after the WRKY conserved amino acid sequence in the N-terminus of the protein) were significantly up- and downregulated in a constant and robust manner (**Supplementary Figure 3**; **Supplementary Table 7**).

To complement our analysis, we built a gene network based on the interactions between the DEGs in our RNAseq analysis. Interaction data were obtained from the String database (Szklarczyk et al., 2017) and imported into Cytoscape (Shannon et al., 2003) to visualize the network. Approximately 420 genes grouped in 51 clusters interact with each other (**Figure 4**). The largest clusters correspond to ribosome and translation (43), RNA metabolic process (36), response to stimulus (24), ubiquitin mediated proteolysis (15), and oxidation-reduction process (12). Other smaller clusters correspond to cellular macromolecule metabolic process (10), protein transport (10), nucleic acid metabolism and the regulation of gene expression (10), vesicle-mediated transport (10), and others (**Figure 4**; **Supplementary Table 8**). Interestingly, there are some genes in the network (orange rhombus in **Figure 4**) that connect one or more clusters, reflecting the high degree of interaction between the components of this network.

Proteomic Analysis of *DcLCYB1*-Expressing Lines

In our proteomics experiment, the results from the PCA showed that replicates within the transgenic and wild type genotypes grouped together while the differences between the wild type and transgenic groups were large (**Figure 5A**), suggesting a considerable change in the proteome of the transgenic lines compared with the wild type. From the ∼2,900 POTs identified in our experiment (**Supplementary Table 9**), the chloroplast was the compartment where the highest number of proteins was identified (∼31.5%; **Supplementary Figure 4**), followed by the cytoplasm (∼15–20%), mitochondria (6.9%), and nucleus (6.9%; **Supplementary Figure 4**; **Supplementary Table 10**). This pattern was also observed for the up- (∼32–35%) and downregulated (∼34–35%) proteins measured for all the transgenic lines (**Supplementary Table 10**). Unfortunately, it was not possible to detect the *DcLCYB1* protein in our analysis. However, the endogenous *Nt*LCYB showed an increase between 10 and 30%; however, it was significant

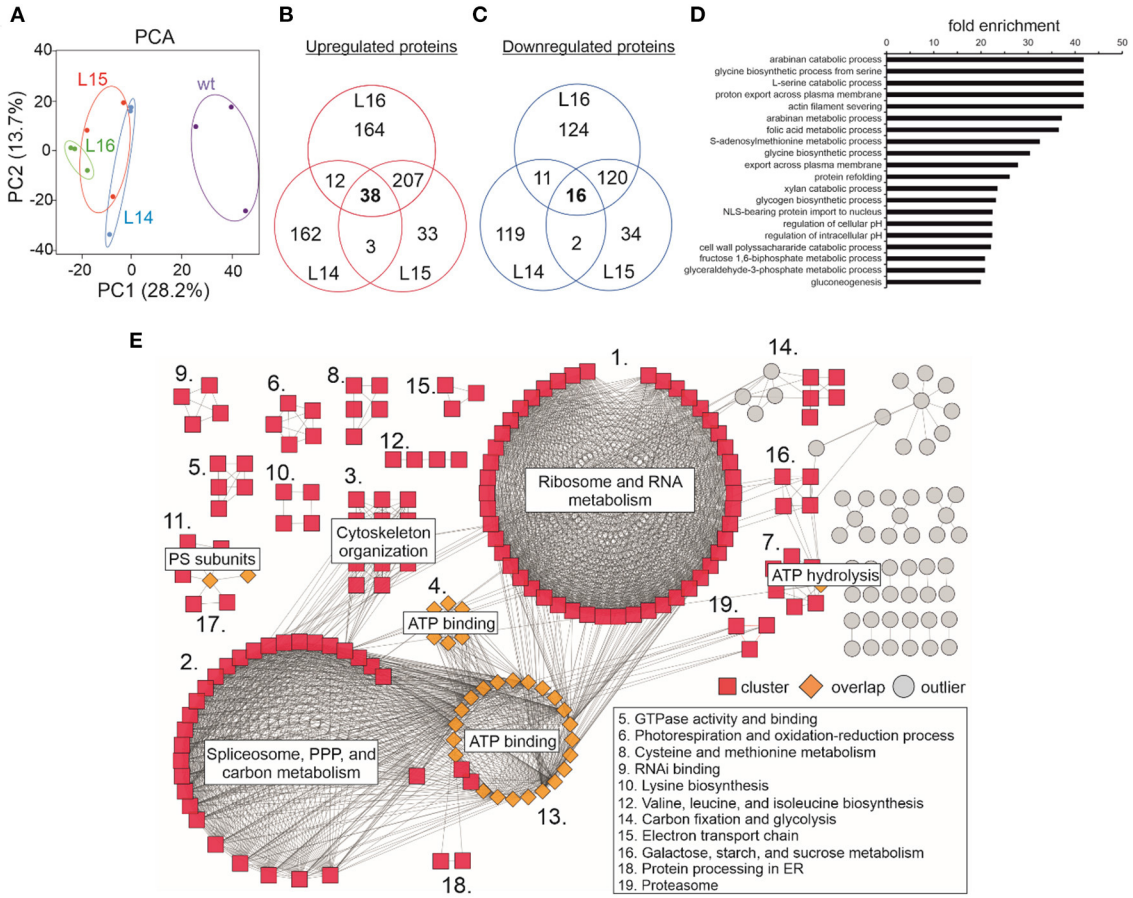

FIGURE 5 | Effect of the expression of the *DcLCYB1* gene in total leaf proteome of transgenic tobacco lines. **(A)** Principal component analysis (PCA) of wild type and transgenic *DcLCYB1* lines. **(B,C)** Venn diagrams of proteins with increased and reduced abundance in the *DcLCYB1* transgenic lines (using POT data). **(D)** GO (biological process) enrichment of significantly changing (increased and reduced abundance) proteins (using the ATG codes) in at least two of the three transgenic *DcLCYB1* lines (top 20 processes are shown). **(E)** Protein network representation of proteins changing significantly (increased and reduced abundance) in the *DcLCYB1* transgenic lines. The network comprises 214 highly interacting proteins. Protein abundance was quantified by LC-MS/MS and protein intensity was log2 transformed and the linear model for microarray analysis (limma) R package (Ritchie et al., 2015) was used for comparative analysis ($p \leq 0.05$). Three biological replicates for each genotype (wt, L14, L15, and L16) were used for shotgun proteomics ($n = 3$).

only for line L16 (**Supplementary Table 9**). Nevertheless, 260 proteins showed increased abundance (**Figure 5B**), while 149 showed decreased abundance in at least two of the three transgenic lines (**Figure 5C**). In addition, (GO) enrichment analysis revealed processes such as amino acid metabolic processes (e.g., glycine and serine), fructose 1,6-biphosphate and glyceraldehyde 3-phosphate metabolic processes, and gluconeogenesis (among others) with at least 20-fold enrichment (**Figure 5D**). In order to integrate all this information, we used the proteins overlapping in at least two lines (409) and built a protein–protein interaction network by combining the String database (**Supplementary Table 11**) and Cytoscape software for visualization (Shannon et al., 2003; Szklarczyk et al., 2017). Around 214 proteins showed a high degree of interaction (see the Material and Methods section; **Figure 5E**; **Supplementary Table 12**). The network revealed three main larger clusters containing the proteins involved mostly in ribosome and RNA metabolism, spliceosome, pentose phosphate pathway (PPP) and carbon metabolism, and ATP binding, respectively. Interestingly, almost all the proteins comprising the ATP binding cluster interact with proteins of the other two larger clusters, suggesting the ATP binding function as a nexus between these other two larger clusters (**Figure 5E**). Other smaller clusters contain the proteins involved in cytoskeleton organization, ATP hydrolysis, photosystems subunits, photorespiration and oxidation-reduction process, amino acid metabolism, RNA binding, carbon fixation, and glycolysis, among others (**Figure 5E**; **Supplementary Table 12**)

Metabolomics Analyses Reveal Changes in Secondary Metabolites and Lipids

Because of significant changes in many of the genes and proteins involved in secondary metabolism in the transcriptome and proteome of the transgenic lines, we decided to determine changes in the secondary metabolites through a LC-MS analysis. We identified significant increases in acetylsalicylic

FIGURE 6 | Metabolomic alterations in *DcLCYB1*-expressing tobacco lines. **(A)** The heat map represents the ratio of transgenic lines and wild type (fold change) of 46 secondary metabolites measured in the experiment. Asterisks indicate significant changes (nonpaired two-tailed student *t*-test, $p \leq 0.05$; $n = 6$ biological replicates). **(B)** Venn diagram showing lipid number significantly changed in the transgenic *DcLCYB1* lines. **(C)** Heatmap representing the 75 of lipids changing significantly in all the transgenic lines. Significant differences were determined using nonpaired two-tailed student *t*-test ($p \leq 0.05$; $n = 6$ biological replicates).

acid, flavin mononucleotide, O-acetyl-L-homoserine, quercetin 3-O-glucoside 7-O rhamnoside, quinic acid (3-caffeoyl), and one acyclic diterpene glycoside in all transgenic lines (**Figure 6A**). In addition, other metabolites were increased (e.g., adenine, proline, Pro-Glu) or decreased (e.g., nicotine) in one or two transgenic lines (**Figure 6A**). Finally, we analyzed lipid composition in the wild type and *DcLCYB1* transgenic lines because β-carotene and polar carotenoids (xanthophylls) rigidify

the fluid phase of the membranes and limit oxygen penetration to the hydrophobic membrane core, which is susceptible to oxidative degradation (Subczynski et al., 1991; Berglund et al., 1999). Thus, increases in β-carotene and xanthophylls in our transgenic lines might influence lipid composition. Interestingly, 75 lipid species were significantly changed in all three lines (**Figure 6B**). Small but significant decreases (∼2–5%) in the lipid composition of monogalactosyldiacylglycerol (MGDG) and digalactosyldiacylglycerol (DGDG) were detected in the transgenic lines compared with the wild type (**Figure 6C**; **Supplementary Tables 14**, **15**). By contrast, a general increase in phosphatidylethanolamine (PE), triacylglycerides (TAG), and phosphatidylserine (PS) was found in the transgenic lines compared with the wild type (**Figure 6C**; **Supplementary Tables 14**, **15**).

Plant Stress Tolerance Is Enhanced in *DcLCYB1*-Expressing Lines

Considering the great number of upregulated genes related to abiotic stress (**Figure 3B**), we decided to challenge our transgenic lines to different abiotic stresses, such as high light, salt, and oxidant agents (e.g., catechin and H_2O_2). We decided to asses these stresses due to the fact that enhanced xanthophyll content is reflected in enhanced photoprotection, while higher β-carotene and ABA content favor antioxidant capacity and salt tolerance. Interestingly, our transgenic lines possess the aforementioned features and therefore it is possible that they show enhance tolerance to theses abiotic stresses. Due to the increased hormone content (GAs and ABA) (Moreno et al., 2020) and altered gene expression related to hormone signaling (**Figure 3B**) in these lines, we first characterized the early growth and development of these lines. As expected, radicle emergence and germination were delayed in the transgenic lines compared with the wild type (**Supplementary Figures 5A,B**), reflecting the increased ABA content in these lines. In addition, leaf area and internode length were increased in the transgenic lines compared with the wild type in later developmental stages in plants growing in the greenhouse (**Supplementary Figures 5C,D**), which is well in line with the increased GA content in these lines.

Then, we challenged our transgenic lines and exposed them to different abiotic stresses. First, tobacco leaf discz were exposed to high light intensity (see the Material and Methods section), and the autoluminescence was measured. Quantification of the autoluminescence in the leaf discz reflects the accumulation of lipid peroxidation in the leaf. The tobacco leaf discz from the transgenic lines remained green, while the wild type bleach (**Figure 7A**) suggesting increased tolerance to high light intensity in the transgenic lines. In addition, lipid peroxide accumulation in the transgenic lines was approximately four times lower than in the wild type (**Figure 7B**). Second, we exposed tobacco seedlings to different salt concentrations (100 and 150 mM) and observed their phenotype. Interestingly, all transgenic lines showed higher biomass in both salt concentrations, and L14 was the line with the highest salt tolerance (**Figures 7C,D**). Third, we exposed tobacco seedlings to catechin and H_2O_2 (Scarpeci et al., 2008; Kaushik et al., 2010), two well-characterized oxidant agents. The transgenic lines showed higher plant biomass under control (mock), catechin, and H_2O_2 treatments compared with the wild type (**Figures 7E,F**; **Supplementary Figure 5E**). In addition, the leaf area of cotyledons and the first four leaves were quantified in the wild type and transgenic lines under control and stress conditions. In general, the transgenic lines showed a bigger leaf area than the wild type under control conditions and under oxidative stress (**Supplementary Figure 5F**). Taken together, these results showed enhanced stress tolerance in the transgenic lines, which is reflected in a higher biomass under different stress conditions.

DISCUSSION

Carotenoids are important isoprenoid molecules involved in the essential functions for plant growth and development (e.g., photosynthesis, photoprotection, ROS-scavenging). Moreover, carotenoids (e.g., β-carotene) are the precursors of plant hormones (e.g., ABA and SLs). Thus, manipulation of carotenoid metabolism can influence hormonal content (e.g., GA, ABA) and trigger growth and developmental responses in addition to the expected changes in pigment accumulation (Moreno et al., 2020). In the current study, we showed the impact of *DcLCYB1* gene expression at the transcriptome, proteome, and metabolic levels of our previously published *DcLCYB1* tobacco lines (Moreno et al., 2020), attempting to explain how these changes support higher biomass and stress tolerance. *DcLCYB1* tobacco lines showed higher β-carotene, lutein/zeaxanthin, and violaxanthin content, which resulted in higher ABA but also indirectly in higher GA content. Increased hormone content altered plant architecture (**Figures 1A,B**), resulting in enhanced photosynthetic efficiency and plant yield in these lines (Moreno et al., 2020). Enhanced carotenoid and hormone content, photosynthetic efficiency, and plant yield can be very desirable traits in crops, making the genetic manipulation of the carotenoid pathway—particularly of the *LCYB* gene—a promising target for crop improvement. However, additional information at the molecular level (transcriptome, proteome, and the overall metabolism) is needed to complete the analysis of these lines before exporting this bioengineering to crops.

At the transcriptome level, *DcLCYB1* expression caused genetic changes that extended beyond the chloroplast (e.g., cytosol, nucleus; **Supplementary Figure 1**), which is the organelle where the LCYB protein is located and where it plays a key role in carotenoid synthesis. Moreover, the expression of ∼2,000 genes changed significantly in the transgenic lines, raising the question of how a single gene transformation with a gene encoding an enzyme of the carotenoid pathway can trigger this response. Interestingly, the cytosol and nucleus were the other compartments with the highest number of genes that changed significantly (**Supplementary Figure 1**). The cytosol and nucleus are compartments in which transcription factors are localized and can induce changes in gene expression that favor stress tolerance, growth, and development (Aida et al., 1997; Kim et al., 2003; Tran et al., 2004; Wu et al., 2009; Beltramino et al., 2018; D'Alessandro et al., 2018). This suggests a plastid-to-nucleus

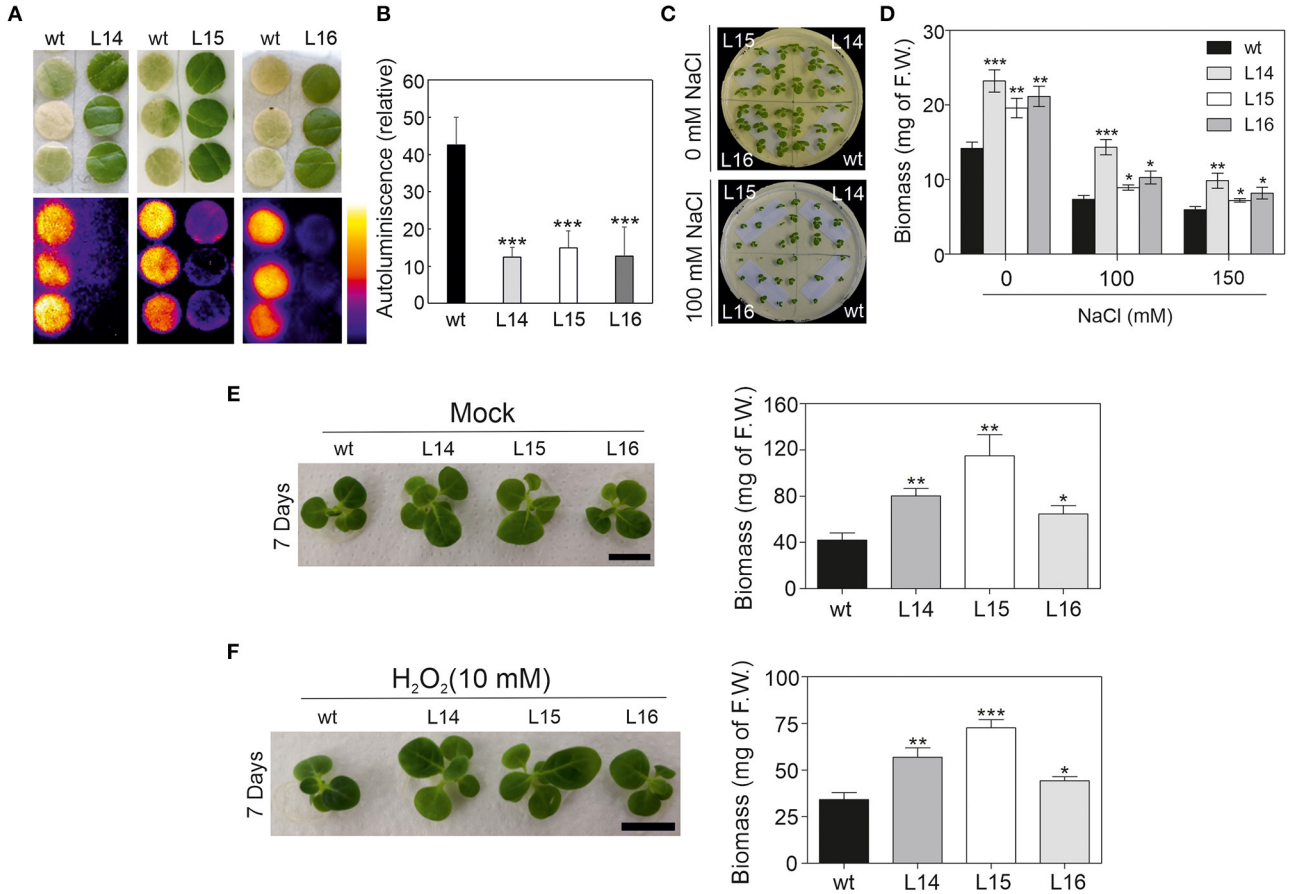

FIGURE 7 | High light, salt, and oxidative stress response in *DcLCYB1* tobacco lines. **(A)** Lipid peroxidation analysis by imaging of the wild type and lines L14, L15, and L16 ($n = 3$). **(B)** Quantification of the relative autoluminiscence of the wild type and transgenic *DcLCYB1* lines after stress from a high amount of light. **(C)** NaCl control (upper panel) and treatment (100 mM; bottom panel) of wild type and transgenic lines. **(D)** Biomass quantification (F.W.) of wild type and transgenic lines at 0, 100, and 150 mM of NaCl treatment. **(E,F)** Oxidant agents (mock and H_2O_2) treatments of wild type and transgenic lines. Two-week-old seedlings grown in liquid MS media were transferred to liquid MS supplemented with water (mock) and H_2O_2 (10 mM) and photographed after seven days of treatment. Plant biomass (F.W.) of wild type and transgenic lines was recorded for mock- (E) and H_2O_2-treated (F) plants after seven days. Unpaired student's *t*-test was performed to compare transgenic lines with the wild type. $^*p < 0.05$, $^{**}p < 0.005$, $^{***}p < 0.0005$.

communication that could support the ∼2,000 genes changing significantly in the transgenic lines. In fact, consistent changes in the expression of transcription factors, which could influence the expression of a large number of genes, were detected in our transgenic lines (**Supplementary Table 7**). For instance, the expression of the *bZIP12* transcription factor increased ∼40% in the transgenic lines (**Figure 8**). This transcription factor was reported to enhance salt tolerance in rice (Hossain et al., 2010) and is in line with the enhanced salt tolerance shown in our transgenic lines. In addition, a NAC [ATAF1 (activating factor 1)/NAC002] transcription factor was shown to mediate the responses to abiotic stress in Arabidopsis (Wu et al., 2009). Moreover, ATAF1 regulates and promotes salt tolerance in rice (Liu et al., 2016). In rice, the *ATAF1* overexpressors, the *DEHYDRIN* and *LEA* (e.g., *OsLEA3*) genes, are induced. These genes contribute to the salt tolerance mechanism in rice and Arabidopsis (Chourey et al., 2003). In our transgenic lines, upregulation of *DEHYDRIN* (∼200% increase) and *LEA* (230% increase) as a response to increased *ATAF1* expression (∼40%; **Figure 8**) might have contributed to the enhanced salt tolerance in our plants. In addition, *ATAF1* is a positive regulator of ABA synthesis (Jensen et al., 2013). Indeed, enhanced *ATAF1* expression in our transgenic lines is in line with the observed increase in ABA content (Moreno et al., 2020) and enhanced salt tolerance. Another NAC family member (NAP/NAC029) was reported to be involved in salt tolerance, GA-mediated chlorophyll degradation, and leaf senescence (Seok et al., 2017; Lei et al., 2020). Arabidopsis *nap* mutants showed enhanced salt tolerance in plants grown using synthetic media and using soil (Seok et al., 2017). Reduced *NAP* expression (∼55%; **Figure 8**) in our transgenic lines might contribute to the enhanced salt tolerance observed in plants grown on synthetic media supplemented with NaCl (**Figures 7C,D**). Moreover, *NAP* expression promotes leaf senescence and GA-mediated

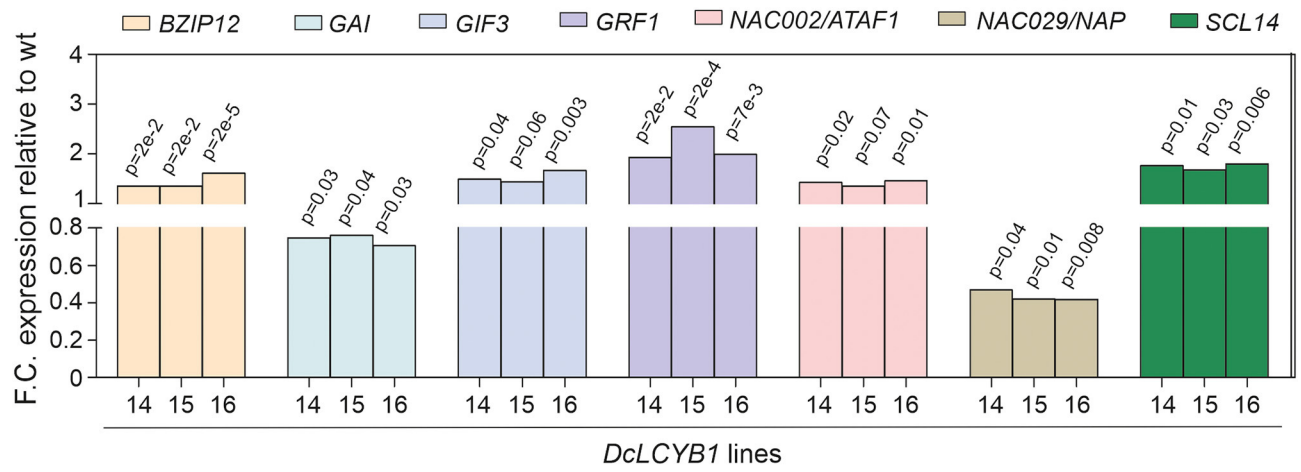

FIGURE 8 | Fold change expression of transcription factors involved in growth, development, and stress response. Transcription factors involved in light and salt responses and in plant growth and development. Gene expression was measured by RNAseq (padjust < 0.05). e: represents 10.

chlorophyll degradation (Lei et al., 2020). Thus, the reduced NAP expression in our transgenic lines might contribute to the observed delayed senescence phenotype and enhanced chlorophyll content found in our tobaccos (Moreno et al., 2020).

The SCARECROW-LIKE protein (SCL14) is a member of the Arabidopsis GRAS family of transcription factors. SCL14 competes with GRX480/ROXY19 for binding the TGAII transcription factors and mediating the activation or inhibition, respectively, of the detoxification response (Ndamukong et al., 2007; Fode et al., 2008; Koster et al., 2012; Huang et al., 2016). Recently, it was shown that SCL14-dependent detoxification is necessary for the resilience of Arabidopsis plants exposed to photooxidative stress (D'Alessandro et al., 2018). In addition, Arabidopsis *scl14* mutants with reduced and enhanced *SCL14* expression showed reduced and enhanced tolerance, respectively, to high light (D'Alessandro et al., 2018). It was shown that β-cyclocitral (β-cc) induces the expression of SCL14, which interacts with TGAII and activates the xenobiotic detoxification response through the NAC002/ATAF1 transcription factor (D'Alessandro et al., 2018; D'Alessandro and Havaux, 2019). Interestingly, our transgenic lines showed enhanced tolerance to high light (**Figures 7A,B**). Moreover, increased expression of the SCL14 (∼80%) and NAC002/ATAF1 (∼40%) transcription factors suggest the activation of the xenobiotic response, resulting in higher tolerance to high light. However, β-cc content did not change in our transgenic lines (Moreno et al., 2020), suggesting the possibility of a β-cc-independent activation of the xenobiotic response. Other members of the GRAS family also showed increased expression in our dataset (SCL9 and SCR), which might be contributing to the high tolerance to high light in our transgenic lines.

Another interesting example is the gibberellic acid insensitive (GAI), which represses GA responses and restrains the normal cell proliferation and expansion that drive plant growth. In our transgenic lines, growth is enhanced because of an increase in GA levels (Moreno et al., 2020). This is correlated with reduced *GAI* gene expression identified by RNAseq in our transgenic lines (**Figure 8**). Reduction of *GAI* allowed for the accumulation of GA, resulting in enhanced plant growth. Furthermore, *GRF (growth regulating factor)-interacting factor3* (*GIF3*) is a member of a small family of transcription coactivators that forms functional complexes with GRFs (Kim et al., 2003; Lee et al., 2009; Lee and Kim, 2014). *GIF3* is required for the cell proliferation activities of lateral organs, including leaves and cotyledons (Kim et al., 2003; Lee et al., 2009). The Arabidopsis *gif1* mutant showed reduced leaf and cotyledon size (Kim and Kende, 2004). Increased *GIF3* expression by ∼50% in our transgenic lines supports the observed increased size in cotyledons and leaves under control and stress conditions (**Supplementary Figures 5C,F**). In the same line of evidence, a GRF (*GRF1*) involved in leaf and cotyledon growth (Kim et al., 2003) was detected in our RNAseq analysis. Arabidopsis mutants with reduced and increased GRF expression showed reduced and increased leaf and cotyledon size, respectively (Kim et al., 2003; Kim and Kende, 2004; Beltramino et al., 2018). Thus, increased *GRF1* expression (up to 150%) in our transgenic lines (**Figure 8**) might contribute to the enhanced growth observed in leaves and cotyledons under normal and stress conditions in our tobacco lines (**Supplementary Figures 5C,F**). In a recent study, an RNAseq analysis showed a broad range of gene targets for GRF1 and GRF3, including the genes involved in plant growth and development, phytohormone biosynthesis and signaling, and the cell cycle (Piya et al., 2020). Moreover, clock core genes and genes with stress- and defense-related functions are the most predominant among the GRF1 and GRF3-bound targets. Additionally, it was shown that GRF1 and GRF3 target molecular nodes of growth-defense antagonism and modulate the levels of defense- and development-related hormones (e.g., ABA) (Piya et al., 2020). This is in line with our RNAseq analysis (**Figure 3B**; **Supplementary Figures 2A,B**), where the expression of more than 100 genes involved in hormone biosynthesis and signaling,

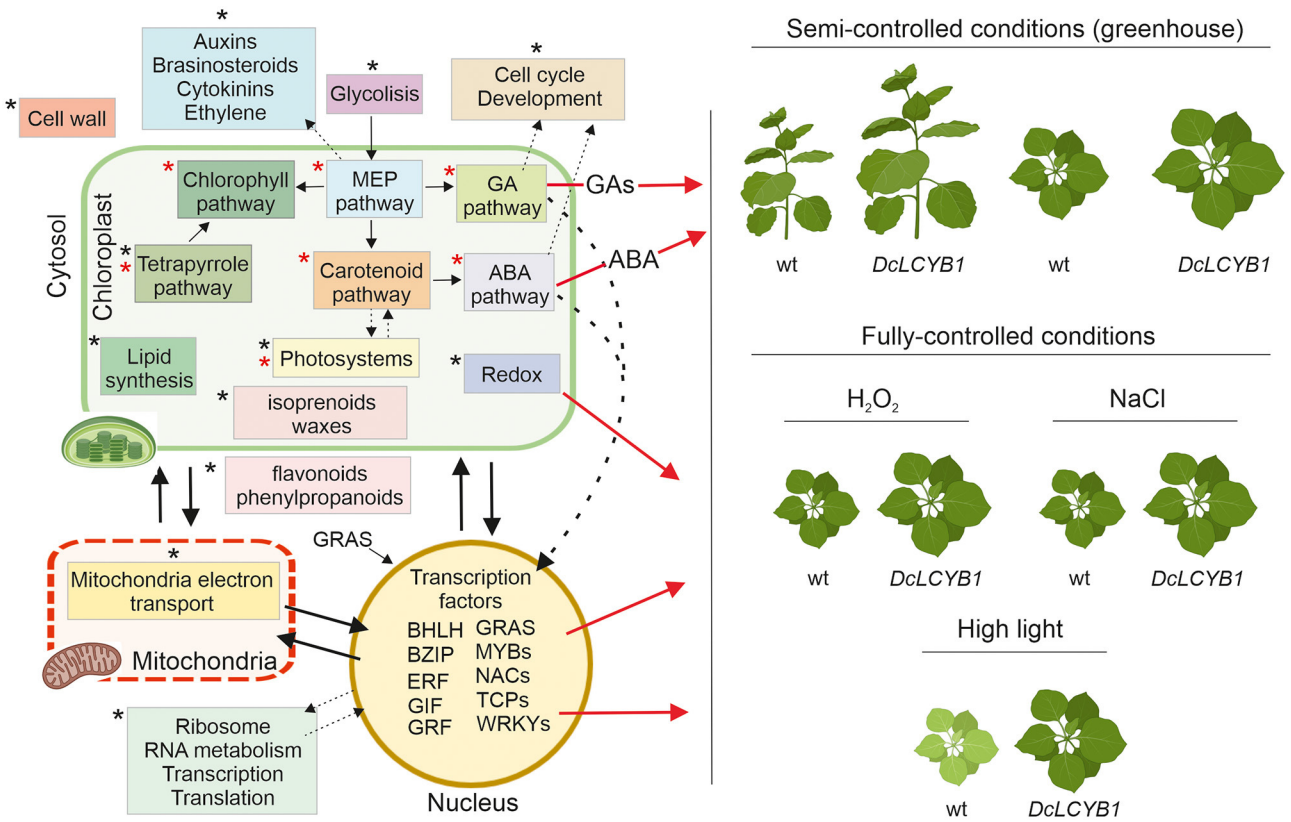

FIGURE 9 | Schematic model representing pathways and processes with changes at transcript, protein, and metabolic level and allowing greater plant biomass and stress resilience in tobacco *DcLCYB1* lines. Expression of *DcLCYB1* results in a reshaping of the tobacco transcriptome, proteome and metabolome affecting processes outside the chloroplast (e.g., mitochondria, nucleus, and cytosol). Previously reported processes that were affected upon expression of *DcLCYB1* (Moreno et al., 2020) are indicated with a red asterisk, while newly identified processes (altered upon *DcLCYB1* expression) with our OMICs strategy are indicated with a black asterisk. Although increased hormone content (e.g., ABA) might have enhanced stress tolerance, here we integrate the genes and proteins that can influence the expression of other genes (e.g., transcription factors) and can trigger signaling cascades involved in stress tolerance, growth, and development. A schematic representation using *Nicotiana benthamiana* plants (available in Biorender) were used to represent the stress response in the *DcLCYB1* lines. The model was build using Biorender (Biorender.com).

cell division, cell cycle, and development was significantly changed in our transgenic lines.

Interestingly, many of the affected processes at the transcript level (RNAseq) were also identified at the proteome level. For instance, the biggest nodes in the protein–protein interaction network correspond to ribosome and RNA metabolism, which comprises the proteins involved in transcription and translation (e.g., ribosomal subunits). The reshaping in those processes might be indicators of higher translation to support the increased/decreased abundance of around 600 proteins in the transgenic lines. Proteins belonging to processes such as photorespiration and redox, amino acid metabolism and biosynthesis, RNA binding, carbon fixation and glycolysis, and electron transport chain reflect a direct impact on the increased/reduced gene expression measured in our RNAseq experiment (**Figures 4**, **5**; **Supplementary Tables 2–6**, **10–12**).

Summarizing and integrating our results, we provide a model that explains the higher yield phenotype and high light, salt, and oxidative stress tolerance observed in our transgenic tobacco lines beyond the previously reported isoprenoid pathways in chloroplast (**Figure 9**). The carotenoid and carotenoid-related pathways influencing phytohormone content or photosynthesis and, thus, impacting plant growth (red asterisks in **Figure 9**) were thought to be the main reason for the higher yield phenotype (Moreno et al., 2020). However, by combining transcriptome, proteome, and metabolome data, we have provided new evidence suggesting other processes and pathways (black asterisks in **Figure 9**), for instance, in the cytosol and nucleus, are involved in this phenomenon. One example is the increased gene expression and protein abundance of glycolytic enzymes, which might be related to the increased GA, carotenoid, and chlorophyll content observed in our tobacco lines. Glycolysis provides the precursor used for isoprenoid synthesis in the MEP pathway, and MEP provides the common precursor (GGPP) for GA, carotenoids, and chlorophyll synthesis. More MEP precursors could lead to higher GGPP content, thus supporting increases in MEP-derived isoprenoid pathways. On the one hand, a great number of genes and proteins involved in cell cycle and development (**Supplementary Tables 6**, **9**) might contribute to the observed growth rate and accelerated development in our tobacco lines.

In addition, the transcription factors involved in plant growth and development (transcription factors GIF3 and GRF1, and GAI growth-related factor) might also contribute to the high-yield phenotype observed under control conditions. Furthermore, the DEGs and proteins involved in auxin, brassinosteroid, cytokinin, and ethylene metabolism might indicate their participation in growth and developmental phenotypes observed in our lines. On the other hand, besides the higher ABA content, the significant changes in transcription factors (localized in the nucleus and cytoplasm) involved in salt (bZIP12, ATAF1, NAP) and tolerance to high light (GRAS SCL14, ATAF1) together with a reshaping at the transcriptome and proteome level of the redox process contribute to the observed higher tolerance to high light, salt, and oxidative stress in our transgenic tobacco lines (**Figure 9**). Interestingly, previous studies have shown that altered hormone content (e.g., ABA) induces the expression of transcription factors and vice versa (Devkar et al., 2020; Piya et al., 2020; Yu et al., 2020), thus activating the signaling cascades that impact plant growth, development, and stress response.

In conclusion, what seemed to be a simple expression of a carotenogenic gene that encodes for an enzyme converting the lycopene into β-carotene resulted in a greater reshaping at transcriptome, proteome, and metabolome levels in different cell compartments to support plant growth, development, and stress tolerance in tobacco. The progress and knowledge generated here will allow us to take this bioengineering to the next level, applying it to crops to generate a new generation of super crops with enhanced photosynthetic efficiency, yield, stress tolerance, and nutritional content.

DATA AVAILABILITY STATEMENT

The datasets presented in this study can be found in online repositories. The names of the repository/repositories and accession number(s) can be found in the article/**Supplementary Material**.

AUTHOR CONTRIBUTIONS

JM and AS conceived the project and wrote the manuscript with input from the coauthors. JM performed the cDNA synthesis, metabolite extraction, and MapMan analysis and analyzed RNAseq data. JM and MK performed the oxidative stress experiments. PS performed salt stress experiments. ES run samples for proteomics and the data deposition. SM-J and JM performed statistical analysis and analyzed and interpreted the data. AS performed the secondary metabolite data analysis. MH performed the photooxidative stress and lipid peroxidation experiments. AF performed the mapping of the NiTAB identifiers into Arabidopsis AGI codes and data deposition. UL performed lipid data analysis. All authors contributed to the article and approved the submitted version.

ACKNOWLEDGMENTS

We want to thank Prof. Lothar Willmitzer for support and discussion, Änne Michaelis for technical assistance, Dr. Michael Tillich and Dr. Ralph Bock for providing access to the POTbaseMS for proteomics analysis, and the Max-Planck-Institut für Molekulare Pflanzenphysiologie Green Team for plant cultivation.

SUPPLEMENTARY MATERIAL

The Supplementary Material for this article can be found online at: https://www.frontiersin.org/articles/10.3389/fpls.2021.624365/full#supplementary-material

REFERENCES

Aida, M., Ishida, T., Fukaki, H., Fujisawa, H., and Tasaka, M. (1997). Genes involved in organ separation in Arabidopsis: an analysis of the cup-shaped cotyledon mutant. *Plant Cell* 9, 841–857. doi: 10.1105/tpc.9.6.841

Alder, A., Jamil, M., Marzorati, M., Bruno, M., Vermathen, M., Bigler, P., et al. (2012). The path from beta-carotene to carlactone, a strigolactone-like plant hormone. *Science* 335, 1348–1351. doi: 10.1126/science.1218094

Ampomah-Dwamena, C., Thrimawithana, A. H., Dejnoprat, S., Lewis, D., Espley, R. V., and Allan, A. C. (2019). A kiwifruit (Actinidia deliciosa) R2R3-MYB transcription factor modulates chlorophyll and carotenoid accumulation. *New Phytol.* 221, 309–325. doi: 10.1111/nph.15362

Bartley, G. E., and Scolnik, P. A. (1995). Plant carotenoids: pigments for photoprotection, visual attraction, and human health. *Plant Cell* 7, 1027–1038. doi: 10.1105/tpc.7.7.1027

Beltramino, M., Ercoli, M. F., Debernardi, J. M., Goldy, C., Rojas, A. M. L., Nota, F., et al. (2018). Robust increase of leaf size by *Arabidopsis thaliana* GRF3-like transcription factors under different growth conditions. *Sci. Rep.* 8:13447. doi: 10.1038/s41598-018-29859-9

Berglund, A. H., Nilsson, R., and Liljenberg, C. (1999). Permeability of large unilamellar digalactosyldiacylglycerol vesicles for protons and glucose - influence of alpha-tocopherol, beta-carotene, zeaxanthin and cholesterol. *Plant Physiol. Biochem.* 37, 179–186. doi: 10.1016/S0981-9428(99)80032-1

Birtic, S., Ksas, B., Genty, B., Mueller, M. J., Triantaphylides, C., and Havaux, M. (2011). Using spontaneous photon emission to image lipid oxidation patterns in plant tissues. *Plant J.* 67, 1103–1115. doi: 10.1111/j.1365-313X.2011.04646.x

Chen, X., Han, H., Jiang, P., Nie, L., Bao, H., Fan, P., et al. (2011). Transformation of beta-lycopene cyclase genes from *Salicornia europaea* and Arabidopsis conferred salt tolerance in Arabidopsis and tobacco. *Plant Cell Physiol.* 52, 909–921. doi: 10.1093/pcp/pcr043

Chourey, K., Ramani, S., and Apte, S. K. (2003). Accumulation of LEA proteins in salt (NaCl) stressed young seedlings of rice (Oryza sativa L.) cultivar Bura Rata and their degradation during recovery from salinity stress. *J. Plant Physiol.* 160, 1165–1174. doi: 10.1078/0176-1617-00909

Chung, M. Y., Vrebalov, J., Alba, R., Lee, J., McQuinn, R., Chung, J. D., et al. (2010). A tomato (*Solanum lycopersicum*) APETALA2/ERF gene, SlAP2a, is a negative regulator of fruit ripening. *Plant J.* 64, 936–947. doi: 10.1111/j.1365-313X.2010.04384.x

Cox, J., and Mann, M. (2008). MaxQuant enables high peptide identification rates, individualized p.p.b.-range mass accuracies and proteome-wide protein quantification. *Nat. Biotechnol.* 26, 1367–1372. doi: 10.1038/nbt.1511

D'Alessandro, S., and Havaux, M. (2019). Sensing beta-carotene oxidation in photosystem II to master plant stress tolerance. *New Phytol.* 223, 1776–1783. doi: 10.1111/nph.15924

D'Alessandro, S., Ksas, B., and Havaux, M. (2018). Decoding beta-cyclocitral-mediated retrograde signaling reveals the role of a detoxification response

in plant tolerance to photooxidative stress. *Plant Cell* 30, 2495–2511. doi: 10.1105/tpc.18.00578

D'Ambrosio, C., Giorio, G., Marino, I., Merendino, A., Petrozza, A., Salfi, L., et al. (2004). Virtually complete conversion of lycopene into beta-carotene in fruits of tomato plants transformed with the tomato lycopene beta-cyclase (tlcy-b) cDNA. *Plant Sci.* 166, 207–214. doi: 10.1016/j.plantsci.2003.09.015

Davison, P. A., Hunter, C. N., and Horton, P. (2002). Overexpression of beta-carotene hydroxylase enhances stress tolerance in Arabidopsis. *Nature* 418, 203–206. doi: 10.1038/nature00861

Devkar, V., Thirumalaikumar, V. P., Xue, G. P., Vallarino, J. G., Tureckova, V., Strnad, M., et al. (2020). Multifaceted regulatory function of tomato SlTAF1 in the response to salinity stress. *New Phytol.* 225, 1681–1698. doi: 10.1111/nph.16247

Fode, B., Siemsen, T., Thurow, C., Weigel, R., and Gatz, C. (2008). The arabidopsis GRAS protein SCL14 interacts with class II TGA transcription factors and is essential for the activation of stress-inducible promoters. *Plant Cell* 20, 3122–3135. doi: 10.1105/tpc.108.058974

Fraser, P. D., and Bramley, P. M. (2004). The biosynthesis and nutritional uses of carotenoids. *Prog. Lipid Res.* 43, 228–265. doi: 10.1016/j.plipres.2003.10.002

Fraser, P. D., Truesdale, M. R., Bird, C. R., Schuch, W., and Bramley, P. M. (1994). Carotenoid biosynthesis during tomato fruit development (evidence for tissue-specific gene expression). *Plant Physiol.* 105, 405–413. doi: 10.1104/pp.105.1.405

Giavalisco, P., Li, Y., Matthes, A., Eckhardt, A., Hubberten, H. M., Hesse, H., et al. (2011). Elemental formula annotation of polar and lipophilic metabolites using (13) C, (15) N and (34) S isotope labelling, in combination with high-resolution mass spectrometry. *Plant J.* 68, 364–376. doi: 10.1111/j.1365-313X.2011.04682.x

Gotz, T., Sandmann, G., and Romer, S. (2002). Expression of a bacterial carotene hydroxylase gene (crtZ) enhances UV tolerance in tobacco. *Plant Mol. Biol.* 50, 129–142. doi: 10.1023/A:1016072218801

Han, H. P., Li, Y. X., and Zhou, S. F. (2008). Overexpression of phytoene synthase gene from *Salicornia europaea* alters response to reactive oxygen species under salt stress in transgenic Arabidopsis. *Biotechnol. Lett.* 30, 1501–1507. doi: 10.1007/s10529-008-9705-6

Holt, N. E., Zigmantas, D., Valkunas, L., Li, X. P., Niyogi, K. K., and Fleming, G. R. (2005). Carotenoid cation formation and the regulation of photosynthetic light harvesting. *Science* 307, 433–436. doi: 10.1126/science.1105833

Hossain, M. A., Cho, J. I., Han, M., Ahn, C. H., Jeon, J. S., An, G., et al. (2010). The ABRE-binding bZIP transcription factor OsABF2 is a positive regulator of abiotic stress and ABA signaling in rice. *J. Plant Physiol.* 167, 1512–1520. doi: 10.1016/j.jplph.2010.05.008

Huang, L. J., Li, N., Thurow, C., Wirtz, M., Hell, R., and Gatz, C. (2016). Ectopically expressed glutaredoxin ROXY19 negatively regulates the detoxification pathway in *Arabidopsis thaliana*. *BMC Plant Biol.* 16:200. doi: 10.1186/s12870-016-0886-1

Hummel, J., Segu, S., Li, Y., Irgang, S., Jueppner, J., and Giavalisco, P. (2011). Ultra performance liquid chromatography and high resolution mass spectrometry for the analysis of plant lipids. *Front. Plant Sci.* 2:54. doi: 10.3389/fpls.2011.00054

Jain, B. P., and Pandey, S. (2018). WD40 repeat proteins: signalling scaffold with diverse functions. *Protein J.* 37, 391–406. doi: 10.1007/s10930-018-9785-7

Jensen, M. K., Lindemose, S., de Masi, F., Reimer, J. J., Nielsen, M., Perera, V., et al. (2013). ATAF1 transcription factor directly regulates abscisic acid biosynthetic gene NCED3 in *Arabidopsis thaliana*. *FEBS Open Bio.* 3, 321–327. doi: 10.1016/j.fob.2013.07.006

Kang, C., Zhai, H., Xue, L., Zhao, N., He, S., and Liu, Q. (2018). A lycopene beta-cyclase gene, IbLCYB2, enhances carotenoid contents and abiotic stress tolerance in transgenic sweetpotato. *Plant Sci.* 272, 243–254. doi: 10.1016/j.plantsci.2018.05.005

Kaushik, S., Bais, H. P., Biedrzycki, M. L., and Venkatachalam, L. (2010). Catechin is a phytototoxin and a pro-oxidant secreted from the roots of *Centaurea stoebe*. *Plant Signal. Behav.* 5, 1088–1098. doi: 10.4161/psb.5.9.11823

Kim, J. H., Choi, D., and Kende, H. (2003). The AtGRF family of putative transcription factors is involved in leaf and cotyledon growth in Arabidopsis. *Plant J.* 36, 94–104. doi: 10.1046/j.1365-313X.2003.01862.x

Kim, J. H., and Kende, H. (2004). A transcriptional coactivator, AtGIF1, is involved in regulating leaf growth and morphology in Arabidopsis. *Proc. Natl. Acad. Sci. U. S. A.* 101, 13374–13379. doi: 10.1073/pnas.0405450101

Koster, J., Thurow, C., Kruse, K., Meier, A., Iven, T., Feussner, I., et al. (2012). Xenobiotic- and jasmonic acid-inducible signal transduction pathways have become interdependent at the Arabidopsis CYP81D11 promoter. *Plant Physiol.* 159, 391–402. doi: 10.1104/pp.112.194274

Lazar, C., Gatto, L., Ferro, M., Bruley, C., and Burger, T. (2016). Accounting for the multiple natures of missing values in label-free quantitative proteomics data sets to compare imputation strategies. *J. Proteome Res.* 15, 1116–1125. doi: 10.1021/acs.jproteome.5b00981

Lee, B. H., and Kim, J. H. (2014). Spatio-temporal distribution patterns of GRF-INTERACTING FACTOR expression and leaf size control. *Plant Signal. Behav.* 9:e29697. doi: 10.4161/psb.29697

Lee, B. H., Ko, J. H., Lee, S., Lee, Y., Pak, J. H., and Kim, J. H. (2009). The Arabidopsis GRF-INTERACTING FACTOR gene family performs an overlapping function in determining organ size as well as multiple developmental properties. *Plant Physiol.* 151, 655–668. doi: 10.1104/pp.109.141838

Lee, J. M., Joung, J. G., McQuinn, R., Chung, M. Y., Fei, Z., Tieman, D., et al. (2012). Combined transcriptome, genetic diversity and metabolite profiling in tomato fruit reveals that the ethylene response factor SlERF6 plays an important role in ripening and carotenoid accumulation. *Plant J.* 70, 191–204. doi: 10.1111/j.1365-313X.2011.04863.x

Lei, W., Li, Y., Yao, X. H., Qiao, K., Wei, L., Liu, B. H., et al. (2020). NAP is involved in GA-mediated chlorophyll degradation and leaf senescence by interacting with DELLAs in Arabidopsis. *Plant Cell Rep.* 39, 75–87. doi: 10.1007/s00299-019-02474-2

Leister, D. (2003). Chloroplast research in the genomic age. *Trends Genet.* 19, 47–56. doi: 10.1016/S0168-9525(02)00003-3

Liu, L., Shao, Z., Zhang, M., and Wang, Q. (2015). Regulation of carotenoid metabolism in tomato. *Mol. Plant* 8, 28–39. doi: 10.1016/j.molp.2014.11.006

Liu, Y., Sun, J., and Wu, Y. (2016). Arabidopsis ATAF1 enhances the tolerance to salt stress and ABA in transgenic rice. *J. Plant Res.* 129, 955–962. doi: 10.1007/s10265-016-0833-0

Love, M. I., Huber, W., and Anders, S. (2014). Moderated estimation of fold change and dispersion for RNA-seq data with DESeq2. *Genome Biol.* 15:550. doi: 10.1186/s13059-014-0550-8

Ma, N. N., Feng, H. L., Meng, X., Li, D., Yang, D. Y., Wu, C. G., et al. (2014). Overexpression of tomato SlNAC1 transcription factor alters fruit pigmentation and softening. *BMC Plant Biol.* 14:351. doi: 10.1186/s12870-014-0351-y

Martel, C., Vrebalov, J., Tafelmeyer, P., and Giovannoni, J. J. (2011). The tomato MADS-box transcription factor RIPENING INHIBITOR interacts with promoters involved in numerous ripening processes in a COLORLESS NONRIPENING-dependent manner. *Plant Physiol.* 157, 1568–1579. doi: 10.1104/pp.111.181107

Mi, H., Huang, X., Muruganujan, A., Tang, H., Mills, C., Kang, D., et al. (2017). PANTHER version 11: expanded annotation data from gene ontology and reactome pathways, and data analysis tool enhancements. *Nucleic Acids Res.* 45, D183–D189. doi: 10.1093/nar/gkw1138

Moise, A. R., Al-Babili, S., and Wurtzel, E. T. (2014). Mechanistic aspects of carotenoid biosynthesis. *Chem. Rev.* 114, 164–193. doi: 10.1021/cr400106y

Moreno, J. C. (2019). The proteOMIC era: a useful tool to gain deeper insights into plastid physiology. *Theor. Exp. Plant Physiol.* 31, 157–171. doi: 10.1007/s40626-018-0133-2

Moreno, J. C., Cerda, A., Simpson, K., Lopez-Diaz, I., Carrera, E., Handford, M., et al. (2016). Increased *Nicotiana tabacum* fitness through positive regulation of carotenoid, gibberellin and chlorophyll pathways promoted by *Daucus carota* lycopene beta-cyclase (Dclcyb1) expression. *J. Exp. Bot.* 67, 2325–2338. doi: 10.1093/jxb/erw037

Moreno, J. C., Martinez-Jaime, S., Schwartzmann, J., Karcher, D., Tillich, M., Graf, A., et al. (2018). Temporal proteomics of inducible RNAi lines of Clp protease subunits identifies putative protease substrates. *Plant Physiol.* 176, 1485–1508. doi: 10.1104/pp.17.01635

Moreno, J. C., Mi, J., Agrawal, S., Kossler, S., Tureckova, V., Tarkowska, D., et al. (2020). Expression of a carotenogenic gene allows faster biomass production by redesigning plant architecture and improving photosynthetic efficiency in tobacco. *Plant J.* 103, 1967–1984. doi: 10.1111/tpj.14909

Moreno, J. C., Pizarro, L., Fuentes, P., Handford, M., Cifuentes, V., and Stange, C. (2013). Levels of lycopene beta-cyclase 1 modulate carotenoid

gene expression and accumulation in *Daucus carota*. *PLoS ONE* 8:e58144. doi: 10.1371/journal.pone.0058144

Murashige, T., and Skoog, F. (1962). A revised medium for rapid growth and bio assays with tobacco tissue cultures. *Physiol. Plant* 15, 473–497. doi: 10.1111/j.1399-3054.1962.tb08052.x

Ndamukong, I., Al Abdallat, A., Thurow, C., Fode, B., Zander, M., Weigel, R., et al. (2007). SA-inducible Arabidopsis glutaredoxin interacts with TGA factors and suppresses JA-responsive PDF1.2 transcription. *Plant J.* 50, 128–139. doi: 10.1111/j.1365-313X.2007.03039.x

Nisar, N., Li, L., Lu, S., Khin, N. C., and Pogson, B. J. (2015). Carotenoid metabolism in plants. *Mol. Plant* 8, 68–82. doi: 10.1016/j.molp.2014.12.007

Niyogi, K. K., Bjorkman, O., and Grossman, A. R. (1997). The roles of specific xanthophylls in photoprotection. *Proc. Natl. Acad. Sci. U. S. A.* 94, 14162–14167. doi: 10.1073/pnas.94.25.14162

Olson, J. A. (1996). Benefits and liabilities of vitamin A and carotenoids. *J. Nutr.* 126, 1208S−1212S. doi: 10.1093/jn/126.suppl_4.1208S

Perez-Riverol, Y., Csordas, A., Bai, J., Bernal-Llinares, M., Hewapathirana, S., Kundu, D. J., Inuganti, A., et al. (2019). The PRIDE database and related tools and resources in 2019: improving support for quantification data. *Nucleic Acids Res.* 47, D442–D450. doi: 10.1093/nar/gky1106

Piya, S., Liu, J., Burch-Smith, T., Baum, T. J., and Hewezi, T. (2020). A role for Arabidopsis growth-regulating factors 1 and 3 in growth-stress antagonism. *J. Exp. Bot.* 71, 1402–1417. doi: 10.1093/jxb/erz502

Rao, A. V., and Rao, L. G. (2007). Carotenoids and human health. *Pharmacol. Res.* 55, 207–216. doi: 10.1016/j.phrs.2007.01.012

Ritchie, M. E., Phipson, B., Wu, D., Hu, Y., Law, C. W., Shi, W., et al. (2015). limma powers differential expression analyses for RNA-sequencing and microarray studies. *Nucleic Acids Res.* 43:e47. doi: 10.1093/nar/gkv007

Ruiz-Sola, M. A., and Rodriguez-Concepcion, M. (2012). Carotenoid biosynthesis in Arabidopsis: a colorful pathway. *Arabidopsis Book* 10:e0158. doi: 10.1199/tab.0158

Sagawa, J. M., Stanley, L. E., LaFountain, A. M., Frank, H. A., Liu, C., and Yuan, Y. W. (2016). An R2R3-MYB transcription factor regulates carotenoid pigmentation in *Mimulus lewisii* flowers. *New Phytol.* 209, 1049–1057. doi: 10.1111/nph.13647

Salem, M. A., Juppner, J., Bajdzienko, K., and Giavalisco, P. (2016). Protocol: a fast, comprehensive and reproducible one-step extraction method for the rapid preparation of polar and semi-polar metabolites, lipids, proteins, starch and cell wall polymers from a single sample. *Plant Methods* 12:45. doi: 10.1186/s13007-016-0146-2

Scarpeci, T. E., Zanor, M. I., Carrillo, N., Mueller-Roeber, B., and Valle, E. M. (2008). Generation of superoxide anion in chloroplasts of *Arabidopsis thaliana* during active photosynthesis: a focus on rapidly induced genes. *Plant Mol. Biol.* 66, 361–378. doi: 10.1007/s11103-007-9274-4

Schwartz, S. H., Tan, B. C., Gage, D. A., Zeevaart, J. A., and McCarty, D. R. (1997). Specific oxidative cleavage of carotenoids by VP14 of maize. *Science* 276, 1872–1874. doi: 10.1126/science.276.5320.1872

Seok, H. Y., Woo, D. H., Nguyen, L. V., Tran, H. T., Tarte, V. N., Mehdi, S. M., et al. (2017). Arabidopsis AtNAP functions as a negative regulator via repression of AREB1 in salt stress response. *Planta* 245, 329–341. doi: 10.1007/s00425-016-2609-0

Shannon, P., Markiel, A., Ozier, O., Baliga, N. S., Wang, J. T., Ramage, D., et al. (2003). Cytoscape: a software environment for integrated models of biomolecular interaction networks. *Genome Res.* 13, 2498–2504. doi: 10.1101/gr.1239303

Shi, Y., Guo, J., Zhang, W., Jin, L., Liu, P., Chen, X., et al. (2015). Cloning of the Lycopene beta-cyclase gene in *Nicotiana tabacum* and its overexpression confers salt and drought tolerance. *Int. J. Mol. Sci.* 16, 30438–30457. doi: 10.3390/ijms161226243

Smith, T. F., Gaitatzes, C., Saxena, K., and Neer, E. J. (1999). The WD repeat: a common architecture for diverse functions. *Trends Biochem. Sci.* 24, 181–185. doi: 10.1016/S0968-0004(99)01384-5

Subczynski, W. K., Markowska, E., and Sielewiesiuk, J. (1991). Effect of polar carotenoids on the oxygen diffusion-concentration product in lipid bilayers - an epr spin label study. *Biochim. Biophys. Acta* 1068, 68–72. doi: 10.1016/0005-2736(91)90061-C

Szklarczyk, D., Morris, J. H., Cook, H., Kuhn, M., Wyder, S., Simonovic, M., et al. (2017). The STRING database in 2017: quality-controlled protein-protein association networks, made broadly accessible. *Nucleic Acids Res.* 45, D362–D368. doi: 10.1093/nar/gkw937

Tanz, S. K., Castleden, I., Hooper, C. M., Vacher, M., Small, I., and Millar, H. A. (2013). SUBA3: a database for integrating experimentation and prediction to define the SUBcellular location of proteins in Arabidopsis. *Nucleic Acids Res.* 41, D1185–1191. doi: 10.1093/nar/gks1151

Thimm, O., Blasing, O., Gibon, Y., Nagel, A., Meyer, S., Kruger, P., et al. (2004). MAPMAN: a user-driven tool to display genomics data sets onto diagrams of metabolic pathways and other biological processes. *Plant J.* 37, 914–939.

Tran, L. S., Nakashima, K., Sakuma, Y., Simpson, S. D., Fujita, Y., Maruyama, K., et al. (2004). Isolation and functional analysis of Arabidopsis stress-inducible NAC transcription factors that bind to a drought-responsive cis-element in the early responsive to dehydration stress 1 promoter. *Plant Cell* 16, 2481–2498. doi: 10.1105/tpc.104.022699

Vrebalov, J., Pan, I. L., Arroyo, A. J. M., McQuinn, R., Chung, M., Poole, M., et al. (2009). Fleshy fruit expansion and ripening are regulated by the tomato SHATTERPROOF gene TAGL1. *Plant Cell* 21, 3041–3062. doi: 10.1105/tpc.109.066936

Welsch, R., Maass, D., Voegel, T., Dellapenna, D., and Beyer, P. (2007). Transcription factor RAP2.2 and its interacting partner SINAT2: stable elements in the carotenogenesis of Arabidopsis leaves. *Plant Physiol.* 145, 1073–1085. doi: 10.1104/pp.107.104828

Wisniewski, J. R., Zougman, A., Nagaraj, N., and Mann, M. (2009). Universal sample preparation method for proteome analysis. *Nat. Methods* 6, 359–362. doi: 10.1038/nmeth.1322

Wu, Y., Deng, Z., Lai, J., Zhang, Y., Yang, C., Yin, B., et al. (2009). Dual function of Arabidopsis ATAF1 in abiotic and biotic stress responses. *Cell Res.* 19, 1279–1290. doi: 10.1038/cr.2009.108

Yu, Y., Qian, Y., Jiang, M., Xu, J., Yang, J., Zhang, T., et al. (2020). Regulation mechanisms of plant basic leucine zippers to various abiotic stresses. *Front. Plant Sci.* 11:1258. doi: 10.3389/fpls.2020.01258

Yuan, H., Zhang, J., Nageswaran, D., and Li, L. (2015). Carotenoid metabolism and regulation in horticultural crops. *Hortic. Res.* 2:15036. doi: 10.1038/hortres.2015.36

Zhu, F., Luo, T., Liu, C. Y., Wang, Y., Yang, H. B., Yang, W., et al. (2017). An R2R3-MYB transcription factor represses the transformation of alpha- and beta-branch carotenoids by negatively regulating expression of CrBCH2 and CrNCED5 in flavedo of *Citrus reticulate*. *New Phytol.* 216, 178–192. doi: 10.1111/nph.14684

Zhu, M. K., Chen, G. P., Zhang, J. L., Zhang, Y. J., Xie, Q. L., Zhao, Z. P., et al. (2014a). The abiotic stress-responsive NAC-type transcription factor SlNAC4 regulates salt and drought tolerance and stress-related genes in tomato (*Solanum lycopersicum*). *Plant Cell Rep.* 33, 1851–1863. doi: 10.1007/s00299-014-1662-z

Zhu, M. K., Chen, G. P., Zhou, S., Tu, Y., Wang, Y., Dong, T. T., et al. (2014b). A new tomato NAC (NAM/ATAF1/2/CUC2) transcription factor, SlNAC4, functions as a positive regulator of fruit ripening and carotenoid accumulation. *Plant Cell Physiol.* 55, 119–135. doi: 10.1093/pcp/pct162

Conflict of Interest: The authors declare that the research was conducted in the absence of any commercial or financial relationships that could be construed as a potential conflict of interest.

frontiers in Plant Science

ORIGINAL RESEARCH
published: 12 May 2021
doi: 10.3389/fpls.2021.647507

Transformation of Long-Lived Albino *Epipremnum aureum* 'Golden Pothos' and Restoring Chloroplast Development

Chiu-Yueh Hung[1†], Jianhui Zhang[1†], Chayanika Bhattacharya[1], Hua Li[1], Farooqahmed S. Kittur[1], Carla E. Oldham[1], Xiangying Wei[2], Kent O. Burkey[3], Jianjun Chen[4] and Jiahua Xie[1]*

[1] Department of Pharmaceutical Sciences, Biomanufacturing Research Institute and Technology Enterprise, North Carolina Central University, Durham, NC, United States, [2] Institute of Oceanography, Minjiang University, Fuzhou, China, [3] USDA-ARS Plant Science Research Unit, Department of Crop and Soil Sciences, North Carolina State University, Raleigh, NC, United States, [4] Environmental Horticulture Department, Mid-Florida Research and Education Center, University of Florida, Apopka, FL, United States

OPEN ACCESS

Edited by:
Clelia De-la-Peña, Scientific Research Center of Yucatán (CICY), Mexico

Reviewed by:
Yanjun Dong, Shanghai Normal University, China
Sam-Geun Kong, Kongju National University, South Korea

***Correspondence:**
Jiahua Xie
jxie@nccu.edu

† These authors have contributed equally to this work

Specialty section:
This article was submitted to Plant Cell Biology, a section of the journal Frontiers in Plant Science

Received: *30 December 2020*
Accepted: *19 April 2021*
Published: *12 May 2021*

Citation:
Hung C-Y, Zhang J, Bhattacharya C, Li H, Kittur FS, Oldham CE, Wei X, Burkey KO, Chen J and Xie J (2021) Transformation of Long-Lived Albino Epipremnum aureum 'Golden Pothos' and Restoring Chloroplast Development. Front. Plant Sci. 12:647507. doi: 10.3389/fpls.2021.647507

Chloroplasts are organelles responsible for chlorophyll biosynthesis, photosynthesis, and biosynthesis of many metabolites, which are one of key targets for crop improvement. Elucidating and engineering genes involved in chloroplast development are important approaches for studying chloroplast functions as well as developing new crops. In this study, we report a long-lived albino mutant derived from a popular ornamental plant *Epipremnum aureum* 'Golden Pothos' which could be used as a model for analyzing the function of genes involved in chloroplast development and generating colorful plants. Albino mutant plants were isolated from regenerated populations of variegated 'Golden Pothos' whose albino phenotype was previously found to be due to impaired expression of *EaZIP*, encoding Mg-protoporphyrin IX monomethyl ester cyclase. Using petioles of the mutant plants as explants with a traceable *sGFP* gene, an efficient transformation system was developed. Expressing Arabidopsis *CHL27* (a homolog of *EaZIP*) but not *EaZIP* in albino plants restored green color and chloroplast development. Interestingly, in addition to the occurrence of plants with solid green color, plants with variegated leaves and pale-yellow leaves were also obtained in the regenerated populations. Nevertheless, our study shows that these long-lived albino plants along with the established efficient transformation system could be used for creating colorful ornamental plants. This system could also potentially be used for investigating physiological processes associated with chlorophyll levels and chloroplast development as well as certain biological activities, which are difficult to achieve using green plants.

Keywords: albino, *Epipremnum aureum* 'Golden Pothos', Mg-protoporphyrin IX monomethyl ester cyclase, long-lived, chlorophyll biosynthesis, chloroplast development, Agrobacterium-mediated transformation

INTRODUCTION

In plants, chloroplasts are important organelles, responsible for producing pigments, harvesting solar energy and generating various metabolites (Block et al., 2007; Terry and Smith, 2013; Pogson et al., 2015). Chloroplast biogenesis and functions require 2,500–3,500 proteins (Peltier et al., 2002; Block et al., 2007; Woodson and Chory, 2008), but its genome only encodes ∼100 proteins (Martin et al., 2002). The remaining over 95% of proteins are encoded by nuclear genes, which are synthesized in the cytosol and then imported into proplastids for chloroplast biogenesis, development, and function (Abdallah et al., 2000; Kleine et al., 2009; Pogson et al., 2015). Thus, understanding the roles of individual genes encoded by two separate genomes, their coordinated expressions, and the translocation of nuclear-encoded proteins during chloroplast development is fundamentally important for genetic engineering of plants in order to improve photosynthetic efficiency, plant growth, and seed and natural product production (Woodson and Chory, 2008; Bölter, 2018; Zoschke and Bock, 2018; Boehm and Bock, 2019).

So far, determining the roles of most nuclear-encoded plastid genes and elucidating mutual regulation of genes from two genomes during the chloroplast biogenesis and development remain big challenges because of the complexity and the lack of an effective experimental platform. Various experimental systems, such as dark-grown etiolated seedlings, various types of color-defective mutants including albino, variegated, and chemical/physical induced mutants, have been used for aforementioned studies (McCormac and Terry, 2004; Yu et al., 2007; Pogson et al., 2015; Zoschke et al., 2017). Among them, etiolated seedlings have been widely used to study the chloroplast biogenesis by monitoring the greening process in cotyledon cells upon exposure to light (Sinclair et al., 2017; Gommers and Monte, 2018; Armarego-Marriott et al., 2020). However, the transition from proplastids to chloroplasts is very quick and complex (Block et al., 2007; Woodson and Chory, 2008; Pogson et al., 2015; Bölter, 2018; Zoschke and Bock, 2018), and the expression of genes from both plastid and nuclear genomes is sharply induced (Jiao et al., 2007; Chen et al., 2010; Jing and Lin, 2020), which poses a problem to study spatially and temporally coordinated expressions of these genes during the chloroplast biogenesis.

Albino plants are also commonly used for studying chloroplast development and function. Previous studies show that albino plants derived from mutation together with their green counterparts are ideal genetic materials for identifying mutated genes involved in the chloroplast biogenesis and development. This has been demonstrated in a variety of albino mutants, such as barley *albostrians* (Hess et al., 1994; Li et al., 2019), maize *iojap* (Han et al., 1992), and *white seedling 3* (Hunter et al., 2018), Arabidopsis *seedling plastid development1* (Ruppel et al., 2011), as well as T-DNA insertion mutants Arabidopsis *pap3, pap6,* and *pap7* (Steiner et al., 2011), rice *albino Leaf1* (Zhang et al., 2016) and *albino Leaf2* (Liu et al., 2016), and tomato *wls-2297* (García-Alcázar et al., 2017). Albino mutants are also considered as ideal materials for studying mechanisms underlying chloroplast biogenesis and development (Dunford and Walden, 1991; Pfalz and Pfannschmidt, 2012; Hayashi-Tsugane et al., 2014; Yang et al., 2019). Some of them have been used to shed the light on pathways involved in chloroplast biogenesis, such as the retrograde signaling (Bradbeer et al., 1979; Börner, 2017), plastid protein import machinery (Shipman-Roston et al., 2010; Li et al., 2019), and light signal regulated genes in albino plants (Grübler et al., 2017). Chemically induced and tissue culture-derived albino plants have been used to understand the development of stomatal complex (Hernández-Castellano et al., 2020), stomatal opening and functioning (Roelfsema et al., 2006), the role of blue or red light in regulating flowering (Jabben and Deitzer, 1979; Bavrina et al., 2002), and the effects of carotenoid-derived molecules on root development patterning (Van Norman et al., 2014). Although albino plants occur in nature and can also be obtained in laboratory through somaclonal variation by cell and tissue culture, induction by physical and chemical mutagenesis, and genetic engineering, a distinct characteristic of the albino plants is that the majority of them are usually short-lived even though they are maintained on culture media with high sucrose (Dunford and Walden, 1991; Zubko and Day, 1998; Ruppel et al., 2011; Steiner et al., 2011; García-Alcázar et al., 2017). The short-lived nature of these plants is a shortcoming for their applications as an experimental platform to study the coordinated expressions of nuclear and plastid genes.

Long-lived albino plants having capacity to be switched from aberrant plastids to functional chloroplasts are desirable. Because they could be used as an experimental platform for investigating genes related to the chloroplast development and monitoring the translocation of nuclear-encoded plastid proteins during the greening process. Moreover, long-lived albino plants could be useful to solve certain biological questions where chlorophyll effects should be avoided. Recently, plants are emerging as alternative expression system to replace mammalian one for producing a diverse range of biopharmaceuticals (Xu et al., 2012; Moon et al., 2020). The long-lived albino plants can also be an ideal expression system to express high-value compounds and therapeutic proteins to avoid chlorophyll interference during the purification process (Wilken and Nikolov, 2012; Mellor et al., 2018). However, there are no reports on long-lived albino plants with exception of three recent studies from perennial Agave (*Agave angustifolia* Haw.) in which created albino plants are surely long-lived even though their life span was not indicated (Duarte-Aké et al., 2016; Us-Camas et al., 2017; Hernández-Castellano et al., 2020). One possibility for the lack of long-lived albino plants could be due to the life span of their parental species since most of albino mutants are derived from either annual or biennial plant species. Thus, we postulated that using perennial, vegetatively growing, non-flowering and long-lived pothos plants (*Epipremnum aureum*) (Hung and Xie, 2009; Hung et al., 2016) to develop albino plants could be a better choice. To this end, we regenerated albino plants from a variegated variety 'Golden Pothos' by tissue culture techniques (Hung and Xie, 2009). Regenerated albino plants (**Figure 1A**) have been propagated and maintained for more than 11 years in our laboratory despite being rootless. Our previous studies indicated that they have impaired expression of *EaZIP* encoding

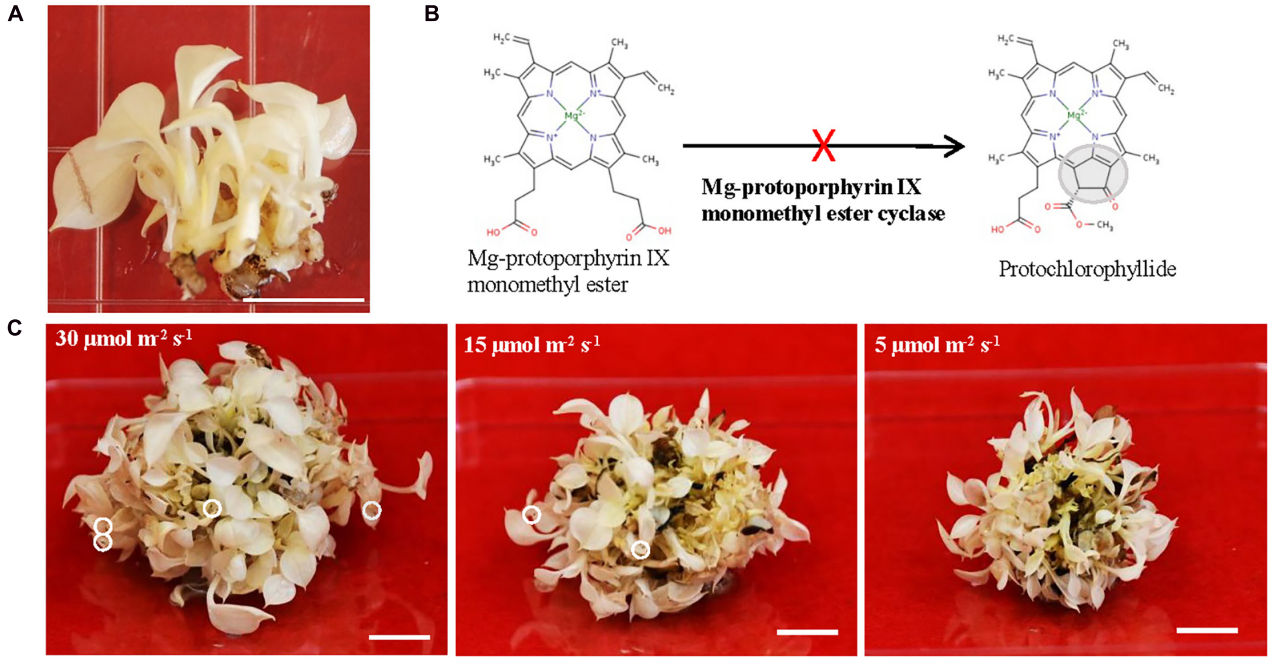

FIGURE 1 | The growth of albino plants and the involvement of *EaZIP*. **(A)** Albino plantlets. **(B)** Impaired *EaZIP* in chlorophyll biosynthesis pathway. **(C)** Albino plantlets were grown under ~30, 15, and 5 μmol m^{-2} s^{-1} light intensity at 23°C for 4 weeks. The white circle indicates damaged leaf-tip. Bar = 1 cm.

Mg-protoporphyrin IX monomethyl ester (MPE) cyclase, a key enzyme in the chlorophyll biosynthesis pathway (**Figure 1B**; Hung et al., 2010). Impaired expression of MPE cyclase is thought to cause defective leaf color and result in colorless plastids in various plant species (Tottey et al., 2003; Liu et al., 2004; Rzeznicka et al., 2005; Hung et al., 2010).

In view of the importance of MPE cyclase, we hypothesized that compensating *EaZIP* expression in regenerated albino plants would potentially synthesize sufficient chlorophylls for plastid development and restore the normal green phenotype. In the present study, we first expressed traceable *sGFP* gene (Chiu et al., 1996) in albino plants for developing a transformation method. We then overexpressed *EaZIP* driven by a constitutive promoter CaMV35S (*35S:EaZIP*) in albino plants to restore the normal green phenotype. However, it did not generate any green transgenic plants. When Arabidopsis *CHL27*, a homolog of *EaZIP*, driven by the CaMV35S promoter (*35S:CHL27*) was expressed, both the defective color and dysfunctional chloroplast development were restored in albino plants. Intriguingly, expressing *CHL27* in albino plants produced various leaf colors of regenerated transgenic plants. For ornamental plants, color is one of the most important traits to add value to a new cultivar (Chen et al., 2005). Generally, colorful ornamental plants are produced from green plants via natural or artificial mutation, somaclonal variation, or genetic engineering (Marcotrigiano, 1997; Van Harten, 1998; Chen and Henny, 2006; Zhao et al., 2012). The present study presents a new strategy for producing colorful plants by genetically engineering of long-lived albino plants. Potential mechanisms of developing different color plants and application of long-lived albino plants were discussed.

MATERIALS AND METHODS

Plant Maintenance

Albino plantlets were derived from variegated leaves of *E. aureum* 'Golden Pothos' by tissue culture techniques (Hung and Xie, 2009). They were propagated in a maintenance medium containing MS salts with vitamins (Research Products International, Mount Prospect, IL, United States), 10 mg/L ascorbic acid, 25 g/L sucrose, and 5 g/L agar with pH adjusted to 5.6 and grown at 23°C under a constant light intensity of 5 μmol m^{-2} s^{-1}. The plantlets were maintained by transferring onto fresh medium once a month. To observe the effects of light intensity on their growth, equal-sized clusters of albino plantlets were cultured on the maintenance medium at 23°C under full spectrum light with the intensities of 30, 15, and 5 μmol m^{-2} s^{-1}, respectively for a month before they were photographed. Regenerated green transgenic plants were transplanted to soil after rooting.

Creation of Genetic Cassettes

The *sGFP* genetic cassette, CEJ899, was kindly provided by Professor Deyu Xie of North Carolina State University. The *EaZIP* genetic cassette, CEJ1260, was created by replacing *GUS* in commercial vector pBI121 (Clontech, Mountain View, CA, United States) with *EaZIP* coding region (Accession #: FJ666046) (Hung et al., 2010). The *CHL27* genetic cassette, CEJ1264, was created by replacing *GUS* in pBI121 with *Arabidopsis thaliana CHL27* coding region (Accession #:

NM_115553) (Salanoubat et al., 2000). The sequence alignment of cDNAs of *EaZIP* and Arabidopsis *CHL27* is presented in **Supplementary Figure 1**. After cloning, both inserted genes were sequenced for validation before used for transformation. Each plasmid DNA was introduced into *Agrobacterium tumefaciens* strain LBA4404 using the freeze–thaw method (Holsters et al., 1978).

Plant Transformation

For *Agrobacterium*-mediated transformation, our previous transformation system developed for green *E. aureum* 'Jade' (Zhao et al., 2013b) was modified. Briefly, petiole segments were excised from albino plantlets and infected with *Agrobacterium* solution (OD_{600} of 0.8) containing 100 μM acetosyringone for 10 min. Then infected petiole segments were co-cultured on induction medium containing MS salts with vitamins (Research Products International), 2 mg/L *N*-(2-chloro-4-pyridl)-*N*'-phenylurea (CPPU), 0.2 mg/L α-naphthalene acetic acid (NAA), 10 mg/L ascorbic acid, 25 g/L sucrose, and 5 g/L agar (pH 5.6) in the dark. After 7-day co-culture, they were transferred onto the selection medium which is the induction medium with additional 75 mg/L kanamycin and 100 mg/L Timentin. Only one callus from each explant was isolated for the regeneration. Induced calli were transferred onto regeneration medium which is the selection medium without hormones.

Genomic DNA PCR, RT-PCR, and qRT-PCR

Shoots maintained on regeneration medium were harvested and stored at −80°C for genomic DNA and total RNA isolation. The DNeasy Plant Mini Kit (Qiagen, Germantown, MD, United States) was used for isolating genomic DNA. The RNeasy Plant Mini Kit (Qiagen) was used for isolating total RNA. Further treatment of DNase I and first strand cDNA synthesis were performed using SuperScript™ IV VILO™ master mix with ezDNase™ enzyme (Invitrogen, Carlsbad, CA, United States). For PCR and RT-PCR, the reactions were carried out with *Taq* DNA polymerase (Sigma Aldrich, St. Louis, MO, United States) and specific primers: NPTIIF 5′-AAGATGGATTGCACGCAGGTTC-3′ and NPTIIR 5′-ACGGGTAGCCAACGCTATGTC-3′ for the *nptII*; GFPF 5′-GAGCTGGACGGCGACGTAAA-3′ and GFPR 5′-GTGTCGCCCTCGAACTTCAC-3′ for the *GFP*; EaZIPF 5′-ACGAAGGCTAGGCAGTACAC-3′ and NosR1 5′-AAATGTATAATTGCGGGACTCT-3′ for the *EaZIP*; and CHL27F 5′-ACAACCAGACACATTTCGTGA-3′ and CHL27R 5′-ACGTCGACGAGCTCCTAATAGA-3′ for the *CHL27*. For qRT-PCR, the procedure was the same as described previously (Hung et al., 2016), while the specific primers are EaZIP-qF 5′-AGACTGAAGACATTCCCCTGGTAA-3′ and EaZIP-qR 5′-CTCAGAGACTAGTGCTGCGATGA-3′ for the *EaZIP*; and CHL27-qF 5′-GTGGTTCGGTTTGTCTCGAT-3′ and CHL27-qR 5′-ACGTCGACGAGCTCCTAATAGA-3′ for the *CHL27*. The QuantumRNA™ 18S Internal Standards (Ambion, Austin, TX, United States) was used as an endogenous control.

GFP Imaging and Transmission Electron Microscopy (TEM) Analysis

The GFP fluorescence detected in transgenic plants were captured under fluorescence microscope (Keyence, Osaka, Japan). To observe the chloroplast ultra-structures in leaf tissues, TEM analysis was performed at the Center for Electron Microscopy of North Carolina State University. Fully expanded young leaves from baby jar grown plants were cut into 1 mm^3 blocks and then fixed in 3% glutaraldehyde in 0.05 M KPO_4 buffer, pH 7 at 4°C. All samples were rinsed in three 30-min changes of cold 0.05 M KPO_4 buffer, pH 7, then post-fixed in 2% OsO_4 in the same buffer at 4°C in the dark. After dehydrated with graded series of ethanol (30, 50, 70, 95, and 100%), samples were infiltrated with Spurr's resin (Ladd Research Industries, Williston, VT, United States), flat embedded and cured at 70°C overnight. Samples were sectioned with a Leica UC6rt ultramicrotome (Leica Microsystems, Wetzlar, Germany) and placed onto 200-mesh grids. The grids were then stained with 4% aqueous uranyl acetate in the dark at 25°C followed by three times of warm distilled water (40°C) washes and 1 min in Reynold's lead citrate followed by three more warm distilled water washes. All sections were observed under a JEOL JEM 1200EX transmission electron microscope (JEOL, Peabody, MA, United States). Images were captured using a Gatan Erlangshen Model 785 ES1000W camera and Digital Micrograph software (Gatan, Pleasanton, CA, United States).

Immunoblotting Analysis

For detecting the presence of GFP protein in transgenic lines, the total proteins were first extracted from mature leaf tissues using the Plant Total Protein Extraction kit (Sigma-Aldrich). The protein extract was then subjected to SDS-PAGE. They were heated with NuPAGE™ LDS sample buffer containing 10% reducing agent (500 mM DTT) at 70°C for 10 min, then analyzed under a NuPAGE™ 4–12% Bis-Tris gel with a MES SDS running buffer containing antioxidant as instructed by the manufacturer. For immunoblotting, proteins were transferred onto a PVDF membrane (Bio-Rad, Hercules, CA, United States). The membrane was then blocked at 25°C for 1 h with 15% (w/v) dry milk dissolved in PBST. It was then incubated at 25°C for 1 h with 1:200 diluted primary antibody anti-GFP (B-2) (sc-9996; Santa Cruz Biotechnology, Dallas, TX, United States) followed by incubation in the secondary antibody Goat anti-Rabbit IgG horseradish peroxidase conjugate (Bio-Rad). The luminescent signals were generated after incubation with SuperSignal® West Pico Chemiluminescent substrate (Pierce biotechnology, Rockford, IL, United States) and captured by Kodak Biomax X-ray film (PerkinElmer, Waltham, MA, United States). For staining the PVDF membrane, 0.2% (w/v) Amido Black 10B (MP Biomedicals, Santa Ana, CA, United States) in 10% (v/v) acidic acid was used.

Measurement of Chlorophylls

For extracting chlorophylls, the mature leaf tissues were first ground in liquid nitrogen then resuspended in 80% acetone as described in Hung and Xie (2009). After centrifugation,

the clear supernatant was collected and diluted 10x in acetone before reading their absorption wavelengths using SpectraMax Plus 384 (Molecular Devices, San Jose, CA, United States). The chlorophyll content was calculated based on the formula described by Hanfrey et al. (1996). All results were presented as the average of three biological replicates ± SD. Statistical significance was analyzed by comparing all pairs using Tukey-kramer HSD ($p < 0.05$).

RESULTS

Albino Plants Are Long-Lived and Grow Well Under Low Light

To explore the potential applications of regenerated albino plants, we optimized their growth conditions in order to have healthy plants for downstream studies. They were propagated and maintained on Murashige and Skoog (MS) medium (Murashige and Skoog, 1962) with 25 g/L sucrose as a carbon source and addition of 10 mg/L ascorbic acid. Ascorbic acid was used as an antioxidant agent, which is due to the notion that albino plants lacking functional chloroplasts are unable to carry out photosynthesis and more sensitive to the photo-oxidation (Spoehr, 1942; Hess et al., 1994; García-Alcázar et al., 2017). Initially, regenerated plants from color defective leaf sectors were pale yellow and had rooting capacity (Hung and Xie, 2009). However, they gradually lost pale yellow color and rooting capacity, and became albino plants without roots (**Figure 1A**). We found that they grew slowly but well under low light (5 μmol m^{-2} s^{-1}) on MS medium with addition of 10 mg/L ascorbic acid. Although growths were much faster under high light conditions (15 and 30 μmol m^{-2} s^{-1}), there were signs of cell damage on the tip of leaves (**Figure 1C**). Because of the high light associated cell damage, low light conditions were chosen for growth and maintenance. Since then they have grown and been successfully propagated for more than 11 years and could be considered as long-lived albino plants in comparison with other known albino plants (Hess et al., 1994; Ruppel et al., 2011; Liu et al., 2016; Zhang et al., 2016; García-Alcázar et al., 2017).

Albino Plants Can Be Easily Transformed With a High Transformation Efficiency

After establishing the optimal growth conditions for the albino plants, a transformation system to produce stable albino transgenic plants was developed. We adopted our previous *Agrobacterium*-mediated transformation system developed for green pothos plants (Zhao et al., 2013b) with three major changes. Briefly, *nptII* was used to replace *hpt* as a selection gene (**Figure 2A**), 75 mg/L kanamycin was used for screening transgenic plants, and ascorbic acid was supplemented into induction, selection and regeneration media to prevent oxidative damage.

Transformation results showed that visible kanamycin resistant calli first appeared after 4 weeks on selection medium (**Figure 2B**). The average callus induction rate observed after 8 weeks of subculture was ∼52% (**Table 1**), which was higher than green pothos plants (Zhao et al., 2013b). After growing for an additional 4–6 weeks, calli were transferred onto a regeneration medium. After about 2 weeks, newly regenerated white shoots appeared (**Figure 2B**). To confirm the presence of transgenes *sGFP* and *nptII* in these regenerated white shoots, seven independent kanamycin-resistant lines (**Figure 2C**) were examined by PCR and the results showed that both genes were detected in all lines (**Figure 2D**). To confirm the expression of *sGFP*, RT-PCR and immunoblotting analyses were performed. The expression of *sGFP* was confirmed in all seven lines by RT-PCR (**Figure 2E**). Immunoblotting results based on equal loading of total proteins further confirmed the presence of GFP protein in five out of seven lines which had high transcript levels (**Figure 2F**). The GFP fluorescence was also observed in regenerated plants (**Figure 2G**). These results indicate that albino plants can be stably transformed with a high transformation efficiency.

Overexpressing *EaZIP* Did Not Change the Albino Phenotype

Our previous study suggested that no expression of *EaZIP* could be responsible for the loss of green color in albino plants (Hung et al., 2010). We found that the albino plants accumulated MPE, the substrate of the MPE cyclase, when they were fed with 5-aminolevulinic acid, the first committed intermediate of the porphyrin synthesis pathway. These results indicate that the albino plants lack functional MPE cyclase. Our previous cloning effort obtained an *EaZIP* from green pothos (Hung et al., 2010), which lacks a sequence region encoding a *N*-terminal chloroplast transit peptide (cTP). When overexpressing the cloned *EaZIP* in wild type tobacco plants which carry the *NtZIP* also lacking 5′-end sequence coding for a cTP (Liu et al., 2004), surprisingly we found transgenic plants showing variegated phenotype (Guan et al., 2017). However, whether the cloned *EaZIP* is a functional version or not has not been tested. To determine if overexpression of the *EaZIP* could restore green color, we first overexpressed *EaZIP* in albino plants (**Figure 3A**).

Following *EaZIP* overexpression, no green shoots were observed among all regenerated plantlets. These regenerants were derived from 31 independent kanamycin-resistant calli grown with or without light exposure (**Table 1**), even though the growth of kanamycin-resistant calli and regenerated shoots was robust (**Figure 3B**) with a high transformation rate of 69% (**Table 1**). To confirm the presence and expression of transgenes in these regenerated plantlets, PCR and RT-PCR were performed. The presence and expression of *EaZIP* were confirmed in all selected seven lines (**Figures 3C,D**). The finding that overexpressing *EaZIP* was unable to restore the chlorophyll production complements with our previous study that overexpressing the *EaZIP* caused normal green tobacco plants to become variegated (Guan et al., 2017). The results from these two studies implied that the cloned *EaZIP* might be defective. One possible reason might be the lack of cTP. For

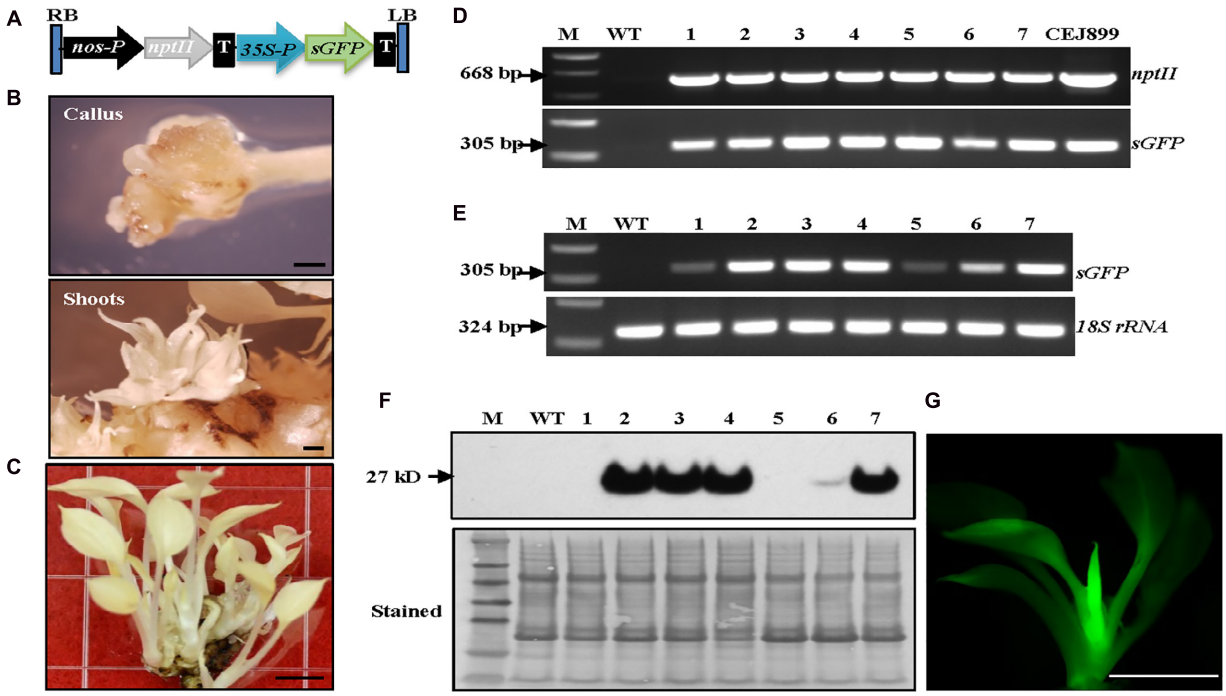

FIGURE 2 | Establishment of *Agrobacterium*-mediated transformation system in albino plants expressing *sGFP*. **(A)** Genetic cassette CEJ899 with *sGFP* driven by CaMV35S promoter (35S-P) and *nptII* driven by *nos* promoter (nos-P). T, nos terminator; RB, right border; LB, left border. **(B)** Induced calli and shoots. Bar = 1 mm. **(C)** Regenerated transgenic plantlets. Bar = 5 mm. **(D)** Genomic DNA PCR and **(E)** RT-PCR of seven individual transgenic lines (1–7) amplified by specific primer pairs for *nptII* and *sGFP*, respectively, using *18S rRNA* as an internal control. M, molecular marker; WT, wild-type albino plant. **(F)** Immunoblot against anti-GFP. Stained blot shows equal protein loading. **(G)** GFP fluorescence of a transgenic plantlet. Bar = 5 mm.

TABLE 1 | The induction rates of kanamycin-resistant calli and subsequently regenerated shoots.

Transgene	Batch	No. of explants	No. of explants with calli	Callus induction rate (%)	Average ± SD (%)	No. of tested calli*	No. of tested calli with green shoots	No. of tested calli with white shoots	Shoot induction rate (%)
sGFP	I	62	33	53.2					
	II	35	10	28.6	51.7 ± 22.4	17 (26%)	0	17	100
	III	30	22	73.3					
EaZIP	I	32	21	65.6					
	II	36	29	80.6	69.2 ± 10.1	31 (45%)	0	31	100
	III	31	19	61.3					
CHL27	I	40	35	87.5					
	II	35	30	85.7	88.1 ± 2.8	22 (23%)	17	5	100
	III	34	31	91.2					

**Calli obtained from batch I, II and III were randomly selected for the shoot induction experiment.*

further testing, using a functional Arabidopsis *CHL27* with a cTP (Tottey et al., 2003) could be an alternative.

Introducing Arabidopsis *CHL27* in Albino Plants Restored Chlorophyll Biosynthesis

The function of Arabidopsis *CHL27* has been fully characterized (Tottey et al., 2003). We reasoned that expressing *CHL27* in albino plants might restore chlorophyll biosynthesis. Positive results would demonstrate that the impaired expression of *EaZIP* could be responsible for albino phenotype. To test this hypothesis, we created a genetic cassette by replacing *EaZIP* with *CHL27* (**Figure 4A**). The transformation rate was high at ∼88% (**Table 1**). When 22 kanamycin-resistant calli with 0.5–1 cm diameters were exposed to light for approximately 2 weeks, cells with green color started to appear (**Figure 4B**), and subsequently green shoots emerged (**Figure 4B**) in 17 individual calli (**Table 1**). Rooting capacity was also recovered in *CHL27* transgenic plants, which allowed them to grow well in soil (**Figure 4D**). To confirm these green shoots (**Figure 4C**) expressing *CHL27*, PCR, and RT-PCR were performed in seven lines. The PCR and RT-PCR

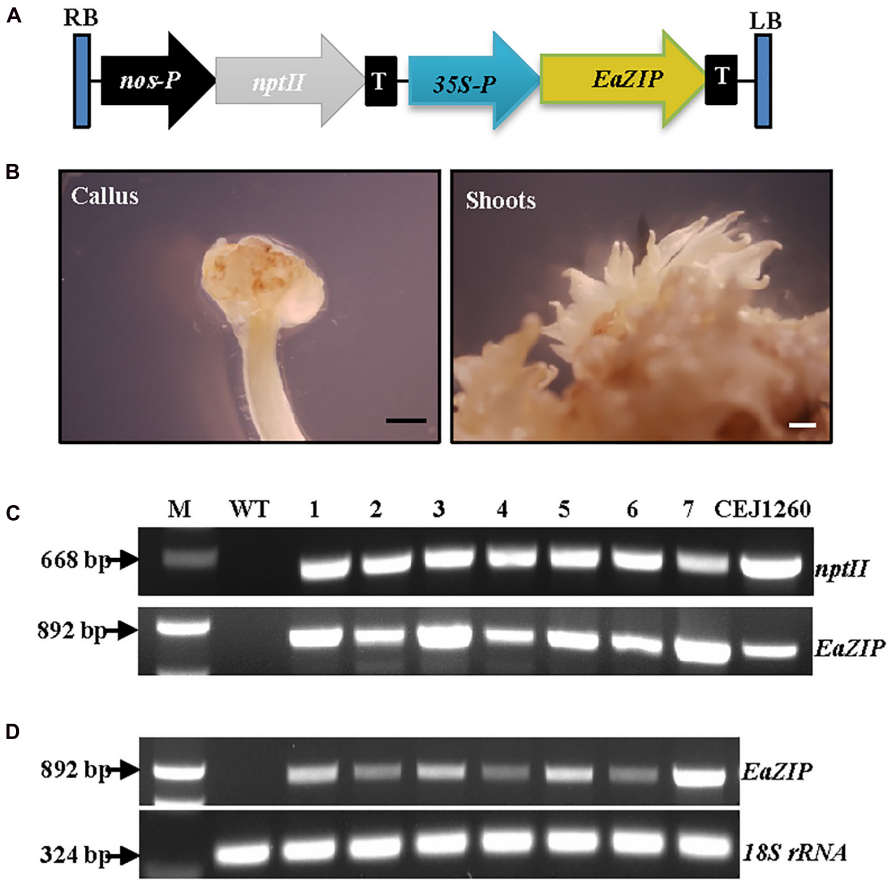

FIGURE 3 | Overexpression of *EaZIP* in albino plants. **(A)** Genetic cassette CEJ1260 with *EaZIP* driven by CaMV35S promoter (35S-P). The remaining annotations are the same as in **Figure 2A**. **(B)** Induced calli and shoots. Bar = 1 mm. **(C)** Genomic DNA PCR and **(D)** RT-PCR of seven individual transgenic lines (1–7) amplified by specific primer pairs for *nptII* and *EaZIP*, respectively, using *18S rRNA* as an internal control. M, molecular marker; WT, wild-type albino plant.

results showed that all green shoots carried (**Figure 4E**) and expressed (**Figure 4F**) *CHL27*. These results confirm that the cTP is required and a functional form of *EaZIP* with cTP may be present in green pothos cells.

The Leaf Color and Chlorophyll Levels of Created Transgenic Plants Correlate Well With the Expression of *CHL27*

We observed that the majority of regenerated shoots derived from the same transgenic callus had three types of leaves: pure green (PG), variegated (V), and pale yellow (PY) (**Figure 4C**). Different leaf colors appeared in regenerated plants were relatively stable when they grew under the same growth conditions (**Figure 5**). This phenomenon, however, did not appear in tissue culture regenerated pothos green and albino plants (**Figure 6**) where calli derived from green or albino explants generated uniform green or white color shoots. To determine whether the leaf color correlates with the expression of *CHL27*, three types (PG, V, and PY) of transgenic plants from the same transgenic line (**Figure 7**) were used to measure the contents of chlorophylls and quantify the expression levels of *CHL27*. Their ultra-structures of leaf cells were also examined since chlorophylls are required for chloroplast biogenesis, such as for assembly and maintenance of photosynthetic apparatus and stacking of thylakoid membranes (Eckhardt et al., 2004; Block et al., 2007).

The results showed that the chlorophyll *a* and *b* levels in PG transgenic plants were 3.4 and 1.25 mg/g FW, respectively (**Table 2**). They were elevated from undetectable in initial wild-type albino plants to 64% of levels found in pothos green plants regenerated from tissue culture. Although the total contents of chlorophylls were less, the chlorophyll *a*/*b* ratio was the same as in pothos green plants (**Table 2**). The chlorophyll *a* and *b* levels of V (1.72 and 0.86 mg/g FW) and PY (0.28 and 0.03 mg/g FW) transgenic plants were lower than those of pothos green and PG transgenic plants, but higher than those of wild-type albino plants. In addition, the chlorophyll *a*/*b* ratios of PY transgenic plants were in average of 8.14 which was abnormal compared to green plants ranging around 2.7 (**Table 2**). The stable chlorophyll *a*/*b* ratio is important and thought to be very critical to acclimate to changes in light conditions (Rudiger, 2002). When the expression levels of *CHL27* were quantified by qRT-PCR in three types of transgenic plants as well as wild-type green and albino plants,

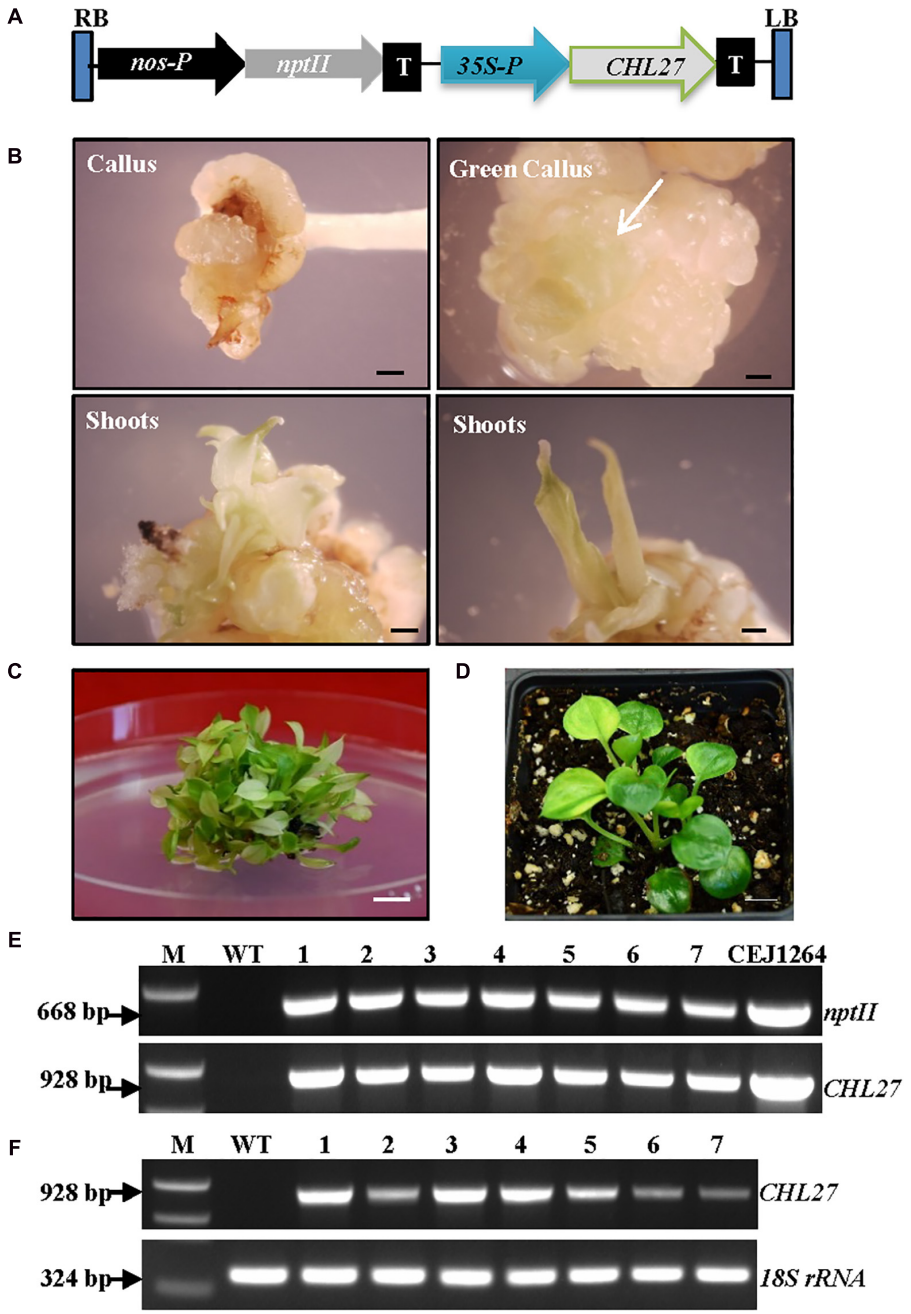

FIGURE 4 | Expression of *CHL27* in albino plants. **(A)** Genetic cassette CEJ1264 with *CHL27* driven by CaMV35S promoter (35S-P). The remaining annotations are the same as in **Figure 2A**. **(B)** Induced calli from petiole explant, and propagated green calli (white arrow) and shoots. Bar = 1 mm. **(C)** Mixed green and pale yellow shoots. Bar = 1 cm. **(D)** Regenerated green *CHL27* transgenic plant. Bar = 1 cm. **(E)** Genomic DNA PCR and **(F)** RT-PCR of seven individual transgenic lines (1–7) amplified by specific primer pairs for *nptII* and *CHL27*, respectively, using *18S rRNA* as an internal control. M, molecular marker; WT, wild-type albino plant.

the levels of PG transgenic plants were 3.7- and 6.2-fold higher than those of V and PY plants, respectively (**Table 3**). As for pothos endogenous *EaZIP*, qRT-PCR result showed that comparing to pothos green plants, none of the wild type albino and *CHL27* PG, V and PY transgenic plants had detectable *EaZIP* (**Table 3**). These results further indicate that transgenic plants with different colors correlate well the restored levels of chlorophylls, which were indeed contributed from the level of *CHL27* expression.

When ultra-structures were examined under the TEM, leaf cells from PG transgenic plants exhibited normal chloroplasts (**Figure 7**) but had fewer grana and more unstacked thylakoids compared to those of pothos green plants (**Figure 6A**). Leaf cells of V transgenic plants had completely developed

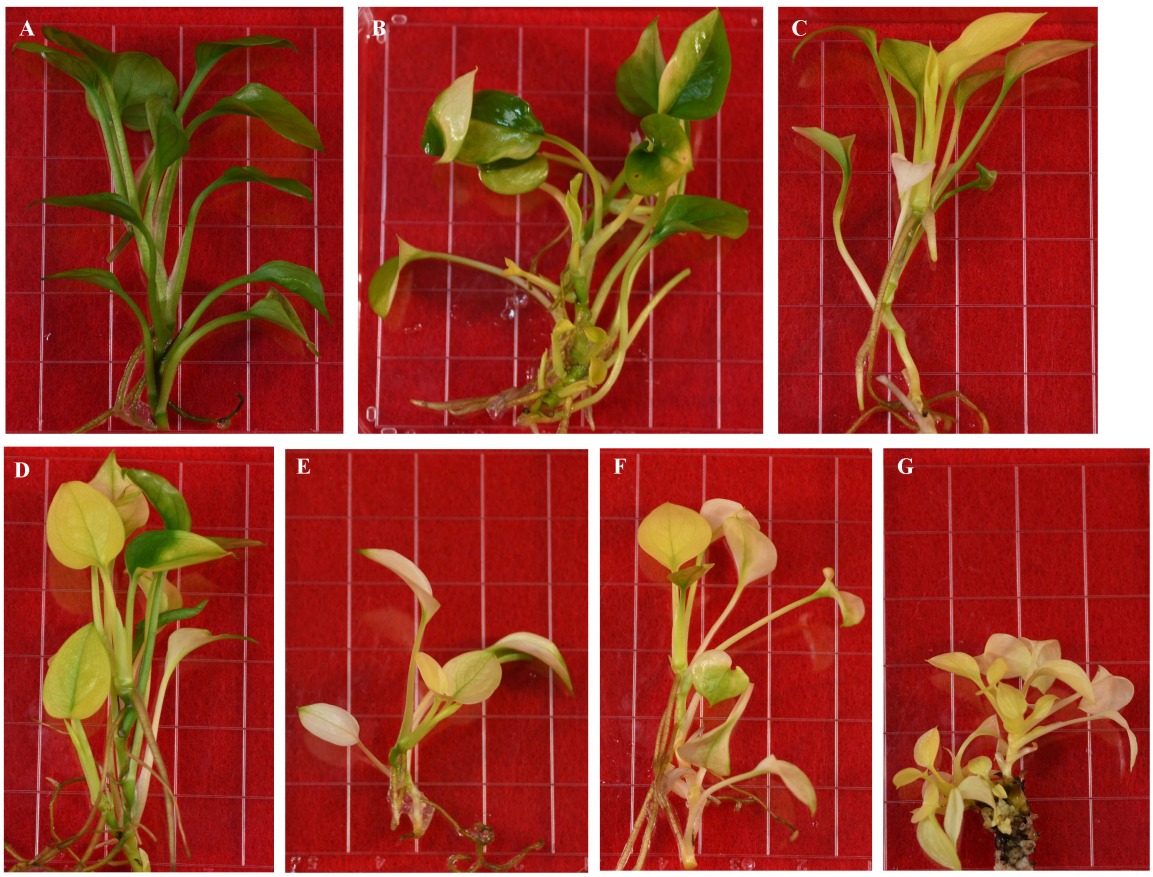

FIGURE 5 | Regenerated transgenic plants from the same transformed callus expressing Arabidopsis *CHL27*. **(A)** Pure green. **(B–D)** Variegated. **(E–G)** Pale yellow.

chloroplasts, but only a few developed thylakoids. As for leaf cells of PY transgenic plants, they contained partially developed chloroplasts (**Figure 7**), which were different from those in wild-type albino leaf cells with only plastids (**Figure 6B**). Both partially developed chloroplasts in PY transgenic plants and plastids in wild-type albino plants did not have developed thylakoids. The numbers of thylakoids and the degrees of their stacking correlate with the chlorophyll *a* and *b* contents in these three types of *CHL27* transgenic plants, which agrees with the important roles of chlorophyll *a* and *b* in chloroplast development. These results prove that both defective color and dysfunctional chloroplast development in albino plants can be restored by compensating the loss of MPE cyclase.

DISCUSSION

The present study demonstrates that albino plants regenerated from *E. aureum* 'Golden Pothos' are long-lived when maintained in a modified MS culture medium under low light conditions (**Figure 1**). Albino plants occur in a wide range of plants including Arabidopsis (Ruppel et al., 2011), maize (Han et al., 1992; Hunter et al., 2018), barley (Hess et al., 1994; Li et al., 2019), rice (Liu et al., 2016; Zhang et al., 2016), tomato (García-Alcázar et al., 2017), Agave (Duarte-Aké et al., 2016; Us-Camas et al., 2017), *Artemisia vulgaris* (Knudson and Lindstrom, 1919; Spoehr, 1942), *Sequoia sempervirens* (Pittermann et al., 2018), *Cucumis sativus* (Yan et al., 2020), and *Pyrola japonica* (Shutoh et al., 2020). However, none was reported to have extended life span as the albino pothos. Although *S. sempervirens* and *P. japonica* can survive for a prolonged time, albino shoots of the former were derived from sprouts while the latter had symbiotic relationships with fungi. The longest individual albino plants survived on culture medium are Agave plants (∼5 years) (Duarte-Aké et al., 2016; Hernández-Castellano et al., 2020), followed by *A. vulgaris* with a life span of 3 months (Rischkow and Bulanowa, 1931) and maize plants of less than 4 months (Spoehr, 1942) while the former one should be long-lived. A consensus is drawn that individual albino plants are unable to perform photosynthesis; hence they die after stored energy is exhausted. Unlike albino pothos and Agave, most albino plants could not live long for years even though they are maintained on culture media with high sucrose (Dunford and Walden, 1991; Zubko and Day, 1998; Ruppel et al., 2011; Steiner et al., 2011; García-Alcázar et al., 2017), which raises a question concerning the involvement of other factors besides photosynthesis as a sole factor. One possible factor could be the life span of parental plants since most of them

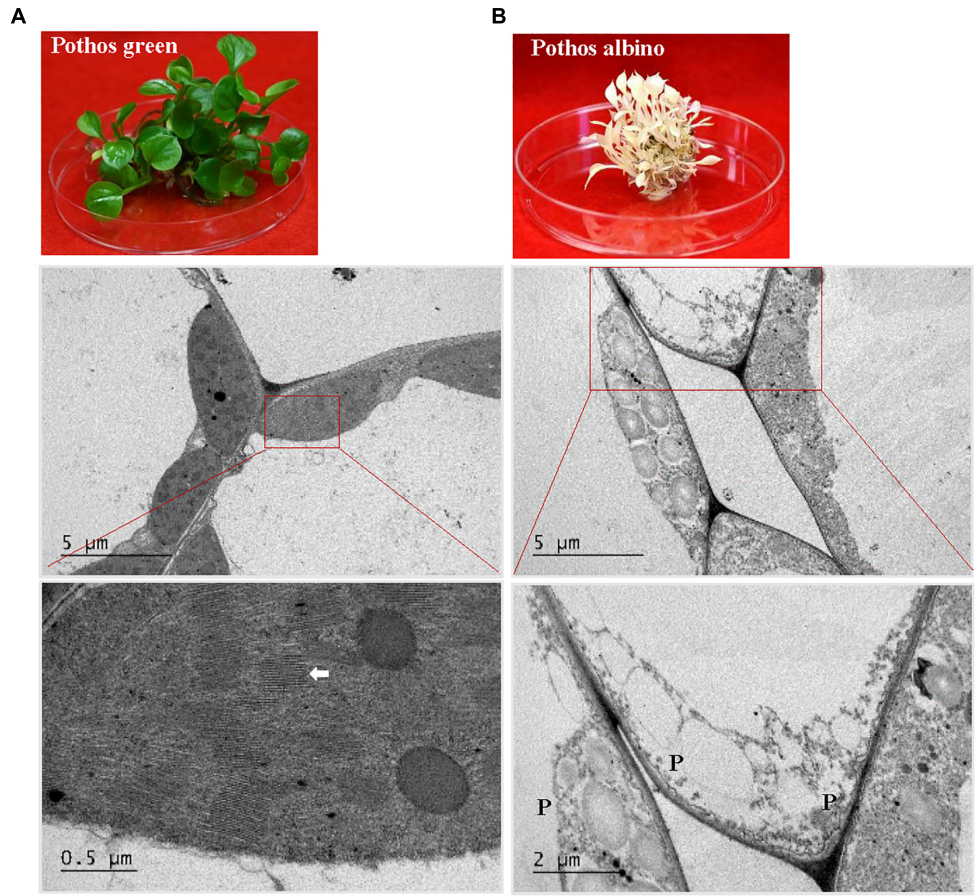

FIGURE 6 | TEM analysis of chloroplast development in 'Pothos' wild type leaf cells. **(A)** 'Pothos' green and **(B)** albino plants from tissue culture (above) and TEM of their leaf cells (below). Red lines indicate the enlarged area. White arrow: detailed thylakoids; P: plastid.

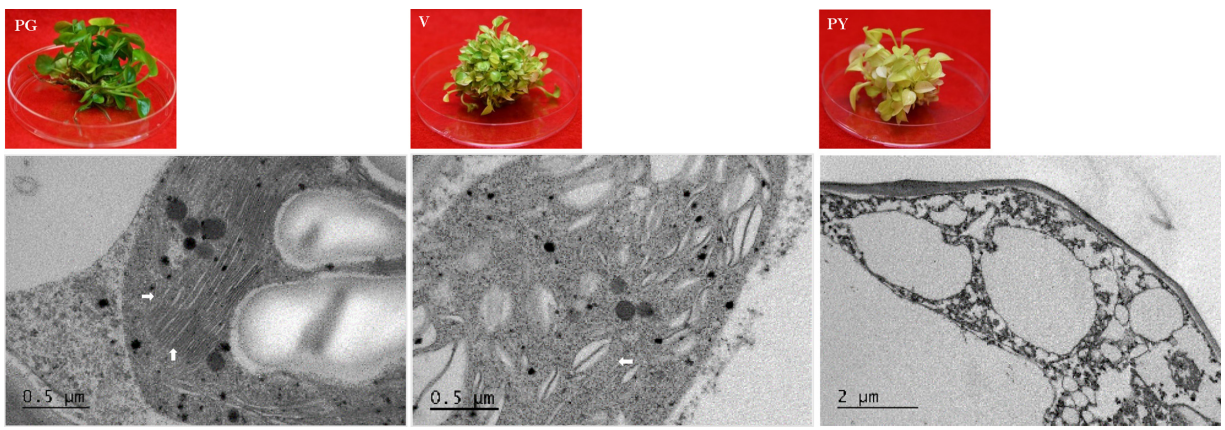

FIGURE 7 | TEM analysis of chloroplast development in 'Pothos' transgenic leaf cells. *CHL27* transgenic plants from single transformation event with pure green (PG), variegated (V) and pale yellow (PY) leaf colors (left), and TEM (right) of their thylakoids (marked by white arrows).

are annual and biennial species while 'Golden Pothos' plants are vegetatively growing and non-flowering perennial vines (Hung et al., 2016). Other factors could be the ability of plants to tolerate low light and absorb nutrients. Pothos plants are produced as houseplants for indoor decoration, and they are able to grow under low light conditions with limited nutrient supply (Chen et al., 2005). Other albino plants, such as *A. vulgaris* and maize inherently require high light intensity and abundant nutrient

TABLE 2 | Chlorophyll *a* and *b* contents*.

FW (mg/g)	Pothos green	Pothos albino	PG	V	PY
Chl *a*	5.32 ± 0.80^{a}	0.01 ± 0.01^{d}	3.40 ± 0.64^{b}	1.72 ± 0.08^{c}	0.28 ± 0.05^{d}
Chl *b*	1.94 ± 0.06^{a}	0.01 ± 0.01^{d}	1.25 ± 0.22^{b}	0.86 ± 0.05^{c}	0.03 ± 0.02^{d}
Chl *a* + *b*	7.26 ± 0.83^{a}	0.02 ± 0.02^{d}	4.65 ± 0.85^{b}	2.59 ± 0.11^{c}	0.31 ± 0.07^{d}
Chl *a*/*b*	2.74	0.59	2.71	1.99	8.14

**Data represent the average of biological replicates ± SD (n = 3). Different letters represent significant differences at $p < 0.05$ level.*

supply to grow. Once they are unable to conduct photosynthesis, they had little ability to absorb sugar and other nutrients from *in vitro* culture conditions as little increase in their fresh weight was observed (Rischkow and Bulanowa, 1931; Spoehr, 1942), thus they died in 3–4 months. Although albino pothos plants lost their ability to form roots during the continuous subculture, they grew well with a vigorous regeneration of new shoots in the modified MS culture medium, indicating that the albino pothos plants are able to absorb sugar and nutrients from the culture medium.

The albino pothos plants not only survived more than 11 years but also can be used for regeneration. Moreover, its active regeneration can be used for genetic transformation of a foreign gene with great efficiency. The defective color, dysfunctional chloroplast development and rooting capacity were restored by expressing Arabidopsis *CHL27*. The expression of *CHL27* resulted in the restoration of complete green as well as variegated plants. Pothos is among the most popular houseplants used in indoor conditions for decoration (Henny and Chen, 2003). Its interior use has been shown to abate indoor air pollutants (Sawada and Oyabu, 2008; Tada et al., 2010). Thus, there is increasing demand for new pothos cultivars around the world. However, due to its non-flowering nature, new cultivars cannot be developed through hybridization (Henny and Chen, 2003). Thus far, only four pothos cultivars in the market (Zhao et al., 2013a). The present study showed that using albino plants as materials, plants with different leaf colors can be produced, and the degree of color restoration is dependent on the level of *CHL27* expression. Additionally, these albino plants could also be used directly to express color related genes, such as Arabidopsis PAP1 (production of anthocyanin pigment 1) gene (*AtPAP1*) for red/purple color (He et al., 2017), and Chinese cabbage *BrMYB2* gene for purple color (He et al., 2020), to produce colorful plants. Thus, this established system could be used to generate different types of transgenic plants for developing new colorful pothos cultivars.

TABLE 3 | Quantitative RT-PCR of *CHL27* and *EaZIP**.

Samples	*CHL27* Δ Ct (n = 3)	Fold changes	*EaZIP* ΔCt (n = 3)	Fold changes
Pothos green	ND	–	9.1 ± 1.9	1
Pothos albino	ND	–	21.9 ± 2.7	−7287.7
PG	9.3 ± 0.8	1	21.4 ± 0.8	−5093.8
V	11.1 ± 0.2	−3.7	22.3 ± 0.9	−9567.4
PY	11.8 ± 0.3	−6.2	22.9 ± 1.3	−13840.3

**The data represent the average of ΔCt compared to their internal control ± SD (n = 3). Fold change is determined as $2^{(\Delta\Delta ct)}$ and calculated using PG as 1 for CHL27, and pothos green control as 1 for EaZIP. Negative fold change indicates reduced gene expression. ND: not detected.*

It is unclear at this time why the same transformation resulted in different types of plants. One possibility could be inappropriate coordination or interactions between the expressed foreign *CHL27* nuclear genes and other endogenous genes. This study show that overexpressing *EaZIP* failed to restore green color in transgenic plants (**Figure 3**). This failure could be attributed to the *EaZIP* cDNA without 5′-end sequence coding for the cTP. This *EaZIP* without cTP was initially cloned from green pothos through 5′RACE-PCR techniques (Hung et al., 2010). The expression of this *EaZIP* in green-leaved tobacco produced variegated transgenic plants (Guan et al., 2017). In addition to this cTP-lacking *EaZIP*, pothos might have a functional form of *EaZIP* with sequences encoding the *N*-terminal cTP. The interactions of *CHL27* with functional and non-functional *EaZIP* may cause the variation among the transgenic populations. Other possibilities could be epigenetic effects as reported in Agave plants (Duarte-Aké et al., 2016; Us-Camas et al., 2017). DNA methylation has been found to be intensive in pothos (Chen, unpublished data), it is possible that epigenetics through methylation is implicated the variation among regenerated plants. Future research is warranted to identify the underlying mechanisms.

As far as is known, this is the first report of successful stable transformation of an albino plant. In addition to be used for new pothos cultivar development, the albino plants along with the established transformation system could be valuable for studying critical events in chloroplast development. One example of such applications is to create inducible transgenic albino plants by controlling the expression levels of *CHL27* or a functional form of *EaZIP* under an inducible promoter. These inducible transgenic albino plants, which would keep white color under un-induced conditions but turn green under induced conditions, can be used as an experimental platform to study nuclear genes for plastid involved in chloroplast biogenesis and development. Those could be *E. aureum* genes or genes from different species with the exception of some species-specifically regulated. With this inducible platform, co-expression of a test gene with a fluorescent protein tag can be observed in co-transformed cells/tissues via live-cell imaging techniques (Wada and Suetsugu, 2004; Day and Davidson, 2009). Inducible co-transformed albino plants could be used not only to study the expression site(s) of the test gene but also to monitor the translocation process of its encoded protein during the chloroplast biogenesis under induced conditions. These albino plants could also be used to unravel biological questions, such as the effects of pigments on root development

and light quality on plant development, where chlorophyll effects must be avoided or controlled as demonstrated previously (Jabben and Deitzer, 1979; Bavrina et al., 2002; Roelfsema et al., 2006; Van Norman et al., 2014). Recently, plants are becoming a promising expression system to produce a diverse range of biopharmaceuticals (Xu et al., 2012; Moon et al., 2020). Likewise, they can also be used to express high-value compounds and therapeutic proteins to facilitate downstream purification process without chlorophyll interference (Wilken and Nikolov, 2012; Mellor et al., 2018).

DATA AVAILABILITY STATEMENT

The original contributions presented in the study are included in the article/**Supplementary Material**, further inquiries can be directed to the corresponding author.

AUTHOR CONTRIBUTIONS

C-YH and JX conceived and designed the experiments. C-YH, JZ, CB, HL, FK, and XW performed the experiments. C-YH, CEO, KOB, JC, and JX analyzed the data. C-YH, JC, and JX wrote the article with contributions of all authors. All authors read and approved the manuscript, contributed to the article, and approved the submitted version.

FUNDING

Research conducted in these studies was supported by National Science Foundation grant (HRD-1400946) to JX and CEO, and National Institute of General Medical Sciences grant (SC1GM111178-01A1) to JX.

ACKNOWLEDGMENTS

We thank Valerie Lapham for the help of electron microscopy.

SUPPLEMENTARY MATERIAL

The Supplementary Material for this article can be found online at: https://www.frontiersin.org/articles/10.3389/fpls.2021.647507/full#supplementary-material

Supplementary Figure 1 | Sequence alignment of the cDNAs of *EaZIP* (without cTP) (Accession #: FJ666046) and Arabidopsis *CHL27* (Accession #: NM_115553).

REFERENCES

Abdallah, F., Salamini, F., and Leister, D. (2000). A prediction of the size and evolutionary origin of the proteome of chloroplasts of Arabidopsis. *Trends Plant Sci.* 5, 141–142. doi: 10.1016/s1360-1385(00)01574-0

Armarego-Marriott, T., Sandoval-Ibañez, O., and Kowalewska, Ł (2020). Beyond the darkness: recent lessons from etiolation and de-etiolation studies. *J. Exp. Bot.* 71, 1215–1225. doi: 10.1093/jxb/erz496

Bavrina, T. V., Lozhnikova, V. N., Culafic, L., and Zhivanovich, B. (2002). Flowering of cultivated green and SAN 9789-treated *Chenopodium rubrum* plants exposed to white, blue, and red light. *Russ. J. Plant Physiol.* 49, 460–464. doi: 10.1023/A:1016347622722

Block, M. A., Douce, R., Joyard, J., and Rolland, N. (2007). Chloroplast envelope membranes: a dynamic interface between plastids and the cytosol. *Photosynth. Res.* 92, 225–244. doi: 10.1007/s11120-007-9195-8

Boehm, C. R., and Bock, R. (2019). Recent advances and current challenges in synthetic biology of the plastid genetic system and metabolism. *Plant Physiol.* 179, 794–802. doi: 10.1104/pp.18.00767

Bölter, B. (2018). En route into chloroplasts: preproteins' way home. *Photosynth. Res.* 138, 263–275. doi: 10.1007/s11120-018-0542-8

Börner, T. (2017). The discovery of plastid-to-nucleus retrograde signaling—a personal perspective. *Protoplasma* 254, 1845–1855. doi: 10.1007/s00709-017-1104-1

Bradbeer, J. W., Atkinson, Y. E., Börner, T., and Hagemann, R. (1979). Cytoplasmic synthesis of plastid polypeptides may be controlled by plastid-synthesised RNA. *Nature* 279, 816–817. doi: 10.1038/279816a0

Chen, J., and Henny, R. J. (2006). "Somaclonal variation: an important source for cultivar development of floriculture crops," in *Floriculture, Ornamental and Plant Biotechnology*, ed. J. A. Teixeira da Silva, (London, UK: Global Science Books), 244–253.

Chen, J., McConnell, D. B., Norman, D. J., and Henny, R. J. (2005). The foliage plant industry. *Hort Rev.* 31, 45–110. doi: 10.1002/9780470650882.ch2

Chen, M., Galvão, R. M., Li, M., Burger, B., Bugea, J., Bolado, J., et al. (2010). Arabidopsis HEMERA/pTAC12 initiates photomorphogenesis by phytochromes. *Cell* 141, 1230–1240. doi: 10.1016/j.cell.2010.05.007

Chiu, W., Niwa, Y., Zeng, W., Hirano, T., Kobayashi, H., and Sheen, J. (1996). Engineered GFP as a vital reporter in plants. *Curr. Biol.* 6, 325–330. doi: 10.1016/S0960-9822(02)00483-9

Day, R. N., and Davidson, M. W. (2009). The fluorescent protein palette: tools for cellular imaging. *Chem. Soc. Rev.* 38, 2887–2921. doi: 10.1039/b901966a

Duarte-Aké, F., Castillo-Castro, E., Pool, F. B., Espadas, F., Santamaría, J. M., Robert, M. L., et al. (2016). Physiological differences and changes in global DNA methylation levels in *Agave angustifolia* Haw. albino variant somaclones during the micropropagation process. *Plant Cell Rep.* 35, 2489–2502. doi: 10.1007/s00299-016-2049-0

Dunford, R., and Walden, R. M. (1991). Plastid genome structure and plastid-related transcript levels in albino barley plants derived from another culture. *Curr. Genet.* 20, 339–347. doi: 10.1007/BF00318524

Eckhardt, U., Grimm, B., and Hortensteiner, S. (2004). Recent advances in chlorophyll biosynthesis and breakdown in higher plants. *Plant Mol. Biol.* 56, 1–14. doi: 10.1007/s11103-004-2331-3

García-Alcázar, M., Giménez, E., Pineda, B., Capel, C., García-Sogo, B., Sánchez, S., et al. (2017). Albino T-DNA tomato mutant reveals a key function of 1-deoxy-D-xylulose-5-phosphate synthase (DXS1) in plant development and survival. *Sci. Rep.* 7:45333. doi: 10.1038/srep45333

Gommers, C. M., and Monte, E. (2018). Seedling establishment: a dimmer switch-regulated process between dark and light signaling. *Plant physiol.* 176, 1061–1074. doi: 10.1104/pp.17.01460

Grübler, B., Merendino, L., Twardziok, S. O., Mininno, M., Allorent, G., Chevalier, F., et al. (2017). Light and plastid signals regulate different sets of genes in the albino mutant pap7-1. *Plant Physiol.* 175, 1203–1219. doi: 10.1104/pp.17.00982

Guan, X., Li, Z., Zhang, Z., Wei, X., Xie, J., Chen, J., et al. (2017). Overexpression of an *EaZIP* gene devoid of transit peptide sequence induced leaf variegation in tobacco. *PLoS ONE* 12:e0175995. doi: 10.1371/journal.pone.0175995

Han, C. D., Coe, E. H. Jr., and Martienssen, R. A. (1992). Molecular cloning and characterization of iojap (ij), a pattern striping gene of maize. *EMBO J.* 11, 4037–4046. doi: 10.1002/j.1460-2075.1992.tb05497.x

Hanfrey, C., Fife, M., and Buchanan-Wollaston, V. (1996). Leaf senescence in *Brassica napus*: expression of genes encoding pathogenesis-related proteins. *Plant Mol. Biol.* 30, 597–609. doi: 10.1007/BF00049334

Hayashi-Tsugane, M., Takahara, H., Ahmed, N., Himi, E., Takagi, K., Iida, S., et al. (2014). A mutable albino allele in rice reveals that formation of thylakoid membranes requires the *SNOW-WHITE LEAF1* gene. *Plant Cell Physiol.* 55, 3–15. doi: 10.1093/pcp/pct149

He, X., Li, Y., Lawson, D., and Xie, D. Y. (2017). Metabolic engineering of anthocyanins in dark tobacco varieties. *Physiol. Plant* 159, 2–12. doi: 10.1111/ppl.12475

He, Q., Wu, J., Xue, Y., Zhao, W., Li, R., and Zhang, L. (2020). The novel gene *BrMYB2*, located on chromosome A07, with a short intron 1 controls the purple-head trait of Chinese cabbage (*Brassica rapa* L.). *Hortic. Res.* 7:97. doi: 10.1038/s41438-020-0319-z

Henny, R. J., and Chen, J. J. (2003). *Plant Breeding Reviews: Cultivar Development of Ornamental Foliage Plants*, Vol. 23. Oxford: John Wiley & Sons, 245–290.

Hernández-Castellano, S., Garruña-Hernández, R., Us-Camas, R., Kú-Gonzalez, Á, and De-la-Peña, C. (2020). *Agave angustifolia* albino plantlets lose stomatal physiology function by changing the development of the stomatal complex due to a molecular disruption. *Mol. Genet. Genom.* 295, 787–805. doi: 10.1007/s00438-019-01643-y

Hess, W. R., Müller, A., Nagy, F., and Börner, T. (1994). Ribosome-deficient plastids affect transcription of light-induced nuclear genes: genetic evidence for a plastid-derived signal. *Mol. Gen. Genet.* 242, 305–312. doi: 10.1007/BF00280420

Holsters, M., De Waele, D., Depicker, A., Messens, E., Van Montagu, M., and Schell, J. (1978). Transfection and transformation of *Agrobacterium tumefaciens*. *Mol. Gen. Genet.* 163, 181–187. doi: 10.1007/BF00267408

Hung, C. Y., and Xie, J. H. (2009). A comparison of plants regenerated from a variegated *Epipremnum aureum*. *Biol. Plant* 53, 610–616. doi: 10.1007/s10535-009-0112-1

Hung, C. Y., Sun, Y. H., Chen, J., Darlington, D. E., Williams, A. L., Burkey, K. O., et al. (2010). Identification of a Mg-protoporphyrin IX monomethyl ester cyclase homologue, EaZIP, differentially expressed in variegated *Epipremnum aureum* 'Golden Pothos' is achieved through a unique method of comparative study using tissue regenerated plants. *J. Exp. Bot.* 61, 1483–1493. doi: 10.1093/jxb/erq020

Hung, C. Y., Qiu, J., Sun, Y. H., Chen, J., Kittur, F. S., Henny, R. J., et al. (2016). Gibberellin deficiency is responsible for shy-flowering nature of *Epipremnum aureum*. *Sci. Rep.* 6:28598. doi: 10.1038/srep28598

Hunter, C. T., Saunders, J. W., Magallanes-Lundback, M., Christensen, S. A., Willett, D., Stinard, P. S., et al. (2018). Maize w3 disrupts homogentisate solanesyl transferase (ZmHst) and reveals a plastoquinone-9 independent path for phytoene desaturation and tocopherol accumulation in kernels. *Plant J.* 93, 799–813. doi: 10.1111/tpj.13821

Jabben, M., and Deitzer, G. F. (1979). Effects of the herbicide San-9789 on photomorphogenic responses. *Plant Physiol.* 63, 481–485. doi: 10.1104/pp.63.3.481

Jiao, Y., Lau, O. S., and Deng, X. W. (2007). Light-regulated transcriptional networks in higher plants. *Nat. Rev. Genet.* 8, 217. doi: 10.1038/nrg2049

Jing, Y., and Lin, R. (2020). Transcriptional regulatory network of the light signaling pathways. *New Phytol.* 227, 683–697. doi: 10.1111/nph.16602

Kleine, T., Voigt, C., and Leister, D. (2009). Plastid signaling to the nucleus: messengers still lost in the mists? *Trends Genet.* 25, 185–192. doi: 10.1016/j.tig.2009.02.004

Knudson, L., and Lindstrom, E. W. (1919). Influence of sugars on the growth of albino plants. *Am. J. Bot.* 6, 401–405.

Li, M., Hensel, G., Mascher, M., Melzer, M., Budhagatapalli, N., Rutten, T., et al. (2019). Leaf variegation and impaired chloroplast development caused by a truncated CCT domain gene in albostrians barley. *Plant Cell* 31, 1430–1445. doi: 10.1105/tpc.19.00132

Liu, N., Yang, Y. T., Liu, H. H., Yang, G. D., Zhang, N. H., and Zheng, C. C. (2004). NTZIP antisense plants show reduced chlorophyll levels. *Plant Physiol. Biochem.* 42, 321–327. doi: 10.1016/j.plaphy.2004.02.007

Liu, C., Zhu, H., Xing, Y., Tan, J., Chen, X., Zhang, J., et al. (2016). Albino Leaf 2 is involved in the splicing of chloroplast group I and II introns in rice. *J. Exp. Bot.* 67, 5339–5347. doi: 10.1093/jxb/erw296

Marcotrigiano, M. (1997). Chimeras and variegation: patterns of deceit. *HortScience* 32, 773–784. doi: 10.21273/HORTSCI.32.5.773

Martin, W., Rujan, T., Richly, E., Hansen, A., Cornelsen, S., Lins, T., et al. (2002). Evolutionary analysis of Arabidopsis, cyanobacterial, and chloroplast genomes reveals plastid phylogeny and thousands of cyanobacterial genes in the nucleus. *Proc. Natl. Acad. Sci. U S A* 99, 12246–12251. doi: 10.1073/pnas.182432999

McCormac, A. C., and Terry, M. J. (2004). The nuclear genes Lhcb and HEMA1 are differentially sensitive to plastid signals and suggest distinct roles for the GUN1 and GUN5 plastid-signalling pathways during de-etiolation. *Plant J.* 40, 672–685. doi: 10.1111/j.1365-313X.2004.02243.x

Mellor, S. B., Behrendorff, J. B., Nielsen, A. Z., Jensen, P. E., and Pribil, M. (2018). Non-photosynthetic plastids as hosts for metabolic engineering. *Essays Biochem.* 62, 41–50. doi: 10.1042/EBC20170047

Moon, K. B., Park, J. S., Park, Y. I., Song, I. J., Lee, H. J., Cho, H. C., et al. (2020). Development of systems for the production of plant-derived biopharmaceuticals. *Plants* 9:30. doi: 10.3390/plants9010030

Murashige, T., and Skoog, F. (1962). A revised medium for rapid growth and bioassays with tobacco tissue cultures. *Physiol. Plant.* 15, 473–479. doi: 10.1111/j.1399-3054.1962.tb08052.x

Peltier, J. B., Emanuelsson, O., Kalume, D. E., Ytterberg, J., Friso, G., Rudella, A., et al. (2002). Central functions of the lumenal and peripheral thylakoid proteome of Arabidopsis determined by experimentation and genome-wide prediction. *Plant Cell* 14, 211–236. doi: 10.1105/tpc.010304

Pfalz, J., and Pfannschmidt, T. (2012). Essential nucleoid proteins in early chloroplast development. *Trends Plant Sci.* 18, 186–194. doi: 10.1016/j.tplants.2012.11.003

Pittermann, J., Cowan, J., Kaufman, N., Baer, A., Zhang, E., and Kuty, D. (2018). The water relations and xylem attributes of albino redwood shoots (*Sequoia sempervirens* (D. Don.) Endl.). *PLoS ONE* 13:e0191836. doi: 10.1371/journal.pone.0191836

Pogson, B. J., Ganguly, D., and Albrecht-Borth, V. (2015). Insights into chloroplast biogenesis and development. *Biochim. Biophys. Acta Bioenerg.* 1847, 1017–1024. doi: 10.1016/j.bbabio.2015.02.003

Rischkow, V., and Bulanowa, M. (1931). Uber sterile kulturen von Albinos. *Planta* 12, 144–146.

Roelfsema, M. R. G., Konrad, K. R., Marten, H., Psaras, G. K., Hartung, W., and Hedrich, R. (2006). Guard cells in albino leaf patches do not respond to photosynthetically active radiation, but are sensitive to blue light, CO_2 and abscisic acid. *Plant Cell. Environ.* 29, 1595–1605. doi: 10.1111/j.1365-3040.2006.01536.x

Rudiger, W. (2002). Biosynthesis of chlorophyll b and the chlorophyll cycle. *Photosynth. Res.* 74, 187–193. doi: 10.1023/A:1020959610952

Ruppel, N. J., Logsdon, C. A., Whippo, C. W., Inoue, K., and Hangarter, R. P. (2011). A mutation in Arabidopsis *SEEDLING PLASTID DEVELOPMENT1* affects plastid differentiation in embryo-derived tissues during seedling growth. *Plant Physiol.* 155, 342–353. doi: 10.1104/pp.110.161414

Rzeznicka, K., Rzeznicka, K., Walker, C. J., Westergren, T., Kannangara, C. G., von Wettstein, D., et al. (2005). *Xantha-l* encodes a membrane subunit of the aerobic Mg-protoporphyrin IX monomethyl ester cyclase involved in chlorophyll biosynthesis. *Proc. Natl. Acad. Sci. U S A* 102, 5886–5891. doi: 10.1073/pnas.0501784102

Salanoubat, M., Lemcke, K., Rieger, M., Ansorge, W., Unseld, M., Fartmann, B., et al. (2000). Sequence and analysis of chromosome 3 of the plant *Arabidopsis thaliana*. *Nature* 408, 820–822. doi: 10.1038/35048706

Sawada, A., and Oyabu, Y. (2008). Purification characteristics of pothos for airborne chemicals in growing conditions and its evaluation. *Atmospheric Environ.* 42, 594–602. doi: 10.1016/j.atmosenv.2007.10.028

Shipman-Roston, R. L., Ruppel, N. J., Damoc, C., Phinney, B. S., and Inoue, K. (2010). The significance of protein maturation by plastidic type I signal peptidase 1 for thylakoid development in Arabidopsis chloroplasts. *Plant Physiol.* 152, 1297–1308. doi: 10.1104/pp.109.151977

Shutoh, K., Tajima, Y., Matsubayashi, J., Tayasu, I., Kato, S., Shiga, T., et al. (2020). Evidence for newly discovered albino mutants in a pyroloid: implication for the nutritional mode in the genus *Pyrola*. *Amer. J. Bot.* 107, 650–657. doi: 10.1002/ajb2.1462

Sinclair, S. A., Larue, C., Bonk, L., Khan, A., Castillo-Michel, H., Stein, R. J., et al. (2017). Etiolated seedling development requires repression of photomorphogenesis by a small cell-wall-derived dark signal. *Curr. Biol.* 27, 3403–3418. doi: 10.1016/j.cub.2017.09.063

Spoehr, H. A. (1942). The culture of albino maize. *Plant Physiol.* 17:397. doi: 10.1104/pp.17.3.397

Steiner, S., Schröter, Y., Pfalz, J., and Pfannschmidt, T. (2011). Identification of essential subunits in the plastid-encoded RNA polymerase complex reveals building blocks for proper plastid development. *Plant physiol.* 157, 1043–1055. doi: 10.1104/pp.111.184515

Tada, Y., Tanaka, Y., and Matsuzaki, T. (2010). Isolation and characterization of formaldehyde-responsive genes from golden pothos (*Epipremnum aureum*). *Plant Biotechnol.* 27, 325–331. doi: 10.5511/plantbiotechnology.27.325

Terry, M. J., and Smith, A. G. (2013). A model for tetrapyrrole synthesis as the primary mechanism for plastid-to-nucleus signaling during chloroplast biogenesis. *Front. Plant Sci.* 4:14. doi: 10.3389/fpls.2013.00014

Tottey, S., Block, M. A., Allen, M., Westergren, T., Albrieux, C., Scheller, H. V., et al. (2003). Arabidopsis CHL27, located in both envelope and thylakoid membranes, is required for the synthesis of protochlorophyllide. *Proc. Natl. Acad. Sci.U S A* 100, 16119–16124. doi: 10.1073/pnas.2136793100

Us-Camas, R., Castillo-Castro, E., Aguilar-Espinosa, M., Limones-Briones, V., Rivera-Madrid, R., Robert-Díaz, M. L., et al. (2017). Assessment of molecular and epigenetic changes in the albinism of *Agave angustifolia* Haw. *Plant Sci.* 263, 156–167. doi: 10.1016/j.plantsci.2017.07.010

Van Harten, A. M. (1998). *Mutation Breeding: Theory and Practical Aapplication*. Cambridge, UK: Cambridge University Press.

Van Norman, J. M., Zhang, J., Cazzonelli, C. I., Pogson, B. J., Harrison, P. J., Bugg, T. D., et al. (2014). Periodic root branching in Arabidopsis requires synthesis of an uncharacterized carotenoid derivative. *Proc. Natl. Acad. Sci. U S A* 111, E1300–E1309. doi: 10.1073/pnas.1403016111

Wada, M., and Suetsugu, N. (2004). Plant organelle positioning. *Curr. Opin. Plant Biol.* 7, 626–631. doi: 10.1016/j.pbi.2004.09.005

Wilken, L. R., and Nikolov, Z. L. (2012). Recovery and purification of plant-made recombinant proteins. *Biotechnol. Adv.* 30, 419–433. doi: 10.1016/j.biotechadv.2011.07.020

Woodson, J. D., and Chory, J. (2008). Coordination of gene expression between organellar and nuclear genomes. *Nat. Rev. Genet.* 9, 383–395. doi: 10.1038/nrg2348

Xu, J., Dolan, M. C., Medrano, G., Cramer, C. L., and Weathers, P. J. (2012). Green factory: plants as bioproduction platforms for recombinant proteins. *Biotechnol. Adv.* 30, 1171–1184. doi: 10.1016/j.biotechadv.2011.08.020

Yan, J., Liu, B., Cao, Z., Sun, P., Liu, W., Liang, Z., et al. (2020). A novel cucumber albino mutant caused by chloroplast development deficiency. doi: 10.21203/rs.3.rs-20991/v1

Yang, E. J., Yoo, C. Y., Liu, J., Wang, H., Cao, J., Li, F. W., et al. (2019). NCP activates chloroplast transcription by controlling phytochrome-dependent dual nuclear and plastidial switches. *Nat. Commun.* 10:2630. doi: 10.1038/s41467-019-10517-1

Yu, F., Fu, A., Aluru, M., Park, S., Xu, Y., Liu, H., et al. (2007). Variegation mutants and mechanisms of chloroplast biogenesis. *Plant Cell Environ.* 30, 350–365. doi: 10.1111/j.1365-3040.2006.01630.x

Zhang, Z., Tan, J., Shi, Z., Xie, Q., Xing, Y., Liu, C., et al. (2016). Albino Leaf1 that encodes the sole octotricopeptide repeat protein is responsible for chloroplast development. *Plant Physiol.* 171, 1182–1191. doi: 10.1104/pp.16.00325

Zhao, J., Li, Z. T., Chen, J., Henny, R. J., Gray, D. J., and Chen, J. (2013a). Purple-leaved *Ficus lyrata* plants produced by overexpressing a grapevine *VvMybA1* gene. *Plant Cell Rep.* 32, 1783–1793. doi: 10.1007/s00299-013-1491-5

Zhao, J., Li, Z. T., Cui, J., Henny, R. J., Gray, D. J., Xie, J., et al. (2013b). Efficient somatic embryogenesis and *Agrobacterium*-mediated transformation of pothos (*Epipremnum aureum*) 'Jade'. *Plant Cell Tiss. Organ Cult.* 114, 237–247. doi: 10.1007/s11240-013-0319-x

Zhao, J., Zhang, Q., Xie, J., Hung, C., Cui, J., Henny, R. J., et al. (2012). Plant regeneration via direct somatic embryogenesis from leaf and petiole explants of *Epipremnum aureum* 'Marble Queen' and characterization of selected variants. *Acta Physiol. Plant.* 34, 1461–1469. doi: 10.1007/s11738-012-0944-8

Zoschke, R., Chotewutmontri, P., and Barkan, A. (2017). Translation and co-translational membrane engagement of plastid-encoded chlorophyll-binding proteins are not influenced by chlorophyll availability in maize. *Front. Plant Sci.* 8:385. doi: 10.3389/fpls.2017.00385

Zoschke, R., and Bock, R. (2018). Chloroplast translation: structural and functional organization, operational control, and regulation. *Plant Cell* 30, 745–770. doi: 10.1105/tpc.18.00016

Zubko, M. K., and Day, A. (1998). Stable albinism induced without mutagenesis: a model for ribosome-free plastid inheritance. *Plant J.* 15, 265–271.

Conflict of Interest: The authors declare that the research was conducted in the absence of any commercial or financial relationships that could be construed as a potential conflict of interest.

frontiers in Plant Science

REVIEW
published: 26 July 2021
doi: 10.3389/fpls.2021.691295

Nanotechnology Approaches for Chloroplast Biotechnology Advancements

*Gregory M. Newkirk[1,2], Pedro de Allende[1], Robert E. Jinkerson[1,3] and Juan Pablo Giraldo[1]**

[1]Department of Botany and Plant Sciences, University of California, Riverside, Riverside, CA, United States, [2]Department of Microbiology and Plant Pathology, University of California, Riverside, Riverside, CA, United States, [3]Department of Chemical and Environmental Engineering, University of California, Riverside, Riverside, CA, United States

Photosynthetic organisms are sources of sustainable foods, renewable biofuels, novel biopharmaceuticals, and next-generation biomaterials essential for modern society. Efforts to improve the yield, variety, and sustainability of products dependent on chloroplasts are limited by the need for biotechnological approaches for high-throughput chloroplast transformation, monitoring chloroplast function, and engineering photosynthesis across diverse plant species. The use of nanotechnology has emerged as a novel approach to overcome some of these limitations. Nanotechnology is enabling advances in the targeted delivery of chemicals and genetic elements to chloroplasts, nanosensors for chloroplast biomolecules, and nanotherapeutics for enhancing chloroplast performance. Nanotechnology-mediated delivery of DNA to the chloroplast has the potential to revolutionize chloroplast synthetic biology by allowing transgenes, or even synthesized DNA libraries, to be delivered to a variety of photosynthetic species. Crop yield improvements could be enabled by nanomaterials that enhance photosynthesis, increase tolerance to stresses, and act as nanosensors for biomolecules associated with chloroplast function. Engineering isolated chloroplasts through nanotechnology and synthetic biology approaches are leading to a new generation of plant-based biomaterials able to self-repair using abundant CO_2 and water sources and are powered by renewable sunlight energy. Current knowledge gaps of nanotechnology-enabled approaches for chloroplast biotechnology include precise mechanisms for entry into plant cells and organelles, limited understanding about nanoparticle-based chloroplast transformations, and the translation of lab-based nanotechnology tools to the agricultural field with crop plants. Future research in chloroplast biotechnology mediated by the merging of synthetic biology and nanotechnology approaches can yield tools for precise control and monitoring of chloroplast function *in vivo* and *ex vivo* across diverse plant species, allowing increased plant productivity and turning plants into widely available sustainable technologies.

Keywords: plant nanobiotechnology, nano-enabled agriculture, chloroplast bioengineering, nanosensors, targeted delivery

OPEN ACCESS

Edited by:
Patricia León, National Autonomous University of Mexico, Mexico

Reviewed by:
Sangram Keshari Lenka, TERI Deakin Nanobiotechnology Centre, India
Jeff Wolt, Iowa State University, United States

****Correspondence:***
Juan Pablo Giraldo
juanpablo.giraldo@ucr.edu

Specialty section:
This article was submitted to Plant Biotechnology, a section of the journal Frontiers in Plant Science

Received: *06 April 2021*
Accepted: *28 June 2021*
Published: *26 July 2021*

Citation:
Newkirk GM, de Allende P, Jinkerson RE and Giraldo JP (2021) Nanotechnology Approaches for Chloroplast Biotechnology Advancements. Front. Plant Sci. 12:691295. doi: 10.3389/fpls.2021.691295

INTRODUCTION

Chloroplast biotechnology has the potential to help alleviate the main challenges of this century by lowering renewable biofuels cost, increasing food production, and increasing productivity per plant. Currently, the cost of renewable energy through biofuels is not competitive against fossil fuels (Medipally et al., 2015; Mu et al., 2020; Lo et al., 2021; Scown et al., 2021). The current goal of the Bioenergy Technologies Office Advanced Algal Systems program within the Department of Energy is $2.5–3 gallon of gas equivalent for renewable algal biofuels by 2030, while current gasoline prices remain relatively low at $2.18 per gallon (BETO Publications, 2020; Fuel Prices, n.d.). Additionally, due to the rapidly growing world population, food production must increase by more than 50% in the coming decades with a more limited amount of arable and productive land and under a changing climate (Hatfield et al., 2011; Xu et al., 2013; Masson-Delmotte et al., 2018; Lowry et al., 2019). The "Green Revolution" in plant and molecular biology led to a significant increase in food productivity (Long et al., 2015). However, chloroplast biotechnology efforts toward increasing food production have been impaired by the inability to take full advantage of emergent research progress in synthetic biology and nanotechnology.

Stifling the ability to explore synthetic biology tools for the advancement of chloroplast biotechnology are the low chloroplast transformation rate, low number of species capable of having their chloroplast genomes transformed, and labor intensive culturing of calli – unorganized plant cells – and screening of phenotypes for homoplasmy. When compared to the rates of nuclear transformation within the same plant species, chloroplast transformation is a significant limitation. In-depth reviews of chloroplast transformation have been written by Day and Goldschmidt-Clermont (2011) and Bock (2015). Since its introduction, particle bombardment has been the standard method of chloroplast transformation across multiple plant species (Przibilla et al., 1991). This method attaches DNA to microparticles of gold or tungsten and, using a biolistic delivery system, propels the DNA-attached particle, *via* high-pressure helium gas, toward the plant cell. A significant downside to particle bombardment is that it requires specialized equipment and has a low transformation throughput. Accessibility, however, is limited to those plants for which protoplasts can be readily obtained (O'Neill et al., 1993). A more recent addition to the chloroplast transformation toolkit, a glass-bead vortex method has been demonstrated for green algae, but it does have lower rates when compared to particle bombardment (Economou et al., 2014; Wannathong et al., 2016). Despite these advances, relatively few plant species can have their chloroplast transformed with *Arabidopsis* being a very recent addition by Yu et al. in the Maliga Lab (Yu et al., 2017). Land plants routinely need species-specific bombardment procedures, vectors, and selectable markers. Increasing the number of species amenable to chloroplast transformation would have a significant research impact on broadening the number of crop plants that can be made more productive by bioengineering. A further hurdle is that any current chloroplast transformation method creates heterogenous chloroplast genomes, which must subsequently be driven to homoplasmy. Chloroplast genome replication, through cell division, is one way of producing and confirming a homogenous chloroplast genome. However, continuous calli culturing is a laborious and tedious manual process. Chloroplast transformation problems could be alleviated by a biomolecule delivery chassis that targets specific germline or meristematic plant cells and removes the tissue culture bottleneck. The benefits of a universal chloroplast transformation tool for diverse plant species could improve research in plant biology and have significant impacts on agriculture, the biopharmaceutical industry, and sustainable materials.

Advances in chloroplast biotechnology have broader impacts on medicine, fuel, food, bioplastics, and chemicals and may open new frontiers of crop development (Maliga and Bock, 2011). These chloroplast products become compartmentalized, which means they have unique abilities to produce advanced biopharmaceuticals like cancer-killing immunotoxins that would normally kill eukaryotic cells (Tran et al., 2013). Also, algal chloroplasts can produce high-value proteins like human growth hormones (Wannathong et al., 2016). Several reviews of biopharmaceuticals capable of being made within chloroplasts include Adem et al. (2017) and Dyo and Purton (2018). Additionally, chloroplasts can produce renewable fuel that is environmentally sustainable by utilizing carbon within the atmosphere rather than ecological carbon sinks (Medipally et al., 2015). A significant advantage of algae biofuels is that the biodiesel produced can work with existing gas infrastructure with slight modifications. The benefits of algal biofuels from advances in synthetic biology have been reviewed by Georgianna and Mayfield (2012). Chloroplast biotechnology advances also are leading to improvements in food crop productivity (Parry et al., 2013) of algae-based food products (Dawczynski et al., 2007). There are new frontiers of materials made from non-petroleum-based foam, where bioplastics are being used to make algae-based products from the starch made within chloroplasts (Mathiot et al., 2019). Through synthetic biology and the addition of artificial intelligence algorithms *via* deep learning, there could be even more opportunities for novel chemicals and crop improvements (Wang et al., 2020). To fulfill these chloroplast biotechnology breakthroughs, knowledge gaps in our current understanding of delivering synthetic biology tools must be addressed and molecular biology tools developed to be universal and more efficient.

Nanotechnology is providing tools to enable plant biology researchers for a better understanding of chloroplast molecular biology and genetics, by offering modular delivery chassis for chemicals and biomolecules, nanosensors, and nanotherapeutics that are customizable with targeted and controlled capabilities. Nanomaterials are particles within a size range of 1–100 nanometer scale and varying shapes, aspect ratios, charge, and surface chemistry. These nanoparticles can also be made up of diverse materials for biological applications including silica, gold, carbon, and polymers. Nanoparticles can be coated or loaded with biomolecules for delivery of cargo that can be targeted to plant cells and organelles, such as chloroplasts, by modifying their size and charge (Avellan et al., 2019;

Hu et al., 2020) and biorecognition coatings (Santana et al., 2020). For example, single-walled carbon nanotubes (SWCNTs) can be coated with a single-stranded DNA for delivery to chloroplasts (Giraldo et al., 2014) with polyethylenimine for an overall positive charge to facilitate binding and release of plasmid DNA into the nucleus of a mature land plant (Demirer et al., 2019b) or with chitosan for the delivery and plasmid DNA to the chloroplast of a mature land plant (Kwak et al., 2019). Nanoparticles can also be fabricated with fluorescent properties such as carbon nanotubes and quantum dots for research on plant signaling, stress communication, and environmental monitoring (Giraldo et al., 2019). While knowledge of nanoparticle interactions with plants has increased in technological prowess, research into studying and engineering plants with nanomaterials are still in infancy.

This review focuses on nanotechnology uses that advance our understanding of chloroplast biotechnology (**Figure 1**). We discuss the current knowledge of the interactions between chloroplasts and nanomaterials, how plastid synthetic biology can synergize with nanotechnology approaches, nanomaterials' impact on crop performance monitoring and improvement, and how nanotechnology can turn chloroplasts into manufacturing technologies.

CHLOROPLAST-NANOPARTICLE INTERACTIONS

Nanoparticle interactions with chloroplasts for biotechnology applications have been researched with isolated chloroplasts (Wong et al., 2016), plant protoplasts (Lew et al., 2018), and in leaves of land plants (Hu et al., 2020), but knowledge gaps remain on how nanomaterial properties, such as size, charge, hydrophobicity, and plant biomolecule coatings and coronas, influence interactions with land plants and green algae biosurfaces including the plant cuticle and cell wall and outer algae matrix, respectively. Although recent studies have improved our understanding of translocation of nanoparticles through chloroplast galactolipid-based membranes, how nanoparticle and membrane physical and chemical properties impact uptake into chloroplasts is not well understood.

Plant cell and organelle biosurfaces represent obstacles for delivering nanoparticles with their cargo into chloroplasts (**Figure 2**). Current standard particle delivery methods, such as particle bombardment, rely on pressure and force to deliver microcarriers to the chloroplast genome (Economou et al., 2014). More recently, nanomaterials have been delivered to chloroplasts by spontaneous penetration of lipid membranes *via* diffusion *in vitro*, leaf infiltration using a needleless syringe, and topical foliar delivery mediated by surfactants (Giraldo et al., 2014; Wong et al., 2016; Lew et al., 2018; Hu et al., 2020). The main barriers for entry into the chloroplast genome that nanoparticles must overcome are the plant cell wall, the plant cell membrane, the cytosol, and the chloroplast double membrane; in algae, there can also be an outer epilithic algal matrix (Kramer et al., 2014). Each of these plant biosurfaces represents various physical and chemical barriers that can limit nanoparticle uptake by size, charge, hydrophobicity, and other properties.

The plant cell wall comprises pectin, cross-linking glycan, and cellulose microfibrils (Barros et al., 2015) and is the first significant barrier to entry into the plant cell. The role of plant cell wall pore size, charge, and hydrophobicity have in limiting nanoparticle entry into cells has been recently reported but is not well understood. Nanoparticles up to 18 nm were capable of permeating cotton leaf cells, while nanoparticles larger than 8 nm could not permeate the maize leaf cells (Hu et al., 2020). This study, based on high spatial and temporal resolution confocal fluorescence microscopy, suggests that hydrophilic nanoparticles with a positive charge and less than 20 or 10 nm depending on plant type and leaf anatomy are more efficiently delivered into plant cells and chloroplasts. However, other studies have observed amphiphilic nanoparticles up to 40 nm to translocate across leaf cells and into other plant organs (Avellan et al., 2019). Additionally, studies of poly- and mono-dispersed poly(lactic-co-glycolic) acid nanoparticles have reported that the cell wall inhibits uptake in grapevine cells over 50 nm while the plasma membrane is permeable from 500 to 600 nm with the same nanoparticles (Palocci et al., 2017).

The cell membrane, which is a lipid bilayer composed of phospholipids, carbohydrates, and proteins, represents another barrier of entry into plant cells. Highly charged nanoparticles have been reported to cross both the plasma membrane and chloroplast envelopes (Giraldo et al., 2014; Wong et al., 2016; Lew et al., 2018). Passive penetration rather than energy-dependent endocytosis is hypothesized as the mechanism for nanoparticle uptake. The lipid exchange envelope penetration (LEEP) model proposes a disruption of the lipid bilayer by the ionic cloud surrounding nanoparticles (**Figure 2B**; Lew et al., 2018). Modeling studies of nanoparticle uptake by chloroplasts highlight the importance of nanoparticle charge. However, these models need to incorporate a variety of biosurfaces in plants such as plant cell wall, where nanoparticles encounter *in planta*. Furthermore, nanoparticles with varying hydrophobicities and biomolecules coatings and coronas have not been accounted for in the modeling efforts of chloroplast nanoparticle interactions. Recent evidence suggests that nanoparticles coated with a chloroplast guiding peptide do not require the high charge predicted by the LEEP model for targeting chloroplasts at high levels of more than 75% in *Arabidopsis* leaf mesophyll cells (Santana et al., 2020).

After crossing the cell wall and membrane, nanoparticles must then pass through the cytosol, containing a variety of different biomolecules, including proteins. Nanoparticles passing through the cytosol are expected to be coated with biomolecule coronas, but this is poorly understood within plants. Recently, Prakash and Deswal (2020) demonstrated that gold nanoparticles interfaced with plant extracts from *Brassica juncea* formed protein coronas increasing the nanoparticle surface charge by approximately 30% after 36 h of interaction. Mass spectrometry showed that 27% of the hard corona formation around the gold nanoparticle comes from the plant energy-yielding pathways including glycolysis, photosynthesis, and ATP synthesis

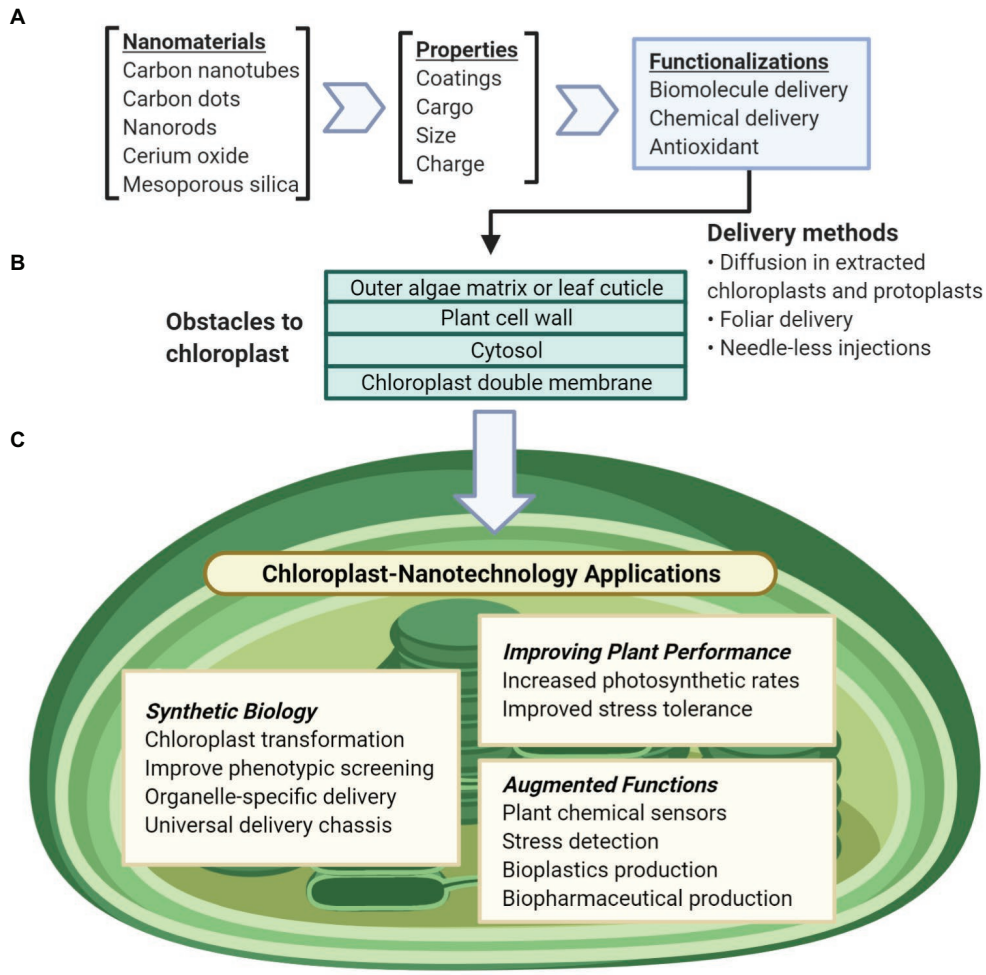

FIGURE 1 | Overview of nanotechnology approaches for chloroplast biotechnology. **(A)** Nanomaterial properties can be modularly tuned for a variety of functions including biomolecule and chemical delivery, biosensors, antioxidants. **(B)** Nanomaterials can be delivered to chloroplasts in liquid suspensions by passive intake without mechanical aid or through needleless-syringes and foliar spray. To reach the chloroplast, these particles pass through obstacles of the plant cell including the outer leaf cuticle or the glycoprotein-rich extracellular matrix of algae, the plant cell wall, the plant cell membrane, the cell cytosol, and lastly the chloroplast double membranes. **(C)** Nanotechnology applications for understanding and engineering chloroplasts include synthetic biology research, improving chloroplast function, or enabling non-native abilities for chloroplasts.

(Prakash and Deswal, 2020). In comparison, a study on nanoparticle coronas with human plasma highlights that irrespective of the nanoparticle material, the coronas formed were dependent on size and surface engineering (Lundqvist et al., 2008). Research performed in mouse models reports that the wild-type *Tobacco mosaic virus* had a higher accumulation of proteins than synthetic nanoparticles, promoting faster clearance from the body (Pitek et al., 2016). This study also found that the choice of targeting ligand and surface engineering, e.g., coatings, can drastically alter the distribution and biocompatibility of the nanoparticles in living systems. These studies in non-plant systems indicate that protein, lipid, and carbohydrate coronas should be crucial to tune interactions with plant cells and organelles.

The last obstacles to reaching the chloroplast are its double lipid bilayers, referred to as the chloroplast membranes. The chloroplast membranes are formed by galactolipids and are highly dynamic (Block et al., 2007). Chemical interactions of nanomaterials with phospholipid-based membranes of eukaryotic cells have been thoroughly studied (Sanchez et al., 2012; Wu et al., 2013; Wang et al., 2016; Lew et al., 2018). However, there are no studies of nanomaterial interactions with the galactolipid-based membranes that form the majority of the chloroplast envelopes. Highly positively or negatively charged nanoparticles interact with the exposed lipids, allowing diffusion and eventual kinetic trapping into isolated chloroplasts without mechanical aid (**Figure 2A**; Wong et al., 2016). These nanoparticles can be larger than chloroplast porin's diameter of 2.5–3 nm, and channel proteins, including mechanosensitive channels, have the largest diameter in chloroplast membranes (Ganesan et al., 2018). High and low aspect ratio nanomaterials, such as carbon nanotubes and carbon dots, respectively, are capable of penetrating plant cells and chloroplasts with high efficiency (Giraldo et al., 2014; Wong et al., 2016; Hu et al., 2020;

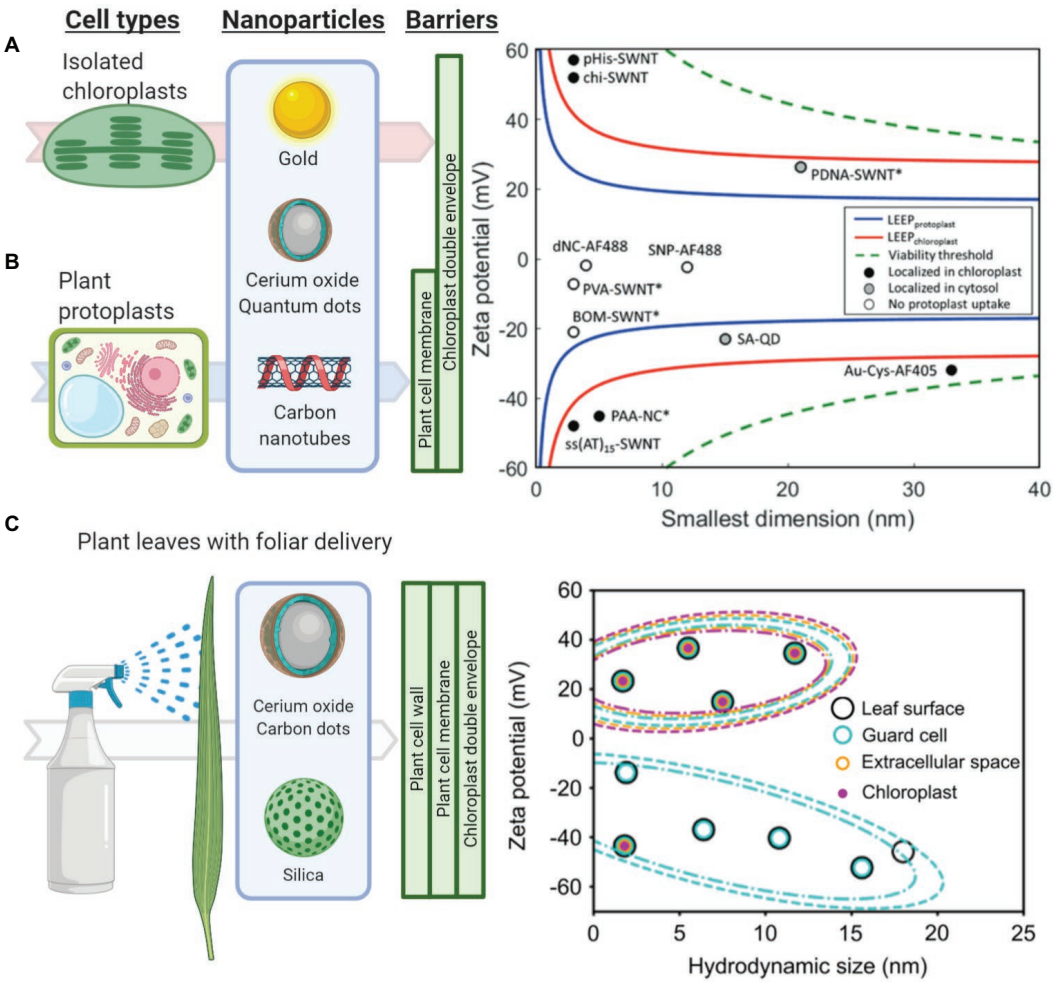

FIGURE 2 | Understanding and modeling nanoparticle-chloroplast interactions. **(A)** The lipid exchange envelope penetration (LEEP) model was developed on isolated plant chloroplasts. It predicts that highly charged nanoparticles localize within chloroplasts while more neutrally charged nanoparticles are unable to enter these organelles (Reprinted with permission from Wong et al., 2016). **(B)** Similarly, the LEEP model for isolated plant protoplasts that includes a plant cell membrane as a barrier, predicts that nanomaterial charge magnitude determines whether particles enter plant protoplasts or localize in the cytosol or chloroplasts (Reprinted with permission from Lew et al., 2018). **(C)** Systematic studies of foliar delivery of nanoparticles of various sizes and charges *in planta* indicated that there is a size limit for uptake in leaf cells in which highly positively charged nanoparticles were more efficiently delivered into these organelles (Reprinted with permission from Hu et al., 2020).

Santana et al., 2020). However, the role of nanomaterial aspect ratio on entry into cells and chloroplasts has not been systematically explored with nanomaterials having precise control of aspect ratios. Gold, silica, and polymer nanostructures could aid in understanding the role of nanoparticle aspect ratio on interactions with chloroplast envelopes.

NANOTECHNOLOGY CARGO DELIVERY APPROACHES TO ENABLE CHLOROPLAST SYNTHETIC BIOLOGY

Developing a universal and efficient chassis for biomolecule delivery into chloroplasts may unleash synthetic biology research progress into novel photosynthetic organisms, their molecular pathways and enable high-value biomolecule production. The advanced regulatory and expression logic systems constructed through synthetic biology are stymied by the inability to deliver biomolecules to chloroplasts. Ideally, this delivery chassis would cause little to no toxicity to the organism and have the ability to carry a variety of biomolecules (Vazquez-Vilar et al., 2018). Current approaches to deliver DNA to chloroplasts through force *via* particle bombardment work for a small number of organisms – nine species are shown with stable and reproducible plastid transformation (Bock, 2015) plus recently *Arabidopsis thaliana* (Yu et al., 2017) – but cannot be targeted to specific organelles. The standard gold or tungsten microcarriers used for chloroplast transformation in the gene gun system are 0.6–1.6 μm in diameter (**Figure 3**). These microcarriers have coatings that are not fully customizable, cannot be directed to specific organelles, or used without forced mechanical aid. Despite these limitations of current microcarriers and low

transformation efficiency, synthetic biology has made enormous strides in plant biology research.

Despite being a relatively new field of research, synthetic biology has enabled the discovery of multiple new chemicals, exploration of advanced protein expression regulation, and production of novel high-value proteins like biopharmaceuticals within chloroplasts. These advancements in chloroplast biotechnology have been discussed in seminal reviews (Bock, 2015; Boehm and Bock, 2019). New research that is enabling chloroplast biotechnology includes the ability to monitor the expression of proteins *in vivo* through a luciferase reporter (Matsuo et al., 2006), gene activation can be enabled through a site-specific recombinase (Tungsuchat-Huang et al., 2011), a synthetic riboswitch (Verhounig et al., 2010), and metabolic pathway engineering is possible through synthetic multigene operons (Lu et al., 2013). These approaches may, in the future, be used in combination with nanotechnology approaches within diverse wild-type plants, for which currently there are no transformation and genome modification protocols available. Containing these new molecular and genetic regulatory mechanisms and proteins are possible through chloroplast biotechnology. As shown in the green algae *Chlamydomonas reinhardtii*, codon reassignment allows an additional avenue for biocontainment (Young and Purton, 2016). Biocontainment within chloroplasts may allow researchers to rapidly and specifically produce proteins within wild-type strains at specific time periods for a better understanding of nuclear-chloroplast protein expression and regulation. In addition, synthetic biology may be further enabled by a chloroplast transformation with large mutant libraries for the entire plastid genome. Facile *in vivo* assembly of chloroplast transformation vectors have been developed for plastid engineering (Wu et al., 2017a). The first fully exogenous plastid transformation has been completed in *C. reinhardtii* (O'Neill et al., 2012). The *in situ* ability of nanotechnology DNA delivery may enable new directed evolution approaches to screen large mutant libraries. Synthetic biology has made strides in research in a short amount of time, and new research done in nanotechnology may help to bolster it into new plant species.

Nanotechnology approaches are allowing the genetic modification for the expression of proteins and the specific delivery of cargoes to chloroplasts in wild-type plants. Chloroplast transformations currently must be performed with somatic or embryonic plant callus material and must be screened for heterogeneity in their genomes. This callus culturing stage requires manual labor and lengthy growth periods. New nanotechnology approaches are focusing on using mature land plants for the expression of exogenous DNA, which in turn may lead to the development of chloroplast transformations without calli culturing through targeted delivery into germline or meristematic tissues. Nuclear expression of exogenous DNA

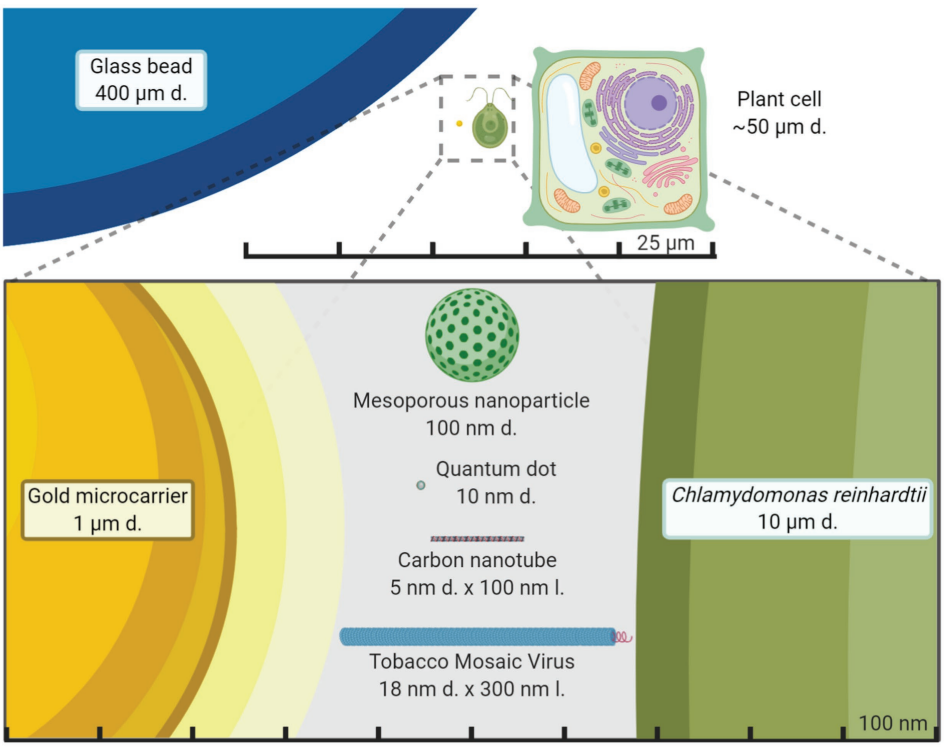

FIGURE 3 | Size comparison of nanomaterials to other exogenous biomolecule delivery systems. Average plant cell and the green alga *Chlamydomonas reinhardtii* size are compared to chloroplast transformation carriers in the micrometer and nanometer scale. Gold microcarriers are standardly used in chloroplast transformations of both land plants and green algae through particle bombardment while the glass beads are used in a vortex-based protocol for *C. reinhardtii*. It becomes starkly apparent just how smaller nanoparticles are compared to standard microcarriers and potentially less disruptive for plant cells. The figure is made to scale.

mediated by SWCNT has been assessed with a green fluorescent protein (Demirer et al., 2019a). Interestingly, the nuclear genomes seemed to not have been transformed as the incorporation of the exogenous DNA was not observed. A yellow fluorescent protein has also been transiently expressed from chloroplasts in mature *Eruca sativa*, *Nasturtium officinale*, *Nicotiana tabacum*, and *Spinacia oleracea* plants through SWCNT mediated delivery of exogenous plasmid DNA (**Figure 4A**; Kwak et al., 2019). One major advantage of nanoparticles is the ability to functionalize them with biomolecules for targeted and controlled delivery. A chloroplast targeting peptide allowed quantum dots to selectively target these organelles and to deliver chemical cargoes (**Figure 4B**; Santana et al., 2020). These nanotechnology advances in biomolecule delivery can act as promising tools for plant biology research and widespread use in crop biotechnology.

CROP IMPROVEMENTS THROUGH CHLOROPLAST NANOBIOTECHNOLOGY

Agriculture demands more precise monitoring of plant health, increasing crop productivity, and efficiently delivering agrochemicals with lessening amounts of harmful environmental runoff. Chloroplasts are sites of photosynthesis, assimilation of nutrients, including nitrogen and phosphorus (Merchant et al., 2006; Carmo-Silva et al., 2015), and function as signaling organelles involved in plant stress responses (Van Aken et al., 2016; Su et al., 2019). More precise monitoring and improvement of photosynthesis, nutrient delivery to the sites of assimilation, stress responses, and plant health would allow higher crop yields. Some of these needs were met in the "Green Revolution" with molecular biology and genetics advancements that allowed higher crop productivity. However, chloroplast transformation-based approaches have not been reproducibly developed in most crops that feed the world (Bock, 2015).

Recent advances in nanosensors research may allow nanotechnology-based devices that monitor plant's health in real-time before detrimental symptoms occur. A full review of this topic discusses nanotechnology approaches for smart plant sensors (Giraldo et al., 2019), including nanosensors for monitoring plant health, detecting molecules related to photosynthesis, and reporting chemicals in the environment to electronic imaging devices already in use in phenotyping and agricultural operations. Current standard technologies that monitor plant function, stress, and photosynthesis rely on remote sensing tools to measure chlorophyll fluorescence or gas analyzers to quantify CO_2 assimilation (Pérez-Bueno et al., 2019). Recently, carbon nanotubes were functionalized to sense H_2O_2, a key signaling molecule generated by chloroplasts and associated with plant stress (Wu et al., 2020). The H_2O_2 was monitored in real-time and within the plant physiological range through a near-infrared camera (**Figures 5A,B**). Multiplexed sensing of several plants signaling molecules associated with plant health, such as NO, glucose, and $Ca^{2+,}$ among others, could allow for both monitoring plant stress status and identification of types of stress experienced. New research in nanotechnology has demonstrated the ability to use fluorescent quantum dots to monitor glucose, a direct product of chloroplast photosynthesis, through a Raspberry Pi camera in laboratory conditions in wild-type *Arabidopsis* plants (**Figure 5C**; Li et al., 2018). Previous approaches were only able to monitor glucose through genetically modified plant model systems. Plants embedded with nanosensors can also be engineered into environmental sensors for chemicals in groundwater with the use of remote near-infrared cameras. These plant nanosensors can detect small amounts of molecules in the environment such as those present in explosives (Wong et al., 2017). Although carbon nanotubes and quantum dots raise environmental toxicity concerns, improved knowledge in plant-nanoparticle interactions is leading to more precise control of the spatial and temporal distribution of nanomaterials in plant organs, such as leaves, for reducing exposure to humans and the environment (Wang et al., 2008; Williams et al., 2014). Alternatively, sentinel plants with nanosensors may be deployed throughout an area to determine what other plants within that crop field are experiencing.

Bolstering chloroplast biotechnology through nanotechnology also may come through engineering photosynthesis in plants. Semiconducting SWCNTs have been shown to increase photosynthetic activity in mature plants (**Figure 6A**; Giraldo et al., 2014). The mechanisms of increased photosynthetic rates in land plants suggest that expanding the range of chloroplast pigment absorption to the near-infrared is a route for improving photosynthesis and is an avenue for new research. Nanotechnology approaches are enabling the improvement of wild-type plants without genetic modification by increasing their ability to scavenge reactive oxygen species (ROS) that are accumulated under abiotic and biotic stresses. Cerium oxide nanoparticles catalytically reduce hydroxyl radicals in *A. thaliana* leaves, a novel ability in plants (**Figure 6B**; Wu et al., 2018). This augmented hydroxyl radical scavenging capability improves plant stress tolerance by enhancing potassium mesophyll retention, which is a key trait associated with salt stress. Stressed plants interfaced with cerium oxide nanoparticles have higher carbon asssimilation rates, photosystem II quantum yields, and quantum efficiency of CO_2 relative to controls without nanoparticles (**Figures 6C–F**; Wu et al., 2017b, 2018). Reducing ROS through nanomaterials is a promising mechanism for improving or maintaining plant productivity under stress environments in the field. While both of these examples are in the lab environment with a plant model species, they give an important stepping stone to future applications in the field in crop plant species.

FUTURE RESEARCH IN CHLOROPLAST NANOBIOTECHNOLOGY

Research into chloroplast biotechnology through nanotechnology approaches may take guidance from previous research breakthroughs in the biomedical field, lead to new discoveries through improved synthetic biology tools, and enable innovative ways of human-plant interactions, all while managing environmental impacts for applications in crops. Future chloroplast nanobiotechnology applications will range from targeted delivery of agrochemicals, plastid transformation and genome editing, nanosensors for monitoring signaling molecules,

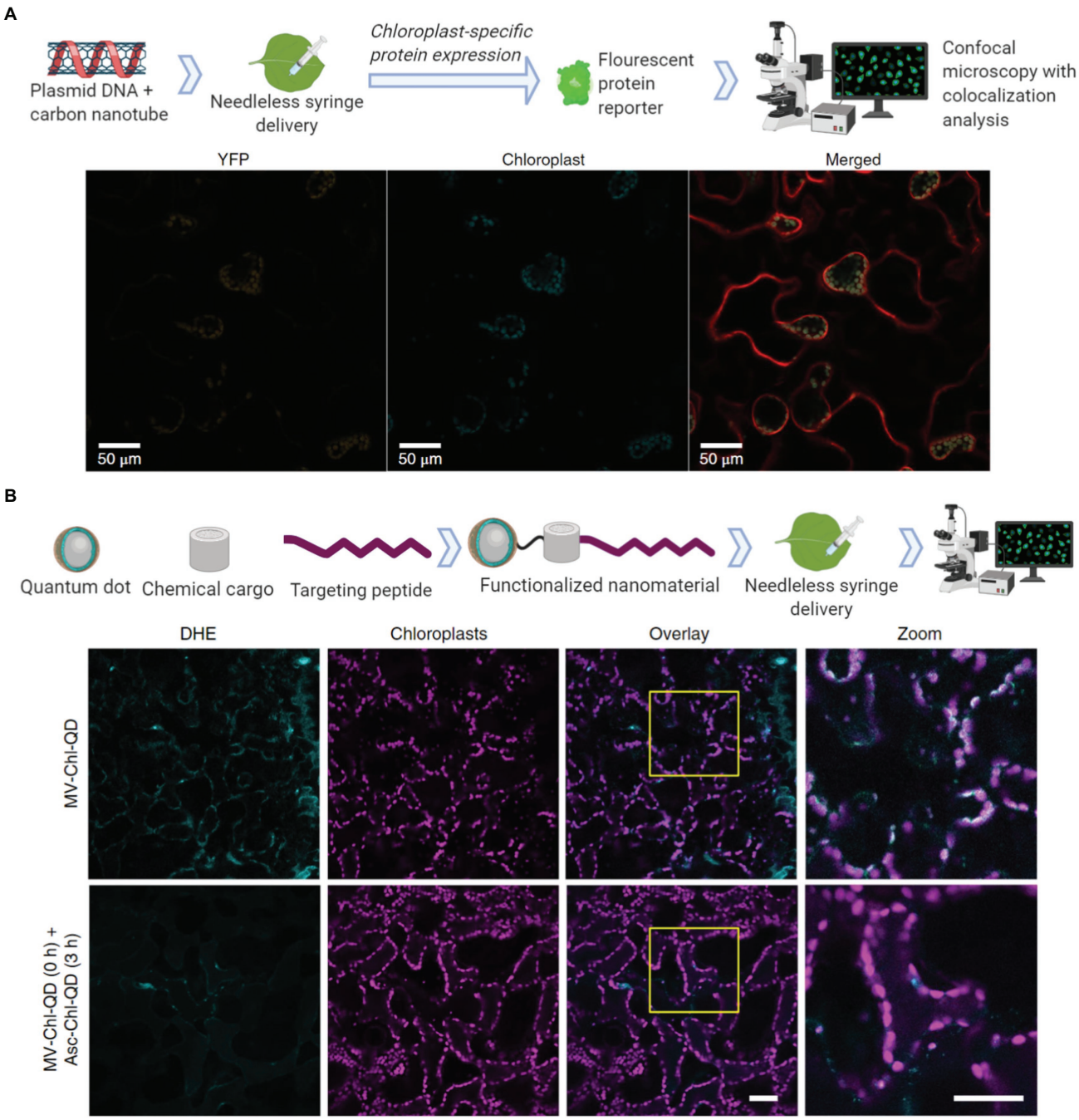

FIGURE 4 | Nanomaterial mediated delivery of DNA and chemical cargoes to chloroplasts. **(A)** Single walled carbon nanotubes coated with chitosan carry plasmid DNA to chloroplasts. The nanomaterials are infiltrated into leaf mesophyll cells with a needless syringe. Confocal microscopy was then used for colocalization analysis 2–3 days post-infiltration by measuring the chloroplast-specific fluorescent protein (YFP) expressed within the mesophyll cells of tobacco plants (Material from Kwak et al., 2019). **(B)** Quantum dots with molecular baskets target the delivery of a chemical cargo to chloroplasts guided by a peptide recognition motif (Chl-QD). These functionalized nanomaterials were then loaded with methyl viologen (paraquat; MV-Chl-QD) to generate superoxide anion within chloroplasts or ascorbic acid (Asc-Chl-QD) to scavenge the superoxide anion. By monitoring reactive oxygen species (ROS) through the DHE dye using confocal microscopy, the targeted nanomaterials were shown to specifically induce and scavenge ROS *in vivo* in chloroplasts. Scale bar, 40 µM (Material from Santana et al., 2020).

improvement of plant photosynthesis, and turning plants into biomanufacturing devices (**Table 1**).

To enable these future applications of nanotechnology for chloroplast biotechnology advancements will require improving our understanding of chloroplast-nanoparticle interactions. The role of nanomaterial hydrophobicity, aspect ratios, and biomolecule coatings on nanoparticle delivery to chloroplasts is not well understood. Hydrophobicity has been reported to

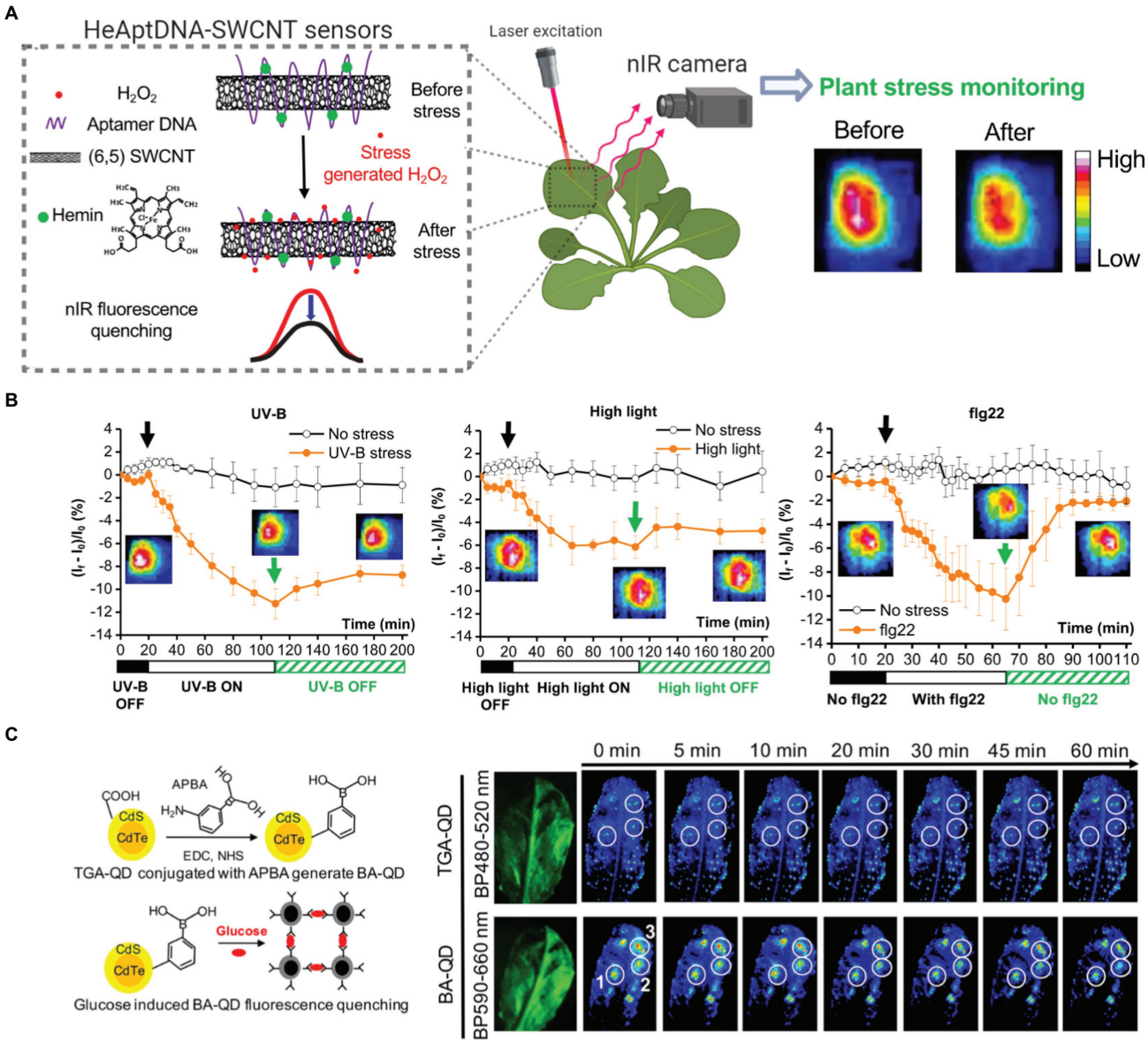

FIGURE 5 | Plant health monitoring by nanotechnology-based sensors. **(A)** Single-walled carbon nanotubes (SWCNTs) can be functionalized with aptamer DNA and hemins to detect H_2O_2, a signaling molecule associated with plant stress. SWCNT sensors report H_2O_2 in real-time by quenching in NIR fluorescence intensity The nanosensor fluorescence changes are monitored by a NIR imaging before and after the stress event. This standoff detection *via* NIR imaging can report stress events within the plant physiological range of H_2O_2 (10–100 μm; Wu et al., 2020). **(B)** SWCNT-based nanosensors allow early detection of stresses from UV-B, high light, and a pathogen-related peptide (flg22; Reprinted with permission from Wu et al., 2020). **(C)** Boronic acid-coated quantum dots (BA-QDs) can act as glucose sensors, a principal product of chloroplast photosynthesis. Standoff glucose detection of *A. thaliana* is enabled by nanosensors excited through UV light and imaged with a Raspberry Pi camera (Reprinted with permission from Li et al., 2018). Thioglycolic acid-coated quantum dots (TGA-QD) act as internal controls that do not respond to glucose.

play a role in altering the distribution of gold nanoparticles in plant leaves (Avellan et al., 2019). Recent studies have also explored how shapes of DNA nanostructures influence the delivery of siRNA-based gene silencing biomolecules in plant leaves (Zhang et al., 2020). Peptide coatings have recently been reported to more precisely guide nanoparticles to chloroplasts in plants (Santana et al., 2020). Future studies in these areas will be a significant step forward in understanding the underlying mechanisms of nanoparticle entry into plant cells and chloroplasts.

Chloroplast transformation is a limiting factor that, if alleviated, could fundamentally transform plant biotechnology research. Plant chloroplast transformation efficiencies are so low that researchers studying RuBisCO, the key protein responsible for CO_2 assimilation during photosynthesis, have relied on bacterial systems instead of using plant or algae systems (Wilson et al., 2018). With efficient chloroplast transformation rates, large libraries could be used for the directed evolution of photosynthetic proteins; genome shuffling could be performed with the entire

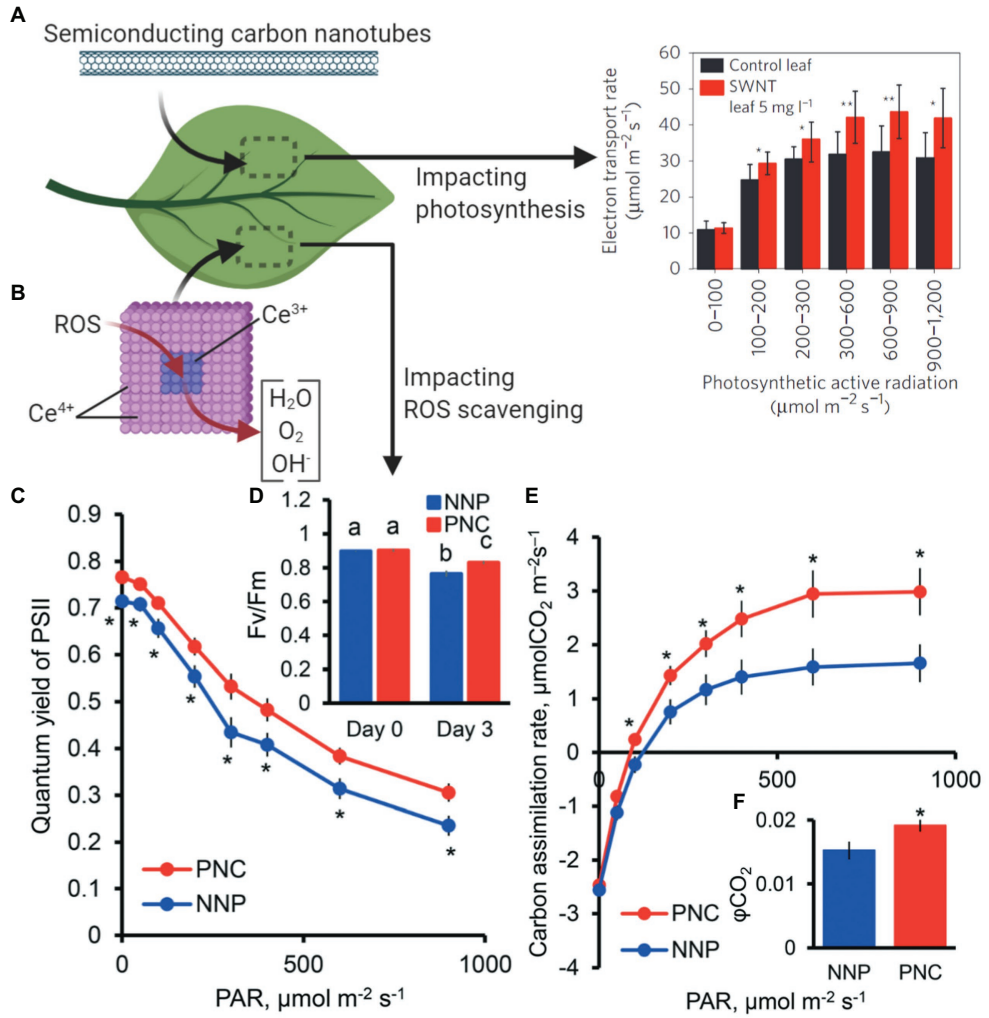

FIGURE 6 | Nanotechnology approaches to improve plant photosynthesis. **(A)** SWCNTs interfaced with plant leaves increase chloroplast photosynthetic activity (Material from Giraldo et al., 2014). **(B)** Cerium oxide nanoparticles catalytically scavenge reactive oxygen species (ROS) in chloroplasts, resulting in enhanced light and carbon reactions of photosynthesis. Stressed plants with poly acrylic-coated cerium oxide nanoparticles (PNC) have higher **(C)** PSII quantum yields, **(D)** maximum PSII efficiency (Fv/Fm), **(E)** carbon assimilation rates, and **(F)** quantum yield of CO_2 relative to controls without nanoparticles (NNP; Reproduced from Wu et al., 2018 with permission from the Royal Society of Chemistry). *$p < 0.05$; **$p < 0.01$. Different lower case letters mean significant differences at $p < 0.05$.

photosynthetic pathway; entire plastid genomes could be synthesized and mutated for increased photosynthetic abilities. For example, directed protein evolution is a strategy that takes advantage of large mutant libraries and yields mutants with a beneficial trait (Zhu et al., 2010; Sinha and Shukla, 2019). Recent research has enabled the simultaneous multiplexed synthesis of 7,000 synthetic genes for two essential genes in *Escherichia coli* (Plesa et al., 2018). While chloroplast transformation efficiencies may never achieve the efficiency of bacteria transformation, the most robust directed evolution experiment of a single chloroplast gene, RuBisCO's *rbcL*, in *C. reinhardtii* was able to yield 80,000 library variants that were selected and screened across multiple chloroplast transformations (Zhu et al., 2010). While researching chloroplast transformation efficiencies, we found that there was a lack of standardization across research articles. Therefore, we are recommending reporting the following parameters to increase the scientific value and reproducibility of chloroplast transformations. Chloroplast transformations should be reported with raw data for (1) the amount and type of DNA used, (2) age and origin of calli, or cell count for algae, (3) amount of calli per plate bombarded, or algae cell count per transformation replicate, (4) transformants per replicate and total number before and after genetic screening, and (5) the transformation efficiency.

New synthetic biology applications and evolutionary strategies could help to bioengineer chloroplast genomes with, for example, improved efficiency through pathway engineering using robust mutant libraries and directed protein evolution. Synthetic genomics, i.e., the construction of chromosomes, is emerging in the last decade as an exciting frontier for minimizing genomes, constructing mosaic chromosomes of two or more species reengineering organelles (Coradini et al., 2020). Synthetic genomics approaches will be bolstered by nanoparticle gene

TABLE 1 | Strengths and weaknesses of nanotechnology approaches for chloroplast biotechnology advancements.

Chloroplast nanobiotechnology applications	Strengths	Weaknesses	Areas of improvement
Chemical delivery	- Targeted delivery - Less runoff into environment - Improvement of agrochemical suspensions	- Environmental impact of biocompatible nanomaterials for targeted delivery is unknown	- Biodegradability studies of targeted nanomaterials - Controlled chemical release
Gene delivery	- Species independent - Gene delivery without specialized equipment - *In situ* gene delivery	- Potential limitation of plasmid DNA size per nanoparticle - Only transient expression shown - Only proof of concept, with GFP expression	- Stable plastid genome transformation enabled by nanomaterials - Targeted gene delivery to chloroplasts for applied research - Inducible expression of exogenous DNA - Overcoming the bottleneck of selectable markers
Nanosensors	- Real-time monitoring of plant signaling molecules - High sensitivity down to single molecule level - Do not photobleach - Near infrared imaging - Species independent	- Available for only a few plant signaling molecules to date - Most studies performed in laboratory conditions	- Targeted sensor delivery to chloroplasts - Multiplexed sensing of plant signaling molecules
Photosynthesis	- Enhancement of light and carbon reactions of photosynthesis - Protecting chloroplast photosynthetic machinery from oxidative stress	- Environmental toxicity of some types of nanomaterials used to boost photosynthesis - Most studies performed in laboratory conditions	- Targeted delivery of nanoparticles to chloroplasts - Develop more biocompatible and biodegradable nanomaterials that improve photosynthesis
Biomanufacturing	- Use of plants as widely accessible, solar powered manufacturing technology - Scalable, low cost manufacturing of biopharmaceuticals and bioplastics *in situ*	- Research and development at very early stage	- Proof of concept of turning plants into biomanufacturing devices using nanotechnology

delivery due to the ability to tune characteristics of the delivery chassis, deliver a wider array of genes for more applications at once, and allow gene delivery to precise organelles. In addition, nanotechnology approaches may be employed for CRISPR-Cas genetic engineering of plants (Demirer et al., 2021). With the chloroplast's DNA repair mechanism nearly exclusively homology-driven, current approaches for plastid genetic engineering rely on delivering antibiotic markers with homologous arms for integration. However, a large problem with chloroplast biotechnology is the lack of strong selectable markers, like spectinomycin, necessary for marker excision through repeated rounds of transformation for chloroplast genetic engineering (Bock, 2015). In the future, CRISPR delivered by nanoparticles may enable new strategies of inducible silencing and increasing expression of exogenous DNA for pathway engineering that move beyond the bottleneck of strong selectable markers.

Nanomaterials can be used to deliver genes that encode proteins that act as sensors or the nanoparticle itself can be used as a sensor, and these approaches could lead to new applications in chloroplast biotechnology research. Through tunable characteristics and various types of nanoparticles, genes can be delivered that detect other proteins in wild-type plant species. For example, nanotechnology approaches for gene delivery of fluorescence resonance energy transfer (FRET) sensors to mature plants without previous genetic modification. In the future, multiplexed sensing of signaling molecules associated with chloroplast function may be possible. Currently, with *C. reinhardtii*, multiplexed stress-based imaging is possible through fluorescent-activated cell sorting (Béchet et al., 2017). In terms of applications to land plants, nanosensors already offer approaches to monitor chloroplast ROS, glucose, and nitric oxide (Giraldo et al., 2019). These plant signaling molecules may be able to be monitored simultaneously for the actuation of devices that promote plant health that are integrated into artificial intelligence deep learning algorithms.

Research into photosynthesis would be bolstered by nanotechnology approaches that allow targeted delivery of nanoparticles that manipulate chloroplast function. Biomolecule delivery of DNA or RNA (Wang et al., 2019) will expand research in the lab into chloroplasts of land plants that are not currently capable of being transformed. While nanotechnology approaches for plant research is a new field, nanoparticles have been used in mammalian systems to deliver biomolecules for the past decades (Shahiwala et al., 2007; Woodward et al., 2007). Their applications may give insights to future research directions in plants. CRISPR/Cas9 genome editing in mammalian cells through mRNA delivery has been demonstrated over the span of months (Liu et al., 2019). Applications in the field of nanoparticles for improving plant photosynthesis under stress will also require studies on environmental toxicity, the longevity

of nanoparticles in the environment, and exposure of those nanoparticles to products for human consumption.

Plants and their chloroplasts potential are just beginning to be explored in terms of manufacturing of biopharmaceuticals, fuels, and materials. Plant chloroplasts within our homes may become 3D printers for high-value biopharmaceuticals (Maliga and Bock, 2011; Jin and Daniell, 2015). Polyhydroxybutyrate, a biodegradable polyester, can be made within the chloroplast and is being researched as a bioplastic (McQualter et al., 2016). Plants themselves could be used as a platform for self-repairing of infrastructure (Lu, 2020). A new class of materials made with extracted spinach chloroplasts stabilized with antioxidant cerium oxide nanoparticles can self-repair using glucose created from photosynthesis (Kwak et al., 2018). Algae and their chloroplasts enable a unique opportunity for renewable biofuels to take advantage of existing gasoline infrastructure and create jet fuel (Mayfield and Golden, 2015). In terms of legislation that is further enabling renewable algal biofuels, algae has officially been included in the latest 2018 Farm Bill in the United States, which enables algae agriculture to receive federal financial assistance for biomass cultivation, farm insurance, loans, carbon capture research and creates a new USDA Algae Agriculture Research Program (Conaway, 2018). These future applications for plants may fundamentally revolutionize our relationship with plants from providing food and materials to intricate partners that facilitate technology access to the world.

CONCLUSION

Nanotechnology offers promising new approaches for some of the hardest challenges in chloroplast biotechnology research. Nanoparticle and plant cell interactions are still an emerging field that needs to be studied, but research has shown promising results in nanoparticles getting past plant cell barriers to their organelles. Knowledge gaps still exist in the exact mechanism of entry of nanoparticles into plant cells and chloroplast envelopes to determine the characteristics needed for a universal delivery cassette for biomolecules that would be applicable across diverse plant species. With current knowledge of plant-nanoparticle interactions, successful nanoparticle-based biomolecule delivery to chloroplasts has been possible. Using these targeted and controlled delivery technologies to bolster the number of applicable species or increase the efficiency of chloroplast transformations is yet to be seen. If increased chloroplast transformation efficiencies were to be realized, emerging synthetic biology-based strategies, such as directed protein evolution, may be able to be deployed within plastid genomes to unlock new potential in productivity and augmented manufacturing capabilities in chloroplasts. Additionally, nanomaterials have already been used to enable chloroplast biotechnology advancements such as sensing specific compounds, increasing photosynthetic rates, and decreasing stress-related molecules' accumulation. Taken together, chloroplast biology and biotechnology research have challenges that can be uniquely addressed with nanotechnology approaches for increasing crop productivity and realizing the next generation of chloroplast-related biomanufacturing.

AUTHOR CONTRIBUTIONS

All authors listed have made a substantial, direct and intellectual contribution to the work, and approved it for publication.

FUNDING

This work was supported by the National Science Foundation under grant no. 1911763 to JG and the National Defense Science and Engineering Graduate Fellowship Program to GN.

ACKNOWLEDGMENTS

All figures were made on BioRender.com.

REFERENCES

Adem, M., Beyene, D., and Feyissa, T. (2017). Recent achievements obtained by chloroplast transformation. *Plant Methods* 13:30. doi: 10.1186/s13007-017-0179-1

Avellan, A., Yun, J., Zhang, Y., Spielman-Sun, E., Unrine, J. M., Thieme, J., et al. (2019). Nanoparticle size and coating chemistry control foliar uptake pathways, translocation, and leaf-to-rhizosphere transport in wheat. *ACS Nano* 13, 5291–5305. doi: 10.1021/acsnano.8b09781

Barros, J., Serk, H., Granlund, I., and Pesquet, E. (2015). The cell biology of lignification in higher plants. *Ann. Bot.* 115, 1053–1074. doi: 10.1093/aob/mcv046

Béchet, Q., Laviale, M., Arsapin, N., Bonnefond, H., and Bernard, O. (2017). Modeling the impact of high temperatures on microalgal viability and photosynthetic activity. *Biotechnol. Biofuels* 10:136. doi: 10.1186/s13068-017-0823-z

BETO Publications (2020). Integrated Strategies to Enable Lower-Cost Biofuels. Bioenergy Technologies Office. Available at: https://www.energy.gov/eere/bioenergy/beto-publications (Accessed April 2, 2021).

Block, M. A., Douce, R., Joyard, J., and Rolland, N. (2007). Chloroplast envelope membranes: a dynamic interface between plastids and the cytosol. *Photosynth. Res.* 92, 225–244. doi: 10.1007/s11120-007-9195-8

Bock, R. (2015). Engineering plastid genomes: methods, tools, and applications in basic research and biotechnology. *Annu. Rev. Plant Biol.* 66, 211–241. doi: 10.1146/annurev-arplant-050213-040212

Boehm, C. R., and Bock, R. (2019). Recent advances and current challenges in synthetic biology of the plastid genetic system and metabolism. *Plant Physiol.* 179, 794–802. doi: 10.1104/pp.18.00767

Carmo-Silva, E., Scales, J. C., Madgwick, P. J., and Parry, M. A. J. (2015). Optimizing Rubisco and its regulation for greater resource use efficiency. *Plant Cell Environ.* 38, 1817–1832. doi: 10.1111/pce.12425

Conaway, K. M. (2018). Agriculture improvement act of 2018. Available at: https://www.congress.gov/bill/115th-congress/house-bill/2 (Accessed April 1, 2021).

Coradini, A. L. V., Hull, C. B., and Ehrenreich, I. M. (2020). Building genomes to understand biology. *Nat. Commun.* 11:6177. doi: 10.1038/s41467-020-19753-2

Dawczynski, C., Schäfer, U., Leiterer, M., and Jahreis, G. (2007). Nutritional and toxicological importance of macro, trace, and ultra-trace elements in algae food products. *J. Agric. Food Chem.* 55, 10470–10475. doi: 10.1021/jf0721500

Day, A., and Goldschmidt-Clermont, M. (2011). The chloroplast transformation toolbox: selectable markers and marker removal. *Plant Biotechnol. J.* 9, 540–553. doi: 10.1111/j.1467-7652.2011.00604.x

Demirer, G. S., Silva, T. N., Jackson, C. T., Thomas, J. B., Ehrhardt, D. W., Rhee, S. Y., et al. (2021). Nanotechnology to advance CRISPR-Cas genetic

engineering of plants. *Nat. Nanotechnol.* 16, 243–250. doi: 10.1038/s41565-021-00854-y

Demirer, G. S., Zhang, H., Goh, N. S., González-Grandío, E., and Landry, M. P. (2019a). Carbon nanotube-mediated DNA delivery without transgene integration in intact plants. *Nat. Protoc.* 14, 2954–2971. doi: 10.1038/s41596-019-0208-9

Demirer, G. S., Zhang, H., Matos, J. L., Goh, N. S., Cunningham, F. J., Sung, Y., et al. (2019b). High aspect ratio nanomaterials enable delivery of functional genetic material without DNA integration in mature plants. *Nat. Nanotechnol.* 14, 456–464. doi: 10.1038/s41565-019-0382-5

Dyo, Y. M., and Purton, S. (2018). The algal chloroplast as a synthetic biology platform for production of therapeutic proteins. *Microbiology* 164, 113–121. doi: 10.1099/mic.0.000599

Economou, C., Wannathong, T., Szaub, J., and Purton, S. (2014). "A simple, low-cost method for chloroplast transformation of the green alga *Chlamydomonas reinhardtii*," in *Chloroplast Biotechnology: Methods and Protocols*. ed. P. Maliga (Totowa, NJ: Humana Press), 401–411.

Fuel Prices (n.d.). Available at: https://afdc.energy.gov/fuels/prices.html (Accessed April 2, 2021).

Ganesan, I., Shi, L.-X., Labs, M., and Theg, S. M. (2018). Evaluating the functional pore size of chloroplast TOC and TIC protein translocons: import of folded proteins. *Plant Cell* 30, 2161–2173. doi: 10.1105/tpc.18.00427

Georgianna, D. R., and Mayfield, S. P. (2012). Exploiting diversity and synthetic biology for the production of algal biofuels. *Nature* 488, 329–335. doi: 10.1038/nature11479

Giraldo, J. P., Landry, M. P., Faltermeier, S. M., McNicholas, T. P., Iverson, N. M., Boghossian, A. A., et al. (2014). Plant nanobionics approach to augment photosynthesis and biochemical sensing. *Nat. Mater.* 13, 400–408. doi: 10.1038/nmat3890

Giraldo, J. P., Wu, H., Newkirk, G. M., and Kruss, S. (2019). Nanobiotechnology approaches for engineering smart plant sensors. *Nat. Nanotechnol.* 14, 541–553. doi: 10.1038/s41565-019-0470-6

Hatfield, J. L., Boote, K. J., Kimball, B. A., Ziska, L. H., Izaurralde, R. C., Ort, D., et al. (2011). Climate impacts on agriculture: implications for crop production. *Agron. J.* 103, 351–370. doi: 10.2134/agronj2010.0303

Hu, P., An, J., Faulkner, M. M., Wu, H., Li, Z., Tian, X., et al. (2020). Nanoparticle charge and size control foliar delivery efficiency to plant cells and organelles. *ACS Nano* 14, 7970–7986. doi: 10.1021/acsnano.9b09178

Jin, S., and Daniell, H. (2015). The engineered chloroplast genome just got smarter. *Trends Plant Sci.* 20, 622–640. doi: 10.1016/j.tplants.2015.07.004

Kramer, M. J., Bellwood, D. R., and Bellwood, O. (2014). Large-scale spatial variation in epilithic algal matrix cryptofaunal assemblages on the Great Barrier Reef. *Mar. Biol.* 161, 2183–2190. doi: 10.1007/s00227-014-2495-6

Kwak, S.-Y., Giraldo, J. P., Lew, T. T. S., Wong, M. H., Liu, P., Yang, Y. J., et al. (2018). Polymethacrylamide and carbon composites that grow, strengthen, and self-repair using ambient carbon dioxide fixation. *Adv. Mater.* 30:e1804037. doi: 10.1002/adma.201804037

Kwak, S.-Y., Lew, T. T. S., Sweeney, C. J., Koman, V. B., Wong, M. H., Bohmert-Tatarev, K., et al. (2019). Chloroplast-selective gene delivery and expression in planta using chitosan-complexed single-walled carbon nanotube carriers. *Nat. Nanotechnol.* 14, 447–455. doi: 10.1038/s41565-019-0375-4

Lew, T. T. S., Wong, M. H., Kwak, S.-Y., Sinclair, R., Koman, V. B., and Strano, M. S. (2018). Rational design principles for the transport and subcellular distribution of nanomaterials into plant protoplasts. *Small* 14:e1802086. doi: 10.1002/smll.201802086

Li, J., Wu, H., Santana, I., Fahlgren, M., and Giraldo, J. P. (2018). Standoff optical glucose sensing in photosynthetic organisms by a quantum dot fluorescent probe. *ACS Appl. Mater. Interfaces* 10, 28279–28289. doi: 10.1021/acsami.8b07179

Liu, J., Chang, J., Jiang, Y., Meng, X., Sun, T., Mao, L., et al. (2019). Fast and efficient CRISPR/Cas9 genome editing in vivo enabled by bioreducible lipid and messenger RNA nanoparticles. *Adv. Mater.* 31:e1902575. doi: 10.1002/adma.201902575

Lo, S. L. Y., How, B. S., Leong, W. D., Teng, S. Y., Rhamdhani, M. A., and Sunarso, J. (2021). Techno-economic analysis for biomass supply chain: a state-of-the-art review. *Renew. Sust. Energ. Rev.* 135:110164. doi: 10.1016/j.rser.2020.110164

Long, S. P., Marshall-Colon, A., and Zhu, X.-G. (2015). Meeting the global food demand of the future by engineering crop photosynthesis and yield potential. *Cell* 161, 56–66. doi: 10.1016/j.cell.2015.03.019

Lowry, G. V., Avellan, A., and Gilbertson, L. M. (2019). Opportunities and challenges for nanotechnology in the agri-tech revolution. *Nat. Nanotechnol.* 14, 517–522. doi: 10.1038/s41565-019-0461-7

Lu, G. (2020). A review of recent research on bio-inspired structures and materials for energy absorption applications. *Compos. B. Eng.* 181:107496. doi: 10.1016/j.compositesb.2019.107496

Lu, Y., Rijzaani, H., Karcher, D., Ruf, S., and Bock, R. (2013). Efficient metabolic pathway engineering in transgenic tobacco and tomato plastids with synthetic multigene operons. *Proc. Natl. Acad. Sci. U. S. A.* 110, E623–E632. doi: 10.1073/pnas.1216898110

Lundqvist, M., Stigler, J., Elia, G., Lynch, I., Cedervall, T., and Dawson, K. A. (2008). Nanoparticle size and surface properties determine the protein corona with possible implications for biological impacts. *Proc. Natl. Acad. Sci. U. S. A.* 105, 14265–14270. doi: 10.1073/pnas.0805135105

Maliga, P., and Bock, R. (2011). Plastid biotechnology: food, fuel, and medicine for the 21st century. *Plant Physiol.* 155, 1501–1510. doi: 10.1104/pp.110.170969

Masson-Delmotte, V., Zhai, P., Pörtner, H. O., Roberts, D., Skea, J., Shukla, P. R., et al. (eds.) (2018). IPCC, 2018: Global Warming of 1.5°C. An IPCC Special Report on the impacts of global warming of 1.5°C above pre-industrial levels and related global greenhouse gas emission pathways, in the context of strengthening the global response to the threat of climate change, sustainable development, and efforts to eradicate poverty. Intergovernmental Panel on Climate Change. Available at: https://www.ipcc.ch/sr15/ (Accessed December 5, 2018).

Mathiot, C., Ponge, P., Gallard, B., Sassi, J.-F., Delrue, F., and Le Moigne, N. (2019). Microalgae starch-based bioplastics: screening of ten strains and plasticization of unfractionated microalgae by extrusion. *Carbohydr. Polym.* 208, 142–151. doi: 10.1016/j.carbpol.2018.12.057

Matsuo, T., Onai, K., Okamoto, K., Minagawa, J., and Ishiura, M. (2006). Real-time monitoring of chloroplast gene expression by a luciferase reporter: evidence for nuclear regulation of chloroplast circadian period. *Mol. Cell. Biol.* 26, 863–870. doi: 10.1128/MCB.26.3.863-870.2006

Mayfield, S., and Golden, S. S. (2015). Photosynthetic bio-manufacturing: food, fuel, and medicine for the 21st century. *Photosynth. Res.* 123, 225–226. doi: 10.1007/s11120-014-0063-z

McQualter, R. B., Bellasio, C., Gebbie, L. K., Petrasovits, L. A., Palfreyman, R. W., Hodson, M. P., et al. (2016). Systems biology and metabolic modelling unveils limitations to polyhydroxybutyrate accumulation in sugarcane leaves; lessons for C4 engineering. *Plant Biotechnol. J.* 14, 567–580. doi: 10.1111/pbi.12399

Medipally, S. R., Yusoff, F. M., Banerjee, S., and Shariff, M. (2015). Microalgae as sustainable renewable energy feedstock for biofuel production. *Biomed. Res. Int.* 2015:519513. doi: 10.1155/2015/519513

Merchant, S. S., Allen, M. D., Kropat, J., Moseley, J. L., Long, J. C., Tottey, S., et al. (2006). Between a rock and a hard place: trace element nutrition in *Chlamydomonas*. *Biochim. Biophys. Acta* 1763, 578–594. doi: 10.1016/j.bbamcr.2006.04.007

Mu, D., Xin, C., and Zhou, W. (2020). "Chapter 18 – Life cycle assessment and techno-economic analysis of algal biofuel production," in *Microalgae Cultivation for Biofuels Production*. ed. A. Yousuf (Cambridge, Massachusetts: Academic Press), 281–292.

O'Neill, C., Horváth, G. V., Horváth, E., Dix, P. J., and Medgyesy, P. (1993). Chloroplast transformation in plants: polyethylene glycol (PEG) treatment of protoplasts is an alternative to biolistic delivery systems. *Plant J.* 3, 729–738. doi: 10.1111/j.1365-313X.1993.00729.x

O'Neill, B. M., Mikkelson, K. L., Gutierrez, N. M., Cunningham, J. L., Wolff, K. L., Szyjka, S. J., et al. (2012). An exogenous chloroplast genome for complex sequence manipulation in algae. *Nucleic Acids Res.* 40, 2782–2792. doi: 10.1093/nar/gkr1008

Palocci, C., Valletta, A., Chronopoulou, L., Donati, L., Bramosanti, M., Brasili, E., et al. (2017). Endocytic pathways involved in PLGA nanoparticle uptake by grapevine cells and role of cell wall and membrane in size selection. *Plant Cell Rep.* 36, 1917–1928. doi: 10.1007/s00299-017-2206-0

Parry, M. A. J., Andralojc, P. J., Scales, J. C., Salvucci, M. E., Carmo-Silva, A. E., Alonso, H., et al. (2013). Rubisco activity and regulation as targets for crop improvement. *J. Exp. Bot.* 64, 717–730. doi: 10.1093/jxb/ers336

Pérez-Bueno, M. L., Pineda, M., and Barón, M. (2019). Phenotyping plant responses to biotic stress by chlorophyll fluorescence imaging. *Front. Plant Sci.* 10:1135. doi: 10.3389/fpls.2019.01135

Pitek, A. S., Wen, A. M., Shukla, S., and Steinmetz, N. F. (2016). The protein corona of plant virus nanoparticles influences their dispersion properties, cellular interactions, and in vivo fates. *Small* 12, 1758–1769. doi: 10.1002/smll.201502458

Plesa, C., Sidore, A. M., Lubock, N. B., Zhang, D., and Kosuri, S. (2018). Multiplexed gene synthesis in emulsions for exploring protein functional landscapes. *Science* 359, 343–347. doi: 10.1126/science.aao5167

Prakash, S., and Deswal, R. (2020). Analysis of temporally evolved nanoparticle-protein corona highlighted the potential ability of gold nanoparticles to stably interact with proteins and influence the major biochemical pathways in *Brassica juncea*. *Plant Physiol. Biochem.* 146, 143–156. doi: 10.1016/j.plaphy.2019.10.036

Przibilla, E., Heiss, S., Johanningmeier, U., and Trebst, A. (1991). Site-specific mutagenesis of the D1 subunit of photosystem II in wild-type Chlamydomonas. *Plant Cell* 3, 169–174. doi: 10.1105/tpc.3.2.169

Sanchez, V. C., Jachak, A., Hurt, R. H., and Kane, A. B. (2012). Biological interactions of graphene-family nanomaterials: an interdisciplinary review. *Chem. Res. Toxicol.* 25, 15–34. doi: 10.1021/tx200339h

Santana, I., Wu, H., Hu, P., and Giraldo, J. P. (2020). Targeted delivery of nanomaterials with chemical cargoes in plants enabled by a biorecognition motif. *Nat. Commun.* 11:2045. doi: 10.1038/s41467-020-15731-w

Scown, C. D., Baral, N. R., Yang, M., Vora, N., and Huntington, T. (2021). Technoeconomic analysis for biofuels and bioproducts. *Curr. Opin. Biotechnol.* 67, 58–64. doi: 10.1016/j.copbio.2021.01.002

Shahiwala, A., Vyas, T. K., and Amiji, M. M. (2007). Nanocarriers for systemic and mucosal vaccine delivery. *Recent Pat. Drug Deliv. Formul.* 1, 1–9. doi: 10.2174/187221107779814140

Sinha, R., and Shukla, P. (2019). Current trends in protein engineering: updates and progress. *Curr. Protein Pept. Sci.* 20, 398–407. doi: 10.2174/1389203720666181119120120

Su, T., Li, W., Wang, P., and Ma, C. (2019). Dynamics of peroxisome homeostasis and its role in stress response and signaling in plants. *Front. Plant Sci.* 10:705. doi: 10.3389/fpls.2019.00705

Tran, M., Henry, R. E., Siefker, D., Van, C., Newkirk, G., Kim, J., et al. (2013). Production of anti-cancer immunotoxins in algae: ribosome inactivating proteins as fusion partners. *Biotechnol. Bioeng.* 110, 2826–2835. doi: 10.1002/bit.24966

Tungsuchat-Huang, T., Slivinski, K. M., Sinagawa-Garcia, S. R., and Maliga, P. (2011). Visual spectinomycin resistance (aadA(au)) gene for facile identification of transplastomic sectors in tobacco leaves. *Plant Mol. Biol.* 76, 453–461. doi: 10.1007/s11103-010-9724-2

Van Aken, O., De Clercq, I., Ivanova, A., Law, S. R., Van Breusegem, F., Millar, A. H., et al. (2016). Mitochondrial and chloroplast stress responses are modulated in distinct touch and chemical inhibition phases. *Plant Physiol.* 171, 2150–2165. doi: 10.1104/pp.16.00273

Vazquez-Vilar, M., Orzaez, D., and Patron, N. (2018). DNA assembly standards: setting the low-level programming code for plant biotechnology. *Plant Sci.* 273, 33–41. doi: 10.1016/j.plantsci.2018.02.024

Verhounig, A., Karcher, D., and Bock, R. (2010). Inducible gene expression from the plastid genome by a synthetic riboswitch. *Proc. Natl. Acad. Sci. U. S. A.* 107, 6204–6209. doi: 10.1073/pnas.0914423107

Wang, H., Cimen, E., Singh, N., and Buckler, E. (2020). Deep learning for plant genomics and crop improvement. *Curr. Opin. Plant Biol.* 54, 34–41. doi: 10.1016/j.pbi.2019.12.010

Wang, J. W., Grandio, E. G., Newkirk, G. M., Demirer, G. S., Butrus, S., Giraldo, J. P., et al. (2019). Nanoparticle-mediated genetic engineering of plants. *Mol. Plant* 12, 1037–1040. doi: 10.1016/j.molp.2019.06.010

Wang, J., Zhang, X., Chen, Y., Sommerfeld, M., and Hu, Q. (2008). Toxicity assessment of manufactured nanomaterials using the unicellular green alga *Chlamydomonas reinhardtii*. *Chemosphere* 73, 1121–1128. doi: 10.1016/j.chemosphere.2008.07.040

Wang, Z., Zhu, W., Qiu, Y., Yi, X., von dem Bussche, A., Kane, A., et al. (2016). Biological and environmental interactions of emerging two-dimensional nanomaterials. *Chem. Soc. Rev.* 45, 1750–1780. doi: 10.1039/c5cs00914f

Wannathong, T., Waterhouse, J. C., Young, R. E. B., Economou, C. K., and Purton, S. (2016). New tools for chloroplast genetic engineering allow the synthesis of human growth hormone in the green alga *Chlamydomonas reinhardtii*. *Appl. Microbiol. Biotechnol.* 100, 5467–5477. doi: 10.1007/s00253-016-7354-6

Williams, R. M., Taylor, H. K., Thomas, J., Cox, Z., Dolash, B. D., and Sooter, L. J. (2014). The effect of DNA and sodium cholate dispersed single-walled carbon nanotubes on the green algae *Chlamydomonas reinhardtii*. *J. Nanosci. Nanotechnol.* 2014:419382. doi: 10.1155/2014/419382

Wilson, R. H., Martin-Avila, E., Conlan, C., and Whitney, S. M. (2018). An improved *Escherichia coli* screen for Rubisco identifies a protein-protein interface that can enhance CO2-fixation kinetics. *J. Biol. Chem.* 293, 18–27. doi: 10.1074/jbc.M117.810861

Wong, M. H., Giraldo, J. P., Kwak, S.-Y., Koman, V. B., Sinclair, R., Lew, T. T. S., et al. (2017). Nitroaromatic detection and infrared communication from wild-type plants using plant nanobionics. *Nat. Mater.* 16, 264–272. doi: 10.1038/nmat4771

Wong, M. H., Misra, R. P., Giraldo, J. P., Kwak, S.-Y., Son, Y., Landry, M. P., et al. (2016). Lipid exchange envelope penetration (LEEP) of nanoparticles for plant engineering: a universal localization mechanism. *Nano Lett.* 16, 1161–1172. doi: 10.1021/acs.nanolett.5b04467

Woodward, J., Kennel, S. J., Mirzadeh, S., Dai, S., and Rondinone, A. J. (2007). Biodistribution of radioactive Cd 125m Te/ZnS nanoparticles targeted with antibody to murine lung endothelium. *Nanotechnology* 18:175103. doi: 10.1088/0957-4484/18/17/175103

Wu, H., Nißler, R., Morris, V., Herrmann, N., Hu, P., Jeon, S.-J., et al. (2020). Monitoring plant health with near-infrared fluorescent H_2O_2 nanosensors. *Nano Lett.* 20, 2432–2442. doi: 10.1021/acs.nanolett.9b05159

Wu, Y.-L., Putcha, N., Ng, K. W., Leong, D. T., Lim, C. T., Loo, S. C. J., et al. (2013). Biophysical responses upon the interaction of nanomaterials with cellular interfaces. *Acc. Chem. Res.* 46, 782–791. doi: 10.1021/ar300046u

Wu, H., Shabala, L., Shabala, S., and Giraldo, J. P. (2018). Hydroxyl radical scavenging by cerium oxide nanoparticles improves *Arabidopsis* salinity tolerance by enhancing leaf mesophyll potassium retention. *Environ. Sci. Nano.* 5, 1567–1583. doi: 10.1039/C8EN00323H

Wu, H., Tito, N., and Giraldo, J. P. (2017b). Anionic cerium oxide nanoparticles protect plant photosynthesis from abiotic stress by scavenging reactive oxygen species. 11, 11283–11297. doi: 10.1021/acsnano.7b05723

Wu, Y., You, L., Li, S., Ma, M., Wu, M., Ma, L., et al. (2017a). *In vivo* assembly in *Escherichia coli* of transformation vectors for plastid genome engineering. *Front. Plant Sci.* 8:1454. doi: 10.3389/fpls.2017.01454

Xu, Z., Shimizu, H., Yagasaki, Y., Ito, S., Zheng, Y., and Zhou, G. (2013). Interactive effects of elevated CO_2, drought, and warming on plants. *J. Plant Growth Regul.* 32, 692–707. doi: 10.1007/s00344-013-9337-5

Young, R. E. B., and Purton, S. (2016). Codon reassignment to facilitate genetic engineering and biocontainment in the chloroplast of *Chlamydomonas reinhardtii*. *Plant Biotechnol. J.* 14, 1251–1260. doi: 10.1111/pbi.12490

Yu, Q., Lutz, K. A., and Maliga, P. (2017). Efficient plastid transformation in *Arabidopsis*. *Plant Physiol.* 175, 186–193. doi: 10.1104/pp.17.00857

Zhang, H., Zhang, H., Demirer, G. S., González-Grandío, E., Fan, C., and Landry, M. P. (2020). Engineering DNA nanostructures for siRNA delivery in plants. *Nat. Protoc.* 15, 3064–3087. doi: 10.1038/s41596-020-0370-0

Zhu, G., Kurek, I., and Liu, L. (2010). "Chapter 20 – Engineering photosynthetic enzymes involved in CO_2-assimilation by gene shuffling," in *The Chloroplast: Basics and Applications*. eds. C. A. Rebeiz, C. Benning, H. J. Bohnert, H. Daniell, J. K. Hoober, H. K. Lichtenthaler et al. (Dordrecht: Springer Netherlands), 307–322.

Conflict of Interest: The authors declare that the research was conducted in the absence of any commercial or financial relationships that could be construed as a potential conflict of interest.

Publisher's Note: All claims expressed in this article are solely those of the authors and do not necessarily represent those of their affiliated organizations, or those of the publisher, the editors and the reviewers. Any product that may be evaluated in this article, or claim that may be made by its manufacturer, is not guaranteed or endorsed by the publisher.

frontiers in Plant Science

ORIGINAL RESEARCH
published: 23 August 2021
doi: 10.3389/fpls.2021.717952

Mass Production of Virus-Like Particles Using Chloroplast Genetic Engineering for Highly Immunogenic Oral Vaccine Against Fish Disease

Yoichi Nakahira[1,2], Kaori Mizuno[3], Hirofumi Yamashita[3], Minami Tsuchikura[1], Kaoru Takeuchi[4], Takashi Shiina[5,6] and Hidemasa Kawakami[3]*

[1]College of Agriculture, Ibaraki University, Ami, Japan, [2]United Graduate School of Agricultural Science, Tokyo University of Agriculture and Technology, Fuchu, Japan, [3]Ehime Fisheries Research Center, Ehime, Japan, [4]Laboratory of Environmental Microbiology, Division of Basic Medicine, Faculty of Medicine, University of Tsukuba, Tsukuba, Japan, [5]Graduate School of Life and Environmental Sciences, Kyoto Prefectural University, Kyoto, Japan, [6]Department of Applied Biological Sciences, Faculty of Agriculture, Setsunan University, Hirakata, Japan

OPEN ACCESS

Edited by:
Thomas D. Sharkey, Michigan State University, United States

Reviewed by:
Fumihiko Sato, Kyoto University, Japan
Edward Alexander Espinoza Sánchez, Universidad Autónoma de Chihuahua, Mexico

***Correspondence:**
Yoichi Nakahira
yoichi.nakahira.41@vc.ibaraki.ac.jp

Specialty section:
This article was submitted to Plant Biotechnology, a section of the journal Frontiers in Plant Science

Received: *31 May 2021*
Accepted: *12 July 2021*
Published: *23 August 2021*

Citation:
Nakahira Y, Mizuno K, Yamashita H, Tsuchikura M, Takeuchi K, Shiina T and Kawakami H (2021) Mass Production of Virus-Like Particles Using Chloroplast Genetic Engineering for Highly Immunogenic Oral Vaccine Against Fish Disease. Front. Plant Sci. 12:717952. doi: 10.3389/fpls.2021.717952

Nervous necrosis virus (NNV) is the causative agent of viral nervous necrosis (VNN), which is one of the most serious fish diseases leading to mass mortality in a wide range of fish species worldwide. Although a few injectable inactivated vaccines are commercially available, there is a need for more labor-saving, cost-effective, and fish-friendly immunization methods. The use of transgenic plants expressing pathogen-derived recombinant antigens as edible vaccines is an ideal way to meet these requirements. In this study, chloroplast genetic engineering was successfully utilized to overexpress the red-spotted grouper NNV capsid protein (RGNNV-CP). The RGNNV-CP accumulated at high levels in all young, mature, and old senescent leaves of transplastomic tobacco plants (averaging approximately 3 mg/g leaf fresh weight). The RGNNV-CP efficiently self-assembled into virus-like particles (RGNNV-VLPs) in the chloroplast stroma of the transgenic lines, which could be readily observed by *in situ* transmission electron microscopy. Furthermore, intraperitoneal injection and oral administration of the crudely purified protein extract containing chloroplast-derived RGNNV-VLPs provided the sevenband grouper fish with sufficient protection against RGNNV challenge, and its immunogenicity was comparable to that of a commercial injectable vaccine. These findings indicate that chloroplast-derived VLP vaccines may play a promising role in the prevention of various diseases, not only in fish but also in other animals, including humans.

Keywords: red-spotted grouper nervous necrosis virus (RGNNV), virus-like particles (VLPs), chloroplast genetic engineering, oral vaccine, aquaculture

INTRODUCTION

According to a report by the Food and Agriculture Organization of the United Nations (FAO), global fish production reached 179 million tons in 2018, with first-hand sales estimated at USD 401 billion, and is projected to increase further over the next decade. In 2018, aquaculture accounted for 46% of global fish production (82 million tons), but its contribution is expected to be even greater in the future, as 34.2% of fish stocks are currently captured at biologically

unsustainable levels (FAO, 2020). There are several factors that hinder the sustainable development of the aquaculture sector, but one of the major challenges is the prevention and control of infectious diseases. Disease outbreaks can cause enormous economic losses in the aquaculture industry. There are a wide range of pathogens that can cause serious diseases in aquaculture, including viruses, bacteria, protozoa, and metazoans (Lafferty et al., 2015). Antibiotics have been widely used in aquaculture to prevent and treat bacterial infections, but the overuse and misuse of antibiotics have led to the spread of antibiotic-resistant strains that pose health risks to humans (Reverter et al., 2020). In addition, antibiotics are ineffective against pathogens other than bacteria. Therefore, vaccines are better alternatives to antibiotics.

Viral nervous necrosis (VNN), also known as viral encephalopathy and retinopathy (VER) is one of the most serious infectious diseases in aquaculture. It affects a wide range of hosts, including 177 susceptible marine species, 62 of which have been reported to be prevalent (Bandín and Souto, 2020). VNN frequently causes mass mortality in the larval and juvenile stages of fish (Munday and Nakai, 1997), leading to serious economic losses. Therefore, the development of a highly immunogenic, cost-effective, and labor-saving VNN vaccine is of great interest to the aquaculture industry. The causative agent of VNN is the nervous necrosis virus (NNV), which belongs to the genus *Betanodavirus*. NNV is a small, non-enveloped icosahedral virus that contains two positive-sense single-stranded RNA molecules, RNA1 (3.1 kb) and RNA2 (1.4 kb), encoding the RNA-dependent RNA polymerase and the capsid protein respectively (Low et al., 2017). Based on the phylogenetic analysis of the partially variable sequences within the RNA2, betanodaviruses have been classified into four major genotypes: striped jack NNV (SJNNV), tiger puffer NNV (TPNNV), red-spotted grouper NNV (RGNNV), and barfin flounder NNV (BFNNV) (Nishizawa et al., 1997). Of these, RGNNV is the most prevalent and has the highest number of susceptible species (Bandín and Souto, 2020).

To date, several potential vaccines against VNN have been proposed, including inactivated vaccines, DNA vaccines, synthetic peptides derived from NNV capsid protein (NNV-CP), recombinant subunit vaccines, and virus-like particles (VLPs) (Costa and Thompson, 2016; Bandín and Souto, 2020). However, among them, only a few formalin-inactivated vaccines against the RGNNV genotype have been licensed, including one for sevenband grouper in Japan (Costa and Thompson, 2016) and two for sea bass in the Mediterranean market (Bandín and Souto, 2020). Commercially available injectable vaccines provide sufficient protective immunogenicity against VNN, but the parenteral method of vaccination is laborious, expensive, stresses the fish, and is not applicable to small fish in the larval or juvenile stages. In contrast, oral administration of vaccines is an ideal immunization method for fish because it is labor-saving, inexpensive, and fish-friendly, and can be applied to any size of fish. Although injection is the only recommended route of administration for all commercially available VNN vaccines, oral administration of a formalin-inactivated vaccine with a capsaicin adjuvant has been reported to confer significant protective immunity against VNN in fish (Gaafar et al., 2018). However, the use of capsaicin in combination with an inactivated VNN vaccine may not be feasible because currently available commercial vaccines are more expensive compared to the wholesale price of fish. Therefore, there is an impending need for alternative cost-effective vaccines.

VLPs are composed of one or more structural proteins that self-assemble to mimic the shape and size of the native virions but do not contain the viral genetic materials required for replication. VLPs are one of the most promising vaccine candidates because they are safer than infectious attenuated and inactivated vaccines and can effectively elicit humoral and cellular immune responses (Lua et al., 2014; Charlton Hume et al., 2019; Nooraei et al., 2021). To date, several VLP-based vaccines against human diseases are commercially available, including vaccines against hepatitis B virus (HBV), human papillomavirus (HPV), and hepatitis E virus (HEV) (Lua et al., 2014; Nooraei et al., 2021). In addition, the use of VLPs against animal diseases, including fish, is also being explored as a highly immunogenic and cost-effective vaccine candidate (Liu et al., 2012; Jeong et al., 2020).

NNV-CP is the only structural protein of NNV that can self-assemble into VLPs. Several potential VLP vaccines against VNN have been reported, including NNV-VLPs produced in insect cells using a baculovirus expression system (Lin et al., 2001; Thiéry et al., 2006), *Escherichia coli* (Liu et al., 2006; Lai et al., 2014; Lin et al., 2016; Chien et al., 2018), and yeast (Wi et al., 2015; Cho et al., 2017). Among them, orange-spotted grouper NNV (OSGNNV)-VLPs derived from *E. coli* (Chien et al., 2018) and RGNNV-VLPs expressed in yeast (Cho et al., 2017) have been demonstrated to confer protective immunity against NNV challenges in fish not only by injection but also by oral administration, indicating that recombinant VLPs could be promising oral vaccines against VNN. However, such a VLP vaccine is not commercially available yet. Since the microbial production of NNV-VLPs and the subsequent purification process are costly, an oral VLP vaccine may not be affordable.

Over the last three decades, plants have been utilized as bioreactors in the "plant molecular farming" process to produce biopharmaceuticals, such as antibodies, vaccines, growth factors, and cytokines (Lomonossoff and D'Aoust, 2016; Mahmood et al., 2020; Tusé et al., 2020). Although only a limited number of plant-derived recombinant biopharmaceuticals have been commercially approved, plant molecular farming offers several advantages over other bioreactors, including cost-effectiveness, scalability, and lower risk of contamination by bacterial endotoxins or animal pathogens (Lomonossoff and D'Aoust, 2016; Mahmood et al., 2020; Tusé et al., 2020). Plant-based protein expression systems can be divided into two types: conventional stable transformation, where transgenes are introduced into the nuclear or chloroplast genome, and transient gene expression, using *Agrobacterium*-mediated infiltration or plant virus-based vectors. Although generating stable transformants is time-consuming and labor-intensive, edible host plants

expressing the desired recombinant antigen can be administered directly as oral vaccines without any purification process (Hernández et al., 2014). This is an attractive feature for the development of highly immunogenic, labor-saving, and cost-effective vaccines for animals, including fish (Clarke et al., 2013; Shahid and Daniell, 2016). Conversely, transient expression systems can produce recombinant proteins rapidly and in large quantities and are suitable to produce injectable vaccines that require the purification of recombinant antigens (Lomonossoff and D'Aoust, 2016; Mahmood et al., 2020; Tusé et al., 2020). Using transient expression systems, a variety of potential VLP-based vaccines against human diseases have been developed (Marsian and Lomonossoff, 2016; Rybicki, 2020), some of which are in clinical trials, including SARS-CoV2 vaccine candidates (Mahmood et al., 2020; Tusé et al., 2020; Shohag et al., 2021).

Taking advantage of plant molecular farming, it has been reported that transient expression of Atlantic cod NNV (ACNNV)-CP in *Nicotiana benthamiana* leaves causes the capsid protein to self-assemble into ACNNV-VLPs (Marsian et al., 2019). Furthermore, purified ACNNV-VLPs were able to partially protect sea bass from NNV challenge, suggesting that plant-derived NNV-VLPs could be candidates for VNN vaccines. However, the yield of ACNNV-VLPs obtained by transient expression in tobacco leaves was still low (10 mg of purified VLPs from 1 kg of fresh weight leaves), and the immunogenicity of plant-derived ACNNV-VLPs by oral administration has not yet been evaluated (Marsian et al., 2019).

Chloroplast genetic engineering (plastid transformation) has several advantages over nuclear transformation, the most distinctive of which is the ability to integrate transgenes into the entire highly polyploid chloroplast genomes (up to 10,000 copies per cell), resulting in extremely high levels of exogenous protein expression (Cardi et al., 2010; Jin and Daniell, 2015; Fuentes et al., 2018). In most cases, the accumulation levels of recombinant proteins expressed in transplastomic plants are 10–100 times higher than those expressed in nuclear transformants and can even reach more than 70% of the total soluble protein (TSP) (Oey et al., 2009; Castiglia et al., 2016). Further advantages of plastid transformation include the absence of positional effects and gene silencing, expression of multiple transgenes in an operon, and containment of the transgenes by maternal inheritance of the plastid genomes (Cardi et al., 2010; Jin and Daniell, 2015; Fuentes et al., 2018). Chloroplast genetic engineering has been applied to the production of high value-adding proteins, such as vaccine antigens, biopharmaceuticals, and industrial enzymes, as well as to the improvement of crop traits and metabolic engineering. In particular, various studies have reported the production of recombinant antigens derived from human and animal pathogens, and several studies have shown that oral administration of antigen vaccines expressed in crops with edible leaves, such as lettuce, can provide sufficient immunogenicity (Arlen et al., 2008; Davoodi-Semiromi et al., 2010; Yácono et al., 2012; Lakshmi et al., 2013; Daniell et al., 2019). Although examples of chloroplast-expressed VLPs are limited to those derived from human papillomavirus type 16 (HPV-16) (Fernández-San Millán et al., 2008; Lenzi et al., 2008; Waheed et al., 2011), dengue serotype 3 virus (Kanagaraj et al., 2011), and poliovirus serotype 2 (Daniell et al., 2019), it has been reported that HPV-16 L1 capsid protein accumulates at high levels (24% of TSP) in transplastomic tobacco plants and self-assembled into VLPs, which were highly immunogenic when injected intraperitoneally into mice (Fernández-San Millán et al., 2008). These results suggest that chloroplast genetic engineering may be a promising platform for the high-yield production of immunogenic VLP-based vaccines.

In this study, we generated transplastomic tobacco plants overexpressing the RGNNV capsid protein (RGNNV-CP), which could successfully self-assemble into VLPs (RGNNV-VLPs) in the chloroplast stroma. Both intraperitoneal injection and oral administration of chloroplast-derived RGNNV-VLPs to fish (sevenband grouper) showed high immunogenicity against NNV challenge.

MATERIALS AND METHODS

Plant Growth Conditions

Tobacco (*Nicotiana tabacum* cv. Xanthi) plants were grown aseptically on Murashige-Skoog (MS) medium containing 3% (w/v) sucrose and 0.8% (w/v) agar at 25°C under a light–dark cycle with a 16-h light period (50 μmol photons m^{-2} s^{-1}) and an 8-h dark period. Soil-grown tobacco plants were cultivated in a phytotron (Koitotoron SBH2515A, Koito Industries Co., Yokohama, Japan) using sunlight and natural daylengths with a temperature cycle of 12 h at 26°C and 12 h at 23°C.

Construction of the Plastid Transformation Vector

To construct a universal plastid transformation vector for tobacco plants, the homologous DNA fragment corresponding to a part of the tobacco plastid *rrn16-rrn23* region [nucleotides 103441-107302 in *N. tabacum* chloroplast genome DNA (GenBank accession number Z00044.2)] was amplified by PCR using total cellular tobacco DNA as a template with the following primer pair: ADLF (5'-CACTCTGCTGGGCCGACACTGACAC-3') and ADLR (5'-CACTAGCCGACCTTGACCCCTGTT-3'), and inserted into *Pvu*II-digested pBluescript II KS (+) (Stratagene). The resulting plasmid was then digested with *Pvu*II, which recognizes the intergenic spacer region between tobacco plastid *trnI* and *trnA*, and the spectinomycin resistance gene (*aadA*), driven by the tobacco plastid P*rrn* promoter (nucleotides 102553-102728 in Z00044.2) and the bacteriophage T7 gene 10 leader sequence (G10L), was inserted into the *Pvu*II-digested site to obtain the universal plastid transformation vector, p16S-aadA-23S(T).

The cDNA encoding RGNNV-CP was derived from RNA2 of the RGNNV strain SG2001Nag (GenBank accession number AB373029). A DNA fragment consisting of the coding sequence of RGNNV-CP (nucleotides 27-1043 in AB373029) with codon usage optimized for plastid expression (*RGNNV-CPpt*) and the subsequent 3' non-coding region (3' NCR) from the RNA2 of RGNNV, flanked by *Nco*I and *Xba*I sites, was synthesized by Eurofins Genomics (Tokyo, Japan). The synthetic DNA fragment was cloned into the pPpsbA-TpsbA(R), harboring the tobacco

plastid *psbA*-derived promoter and subsequent 5'-untranslated region (5'-UTR; complement of nucleotides 1595-1811 in Z00044.2; P*psbA*), a multiple cloning site, and 3'-UTR of tobacco *psbA* (complement of nucleotides 142-535 in Z00044.2; T*psbA*). The resulting expression cassette, P*psbA*::*RGNNV-CPpt*::RNA2-3' NCR::T*psbA*, was cut out with *Pst*I and *Sal*I and inserted into p16S-aadA-23S(T), which has cognate restriction sites just downstream of *aadA*, to obtain the plastid transformation vector, pRGNNV1. The nucleotide sequence of the final construct was confirmed by dye-terminator sequencing.

Generation of Transplastomic Tobacco Plants

Plastid transformation was performed as described in previous studies (Nakahira et al., 2013; Kikuchi et al., 2018). Gold particles (0.6 μm) coated with pRGNNV1 plasmid DNA were delivered into young tobacco leaves cultured *in vitro* using the Biolistic® PDS1000/He particle delivery system (Bio-Rad, Hercules, CA, United States). The bombarded leaves were kept in the dark at 25°C for 3 days, then cut into small pieces (~0.25 cm^2), and placed onto RMOP agar medium [MS medium containing 3% (w/v) sucrose, 0.8% (w/v) agar, 0.1 mg/L 1-naphthaleneacetic acid, 1 mg/L N^6-benzyladenine, 1 mg/L thiamine, 100 mg/L inositol] supplemented with 200 mg/L spectinomycin dihydrochloride as a selective agent. In tobacco plasmid transformation, it is common to use 500 mg/L spectinomycin dihydrochloride in all selection rounds, but we experienced low efficiency in acquiring resistant shoots or calli when 500 mg/L spectinomycin dihydrochloride was used in primary selection. Therefore, in our research group, the use of 200 mg/L spectinomycin dihydrochloride for primary selection was kept as a standard condition (Nakahira et al., 2013; Kikuchi et al., 2018). Resistant shoots and calli were transferred onto RMOP agar medium containing 500 mg/L spectinomycin dihydrochloride for the second selection. The obtained shoots were subjected to total cellular DNA extraction, as described previously (Kikuchi et al., 2018). To confirm that *RGNNV-CPpt* was correctly introduced into the specific region of the plastid genome, PCR-based genotyping was performed using the total cellular DNA as a template with the primer pair 1: ADL-F3 (5'-CGGGGGGGACCACCACGGCT-3') and ADL-R3 (5'-AGGGTT GAAGGGAGATAGTGCATCA-3'), and primer pair 2: RGNNV-Fd1 (5'-CCATGGTAAGAAAAGGAGAAAAAAAATTAGC-3') and Sal-TpsbA-Rv (5'-GTCGACCGAATATAGCTCTTCTTTCTTA TT-3'). The amplification program using primer pairs 1 and 2 was as follows: 94°C for 1 min, followed by 30 cycles at 94°C for 30 s, 53°C for 30 s, and 72°C for 2 min. The transgenic lines confirmed by genotyping were subjected to two more rounds of regeneration cycles on RMOP agar medium containing 500 mg/L spectinomycin dihydrochloride to achieve homoplasmy and finally rooted on MS medium supplemented with 3% (w/v) sucrose, 0.8% (w/v) agar, and 500 mg/L spectinomycin dihydrochloride.

Southern Blot Analysis

Total cellular DNA was extracted from wild-type and transplastomic tobacco leaves using the DNeasy Plant Mini Kit (QIAGEN, Valencia, CA, United States) according to the manufacturer's instructions. One microgram of total cellular DNA was digested with *Xmn*I, separated by 1% (w/v) agarose gel electrophoresis, and transferred to an Amersham Hybond-N^+ positively charged nylon membrane (GE Healthcare, Chicago, IL, United States). The DNA probe covering a part of the tobacco plastid *rrn16-rrn23* operon was generated using the PCR DIG Probe Synthesis Kit (Roche/Merck KGaA, Darmstadt, Germany) with wild-type tobacco total cellular DNA as a template and a primer pair: ADL-F2 (5'-CCCCTTTTTT ACGTCCCCATGTTCC-3') and ADL-R2 (5'-GCCTTTCCTCG TTTGAACCTCGCCC-3'). The amplification program was as follows: 95°C for 2 min, followed by 30 cycles at 95°C for 30 s, 58°C for 30 s, 72°C for 1 min, and 72°C for 7 min. Hybridization was performed overnight at 60°C using DIG Easy Hyb (Roche/Merck KGaA, Darmstadt, Germany). The hybridized membrane was then washed, and the probe DNA was detected using a DIG Luminescent Detection Kit (Roche/Merck KGaA, Darmstadt, Germany) according to the manufacturer's instructions. Immunodetectable bands on the membrane were visualized using the Chemiluminescence Imaging System, FUSION SL4 (Vilber-Lourmat, France).

SDS-PAGE and Western Blot Analysis

To extract total cellular proteins from leaves of wild-type and transplastomic tobacco plants grown on MS medium or in soil, leaf material (200 mg) was homogenized in 1 ml of pre-chilled phosphate-buffered saline (PBS) (pH 7.4). The homogenate was centrifuged at 20,000 × *g* for 5 min at 4°C, and the supernatant was collected as a soluble fraction. The resulting pellet was resuspended in an equal volume of PBS and 2× Laemmli Sample Buffer (Bio-Rad, Hercules, CA, United States), and centrifuged at 20,000 × *g* for 5 min at 4°C. The resulting supernatant was collected as the insoluble fraction. The protein concentration in the soluble fraction (total soluble protein; TSP) was quantified using BCA Protein Assay Kit (TaKaRa Bio Inc., Kusatsu, Japan) according to the manufacturer's instructions. The protein extracts were separated by 12.5% or 13% sodium dodecyl sulfate-polyacrylamide gel electrophoresis (SDS-PAGE) and subjected to Coomassie Brilliant Blue (CBB) staining or Western blot analysis. For Western blot analysis, proteins were transferred to polyvinylidene difluoride (PVDF) membranes (Hybond P; GE Healthcare, Chicago, IL, United States). After blocking, the blots were incubated for 1 h with a custom-made rabbit antiserum against a mixture of two synthetic peptides derived from amino acid residues 170-180 and 209-220 of RGNNV-CP, purchased from Eurofins Genomics (Tokyo, Japan), and then washed with T-PBS [PBS containing 0.1% (w/v) Tween-20]. The blots were then incubated with anti-rabbit IgG and HRP-linked antibody (Cell Signaling Technology, Danvers, MA, United States) at a dilution of 1:20,000 for 1 h. After washing the membranes with T-PBS, immunoblot detection was performed using a Chemiluminescence Imaging System (FUSION SL4, Vilber-Lourmat, France) and ECL Prime Western blotting detection reagent (GE Healthcare, Chicago, IL, United States). The expression levels of RGNNV-CP were quantified by densitometric analysis using Fusion-Capt software (Vilber Lourmat, France).

Expression and Purification of RGNNV-VLPs in *Escherichia coli*

DNA fragments flanked by *Nco*I and *Not*I sites encoding the codon-optimized *RGNNV-CP* for expression in *E. coli* (*RGNNV-CPec*) or its variant with a 6×His tag at the C-terminus (*RGNNV-CPec-(GGGS)$_3$-His$_6$*) were synthesized by Eurofins Genomics (Tokyo, Japan). Synthetic DNA fragments (*RGNNV-CPec* and *RGNNV-CPec-(GGGS)$_3$-His$_6$*) were inserted into pET-28a (Novagen; Merck KGaA, Darmstadt, Germany) digested with *Nco*I and *Not*I to obtain pET-RGNNV and pET-RGNNV-His, respectively.

The pET-RGNNV or pET-RGNNV-His was expressed in *E. coli* BL21 (DE3), and the cells were cultured in Luria-Bertani (LB) broth containing 20 mg/ml kanamycin at 37°C until the OD at 600 nm reached 0.3–0.6. To induce gene expression, isopropyl β-D-thiogalactopyranoside (IPTG) was added to a final concentration of 1 mM, and the cells were cultured at 30°C for 2 h. Cells were harvested and disrupted in PBS using a sonicator (Sonifier SFX250, Branson, Danbury, CT, United States). After centrifugation, the resulting supernatant was layered on a 30% (w/w) sucrose cushion and ultracentrifuged at 250,000 × *g* for 60 min at 4°C using a Beckman TLS-55 swinging bucket rotor (Beckman Coulter Inc., Brea, CA, United States). The resulting pellet was resuspended in PBS and then layered onto a 10–40% (w/w) discontinuous sucrose gradient and ultracentrifuged at 250,000 × *g* for 20 min at 4°C using a Beckman TLS-55 swinging bucket rotor. The collected fractions were analyzed by SDS-PAGE to confirm the fractions enriched with RGNNV-VLPs. The desired fractions containing RGNNV-VLPs were diafiltrated and concentrated using the Amicon Ultra-15 Centrifugal Filter Unit [10,000 molecular weight cutoff (MWCO); Merck KGaA, Darmstadt, Germany], according to the manufacturer's instructions.

Purification of Plant-Derived RGNNV-VLPs

Mature leaves (200 mg leaf fresh weight) from transplastomic tobacco plants were homogenized in 1 ml of pre-chilled PBS (pH 7.4). After centrifugation at 20,000 × *g* for 20 min at 4°C, the resulting supernatant was layered onto a 10–40% (w/w) discontinuous sucrose gradient and centrifuged at 141,000 × *g* for 3 h at 4°C using a Beckman SW28 swinging bucket rotor (Beckman Coulter Inc., Brea, CA, United States). The collected fractions were analyzed by SDS-PAGE to confirm the fractions enriched with RGNNV-VLPs. The desired fractions containing RGNNV-VLPs were diafiltrated and concentrated using the Amicon Ultra-15 Centrifugal Filter Unit (10,000 MWCO; Merck KGaA, Darmstadt, Germany), according to the manufacturer's instructions.

Transmission Electron Microscopy (TEM)

For negative staining, RGNNV-VLPs purified from *E. coli* or tobacco plants were diluted to 0.8 mg/ml, placed on freshly glow-discharged copper grids coated with carbon (Excel support film, 200 mesh, Nisshin EM Co., Tokyo, Japan), and allowed to dry completely. The grids were rinsed with water, negatively stained with 2% (w/v) uranyl acetate, and then dried. Micrographs were obtained using a transmission electron microscope (JEOL JEM-1400, Tokyo, Japan) operating at 80 kV. Digital images were captured using a charge-coupled device (CCD) camera (EM-14321DCAM; Hamamatsu Photonics K. K., Hamamatsu, Japan).

For ultrastructural observations, mature tobacco leaf samples were fixed with 2% paraformaldehyde (PFA) and 2% glutaraldehyde (GA) in 0.05 M cacodylate buffer (pH 7.4) overnight at 4°C. After fixation, the samples were washed with 0.05 M cacodylate buffer and post-fixed with 2% OsO_4 in 0.05 M cacodylate buffer for 3 h. The samples were then dehydrated overnight in a series of graded ethanol solutions, infiltrated with propylene oxide (PO), placed in a 50:50 mixture of PO and resin (Quetol-651; Nisshin EM Co., Tokyo, Japan) for 3 h, then transferred to a 100% resin, and polymerized at 60°C for 48 h. The polymerized resins were cut into 80-nm ultrathin sections with a diamond knife using an ultramicrotome (Ultracut UCT; Leica, Vienna, Austria), and the sections were mounted on copper grids and counterstained with 2% uranyl acetate and Lead stain solution (Sigma-Aldrich Co., Tokyo, Japan). The grids were observed using a transmission electron microscope (JEM-1400Plus; JEOL Ltd., Tokyo, Japan) at an acceleration voltage of 100 kV. Digital images were captured using a CCD camera (EM-14830RUBY2; JEOL Ltd., Tokyo, Japan).

Fish

Hatchery-reared young sevenband grouper (*Epinephelus septemfasciatus*) with an average body weight of 25.8 g were immunized intraperitoneally and orally with crudely purified protein extracts from tobacco mature leaves. Fish were reared at approximately 25°C in 1 m^3 tanks with a flow-through system, using water previously disinfected with ultraviolet (UV) light. All animal experiments were conducted in accordance with "Fundamental Guidelines for Proper Conduct of Animal Experiment and Related Activities in Academic Research Institutions under the jurisdiction of the Ministry of Education, Culture, Sports, Science and Technology (Notice No. 711)" and approved by the Ehime Fisheries Research Center. Prior to immunization experiments, 20 fish from the fish stock were randomly sampled and their brains were subjected to reverse transcriptase-polymerase chain reaction (RT-PCR) test for detecting betanodavirus as described by Nishioka et al. (2016). No positive PCR products were detected in any of the examined fish.

Virus

The SGEhi00 strain of RGNNV genotype (Yamashita et al., 2005) was propagated in E-11 cells in Leibovitz's L-15 medium (Thermo Fisher Scientific, Waltham, MA, United States) supplemented with 5% fetal bovine serum (FBS) (Thermo Fisher Scientific, Waltham, MA, United States) at 25°C. Viral infectivity titers were determined and stored at −80°C until use, as described by Iwamoto et al. (2000).

Immunization of Fish

Sevenband groupers were immunized by intraperitoneal injection or oral administration of crudely purified protein extracts from

wild-type and transplastomic tobacco leaves. Mature leaves were homogenized in pre-chilled PBS and centrifuged at 20,000 × *g* for 20 min at 4°C. The resulting supernatants were filtered using a filter (Millex-GP Syringe Filter Unit, 0.22 μm, polyethersulfone, 33 mm, gamma sterilized; Merck KGaA, Darmstadt, Germany) to remove cell debris. The filtrate was diafiltrated with PBS using an Amicon Ultra-15 Centrifugal Filter Unit (10,000 MWCO; Merck KGaA, Darmstadt, Germany) to reduce the contamination of alkaloids such as nicotine. The concentration of recovered proteins was quantified using BCA Protein Assay Kit (TaKaRa Bio Inc., Kusatsu, Japan), and the protein samples were diluted to 2 mg/ml in PBS and stored at −80°C until use.

A total of 280 fish were randomly divided into seven groups (approximately 40 fish per group). For parenteral vaccination, fish were immunized intraperitoneally with crudely purified protein extracts (200 μg/fish) from wild-type or transplastomic tobacco leaves, a commercial formalin-inactivated virus vaccine (OceanTect VNN; Nisseiken Co., Ltd., Ome, Japan) as positive control, or PBS as negative control. For oral vaccination, fish were fed commercial diets supplemented with crudely purified protein extracts from wild-type or transgenic tobacco leaves (200 μg/fish) or PBS (0.1 ml/fish) as a negative control, once a day for five consecutive days. After immunization, the experimental fish were transferred to 45 L plastic tanks at 25°C (±1.0°C), supplied with UV-treated water, and fed with commercial pellets once a day. On day 21 after immunization, blood samples were collected from the caudal veins of 8–10 fish per group to measure anti-RGNNV neutralizing antibody levels, and the remaining fish were subjected to a viral challenge test.

Viral Challenge Test

Fish were intramuscularly challenged with RGNNV (SGEhi00 strain) at a dose of $10^{3.3}$ $TCID_{50}$ per fish. The experimental fish were reared in 45 L tanks at 25°C (±1.0°C) for 14 days after challenging with virus and monitored for mortality. The relative percent survival (RPS; Amend, 1981) was calculated from the cumulative mortality using the following formula:

$$RPS = \left\{1 - \left(\frac{\%mortality\ of\ experimental\ group}{\%mortality\ of\ control\ group}\right)\right\} \times 100$$

Virus-Neutralizing Antibody Assay

Anti-RGNNV neutralizing antibody titers in sera were measured using E-11 cells and SGEhi00 strains, as described by Yamashita et al. (2005). The detection limit for antibody titer was 1:80.

Statistical Analysis

The cumulative mortality and morbidity of fish after the RGNNV challenge were analyzed using Fisher's exact probability test. The levels of anti-RGNNV neutralizing antibodies between the vaccinated and PBS-control fish groups were tested by Student's *t*-test. Statistical significance was set at $p < 0.05$.

RESULTS

Construction of Plastid Transformation Vector and Generation of Transplastomic Tobacco Plants

The plastid transformation vector pRGNNV1 was constructed to transform the chloroplast genomes. This vector contains a synthetic *RGNNV-CP* gene (*RGNNV-CPpt*) with codon usage optimized for expression in plastids. The coding region of *RGNNV-CPpt* was designed to be followed by a 3' non-coding region (3' NCR) derived from the RNA2 genome of RGNNV. The 3' NCR has been reported to be required for high expression of RGNNV-CP in avian cell lines (Huang et al., 2007). To further increase the expression level of *RGNNV-CPpt*, the transgene was driven by a promoter derived from tobacco plastid *psbA* and its subsequent 5'-untranslated region (5'-UTR), and the transcript was stabilized by the 3'-UTR of tobacco plastid *psbA*. This expression cassette was inserted into the *trnI-trnA* intergenic region derived from the tobacco plastid DNA on the universal plastid transformation vector p16S-aadA-23S(T) with the spectinomycin resistance gene, *aadA*, as a selectable marker, to obtain pRGNNV1 (**Figure 1A**).

Plastid transformation was carried out by the biolistic method using pRGNNV1, and 36 bombardments resulted in 11 independent spectinomycin-resistant shoots/calli. Shoots regenerated after the second round of selection with spectinomycin were genotyped by PCR using a primer pair (ADL-F3 and ADL-R3) to infer site-specific incorporation of the transgene and another primer pair (RGNNV-Fd1 and Sal-TpsbA) to confirm the presence of the transgene. The results demonstrated that three of the regenerating shoots were PCR-positive, and that six were PCR-negative and considered to be spontaneous mutants (data not shown). For the remaining two regenerating shoots, the presence of the transgene was confirmed, but it was not targeted to the *trnI-trnA* intergenic region (data not shown). In both the shoots, the transgene may have been mis-targeted due to homologous recombination *via* the *psbA* promoter and/or the 5'-, 3'-UTR of *psbA* used in the expression cassette. After the three positive shoots were subjected to two more rounds of regeneration cycles on RMOP agar medium containing 500 mg/L spectinomycin dihydrochloride to achieve homoplasmy, they were finally rooted on MS agar medium supplemented with 500 mg/L spectinomycin dihydrochloride. Two of the three lines showed a normal phenotype, but one line exhibited abnormal leaf morphology with rounding and unevenness, probably due to somatic mutation caused by tissue culture. Therefore, two independent transformants with normal phenotypes (RGNNV1-1 and RGNNV1-2) were subjected to further analysis.

To verify the site-specific integration into the plastid genome and to confirm homoplasmy, Southern blot analysis was performed using a probe covering the flanking region (**Figure 1A**). The expected size of DNA fragments digested with *Xmn*I was 2.3 kb and 5.3 kb for wild-type and the transformed plastid DNA, respectively (**Figure 1A**). There was no detectable 2.3 kb band in the two transgenic lines, indicating that all copies of the plastid genome were

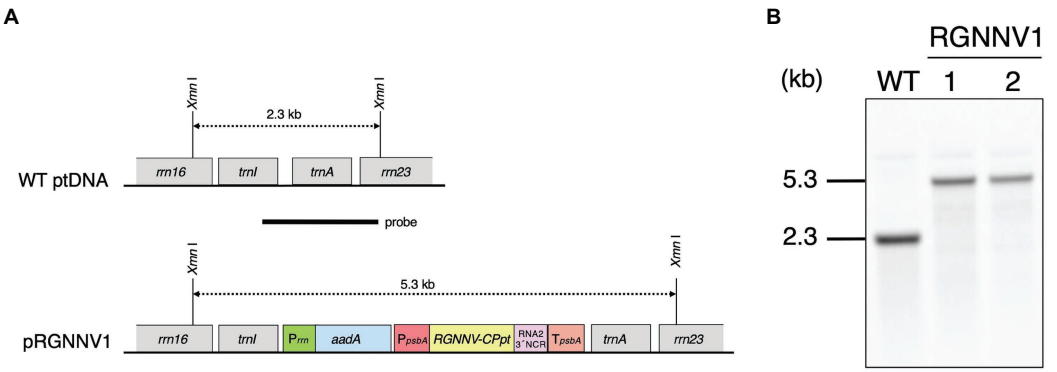

FIGURE 1 | Generation of transplastomic tobacco plants expressing RGNNV capsid protein (RGNNV-CP). **(A)** Physical map of the target region in the plastid genome (WT ptDNA) and schematic diagram of the chloroplast transformation vector, pRGNNV1 (construct not drawn to scale). Synthetic DNA covering the codon-optimized *RGNNV-CP* (*RGNNV-CPpt*) and the subsequent 3' non-cooding regioon (3' NCR) derived from the RNA2 genome of red-spotted grouper NNV (RGNNV) is driven by the tobacco plastid *psbA* promoter and its 5'-UTR (P*psbA*), and the transcript is designed to be stabilized by the 3'-UTR of tobacco plastid *psbA* (T*psbA*). The selectable marker gene *aadA* is under the control of the tobacco plastid ribosomal RNA operon promoter (P*rrn*). The transgenes are targeted to the intergenic spacer region between *trnI* and *trnA* in the tobacco plastid genome. The location of the probe used in Southern blot analysis is shown as a black bar. The wild-type and the transgenic chloroplast genomes give rise to hybridization signals corresponding to 2.3 kb and 5.3 kb *Xmn*I-*Xmn*I DNA fragments, respectively. **(B)** Southern blot analysis of two independent transgenic lines (RGNNV1-1 and RGNNV1-2). Total cellular DNA was digested with *Xmn*I and subjected to hybridization analysis with a DIG-labeled probe shown in **(A)**.

transformed (**Figure 1B**). The resulting homoplasmic T_0 lines were grown in soil for seed collection, and T_1 generation plants were used for all subsequent analyses.

High-Level Expression of RGNNV-CP in Transplastomic Tobacco Plants

When grown on MS agar medium supplemented with sucrose as a carbon source, the two transplastomic lines (RGNNV1-1 and RGNNV1-2) grew normally and showed a visible phenotype similar to that of the wild-type plants (**Figure 2A**). Protein extracts from mature leaves of wild-type and transgenic plants grown on the synthetic medium were subjected to SDS-PAGE followed by CBB staining. Protein extracts from the transgenic plants showed a specific band of approximately 37 kDa, which is expected for RGNNV-CP, mainly as a soluble protein, and its accumulation level was higher than that of the large subunit of Rubisco (RbcL) (**Figure 2B**).

When the transplastomic plants were grown in soil, they showed a weak pale green phenotype (**Figure 3B**) and significant growth retardation compared to wild-type plants (**Figure 3A**), but eventually grew to the same height as the wild-type plants, and viable seeds were obtained. Total soluble protein (TSP) extracted from mature leaves of soil-grown plants was analyzed by SDS-PAGE followed by CBB staining. As a result, a prominent band of approximately 37 kDa, corresponding to the expected molecular weight of RGNNV-CP, was specifically detected in the extracts of two independent transgenic lines (RGNNV1-1 and RGNNV1-2), which was not found in the wild-type plant extracts (**Figure 3C**). Since the biosynthetic capacity of proteins decreases with leaf age, we evaluated the stability of RGNNV-CP by examining the RGNNV-CP accumulation in each leaf. The results showed that the accumulation of most proteins, including RbcL, gradually decreased with senescence, while RGNNV-CP was highly expressed in young leaves and stably accumulated in mature and old senescent leaves (**Figure 4A**). To further confirm that the 37-kDa band was derived from *RGNNV-CPpt*, Western blot analysis was performed using an antiserum against a mixture of two synthetic peptides derived from RGNNV-CP. The results showed that the 37-kDa protein in transplastomic plants was identical to the gene product of *RGNNV-CPpt*, and no signal was obtained in wild-type plants (**Figure 4C**). The accumulation level of RGNNV-CP was quantified by Western blot analysis using a dilution series of the His-tagged RGNNV-CP recombinant protein expressed and purified in *E. coli* as a standard. Three independent experiments showed that RGNNV-CP accounted for 10.2, 20.1, and 22.7% of TSP in young, mature, and old senescent leaves of the transgenic plants, respectively (**Figure 4C**). Based on the protein content extracted from the leaves, the production yield of RGNNV-CP was estimated to be 3.5, 3.4, and 2.3 mg/g leaf fresh weight in young, mature, and old senescent leaves of the transplastomic plants, respectively.

RGNNV-CP Efficiently Self-Assembles Into VLPs in Chloroplast Stroma

RGNNV-CP was expressed in large amounts in the transplastomic plants and showed high stability even in old senescent leaves, suggesting that the recombinant protein was present in tobacco chloroplasts as VLPs. To confirm this, TSP extracted from the transgenic plants was analyzed by sucrose sedimentation. Among the 10 fractions recovered (fraction 1 obtained from the top of the tube), Rubisco was enriched in fractions 2 and 3, whereas RGNNV-CP was detected in fractions 6–10 with higher molecular weight (**Figure 5A**). This result is consistent with the fact that the Rubisco holoenzyme in tobacco plants is a 550 kDa RbcL8RbcS8 form (Wostrikoff and Stern, 2007), whereas 180

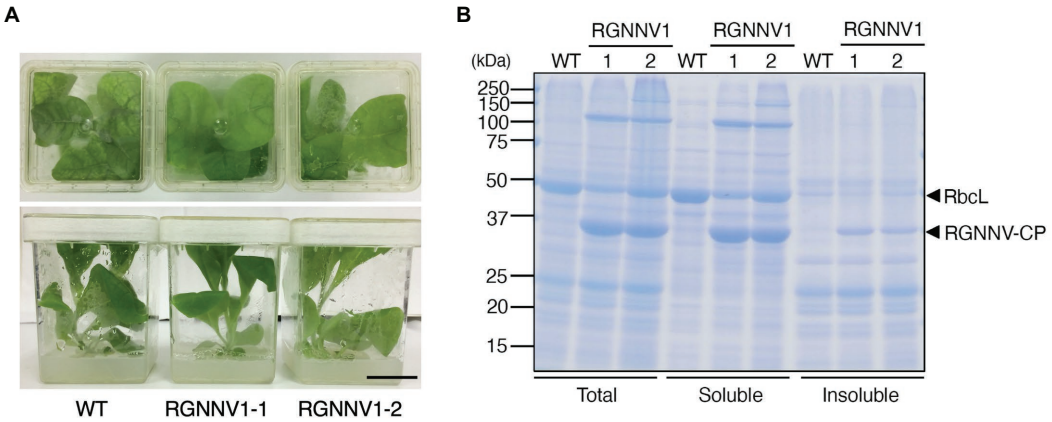

FIGURE 2 | Transplastomic plants expressing RGNNV-CP grown under photoheterotrophic conditions. **(A)** Phenotype of wild-type (WT) and transplastomic (RGNNV1-1 and RGNNV1-2) plants grown on MS agar medium containing 3% (w/v) sucrose as carbon source. Bar = 3 cm. **(B)** Detection of RGNNV-CP accumulated in transplastomic plants (RGNNV1-1 and RGNNV1-2) by Coomassie Brilliant Blue (CBB) staining. Total, soluble, and insoluble protein extracts from 1.5 mg of fresh leaf were separated by 12.5% sodium dodecyl sulfate-polyacrylamide gel electrophoresis (SDS-PAGE) gel and stained with CBB. The 37-kDa and 55-kDa bands correspond to RGNNV-CP and large subunit of Rubisco (RbcL), respectively.

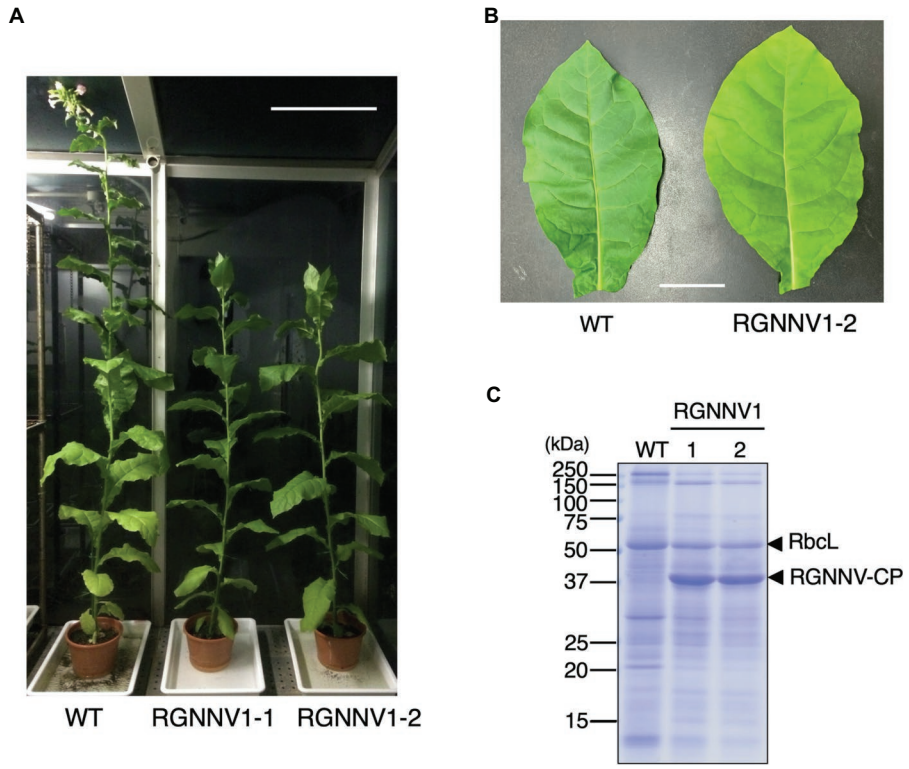

FIGURE 3 | Transplastomic plants expressing RGNNV-CP grown under photoautotrophic conditions. **(A)** Soil-grown wild-type (WT) and transplastomic (RGNNV1-1 and RGNNV1-2) plants were cultivated in a phytotron using sunlight and natural daylength, with a temperature cycle of 12 h at 26°C and 12 h at 23°C. Bar = 30 cm. **(B)** Mature leaves of WT and RGNNV1-2 plants. Bar = 5 cm. **(C)** Detection of RGNNV-CP accumulated in transplastomic plants (RGNNV1-1 and RGNNV1-2) by CBB staining. Total soluble protein (TSP) extracted from 1.5 mg of fresh leaf was separated by 13% SDS-PAGE gel and stained with CBB.

copies of RGNNV-CP arranged with $T = 3$ symmetry self-assemble into a 6,660-kDa VLP (Bandín and Souto, 2020). When fractions enriched with RGNNV-CP were collected and analyzed by transmission electron microscopy (TEM), spherical particles with a diameter of approximately 25–30 nm were frequently observed (**Figure 5B**). The morphology and size of

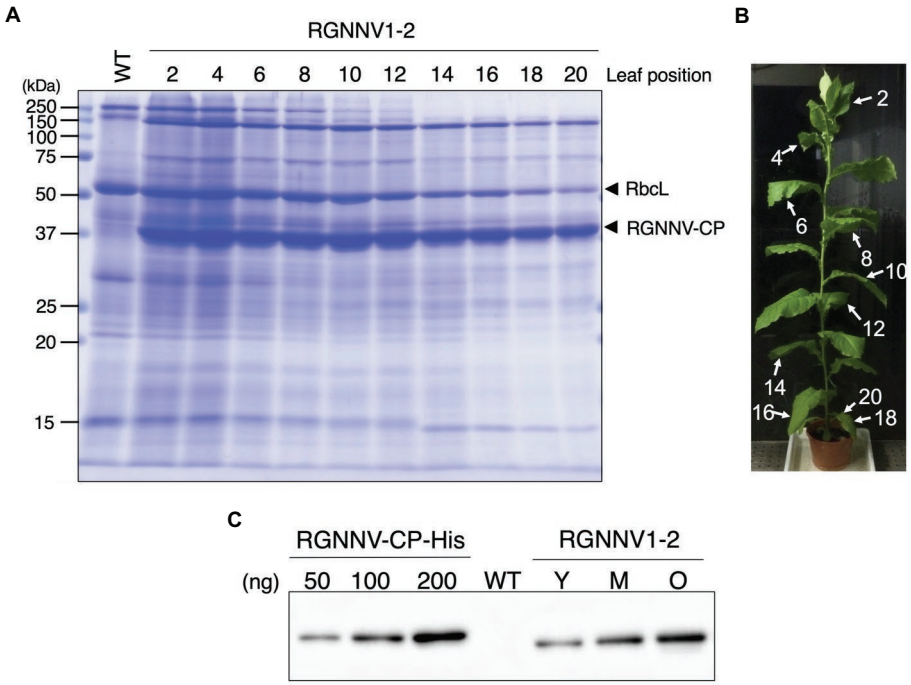

FIGURE 4 | High accumulation of RGNNV-CP in all leaves of the transgenic tobacco plant. **(A)** TSPs extracted from 1.5 mg of different leaves of a transplastomic plant (RGNNV1-2) were separated by 13% SDS-PAGE and stained with CBB. TSP extracted from a mature leaf of wild-type (WT) plant was loaded as a control. **(B)** The RGNNV1-2 plant used for the analysis shown in **(A)**. The leaves were numbered from top to bottom. **(C)** Western blot analysis to detect RGNNV-CP accumulated in the transplastomic plant. TSPs (500 ng) extracted from young (Y), mature (M), and old senescent (O) leaves of RGNNV1-2 correspond to leaf nos. 2, 10, and 20 in **(B)**, respectively, were analyzed. TSP (5,000 ng) extracted from a mature leaf of wild-type (WT) was also loaded as a control. Blots were detected using an antiserum against a mixture of synthetic peptides derived from RGNNV-CP. A dilution series (50, 100, and 200 ng) of purified 6×His-tagged RGNNV-CP (RGNNV-CP-His) expressed in *Escherichia coli* was analyzed as a standard.

the chloroplast-derived RGNNV-VLPs were similar to those expressed in *E. coli* (**Figure 5B**).

To investigate whether RGNNV-VLPs are formed in tobacco chloroplasts, *in situ* TEM observations were performed. Although the grana stacked in the chloroplasts of the transformants tended to be slightly smaller than those of wild-type tobacco, there were no significant differences in chloroplast size or morphology (**Figure 6**). Interestingly, however, the chloroplast stroma of the transplastomic plants contained uniformly dispersed spherical particles with a diameter of approximately 25–30 nm (**Figure 6**). Such structures were not observed in the chloroplasts of the wild-type plants (**Figure 6**). These results indicate that RGNNV-CP can self-assemble into VLPs in tobacco chloroplasts.

Chloroplast-Derived RGNNV-VLPs Are Highly Immunogenic Against RGNNV Challenge

To investigate the immunogenicity of chloroplast-derived RGNNV-VLPs, we planned to conduct a viral challenge test after intraperitoneal injection and oral administration of VLPs to the fish (sevenband grouper). Although it is convenient to use crude TSP extracts containing chloroplast-derived RGNNV-VLPs or lyophilized powder of the transgenic tobacco leaves as vaccine candidates, there are concerns that alkaloid, such as nicotine, contained in tobacco leaves may adversely affect fish or reduce the immunogenicity of chloroplast-derived RGNNV-VLPs. In fact, when *Staphylococcus aureus*-derived antigenic protein (Efb) was expressed in tobacco and lyophilized powder of transgenic leaves was orally administered to mice, transgenic leaves of a low-alkaloid tobacco variety (cv. 81V9) showed significantly higher immunogenicity than the transgenic leaves of a common tobacco variety (cv. Samsun) (Festa et al., 2013). Therefore, ultrafiltration was employed to reduce the alkaloid content of TSP extracted from the wild-type and transplastomic tobacco leaves. Although other methods have been reported to be more effective in removing nicotine from crude protein extracts derived from tobacco leaves (Fu et al., 2010), ultrafiltration using a centrifugal filter device was chosen because it is a simple method and is believed to have less effect on the VLP structure during the purification process. Comparison of the protein composition of TSPs extracted from the leaves of wild-type and transgenic plants before and after the ultrafiltration treatment showed no noticeable differences (**Supplementary Figure S1**). In a preliminary experiment, ultrafiltered protein extracts (200 μg/fish) from wild-type and transplastomic leaves were administered intraperitoneally or orally to sevenband grouper, and no lethal symptoms, abnormal swimming behavior, or reduced growth rate were observed, suggesting that the level of alkaloids remaining in the protein extracts after ultrafiltration was not considered to be harmful to fish.

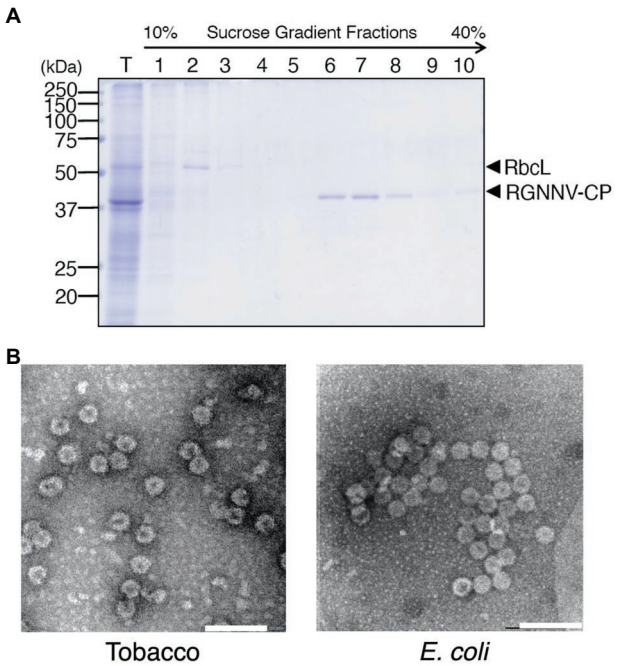

FIGURE 5 | Purification of RGNNV virus-like particles (RGNNV-VLPs) from transplastomic tobacco plants. **(A)** TSP (T) extracted from mature leaves of transplastomic plants (RGNNV1-2) was analyzed by sucrose gradient sedimentation, and RGNNV-CP in each fraction was detected by CBB staining. Fraction 1 was obtained from the top of the tube. **(B)** Electron micrograph of the RGNNV-CP-enriched fractions recovered by the sucrose gradient sedimentation analysis shown in **(A)**. RGNNV-VLPs derived from the transplastomic tobacco plants (Tobacco) and *E. coli* were visualized by negative staining with 2% (w/v) uranyl acetate and transmission electron microscopy (TEM). Bar = 100 nm.

For injection vaccination, ultrafiltered protein extracts from the transplastomic leaves (200 μg/fish; approximately equivalent to 1.5 μg/fish body weight of RGNNV-CP), the same amount of protein extracts from wild-type leaves, a commercially available formalin-inactivated vaccine, or PBS as a negative control were administrated intraperitoneally to the fish without adjuvant. Twenty-one days post-immunization, the experimental fish were challenged with RGNNV, and mortality was monitored. The results showed that the cumulative mortality of fish immunized with PBS and wild-type tobacco-derived protein extracts was 66.7 and 60.0%, respectively. In contrast, the cumulative mortality of fish groups vaccinated with the commercial vaccine and protein extracts containing chloroplast-derived RGNNV-VLPs was only 10.0 and 3.3%, respectively (**Figure 7**). This indicates that the RPS (Amend, 1981) of the fish injected intraperitoneally with the commercial vaccine and the protein extracts containing chloroplast-derived RGNNV-VLPs was 85.0 and 95.1%, respectively, revealing that the chloroplast-derived RGNNV-VLPs were more immunogenic than the commercial inactivated vaccine (**Table 1**).

For oral vaccination, ultrafiltered protein extracts from the transplastomic leaves (200 μg/fish; approximately equivalent to 1.5 μg/fish body weight of RGNNV-CP), the same amount of protein extracts from wild-type leaves, or PBS were mixed with commercial feed without adjuvant and fed to the fish once a day for five consecutive days. This oral vaccination relied on the fish to voluntarily eat the feed, making it difficult to strictly control the vaccine dosage. However, it is ideal for use at the practical application stage, and the same method has been used to investigate the immunogenicity of *E. coli*-derived OSGNNV-VLPs (Chien et al., 2018) and yeast-derived RGNNV-VLPs (Cho et al., 2017). A commercially available inactivated vaccine was not used in this experiment because it has been reported that it does not show significant immunogenicity when administered orally without adjuvant (Gaafar et al., 2018). As in the case of parenteral vaccination, the experimental fish were challenged with RGNNV 21 days after immunization and then monitored for mortality. The results showed that the cumulative mortality of the fish immunized with PBS and wild-type tobacco-derived protein extracts reached 50 and 66.7%, respectively (**Figure 7**). In contrast, the cumulative mortality of the fish group immunized with the protein extracts containing chloroplast-derived RGNNV-VLPs was only 13.8% (**Figure 7**), and the RPS was calculated to be 72.4% (**Table 1**). It seems counterintuitive that the cumulative mortality of the fish group immunized with wild-type tobacco-derived protein extracts (66.7%) was higher than that of the fish group immunized with PBS (50%), but the difference was not statistically significant (**Table 1**). Furthermore, when the cumulative morbidity was calculated by adding the number of surviving fish showing symptoms of the disease (abnormal swimming) to the number of dead fish, the morbidity of both fish groups immunized with PBS and wild-type tobacco-derived protein extracts was the same at 73.3% (**Table 1**). Therefore, the above results were considered to be due to experimental error and not due to toxic factors other than nicotine. Compared with the cumulative morbidity of the fish group vaccinated with PBS and with wild-type tobacco-derived protein extracts, the cumulative morbidity of the fish vaccinated with the protein extracts containing chloroplast-derived RGNNV-VLPs was significantly lower (13.8%) (**Table 1**), indicating that chloroplast-derived RGNNV-VLPs are immunogenic even when administered orally.

Serum was collected from each group of immunized fish, and the titer of anti-RGNNV neutralizing antibody was measured. The results showed that intraperitoneal injection of protein extracts containing chloroplast-derived RGNNV-VLPs elicited a high level of neutralizing antibodies (1:2600 ± 1913.1; $p < 0.01$). Statistically significant induction of neutralizing antibodies was also observed when the same protein extracts were administered orally (1:138 ± 49.1; $p < 0.01$) and when the commercial inactivated vaccine was administered by injection (1:160 ± 106.5; $p < 0.05$) (**Supplementary Figure S2**). This result is in agreement with the results of the RGNNV challenge test (**Figure 7**).

DISCUSSION

In this study, transgenic tobacco plants producing RGNNV-VLPs, a promising vaccine candidate against VNN, were developed using chloroplast genetic engineering. Consequently, high levels

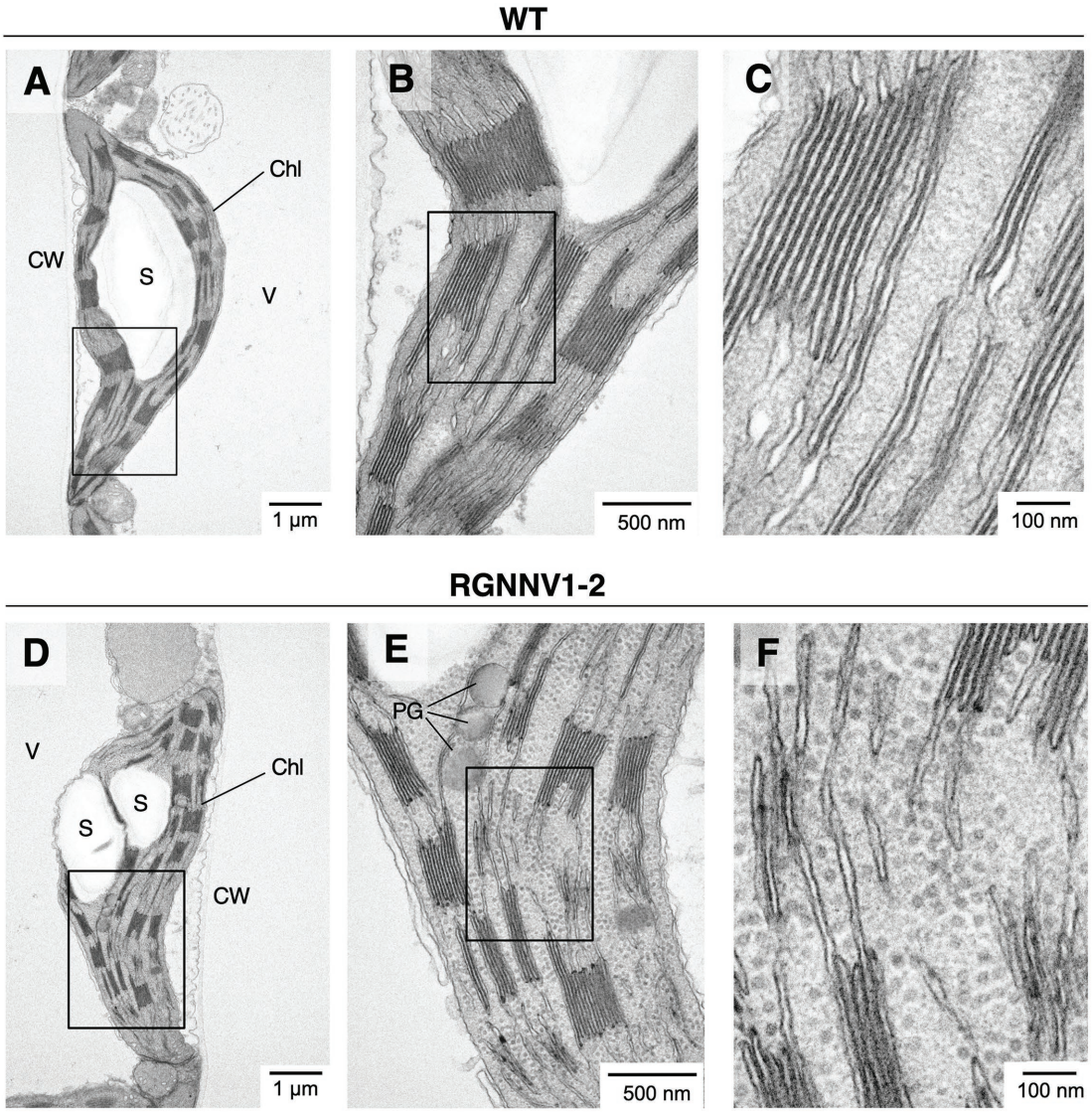

FIGURE 6 | Electron micrographs of RGNNV-VLPs present in high density in chloroplast stroma of transplastomic tobacco plants. *In situ* TEM images of chloroplasts from mature leaves of wild-type [WT; **(A–C)**] and the transplastomic [RGNNV1-2; **(D–F)**] plants. **(B)**, **(C)**, **(E)**, and **(F)** are magnified views of the box regions in **(A)**, **(B)**, **(D)**, and **(E)**, respectively. Chl, chloroplast; S, starch granule; V, vacuole; CW, cell wall; and PG, plastoglobule.

of RGNNV-CP accumulation (averaging about 3 mg/g leaf fresh weight) were achieved in all young, mature, and old senescent leaves (**Figure 4**). This may be due to the optimization of codon usage of *RGNNV-CP* for expression in chloroplasts, the use of the *psbA* promoter and its 5'-UTR, which are responsible for the high transcriptional and translational activity, respectively, and the utilization of the *psbA* 3'-UTR, which helps stabilize the transcript. A number of reports described successful high expression of transgenes using the *psbA*-derived gene expression cassette (Cardi et al., 2010; Jin and Daniell, 2015). In addition, among the several reports on chloroplast expression of the HPV-16 L1 capsid protein (Fernández-San Millán et al., 2008; Lenzi et al., 2008; Waheed et al., 2011), the highest expression level (24% of TSP) was achieved using a *psbA*-derived gene expression cassette (Fernández-San Millán et al., 2008). However, it is unlikely that the 3' NCR derived from RNA2 of RGNNV, which has been reported to contribute to the high expression of RGNNV-CP in avian cell lines (Huang et al., 2007), is also involved in the high accumulation of RGNNV-CP in chloroplasts. This is because we produced transplastomic tobacco plants expressing RGNNV-CP without the 3' NCR of RNA2 and observed that the accumulation level of RGNNV-CP was comparable to those of RGNNV1-1 and RGNNV1-2 with the 3' NCR (data not shown). Another reason for the high accumulation of RGNNV-CP in all leaves of the transplastomic tobacco plants may be that RGNNV-CP self-assembles into VLPs in the chloroplast stroma with high efficiency (**Figures 5, 6**), and the resulting higher-order molecular

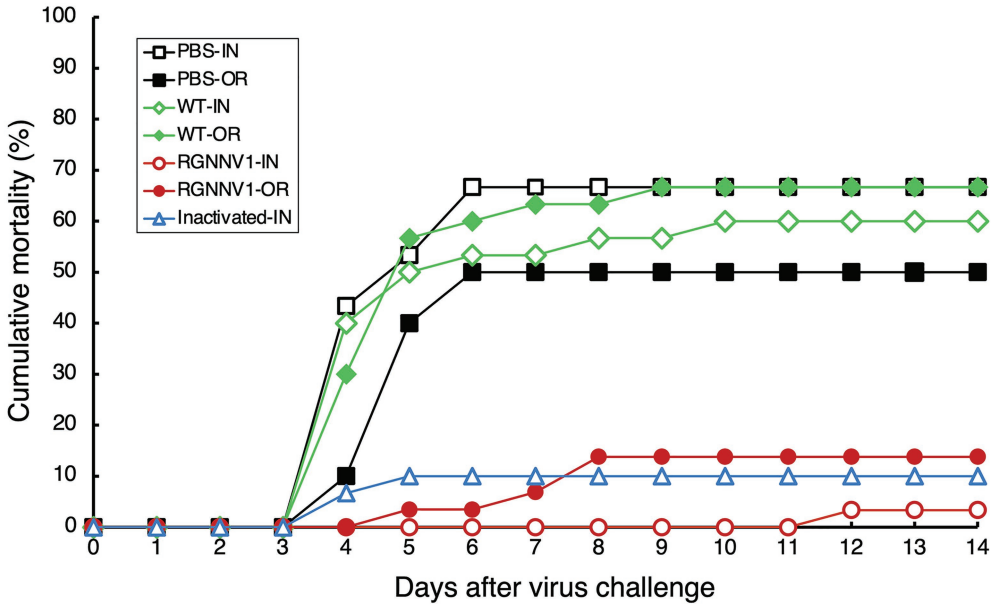

FIGURE 7 | Cumulative mortality after RGNNV challenge in sevenband grouper immunized with chloroplast-derived RGNNV-VLPs. Fish were vaccinated with PBS as control, crudely purified protein extracts from mature leaves of wild-type (WT) or the transplastomic (RGNNV1) tobacco plants, or a commercial inactivated vaccine (Inactivated) by intraperitoneal injection (IN) or oral administration (OR). On day 21 after immunization, the fish were challenged by intramuscular injection with RGNNV at a dose of $10^{3.3}$ $TCID_{50}$ per fish and observed for an additional 14 days.

TABLE 1 | Immunogenicity of chloroplast-derived RGNNV-VLPs against RGNNV-challenge in sevenband grouper fish.

Fish group[a]	Cumulative mortality (%) [No. of dead/No. of challenged]	RPS[b] (%)	Cumulative morbidity (%) [(No. of dead + No. of showing abnormal swimming)/No. of challenged]
PBS-IN	66.7 [20/30]		66.7 [(20 + 0)/30]
WT-IN	60.0 [18/30]	10.0	70.0 [(18 + 3)/30]
RGNNV1-IN	3.3 [1/30]*	95.1	3.3 [(1 + 0)/30]*
Inactivated-IN	10.0 [3/30]*	85.0	20.0 [(3 + 3)/30]*
PBS-OR	50.0 [15/30]		73.3 [(15 + 7)/30]
WT-OR	66.7 [20/30]	−33.4	73.3 [(20 + 2)/30]
RGNNV1-OR	13.8 [4/29]*	72.4	13.8 [(4 + 0)/29]*

[a]Fish were vaccinated with PBS as a control, crudely purified protein extracts from mature leaves of wild-type (WT) or transplastomic (RGNNV1) tobacco plants, or a commercial inactivated vaccine (Inactivated) by intraperitoneal injection (IN) or oral administration (OR). On day 21 after immunization, the fish were challenged by intramuscular injection with RGNNV at a dose of $10^{3.3}$ $TCID_{50}$ per fish and observed for an additional 14 days.

[b]RPS, Relative percent survival.

**$p < 0.01$.*

structures are resistant to proteolysis in chloroplasts. In this study, we investigated the accumulation level of RGNNV-CP in the T_1 generation plants. Since one of the advantages of plastid transformation is the absence of gene silencing, as seen in nuclear transformants, high expression levels are likely to be maintained in successive generations. Nevertheless, actual confirmation of the above is essential for future practical applications.

The expression levels of RGNNV-CP in the transplastomic tobacco plants generated in this study (averaging about 3 mg/g leaf fresh weight) are more than 100-fold higher compared to the productivity of ACNNV-VLPs transiently expressed in tobacco leaves (10 mg/kg leaf fresh weight) in a previous study (Marsian et al., 2019). Prior to this study, the expression of NNV-CP using chloroplast genetic engineering in tobacco has been reported, where, unlike our transformants, *NNV-CP* was transcribed by the rice plastid-derived *clpP* promoter, and the accumulation of NNV-CP in transplastomic tobacco plants was confirmed by Western blot analysis, however, quantitative analysis of expression levels has not been performed (Cho et al., 2018). Although a simple comparison cannot be made, it is likely that the transplastomic plants developed in this study, which expressed *RGNNV-CP* using the *psbA*-derived gene expression cassette, accumulated higher levels of the target capsid protein than the transgenic plants in the previous study. One rationale for this is that the *psbA* promoter shows much higher transcriptional activity than the *clpP* promoter in chloroplasts (Legen et al., 2002). Furthermore, the yield of RGNNV-CP

produced by the transplastomic tobacco plants in this study (averaging approximately 3 g/kg leaf fresh weight) was comparable to or better than that of 100 mg of OSGNNV-VLPs purified from 1 L of *E. coli* culture (Chien et al., 2018) and 60 mg of RGNNV-CP expressed in 1 L of yeast culture (Jeong et al., 2020). However, it is difficult to directly compare the immunogenicity of chloroplast-derived RGNNV-VLPs with that of VLP vaccines expressed in *E. coli* or yeast. This is because the conditions for each virus challenge test are different, including the species and age of the fish, dose, frequency, interval of administration of the VLP vaccines, and the titer of the virus that infected the fish (Cho et al., 2017; Chien et al., 2018).

The RGNNV challenge of sevenband grouper vaccinated by intraperitoneal injection demonstrated that crudely purified protein extracts containing chloroplast-derived RGNNV-VLPs (RPS = 95.1) were more immunogenic than the commercial inactivated vaccine (RPS = 85.0) (**Figure 7** and **Table 1**). This result is consistent with the induction of extremely high levels of neutralizing antibodies against RGNNV in the fish group vaccinated with chloroplast-derived RGNNV-VLPs (**Supplementary Figure S2**). Furthermore, oral administration of chloroplast-derived RGNNV-VLPs also showed significant immunogenicity (RPS = 72.4), although it was lower than that of parenteral administration. However, the variables influencing oral immunization (dose, number of doses, and administration interval) have not been optimized, and future studies are needed to improve the immunogenicity of orally administered chloroplast-derived RGNNV-VLPs. It should also be noted that the levels of neutralizing antibodies elicited by oral administration of chloroplast-derived RGNNV-VLPs and by injection of a commercially available inactivated vaccine were lower than expected (**Supplementary Figure S2**), and the results could not clearly explain the high RPS values in the RGNNV challenge test (**Figure 7** and **Table 1**). Similar contradictory results were reported when sea bass was immunized by injection of ACNNV-VLPs transiently expressed in tobacco leaves. In a previous study, parenteral administration of plant-derived VLPs to fish provided some protection against NNV, but failed to induce statistically significant anti-NNV antibodies (Marsian et al., 2019). One hypothesis to explain these seemingly contradictory results is that injection or oral administration of an inactivated or VLP vaccine against NNV in fish may activate the humoral and cellular immune systems simultaneously. This is because it has been reported that immunization of fish with inactivated or VLP-based vaccines not only induces neutralizing antibodies against NNV, but also activates the expression of genes associated with cellular immunity against betanodavirus infection (Kai et al., 2014; Lai et al., 2014).

Immersion vaccination is an alternative immunization method other than injection or oral administration and is suitable for mass vaccination of fish that are too small for vaccination by injection (Bøgwald and Dalmo, 2019). Immersion vaccination of fish with OSGNNV-VLPs derived from *E. coli* has been reported to be more immunogenic than injection, however, the dose of OSGNNV-VLPs required to confer significant protective immunity by immersion was approximately 125 times higher than that of injection (Chien et al., 2018), making it difficult to reduce the cost of the vaccine. Although immersion vaccination of fish with chloroplast-derived RGNNV-VLPs has not been investigated, the high yield of RGNNV-VLPs produced by transplastomic tobacco plants in this study suggests that immersion administration of chloroplast-derived RGNNV-VLPs may be an affordable vaccination method.

In this study, we have shown that chloroplast genetic engineering is a promising platform for the mass production of highly immunogenic RGNNV-VLP vaccines. However, it will not be easy to commercialize the transplastomic plants developed in the present study. Crude protein extracts from tobacco leaves contain alkaloids, such as nicotine, which must be removed before vaccination, but the cost of the purification process is thought to be an obstacle to practical application. Even though the use of low-alkaloid tobacco as a host plant is possible, given consumer psychology, the use of a non-edible plant as an oral vaccine may not be socially acceptable. One possible solution to this problem is to develop transplastomic plants that express large amounts of RGNNV-CP using leafy greens as host plants. Lettuce is a representative leafy vegetable for which a reproducible chloroplast transformation method has been established. Lettuce transplastomic plants expressing various recombinant antigens derived from human and animal pathogens have been developed. Some studies have demonstrated that recombinant antigens can be maintained in lyophilized transgenic lettuce leaves for a long time at ambient temperature, and specific antibodies against the antigens were induced in mice by oral administration of lyophilized plant materials (Davoodi-Semiromi et al., 2010; Lakshmi et al., 2013; Daniell et al., 2019). Fortunately, it has been reported that RGNNV-VLPs can maintain their immunogenicity even after lyophilization (Lan et al., 2018). Therefore, lyophilized powder of transplastomic lettuce leaves expressing RGNNV-VLPs mixed with feed pellets and orally administered to fish would be an ideal method of VNN vaccination. We are currently working on the generation of transplastomic lettuce plants overexpressing RGNNV-CP.

In the present study, we successfully expressed RGNNV-VLPs with sufficient immunogenicity in tobacco chloroplasts, suggesting that plastid transformation may be effective for mass production of VLP vaccines against other fish diseases caused by non-enveloped viruses, such as infectious pancreatic necrosis virus (IPNV) (Jeong et al., 2020). The same is likely to be true for the manufacture of VLP vaccines for the prevention of viral diseases affecting humans and animals. While most reports on the production of VLP vaccines in plants have utilized stable nuclear transformation or transient expression systems (Marsian and Lomonossoff, 2016; Rybicki, 2020), the use of chloroplast genetic engineering may also be worth considering.

Since VLPs are particulate and have a high density of capsid proteins on their surface, attempts have been made to display heterologous antigens on the surface of VLPs by genetic fusion or chemical conjugation to generate more immunogenic vaccines (Chen and Lai, 2013; Rybicki, 2020). RGNNV-VLPs may serve as attractive carriers for displaying foreign antigens. This is because it has been reported that when foreign peptides were fused to the C-terminus of OGNNV-CP, which is 100% identical in amino acid sequence to RGNNV-CP, and expressed in *E. coli*, the modified OGNNV-CPs were able to self-assemble into

stable VLPs displaying a high density of foreign peptides (Xie et al., 2016). If similar improvements can be applied to chloroplast-expressed RGNNV-VLPs, they could provide a versatile platform for the development of affordable vaccines against various fish diseases caused by enveloped viruses, bacteria, protozoa, and metazoans. Furthermore, a previous study by another group reported that oral administration of lyophilized powder of transplastomic tobacco leaves expressing NNV-CP induced significant NNV-CP-specific IgA and IgG responses in immunized mice (Cho et al., 2018), suggesting that chloroplast-derived RGNNV-VLPs may also play a promising role in disease prevention in mammals, including humans.

CONCLUSION

The results of the present study show that chloroplast genetic engineering is a promising platform for the high-yield production of RGNNV-VLPs, which can confer high immunity to fish by injection or oral administration. In the future, if leafy vegetables such as lettuce overproducing RGNNV-VLPs can be generated by plastid transformation, they could be commercialized as ideal oral vaccines that are cost-effective, labor-saving, and fish-friendly. Further research on the production and improvement of VLPs using chloroplast genetic engineering, not limited to RGNNV-VLPs, may provide an impetus for the development of affordable oral vaccines to prevent infectious and chronic diseases in animals and humans.

DATA AVAILABILITY STATEMENT

The original contributions presented in the study are included in the article/**Supplementary Material**, and further inquiries can be directed to the corresponding author.

AUTHOR CONTRIBUTIONS

YN made substantial contributions to the conception and design of this work, the generation and analysis of transgenic plants, the interpretation of the results, and the preparation of the manuscript. TS and MT helped in the generation and analysis of transgenic plants, respectively. KT performed the expression and purification of *E. coli*-derived RGNNV-VLPs and TEM observations of the purified VLPs. KM, HY, and HK conducted fish experiments. All authors approved the final version of the manuscript.

FUNDING

This study was supported by a Grant-in-Aid for Scientific Research to YN (Grant Nos. 15K14912, 18K19162, and 20K07524), KT (Grant Nos. 18K19162 and 20K07524), and TS (Grant Nos. 17H03968, 19H04731, and 21K06238) from the Japan Society for the Promotion of Science (JSPS), and the Adaptable and Seamless Technology Transfer Program through Target-driven R&D (A-STEP) to YN (Grant Nos. AS242Z01579N and JPMJTM19EE), and HK (Grant No. JPMJTM19EE) from the Japan Science and Technology Agency (JST).

ACKNOWLEDGMENTS

We thank Dr. Munehiko Asayama, Dr. Toshihiro Nakai, Dr. Yuzuru Tozawa, Dr. Koji Uetsuka, and Dr. Akashi Kuroda for their helpful advice, and the Gene Research Center, Ibaraki University, for allowing us to use the experimental equipment.

SUPPLEMENTARY MATERIAL

The Supplementary Material for this article can be found online at: https://www.frontiersin.org/articles/10.3389/fpls.2021.717952/full#supplementary-material

Supplementary Figure S1 | To examine the immunogenicity of chloroplast-derived RGNNV-VLPs, crudely purified protein extracts were prepared from wild-type (WT) or the transplastomic (RGNNV1-2) tobacco plants. TSP extracted from mature leaves of WT or RGNNV1-2 plants was ultrafiltrated using a centrifugal filter device to reduce the contamination of alkaloids, such as nicotine. The protein samples (10 μg) before ultrafiltration (Crude) and after ultrafiltration (Ultrafiltrated) were separated by 13% SDS-PAGE and stained with CBB.

Supplementary Figure S2 | Anti-RGNNV neutralizing titers in sevenband grouper immunized with chloroplast-derived RGNNV-VLPs. Fish were vaccinated with PBS as control, crudely purified protein extracts from mature leaves of wild-type (WT) or the transplastomic (RGNNV1) tobacco plants, or a commercial inactivated vaccine (Inactivated) by intraperitoneal injection (Injection) or oral administration (Oral). After 21 days post-immunization, sera were collected from the caudal veins of fish (n = 8 for PBS-Injection and WT-Oral; n = 9 for Inactivated-Injection; n = 10 for WT-Injection, RGNNV1-Injection, PBS-Oral, and RGNNV1-Oral). Titer 0 indicates 1:80 or lower. $^{*}p < 0.01$; $^{**}p < 0.05$.

REFERENCES

Amend, D. F. (1981). "Potency testing of fish vaccines," in *Fish Biologics: Serodiagnostics and Vaccines. Development in Biological Standardization*. eds. D. P. Anderson and H. Hennessen (Basel: Karger), 447–454.

Arlen, P. A., Singleton, M., Adamovicz, J. J., Ding, Y., Davoodi-Semiromi, A., and Daniell, H. (2008). Effective plague vaccination via oral delivery of plant cells expressing F1-V antigens in chloroplasts. *Infect. Immun.* 76, 3640–3650. doi: 10.1128/IAI.00050-08

Bandín, I., and Souto, S. (2020). Betanodavirus and VER disease: A 30-year research review. *Pathogens* 9:106. doi: 10.3390/pathogens9020106

Bøgwald, J., and Dalmo, R. A. (2019). Review on immersion vaccines for fish: an update 2019. *Microorganisms* 7:627. doi: 10.3390/microorganisms7120627

Cardi, T., Lenzi, P., and Maliga, P. (2010). Chloroplasts as expression platforms for plant-produced vaccines. *Expert Rev. Vaccines* 9, 893–911. doi: 10.1586/erv.10.78

Castiglia, D., Sannino, L., Marcolongo, L., Ionata, E., Tamburino, R., De Stradis, A., et al. (2016). High-level expression of thermostable cellulolytic enzymes in

tobacco transplastomic plants and their use in hydrolysis of an industrially pretreated *Arundo donax* L. biomass. *Biotechnol. Biofuels* 9:154. doi: 10.1186/s13068-016-0569-z

Charlton Hume, H. K., Vidigal, J., Carrondo, M. J. T., Middelberg, A. P. J., Roldão, A., and Lua, L. H. L. (2019). Synthetic biology for bioengineering virus-like particle vaccines. *Biotechnol. Bioeng.* 116, 919–935. doi: 10.1002/bit.26890

Chen, Q., and Lai, H. (2013). Plant-derived virus-like particles as vaccines. *Hum. Vaccin. Immunother.* 9, 26–49. doi: 10.4161/hv.22218

Chien, M. H., Wu, S. Y., and Lin, C. H. (2018). Oral immunization with cell-free self-assembly virus-like particles against orange-spotted grouper nervous necrosis virus in grouper larvae, *Epinephelus coioides*. *Vet. Immunol. Immunopathol.* 197, 69–75. doi: 10.1016/j.vetimm.2018.01.012

Cho, S. Y., Kim, H. J., Lan, N. T., Han, H. J., Lee, D. C., Hwang, J. Y., et al. (2017). Oral vaccination through voluntary consumption of the convict grouper *Epinephelus septemfasciatus* with yeast producing the capsid protein of red-spotted grouper nervous necrosis virus. *Vet. Microbiol.* 204, 159–164. doi: 10.1016/j.vetmic.2017.04.022

Cho, H. S., Seo, J. Y., Park, S. I., Kim, T. G., and Kim, T. J. (2018). Oral immunization with recombinant protein antigen expressed in tobacco against fish nervous necrosis virus. *J. Vet. Med. Sci.* 80, 272–279. doi: 10.1292/jvms.16-0408

Clarke, J. L., Waheed, M. T., Lössl, A. G., Martinussen, I., and Daniell, H. (2013). How can plant genetic engineering contribute to cost-effective fish vaccine development for promoting sustainable aquaculture? *Plant Mol. Biol.* 83, 33–40. doi: 10.1007/s11103-013-0081-9

Costa, J. Z., and Thompson, K. D. (2016). Understanding the interaction between Betanodavirus and its host for the development of prophylactic measures for viral encephalopathy and retinopathy. *Fish Shellfish Immunol.* 53, 35–49. doi: 10.1016/j.fsi.2016.03.033

Daniell, H., Rai, V., and Xiao, Y. (2019). Cold chain and virus-free oral polio booster vaccine made in lettuce chloroplasts confers protection against all three poliovirus serotypes. *Plant Biotechnol. J.* 17, 1357–1368. doi: 10.1111/pbi.13060

Davoodi-Semiromi, A., Schreiber, M., Nalapalli, S., Verma, D., Singh, N. D., Banks, R. K., et al. (2010). Chloroplast-derived vaccine antigens confer dual immunity against cholera and malaria by oral or injectable delivery. *Plant Biotechnol. J.* 8, 223–242. doi: 10.1111/j.1467-7652.2009.00479.x

FAO (2020). The State of World Fisheries and Aquaculture 2020. Available at: http://www.fao.org/publications/card/en/c/CA9229EN (Accessed May 22, 2021).

Fernández-San Millán, A., Ortigosa, S. M., Hervás-Stubbs, S., Corral-Martínez, P., Seguí-Simarro, J. M., Gaétan, J., et al. (2008). Human papillomavirus L1 protein expressed in tobacco chloroplasts self-assembles into virus-like particles that are highly immunogenic. *Plant Biotechnol. J.* 6, 427–441. doi: 10.1111/j.1467-7652.2008.00338.x

Festa, M., Brun, P., Piccinini, R., Castagliuolo, I., Basso, B., and Zecconi, A. (2013). *Staphylococcus aureus* Efb protein expression in *Nicotiana tabacum* and immune response to oral administration. *Res. Vet. Sci.* 94, 484–489. doi: 10.1016/j.rvsc.2012.10.012

Fu, H., Machado, P. A., Hahm, T. S., Kratochvil, R. J., Wei, C. I., and Lo, Y. M. (2010). Recovery of nicotine-free proteins from tobacco leaves using phosphate buffer system under controlled conditions. *Bioresour. Technol.* 101, 2034–2042. doi: 10.1016/j.biortech.2009.10.045

Fuentes, P., Armarego-Marriott, T., and Bock, R. (2018). Plastid transformation and its application in metabolic engineering. *Curr. Opin. Biotechnol.* 49, 10–15. doi: 10.1016/j.copbio.2017.07.004

Gaafar, A. Y., Yamashita, H., Istiqomah, I., Kawato, Y., Ninomiya, K., Younes, A. E., et al. (2018). An oral vaccination method with the aid of capsaicin against viral nervous necrosis (VNN). *Fish Pathol.* 53, 110–113. doi: 10.3147/jsfp.53.110

Hernández, M., Rosas, G., Cervantes, J., Fragoso, G., Rosales-Mendoza, S., and Sciutto, E. (2014). Transgenic plants: a 5-year update on oral antipathogen vaccine development. *Expert Rev. Vaccines* 13, 1523–1536. doi: 10.1586/14760584.2014.953064

Huang, J. N., Lin, L., Weng, S. P., and He, J. G. (2007). High expression of capsid protein of red-spotted grouper nervous necrosis virus in an avian cell line requires viral RNA2 non-coding regions. *J. Fish Dis.* 30, 439–444. doi: 10.1111/j.1365-2761.2007.00818.x

Iwamoto, T., Nakai, T., Mori, K., Arimoto, M., and Furusawa, I. (2000). Cloning of the fish cell line SSN-1 for piscine nodaviruses. *Dis. Aquat. Org.* 43, 81–89. doi: 10.3354/dao043081

Jeong, K. H., Kim, H. J., and Kim, H. J. (2020). Current status and future directions of fish vaccines employing virus-like particles. *Fish Shellfish Immunol.* 100, 49–57. doi: 10.1016/j.fsi.2020.02.060

Jin, S., and Daniell, H. (2015). The engineered chloroplast genome just got smarter. *Trends Plant Sci.* 20, 622–640. doi: 10.1016/j.tplants.2015.07.004

Kai, Y. H., Wu, Y. C., and Chi, S. C. (2014). Immune gene expressions in grouper larvae (*Epinephelus coioides*) induced by bath and oral vaccinations with inactivated Betanodavirus. *Fish Shellfish Immunol.* 40, 563–569. doi: 10.1016/j.fsi.2014.08.005

Kanagaraj, A. P., Verma, D., and Daniell, H. (2011). Expression of dengue-3 premembrane and envelope polyprotein in lettuce chloroplasts. *Plant Mol. Biol.* 76, 323–333. doi: 10.1007/s11103-011-9766-0

Kikuchi, S., Asakura, Y., Imai, M., Nakahira, Y., Kotani, Y., Hashiguchi, Y., et al. (2018). A Ycf2-FtsHi heteromeric AAA-ATPase complex is required for chloroplast protein import. *Plant Cell* 30, 2677–2703. doi: 10.1105/tpc.18.00357

Lafferty, K. D., Harvell, C. D., Conrad, J. M., Friedman, C. S., Kent, M. L., Kuris, A. M., et al. (2015). Infectious diseases affect marine fisheries and aquaculture economics. *Annu. Rev. Mar. Sci.* 7, 471–496. doi: 10.1146/annurev-marine-010814-015646

Lai, Y. X., Jin, B. L., Xu, Y., Huang, L. J., Huang, R. Q., Zhang, Y., et al. (2014). Immune responses of orange-spotted grouper, *Epinephelus coioides*, against virus-like particles of Betanodavirus produced in *Escherichia coli*. *Vet. Immunol. Immunopathol.* 157, 87–96. doi: 10.1016/j.vetimm.2013.10.003

Lakshmi, P. S., Verma, D., Yang, X., Lloyd, B., and Daniell, H. (2013). Low cost tuberculosis vaccine antigens in capsules: expression in chloroplasts, bio-encapsulation, stability and functional evaluation *in vitro*. *PLoS One* 8:e54708. doi: 10.1371/journal.pone.0054708

Lan, N. T., Kim, H. J., Han, H. J., Lee, D. C., Kang, B. K., Han, S. Y., et al. (2018). Stability of virus-like particles of red-spotted grouper nervous necrosis virus in the aqueous state, and the vaccine potential of lyophilized particles. *Biologicals* 51, 25–31. doi: 10.1016/j.biologicals.2017.11.002

Legen, J., Kemp, S., Krause, K., Profanter, B., Herrmann, R. G., and Maier, R. M. (2002). Comparative analysis of plastid transcription profiles of entire plastid chromosomes from tobacco attributed to wild-type and PEP-deficient transcription machineries. *Plant J.* 31, 171–188. doi: 10.1046/j.1365-313X.2002.01349.x

Lenzi, P., Scotti, N., Alagna, F., Tornesello, M. L., Pompa, A., Vitale, A., et al. (2008). Translational fusion of chloroplast-expressed human papillomavirus type 16 L1 capsid protein enhances antigen accumulation in transplastomic tobacco. *Transgenic Res.* 17, 1091–1102. doi: 10.1007/s11248-008-9186-3

Lin, C. S., Lu, M. W., Tang, L., Liu, W., Chao, C. B., Lin, C. J., et al. (2001). Characterization of virus-like particles assembled in a recombinant baculovirus system expressing the capsid protein of a fish nodavirus. *Virology* 290, 50–58. doi: 10.1006/viro.2001.1157

Lin, K., Zhu, Z., Ge, H., Zheng, L., Huang, Z., and Wu, S. (2016). Immunity to nervous necrosis virus infections of orange-spotted grouper (*Epinephelus coioides*) by vaccination with virus-like particles. *Fish Shellfish Immunol.* 56, 136–143. doi: 10.1016/j.fsi.2016.06.056

Liu, F., Ge, S., Li, L., Wu, X., Liu, Z., and Wang, Z. (2012). Virus-like particles: potential veterinary vaccine immunogens. *Res. Vet. Sci.* 93, 553–559. doi: 10.1016/j.rvsc.2011.10.018

Liu, W., Hsu, C. H., Chang, C. Y., Chen, H. H., and Lin, C. S. (2006). Immune response against grouper nervous necrosis virus by vaccination of virus-like particles. *Vaccine* 24, 6282–6287. doi: 10.1016/j.vaccine.2006.05.073

Lomonossoff, G. P., and D'Aoust, M. A. (2016). Plant-produced biopharmaceuticals: A case of technical developments driving clinical deployment. *Science* 353, 1237–1240. doi: 10.1126/science.aaf6638

Low, C. F., Syarul Nataqain, B., Chee, H. Y., Rozaini, M. Z. H., and Najiah, M. (2017). *Betanodavirus*: Dissection of the viral life cycle. *J. Fish Dis.* 40, 1489–1496. doi: 10.1111/jfd.12638

Lua, L. H., Connors, N. K., Sainsbury, F., Chuan, Y. P., Wibowo, N., and Middelberg, A. P. (2014). Bioengineering virus-like particles as vaccines. *Biotechnol. Bioeng.* 111, 425–440. doi: 10.1002/bit.25159

Mahmood, N., Nasir, S. B., and Hefferon, K. (2020). Plant-based drugs and vaccines for COVID-19. *Vaccine* 9:15. doi: 10.3390/vaccines9010015

Marsian, J., Hurdiss, D. L., Ranson, N. A., Ritala, A., Paley, R., Cano, I., et al. (2019). Plant-made nervous necrosis virus-like particles protect fish against disease. *Front. Plant Sci.* 10:880. doi: 10.3389/fpls.2019.00880

Marsian, J., and Lomonossoff, G. P. (2016). Molecular pharming - VLPs made in plants. *Curr. Opin. Biotechnol.* 37, 201–206. doi: 10.1016/j.copbio.2015.12.007

Munday, B. L., and Nakai, T. (1997). Nodaviruses as pathogens in larval and juvenile marine finfish. *World J. Microbiol. Biotechnol.* 13, 375–381. doi: 10.1023/A:1018516014782

Nakahira, Y., Ishikawa, K., Tanaka, K., Tozawa, Y., and Shiina, T. (2013). Overproduction of hyperthermostable β-1,4-endoglucanase from the archaeon *Pyrococcus horikoshii* by tobacco chloroplast engineering. *Biosci. Biotechnol. Biochem.* 77, 2140–2143. doi: 10.1271/bbb.130413

Nishioka, T., Sugaya, T., Kawato, Y., Mori, K., and Nakai, T. (2016). Pathogenicity of striped jack nervous necrosis virus (SJNNV) isolated from asymptomatic wild Japanese jack mackerel *Trachurus japonicus*. *Fish Pathol.* 51, 176–183. doi: 10.3147/jsfp.51.176

Nishizawa, T., Furuhashi, M., Nagai, T., Nakai, T., and Muroga, K. (1997). Genomic classification of fish nodaviruses by molecular phylogenetic analysis of the coat protein gene. *Appl. Environ. Microbiol.* 63, 1633–1636. doi: 10.1128/aem.63.4.1633-1636.1997

Nooraei, S., Bahrulolum, H., Hoseini, Z. S., Katalani, C., Hajizade, A., Easton, A. J., et al. (2021). Virus-like particles: preparation, immunogenicity and their roles as nanovaccines and drug nanocarriers. *J. Nanobiotechnol.* 19:59. doi: 10.1186/s12951-021-00806-7

Oey, M., Lohse, M., Kreikemeyer, B., and Bock, R. (2009). Exhaustion of the chloroplast protein synthesis capacity by massive expression of a highly stable protein antibiotic. *Plant J.* 57, 436–445. doi: 10.1111/j.1365-313X.2008.03702.x

Reverter, M., Sarter, S., Caruso, D., Avarre, J. C., Combe, M., Pepey, E., et al. (2020). Aquaculture at the crossroads of global warming and antimicrobial resistance. *Nat. Commun.* 11:1870. doi: 10.1038/s41467-020-15735-6

Rybicki, E. P. (2020). Plant molecular farming of virus-like nanoparticles as vaccines and reagents. *Wiley Interdiscip. Rev. Nanomed. Nanobiotechnol.* 12:e1587. doi: 10.1002/wnan.1587

Shahid, N., and Daniell, H. (2016). Plant-based oral vaccines against zoonotic and non-zoonotic diseases. *Plant Biotechnol. J.* 14, 2079–2099. doi: 10.1111/pbi.12604

Shohag, M. J. I., Khan, F. Z., Tang, L., Wei, Y., He, Z., and Yang, X. (2021). COVID-19 crisis: how can plant biotechnology help? *Plants* 10:352. doi: 10.3390/plants10020352

Thiéry, R., Cozien, J., Cabon, J., Lamour, F., Baud, M., and Schneemann, A. (2006). Induction of a protective immune response against viral nervous necrosis in the European sea bass *Dicentrarchus labrax* by using Betanodavirus virus-like particles. *J. Virol.* 80, 10201–10207. doi: 10.1128/JVI.01098-06

Tusé, D., Nandi, S., McDonald, K. A., and Buyel, J. F. (2020). The emergency response capacity of plant-based biopharmaceutical manufacturing-what it is and what it could be. *Front. Plant Sci.* 11:594019. doi: 10.3389/fpls.2020.594019

Waheed, M. T., Thönes, N., Müller, M., Hassan, S. W., Razavi, N. M., Lössl, E., et al. (2011). Transplastomic expression of a modified human papillomavirus L1 protein leading to the assembly of capsomeres in tobacco: a step towards cost-effective second-generation vaccines. *Transgenic Res.* 20, 271–282. doi: 10.1007/s11248-010-9415-4

Wi, G. R., Hwang, J. Y., Kwon, M. G., Kim, H. J., Kang, H. A., and Kim, H. J. (2015). Protective immunity against nervous necrosis virus in convict grouper *Epinephelus septemfasciatus* following vaccination with virus-like particles produced in yeast *Saccharomyces cerevisiae*. *Vet. Microbiol.* 177, 214–218. doi: 10.1016/j.vetmic.2015.02.021

Wostrikoff, K., and Stern, D. (2007). RuBisCO large-subunit translation is autoregulated in response to its assembly state in tobacco chloroplasts. *Proc. Natl. Acad. Sci. U. S. A.* 104, 6466–6471. doi: 10.1073/pnas.0610586104

Xie, J., Li, K., Gao, Y., Huang, R., Lai, Y., Shi, Y., et al. (2016). Structural analysis and insertion study reveal the ideal sites for surface displaying foreign peptides on a Betanodavirus-like particle. *Vet. Res.* 47:16. doi: 10.1186/s13567-015-0294-9

Yácono, M. D. L., Farran, I., Becher, M. L., Sander, V., Sánchez, V. R., Martín, V., et al. (2012). A chloroplast-derived *Toxoplasma gondii* GRA4 antigen used as an oral vaccine protects against toxoplasmosis in mice. *Plant Biotechnol. J.* 10, 1136–1144. doi: 10.1111/pbi.12001

Yamashita, H., Fujita, Y., Kawakami, H., and Nakai, T. (2005). The efficacy of inactivated virus vaccine against viral nervous necrosis (VNN). *Fish Pathol.* 40, 15–21. doi: 10.3147/jsfp.40.15

Conflict of Interest: The authors declare that the research was conducted in the absence of any commercial or financial relationships that could be construed as a potential conflict of interest.

Publisher's Note: All claims expressed in this article are solely those of the authors and do not necessarily represent those of their affiliated organizations, or those of the publisher, the editors and the reviewers. Any product that may be evaluated in this article, or claim that may be made by its manufacturer, is not guaranteed or endorsed by the publisher.

frontiers in Plant Science

ORIGINAL RESEARCH
published: 26 August 2021
doi: 10.3389/fpls.2021.677553

Daucus carota DcPSY2 and *DcLCYB1* as Tools for Carotenoid Metabolic Engineering to Improve the Nutritional Value of Fruits

*Daniela Arias[1], Anita Arenas-M[2], Carlos Flores-Ortiz[1], Clio Peirano[1], Michael Handford[1] and Claudia Stange[1]**

[1] Centro de Biología Molecular Vegetal, Facultad de Ciencias, Universidad de Chile, Ñuñoa, Chile, [2] Laboratorio de Nutrición y Genómica de Plantas, Instituto de Bioquímica y Microbiología, Facultad de Ciencias, Universidad Austral de Chile, Valdivia, Chile

Carotenoids are pigments with important nutritional value in the human diet. As antioxidant molecules, they act as scavengers of free radicals enhancing immunity and preventing cancer and cardiovascular diseases. Moreover, α-carotene and β-carotene, the main carotenoids of carrots (*Daucus carota*) are precursors of vitamin A, whose deficiency in the diet can trigger night blindness and macular degeneration. With the aim of increasing the carotenoid content in fruit flesh, three key genes of the carotenoid pathway, phytoene synthase (*DcPSY2)* and lycopene cyclase (*DcLCYB1)* from carrots, and carotene desaturase (*XdCrtI)* from the yeast *Xanthophyllomyces dendrorhous*, were optimized for expression in apple and cloned under the *Solanum chilense* (tomatillo) polygalacturonase (PG) fruit specific promoter. A biotechnological platform was generated and functionally tested by subcellular localization, and single, double and triple combinations were both stably transformed in tomatoes (*Solanum lycopersicum* var. Microtom) and transiently transformed in Fuji apple fruit flesh (*Malus domestica*). We demonstrated the functionality of the *S. chilense* PG promoter by directing the expression of the transgenes specifically to fruits. Transgenic tomato fruits expressing *DcPSY2*, *DcLCYB1*, and *DcPSY2-XdCRTI*, produced 1.34, 2.0, and 1.99-fold more total carotenoids than wild-type fruits, respectively. Furthermore, transgenic tomatoes expressing *DcLCYB1*, *DcPSY2-XdCRTI*, and *DcPSY2-XdCRTI-DcLCYB1* exhibited an increment in β-carotene levels of 2.5, 3.0, and 2.57-fold in comparison with wild-type fruits, respectively. Additionally, Fuji apple flesh agroinfiltrated with *DcPSY2* and *DcLCYB1* constructs showed a significant increase of 2.75 and 3.11-fold in total carotenoids and 5.11 and 5.84-fold in β-carotene, respectively whereas the expression of *DcPSY2-XdCRTI* and *DcPSY2-XdCRTI-DcLCYB1* generated lower, but significant changes in the carotenoid profile of infiltrated apple flesh. The results in apple demonstrate that *DcPSY2* and *DcLCYB1* are suitable biotechnological genes to increase the carotenoid content in fruits of species with reduced amounts of these pigments.

Keywords: carotenoid, *Malus domestica*, *Solanum lycopersicum*, *DcPSY2*, *DcLCYB1*, *Daucus carota*, transgenic tomatoes, metabolic engineering

Edited by:
Patricia León, National Autonomous University of Mexico, Mexico

Reviewed by:
Barbara Molesini, University of Verona, Italy
Sangram Keshari Lenka, TERI-Deakin Nanobiotechnology Centre, India

***Correspondence:**
Claudia Stange
cstange@uchile.cl

Specialty section:
This article was submitted to Plant Biotechnology, a section of the journal Frontiers in Plant Science

Received: *07 March 2021*
Accepted: *26 May 2021*
Published: *26 August 2021*

Citation:
Arias D, Arenas-M A, Flores-Ortiz C, Peirano C, Handford M and Stange C (2021) Daucus carota DcPSY2 and DcLCYB1 as Tools for Carotenoid Metabolic Engineering to Improve the Nutritional Value of Fruits. Front. Plant Sci. 12:677553. doi: 10.3389/fpls.2021.677553

INTRODUCTION

Carotenoids are natural lipophilic pigments produced by plant plastids that play important roles in light harvesting during photosynthesis and in protecting the photosynthetic apparatus against excessive light radiation. These secondary metabolites also normally accumulate in fruits, flowers and seeds, providing them yellow, orange, and red colors to facilitate pollination and seed dispersal (Rosas-Saavedra and Stange, 2016). Carotenoids are substrates for the biosynthesis of hormones that are crucial for plant physiology such as abscisic acid (ABA) and strigolactones, involved in the stress and developmental signaling responses (Walter and Strack, 2011; Beltran and Stange, 2016). Several plastidial enzymes have been identified that are essential for carotenoid synthesis. Phytoene synthase (PSY) catalyzes the first step and is the key regulatory point controlling flux through the pathway (**Figure 1**). The carotenoid pathway has been thoroughly described (Alcaíno et al., 2016). Briefly, the condensation of three molecules of isopentyl pyrophosphate (IPP) with one molecule of di-methylallyl pyrophosphate (DMAPP) generates the geranylgeranyl diphosphate (GGPP) precursor. The condensation of two molecules of GGPP, carried out by PSY, yields phytoene (C40). This is the first committed step in carotenoid synthesis, which is also highly regulated. In plants, colorless phytoene undergoes several steps of desaturation and isomerization by phytoene desaturase (PDS), ζ–carotene desaturase (ZDS), carotenoid isomerase (CRTISO) and ζ–carotene isomerase (ζ-ISO) (Isaacson et al., 2002, 2004; Lu and Li, 2008). To produce lycopene in bacteria and yeast, the four enzymatic steps from phytoene to lycopene mentioned above are carried out by a single enzyme (CRTI) (Alcaíno et al., 2016). Subsequently, lycopene is cyclized by lycopene β-cyclase (LCYB) producing β-carotene, whereas for α-carotene production, both LCYB and lycopene ε-cyclase (LCYE) are required. Then, the hydroxylation of α-carotene produces lutein, a yellowish pigment that is abundant in leaves (Hornero-Méndez and Britton, 2002; Bang et al., 2007; Misawa, 2011; **Figure 1**). Two subsequent hydroxylations of β-carotene, catalyzed by carotenoid β-hydroxylase (CHYB) produce zeaxanthin, which can be epoxidized by zeaxanthin epoxidase (ZEP) to form violaxanthin, which can be used by violaxanthin de-epoxidase (VDE) to regenerate zeaxanthin (Cazzonelli and Pogson, 2010; Cazzonelli, 2011; Moise et al., 2014). Finally, violaxanthin is the precursor for ABA, which is produced in the cytoplasm (**Figure 1**). In mammals, carotenoids possess antioxidant activity by quenching reactive oxygen species (ROS) (Stahl and Sies, 2003) thus decreasing the risk of developing certain diseases caused by oxidative stress (Malone, 1991; Byers and Perry, 1992; Voorrips et al., 2000; Holick et al., 2002) including cancer, atheromas in vascular diseases, aging and macular degeneration (Marnett, 1987; Mordi, 1993; Bartley and Scolnik, 1995; Rao and Rao, 2007). Carotenoids are also precursors of vitamin A. Specifically, the most relevant provitamin A carotenoids, given their high antioxidant activity and wide distribution in food, are α- and β-carotene, some xanthophylls such as β-cryptoxanthin and some *apo*-carotenoids (Mínguez-Mosquera and Hornero-Méndez, 1997). Of these, β-carotene presents the highest provitamin A activity since each molecule produces two retinal molecules that are then reduced to vitamin A (retinol). Vitamin A is converted into the visual pigment rhodopsin (retinal), in the retina of the eye, and acts as a co-regulator of gene expression (retinoic acid) (Zhu et al., 2013). Vitamin A is also required for cell growth and for healthy immunity, among other physiological processes (Olson, 1996). Therefore, increasing the carotenoid content in crop plants to improve nutritional value and benefits for human health has been a major goal of many research programs worldwide. Over the last four decades, significant progress has been made in the manipulation of carotenoid content and composition in a large number of crops by either genetic engineering or conventional breeding (Fraser et al., 1999, 2009; Giuliano et al., 2008; Rosati et al., 2009; Farré et al., 2010, 2011; Ye and Bhatia, 2012; Giuliano, 2014). Conventional and assisted breeding have successfully enhanced β-carotene levels in maize, sweet potato and cassava, benefiting human health in several countries (Ceballos et al., 2013; Pixley et al., 2013). Genetic engineering also allows nutritional traits to be targeted to specific organs (e.g., cereal seeds) and multiple traits can be combined in the same plants without complex breeding programs (Naqvi et al., 2009, 2010). Other examples of efficient enhancement of carotenoids through metabolic engineering have been obtained in agronomical relevant crops (Alós et al., 2016), such as rice (Paine et al., 2005), tomato (D'Ambrosio et al., 2004), potato (Diretto et al., 2006), carrot (Jayaraj et al., 2008), canola (Shewmaker et al., 1999; Ravanello et al., 2003), cassava (Failla et al., 2012), sorghum (Lipkie et al., 2013), orange (Pons et al., 2014), and apple (Arcos et al., 2020).

Apple (*Malus domestica*) is one of the most widely produced fruits in the world and is consumed not only as a fresh fruit but also in processed forms, such as juice and jam[1] (Harker et al., 2003). As well as improving nutritional value, fruit color is one of the major aims of apple breeding because it provides novel appearances and influences consumer preferences (Yuan et al., 2014). The accumulation of anthocyanins and carotenoids in the skin and pulp are responsible for color in mature fruits (Telias et al., 2011; Cerda et al., 2020). However, commercial varieties such as "Royal Gala" and "Fuji" present low levels of carotenoids in the flesh reaching about 2-6 μg/g fresh weight (FW; Ampomah-Dwamena et al., 2012; Cerda et al., 2020). Specifically, the flesh of Fuji fruits accumulates around 1.8 μg/g FW in total carotenoids (Arcos et al., 2020), 0.04–0.22 μg/g dry weight (DW) of lutein and 0.79–1.14 μg/g DW of β-carotene (Delgado-Pelayo et al., 2014). Low carotenoid levels can be ascribed to reduced biosynthesis, deficient accumulation, and/or efficient degradation. Previous studies determined that the PSY enzyme in apple is codified by a family of genes with different levels of expression in fruit flesh (Ampomah-Dwamena et al., 2012; Cerda et al., 2020) and that the most expressed *PSY* genes are functional (Ampomah-Dwamena et al., 2015; Cerda et al., 2020) suggesting that the synthesis pathway is not the limiting step for carotenoid accumulation. In addition, the ectopic expression of the Arabidopsis 1-deoxy-D-xylulose 5-phosphate reductoisomerase (*AtDXR)* in Fuji apple, a gene

[1]http://faostat.fao.org

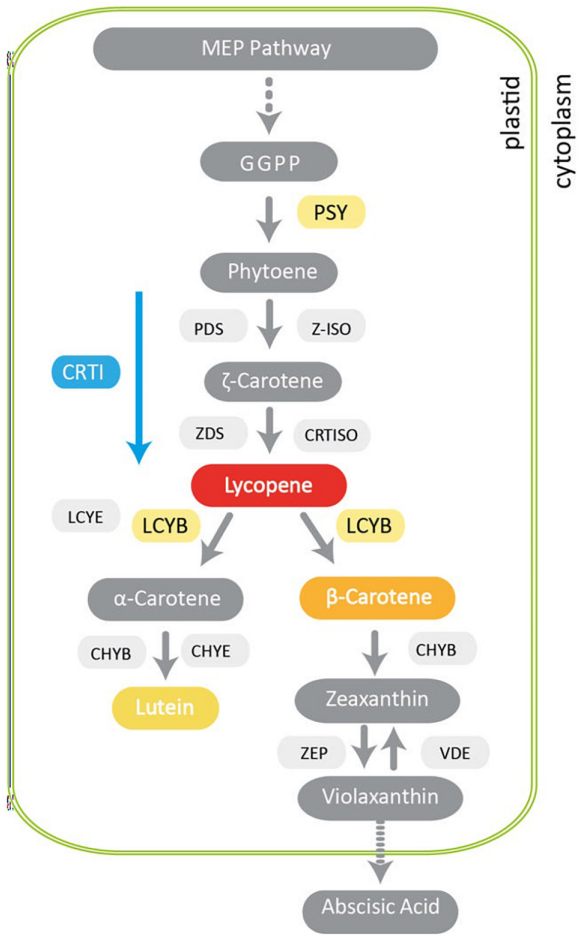

FIGURE 1 | The main steps of carotenoid biosynthesis and related pathways in plants. The methylerythritol 4-phosphate (MEP) pathway produces isoprenoids in plastids leading to the production of geranylgeranyl pyrophosphate (GGPP). Phytoene synthase (PSY) is the first enzyme in the carotenogenic pathway and produces phytoene. In plants, phytoene is then desaturated and isomerized by phytoene desaturase (PDS), ζ–carotene desaturase (ZDS), ζ–carotene isomerase (Z-ISO) and prolycopene isomerase (CRTISO) forming lycopene. In bacteria, these reactions are carried out by a single multifunctional enzyme, phytoene desaturase (CRTI). β-carotene is produced if lycopene is cyclized only by lycopene β-cyclase (LCYB) whilst α-carotene is produced if both LCYB and lycopene ε-cyclase (LCYE) are involved. β-carotene hydroxylase (CHYB) and ε-carotene hydroxylase (CHYE) produce lutein. CHYB produces zeaxanthin, which can be converted into violaxanthin by zeaxanthin epoxidase (ZEP). The reverse step can be carried out by violaxanthin de-epoxidase (VDE). Violaxanthin is the precursor of abscisic acid. Dotted arrows indicate multiple enzymatic reactions. Solid gray arrows represent different steps of the carotenogenic pathway. The blue arrow indicates consecutive desaturations carried out by bacterial CRTI.

participating in the synthesis of carotenoid precursors, produces a threefold rise in total and individual carotenoids in leaves (Arcos et al., 2020). This information led to the proposal that apple is a potential target to become a functional food with high pro-vitamin A and antioxidant components, when genes that codify for biosynthetic enzymes are expressed. Therefore, this work focused on the generation of a biotechnological platform for the rapid functional assessment of whether specific biosynthetic genes can be used to increase the content of provitamin A in fruits. This platform initially uses tomato fruits as a model, before final testing in apples.

Fruits and vegetables are the main sources of carotenoids, and among these, the orange carrot stands out. To generate the biotechnological platform, we chose *PSY2* and *LCYB1* from *Daucus carota* and *CrtI* from *Xanthophyllomyces dendrorhous.* Carrot accumulates high levels of α and β-carotene in its taproot, similar to *X. dendrorhous*, a yeast that is able to accumulate as much as 0.5% DW in astaxanthin, a ketocarotenoid produced from β-carotene (Niklitschek et al., 2008). Carrot presents two paralogs for *PSY* and *LCYB* genes (Just et al., 2007). *DcPSY2* and *DcLCYB1* are highly expressed in carrot leaves and tap roots during plant development (Fuentes et al., 2012; Simpson et al., 2016), suggesting functional roles for carotenoid synthesis. However, no functional characterization for *DcPSY2* has been published yet. Nevertheless, in the case of *DcLCYB1*, its overexpression results in 2–10 fold more carotenoids in transgenic tobacco (Moreno et al., 2016, 2020), and a threefold increase in carrots (Moreno et al., 2013). Indeed, DcLCYB1 also presents a plastidial localization (Moreno et al., 2013). Regarding *XdCrtI*, it codifies the enzyme that catalyzes the conversion of phytoene into lycopene in *X. dendrorhous* (Niklitschek et al., 2008). Although several studies have used *CrtI* from *Erwinia uredevora* to modify the synthesis of carotenoids in plants, as well as the use of other bacterial carotenogenic genes orthologous to *PSY* (*CrtB*) and *LCYB* (*CrtY*) (Römer et al., 2000; Ye et al., 2000; Fraser et al., 2002; Paine et al., 2005; Diretto et al., 2007), *XdCrtI* has yet to be used to increase carotenoids for this purpose. Here, we describe the design and development of carotenogenic gene expression vectors (pCP-CG) that utilize single or combinations of *DcPSY2* and *DcLCYB1* carrot carotenogenic genes and *XdCrtI* from yeast to increase the carotenoid level in apples. To guide transgenic gene expression, the selection of a suitable promoter is essential. In the case of fruits, one of the enzymes that participates in fruit ripening is polygalacturonase (PG), a hydrolase responsible for the degradation of polyuronides or pectins in the cell wall (DellaPenna et al., 1986). PG accumulates during fruit ripening, due to transcriptional activation of the *PG* gene (Sheehy et al., 1987; DellaPenna et al., 1989). The tomato PG promoter (pPG) was characterized by Montgomery et al. (1993), who showed that the first 806 pb upstream of the transcription start site are sufficient to confer fruit flesh (pulp) specific expression. Therefore, in this study, the carotenoid biosynthetic genes were cloned under the pPG from *Solanum chilense* (tomatillo). Once the biotechnological platform was built, the functionality of the vectors was evaluated through subcellular localization, by stable transformation of *Solanum lycopersicum* cv. Microtom and by transient expression in *M. domestica*. The results demonstrate that the pCP-CG vectors, specially pPSY2 and pLCYB1, increment the total carotenoid and β-carotene levels in tomatoes and/or apple fruits, proving their suitability in genetic engineering programs for the improvement of nutritional quality and color traits.

MATERIALS AND METHODS

Vector Construction

pCP vector construction was based on a backbone from the pB7FWG2-AtDXR vector, which includes the p35S:DXR:GFP:T35S cassette (Perello et al., 2016, kindly provided by Dr. Manuel Rodriguez-Concepción, CRAG-CSIC, Spain). This cassette was obtained after a double digestion with *Xba*I and *Sac*I. The backbone fragment of 7,854 bp contains the RB and LB of the T-DNA and the *BAR* gene for BASTA or glufosinate (herbicide) resistance in plants. A specifically designed Multicloning Site (MCS) of 141 bp including *Eco*RI, *Apa*I, *Pst*I, *Avr*II, *Eco*RV, *Bsp*EI, *Nco*I, and *Bgl*II restriction sites flanked by *Xba*I and *Sac*I was synthesized by Genescript (United States[2]). The MCS was cloned in the *Xba*I and *Sac*I sites of the backbone to yield a new and royalty-free binary vector, named pCP that confers resistance to BASTA herbicide (**Supplementary Figure 1**, 201403013, Inapi, Chile).

DNA sequences of carrot *PSY2* (DQ192187) and *LCYB1* (DQ192190), and *CrtI* (gi.68250374) of *X. dendrorhous*, were optimized based on *M. domestica* codon usage by means of the OPTIMIZER software[3]. The *M. domestica* table obtained from[4] was used as a reference set. Vector NTI software was used to verify the correct reading frame of the constructs as well as the amino acid homology with the native sequences encoded by *PSY2, CrtI,* and *LCYB1*. The FGENESH 2.6 gene prediction program was also employed, selecting the item "organism dicotyledonous plants[5]". A plastidial signal peptide (tp) (171 bp) from the small subunit of pea Ribulose Bisphosphate Carboxylase Oxygenase (RUBISCO; EC 4.1.1.39 Seq ID X00806) was included at the 5′ NTR of *XdCrtI* to direct the encoded protein to these organelles (**Figure 2**). A 806 bp fragment of the tomato (*S. chilense*, tomatillo) PG promoter (pPG) was selected to direct the expression of each gene. A 277 bp fragment of the *Agrobacterium tumefaciens* nopaline synthase terminator (NosT) was included at the 3′ end of each coding sequence (Accession number V00087[6]). The sequences of interest, including pPG:DcPSY2:NosT, pPG:DcLCYB1:NosT, and pPG:tp:XdCrtI:NosT were synthesized and cloned in the pUC57 vector by GeneScript (United States). Afterward, pUC57:pPG:DcPSY2:NosT was digested with *Spe*I, pUC57:pPG:DcLCYB1:NosT with *Avr*II and pPG:tp:XdCrtI:NosT with *Xho*I, and each cassette was cloned into the MCS of pCP producing the single (pPSY2 and pLCYB1), double (pPSY2-CRTI) and triple vectors (pPSY2-CRTI-LCYB), collectively called pCP-CG vectors (**Figure 2**). Each vector was verified through sequencing (Macrogen Co.) and transformed into *Agrobacterium tumefaciens* (GV3101 strain). Positive clones were selected and used for stable transformation of *S. lycopersicum* var. Microtom and for transient transformation of *M. domestica* var. Fuji.

[2]http://www.genscript.com

[3]http://genomes.urv.es/OPTIMIZER/

[4]http://www.kazusa.or.jp

[5]http://linux1.softberry.com

[6]http://www.ncbi.nlm.nih.gov/nuccore/V00087

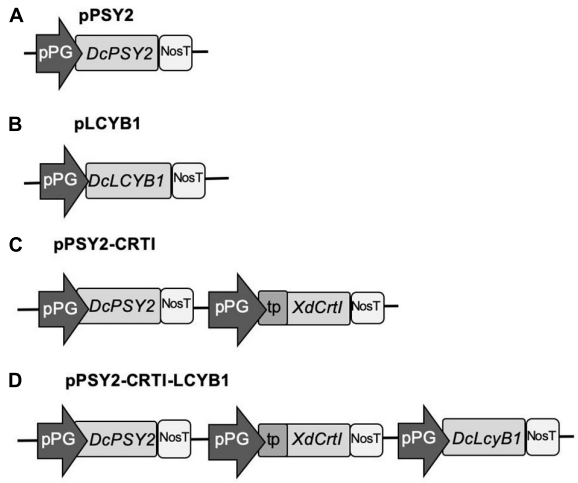

FIGURE 2 | pCP-CG constructs used for the functional assessment of DcPSY2, DcLCYB1, and XdCRTI. The pCP backbone is derived from pB7FWG2.0, with the incorporation of a specifically designed Multiple Cloning Site (MCS; see **Supplementary Figure 1**). Different carotenogenic genes were cloned into the MCS, under the control of the tomato polygalacturonase promoter (pPG) and the Nos terminator (NosT). **(A)** pPSY2. The single gene and fruit-specific expression cassette PG:DcPSY2 was chemically synthesized and cloned into pCP. **(B)** pLCYB1. The single gene and fruit-specific expression cassette PG:DcLCYB2 was chemically synthesized and cloned into pCP. **(C)** pPSY2-CRTI. A double gene and fruit-specific expression cassette including the PG promoter driving the XdCRTI gene fused to a transit peptide (PG:tpXdCRTI) was chemically synthesized and cloned into pPSY2. **(D)** pPSY2-CRTI-LCYB1. The single gene and fruit-specific expression cassette PG:DcLCYB2 was cloned into pPSY2-CRTI.

Subcellular Localization of *DcPSY2* and *XdCrtI*

For the subcellular localization analysis, the full-length and optimized for *M. domestica DcPSY2* and *XdCrtI* sequences were amplified, including the PG promoter but excluding the stop codon from the previously sequenced pPSY2 and pPSY2-CRTI clones using primers listed in **Supplementary Table 1**. Amplicons were subcloned into pCR8/GW/TOPO (Invitrogen) and thereafter recombined into the binary vector pMDC107 (Curtis and Grossniklaus, 2003) in order to express the chimeric proteins DcPSY2:GFP and tp:XdCRTI:GFP, both under the control of pPG. As controls, the pPG:GFP (cloned in pCAMBIA 1302, Abcam) and the empty pMDC107 vector were included (**Supplementary Figure 2**). The constructs were transiently expressed by agroinfiltration in *Nicotiana tabacum* (tobacco) leaves and tomato fruits at breaker stage. *A. tumefaciens* suspensions containing the pPG:DcPSY2:GFP, pPG:tp:XdCRTI:GFP and both control constructs were infiltrated into 2 months old tobacco leaves and into the tomato fruit flesh following previously described protocols (Moreno et al., 2013; Arcos et al., 2020). Plants and fruits were maintained at 20–22°C, 30–50% humidity and while tobacco plants were kept under a 16 h white light photoperiod, tomato fruits were kept in the darkness for 4 days. Then, the infiltrated areas of the leaves and fruits were analyzed for GFP and chlorophyll fluorescence

using a confocal LSM510 microscope. Images were processed with LSM5 Image Browser.

Tomato Stable Transformation and *in vitro* Culture

Solanum lycopersicum var. Microtom was cultivated *in vitro* in solidified Murashige and Skoog (MS: 4.4 g/L MS salts, 20 g/L sucrose, and 0.7% agar-agar) medium and transformed according to a previous report (Pino et al., 2010). Briefly, cotyledons of *in vitro* 8–10 days post-germination seedlings were cut and dipped into an *A. tumefaciens* culture containing the respective genetic construct for 15–20 min, and then transferred into a co-culture medium (4.4 g/L MS salts, 30 g/L sucrose, 6 g/L agar-agar, and 100 μM acetosyringone) for 2 days in darkness at 25°C (**Supplementary Figure 3**). The explants were then transferred to the Induction medium (4.4 g/L MS salts, 100 mg/L Myo-Inositol, 30 g/L sucrose, 6 g/L agar, 5 μM BAP, 0.3 mg/L BASTA, and 400 mg/L Timentin) for callus induction and initial shoot development which started between 4 and 6 weeks post-transformation. The new shoots were transferred to Elongation medium (4.4 g/L MS salts, 100 mg/L Myo-Inositol, 15 g/L sucrose, 6 g/L agar, 0.5 mg/L BASTA, and 400 mg/L Timentin). After 2 months, 4–6 cm high plants developed several branches and a minimum of 4–5 leaves. Then, the shoots were transferred to Rooting medium (4.4 g/L MS salts, 100 mg/L Myo-Inositol, 15 g/L sucrose, 6 g/L agar, 0.5 mg/L BASTA, 400 mg/L Timentin, and 5 mg/L IBA) for 2 weeks. Three months-old plants developed a root system including primary and secondary roots, following which they were acclimated to greenhouse conditions (photoperiod of 16 h light/8 h darkness and illuminated with white fluorescent light; 150 $\mu mol/m^2$ s at 22–25°C) in plastic pots (20 × 10 cm) containing a mix of soil and vermiculite (2:1), until they finally reached maturity and started producing fruits approximately 1 month later. Mature T1 plants were used for further analysis (**Supplementary Figure 3**).

RNA Extraction and Quantitative Expression Analysis

Tomato RNA extraction was performed as described in Meisel et al. (2005). Briefly, mesocarps from five transgenic tomatoes (500 mg) were ground in liquid nitrogen and divided to perform three independent RNA extractions. The powder was then mixed with extraction buffer (2% CTAB, 2% PVP40, 25 mM EDTA, 2 M NaCl, 100 mM Tris–HCl, 0.05% spermidine, and 2% B-mercaptoethanol) at 65°C for 15 min. The samples were centrifuged and the phase containing the RNA was precipitated with 10 M LiCl overnight at 4°C. After centrifugation at 12,000*g* during 20 min, samples were resuspended in 20 μL of DEPC water. Genomic DNA traces were eliminated by a 40 min DNase I (Fermentas) treatment. For cDNA synthesis, 2 μg of DNA-free RNA were incubated with 1.5 μL of 10 μM oligo AP (**Supplementary Table 1**) and 8.3 μL of RT mixture (0.5 μL of RNase Inhibitor Ribolock, Fermentas), 1 μL of 10 mM dNTPs (Fermentas), 2.8 μL of 25 mM $MgCl_2$, and 4 μL of 5× RT Improm II buffer (Promega) for 5 min at 70°C. Then, the samples were incubated for 5 min on ice. Subsequently, 1.2 μL of RT Improm II was added to continue with cDNA synthesis according to RT Improm II manufacturer's instructions. For conventional expression analysis (**Supplementary Figure 4**), PCR reactions (28–35 cycles) were performed using Taq DNA polymerase (New England BioLabs) according to the manufacturer's recommendations and an annealing temperature adjusted to each set of primers (**Supplementary Table 1**) and using *SlPSY* to show the cDNA quality. Quantitative expression analysis (qRT-PCR) was performed in a LightCycler system (MX3000P, Stratagene), using SYBR Green double strand DNA binding dye, as described in Fuentes et al., 2012). Specific primers for optimized *DcPSY2*, *DcLCYB1*, and *XdCRTI* were used (**Supplementary Table 1**), based on the optimized sequences (**Supplementary Material**). *Actin* was selected as reference gene. Each qRT-PCR reaction was performed with three biological and two technical replicates. In all cases, the reaction specificities were tested with melting gradient dissociation curves and non-template controls (NTC).

Transient Transformation of Apple Fruits

Transient transformation of apples fruits was performed according to Arcos et al. (2020) with modifications. Fuji apple fruits at the mature green stage were infiltrated using the *Agrobacterium*-injection strategy containing the genetic construct of interest (pPSY2, pLCBY1, pPSY2-CRTI, or pPSY2-CRTI-LCYB1) and controls (WT). Each construct was infiltrated into a quarter of three fruits to have three biological replicas. Briefly, 30 mL of bacterial cultures in LB medium supplemented with Rifampicin (50 mg/L) and Spectinomycin (50 mg/L) were grown overnight at 28°C with agitation until an optical density (600 nm) of 0.2–0.3. The cultures were centrifuged, and the pellet resuspended in 30 mL of infiltration medium (10 mM $MgSO_4$, 10 mM MES, 10 mM $MgCl_2$). The culture was then infiltrated into the fruit flesh with a tuberculin syringe to a depth of 0.5 cm. For each apple, one half of the fruit was homogeneously agroinfiltrated. Agroinfiltrated fruits were maintained in an incubator with a photoperiod of 18 h light/6 h darkness, at 20–22°C and 30–50% of humidity. After 7 and 14 days post-infiltration, samples were taken for carotenoid quantification.

Carotenoid Extraction and Quantification From Tomato and Apple Fruits

Mesocarps from five transgenic tomatoes (500 mg) of each line of approximately 40–45 days post-flowering were ground in liquid nitrogen and divided to carry out three independent carotenoid extractions. For transient analysis, three independent apple fruits were agroinfiltrated with each construct including both controls, and after 7 and 14 days, 300 mg of infiltrated flesh of each apple were ground in liquid nitrogen independently. In all cases, each sample was measured twice, by adding 4 mL of hexane:acetone:ethanol (2:1:1) to obtain an homogeneous mixture. This solution was transferred to a tube, shaken for 2 min, incubated on ice and darkness for a further 2 min, and then centrifuged at 10.000 rpm for 10 min at 4°C. Finally, the carotenoids were recovered from the upper phase and dried using gaseous nitrogen. Once dried, the samples were stored at −80°C or resuspended in 2 mL of acetone for carotenoid

quantification. All extractions were carried out in on ice and in dim light conditions. Total carotenoids were quantified was carried out using a Shimadzu spectrophotometer at 474, 645/662 (chlorophyll *a* and *b* contribution) and at 520/750 nm (for turbidity). Quantification of individual carotenoids was undertaken in a Reverse Phase High Performance Liquid Chromatography (RP-HPLC) using a RP−18 Lichrocart 125−4 reverse phase column (Merck®). Pigment composition was determined according to Lichtenthaler and Buschmann (2001). The mobile phase was acetonitrile:methanol:isopropyl alcohol (85:10:5) with a 1.5 mL/min flow rate at room temperature in isocratic conditions. Carotenoid and chlorophyll concentrations were calculated according to the total pigments obtained at 474 nm by spectrophotometry, by retention times, absorption spectra and purity of the peaks, as described in Fuentes et al. (2012) and corroborated with the Carotenoids Handbook (Britton, 1995; Britton et al., 2004).

RESULTS

Modifications of Carotenogenic Genes and Functional Analysis of pCP-CG Vectors by Subcellular Localization

To generate the biotechnological platform to boost carotenoid content in apples, we chose *PSY2* and *LCYB1* from *D. carota* and *CrtI* from *X. dendrorhous.* The codon usage of each gene was optimized to maximize expression in apples (**Supplementary Material**).

The *XdCrtI* was destined to plastids using the transit peptide (tp) of the RUBISCO small subunit (**Supplementary Material**). This transit peptide has been used to direct *Erwinia uredovora* CrtI to tobacco leaf plastids, as determined by immunolocalization with gold particles (Misawa et al., 1993). We also amplified a 806 bp fragment upstream of the transcription start site of the PG promoter from *S. chilense* (tomatillo) (**Supplementary Material**) in order to direct expression of the carotenogenic genes to fruits. Using the different modules – the three carotenogenic genes, the tp and the PG promoter – four pCP-CG vectors were generated with different gene combinations, as described in section "Materials and Methods" (**Figure 2**).

Subsequently, we determined the correct plastid location of DcPSY2 and tp:XdCrtI; that of DcLCYB1:GFP has been reported previously (Moreno et al., 2013). Therefore, pPG:PSY2:GFP and pPG:tp:XdCrtI:GFP were transiently expressed in tomato fruits at breaker stage where both chloroplasts and chromoplasts are present in the flesh of the fruit. GFP fluorescence showed that DcPSY2:GFP had a speckled distribution (**Figure 3a**). This signal colocalized with the emission of chlorophyll (**Figures 3b,c**), strongly suggesting that DcPSY2:GFP has a chloroplastic localization. Similarly, GFP signal from tp:XdCrtI:GFP exhibited a distribution pattern of discrete foci (**Figure 3e**), which colocalized with the autofluorescence from chlorophyll (**Figures 3f,g**). Therefore, this result showed that the plastidial tp from the pea RUBISCO small subunit was functional in tomato. Considering that the GFP fluorescence distribution following infiltration with the control pPG:GFP construct was cytoplasmic in fruits, and much reduced in tobacco leaves (**Supplementary Figure 2**), we demonstrated the fruit specificity of the PG promoter from *S. chilense*. Overall, these results show that DcPSY2:GFP and tp:XdCrtI:GFP are chloroplastic.

Stable Transformation of *S. lycopersicum* With the pCP-CG Vectors Produce Fruits With Higher Carotenoid Contents

The functional characterization of pPSY2, pLCYB1, pPSY2-CRTI, and pPSY2-CRTI-LCYB1 vectors was carried out by stable transformation of *S. lycopersicum* var. Microtom. The *in vitro* transformation and regeneration culture to obtain transgenic plants was adapted from the protocol described in Pino et al. (2010) and summarized in Suppplementary **Figure 3**. During plant development, no phenotypic differences were noticeable with respect to WT tomato plants, except in the case of those transformed with pPSY2-CRTI-LCYB1 that showed dramatic alterations at all stages during the regeneration process (Suppplementary **Figure 3**). These lines exhibited a slower induction of shoots and their vegetative development was also delayed in comparison with the other transgenic lines. Interestingly, these lines produced tomatoes when they were still *in vitro*, about 2 months after the regeneration process started. This was significantly earlier in comparison with the WT and other transformed lines, which only produced fruits once they were in soil in greenhouse conditions.

Transformed tomato plants were subjected to molecular analysis to select transgenic lines once they were acclimated to the greenhouse conditions, except for pPSY2-CRTI-LCYB1. Twelve pPSY2 lines, seven pLCYB1 lines, and eight pPSY2-CRTI lines were transgenic, based on the respective transgene amplification (data not shown). At fructification, tomato fruits from untransformed WT plants, as well as from lines transformed with pPSY2, pLCYB1, and pPSY2-CRTI were observed at different developmental and ripening stages ranging from incipient green fruits to red, fully mature fruits; no significant differences between them in terms of size and ripening time were noted, and all were similar to previous reports (Fraser et al., 2002; Apel and Bock, 2009). However, in the case of the pPSY2-CRTI-LCYB1 construct, it was not possible to regenerate fully developed plants; instead stem-like structures were obtained with a reduced number of incipiently developed leaves. Nonetheless, these plants showed an accelerated flower development with fully functional flowers that yielded fruits during *in vitro* culture (Suppplementary **Figure 3**). Since the tissue was limited, molecular analysis of these fruits was challenging. Thus, transgene expression was confirmed when some of these fruits reached maturity. We determined that fruits of seven pPSY2 lines, five pLCYB1 lines and seven pPSY2-CRTI lines expressed the transgene (**Supplementary Figure 4**), and three of each were selected for qRTPCR and phenotypic analysis (**Figure 4**) and carotenoid quantification (**Figure 5**). As explained above, it was not possible to regenerate fully developed lines transformed with pPSY2-CRTI-LCYB1. Therefore, the

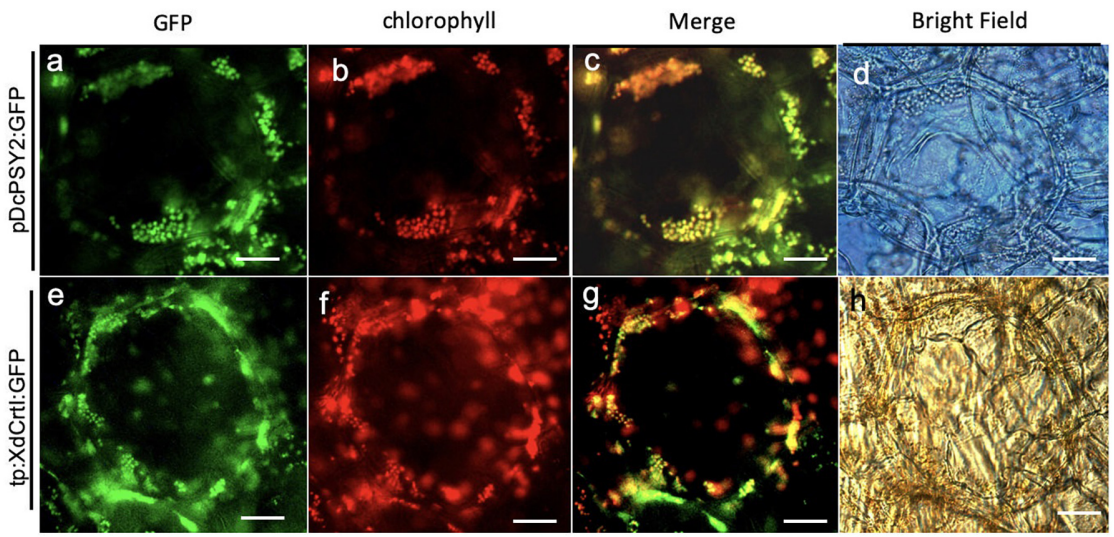

FIGURE 3 | Subcellular localization of DcPSY2 and XdCRTI. Transient transformation of tomato fruits agroinfiltrated with DcPSY2:GFP or XdCrtI:GFP fused to a transit peptide (tp). The expression of both constructs was driven by the pPG promoter. Fluorescence was observed 4 days after transient transformation. **(a)** GFP fluorescence of DcPSY2:GFP. **(b)** Chlorophyll autofluorescence of **(a)**. **(c)** Merge of panels **(a,b)**, showing colocalization of chlorophyll and the GFP signal. **(d)** Bright field of **(a–c)**. **(e)** GFP fluorescence of tp:XdCRTI:GFP. **(f)** Chlorophyll autofluorescence of **(e)**. **(g)** Merge of panels **(e,f)**, showing colocalization of chlorophyll and GFP signal. **(h)** Bright field of **(e–g)**. The TRITC filter U-N31001 was used for visualizing GFP fluorescence, with an excitation wavelength between 465 and 495 nm. Emission was collected between 513 and 556 nm. Chlorophyll autofluorescence was assessed by using a U-MNG2 filter, with an excitation wavelength between 530 and 550 nm and emission collected at 590 nm. Scale bar = 50 μm.

expression analysis was performed with a group of tomatoes obtained from *in vitro* culture and not from individual transgenic lines (**Figure 4** and **Supplementary Figure 4**).

For these evaluations, five mature fruits of each line were harvested and phenotypically analyzed. Fully ripe WT tomato fruits (2.2 ± 0.3 cm diameter) have a homogeneous red exocarp, are firm to the touch and have a central pedicel surrounded by several sepals (**Figure 4a**). Transverse sections showed a red fleshy mesocarp and endocarp with several yellowish seeds embedded in a locular cavity (**Figure 4a.1**). Transgenic tomato fruits from pPSY2 (**Figures 4b,b.1**), pLCYB1 (**Figures 4c,c.1**), and pPSY2-CRTI (**Figures 4d,d.1**) were phenotypically similar to fruits from WT plants (2.4 ± 0.3 cm diameter). On the other hand, pPSY2-CRTI-LCYB1 transgenic fruits exhibited a pale orange color at the ripening stage (**Figures 4e,e.1**), unlike the fruits of the WT and other transgenic lines, which turned red. In addition to the color difference, these transgenic fruits did not develop seeds and were therefore sterile lines (**Figure 4e.1**). Quantitative expression analysis showed that pPSY2 lines (P6, P14, and P16) present between 2.8 and 9.8-fold of *PSY2* expression, pLCYB1 lines (L3, L5, and L6) present between 12 and 45.2-fold *LCYB1* expression (**Figures 4f,e**, respectively), whereas pPSY-CRTI lines (PC3, PC4, and PC5) present between 3.6 and 300-fold expression of *PSY2* and 0.2 and 1.2-fold *CRTI* expression (**Figure 4h**). In the case of the transgenic pPSY2-CRTI-LCYB1 fruits, *CRTI* expression was significantly lower than that of *PSY2* and *LCYB1* (**Figure 4i**).

Regarding the total content of carotenoids, and compared to WT plants, the pPSY2 lines present a 1.21–1.34-fold increase, pLCYB1 lines present a 1.7-2-fold increase, and pPSY2-CRTI lines showed a 1.21–1.99-fold increase whilst pPSY2-CRTI-LCYB1 lines had a 2.9-fold decrease (**Figure 5**). This suggests that the expression of *LCYB1* is sufficient to enhance the total carotenoid content in fruits and that the simultaneous expression of these three transgenes negatively modulates the carotenoid pathway, reducing the total carotenoid content in tomato fruits (**Figure 5**).

Analysis of the individual carotenoid profiles revealed that transgenic tomatoes from the pPSY2 lines had up to 1.25-fold more lycopene, and only one line presented a 2.5-fold increase in β-carotene and two had a 1.27-fold increment in α-carotene with respect to WT (**Figure 5A**). Transgenic fruits from the pLCYB1 lines had a 1.75–2.0-fold increase in lycopene, 2.12–2.5-fold increase in β-carotene, and 1.36-2.27 fold increment in α-carotene with respect to the WT (**Figure 5B**). Fruits of pPSY2:CRTI lines presented a 1.87-1.95-fold increase in lycopene, two to threefold increase in β-carotene and 1.4-1.75-fold increment in α-carotene with respect to WT (**Figure 5C**), whereas pPSY2-CRTI-LCYB1 transgenic tomatoes present 3.6-fold less lycopene, a 2.57-fold increment in β-carotene, and 7.3-fold less α-carotene compared to untransformed controls (**Figure 5D**). The orange coloration phenotype of these tomatoes could be due to the combination of a reduced amount of red lycopene together with an increment in orange β-carotene (**Figure 4e**). These results suggest that the expression of carrot carotenogenic genes is capable of modulating carotenoid synthesis in a fruit that naturally accumulates large amounts of these pigments. Moreover, the increase in carotenoid content does not directly correlate with the expression level, as exemplified by comparing pPSY2 and pPSY2-CRTI lines.

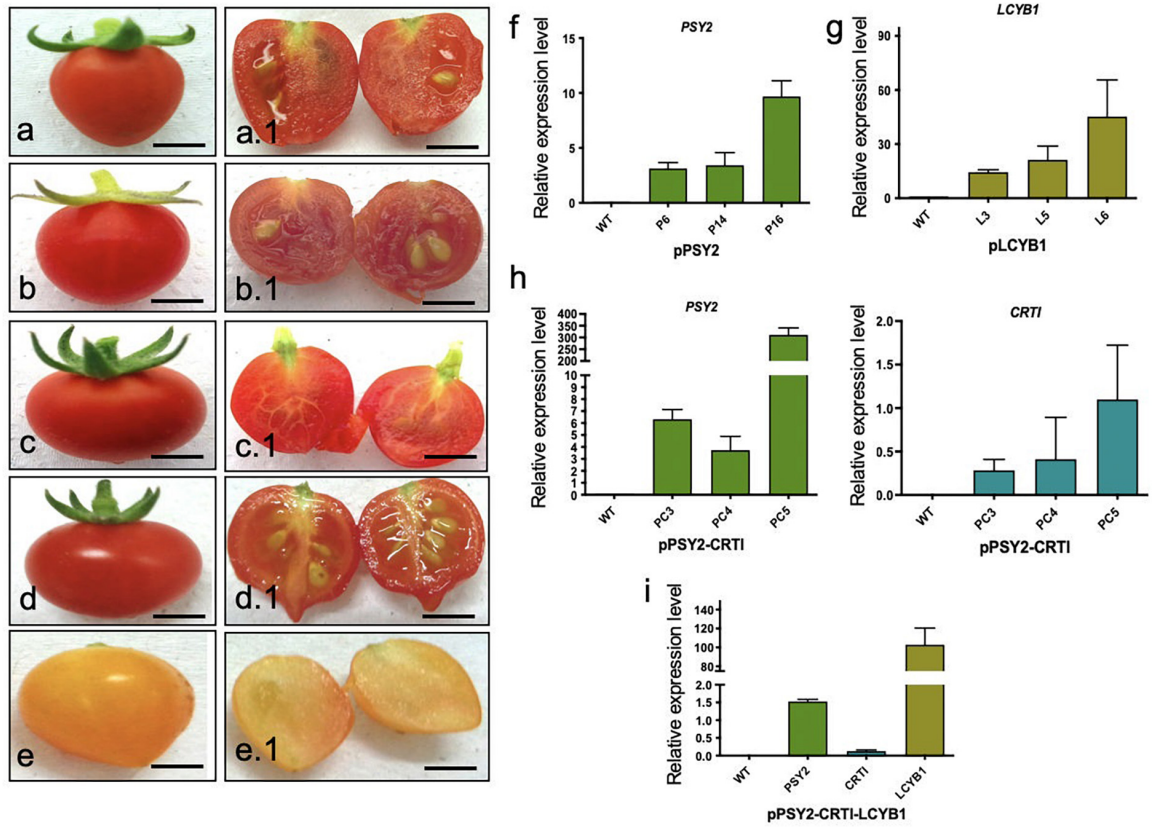

FIGURE 4 | Fruit phenotypes and expression analysis in T1 transgenic fruits. **(a)** Representative WT tomato fruit. **(a.1)** Cross-section of **(a)**. **(b)** Representative tomato fruit from pPSY2 line. **(b.1)** Cross-section of **(b)**. **(c)** Representative tomato fruit from pLCYB1 line. **(c.1)** Cross-section of **(c)**. **(c)** Representative tomato fruit from pPSY2-CRTI line. **(d.1)** Cross-section of **(d)**. **(e)** Tomato fruit from pPSY2-CRTI-LCYB2. **(e.1)** cross-section of **(e)**. Scale bar = 1 cm. **(f)** q-RTPCR in fruits of pPSY2, **(g)** pLCYB1, **(h)** pPSY2-CRTI, and **(i)** pPSY2-CRTI-LCYB1 transgenic lines. The relative expression was normalized to that of the *Actin* gene of *S. lycopersicum*. The expression analysis was performed with three biological replicas (cDNAs) from five fruits, each measured twice.

Interestingly, pLCYB1 was the genetic construct that triggered the highest increase in carotenoid content, constituting the most promising tool for future experiments.

Carotenoid Quantification in Apple Fruits After Transient Expression of pCP-CG Vectors

In order to test if the pCP-CG constructs were able to modify the content of carotenoids in apple, transient assays were carried out in Fuji fruits at breaker stage (Suppplementary **Figure 5**). At 7 and 14 days post-agroinfiltration, tissue samples were taken for carotenoid analysis. After 7 days of incubation, apples agroinfiltrated with pPSY2 and pLCYB1 showed an increase of 1.65 to 1.50-fold in total carotenoid content (4.3 and 3.94 μg/gFW, respectively) in comparison to non-agroinfiltrated (WT) apples (2.61 μg/gFW) (**Table 1**). Carotenoid profile analysis revealed that for these constructs, the lutein levels remain stable with respect to the control (**Table 1**). On the contrary, the β-carotene content almost doubles (to 3.51 μg/gFW in pPSY2 and to 3.30 μg/gFW in pLCYB1), respect to the WT apple fruits (1.81 μg/gFW) (**Table 1**). Fruits agroinfiltrated with pPSY2-CRTI showed a significant increment in total carotenoids and β-carotene of 1.17- and 1.3-fold (3.05 and 2.35 μg/gFW, respectively) (**Table 1**). Similarly, apple fruits infiltrated with pPSY2-CRTI-LCYB1 exhibited an increment in their total carotenoid (3.07 μg/gFW) and β-carotene (2.23 μg/gFW) content in comparison to control WT fruits, but to a similar or lesser extent in comparison with fruits agroinfiltrated with other pCP-CG constructions (**Table 1**).

Samples taken 14-days post-infiltration revealed that the total carotenoid content doubled in fruits agroinfiltrated with each one of the four pCP-CG constructs in comparison to WT (**Table 1**). Similarly, a significant increase in β-carotene levels was found in the infiltrated fruits with the pCP-CG series (4.78 μg/gFW for pPSY2, 5.47 μg/gFW for pLCYB1, 3.40 μg/gFW for pPSY2-CRTI, and 3.43 μg/gFW for pPSY2-CRTI-LCYB1) in comparison to control WT fruits (0.94 μg/gFW; **Table 1**). On the other hand, the apple fruits transiently transformed with the pCP-CG constructs did not present changes in the lutein content (**Table 1**), maintaining the same correlation observed in the 7-day incubation experiment. Altogether, these results suggest that transient expression of the pCP-CG constructs are functional in apple fruits, and suggest that double or triple constructs with

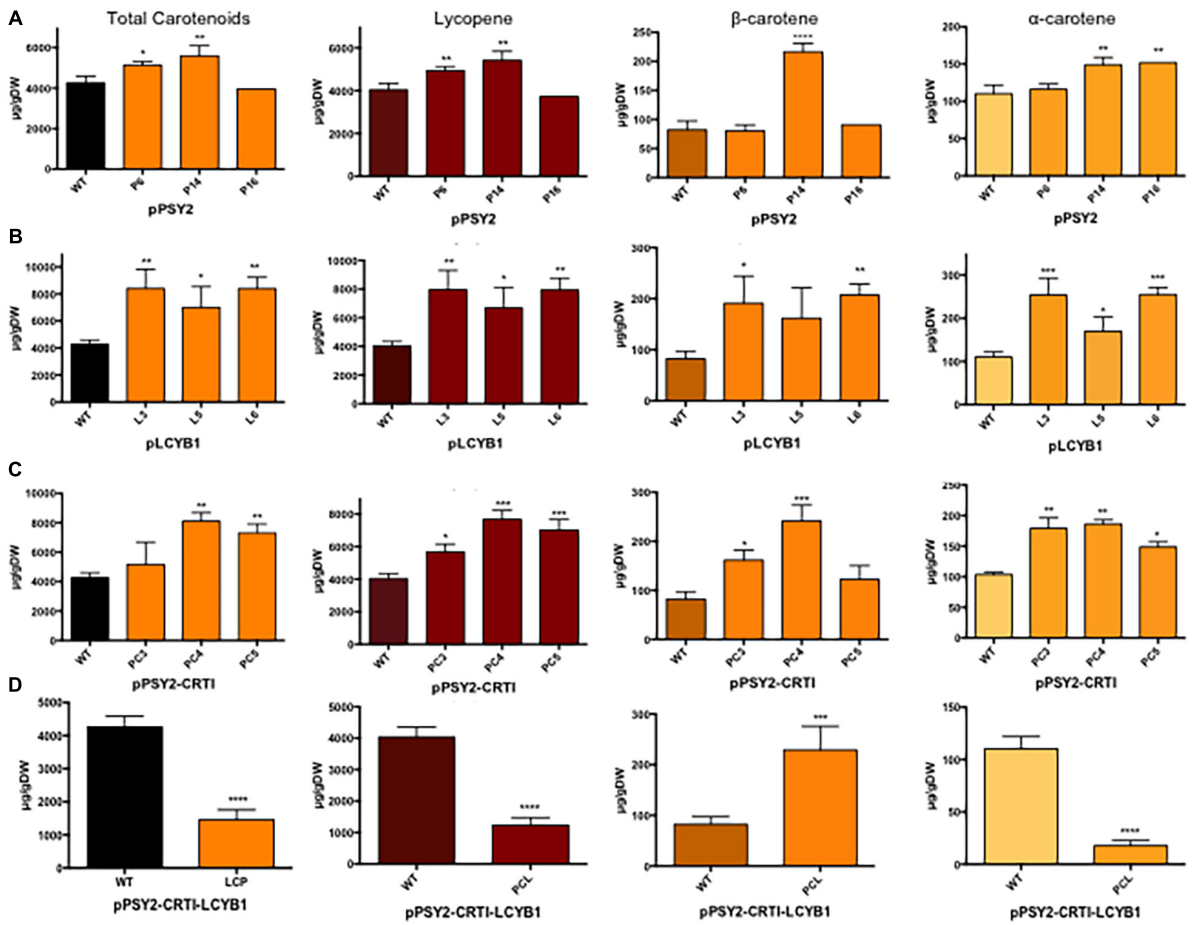

FIGURE 5 | Total and individual carotenoid quantification in pCP-CG transgenic lines. **(A)** pPSY2, **(B)** pLCYB1, **(C)** pPSY2-CRTI, and **(D)** pPSY2-CRTI-LCYB1 transgenic lines. Total carotenoids were quantified in fruits by spectrophotometry at 474 nm and individual carotenoids by HPLC expressed in μg/gDW. Asterisks indicate significant differences respect to the control (WT) determined by one-way ANOVA and Dunnet post-test, $^{*}p < 0.05$, $^{**}p < 0.01$, $^{***}p < 0.001$. In **(D)** the results were analyzed with a two-way *t*-test, $^{****}p < 0.0001$.

genes arranged in tandem do not trigger a synergistic effect on the carotenoid content.

DISCUSSION

Biotechnological Platform

Significant progress has been made in the generation of genetically modified crops with improved carotenoid content and nutritional properties (Alós et al., 2016). With the same goal, we designed and generated a biotechnological platform to evaluate key genes, with the aim of improving the carotenoid content, and thus the nutritional value of apples. The selection of the carotenogenic genes was based on our previous studies regarding carotenoid biosynthesis regulation in carrot, particularly in the taproot, which accumulates up to 1.5 mg/gDW in total carotenoids (Fuentes et al., 2012; Moreno et al., 2013, 2016; Rodriguez-Concepcion and Stange, 2013; Simpson et al., 2016, 2018). We have established that the increment in carotenoids correlates with a significant increase in the expression of almost all carotenogenic genes, especially *DcPSY2, DcZDS2, DcPDS, DcLCYB1, DcLCYE, DcZEP*, and *DcNCED1* (Simpson et al., 2016). The two *PSY* paralogs in carrot, *DcPSY1* and *DcPSY2*, present an induction of 3.2 and 316-fold during carrot tap root development, respectively, whereas *LCYB1* rises by eightfold and *LCYB2* by 100-fold at the mature stage of taproot development (Simpson et al., 2016).

Some of the carotenogenic genes from carrot have been previously characterized, demonstrating that they are functional *in vivo*. Both *DcZDS1* and *DcLCYB1* code for functional enzymes necessary for carrot development and carotenoid synthesis (Moreno et al., 2013; Flores-Ortiz et al., 2020). Total carotenoids rise threefold when *DcLCYB1* is overexpressed in carrot and a 2–10-fold increment when expressed in tobacco, with concomitant increases in chlorophyll content and photosynthetic activity which together have a positive impact on plant fitness (Moreno et al., 2013, 2016, 2020). The ability of LCYB1 to confer these qualities by itself when expressed in plants was the reason for selecting this gene as a candidate to be assessed in the biotechnological platform developed in this

work. On the other hand, *DcPSY2* was selected as previous data suggested that it could play a relevant role during the stress response; we determined that its expression is induced by saline stress and ABA in carrot, and showed that AREB transcription factors bind to the *DcPSY2* promoter (Simpson et al., 2018). Here we demonstrated that DcPSY2:GFP has the expected plastidial subcellular localization (**Figure 3**), and is therefore a possible candidate for boosting carotenoid content in both transgenic pPSY2 tomatoes (**Figure 5A**) and transiently infiltrated apple fruit flesh (**Table 1**). In the case of *XdCrtI*, its functionality was demonstrated by site directed mutagenesis using the double recombinant method in *X. dendrorhous*, whereby the deletion of *XdCrtI* in the homozygous strain causes a completely albino phenotype (Niklitschek et al., 2008). Here we determined that tp:XdCrtI:GFP with the pea small subunit RUBISCO transit peptide was correctly destined to plastids (**Figure 3**) and could be a suitable contender for enhancing total carotenoids and β-carotene when comparing pPSY2 and pPSY2-CRTI transgenic tomatoes (**Figure 5C**). The synthesis of carotenoids requires GGPP, a common precursor also needed for vitamin E (α-tocopherol), gibberellic acid and chlorophyll synthesis. Therefore, re-directing this precursor toward the synthesis of carotenoids by using constitutive promoters can have a negative impact on the metabolism of these other compounds. Consequently, a detrimental effect can be triggered both phenotypically and/or physiologically, with the generation of alterations such as dwarfism (Fray et al., 1995; Sandmann, 2001). A strategy to minimize this risk is to design genetic constructs with genes driven by tissue- or developmental-specific promoters. In this work, a 806 bp fragment of the fruit specific promoter of the tomato PG gene from *S. chilense* was chosen. This promoter has 99% identity to the 4,052–4,818 bp region of the *S. lycopersicum* PG promoter FJ465170.1 (Lau et al., 2009; **Supplementary Figure 6**), and targets specifically the transgenes to fruits (**Figure 3** and **Supplementary Figure 2**). Although the expression of *PG* increases during apple ripening (Janssen et al., 2008), it has been established that the PG promoter does not depend on ethylene, and thus induces ripening in both climacteric fruits such as tomatoes (Lincoln et al., 1987), and non-climacteric fruit such as apples[7]. Importantly, the PG promoter from *S. chilense* is not subjected to intellectual property protection and is therefore available to be used without royalties. As a selection marker, we used *bar* that confers resistance to the BASTA (or phosphinothricin) herbicide. This gene is free of rights, and there are several currently commercialized transgenic plants[8,9] harboring *bar*. The carotenogenic genes used here are also free of rights, even more so after optimizing their nucleotide sequence to make them more different from those native sequences present in carrot and yeast databases. For optimization, the sequence of interest was modified according to the preferential use of codons of the final organism, using the average of the codon usage of ribosomal genes or of a group of highly expressed genes (Puigbò et al., 2007). Here, the codon usage table of 567 mRNAs of *M. domestica* was available, and considered a sufficient population (163,086 codons) to successfully guide the codon usage preference, or at least to discriminate unusual codons (see text footnote 4). In the optimization of *DcPSY2*, *XdCrtI*, and *DcLCYB1*, most codons were conserved, since those used preferentially in carrots and yeast were the same as those in apples. However, there were codons that code for certain amino acids such as Tyr, Thr, Ser, Gln, Asn, Ile, Phe, and Glu where codon optimization was required.

[7]http://www.postharvest.com

[8]www.isaa.org

[9]www.chilebio.cl

Carotenoid Increment in Tomato

Tomato represents a suitable model to evaluate our biotechnological platform designed for the functional assessment of candidate carotenogenic genes. The results obtained through this initial strategy allowed us, in a short period of time, to project possible results that were ultimately used to improve the carotenoid content in apples.

Mature tomato fruits accumulate significant amounts of the reddish lycopene, and very low levels of β-carotene and xanthophylls (Fraser and Bramley, 2004; Liu et al., 2015; D'Andrea and Rodriguez-Concepcion, 2019; Diretto et al., 2020). During ripening, carotenoid levels rise up to 400 times, of which lycopene represents 90% of the total, accumulating approximately 2,000 μg/g DW of this pigment (Fraser et al., 1994, 2002). This large accumulation of carotenoids is associated with several factors such as sink capacity and the activity of some plastidial proteins (Sun et al., 2018; D'Andrea and Rodriguez-Concepcion, 2019). Equally important is the regulatory role of the expression level of carotenogenic genes during ripening such as *PSY1* and *PDS* that present an increase whilst *LCYB* and *LCYE* decrease their expression during ripening (Giuliano et al., 1993; Pecker et al., 1996; Ronen et al., 1999, 2000).

As mentioned above, transgenic tomatoes expressing apple-optimized *DcPSY2*, *DcLCYB1*, and *XdCrtI* showed a dissimilar increase in the levels of total carotenoids, lycopene, β-carotene and lutein (**Figure 5**) which correlated only partially with gene expression (**Figures 4f–i**). Specifically, pPSY2 lines present up to 1.34-fold rises in total carotenoids and 1.25-fold increases in lycopene in P6 and P14 lines, whereas only P14 has a 2.5-fold increase in β-carotene, and P14 and P16 have a 1.27-fold increment in α-carotene (**Figure 5A**); P6 and P14 have the lowest *PSY2* expression level (**Figure 4f**). Nevertheless, this allows us to conclude that *DcPSY2* codes for a functional enzyme capable of increasing carotenoids in tomato fruits but at a moderate level and that a reduced expression level is sufficient to increment β-carotene (P14). Fraser et al., 2002 obtained an increase of up to 2.1 times in the total carotenoid content and lycopene in fruits of the Alisa Craig tomato variety transformed with the *CrtB* gene. This gene codifies a PSY from *E. uredovora*, which was expressed in a fruit-specific manner. These results suggest that DcPSY2 might not be as efficient as CrtB, but this should be confirmed by comparing the same variety of tomato.

Regarding pLCYB1 transgenic lines, they have almost two times more total carotenoids and lycopene and up to 2.5 times more β-carotene and 2.27 times more α-carotene in all transgenic lines (**Figure 5B**). Although L3 presents the lowest expression

level, it is one of the two transgenic lines with the highest carotenoid content together with L6, the line with the highest expression level (**Figures 4g, 5B**). Previous reports have shown that the fruit-specific expression of *AtLCYB* in tomato var. Moneymaker (Rosati et al., 2000) and the constitutive expression of the endogenous *SlLCYB* in tomato var. Red Setter (D'Ambrosio et al., 2004) resulted in an increase of total carotenoid content of 1.6 times and 2 times, respectively, which is similar to the increase we obtained in pLCYB1 tomatoes var. Microtom (**Figure 5**). Regarding individual carotenoids, *AtLCYB* transgenic tomato fruits yielded on average 3.1 times more β-carotene than the control whereas the lycopene content remained constant (Rosati et al., 2000). Similarly, *SlLCYB* transgenic lines presented an increase of over ten times in β-carotene (D'Ambrosio et al., 2004); unlike Rosati et al., 2000, this was accompanied by a 53-fold drop in the lycopene levels (D'Ambrosio et al., 2004). Interestingly, *DcLCYB1* did not produce a detriment in lycopene content and actually produced an increase in α-carotene levels. The expression of *DcLCYB1* alone produces a twofold increment in total carotenoids (**Figure 5B**), similar to transplastomic tomatoes that expressed *LCYB* from *Narcissus pseudonarcissus* that produced a 50% increment in total carotenoids (Apel and Bock, 2009). Expressing *AtLCYB* or *EuCtrY* enabled the enhancement of β-carotene without substantial reductions in lycopene (Rosati et al., 2000; Wurbs et al., 2007). This shows that *DcLCYB1* is at least as equally efficient as *LCYB*s from other species. Indeed, tomatoes from pLCYB1 lines had a higher carotenoid content than tomatoes from the pPSY2 and pPSY2-CRTI lines (**Figure 5**), suggesting that in tomato the endogenous SlPSY, desaturases and isomerases are highly active. Our data revealed that the apple-optimized *XdCrtI* is functional in tomato. pPSY2-CRTI transgenic tomatoes exhibited a larger increase in total carotenoids and lycopene (twofold) in comparison to pPSY2 and also produced up to threefold more β-carotene and up to 1.75-fold more α-carotene compared to WT fruits (**Figure 5C**), especially in PC3 and PC4, the transgenic lines that have the lowest expression level of both *PSY2* and *CRTI*. This suggests that a low expression level is enough to increment the carotenoid level whilst a very high level of expression may not produce a significant increment and sometimes causes a detriment in total or individual carotenoid levels (**Figure 5C**). In previous studies, *EuCrtI* was constitutively expressed in tomato var. Alisa Craig which resulted in a twofold increase in β-carotene levels with a significant reduction in both total carotenoid content and lycopene, producing orange-colored fruits (Römer et al., 2000). This metabolic effect was also due to the induction of endogenous *PDS*, *ZDS*, and *LCYB* and a reduction in PSY1 enzyme activity (Römer et al., 2000). These results suggest that the pPSY2-CRTI construct is more efficient in terms of total carotenoids, lycopene, and lutein production than pPSY2.

The simultaneous expression of three carotenogenic genes in tomatoes has not been previously reported, although it is a strategy that was previously used in rice and potato (Ye et al., 2000; Diretto et al., 2007). Both in rice that simultaneously express *PSY*, *CRTI*, and *LCYB* (Ye et al., 2000) and in potato, that express *Erwinia* CrtB (*PSY*), CrtI, and CrtY (*LCYB*) (Diretto et al., 2007), there were increases in lutein and β-carotene contents in transgenic lines. On the contrary, in our study, the expression of pPSY2-CRTI-LCYB1 in tomatoes produces a significant decrease in total carotenoid content. This decrease correlates with 3.6-fold falls in lycopene and 7.3-fold falls in α-carotene, but not in β-carotene levels, which increased significantly (by 2.57-fold, **Figure 5D**). We propose that these alterations are responsible for the orange phenotype of these transgenic fruits (**Figure 4e**). The decrease in total carotenoids observed in the pPSY1-CRTI-LCYB1 lines, although it is an unexpected result, is similar to that obtained by Römer et al. (2000) in tomatoes expressing 35SCaMV:*CRTI*. Even though there are several reasons that could explain this phenomenon, one hypothesis is that the constitutive and high expression of *CRTI* in transgenic lines, increases the expression levels of *LCYB*, thus causing a concomitant increment in β-carotene synthesis (Römer et al., 2000). A second hypothesis is that the CRTI enzyme is more efficient, delivering either a more abundant or a more suitable substrate to the LCYB

TABLE 1 | Quantification of carotenoids in apple fruits agroinfiltrated with the pCP-CG vectors.

Days post-infiltration	Fuji Apple	Total carotenoid (μg/gFW)				Lutein (μg/gFW)				β-carotene (μg/gFW)			
		Mean	SD	FC	*t*-test	Mean	SD	FC	*t*-test	Mean	SD	FC	*t*-test
7	WT	2.62	0.11	–	–	0.81	0.14	–	–	1.81	0.03	–	–
	pPSY2	4.31	0.32	**1.65**	**	0.79	0.07	–	ns	3.51	0.26	**1.94**	***
	pLCYB1	3.94	0.31	**1.50**	**	0.64	0.11	–	ns	3.30	0.31	**1.82**	**
	pPSY2-CRTI	3.05	0.22	**1.17**	*	0.70	0.10	–	ns	2.35	0.23	**1.30**	*
	pPSY2-LCYB-CRTI	3.08	0.17	**1.18**	*	0.84	0.15	–	ns	2.23	0.18	**1.23**	*
14	WT	2.06	0.30	–	–	1.12	0.16	–	–	0.94	0.19	–	–
	pPSY2	5.67	1.60	**2.75**	*	0.88	0.27	–	ns	4.79	1.37	**5.11**	**
	pLCYB1	6.39	1.33	**3.11**	**	0.92	0.20	–	ns	5.47	1.16	**5.84**	**
	pPSY2-CRTI	4.67	0.77	**2.27**	**	1.27	0.42	–	ns	3.40	0.53	**3.63**	**
	pPSY2-LCYB-CRTI	4.27	0.63	**2.07**	**	0.83	0.06	**−0.74**	*	3.44	0.69	**3.67**	**

Values are means of three biological replicas. "FW" represents Fresh Weight, "SD" Standard deviation and "FC" Fold of Change. Significant levels: $^{*}P < 0.05$; $^{**}P < 0.01$; $^{***}P < 0.001$; ns: not significant; – not considered. The bold values represent the pigments fold of change (FC) between agroinfiltrated apples respect to non-agroinfiltrated apples (WT).

enzyme which then transforms it into β-carotene. These two possibilities are not mutually exclusive and actually together could have a synergistic effect increasing the β-carotene content (Giuliano et al., 2000). In our case, the simultaneous expression of the three key genes may be redirecting the metabolic flux of the carotenoid pathway toward the production of β-carotene at the expense of the α-carotene branch and of the accumulation of those that are synthesized in previous stages, producing fruits with the pale orange appearance. In addition, the dwarf *in vitro* phenotype of these lines can also be explained by the redirection of the metabolic flow of GGPP precursors of the MEP pathway to carotenoid synthesis, with a detriment of the synthesis of gibberellic acid (GA), causing negative effects on the general development and physiology of the plant. GGPP is a precursor shared for the synthesis of carotenoids and for that of several growth regulators such as cytokines, ABA and GA (Cuttriss et al., 2007; Howitt et al., 2007; Rodríguez-Concepción, 2010). GA is an important phytohormone involved in plant development (Yamaguchi, 2008). Tomato plants (var. Alisa Craig) that overexpress *PSY1* under the 35S promoter had fruits with higher levels of lycopene but presented a dwarf phenotype due to reduced levels of GA (Fray et al., 1995).

Taken together, our results allow us to suggest that pLCYB1 is the most suitable option for producing tomato fruits with a higher β-carotene and total carotenoid content.

Carotenoid Increment in Apple Fruits

To evaluate our biotechnological platform, we chose a transient expression assay because it provides a rapid and robust tool for assessing the activity of genetic constructs before undertaking a stable transformation (Sparkes et al., 2006). This is especially relevant in non-model fruits such as apples (Arcos et al., 2020). However, the infiltration of apple fruits has inherent challenges, given their anatomical and physiological characteristics such as large parenchymatous cells with substantial vacuoles (Spolaore et al., 2001). Together with the stage of maturity of the fruits during the infiltration, these factors contribute to making agroinfiltration a highly heterogeneous and complex process (Suppplementary **Figure 5**). Nevertheless, once key steps of the procedure have been standardized, it is a feasible approximation for functional assessment, providing a valuable tool. Our data showed that in Fuji apple fruits, all four pCP-GC constructs were capable of modifying the content of total and individual carotenoids after transient agroinfiltration (**Table 1**). Indeed, the 1.17–2.27-fold increment in total carotenoids obtained with pPSY2-CRTI was similar to those values previously reported by Arcos et al. (2020) with the same genetic construct (2GC) but using a different transient transformation strategy (vacuum infiltration). Interestingly, data at 14-days post-infiltration showed that the total carotenoid content and β-carotene levels were in several cases up to twice and triple, respectively, to those obtained at 7-days post agroinfiltration (**Table 1**). This could be associated with the stability of the enzymes after infiltration as well as the storage mechanism of the pigments once produced. In addition, it shows that apple fruits were capable of continuing the normal ripening process despite the exogenous bacterial application, at least for the periods evaluated. This also allows us to conclude that *DcPSY2* is functional in apple fruits. Moreover, the increments seen in β-carotene also suggest that endogenous carotenogenic genes such as desaturases (PDS and ZDS), isomerases (Z-ISO and CRTISO) and LCYB are functional in apples.

The fact that the single constructs (pPSY2 and pLCYB1) duplicated the content of total carotenoids and β-carotene with respect to the double (pPSY2-CRTI) and triple constructs (pPSY2-CRTI-LCYB1) both at 7 and 14-days post infiltration, suggest that the transgenes in the double or triple constructs might not be properly expressed, or the stability of these transcripts/enzymes could be harmed. It is important to remember that each carotenogenic gene in the pCP constructs is driven by the same promoter, which could generate competition for the same transcription factors, limiting the recruitment of the transcription machinery, especially in the multiple constructs.

These results lead us to propose that apple fruits obtained from stable transformation will also accumulate at least two to three times more carotenoids. However, it is feasible to consider that the increment in the carotenoid levels would be even higher in the flesh considering our previous results, by expressing 35S:AtDXR in Fuji (Arcos et al., 2020). Specifically, leaves of AtDXR transgenic apples displayed up to a threefold rise in total carotenoids (508 mg g^{-1} FW) and in β-carotene (508 mg g^{-1} FW) when compared to wild-type plants, and twofold rises when transiently infiltrated in apple fruits (Arcos et al., 2020). In addition, in the flesh of banana fruits, a 2.3-fold increment in β-carotene was obtained by expressing *PSY1* or *PSY2* directed by a constitutive promoter when compared to the wild-type (Paul et al., 2017), and in kiwi fruit, a 1.3-fold increase in β-carotene was observed by expressing either *GGPPS* or *PSY* (Kim et al., 2010). Regarding the constructs generated, these results suggest that pPSY2 or pLCYB1 are the best candidates for the stable transformation of apples, and possibly for other fruits with pale flesh, in order to improve carotenoid content and thus nutritional properties.

CONCLUSION

1. The PG promoter from *S. chilense* var. tomatillo correctly directs gene expression to fruits in tomato and apple.
2. *DcPSY2* codifies for a functional enzyme with a plastidial localization.
3. All four pCP-CG vectors are able to increase the total carotenoid content, particularly of β-carotene, in tomatoes and apples.
4. Of the pCP-CG vectors, those that possess the carrot carotenogenic genes *DcPSY2* and *DcLCYB1*, would be the best candidates for increasing carotenoids in stably transformed apples.

DATA AVAILABILITY STATEMENT

The original contributions presented in the study are included in the article/**Supplementary Material**, further inquiries can be directed to the corresponding author/s.

AUTHOR CONTRIBUTIONS

AA-M and CS conceived and designed the experiments. DA, AA-M, CF-O, and CP performed the experiments. DA, AA-M, CF-O, MH, and CS wrote the manuscript. All authors contributed to the article and approved the submitted version.

ACKNOWLEDGMENTS

The authors acknowledge Manuel Rodriguez-Concepción (CRAG-CSIC, Spain) for providing the pB7FWG2-AtDXR vector and the Agencia Nacional de Investigación e Innovación (ANID) through the projects Anillo ACT192073, Fondef D10I1022, and Fondecyt 1180747 for financial support.

FUNDING

This study was funded by Programa de Investigación Asociativa (PIA) Anillo ACT192073 and Fondef D10I1022 (CS and MH) and Fondecyt 1180747 (CS) projects.

SUPPLEMENTARY MATERIAL

The Supplementary Material for this article can be found online at: https://www.frontiersin.org/articles/10.3389/fpls.2021.677553/full#supplementary-material

REFERENCES

Alcaíno, J., Baeza, M., and Cifuentes, V. (2016). Carotenoid distribution in nature. *Subcell. Biochem.* 79, 3–33. doi: 10.1007/978-3-319-39126-7_1

Alós, E., Rodrigo, M. J., and Zacarias, L. (2016). Manipulation of carotenoid content in plants to improve human health. *Subcell. Biochem.* 79, 311–343. doi: 10.1007/978-3-319-39126-7_12

Ampomah-Dwamena, C., Dejnoprat, S., Lewis, D., Sutherland, P., Volz, R. K., and Allan, A. C. (2012). Metabolic and gene expression analysis of apple (Malus × domestica) carotenogenesis. *J. Exp. Bot.* 63, 4497–4511. doi: 10.1093/jxb/ers134

Ampomah-Dwamena, C., Driedonks, N., Lewis, D., Shumskaya, M., Chen, X., Wurtzel, E. T., et al. (2015). The phytoene synthase gene family of apple (Malus x domestica) and its role in controlling fruit carotenoid content. *BMC Plant Biol.* 15:185.

Apel, W., and Bock, R. (2009). Enhancement of carotenoid biosynthesis in transplastomic tomatoes by induced lycopene-to-provitamin a conversion. *Plant Physiol.* 151, 59–66. doi: 10.1104/pp.109.140533

Arcos, Y., Godoy, F., Flores-Ortiz, C., Arenas-M, A., and Stange, C. (2020). Boosting carotenoid content in Malus domestica var. Fuji by expressing AtDXR through an Agrobacterium-mediated transformation method. *Biotechnol. Bioeng.* 117, 2209–2222. doi: 10.1002/bit.27358

Bang, H., Kim, S., Leskovar, D., and King, S. (2007). Development of a codominant CAPS marker for allelic selection between canary yellow and red watermelon based on SNP in lycopene β-cyclase (LCYB) gene. *Mol. Breed.* 20, 63–72. doi: 10.1007/s11032-006-9076-4

Bartley, G. E., and Scolnik, P. A. (1995). Plant carotenoids: pigments for photoprotection, visual attraction, and human health. *Plant Cell* 7, 1027–1038. doi: 10.2307/3870055

Beltran, J. C. M., and Stange, C. (2016). Apocarotenoids: a new carotenoid-derived pathway. *Subcell. Biochem.* 79, 239–272. doi: 10.1007/978-3-319-39126-7_9

Britton, G. (1995). Structure and properties of carotenoids in relation to function. *FASEB J.* 9, 1551–1558. doi: 10.1096/fasebj.9.15.8529834

Britton, G., Liaaen-Jensen, H., and Pfander, H. (2004). *Carotenoids Handbook*. Boston: Birkhäuser Basel.

Byers, T., and Perry, G. (1992). Dietary carotenes, vitamin C, and vitamin E as protective antioxidants in human cancers. *Annu. Rev. Nutr.* 12, 139–159. doi: 10.1146/annurev.nu.12.070192.001035

Cazzonelli, C. I. (2011). Carotenoids in nature: insights from plants and beyond. *Funct. Plant Biol.* 38, 833–847. doi: 10.1071/fp11192

Cazzonelli, C. I., and Pogson, B. J. (2010). Source to sink: regulation of carotenoid biosynthesis in plants. *Trends Plant Sci.* 15, 266–274. doi: 10.1016/j.tplants.2010.02.003

Ceballos, H., Morante, N., Sánchez, T., Ortiz, D., Aragón, I., and Chávez, A. L. (2013). Rapid cycling recurrent selection for increased carotenoids content in cassava roots. *Crop Sci.* 53, 2342–2351. doi: 10.2135/cropsci2013.02.0123

Cerda, A., Moreno, J. C., Acosta, D., Godoy, F., Cáceres, J. C., and Cabrera, R. (2020). Functional characterisation and in silico modelling of MdPSY2 variants and MdPSY5 phytoene synthases from Malus domestica. *J. Plant Physiol.* 249, 153166. doi: 10.1016/j.jplph.2020.153166

Curtis, M. D., and Grossniklaus, U. (2003). A gateway cloning vector set for high-throughput functional analysis of genes in planta. *Plant Physiol.* 133, 462–469. doi: 10.1104/pp.103.027979

Cuttriss, A. J., Chubb, A. C., Alawady, A., Grimm, B., and Pogson, B. J. (2007). Regulation of lutein biosynthesis and prolamellar body formation in Arabidopsis. *Funct. Plant Biol.* 34, 663–672. doi: 10.1071/fp07034

D'Ambrosio, C., Giorio, G., Marino, I., Merendino, A., Petrozza, A., Salfi, L., et al. (2004). Virtually complete conversion of lycopene into β-carotene in fruits of tomato plants transformed with the tomato lycopene β-cyclase (tlcy-b) cDNA. *Plant Sci.* 166, 207–214. doi: 10.1016/j.plantsci.2003.09.015

D'Andrea, L., and Rodriguez-Concepcion, M. (2019). Manipulation of plastidial protein quality control components as a new strategy to improve carotenoid contents in tomato fruit. *Front. Plant Sci.* 10:1071.

Delgado-Pelayo, R., Gallardo-Guerrero, L., and Hornero-Méndez, D. (2014). Chlorophyll and carotenoid pigments in the peel and flesh of commercial apple fruits varieties. *Food Res. Int.* 65, 272–281. doi: 10.1016/j.foodres.2014.03.025

DellaPenna, D., Alexander, D. C., and Bennett, A. B. (1986). Molecular cloning of tomato fruit polygalacturonase: analysis of polygalacturonase mRNA levels during ripening. *Proc. Natl. Acad. Sci.* 83, 6420–6424. doi: 10.1073/pnas.83.17.6420

DellaPenna, D., Lincoln, J. E., Fischer, R. L., and Bennett, A. B. (1989). Transcriptional analysis of polygalacturonase and other ripening associated genes in rutgers, rin, nor, and Nr tomato fruit. *Plant Physiol.* 90, 1372–1377. doi: 10.1104/pp.90.4.1372

Diretto, G., Al-Babili, S., Tavazza, R., Papacchioli, V., Beyer, P., and Giuliano, G. (2007). Metabolic engineering of potato carotenoid content through tuber-specific overexpression of a bacterial mini-pathway. *PLoS One* 2:e0000350.

Diretto, G., Frusciante, S., Fabbri, C., Schauer, N., Busta, L., Wang, Z., et al. (2020). Manipulation of β-carotene levels in tomato fruits results in increased ABA content and extended shelf life. *Plant Biotechnol. J.* 18, 1185–1199. doi: 10.1111/pbi.13283

Diretto, G., Tavazza, R., Welsch, R., Pizzichini, D., Mourgues, F., and Papacchioli, V. (2006). Metabolic engineering of potato tuber carotenoids through tuber-specific silencing of lycopene epsilon cyclase. *BMC Plant Biol.* 6:13.

Failla, M. L., Chitchumroonchokchai, C., Siritunga, D., De Moura, F. F., Fregene, M., and Manary, M. J. (2012). Retention during processing and bioaccessibility of β-carotene in high β-carotene transgenic cassava root. *J. Agric. Food Chem.* 60, 3861–3866. doi: 10.1021/jf204958w

Farré, G., Bai, C., Twyman, R. M., Capell, T., Christou, P., and Zhu, C. (2011). Nutritious crops producing multiple carotenoids - a metabolic balancing act. *Trends Plant Sci.* 16, 532–540. doi: 10.1016/j.tplants.2011.08.001

Farré, G., Sanahuja, G., Naqvi, S., Bai, C., Capell, T., and Zhu, C. (2010). Travel advice on the road to carotenoids in plants. *Plant Sci.* 179, 28–48. doi: 10.1016/j.plantsci.2010.03.009

Flores-Ortiz, C., Alvarez, L. M., Undurraga, A., Arias, D., Durán, F., Wegener, G., et al. (2020). Differential role of the two ζ-carotene desaturase paralogs in carrot (*Daucus carota*): ZDS1 is a functional gene essential for plant development and carotenoid synthesis. *Plant Sci.* 291:110327.

Fraser, P. D., and Bramley, P. M. (2004). The biosynthesis and nutritional uses of carotenoids. *Prog. Lipid Res.* 43, 228–265. doi: 10.1016/j.plipres.2003.10.002

Fraser, P. D., Enfissi, E. M. A., and Bramley, P. M. (2009). Genetic engineering of carotenoid formation in tomato fruit and the potential application of systems and synthetic biology approaches. *Arch. Biochem. Biophys.* 483, 196–204. doi: 10.1016/j.abb.2008.10.009

Fraser, P. D., Kiano, J. W., Truesdale, M. R., Schuch, W., and Bramley, P. M. (1999). Phytoene synthase-2 enzyme activity in tomato does not contribute to carotenoid synthesis in ripening fruit. *Plant Mol. Biol.* 40, 687–698.

Fraser, P. D., Romer, S., Shipton, C. A., Mills, P. B., Kiano, J. W., and Misawa, N. (2002). Evaluation of transgenic tomato plants expressing an additional phytoene synthase in a fruit-specific manner. *Proc. Natl. Acad. Sci. U. S. A.* 99, 1092–1097. doi: 10.1073/pnas.241374598

Fraser, P. D., Truesdale, M. R., Bird, C. R., Schuch, W., and Bramley, P. M. (1994). Carotenoid biosynthesis during tomato fruit development. evidence for tissue-specific gene expression. *Plant Physiol.* 105, 405–413. doi: 10.1104/pp.105.1.405

Fray, R. G., Wallace, A., Fraser, P. D., Valero, D., Hedden, P., and Bramley, P. M. (1995). Constitutive expression of a fruit phytoene synthase gene in transgenic tomatoes causes dwarfism by redirecting metabolites from the gibberellin pathway. *Plant J.* 8, 693–701. doi: 10.1046/j.1365-313x.1995.08050693.x

Fuentes, P., Pizarro, L., Moreno, J. C., Handford, M., Rodriguez-Concepcion, M., and Stange, C. (2012). Light-dependent changes in plastid differentiation influence carotenoid gene expression and accumulation in carrot roots. *Plant Mol. Biol.* 79, 47–59. doi: 10.1007/s11103-012-9893-2

Giuliano, G. (2014). Plant carotenoids: genomics meets multi-gene engineering. *Curr. Opin. Plant Biol.* 19, 111–117. doi: 10.1016/j.pbi.2014.05.006

Giuliano, G., Aquilani, R., and Dharmapuri, S. (2000). Metabolic engineering of plant carotenoids. *Trends Plant Sci.* 5, 406–409. doi: 10.1016/s1360-1385(00)01749-0

Giuliano, G., Bartley, G. E., and Scolnik, P. A. (1993). Regulation of carotenoid biosynthesis during tomato development. *Plant Cell* 5, 341–351.

Giuliano, G., Tavazza, R., Diretto, G., Beyer, P., and Taylor, M. A. (2008). Metabolic engineering of carotenoid biosynthesis in plants. *Trends Biotechnol.* 26, 139–145. doi: 10.1016/j.tibtech.2007.12.003

Harker, F. R., Gunson, F. A., and Jaeger, S. R. (2003). The case for fruit quality: an interpretive review of consumer attitudes, and preferences for apples. *Postharvest Biol. Technol.* 28, 333–347. doi: 10.1016/s0925-5214(02)00215-6

Holick, C. N., Michaud, D. S., Stolzenberg-Solomon, R., Mayne, S. T., Pietinen, P., and Taylor, P. R. (2002). Dietary carotenoids, serum β-carotene, and retinol and risk of lung cancer in the alpha-tocopherol, beta-carotene cohort study. *Am. J. Epidemiol.* 156, 536–547. doi: 10.1093/aje/kwf072

Hornero-Méndez, D., and Britton, G. (2002). Involvement of NADPH in the cyclization reaction of carotenoid biosynthesis. *FEBS Lett.* 515, 133–136. doi: 10.1016/s0014-5793(02)02453-5

Howitt, C. A., Pogson, B. J., Cuttriss, A. J., and Mimica, J. L. (2007). "Carotenoids," in *the Structure and Function of Plastids. Advances in Photosynthesis and Respiration*, vol 23, eds R. R. Wise and J. K. Hoober (Dordrecht: Springer).

Isaacson, T., Ohad, I., Beyer, P., and Hirschberg, J. (2004). Analysis in vitro of the enzyme CRTISO establishes a poly-cis-carotenoid biosynthesis pathway in plants. *Plant Physiol.* 136, 4246–4255. doi: 10.1104/pp.104.052092

Isaacson, T., Ronen, G., Zamir, D., and Hirschberg, J. (2002). Cloning of tangerine from tomato reveals a Carotenoid isomerase essential for the production of β-carotene and xanthophylls in plants. *Plant Cell* 14, 333–342. doi: 10.1105/tpc.010303

Janssen, B. J., Thodey, K., Schaffer, R. J., Alba, R., Balakrishnan, L., and Bishop, R. (2008). Global gene expression analysis of apple fruit development from the floral bud to ripe fruit. *BMC Plant Biol.* 8:16. doi: 10.1186/1471-2229-8-16

Jayaraj, J., Devlin, R., and Punja, Z. (2008). Metabolic engineering of novel ketocarotenoid production in carrot plants. *Transgenic Res.* 17, 489–501. doi: 10.1007/s11248-007-9120-0

Just, B. J., Santos, C. A. F., Fonseca, M. E. N., Boiteux, L. S., Oloizia, B. B., and Simon, P. W. (2007). Carotenoid biosynthesis structural genes in carrot (*Daucus carota*): isolation, sequence-characterization, single nucleotide polymorphism (SNP) markers and genome mapping. *Theor. Appl. Genet.* 114, 693–704. doi: 10.1007/s00122-006-0469-x

Kim, M., Kim, S.-C., Song, K. J., Kim, H. B., Kim, I.-J., and Song, E.-Y. (2010). Transformation of carotenoid biosynthetic genes using a micro-cross section method in kiwifruit (*Actinidia deliciosa* cv. Hayward). *Plant Cell Rep.* 29, 1339–1349. doi: 10.1007/s00299-010-0920-y

Lau, J. M., Cooper, N. G., Robinson, D. L., and Korban, S. S. (2009). Sequence and in silico characterization of the tomato polygalacturonase (PG) promoter and terminator region. *Plant Mol. Biol. Rep.* 27, 250–256. doi: 10.1007/s11105-008-0081-0

Lichtenthaler, H. K., and Buschmann, C. (2001). Extraction of photosynthetic tissues: chlorophylls and carotenoids. *Curr. Protoc. Food Anal. Chem.* 1.

Lincoln, J. E., Cordes, S., Read, E., and Fischer, R. L. (1987). Regulation of gene expression by ethylene during Lycopersicon esculentum (tomato) fruit development. *Proc. Natl. Acad. Sci. U. S. A.* 84, 2793–2797. doi: 10.1073/pnas.84.9.2793

Lipkie, T. E., De Moura, F. F., Zhao, Z. Y., Albertsen, M. C., Che, P., and Glassman, K. (2013). Bioaccessibility of carotenoids from transgenic provitamin a biofortified sorghum. *J. Agric. Food Chem.* 61, 5764–5771. doi: 10.1021/jf305361s

Liu, L., Shao, Z., Zhang, M., and Wang, Q. (2015). Regulation of carotenoid metabolism in tomato. *Mol. Plant* 8, 28–39. doi: 10.1016/j.molp.2014.11.006

Lu, S., and Li, L. (2008). Carotenoid metabolism: biosynthesis, regulation, and beyond. *J. Integr. Plant Biol.* 50, 778–785. doi: 10.1111/j.1744-7909.2008.00708.x

Malone, W. F. (1991). Studies evaluating antioxidants and β-carotene as chemopreventives. *Am. J. Clin. Nutr.* 53, 305S–313S.

Marnett, L. J. (1987). Peroxyl free radicals: potential mediators of tumor initiation and promotion. *Carcinogenesis* 8, 1365–1373. doi: 10.1093/carcin/8.10.1365

Meisel, L., Fonseca, B., González, S., Baeza-Yates, R., Cambiazo, V., Campos, R., et al. (2005). A rapid and efficient method for purifying high quality total RNA from peaches (*Prunus persica*) for functional genomics analyses. *Biol. Res.* 38, 83–88.

Mínguez-Mosquera, M. I., and Hornero-Méndez, D. (1997). Changes in provitamin a during paprika processing. *J. Food Prot.* 60, 853–857. doi: 10.4315/0362-028x-60.7.853

Misawa, N. (2011). Carotenoid β-ring hydroxylase and ketolase from marine bacteria - promiscuous enzymes for synthesizing functional xanthophylls. *Mar. Drugs* 9, 757–771. doi: 10.3390/md9050757

Misawa, N., Yamano, S., Linden, H., De Felipe, M. R., Lucas, M., and Ikenaga, H. (1993). Functional expression of the *Erwinia uredovora* carotenoid biosynthesis gene crtl in transgenic plants showing an increase of β-carotene biosynthesis activity and resistance to the bleaching herbicide norflurazon. *Plant J.* 4, 833–840. doi: 10.1046/j.1365-313x.1993.04050833.x

Moise, A. R., Al-Babili, S., and Wurtzel, E. T. (2014). Mechanistic aspects of carotenoid biosynthesis. *Chem. Rev.* 114, 164–193. doi: 10.1021/cr400106y

Montgomery, J., Pollard, V., Deikman, J., and Fischer, R. L. (1993). Positive and negative regulatory regions control the spatial distribution of polygalacturonase transcription in tomato fruit pericarp. *Plant Cell* 5, 1049–1062. doi: 10.2307/3869626

Mordi, R. C. (1993). Mechanism of β-carotene degradation. *Biochem. J.* 292, 310–312. doi: 10.1042/bj2920310

Moreno, J. C., Cerda, A., Simpson, K., Lopez-Diaz, I., Carrera, E., Handford, M., et al. (2016). Increased *Nicotiana tabacum* fitness through positive regulation of carotenoid, gibberellin and chlorophyll pathways promoted by *Daucus carota* lycopene β-cyclase (Dclcyb1) expression. *J. Exp. Bot.* 67, 2325–2338. doi: 10.1093/jxb/erw037

Moreno, J. C., Mi, J., Agrawal, S., Kössler, S., Turečková, V., and Tarkowská, D. (2020). Expression of a carotenogenic gene allows faster biomass production by redesigning plant architecture and improving photosynthetic efficiency in tobacco. *Plant J.* 103, 1967–1984. doi: 10.1111/tpj.14909

Moreno, J. C., Pizarro, L., Fuentes, P., Handford, M., Cifuentes, V., and Stange, C. (2013). Levels of Lycopene β-Cyclase 1 modulate carotenoid gene expression and accumulation in *Daucus carota*. *PLoS One* 8:e0058144.

Naqvi, S., Farré, G., Sanahuja, G., Capell, T., Zhu, C., and Christou, P. (2010). When more is better: multigene engineering in plants. *Trends Plant Sci.* 15, 48–56. doi: 10.1016/j.tplants.2009.09.010

Naqvi, S., Zhu, C., Farre, G., Ramessar, K., Bassie, L., and Breitenbach, J. (2009). Transgenic multivitamin corn through biofortification of endosperm with three vitamins representing three distinct metabolic pathways. *Proc. Natl. Acad. Sci. U. S. A.* 106, 7726–7727.

Niklitschek, M., Alcaíno, J., Barahona, S., Sepúlveda, D., Lozano, C., and Carmona, M. (2008). Genomic organization of the structural genes controlling the astaxanthin biosynthesis pathway of Xanthophyllomyces dendrorhous. *Biol. Res.* 41, 93–108.

Olson, J. A. (1996). Benefits and liabilities of vitamin a and carotenoids. *J. Nutr.* 126(4 Suppl.), 1208S–1212S.

Paine, J. A., Shipton, C. A., Chaggar, S., Howells, R. M., Kennedy, M. J., and Vernon, G. (2005). Improving the nutritional value of golden rice through increased pro-vitamin a content. *Nat. Biotechnol.* 23, 482–487. doi: 10.1038/nbt1082

Paul, J. Y., Khanna, H., Kleidon, J., Hoang, P., Geijskes, J., and Daniells, J. (2017). Golden bananas in the field: elevated fruit pro-vitamin a from the expression of a single banana transgene. *Plant Biotechnol. J.* 15, 520–532. doi: 10.1111/pbi.12650

Pecker, I., Gabbay, R., Cunningham, F. X., and Hirschberg, J. (1996). Cloning and characterization of the cDNA for lycopene beta-cyclase from tomato reveals decrease in its expression during fruit ripening. *Plant Mol. Biol.* 30, 807–819. doi: 10.1007/bf00019013

Perello, C., Llamas, E., Burlat, V., Ortiz-Alcaide, M., Phillips, M. A., and Pulido, P. (2016). Differential subplastidial localization and turnover of enzymes involved in isoprenoid biosynthesis in chloroplasts. *PLoS One* 11:e0150539. doi: 10.1371/journal.pone.0150539

Pino, L. E., Lombardi-Crestana, S., Azevedo, M. S., Scotton, D. C., Borgo, L., and Quecini, V. (2010). The Rg1 allele as a valuable tool for genetic transformation of the tomato "Micro-Tom" model system. *Plant Methods* 6:23. doi: 10.1186/1746-4811-6-23

Pixley, K., Rojas, N. P., Babu, R., Mutale, R., Surles, R., and Simpungwe, E. (2013). "Biofortification of maize with provitamin a carotenoids," in *Carotenoids and Human Health*, ed. S. Tanumihardjo (Totowa, NJ: Humana Press).

Pons, E., Alquézar, B., Rodríguez, A., Martorell, P., Genovés, S., and Ramón, D. (2014). Metabolic engineering of β-carotene in orange fruit increases its in vivo antioxidant properties. *Plant Biotechnol. J.* 12, 17–27. doi: 10.1111/pbi.12112

Puigbò, P., Guzmán, E., Romeu, A., and Garcia-Vallvé, S. (2007). OPTIMIZER: a web server for optimizing the codon usage of DNA sequences. *Nucleic Acids Res.* 35, W126–W131.

Rao, A. V., and Rao, L. G. (2007). Carotenoids and human health. *Pharmacol. Res.* 55, 207–216.

Ravanello, M. P., Ke, D., Alvarez, J., Huang, B., and Shewmaker, C. K. (2003). Coordinate expression of multiple bacterial carotenoid genes in canola leading to altered carotenoid production. *Metab. Eng.* 5, 255–263. doi: 10.1016/j.ymben.2003.08.001

Rodríguez-Concepción, M. (2010). Supply of precursors for carotenoid biosynthesis in plants. *Arch. Biochem. Biophys.* 504, 118–122. doi: 10.1016/j.abb.2010.06.016

Rodriguez-Concepcion, M., and Stange, C. (2013). Biosynthesis of carotenoids in carrot: an underground story comes to light. *Arch. Biochem. Biophys.* 539, 110–116. doi: 10.1016/j.abb.2013.07.009

Römer, S., Fraser, P. D., Kiano, J. W., Shipton, C. A., Misawa, N., and Schuch, W. (2000). Elevation of the provitamin a content of transgenic tomato plants. *Nat. Biotechnol.* 18, 666–669. doi: 10.1038/76523

Ronen, G., Carmel-Goren, L., Zamir, D., and Hirschberg, J. (2000). An alternative pathway to β-carotene formation in plant chromoplasts discovered by map-based cloning of Beta and old-gold color mutations in tomato. *Proc. Natl. Acad. Sci. U. S. A.* 97, 11102–11107. doi: 10.1073/pnas.190177497

Ronen, G., Cohen, M., Zamir, D., and Hirschberg, J. (1999). Regulation of carotenoid biosynthesis during tomato fruit development: expression of the gene for lycopene epsilon-cyclase is down-regulated during ripening and is elevated in the mutant Delta. *Plant J.* 17, 341–351. doi: 10.1046/j.1365-313x.1999.00381.x

Rosas-Saavedra, C., and Stange, C. (2016). Biosynthesis of carotenoids in plants: enzymes and color. *Subcell. Biochem.* 79, 35–69. doi: 10.1007/978-3-319-39126-7_2

Rosati, C., Aquilani, R., Dharmapuri, S., Pallara, P., Marusic, C., and Tavazza, R. (2000). Metabolic engineering of beta-carotene and lycopene content in tomato fruit. *Plant J.* 24, 413–420. doi: 10.1046/j.1365-313x.2000.00880.x

Rosati, C., Diretto, G., and Giuliano, G. (2009). Biosynthesis and engineering of carotenoids and apocarotenoids in plants: state of the art and future prospects. *Biotechnol. Genet. Eng. Rev.* 26, 139–162. doi: 10.7313/upo9781907284489.006

Sandmann, G. (2001). Genetic manipulation of carotenoid biosynthesis: strategies, problems and achievements. *Trends Plant Sci.* 6, 14–17. doi: 10.1016/s1360-1385(00)01817-3

Sheehy, R. E., Pearson, J., Brady, C. J., and Hiatt, W. R. (1987). Molecular characterization of tomato fruit polygalacturonase. *Mol. Gen. Genet.* 208, 30–36. doi: 10.1007/bf00330418

Shewmaker, C. K., Sheehy, J. A., Daley, M., Colburn, S., and Ke, D. Y. (1999). Seed-specific overexpression of phytoene synthase: increase in carotenoids and other metabolic effects. *Plant J.* 20, 401X–412X.

Simpson, K., Cerda, A., and Stange, C. (2016). Carotenoid biosynthesis in *Daucus carota*. *Subcell. Biochem.* 79, 199–217. doi: 10.1007/978-3-319-39126-7_7

Simpson, K., Fuentes, P., Quiroz-Iturra, L. F., Flores-Ortiz, C., Contreras, R., and Handford, M. (2018). Unraveling the induction of phytoene synthase 2 expression by salt stress and abscisic acid in *Daucus carota*. *J. Exp. Bot.* 69, 4113–4126. doi: 10.1093/jxb/ery207

Sparkes, I. A., Runions, J., Kearns, A., and Hawes, C. (2006). Rapid, transient expression of fluorescent fusion proteins in tobacco plants and generation of stably transformed plants. *Nat. Protoc.* 1, 2019–2025. doi: 10.1038/nprot.2006.286

Spolaore, S., Trainotti, L., and Casadoro, G. (2001). A simple protocol for transient gene expression in ripe fleshy fruit mediated by Agrobacterium. *J. Exp. Bot.* 52, 840–850.

Stahl, W., and Sies, H. (2003). Antioxidant activity of carotenoids. *Mol. Aspects Med.* 24, 345–351.

Sun, T., Yuan, H., Cao, H., Yazdani, M., Tadmor, Y., and Li, L. (2018). Carotenoid metabolism in plants: the role of plastids. *Mol. Plant* 11, 58–74. doi: 10.1016/j.molp.2017.09.010

Telias, A., Bradeen, J. M., Luby, J. J., Hoover, E. E., and Allen, A. C. (2011). Regulation of anthocyanin accumulation in apple peel. *Hortic. Rev.* 38, 357–391.

Voorrips, L. E., Goldbohm, R. A., Van Poppel, G., Sturmans, F., Hermus, R. J. J., and Van Den Brandt, P. A. (2000). Vegetable and fruit consumption and risks of colon and rectal cancer in a prospective cohort study: the Netherlands cohort study on diet and cancer. *Am. J. Epidemiol.* 152, 1081–1092. doi: 10.1093/aje/152.11.1081

Walter, M. H., and Strack, D. (2011). Carotenoids and their cleavage products: biosynthesis and functions. *Nat. Prod. Rep.* 28, 663–692. doi: 10.1039/c0np00036a

Wurbs, D., Ruf, S., and Bock, R. (2007). Contained metabolic engineering in tomatoes by expression of carotenoid biosynthesis genes from the plastid genome. *Plant J.* 49, 276–288. doi: 10.1111/j.1365-313x.2006.02960.x

Yamaguchi, S. (2008). Gibberellin metabolism and its regulation. *Annu. Rev. Plant Biol.* 59, 225–251. doi: 10.1146/annurev.arplant.59.032607.092804

Ye, V. M., and Bhatia, S. K. (2012). Pathway engineering strategies for production of beneficial carotenoids in microbial hosts. *Biotechnol. Lett.* 34, 1405–1414.

Ye, X., Al-Babili, S., Andreas, K., Jing, Z., Paola, L., Beyer, P., et al. (2000). Engineering the provitamin a (β-carotene) biosynthetic pathway into (carotenoid-free) rice endosperm. *Science* 287, 303–305. doi: 10.1126/science.287.5451.303

Yuan, K., Wang, C., Wang, J., Xin, L., Zhou, G., and Li, L. (2014). Analysis of the MdMYB1 gene sequence and development of new molecular markers related to apple skin color and fruit-bearing traits. *Mol. Genet. Genom.* 289, 1257–1265. doi: 10.1007/s00438-014-0886-5

Zhu, C., Sanahuja, G., Yuan, D., Farré, G., Arjó, G., and Berman, J. (2013). Biofortification of plants with altered antioxidant content and composition: genetic engineering strategies. *Plant Biotechnol. J.* 11, 129–141. doi: 10.1111/j.1467-7652.2012.00740.x

Conflict of Interest: The authors declare that the research was conducted in the absence of any commercial or financial relationships that could be construed as a potential conflict of interest.

Publisher's Note: All claims expressed in this article are solely those of the authors and do not necessarily represent those of their affiliated organizations, or those of the publisher, the editors and the reviewers. Any product that may be evaluated in this article, or claim that may be made by its manufacturer, is not guaranteed or endorsed by the publisher.

frontiers in Plant Science

REVIEW
published: 31 August 2021
doi: 10.3389/fpls.2021.727118

Engineered Accumulation of Bicarbonate in Plant Chloroplasts: Known Knowns and Known Unknowns

Sarah Rottet[1†], Britta Förster[2†], Wei Yih Hee[1], Loraine M. Rourke[1], G. Dean Price[1,2] and Benedict M. Long[1,2]*

[1]*Realizing Increased Photosynthetic Efficiency (RIPE), The Australian National University, Canberra, ACT, Australia,* [2]*Australian Research Council Centre of Excellence for Translational Photosynthesis, Research School of Biology, The Australian National University, Canberra, ACT, Australia*

OPEN ACCESS

Edited by:
Patricia León, National Autonomous University of Mexico, Mexico

Reviewed by:
Suresh Kumar, Indian Agricultural Research Institute (ICAR), India
Dinakar Challabathula, Central University of Tamil Nadu, India

****Correspondence:***
G. Dean Price
dean.price@anu.edu.au

[†]These authors have contributed equally to this work

Specialty section:
This article was submitted to Plant Biotechnology, a section of the journal Frontiers in Plant Science

Received: *18 June 2021*
Accepted: *06 August 2021*
Published: *31 August 2021*

Citation:
Rottet S, Förster B, Hee WY, Rourke LM, Price GD and Long BM (2021) Engineered Accumulation of Bicarbonate in Plant Chloroplasts: Known Knowns and Known Unknowns. Front. Plant Sci. 12:727118. doi: 10.3389/fpls.2021.727118

Heterologous synthesis of a biophysical CO_2-concentrating mechanism (CCM) in plant chloroplasts offers significant potential to improve the photosynthetic efficiency of C_3 plants and could translate into substantial increases in crop yield. In organisms utilizing a biophysical CCM, this mechanism efficiently surrounds a high turnover rate Rubisco with elevated CO_2 concentrations to maximize carboxylation rates. A critical feature of both native biophysical CCMs and one engineered into a C_3 plant chloroplast is functional bicarbonate (HCO_3^-) transporters and vectorial CO_2-to-HCO_3^- converters. Engineering strategies aim to locate these transporters and conversion systems to the C_3 chloroplast, enabling elevation of HCO_3^- concentrations within the chloroplast stroma. Several CCM components have been identified in proteobacteria, cyanobacteria, and microalgae as likely candidates for this approach, yet their successful functional expression in C_3 plant chloroplasts remains elusive. Here, we discuss the challenges in expressing and regulating functional HCO_3^- transporter, and CO_2-to-HCO_3^- converter candidates in chloroplast membranes as an essential step in engineering a biophysical CCM within plant chloroplasts. We highlight the broad technical and physiological concerns which must be considered in proposed engineering strategies, and present our current status of both knowledge and knowledge-gaps which will affect successful engineering outcomes.

Keywords: CO_2-concentrating mechanism, bicarbonate transport, chloroplast envelope, improving photosynthesis, chloroplast engineering

INTRODUCTION

Crop improvement technologies utilizing synthetic biology approaches have been central to a number of recent advances in photosynthetic output (e.g., Kromdijk et al., 2016; Salesse-Smith et al., 2018; Ermakova et al., 2019; South et al., 2019; Batista-Silva et al., 2020; López-Calcagno et al., 2020). These ambitious aims come at an unprecedented time in human history when agricultural productivity must be rapidly boosted in order to feed future populations (Kromdijk and Long, 2016). In a 2008 review, we discussed the potential of utilizing components of the

CO_2-concentrating mechanism (CCM) of cyanobacteria as a means to improve crop photosynthetic CO_2 fixation (Price et al., 2008), with potential to raise rates of carboxylation at ribulose-1,5-bisphosphate (RuBP) carboxylase/oxygenase (Rubisco) while improving nitrogen and water-use efficiencies (Price et al., 2011a; McGrath and Long, 2014; Rae et al., 2017). In the intervening years great steps forward have been made to address this challenge, yet many uncertainties remain on the path to generating a functional chloroplastic CCM.

The CCMs of proteobacteria, cyanobacteria, and microalgae are comprised of bicarbonate (HCO_3^-) transporters and vectorial CO_2-to-HCO_3^- conversion complexes which, in concert, accumulate a high concentration of HCO_3^- in prokaryotic cells and microalgal chloroplasts (**Figure 1**; Kaplan et al., 1980; Badger and Price, 2003; Moroney and Ynalvez, 2007). As a charged species of inorganic carbon (C_i), HCO_3^- is not freely diffusible through cell membranes (Tolleter et al., 2017), and allows for the generation of an elevated cellular or stromal HCO_3^- pool compared with the external environment (Price and Badger, 1989a). The second chief component of these CCMs are specialized Rubisco compartments called carboxysomes (Rae et al., 2013) and pyrenoids (**Figure 1**; Moroney and Ynalvez, 2007; Mackinder, 2018; Hennacy and Jonikas, 2020) where co-localized carbonic anhydrase (CA) enzymes dehydrate HCO_3^- into CO_2, providing high concentrations of CO_2 as substrate for RuBP carboxylation.

Collectively, these systems are often termed biophysical CCMs since their function utilizes the active movement of C_i across cellular compartments to release it as CO_2 around Rubisco (Giordano et al., 2005). This is distinct from biochemical CCMs found in C_4 and CAM plants, which generally utilize HCO_3^- for the carboxylation of phosphoenolpyruvate into transportable organic acids, prior to spatial or temporal CO_2 re-release and carboxylation by Rubisco.

Modeling has shown that the installation of biophysical CCM HCO_3^- transporters in the inner-envelope membrane

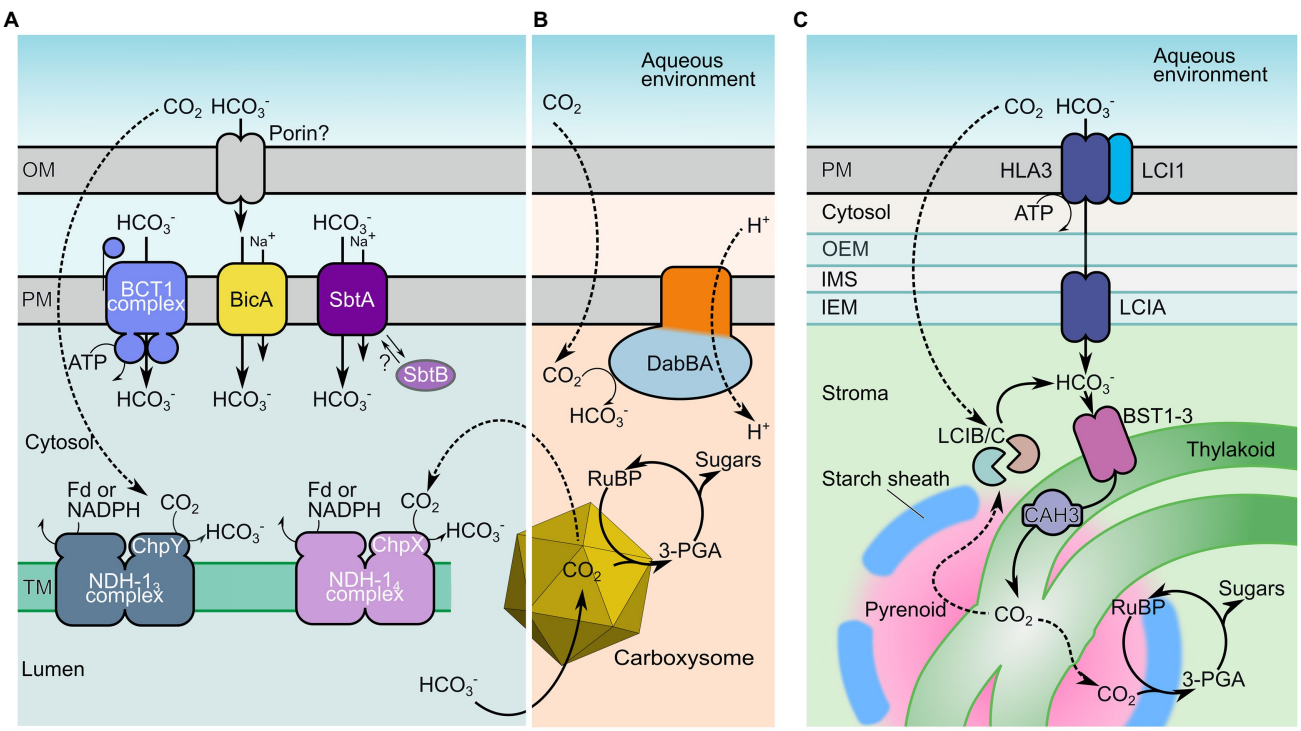

FIGURE 1 | Inorganic carbon uptake components of cyanobacterial, proteobacterial, and microalgal CO_2-concentrating mechanisms (CCMs). Key inorganic carbon transport mechanisms of cyanobacteria **(A)**, proteobacteria **(B)**, and microalgae **(C)** that facilitate elevated cytoplasmic and stromal HCO_3^- concentrations. The HCO_3^- pool is utilized to generate localized high concentrations of CO_2 in specialized Rubisco-containing compartments knowns as carboxysomes **(A,B)** or pyrenoids **(C)**, supporting high carboxylation rates. In cyanobacteria **(A)**, HCO_3^- is potentially supplied to the periplasmic space *via* an outer-membrane (OM) porin, and is directly transferred across the plasma membrane (PM) by the single-protein Na^+-dependent transporters bicarbonate transporter A (BicA) and SbtA, or by the ATP-driven complex BCT1. In addition, cytosolic CO_2, acquired by either diffusion, leakage from the carboxysome or spontaneous dehydration of HCO_3^-, is converted to HCO_3^- by the energy-coupled, vectorial CO_2 pumps NHD-1_3 and NHD-1_4 in the thylakoid membranes (TM). In proteobacteria **(B)**, DabBA plays a similar role, taking advantage of relatively high rates of CO_2 influx from a low-pH external environment to vectorially generate a cytoplasmic HCO_3^- pool (Desmarais et al., 2019). In microalgae (C), HCO_3^- is accumulated *via* a series of transporters located on the PM (LCI1 and presumably ATP-driven HLA3), the chloroplast inner envelope membrane [inner-envelope membrane (IEM); LCIA] and the TM (bestrophins, BST1-3). Thylakoids traverse the Rubisco-containing pyrenoid where the thylakoid lumen-localized carbonic anhydrase (CA) CAH3 is thought to convert HCO_3^- supplied to the thylakoid lumen to CO_2. Analogous to the cyanobacterial system, the LCIB/C complex constitutes a putative, vectorial CA that may recycle any CO_2 arising in the chloroplast stroma back to HCO_3^-. Fd, ferredoxin; RuBP, ribulose-1,5-bisphosphate; 3-PGA, 3-phosphoglycerate; SbtB, SbtA regulator protein; and ChpX/ChpY, NDH-1 complex vectorial CO_2-HCO_3^- domains. Individual transporter proteins are as listed in **Table 1**.

(IEM) of C_3 chloroplasts is sufficient to elevate the chloroplastic C_i, leading to a net improvement in CO_2 available for Rubisco carboxylation and therefore net carbon gain (Price et al., 2011a; McGrath and Long, 2014). This initial step in the conversion of crop plant chloroplasts to a sub-cellular CCM not only provides potential yield gains but is also necessary to generate the required stromal [HCO_3^-] needed for carboxysome or pyrenoid function in the engineering trajectory toward a complete chloroplastic CCM (Price et al., 2013). Therefore, the successful engineering of HCO_3^- accumulation in C_3 stroma is a critical step in this process.

While the idea to generate a C_3 chloroplastic CCM has been considered for some time (Price et al., 2008), the pace of progress in this field highlights a myriad of conceptual and technical challenges associated with achieving such a complex goal. Progress toward the construction of carboxysomes and pyrenoids in C_3 chloroplasts has been made (Lin et al., 2014a; Long et al., 2018; Atkinson et al., 2020), and the transfer of a complete and functional CCM from proteobacteria into Rubisco-dependent *Escherichia coli* (Flamholz et al., 2020) indicates theoretical potential for successful transfer of CCMs to plants. However, hurdles remain in both understanding and constructing CCM components within eukaryotic organelles where system complexity confounds an already difficult engineering task. This is exemplified by reports of the successful expression of HCO_3^- transporters into C_3 chloroplasts, but their lack of function and/or incorrect targeting (Pengelly et al., 2014; Atkinson et al., 2016; Rolland et al., 2016; Uehara et al., 2016, 2020), or lack of functional characterization *in planta* (Nölke et al., 2019), highlights the need to further understand the composite interactions of chloroplast protein targeting, membrane energization, and small molecule passage across the chloroplast envelope.

Herein, we discuss some of the known complexities associated with the engineering task of generating functional HCO_3^- transport systems in C_3 chloroplasts and highlight unknown details, which require ongoing research focus to enable a clearer path to successful elevation of chloroplastic HCO_3^- for increased carboxylation efficiency in crop plants.

CAN HCO_3^- CONCENTRATIONS BE ELEVATED IN A C_3 CHLOROPLAST?

The terrestrial nature of C_3 plants and their appearance in geological history during a period of relatively high atmospheric CO_2 (Flamholz and Shih, 2020) is a possible contributor to the absence of biophysical CCMs from higher plant chloroplasts (Raven et al., 2017). The efficiency of Rubisco carboxylation is hampered by O_2, leading to photorespiratory expenditure of accumulated CO_2 and chemical energy (Busch, 2020). It is assumed that factors selecting for maintenance of relatively high rates of carboxylation, as atmospheric concentrations of CO_2 decreased while O_2 increased approximately 350 million years ago, may have led to a divergence in mechanistic adaptations between aquatic and terrestrial photosynthetic organisms (Flamholz and Shih, 2020; Long et al., 2021). Thus, cyanobacteria and many eukaryotic algae evolved CCMs to overcome these challenges, while emerging terrestrial C_3 plants have maintained a larger investment in Rubisco and evolved to maximize beneficial biochemical contributions from photorespiratory nitrogen and sulfur metabolism (Shi and Bloom, 2021). As a result, terrestrial C_3 plant lineages have not evolved with a capability to elevate chloroplastic C_i concentrations like many of their aquatic counterparts. Indeed, there is good argument that biochemical CCM evolution (e.g., C_4 photosynthesis) would be favored in terrestrial systems over strategies which accumulate HCO_3^- (Flamholz and Shih, 2020). While horizontal gene transfer may have been involved in the evolution of C_4 photosynthesis (Wickell and Li, 2020), there has presumably been very little opportunity or evolutionary pressure for plants to acquire genes from aquatic biophysical CCMs in order to evolve alternative CO_2 fixation strategies. In addition, the slower diffusion of C_i species in aquatic environments compared with plant tissue may confine evolutionary trajectories (Raven et al., 2017; Flamholz and Shih, 2020). This underscores the fact that the C_3 chloroplast has evolved in a gaseous atmosphere and with alternative solutions to Rubisco promiscuity to its aquatic cousins, highlighting that the concept of an engineered chloroplastic CCM is one in which considerable evolutionary complexity must be considered.

When considering any engineering design for enhanced HCO_3^- uptake into C_3 chloroplasts, a reasonable question to ask is whether HCO_3^- can be elevated in this organelle, and if so, how? There is sufficient HCO_3^- in the mesophyll cytoplasm available for transport into chloroplasts (at least 250 μM; Evans and von Caemmerer, 1996). However, a CCM engineering strategy must ensure HCO_3^- can gain passage across both the outer-envelope membrane (OEM) and IEM of the chloroplast. Given that C_3 chloroplasts typically access C_i from the external environment (primarily as the more membrane-permeable CO_2); chloroplast membranes appear not to have specific HCO_3^- transport mechanisms (Rolland et al., 2012). Nonetheless, a number of oxyanions, such as phosphate, nitrate, and sulfate evidently do diffuse through the OEM (Bölter et al., 1999). Notably, simple diffusion of CO_2 through leaf tissue is insufficient to support the supply rates needed for observed rates of CO_2 assimilation by plants (Morison et al., 2005), and it is likely that CO_2 entry into the chloroplast is also facilitated by CO_2-permeable aquaporins (Flexas et al., 2006; Evans et al., 2009; Tolleter et al., 2017; Ermakova et al., 2021) and CA-driven distribution of C_i between predominant species (HCO_3^- and CO_2; Price et al., 1994). Therefore, the facilitated entry of C_i into C_3 chloroplasts is conceptually not counter to contemporary chloroplast function, and on face value would appear beneficial.

In general, solute transport across the chloroplast OEM is considered to be relatively unhindered due to the presence of low-selectivity and large-molecule channel proteins present in this membrane (Bölter et al., 1999; Hemmler et al., 2006; Duy et al., 2007). It is expected that anion passage into the inter-membrane space (IMS), and presumably that of HCO_3^-, occurs *via* at least one of the outer envelope protein channels (OEPs; Duy et al., 2007), with OEP21 a potential route for broad anion uptake into the IMS (**Figure 2**; Hemmler et al., 2006).

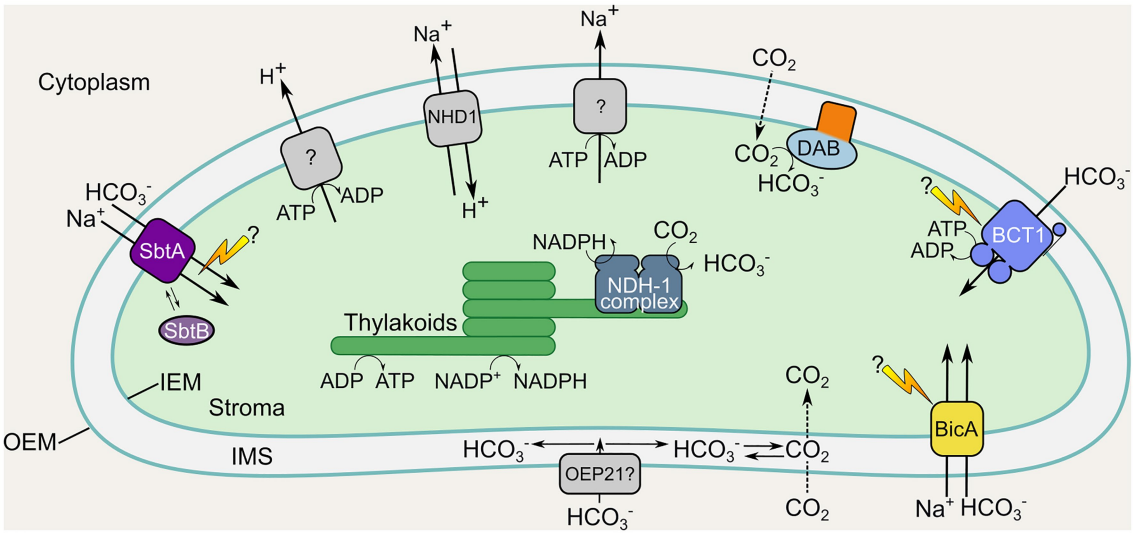

FIGURE 2 | Location and function of inorganic carbon uptake systems in a proposed chloroplastic CCM. Inorganic carbon uptake components from cyanobacteria and proteobacteria proposed for engineering into the chloroplast IEM and thylakoids of terrestrial C_3 plants. Membrane transporters and vectorial CO_2-HCO_3^- conversion complexes from cyanobacteria and proteobacteria are shown in color (see **Figure 1**; **Table 1**). Additional native chloroplastic systems which may support the required energetics and facilitation of active HCO_3^- uptake (including Na^+ and H^+ extrusion systems and the NHD1 Na^+/H^+ antiporter) are shown in gray. The cyanobacterial HCO_3^- transporters BicA and SbtA, as well as the ATP-driven BCT1 complex are targeted to the IEM may require unknown activation processes, indicated by lightning bolts. Note the added complexity of the multi-subunit BCT1 complex requiring protein components in the inter-membrane space (IMS), IEM, and stroma. The cyanobacterial vectorial NDH-1 complex has been suggested on the thylakoid membrane as it likely requires energization by components of the photosynthetic electron transport chain (ETC). The proteobacterial vectorial DAB complex is tentatively depicted on the IEM, but, alternatively, co-localization with the ETC on the thylakoid membrane may be favorable for its energization. The broad-specificity channel protein OEP21 on the outer-envelope membrane (OEM) is depicted as a putative access point for cytoplasmic HCO_3^- uptake into the IMS. Individual transporter proteins are as listed in **Table 1**.

While inward passage through this specific channel may be hampered by triose-phosphate export in the light (Duy et al., 2007), it and other OEPs offer broad selective import into the IMS. Currently, there is no reason to expect that HCO_3^- cannot access the IMS. Nonetheless, it is worthy of consideration, and additional transport mechanisms or solutions should be considered for the elevation of IMS [HCO_3^-] if this becomes a roadblock to the overall strategy. Notably, insertion of an IMS-specific CA would likely generate the requisite HCO_3^- from diffusion of CO_2 in this location (depending on the IMS pH) for utilization by an IEM-localized pump, in the unlikely scenario that insufficient HCO_3^- is present here. The ΔpH across the chloroplast IEM has been measured to be up to 1 pH unit (Demmig and Gimmler, 1983) suggesting that an IMS pH of 7–7.5 is feasible in the light, ensuring that >80% of C_i species would exist as HCO_3^- in the presence of CA.

Assuming sufficient HCO_3^- is available in the IMS from the cytosolic pool, its transport across the IEM into the chloroplast stroma is predicted to be feasible using either high affinity, low flux transporters [e.g., the cyanobacterial sodium-dependent bicarbonate transporter, SbtA, and the ATP driven bicarbonate transporter, BCT1; **Table 1**; **Figures 1, 2**], or low to medium affinity, high flux transporters (e.g., BicA; **Table 1**; **Figures 1, 2**). For the most part, the affinity of these HCO_3^- transporter types falls below the proposed cytosolic [HCO_3^-] (**Table 1**), suggesting that sufficient transport is feasible. Either independently, or in concert, modeling suggests that functional forms of these transporter types should provide net import into the stroma and enable increased CO_2 supply to Rubisco (Price et al., 2011a).

Once HCO_3^- concentrations in the chloroplast are elevated, it is acknowledged that stromal CA is likely to prevent the desired function of a complete chloroplastic CCM, since its action in converting HCO_3^- to CO_2 transforms the C_i pool from one with low membrane permeability to one which can rapidly diffuse away from the site of fixation (Price et al., 2013; McGrath and Long, 2014). This would rob an engineered carboxysome (housing a Rubisco with relatively high K_MCO_2) of its primary C_i substrate, and ectopic CA is known to lead to a high-CO_2-requiring phenotype in cyanobacteria (Price and Badger, 1989a). However, in the development of a simpler CCM with only functional HCO_3^- uptake, stromal CA would provide the rapid, pH-driven development of CO_2 needed in the chloroplast to supply additional CO_2 to Rubisco. The net effect of such a system is the modest elevation of chloroplastic C_i, which leads to enhanced CO_2 availability at Rubisco (Price et al., 2011a; McGrath and Long, 2014).

It is relevant to consider what effects elevated stromal HCO_3^- might have on chloroplast function beyond the capability of supplying increased CO_2 to Rubisco. A role for HCO_3^- as a proton acceptor during water oxidation has been proposed in photosystem II (PSII) function, with HCO_3^- providing stabilizing and protective effects (Shevela et al., 2012). CO_2 formation from HCO_3^- at PSII occurs at a rate that correlates with O_2 evolution at the donor side (somewhat slower at the acceptor side; Shevela et al., 2020). A simplistic viewpoint therefore is

TABLE 1 | Inorganic carbon (C_i) uptake systems relevant to expression of CCMs in chloroplasts.

C_i uptake system	Organism subcellular location	Functional units	Classification	Substrates; Energization	Kinetic properties	References
BicA	*Cyanobacteria*[a] plasma membrane	Homodimer	Sulfate permease (SULP), Solute carrier family (SLC26A)	HCO_3^-/Na^+ symport; dependent on Na^+ gradient	Medium-high flux; low affinity ($k_{0.5}$ 74–353 μM HCO_3^-)	Price et al., 2004; Shelden et al., 2010; Price and Howitt, 2011; Wang et al., 2019
SbtA	*Cyanobacteria*[a] plasma membrane	Possible homotrimer		HCO_3^-/Na^+ symport; dependent on Na^+ gradient	Low flux; high affinity ($k_{0.5}$ 2–38 μM HCO_3^-)	Price et al., 2004, 2011a,b; Du et al., 2014; Förster et al., 2021
BCT1 (*cmpABCD* operon)	*Cyanobacteria*[a] plasma membrane	Five subunit complex: CmpA (substrate binding), 2x CmpB (TMD), CmpC (ATPase: substrate binding fusion), and CmpD (ATPase)	ATP-binding cassette (ABC) transporter	HCO_3^-; ATP hydrolysis[c]	Low flux; high affinity ($k_{0.5}$ 10–15 μM HCO_3^-)	Omata et al., 1999; Koropatkin et al., 2007; Price et al., 2011a
LCIA/Nar1.2	*Chlamydomonas*[b] chloroplast envelope	Unknown	Formate-nitrite transporter family	HCO_3^-; unknown	Unknown	Wang et al., 2015; Atkinson et al., 2016
HLA3	*Chlamydomonas*[b] plasma membrane	Unknown	ABC transporter	HCO_3^-; ATP hydrolysis[c]	Unknown	Gao et al., 2015; Wang et al., 2015; Atkinson et al., 2016
LCI1	*Chlamydomonas*[b] plasma membrane	Unknown	Anion channel	Ci (some evidence for CO_2); unknown	Unknown	Wang et al., 2015; Atkinson et al., 2016; Kono and Spalding, 2020
BST-1 BST-2 BST-3	*Chlamydomonas*[b] thylakoid membrane	BST-1 pentamer	Bestrophin-like proteins, Anion/Cl^-channel family	HCO_3^-; unknown	Unknown	Mukherjee et al., 2019
NHD-1_3	*Cyanobacteria*[a] thylakoid membrane	21 subunit complex: CupS, ChpY (CupA, type II β-CA), NdhD3, and F3 (specialized for CO_2 hydration) NdhA, B, C, E, G-Q, S, V (NDH-1 core, antiporter-like H^+ pumping proteins, Fd binding, PQ binding)	Specialized respiratory NDH-1-type complex, energy-coupled vectorial CA	CO_2; photosynthetic electron transport/ redox-coupled H^+ pumping[c], reduced Fd-dependent	Low flux; high affinity ($k_{0.5}$ 1–2 μM CO_2)	Maeda et al., 2002; Price et al., 2011a; Laughlin et al., 2020; Schuller et al., 2020
NHD-1_4; *ndhA,B,C,D3,E,F3,G-Q,S,V* *chpX/cupB*	*Cyanobacteria*[a] thylakoid membrane	20 subunit complex: ChpX (CupB, type II β-CA), NdhD4, and F4 (specialized for CO_2 hydration) NdhA, B, C, E, G-Q, S, V (NDH-1 core, antiporter-like H^+ pumping proteins, Fd binding, PQ binding)	Specialized respiratory NDH-1-type complex, Energy-coupled vectorial CA	CO_2; photosynthetic electron transport/ redox-coupled H^+ pumping[c], reduced Fd-dependent	High flux; medium affinity ($k_{0.5}$ 10–15 μM CO_2)	Maeda et al., 2002; Price et al., 2011a; Laughlin et al., 2020; Schuller et al., 2020
DAB2; *dabA2*, *dabB2*	*Halothiobacillus neapolitanus* plasma membrane	heterodimer: DabA2 (type II β-CA homolog), DabB2 (H^+ pumping protein homolog)	Energy-coupled vectorial CA	CO_2; cation gradient-coupled[c]	Unknown	Desmarais et al., 2019
LCIB/C; *lciB*, *lciC*	*Chlamydomonas*[b] Chloroplast stroma, pyrenoid periphery	heterodimer: LciB-LciC (β-CA subtype)	Vectorial? CA	CO_2; unknown	Unknown	Duanmu et al., 2009; Wang et al., 2015; Jin et al., 2016

CA, Carbonic anhydrase; Fd, ferredoxin; PQ, plastoquinone; $k_{0.5}$, substrate concentration supporting half-maximum C_i transport activity; TMD, transmembrane domain.
[a]*Identified and characterized in several species incl. Synechococcus elongatus PCC7942, Synechocystis sp. PCC6803, Synechococcus sp. PCC7002, and Thermosynechococcus elongatus.*
[b]*Identified in Chlamydomonas reinhardtii.*
[c]*Energization is to some extent speculative based on structural homology.*

that greater quantities of stromal HCO_3^- may support PSII function rather than having any negative effects, as appears to be the case for cyanobacteria and microalgae. This PSII property highlights potential conversion of HCO_3^- to CO_2 in an engineered chloroplastic CCM, however, and longer-term goals would be to generate systems which recycle stromal CO_2 back to HCO_3^-, whether it is generated through PSII action, anaplerotic reactions, or indeed leakage from an engineered carboxysome or pyrenoid (Price et al., 2013). Nonetheless, CO_2 losses *via* these processes are likely to be minimal within an engineering scheme utilizing a HCO_3^- transporter and a carboxysome, benefiting only marginally from the addition of vectorial CO_2-to-HCO_3^- conversion complexes (McGrath and Long, 2014).

WHICH C_i UPTAKE SYSTEMS COULD FACILITATE CHLOROPLASTIC HCO_3^- ACCUMULATION?

Inorganic carbon acquisition is an essential step in driving a biophysical CCM and for maximizing its efficiency. Acquisition of the predominant C_i species (CO_2 and HCO_3^-) contributes to the accumulation of an intracellular/chloroplastic HCO_3^- pool well above external C_i levels, with up to 1,000-fold increases observed in cyanobacteria (Price, 2011). This can only be achieved by active C_i uptake against a concentration gradient, requiring energy, as opposed to passive diffusional uptake through protein channels such as CO_2 aquaporins (Uehlein et al., 2012; Li et al., 2015). Active C_i uptake systems can be divided into two categories, energy-coupled CAs (also known as vectorial CO_2 pumps or CO_2-to-HCO_3^- conversion systems) and active HCO_3^- transporters. A number of C_i transport systems have been identified through genetic screens of high CO_2 requiring mutants in the microalga *Chlamydomonas* (Spalding, 2008; Fang et al., 2012), several cyanobacteria (Price and Badger, 1989b; Badger and Price, 2003; Price et al., 2008) and, recently non-photosynthetic, CO_2-fixing γ-proteobacteria (Scott et al., 2018; Desmarais et al., 2019), summarized in **Table 1** and Sui et al. (2020).

Cyanobacterial C_i Uptake Systems

In cyanobacteria, five C_i uptake systems have been verified, subsets of which are present in all species (**Figure 1A**; **Table 1**). These transport systems differ in subcellular localization, substrate affinity, flux rates, energization and regulation of gene expression, and transport activity (Price, 2011). These properties somewhat determine their suitability for function in a proposed chloroplastic CCM. Dependent on the species, some C_i uptake systems are constitutively expressed, but in most cases, their expression is controlled by a combination of limiting C_i and light (Badger and Andrews, 1982; Kaplan et al., 1987; McGinn et al., 2003; Price et al., 2011b).

Intracellular CO_2-to-HCO_3^- conversion in cyanobacteria is facilitated by two specialized, thylakoid-located NAD(P)H dehydrogenase (NDH1) complexes related to the respiratory complex-I from mitochondria: the low C_i-inducible, high affinity NDH-1_3, and the constitutive, slightly lower affinity NDH-1_4 complexes (Maeda et al., 2002; Ohkawa et al., 2002). The CO_2 hydration subunits ChpY (CupA) and ChpX (CupB) of NDH-1_3 and NDH-1_4, respectively, convert cytoplasmic CO_2 to HCO_3^-, energized by reduced ferredoxin or NADPH that are generated by photosynthetic electron transport, and hence light-dependent (Ogawa et al., 1985; Maeda et al., 2002; Price et al., 2008; Battchikova et al., 2011). Recently, catalytic properties of the cryo-EM structure of the NDH-1_3 complex have been analyzed applying quantum chemical density modeling to the cryo-EM structure, which has shed light onto putative regulatory mechanisms. CO_2 hydration by NDH-1_3 (and by analogy NDH-1_4) is energetically linked to plastoquinone oxido-reduction coupled to proton-pumping, which controls the opening and closing of the putative CO_2 diffusion channel and lateral removal of H^+ generated in the CO_2 hydration reaction catalyzed by the ChpY (CupA) subunit. This mechanism ensures that the backward reaction, and unfavorable CO_2 release, is prevented (Badger and Price, 2003; Schuller et al., 2020). In plant chloroplasts, we expect such systems would require thylakoid localization for correct function.

Direct transfer of HCO_3^- from the outside into the cytoplasm is facilitated by three types of plasma membrane-located HCO_3^- transporters (**Figure 1**). The high affinity transporters, BCT1 and SbtA, were shown to be newly synthesized upon activation of HCO_3^- uptake, while constitutively expressed BicA was induced without further *de novo* protein synthesis (Sültemeyer et al., 1998; McGinn et al., 2003). The heteromeric BCT1 complex (encoded by the *cmpABCD* operon; **Table 1**) is a high affinity-low flux HCO_3^- transporter (Omata et al., 1999) of the ATP binding cassette (ABC) transporter superfamily, strongly suggesting ATP is used for energization. However, ATPase activity has not yet been demonstrated. BCT1 is composed of the membrane-anchored, substrate-binding protein CmpA, the homodimeric, membrane integral CmpB domain, and the cytoplasmic ATPase subunits CmpC and CmpD. CmpC appears to be a fusion protein which contains both the ATPase moiety and a putative regulatory substrate-binding domain homologous to CmpA. CmpA requires Ca^{2+} as co-ligand for binding of HCO_3^-, yet it is unclear whether Ca^{2+} plays a role in HCO_3^- transport (Koropatkin et al., 2007). The complexity of the proposed subunit localization of BCT1 for chloroplast envelope expression (one subunit in the IMS, one in the IEM, and two in the stroma; see below) provides further plant engineering challenges in addition to correct transporter function.

Both, BicA and SbtA (**Table 1**) are HCO_3^-/Na^+ symporters that require a cell-inward directed Na^+ gradient for HCO_3^- uptake (Shibata et al., 2002; Price et al., 2004), and as single protein transporters are attractive considerations for chloroplast engineering. BicA, a medium affinity-high flux transporter of the SLC26A solute carrier superfamily, is thought to function as a homodimer (Compton et al., 2011; Price and Howitt, 2014; Wang et al., 2019). The high affinity-low flux SbtA transporter, constitutes its own Na^+-dependent HCO_3^- transporter superfamily, and is likely to be active as a trimer (Du et al., 2014; Fang et al., 2021; Förster et al., 2021). These requirements for

Na^+ for HCO_3^- uptake highlight the potential for excessive influx of Na^+ in a chloroplast-based CCM which we discuss below.

Non-photosynthetic Bacterial C_i Uptake Systems

The DAB proteins (encoded by the *dab1* and *dab2* operons) first identified in *Halothiobacillus neapolitanus* are distributed throughout prokaryotic phyla and have been proposed to function as energy-coupled CAs accumulating HCO_3^- in the cytoplasm (Desmarais et al., 2019). A heterodimeric functional unit consists of the cytoplasmic exposed β-CA-like DabA protein coupled to the membrane-integral cation antiporter-like membrane subunit DabB (**Figure 1B**). Vectorial CO_2 hydration by DabA has been hypothesized to be driven by a cation (H^+ or Na^+) gradient but has not yet been proven experimentally (Laughlin et al., 2020). From an engineering standpoint, DAB proteins may represent a viable alternative to $NDH1_{3/4}$ complexes as candidates for CO_2 uptake/recapture in chloroplasts as introduction of only two proteins is required for DABs compared to 20–21 different proteins for $NDH1_{3/4}$ (Price et al., 2019). However, the suitability of DABs to function in chloroplasts will be uncertain until mechanisms of energization/regulation are resolved. In addition, we need to consider that DABs or any vectorial CA will only be effective in the final engineering stages once the endogenous stromal CA has been successfully removed (Price et al., 2011a).

Microalgal C_i Uptake Systems

In *Chlamydomonas*, HCO_3^- transporter genes induced under low C_i include plasma membrane-located HLA3 and LCI1 (**Figure 2**; Kono and Spalding, 2020), the chloroplast envelope-located LCIA (Nar1.2; Wang et al., 2011; Atkinson et al., 2016; Kono and Spalding, 2020), thylakoid membrane-integral bestrophin-like proteins BST1, BST2, and BST3 (Mukherjee et al., 2019), and the chloroplast-located CIA8 (Machingura et al., 2017). In addition, stromal LCIB/C complex and the thylakoid lumenal carbonic anhydrase CAH3 have been implied in CO_2 recapture (reviewed in Mackinder, 2018; Mallikarjuna et al., 2020). Importantly, neither substrate affinities, net accumulation capacity, and energization nor regulatory mechanisms of individual transporters are sufficiently understood to evaluate their suitability for expression in C_3 chloroplasts at this time (**Table 1**). It is highly likely though that HLA3 (**Figure 1C**), as a member of the ABC and transporter family, is energized by ATP hydrolysis (Wang et al., 2015), and heterologous expression of HLA3 or LCIA in *Xenopus* oocytes showed some HCO_3^- uptake activity but were not characterized further (Atkinson et al., 2016).

WHAT ARE THE ENERGETIC AND FUNCTIONAL REQUIREMENTS OF C_i UPTAKE SYSTEMS?

One major challenge for heterologous expression of C_i uptake systems is the regulation of protein function, which encompasses both primary energization and fine-tuning of activity to match dynamic photosynthetic CO_2 assimilation capacity of plant leaves (Price et al., 2013; Rae et al., 2017; Mackinder, 2018). Irrespective of the organism, C_i uptake appears to be controlled at the level of gene expression as well as protein function. While our current knowledge allows us to control expression of transgenes quite effectively, control of protein function in a non-native environment is still vastly empirical and, without greater understanding, far from attaining control by rational design.

Regulation of transporter function appears to be as little understood as energization. Most knowledge has been gathered for the cyanobacterial C_i uptake systems (**Table 1**). In cyanobacteria, as in chloroplasts, elevated HCO_3^- concentration is only beneficial for photosynthetic carbon gain in the light. For maximum efficiency, C_i uptake activity needs to be in tune with day/night cycles and changes in light intensity. In cyanobacteria, CO_2 uptake and HCO_3^- transport are activated within seconds in the light, with CO_2 uptake preceding HCO_3^- uptake (Badger and Andrews, 1982; Price et al., 2008, 2011b), and both SbtA and BicA are inactivated within seconds in the dark (Price et al., 2013; Förster et al., 2021). While a link between light-activation/dark-inactivation of C_i uptake and the state of photosynthetic electron transport and/or to a redox signal has been suggested by Kaplan et al. (1987), the identity of the light signal, signal transduction pathways and sensory/response mechanisms of the C_i uptake proteins are still elusive. Furthermore, protein phosphorylation may play a role in post-translational modulation of HCO_3^- transporter activity (Sültemeyer et al., 1998), and it is uncertain whether the native cyanobacterial regulatory kinases/phosphatases could function correctly in plastids when co-expressed with their transporter targets. This level of regulation dependency needs to be addressed to ensure replication of cyanobacterial-like control of C_i uptake mechanisms in a C_3 system.

Light/Dark Control of C_i Uptake

There is some evidence for redox-regulation of CO_2 uptake by the NDH-1 complexes in cyanobacteria. $NDH1_{3/4}$ function is directly linked to the trans-thylakoid proton motive force and cyclic electron transfer at photosystem I through interaction with ferredoxin and plastoquinone intermediates of the photosynthetic electron transport chain (ETC; Schuller et al., 2020). Light-driven changes in photosynthetic electron transport cause instantaneous changes of the redox state of the ETC which modulates CO_2 fixation *via* changes in NADPH production, ATP synthesis, and the redox-sensitive activation state of the Calvin-Benson-Bassham (CBB) cycle enzymes. In cyanobacteria, oxidizing conditions activate the small, inhibitory CP12 protein and ferredoxin-thioredoxin redox signaling cascades which inhibit the CBB cycle enzymes (*via* thiol-oxidation of cysteines; McFarlane et al., 2019), thus coordinating CO_2 uptake and carboxylation. Given that the ETC and the ferredoxin-thioredoxin-CP12 regulatory system are highly conserved and present in all plant chloroplasts, regulatory features may already be present in chloroplasts if large, multi-gene NDH-1 complexes could be heterologously expressed. However, it is unlikely that

this modus of redox-regulation applies to plasma membrane-located HCO_3^- transporters, which are spatially separated from the ETC and have not been detected among proteins targeted by thioredoxin (Lindahl and Florencio, 2003).

Currently without experimental evidence, other putative redox-sensitive regulatory mechanisms for cyanobacterial C_i uptake, such as eliciting signaling molecules such as Ca^{2+} (Torrecilla et al., 2004; Domínguez et al., 2015), light-stimulated changes in membrane potential (Murvanidze and Glagolev, 1982), and Ca^{2+} sensory phosphorylation relays triggered by light-dark transitions (Mata-Cabana et al., 2012) are speculative. However, regardless of the regulatory mechanism, the main concern remains whether an analogous regulatory system exists in the chloroplast and whether it can interact appropriately with the introduced foreign proteins, or, whether such systems need to be transplanted into chloroplasts alongside C_i uptake systems. Importantly, Ca^{2+} plays a major regulatory role for photosynthesis and related metabolism in chloroplasts and light-dark transitions elicit specific Ca^{2+} responses (Pottosin and Shabala, 2016). Therefore, chloroplasts harbor an extensive Ca^{2+} signaling infrastructure and are part of the whole plant signaling network which includes crosstalk between chloroplastic and cytoplasmic Ca^{2+} signaling responses to environmental stimuli (Navazio et al., 2020). How the incorporation of additional systems, which could have Ca^{2+} dependencies, might impact on overall inter- and intra-cellular signaling is yet to be seen.

So far, evidence for control of HCO_3^- uptake involving interaction of the transporter with regulatory proteins and/or additional co-factors has only emerged for SbtA. Heterologous co-expression of SbtA and its cognate P_{II}-like SbtB proteins in *E. coli* abolished SbtA-mediated HCO_3^- uptake constitutively and formed SbtA:SbtB containing protein complexes (Du et al., 2014). This suggests activity of SbtA can be modulated through binding its respective SbtB (Fang et al., 2021). Effects on SbtA activity have not been observed in low C_i-acclimated, SbtB-deficient cyanobacterial mutants (Förster et al., 2021), although initial C_i acclimation and growth appeared to be compromised in *Synechocystis* sp. PCC6803 (Selim et al., 2018). However, so far, *in vitro* evidence suggest that certain SbtA and SbtB pairs interact in response to adenylate ratios and adenylate energy charge sensed through SbtB (Kaczmarski et al., 2019; Förster et al., 2021), and even though the *in vivo* role of the SbtA-SbtB interaction is not clear yet, co-expression of SbtA and SbtB may be necessary for appropriate functional control in chloroplasts.

Implications for pH Balance, Ion Homeostasis, and Energetic Requirements

While single gene HCO_3^- transporters such as the SbtA HCO_3^-/Na^+ symporters are prime candidates for chloroplast expression (Du et al., 2014), accumulation of HCO_3^- and Na^+ in the stroma in the dark could theoretically lead to pH imbalances and high concentrations of Na^+ impairing chloroplast biochemistry (Price et al., 2008; Mueller et al., 2014; Myo et al., 2020). Cellular pH is tightly regulated to ensure near optimal conditions for biochemical reactions to occur. The cytoplasmic pH in *Arabidopsis* is maintained at about 7.3 (Shen et al., 2013), whereas the chloroplast stroma has been reported to vary between pH 7.2 in the dark to about pH 8 in the light (Höhner et al., 2016). All membrane systems in plant cells possess numerous transport systems (comprised of cation/H^+ and anion/H^+ exchangers) that maintain pH homeostasis in different subcellular compartments, and transmembrane H^+ gradients as a proton motive energy source. In the light, the capacity for pH-regulation and buffering in chloroplasts is likely to accommodate the alkalinization caused by continued HCO_3^- import into the chloroplast. Bicarbonate accumulation in the chloroplast *via* a single transporter type is unlikely to exceed the pool sizes of up to 50 mM measured in CCM-induced and actively photosynthesizing cyanobacteria (Kaplan et al., 1980; Woodger et al., 2005). Moreover, the pH disturbance associated with short-term (~ 5 min) exposure of leaves to high CO_2, which elevated stromal HCO_3^- up to 90 mM in the dark and 120 mM in the light, was counteracted rapidly within seconds (Hauser et al., 1995). However, it is uncertain whether pH buffering is as effective if continued HCO_3^- uptake in the dark were to accumulate substantial HCO_3^- pools without consumption by Rubisco. Consideration must therefore be given to this uncertainty in CCM engineering strategies.

The second potentially confounding issue with expression of the SbtA and BicA transporters on the chloroplast envelope is the influx of Na^+. Assuming a stoichiometry of 1:1 for Na^+ and HCO_3^- co-transport, these transporters could increase chloroplast [Na^+] by at least as much as the [HCO_3^-] mentioned above. In contrast to halophytes which tolerate higher chloroplastic Na^+ concentrations, photosynthesis in glycophytes (including many C_3 crop plants) becomes impaired by subtle elevation of stromal Na^+ from 0.21 to 0.38 mM in *Arabidopsis* (Mueller et al., 2014). The NHD1 Na^+/H^+ antiporter on the chloroplast envelope is active in Na^+ extrusion (**Figure 2**), maintaining a positive Na^+ gradient for other Na^+-dependent carriers on the chloroplast envelope, regulating stromal pH, and contributing to salt tolerance (Höhner et al., 2016; Tsujii et al., 2020). This suggests that, in particular, light/dark regulated Na^+ extrusion and Na^+/HCO_3^- symport need to be synchronized. Thus, boosting Na^+ export systems on the chloroplast envelope may be required to restore ion/pH balance, which could involve overexpression of the endogenous NHD1 or expression of foreign Na^+/H^+ antiporters such as cyanobacterial NhaS proteins (Price et al., 2013).

Unfortunately, regulation of Na^+ fluxes between different compartments of plant cells and the characteristics of Na^+ carriers are not well understood, therefore making it difficult to predict how active HCO_3^- uptake might influence Na^+ fluxes. In addition to the potential over-accumulation of stromal [Na^+], it is not clear whether the cytoplasmic [Na^+] and the magnitude of the Na^+ gradient across the chloroplast envelope will be sufficient for optimal energization of SbtA or BicA and in varying environments. Estimates of cytoplasmic [Na^+] range between 3 and 30 mM (Karley et al., 2000; Tester and Davenport, 2003), which exceeds the $K_{0.5}$ (Na^+ concentration supporting half-maximum HCO_3^- uptake rates) of 1–2 mM Na^+ for SbtA and BicA (Price et al., 2004; Du et al., 2014). Stromal Na^+ concentrations have been reported between 0.2 and 7 mM

(Schröppel-Meier and Kaiser, 1988; Mueller et al., 2014). Therefore, dependent on the plant species and/or environmental conditions, cytoplasmic Na^+ is in the lower concentration range, and the differential between cytoplasm and stroma, could impose limits on HCO_3^- uptake rates depending on substrate availability. However, plants under field conditions experience relatively higher salinity in most agricultural soils than in controlled growth environments, which means we can expect their cells operate at slightly elevated cytoplasmic Na^+ levels (Tester and Davenport, 2003), which renders Na^+ limitation fairly unlikely.

Based on homology to ABC transporters, the cyanobacterial BCT1 and the *Chlamydomonas* HLA3 (**Figures 1A,C**) are thought to be energized by ATP hydrolysis, but the ATP required per HCO_3^- transported has not been determined. Modeled ATP requirements for SbtA and BicA activity, which consume ATP indirectly as costs for proton transport to maintain the Na^+ gradient, project 0.5 and 0.25 ATP, respectively, per HCO_3^- transported (Price et al., 2011a). Particularly at low external C_i, suppression of photorespiration by active HCO_3^- uptake is more ATP cost-effective than typical C_3 photosynthesis, and ATP demand for transporter function should be readily covered by photophosphorylation in the chloroplast. The modeling did not consider additional ATP requirements for synthesis and maintenance of C_i uptake complexes though, since protein accumulation and turnover rates are unknown in both native organisms and chloroplasts, which is a modest pressure onto ATP production compared to the overall daily expenditure in living cells. Recent modeling of proposed pyrenoid-based systems also highlights ATP costs to chloroplastic CCMs; however, these can be limited depending on the engineering strategy (Fei et al., 2021).

HOW CAN WE GET C_i UPTAKE SYSTEMS INTO THE CHLOROPLAST?

The expression of transgenes from the nuclear genome of terrestrial plants is the favored means to introduce a CCM into crop plants due to current difficulties associated with successful insertion of exogenous genes into the chloroplast genomes of some major crops (Hanson et al., 2013). Nonetheless, many proof-of-concept approaches utilize plastome expression to assess CCM components (Lin et al., 2014b; Pengelly et al., 2014; Long et al., 2018). We focus here on strategies relating to the import of nuclear-encoded proteins into chloroplastic membranes and stroma where broader application to the majority of globally important crops is feasible. This approach introduces many complicating challenges when considering the transfer of systems from a cyanobacterium where proteins are targeted to the membrane from the inside, whereas in chloroplast proteins would come from the outside.

Successful transport of HCO_3^- into C_3 plant chloroplasts requires that a transporter will be pumping solute across the chloroplast IEM, into the chloroplast stroma. This sounds simple in principle but implies several assumptions about the transporter are true. Firstly, that it is successfully expressed and targeted to the chloroplast. Secondly, correct direction of the imported protein to the chloroplast IEM occurs. Thirdly, the protein must fold and orient itself in the appropriate manner such that its intended direction of transport is inward to the stroma. Finally, any processes which ensure activation and energization of the transporter must be met (discussed above). Correct targeting of HCO_3^- transporters to the chloroplast IEM has been the subject of several reports in recent years (Atkinson et al., 2016; Rolland et al., 2016, 2017; Uehara et al., 2016, 2020; Nölke et al., 2019), however, correct localization, orientation, and activation of these proteins to ensure favorable function remain an engineering challenge.

Foreign Protein Expression and Targeting

The initial step of expressing foreign genes in transgenic plants is a common point of failure due to a myriad of factors relating to gene positional effects (Pérez-González and Caro, 2019) and silencing (Jackson et al., 2014), codon usage (Nakamura and Sugiura, 2009), promotor and terminator combinations (Beyene et al., 2011; de Felippes et al., 2020), and potential degradation of the precursor protein (Lee et al., 2009; Shen et al., 2017; Hristou et al., 2020). This usually requires the analysis of relatively large numbers of plant transformation events and somewhat laborious testing of gene expression cassettes (often in transient expression systems) to ensure appropriate levels of protein expression can be achieved. We do not provide further discussion on this point but highlight that fine-tuning this aspect of CCM engineering in C_3 plants is not trivial and can heavily impact on the trajectories of engineering approaches.

Once expressed, nuclear encoded proteins targeted to the chloroplasts are translocated as pre-proteins within the cytosol where chaperones, such as Hsp70, Hsp90, and the 14–3-3 protein complex are involved throughout the translocation process (**Figure 3**; May and Soll, 2000; Schwenkert et al., 2011). Proteins translated in the cytosol and destined for the chloroplast either remain unfolded with the help of chaperones (Jarvis, 2008), or can be imported to the chloroplast in a fully-formed state (Ganesan et al., 2018), prior to translocation across the chloroplast envelope. These chaperones are crucial to prevent the premature folding of large proteins and aggregation and/or degradation of pre-proteins (Wojcik and Kriechbaumer, 2021).

Upon reaching the chloroplast, pre-proteins enter through the TIC-TOC pathway and are then directed within the chloroplast to their final destination (e.g., IEM, OEM, stroma, thylakoid membrane, or lumen; **Figure 3**; Oh and Hwang, 2015; Lee et al., 2017; Xu et al., 2020). Noticeably, post-import insertion into the IEM could involve additional processing by the Cpn60/Cpn10 chaperonin complex within the stroma, prior to insertion into the IEM through a membrane bound translocase (SEC2; Li and Schnell, 2006; Li et al., 2017). These various processes are facilitated by the pre-protein chloroplast transit peptide (cTP) which possesses binding sites for chaperones and is crucial for targeting nuclear-encoded proteins into the chloroplast (Ivey et al., 2000; Rial et al., 2000; Lee and Hwang, 2018). Therefore, the types of chaperones that would mediate foreign pre-protein chloroplast import would depend on the cTP used. There is

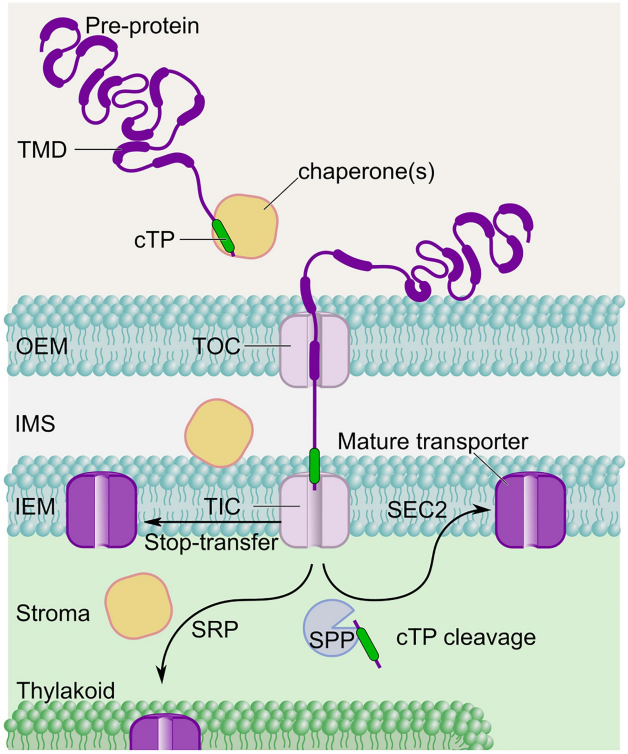

FIGURE 3 | Possible pathways for membrane HCO_3^- transporter insertion in C_3 chloroplasts. For successful targeting to the correct membrane in C_3 chloroplasts, candidate inorganic carbon uptake system proteins need to utilize an appropriate chloroplast targeting peptide (cTP) at the N-terminus of the nuclear-encoded pre-protein. Chaperones co-ordinate transit of membrane pre-proteins to the TIC-TOC translocons enabling initial import into the chloroplast. Here, proteins can undergo a number of localization processes, dependent on sequence motifs and interactions. Proteins destined for the IEM are handled by the stop-transfer or post-import (SEC2) pathways, whereas the signal recognition particle (SRP) pathway is utilized by proteins destined for the thylakoid (Lee et al., 2017). Ultimate localization can be partly driven by transmembrane domain (TMD) sequences (Rolland et al., 2017; Singhal and Fernandez, 2017). The stromal processing peptidase (SPP) must recognize and cleave the cTP in such a way that no functionally disruptive scar is left behind on mature transporters when they reach their proper destination. Very little is known about targeting foreign proteins to the IMS.

currently no understanding of the cyanobacterial chaperone requirements for CCM-related HCO_3^- transporters in their native systems, thus we must rely on host system chaperones for correct folding (if required) in heterologous plant expression. However, Atkinson et al. (2016) and Nölke et al. (2019) have shown successful targeting of microalgal chloroplast membrane transporters, suggesting there is a propensity for direct transfer of proteins from homologous systems with chloroplasts. Notably, the common ancestral origin of cyanobacteria and C_3 plant chloroplasts is partly identified in shared phylogeny of many of their outer membrane proteins (Day and Theg, 2018), and this might suggest potential for successful transfer of cyanobacterial membrane components to the chloroplast IEM. However, the transfer of genes from the plastome to the nucleus during C_3 plant evolution means both the inversion of directional insertion of membrane proteins (Day and Theg, 2018), and the emergence of cTPs to enable protein trafficking through the TIC-TOC complex and to the correct membrane (**Figure 3**; Knopp et al., 2020; Ramundo et al., 2020).

Correct targeting to the chloroplast membranes is further complicated by the presence of additional organelles in plant cells, and dual targeting between chloroplasts and mitochondria is commonly observed (Peeters and Small, 2001; Sharma et al., 2018). This complexity of organelle targeting (Bruce, 2000; Wojcik and Kriechbaumer, 2021) requires specific choice of cTP in proposed photosynthetic engineering strategies, and we suggest that the direction of foreign proteins to the appropriate cellular compartment is unlikely to be a one-size-fits-all solution (Rolland et al., 2017). There are also likely to be protein cargo-specific requirements which determine the choice of cTP for each heterologous membrane protein directed to the chloroplast IEM, thus identifying the need to test and tailor genetic constructs on an individual basis. This strategy is also required to optimize promotor/terminator requirements and is highly relevant in systems where protein stoichiometry (such as for multi-protein complex transporters such as BCT1) may be essential for function.

Successful incorporation of multi-component membrane transporter complexes such as BCT1 (**Figures 1, 2**) will require subunits which lie not only in the IEM, but also in the IMS and the stroma of the chloroplast. Targeting to the IMS has not been well investigated, with few examples in the literature investigating the subject (Kouranov et al., 1999; Vojta et al., 2007). At least two pathways to this location are thought to exist, one where proteins mature in the IMS (e.g., the TIC complex subunit Tic22; Kouranov et al., 1999), and one where proteins transit through the stroma and are then re-inserted into the IMS (e.g., MGD1; Vojta et al., 2007). Which may be the most appropriate pathway and whether foreign proteins can utilize either approach is yet to be described. In contrast, targeting to the stroma has been thoroughly studied and might therefore be the easiest to achieve (reviewed in Li and Chiu, 2010). One aspect worth mentioning is the stromal processing peptidase (SPP) which is known to cleave cTPs from several nuclear-encoded proteins imported into the stroma (**Figure 3**; Richter and Lamppa, 1998, 2002). The complete removal of cTPs is highly desirable in chloroplast engineering, as N-terminal additions to foreign proteins can impede their function. However, successful cTP cleavage may be prevented by cargo protein secondary and tertiary structure. With difficult cargoes, cTPs may need to be extended beyond the cleavage site with a flexible linker which will ultimately leave a scar that might also impede protein function. Notably, however, some novel cTPs have been designed to reduce the proteolytic scars while enhancing targeting of difficult protein cargoes. These engineered cTPs, such as RC2 and PC1 (Shen et al., 2017; Yao et al., 2020) include about 20 residues from its native mature cargo (a spacer to allow translocating factors better access to the cTP) which are followed by a second SPP cleavage site (to allow removal of the additional 20 residues used as spacer). Another approach that has been specifically used for the HCO_3^- transporters SbtA and BicA included a TEV protease cleavage

site after the cTP to enable removal by a heterologously expressed TEV protease (Uehara et al., 2016, 2020).

As mentioned above, the NDH complex may depend on plastoquinone for energization, and if we were to use such a complex for CO_2 recapture, the chloroplast thylakoid membrane would be the destination of choice (**Figure 2**; Long et al., 2016; Price et al., 2019; Hennacy and Jonikas, 2020). While the chloroplast twin arginine translocation, and secretory pathways direct mostly soluble proteins to the thylakoid lumen, it is the chloroplast signal recognition pathway (SRP) that targets membrane proteins to the thylakoid membrane (**Figure 3**; Smeekens et al., 1985; Schnell, 1998; Aldridge et al., 2009; Ouyang et al., 2020; Xu et al., 2020). Note that dual targeting between thylakoid and IEM was encountered when foreign transporters were targeted to the IEM (Pengelly et al., 2014; Rolland et al., 2017). A study on two closely related *Arabidopsis* proteins, SCY1 (thylakoids) and SCY2 (IEM), shed light on the sorting mechanism between IEM and thylakoids. In brief, the N-terminal region of SCY2 alone was not sufficient for exclusive targeting to the IEM. Instead, two internal transmembrane domains (TMDs) were required to achieve unambiguous localization to the IEM with no leakage toward the thylakoid membrane (Singhal and Fernandez, 2017). This study demonstrated that targeting is cargo-dependent. Hence, a more complex engineering of cargo TMDs might be required to successfully target foreign HCO_3^- transporters within the chloroplast (Rolland et al., 2017).

Control of Membrane Protein Orientation

Due to the inverted targeting strategy proposed for cyanobacterial transporters, there is potential for nuclear-encoded membrane proteins to be incorrectly oriented in the chloroplast IEM, even if targeting is successful. Most of the work done to understand membrane protein orientation (i.e., TMD topology) has been carried out in bacteria, establishing the positive-inside rule (Lys and Arg rich loops orient in the cytoplasm; von Heijne, 1986) and the charge-balanced rule (Dowhan et al., 2019). However, little is known about topology determinants in C_3 plant chloroplast membranes. Membrane lipid composition is known to influence the orientation of membrane proteins in the OEM (Schleiff et al., 2001). However, since the lipid composition of the C_3 chloroplast OEM differs from the IEM (Block et al., 2007), it is difficult to draw parallels between their orientation determinants. Interestingly, specific TMDs also appear to affect membrane protein orientation (Viana et al., 2010; Okawa et al., 2014). While changing lipid composition to control orientation is unrealistic in plants (but was achieved in bacteria; Dowhan et al., 2019), rational design of TMDs, and interconnecting loops (Rapp et al., 2007) from HCO_3^- uptake systems might be an option. As shown for the secretory pathway in plant endoplasmic reticulum, membrane protein signal peptides may also play a role in the orientation of some proteins (Wojcik and Kriechbaumer, 2021). Hence, it is reasonable to assume that correct targeting and orientation of membrane proteins in the chloroplast IEM are dependent on both the cargo protein and its targeting sequence (Rolland et al., 2016; Uehara et al., 2016, 2020). As a result, broad screening of targeting peptides for candidate cyanobacterial membrane protein cargos is likely required, both on a case-by-case basis and possibly between heterologous hosts. Membrane protein orientation must therefore be considered when addressing CCM component expression in plant systems and will affect predicted outcomes of functional HCO_3^- uptake assessment in transformed plants.

PERSPECTIVES AND CONCLUSION

Application of synthetic biology approaches to elevate HCO_3^- concentrations in C_3 plant chloroplasts, as a means to enhance Rubisco carboxylation, is an ongoing engineering endeavor among plant biologists. It is, however, a complex task which needs to be considered within a broad framework of molecular and physiological complexity. Efforts to heterologously express candidate HCO_3^- transporters and CO_2-to-HCO_3^- converting complexes in C_3 plants must therefore be contemplated within this context. Therefore, it is critically important that researchers addressing this challenge gather evidence of correct targeting, orientation and processing of protein transporters in plant systems. Functionality should be addressed where possible, and techniques which provide evidence of successful HCO_3^- import (e.g., Tolleter et al., 2017) and elevated leaf-level carboxylation should accompany reports of plant growth and productivity to ensure that predicted physiological outcomes correlate with enhanced growth. In addition to this, greater detail is required on the functional characterization of existing HCO_3^- uptake systems in their native systems (**Table 1**), while an understanding of the broader natural variation in HCO_3^- uptake systems (e.g., Scott et al., 2018; Desmarais et al., 2019) should be accumulated to provide greater options for engineering purposes.

AUTHOR CONTRIBUTIONS

BF generated the table. BML generated the figures. All authors contributed to the article and approved the submitted version.

FUNDING

This work was supported by a sub-award from the University of Illinois as part of the research project Realizing Increased Photosynthetic Efficiency (RIPE) that is funded by the Bill & Melinda Gates Foundation, Foundation for Food and Agriculture Research, and the UK Government's Department for International Development under grant number OPP1172157. We also acknowledge funding support from the Australian Research Council Centre of Excellence for Translational Photosynthesis (CE140100015).

ACKNOWLEDGMENTS

The authors thank Suyan Yee and Nghiem Nguyen for proofreading the final manuscript.

REFERENCES

Aldridge, C., Cain, P., and Robinson, C. (2009). Protein transport in organelles: protein transport into and across the thylakoid membrane. *FEBS J.* 276, 1177–1186. doi: 10.1111/j.1742-4658.2009.06875.x

Atkinson, N., Feike, D., Mackinder, L. C. M., Meyer, M. T., Griffiths, H., Jonikas, M. C., et al. (2016). Introducing an algal carbon-concentrating mechanism into higher plants: location and incorporation of key components. *Plant Biotechnol. J.* 14, 1302–1315. doi: 10.1111/pbi.12497

Atkinson, N., Mao, Y., Chan, K. X., and McCormick, A. J. (2020). Condensation of rubisco into a proto-pyrenoid in higher plant chloroplasts. *Nat. Commun.* 11:6303. doi: 10.1038/s41467-020-20132-0

Badger, M. R., and Andrews, T. J. (1982). Photosynthesis and inorganic carbon usage by the marine cyanobacterium, *Synechococcus* sp. *Plant Physiol.* 70, 517–523. doi: 10.1104/pp.70.2.517

Badger, M. R., and Price, G. D. (2003). CO_2 concentrating mechanisms in cyanobacteria: molecular components, their diversity and evolution. *J. Exp. Bot.* 54, 609–622. doi: 10.1093/jxb/erg076

Batista-Silva, W., da Fonseca-Pereira, P., Martins, A. O., Zsögön, A., Nunes-Nesi, A., and Araújo, W. L. (2020). Engineering improved photosynthesis in the era of synthetic biology. *Plant Commun.* 1:100032. doi: 10.1016/j.xplc.2020.100032

Battchikova, N., Eisenhut, M., and Aro, E. M. (2011). Cyanobacterial NDH-1 complexes: novel insights and remaining puzzles. *Biochim. Biophys. Acta Bioenerg.* 1807, 935–944. doi: 10.1016/j.bbabio.2010.10.017

Beyene, G., Buenrostro-Nava, M. T., Damaj, M. B., Gao, S.-J., Molina, J., and Mirkov, T. E. (2011). Unprecedented enhancement of transient gene expression from minimal cassettes using a double terminator. *Plant Cell Rep.* 30, 13–25. doi: 10.1007/s00299-010-0936-3

Block, M. A., Douce, R., Joyard, J., and Rolland, N. (2007). Chloroplast envelope membranes: a dynamic interface between plastids and the cytosol. *Photosynth. Res.* 92, 225–244. doi: 10.1007/s11120-007-9195-8

Bölter, B., Soll, J., Hill, K., Hemmler, R., and Wagner, R. (1999). A rectifying ATP-regulated solute channel in the chloroplastic outer envelope from pea. *EMBO J.* 18, 5505–5516. doi: 10.1093/emboj/18.20.5505

Bruce, B. D. (2000). Chloroplast transit peptides: structure, function and evolution. *Trends Cell Biol.* 10, 440–447. doi: 10.1016/S0962-8924(00)01833-X

Busch, F. A. (2020). Photorespiration in the context of rubisco biochemistry, CO_2 diffusion and metabolism. *Plant J.* 101, 919–939. doi: 10.1111/tpj.14674

Compton, E. L. R., Karinou, E., Naismith, J. H., Gabel, F., and Javelle, A. (2011). Low resolution structure of a bacterial SLC26 transporter reveals dimeric stoichiometry and mobile intracellular domains. *J. Biol. Chem.* 286, 27058–27067. doi: 10.1074/jbc.M111.244533

Day, P. M., and Theg, S. M. (2018). Evolution of protein transport to the chloroplast envelope membranes. *Photosynth. Res.* 138, 315–326. doi: 10.1007/s11120-018-0540-x

de Felippes, F. F., McHale, M., Doran, R. L., Roden, S., Eamens, A. L., Finnegan, E. J., et al. (2020). The key role of terminators on the expression and post-transcriptional gene silencing of transgenes. *Plant J.* 104, 96–112. doi: 10.1111/tpj.14907

Demmig, B., and Gimmler, H. (1983). Properties of the isolated intact chloroplast at cytoplasmic K^+ concentrations: light-induced cation uptake into intact chloroplasts is driven by an electrical potential difference. *Plant Physiol.* 73, 169–174. doi: 10.1104/pp.73.1.169

Desmarais, J. J., Flamholz, A. I., Blikstad, C., Dugan, E. J., Laughlin, T. G., Oltrogge, L. M., et al. (2019). DABs are inorganic carbon pumps found throughout prokaryotic phyla. *Nat. Microbiol.* 4, 2204–2215. doi: 10.1038/s41564-019-0520-8

Domínguez, D. C., Guragain, M., and Patrauchan, M. (2015). Calcium binding proteins and calcium signaling in prokaryotes. *Cell Calcium* 57, 151–165. doi: 10.1016/j.ceca.2014.12.006

Dowhan, W., Vitrac, H., and Bogdanov, M. (2019). Lipid-assisted membrane protein folding and topogenesis. *Protein J.* 38, 274–288. doi: 10.1007/s10930-019-09826-7

Du, J., Förster, B., Rourke, L., Howitt, S. M., and Price, G. D. (2014). Characterisation of cyanobacterial bicarbonate transporters in *E. coli* shows that SbtA homologs are functional in this heterologous expression system. *PLoS One* 9:e115905. doi: 10.1371/journal.pone.0115905

Duanmu, D., Wang, Y., and Spalding, M. H. (2009). Thylakoid lumen carbonic anhydrase (CAH3) mutation suppresses air-dier phenotype of *LCIB* mutant in *Chlamydomonas reinhardtii*. *Plant Physiol.* 149, 929–937. doi: 10.1104/pp.108.132456

Duy, D., Soll, J., and Philippar, K. (2007). Solute channels of the outer membrane: from bacteria to chloroplasts. *Biol. Chem.* 388, 879–889. doi: 10.1515/BC.2007.120

Ermakova, M., Lopez-Calcagno, P. E., Raines, C. A., Furbank, R. T., and von Caemmerer, S. (2019). Overexpression of the Rieske FeS protein of the cytochrome b_6f complex increases C_4 photosynthesis in *Setaria viridis*. *Commun. Biol.* 2:314. doi: 10.1038/s42003-019-0561-9

Ermakova, M., Osborn, H., Groszmann, M., Bala, S., McGaughey, S., Byrt, C., et al. (2021). Expression of a CO_2-permeable aquaporin enhances mesophyll conductance in the C_4 species *Setaria viridis*. bioRxiv [Preprint]. doi: 10.1101/2021.04.28.441895

Evans, J. R., Kaldenhoff, R., Genty, B., and Terashima, I. (2009). Resistances along the CO_2 diffusion pathway inside leaves. *J. Exp. Bot.* 60, 2235–2248. doi: 10.1093/jxb/erp117

Evans, J. R., and von Caemmerer, S. (1996). Carbon dioxide diffusion inside leaves. *Plant Physiol.* 110, 339–346. doi: 10.1104/pp.110.2.339

Fang, S., Huang, X., Zhang, X., Zhang, M., Hao, Y., Guo, H., et al. (2021). Molecular mechanism underlying transport and allosteric inhibition of bicarbonate transporter SbtA. *Proc. Natl. Acad. Sci. U. S. A.* 118:e2101632118. doi: 10.1073/pnas.2101632118

Fang, W., Si, Y., Douglass, S., Casero, D., Merchant, S. S., Pellegrini, M., et al. (2012). Transcriptome-wide changes in *Chlamydomonas reinhardtii* gene expression regulated by carbon dioxide and the CO_2-concentrating mechanism regulator *CIA5/CCM1*. *Plant Cell* 24, 1876–1893. doi: 10.1105/tpc.112.097949

Fei, C., Wilson, A. T., Mangan, N. M., Wingreen, N. S., and Jonikas, M. C. (2021). Diffusion barriers and adaptive carbon uptake strategies enhance the modeled performance of the algal CO_2-concentrating mechanism. bioRxiv [Preprint]. doi: 10.1101/2021.03.04.433933

Flamholz, A. I., Dugan, E., Blikstad, C., Gleizer, S., Ben-Nissan, R., Amram, S., et al. (2020). Functional reconstitution of a bacterial CO_2 concentrating mechanism in *Escherichia coli*. *elife* 9:e59882. doi: 10.7554/eLife.59882

Flamholz, A., and Shih, P. M. (2020). Cell biology of photosynthesis over geologic time. *Curr. Biol.* 30, R490–R494. doi: 10.1016/j.cub.2020.01.076

Flexas, J., Ribas-Carbó, M., Hanson, D. T., Bota, J., Otto, B., Cifre, J., et al. (2006). Tobacco aquaporin NtAQP1 is involved in mesophyll conductance to CO_2 *in vivo*. *Plant J.* 48, 427–439. doi: 10.1111/j.1365-313X.2006.02879.x

Förster, B., Mukherjee, B., Rourke, L., Kaczmarski, J. A., and Jackson, C. J. (2021). Regulatory adenylnucleotide-mediated binding of the P_{II}-like protein SbtB to the cyanobacterial bicarbonate transporter SbtA is controlled by the cellular energy state. bioRxiv [Preprint]. doi: 10.1101/2021.02.14.431189

Ganesan, I., Shi, L. X., Labs, M., and Theg, S. M. (2018). Evaluating the functional pore size of chloroplast toc and tic protein translocons: import of folded proteins. *Plant Cell* 30, 2161–2173. doi: 10.1105/tpc.18.00427

Gao, H., Wang, Y., Fei, X., Wright, D. A., and Spalding, M. H. (2015). Expression activation and functional analysis of HLA3, a putative inorganic carbon transporter in *Chlamydomonas reinhardtii*. *Plant J.* 82, 1–11. doi: 10.1111/tpj.12788

Giordano, M., Beardall, J., and Raven, J. A. (2005). CO_2 concentrating mechanisms in algae: mechanisms, environmental modulation, and evolution. *Annu. Rev. Plant Biol.* 56, 99–131. doi: 10.1146/annurev.arplant.56.032604.144052

Hanson, M. R., Gray, B. N., and Ahner, B. A. (2013). Chloroplast transformation for engineering of photosynthesis. *J. Exp. Bot.* 64, 731–742. doi: 10.1093/jxb/ers325

Hauser, M., Eichelmann, H., Oja, V., Heber, U., and Laisk, A. (1995). Stimulation by light of rapid pH regulation in the chloroplast stroma *in vivo* as indicated by CO_2 solubilization in leaves. *Plant Physiol.* 108, 1059–1066. doi: 10.1104/pp.108.3.1059

Hemmler, R., Becker, T., Schleiff, E., Bölter, B., Stahl, T., Soll, J., et al. (2006). Molecular properties of Oep21, an ATP-regulated anion-selective solute channel from the outer chloroplast membrane. *J. Biol. Chem.* 281, 12020–12029. doi: 10.1074/jbc.M513586200

Hennacy, J. H., and Jonikas, M. C. (2020). Prospects for engineering biophysical CO_2 concentrating mechanisms into land plants to enhance yields. *Annu. Rev. Plant Biol.* 71, 461–485. doi: 10.1146/annurev-arplant-081519-040100

Höhner, R., Aboukila, A., Kunz, H. H., and Venema, K. (2016). Proton gradients and proton-dependent transport processes in the chloroplast. *Front. Plant Sci.* 7:218. doi: 10.3389/fpls.2016.00218

Hristou, A., Grimmer, J., and Baginsky, S. (2020). The secret life of chloroplast precursor proteins in the cytosol. *Mol. Plant* 13, 1111–1113. doi: 10.1016/j.molp.2020.07.004

Ivey, R. A., Subramanian, C., and Bruce, B. D. (2000). Identification of a Hsp70 recognition domain within the rubisco small subunit transit peptide. *Plant Physiol.* 122, 1289–1299. doi: 10.1104/pp.122.4.1289

Jackson, M. A., Sternes, P. R., Mudge, S. R., Graham, M. W., and Birch, R. G. (2014). Design rules for efficient transgene expression in plants. *Plant Biotechnol. J.* 12, 925–933. doi: 10.1111/pbi.12197

Jarvis, P. (2008). Targeting of nucleus-encoded proteins to chloroplasts in plants. *New Phytol.* 179, 257–285. doi: 10.1111/j.1469-8137.2008.02452.x

Jin, S., Sun, J., Wunder, T., Tang, D., Cousins, A. B., Sze, S. K., et al. (2016). Structural insights into the LCIB protein family reveals a new group of β-carbonic anhydrases. *Proc. Natl. Acad. Sci. U. S. A.* 113, 14716–14721. doi: 10.1073/pnas.1616294113

Kaczmarski, J. A., Hong, N. S., Mukherjee, B., Wey, L. T., Rourke, L., Förster, B., et al. (2019). Structural basis for the allosteric regulation of the SbtA bicarbonate transporter by the P_{II}-like protein, SbtB, from *Cyanobium* sp. PCC7001. *Biochemistry* 58, 5030–5039. doi: 10.1021/acs.biochem.9b00880

Kaplan, A., Badger, M. R., and Berry, J. A. (1980). Photosynthesis and the intracellular inorganic carbon pool in the bluegreen alga *Anabaena variabilis*: response to external CO_2 concentration. *Planta* 149, 219–226. doi: 10.1007/BF00384557

Kaplan, A., Zenvirth, D., Marcus, Y., Omata, T., and Ogawa, T. (1987). Energization and activation of inorganic carbon uptake by light in cyanobacteria. *Plant Physiol.* 84, 210–213. doi: 10.1104/pp.84.2.210

Karley, A. J., Leigh, R. A., and Sanders, D. (2000). Where do all the ions go? The cellular basis of differential ion accumulation in leaf cells. *Trends Plant Sci.* 5, 465–470. doi: 10.1016/s1360-1385(00)01758-1

Knopp, M., Garg, S. G., Handrich, M., and Gould, S. B. (2020). Major changes in plastid protein import and the origin of the Chloroplastida. *iScience* 23:100896. doi: 10.1016/j.isci.2020.100896

Kono, A., and Spalding, M. H. (2020). LCI1, a *Chlamydomonas reinhardtii* plasma membrane protein, functions in active CO_2 uptake under low CO_2. *Plant J.* 102, 1127–1141. doi: 10.1111/tpj.14761

Koropatkin, N. M., Koppenaal, D. W., Pakrasi, H. B., and Smith, T. J. (2007). The structure of a cyanobacterial bicarbonate transport protein, CmpA. *J. Biol. Chem.* 282, 2606–2614. doi: 10.1074/jbc.M610222200

Kouranov, A., Wang, H., and Schnell, D. J. (1999). Tic22 is targeted to the intermembrane space of chloroplasts by a novel pathway. *J. Biol. Chem.* 274, 25181–25186. doi: 10.1074/jbc.274.35.25181

Kromdijk, J., Głowacka, K., Leonelli, L., Gabilly, S. T., Iwai, M., Niyogi, K. K., et al. (2016). Improving photosynthesis and crop productivity by accelerating recovery from photoprotection. *Science* 354, 857–861. doi: 10.1126/science.aai8878

Kromdijk, J., and Long, S. P. (2016). One crop breeding cycle from starvation? How engineering crop photosynthesis for rising CO_2 and temperature could be one important route to alleviation. *Proc. R. Soc. B* 283:20152578. doi: 10.1098/rspb.2015.2578

Laughlin, T. G., Savage, D. F., and Davies, K. M. (2020). Recent advances on the structure and function of NDH-1: the complex I of oxygenic photosynthesis. *Biochim. Biophys. Acta Bioenerg.* 1861:148254. doi: 10.1016/j.bbabio.2020.148254

Lee, D. W., and Hwang, I. (2018). Evolution and design principles of the diverse chloroplast transit peptides. *Mol. Cell* 41, 161–167. doi: 10.14348/molcells.2018.0033

Lee, D. W., Lee, J., and Hwang, I. (2017). Sorting of nuclear-encoded chloroplast membrane proteins. *Curr. Opin. Plant Biol.* 40, 1–7. doi: 10.1016/j.pbi.2017.06.011

Lee, S., Lee, D. W., Lee, Y., Mayer, U., Stierhof, Y. D., Lee, S., et al. (2009). Heat shock protein cognate 70-4 and an E3 ubiquitin ligase, CHIP, mediate plastid-destined precursor degradation through the ubiquitin-26S proteasome system in *Arabidopsis*. *Plant Cell* 21, 3984–4001. doi: 10.1105/tpc.109.071548

Li, H. M., and Chiu, C. C. (2010). Protein transport into chloroplasts. *Annu. Rev. Plant Biol.* 61, 157–180. doi: 10.1146/annurev-arplant-042809-112222

Li, Y., Martin, J. R., Aldama, G. A., Fernandez, D. E., and Cline, K. (2017). Identification of putative substrates of SEC2, a chloroplast inner envelope translocase. *Plant Physiol.* 173, 2121–2137. doi: 10.1104/pp.17.00012

Li, M., and Schnell, D. J. (2006). Reconstitution of protein targeting to the inner envelope membrane of chloroplasts. *J. Cell Biol.* 175, 249–259. doi: 10.1083/jcb.200605162

Li, L., Wang, H., Gago, J., Cui, H., Qian, Z., Kodama, N., et al. (2015). Harpin Hpa1 interacts with aquaporin PIP1;4 to promote the substrate transport and photosynthesis in *Arabidopsis*. *Sci. Rep.* 5:17207. doi: 10.1038/srep17207

Lin, M. T., Occhialini, A., Andralojc, P. J., Devonshire, J., Hines, K. M., Parry, M. A. J., et al. (2014a). β-Carboxysomal proteins assemble into highly organized structures in *Nicotiana* chloroplasts. *Plant J.* 79, 1–12. doi: 10.1111/tpj.12536

Lin, M. T., Occhialini, A., Andralojc, P. J., Parry, M. A. J., and Hanson, M. R. (2014b). A faster rubisco with potential to increase photosynthesis in crops. *Nature* 513, 547–550. doi: 10.1038/nature13776

Lindahl, M., and Florencio, F. J. (2003). Thioredoxin-linked processes in cyanobacteria are as numerous as in chloroplasts, but targets are different. *Proc. Natl. Acad. Sci. U. S. A.* 100, 16107–16112. doi: 10.1073/pnas.2534397100

Long, B. M., Förster, B., Pulsford, S. B., Price, G. D., and Badger, M. R. (2021). Rubisco proton production can drive the elevation of CO_2 within condensates and carboxysomes. *Proc. Natl. Acad. Sci. U. S. A.* 118:e2014406118. doi: 10.1073/pnas.2014406118

Long, B. M., Hee, W. Y., Sharwood, R. E., Rae, B. D., Kaines, S., Lim, Y. L., et al. (2018). Carboxysome encapsulation of the CO_2-fixing enzyme rubisco in tobacco chloroplasts. *Nat. Commun.* 9:3570. doi: 10.1038/s41467-018-06044-0

Long, B. M., Rae, B. D., Rolland, V., Förster, B., and Price, G. D. (2016). Cyanobacterial CO_2-concentrating mechanism components: function and prospects for plant metabolic engineering. *Curr. Opin. Plant Biol.* 31, 1–8. doi: 10.1016/j.pbi.2016.03.002

López-Calcagno, P. E., Brown, K. L., Simkin, A. J., Fisk, S. J., Vialet-Chabrand, S., Lawson, T., et al. (2020). Stimulating photosynthetic processes increases productivity and water-use efficiency in the field. *Nat. Plants* 6, 1054–1063. doi: 10.1038/s41477-020-0740-1

Machingura, M. C., Bajsa-Hirschel, J., Laborde, S. M., Schwartzenburg, J. B., Mukherjee, B., Mukherjee, A., et al. (2017). Identification and characterization of a solute carrier, CIA8, involved in inorganic carbon acclimation in *Chlamydomonas reinhardtii*. *J. Exp. Bot.* 68, 3879–3890. doi: 10.1093/jxb/erx189

Mackinder, L. C. M. (2018). The Chlamydomonas CO_2 -concentrating mechanism and its potential for engineering photosynthesis in plants. *New Phytol.* 217, 54–61. doi: 10.1111/nph.14749

Maeda, S. I., Badger, M. R., and Price, G. D. (2002). Novel gene products associated with NdhD3/D4-containing NDH-1 complexes are involved in photosynthetic CO_2 hydration in the cyanobacterium, *Synechococcus* sp. PCC7942. *Mol. Microbiol.* 43, 425–435. doi: 10.1046/j.1365-2958.2002.02753.x

Mallikarjuna, K., Narendra, K., Ragalatha, R., and Rao, B. J. (2020). Elucidation and genetic intervention of CO_2 concentration mechanism in *Chlamydomonas reinhardtii* for increased plant primary productivity. *J. Biosci.* 45, 1–18. doi: 10.1007/s12038-020-00080-z

Mata-Cabana, A., García-Domínguez, M., Florencio, F. J., and Lindahl, M. (2012). Thiol-based redox modulation of a cyanobacterial eukaryotic-type serine/threonine kinase required for oxidative stress tolerance. *Antioxid. Redox Signal.* 17, 521–533. doi: 10.1089/ars.2011.4483

May, T., and Soll, J. (2000). 14-3-3 proteins form a guidance complex with chloroplast precursor proteins in plants. *Plant Cell* 12, 53–63. doi: 10.2307/3871029

McFarlane, C. R., Shah, N. R., Kabasakal, B. V., Echeverria, B., Cotton, C. A. R., Bubeck, D., et al. (2019). Structural basis of light-induced redox regulation in the Calvin–Benson cycle in cyanobacteria. *Proc. Natl. Acad. Sci. U. S. A.* 116, 20984–20990. doi: 10.1073/pnas.1906722116

McGinn, P. J., Price, G. D., Maleszka, R., and Badger, M. R. (2003). Inorganic carbon limitation and light control the expression of transcripts related to the CO_2-concentrating mechanism in the cyanobacterium *Synechocystis* sp. strain PCC6803. *Plant Physiol.* 132, 218–229. doi: 10.1104/pp.019349

McGrath, J. M., and Long, S. P. (2014). Can the cyanobacterial carbon-concentrating mechanism increase photosynthesis in crop species? A theoretical analysis. *Plant Physiol.* 164, 2247–2261. doi: 10.1104/pp.113.232611

Morison, J. I. L., Gallouët, E., Lawson, T., Cornic, G., Herbin, R., and Baker, N. R. (2005). Lateral diffusion of CO_2 in leaves is not sufficient to support photosynthesis. *Plant Physiol.* 139, 254–266. doi: 10.1104/pp.105.062950

Moroney, J. V., and Ynalvez, R. A. (2007). Proposed carbon dioxide concentrating mechanism in *Chlamydomonas reinhardtii*. *Eukaryot. Cell* 6, 1251–1259. doi: 10.1128/EC.00064-07

Mueller, M., Kunz, H.-H., Schroeder, J. I., Kemp, G., Young, H. S., and Neuhaus, H. E. (2014). Decreased capacity for sodium export out of *Arabidopsis* chloroplasts impairs salt tolerance, photosynthesis and plant performance. *Plant J.* 78, 646–658. doi: 10.1111/tpj.12501

Mukherjee, A., Lau, C. S., Walker, C. E., Rai, A. K., Prejean, C. I., Yates, G., et al. (2019). Thylakoid localized bestrophin-like proteins are essential for

the CO_2 concentrating mechanism of *Chlamydomonas reinhardtii*. *Proc. Natl. Acad. Sci. U. S. A.* 116, 16915–16920. doi: 10.1073/pnas.1909706116

Murvanidze, G. V., and Glagolev, A. N. (1982). Electrical nature of the taxis signal in cyanobacteria. *J. Bacteriol.* 150, 239–244. doi: 10.1128/jb.150.1.239-244.1982

Myo, T., Tian, B., Zhang, Q., Niu, S., Liu, Z., Shi, Y., et al. (2020). Ectopic overexpression of a cotton plastidial Na^+ transporter *GhBASS5* impairs salt tolerance in *Arabidopsis* via increasing Na^+ loading and accumulation. *Planta* 252:41. doi: 10.1007/s00425-020-03445-8

Nakamura, M., and Sugiura, M. (2009). Selection of synonymous codons for better expression of recombinant proteins in tobacco chloroplasts. *Plant Biotechnol.* 26, 53–56. doi: 10.5511/plantbiotechnology.26.53

Navazio, L., Formentin, E., Cendron, L., and Szabò, I. (2020). Chloroplast calcium signaling in the spotlight. *Front. Plant Sci.* 11:186. doi: 10.3389/fpls.2020.00186

Nölke, G., Barsoum, M., Houdelet, M., Arcalís, E., Kreuzaler, F., Fischer, R., et al. (2019). The integration of algal carbon concentration mechanism components into tobacco chloroplasts increases photosynthetic efficiency and biomass. *Biotechnol. J.* 14:e1800170. doi: 10.1002/biot.201800170

Ogawa, T., Miyano, A., and Inoue, Y. (1985). Photosystem-I-driven inorganic carbon transport in the cyanobacterium, *Anacystis nidulans*. *BBA Bioenerg.* 808, 77–84. doi: 10.1016/0005-2728(85)90029-5

Oh, Y. J., and Hwang, I. (2015). Targeting and biogenesis of transporters and channels in chloroplast envelope membranes: unsolved questions. *Cell Calcium* 58, 122–130. doi: 10.1016/j.ceca.2014.10.012

Ohkawa, H., Sonoda, M., Hagino, N., Shibata, M., Pakrasi, H. B., and Ogawa, T. (2002). Functionally distinct NAD(P)H dehydrogenases and their membrane localization in *Synechocystis* sp. PCC6803. *Funct. Plant Biol.* 29, 195–200. doi: 10.1071/pp01180

Okawa, K., Inoue, H., Adachi, F., Nakayama, K., Ito-Inaba, Y., Schnell, D. J., et al. (2014). Targeting of a polytopic membrane protein to the inner envelope membrane of chloroplasts *in vivo* involves multiple transmembrane segments. *J. Exp. Bot.* 65, 5257–5265. doi: 10.1093/jxb/eru290

Omata, T., Price, G. D., Badger, M. R., Okamura, M., Gohta, S., and Ogawa, T. (1999). Identification of an ATP-binding cassette transporter involved in bicarbonate uptake in the cyanobacterium *Synechococcus* sp. strain PCC 7942. *Proc. Natl. Acad. Sci.* 96, 13571–13576. doi: 10.1073/pnas.96.23.13571

Ouyang, M., Li, X., Zhang, J., Feng, P., Pu, H., Kong, L., et al. (2020). Liquid-liquid phase transition drives intra-chloroplast cargo sorting. *Cell* 180, 1144–1159.e20. doi: 10.1016/j.cell.2020.02.045

Peeters, N., and Small, I. (2001). Dual targeting to mitochondria and chloroplasts. *Biochim. Biophys. Acta* 1541, 54–63. doi: 10.1016/S0167-4889(01)00146-X

Pengelly, J. J. L., Föster, B., von Caemmerer, S., Badger, M. R., Price, G. D., and Whitney, S. M. (2014). Transplastomic integration of a cyanobacterial bicarbonate transporter into tobacco chloroplasts. *J. Exp. Bot.* 65, 3071–3080. doi: 10.1093/jxb/eru156

Pérez-González, A., and Caro, E. (2019). Benefits of using genomic insulators flanking transgenes to increase expression and avoid positional effects. *Sci. Rep.* 9:8474. doi: 10.1038/s41598-019-44836-6

Pottosin, I., and Shabala, S. (2016). Transport across chloroplast membranes: optimizing photosynthesis for adverse environmental conditions. *Mol. Plant* 9, 356–370. doi: 10.1016/j.molp.2015.10.006

Price, G. D. (2011). Inorganic carbon transporters of the cyanobacterial CO_2-concentrating mechanism. *Photosynth. Res.* 109, 47–57. doi: 10.1007/s11120-010-9608-y

Price, G. D., and Badger, M. R. (1989a). Expression of human carbonic anhydrase in the cyanobacterium *Synechococcus* PCC7942 creates a high CO_2-requiring phenotype. *Plant Physiol.* 91, 505–513. doi: 10.1104/pp.91.2.505

Price, G. D., and Badger, M. R. (1989b). Isolation and characterization of high CO_2-requiring-mutants of the cyanobacterium Synechococcus PCC7942. *Plant Physiol.* 91, 514–525. doi: 10.1104/pp.91.2.514

Price, G. D., Badger, M. R., and von Caemmerer, S. (2011a). The prospect of using cyanobacterial bicarbonate transporters to improve leaf photosynthesis in C_3 crop plants. *Plant Physiol.* 155, 20–26. doi: 10.1104/pp.110.164681

Price, G. D., Badger, M. R., Woodger, F. J., and Long, B. M. (2008). Advances in understanding the cyanobacterial CO_2-concentrating- mechanism (CCM): functional components, ci transporters, diversity, genetic regulation and prospects for engineering into plants. *J. Exp. Bot.* 59, 1441–1461. doi: 10.1093/jxb/erm112

Price, G. D., and Howitt, S. M. (2011). The cyanobacterial bicarbonate transporter BicA: its physiological role and the implications of structural similarities with human SLC26 transporters. *Biochem. Cell Biol.* 89, 178–188. doi: 10.1139/O10-136

Price, G. D., and Howitt, S. M. (2014). Topology mapping to characterize cyanobacterial bicarbonate transporters: BicA (SulP/SLC26 family) and SbtA. *Mol. Membr. Biol.* 31, 177–182. doi: 10.3109/09687688.2014.953222

Price, G. D., Long, B. M., and Förster, B. (2019). DABs accumulate bicarbonate. *Nat. Microbiol.* 4, 2029–2030. doi: 10.1038/s41564-019-0629-9

Price, G. D., Pengelly, J. J. L., Förster, B., Du, J., Whitney, S. M., von Caemmerer, S., et al. (2013). The cyanobacterial CCM as a source of genes for improving photosynthetic CO_2 fixation in crop species. *J. Exp. Bot.* 64, 753–768. doi: 10.1093/jxb/ers257

Price, G. D., Shelden, M. C., and Howitt, S. M. (2011b). Membrane topology of the cyanobacterial bicarbonate transporter, SbtA, and identification of potential regulatory loops. *Mol. Membr. Biol.* 28, 265–275. doi: 10.3109/09687688.2011.593049

Price, G. D., von Caemmerer, S., Evans, J. R., Yu, J. W., Lloyd, J., Oja, V., et al. (1994). Specific reduction of chloroplast carbonic anhydrase activity by antisense RNA in transgenic tobacco plants has a minor effect on photosynthetic CO_2 assimilation. *Planta* 193, 331–340. doi: 10.1007/BF00201810

Price, G. D., Woodger, F. J., Badger, M. R., Howitt, S. M., and Tucker, L. (2004). Identification of a SulP-type bicarbonate transporter in marine cyanobacteria. *Proc. Natl. Acad. Sci. U. S. A.* 101, 18228–18233. doi: 10.1073/pnas.0405211101

Rae, B. D., Long, B. M., Badger, M. R., and Price, G. D. (2013). Functions, compositions, and evolution of the two types of carboxysomes: polyhedral microcompartments that facilitate CO_2 fixation in cyanobacteria and some proteobacteria. *Microbiol. Mol. Biol. Rev.* 77, 357–379. doi: 10.1128/MMBR.00061-12

Rae, B. D., Long, B. M., Förster, B., Nguyen, N. D., Velanis, C. N., Atkinson, N., et al. (2017). Progress and challenges of engineering a biophysical CO_2-concentrating mechanism into higher plants. *J. Exp. Bot.* 68, 3717–3737. doi: 10.1093/jxb/erx133

Ramundo, S., Asakura, Y., Salome, P. A., Strenkert, D., Boone, M., Mackinder, L., et al. (2020). Co-expressed subunits of dual genetic origin define a conserved supercomplex mediating essential protein import into chloroplasts. *Proc. Natl. Acad. Sci. U. S. A.* 117, 32739–32749. doi: 10.1073/pnas.2014294117

Rapp, M., Seppälä, S., Granseth, E., and von Heijne, G. (2007). Emulating membrane protein evolution by rational design. *Science* 315, 1282–1284. doi: 10.1126/science.1135406

Raven, J. A., Beardall, J., and Sánchez-Baracaldo, P. (2017). The possible evolution and future of CO_2-concentrating mechanisms. *J. Exp. Bot.* 68, 3701–3716. doi: 10.1093/jxb/erx110

Rial, D. V., Arakaki, A. K., and Ceccarelli, E. A. (2000). Interaction of the targeting sequence of chloroplast precursors with Hsp70 molecular chaperones. *Eur. J. Biochem.* 267, 6239–6248. doi: 10.1046/j.1432-1327.2000.01707.x

Richter, S., and Lamppa, G. K. (1998). A chloroplast processing enzyme functions as the general stromal processing peptidase. *Proc. Natl. Acad. Sci. U. S. A.* 95, 7463–7468. doi: 10.1073/pnas.95.13.7463

Richter, S., and Lamppa, G. K. (2002). Determinants for removal and degradation of transit peptides of chloroplast precursor proteins. *J. Biol. Chem.* 277, 43888–43894. doi: 10.1074/jbc.M206020200

Rolland, V., Badger, M. R., and Price, G. D. (2016). Redirecting the cyanobacterial bicarbonate transporters BicA and SbtA to the chloroplast envelope: soluble and membrane cargos need different chloroplast targeting signals in plants. *Front. Plant Sci.* 7:185. doi: 10.3389/fpls.2016.00185

Rolland, N., Curien, G., Finazzi, G., Kuntz, M., Maréchal, E., Matringe, M., et al. (2012). The biosynthetic capacities of the plastids and integration between cytoplasmic and chloroplast processes. *Annu. Rev. Genet.* 46, 233–264. doi: 10.1146/annurev-genet-110410-132544

Rolland, V., Rae, B. D., and Long, B. M. (2017). Setting sub-organellar sights: accurate targeting of multi-transmembrane-domain proteins to specific chloroplast membranes. *J. Exp. Bot.* 68, 5013–5016. doi: 10.1093/jxb/erx351

Salesse-Smith, C. E., Sharwood, R. E., Busch, F. A., Kromdijk, J., Bardal, V., and Stern, D. B. (2018). Overexpression of rubisco subunits with RAF1 increases rubisco content in maize. *Nat. Plants* 4, 802–810. doi: 10.1038/s41477-018-0252-4

Schleiff, E., Tien, R., Salomon, M., and Soll, J. (2001). Lipid composition of outer leaflet of chloroplast outer envelope determines topology of OEP7. *Mol. Biol. Cell* 12, 4090–4102. doi: 10.1091/mbc.12.12.4090

Schnell, D. J. (1998). Protein targeting to the thylakoid membrane. *Annu. Rev. Plant Biol.* 49, 97–126. doi: 10.1146/annurev.arplant.49.1.97

Schröppel-Meier, G., and Kaiser, W. M. (1988). Ion homeostasis in chloroplasts under salinity and mineral deficiency. *Plant Physiol.* 87, 828–832. doi: 10.1104/pp.87.4.828

Schuller, J. M., Saura, P., Thiemann, J., Schuller, S. K., Gamiz-Hernandez, A. P., Kurisu, G., et al. (2020). Redox-coupled proton pumping drives carbon concentration in the photosynthetic complex I. *Nat. Commun.* 11:494. doi: 10.1038/s41467-020-14347-4

Schwenkert, S., Soll, J., and Bölter, B. (2011). Protein import into chloroplasts—how chaperones feature into the game. *Biochim. Biophys. Acta Biomembr.* 1808, 901–911. doi: 10.1016/j.bbamem.2010.07.021

Scott, K. M., Leonard, J. M., Boden, R., Chaput, D., Dennison, C., Haller, E., et al. (2018). Diversity in CO_2-concentrating mechanisms among chemolithoautotrophs from the genera *Hydrogenovibrio*, *Thiomicrorhabdus*, and *Thiomicrospira*, ubiquitous in sulfidic habitats worldwide. *Appl. Environ. Microbiol.* 85, e02096–e02018. doi: 10.1128/AEM.02096-18

Selim, K. A., Haase, F., Hartmann, M. D., Hagemann, M., and Forchhammer, K. (2018). P_{II}-like signaling protein SbtB links cAMP sensing with cyanobacterial inorganic carbon response. *Proc. Natl. Acad. Sci. U. S. A.* 115, E4861–E4869. doi: 10.1073/pnas.1803790115

Sharma, M., Bennewitz, B., and Klösgen, R. B. (2018). Rather rule than exception? How to evaluate the relevance of dual protein targeting to mitochondria and chloroplasts. *Photosynth. Res.* 138, 335–343. doi: 10.1007/s11120-018-0543-7

Shelden, M. C., Howitt, S. M., and Price, G. D. (2010). Membrane topology of the cyanobacterial bicarbonate transporter, BicA, a member of the SulP (SLC26A) family. *Mol. Membr. Biol.* 27, 12–23. doi: 10.3109/09687680903400120

Shen, J., Zeng, Y., Zhuang, X., Sun, L., Yao, X., Pimpl, P., et al. (2013). Organelle pH in the *Arabidopsis* endomembrane system. *Mol. Plant* 6, 1419–1437. doi: 10.1093/mp/sst079

Shen, B. R., Zhu, C. H., Yao, Z., Cui, L. L., Zhang, J. J., Yang, C. W., et al. (2017). An optimized transit peptide for effective targeting of diverse foreign proteins into chloroplasts in rice. *Sci. Rep.* 7:46231. doi: 10.1038/srep46231

Shevela, D., Do, H. N., Fantuzzi, A., Rutherford, A. W., and Messinger, J. (2020). Bicarbonate-mediated CO_2 formation on both sides of photosystem II. *Biochemistry* 59, 2442–2449. doi: 10.1021/acs.biochem.0c00208

Shevela, D., Eaton-Rye, J. J., Shen, J. R., and Govindjee, (2012). Photosystem II and the unique role of bicarbonate: a historical perspective. *Biochim. Biophys. Acta Bioenerg.* 1817, 1134–1151. doi: 10.1016/j.bbabio.2012.04.003

Shi, X., and Bloom, A. (2021). Photorespiration: the futile cycle? *Plan. Theory* 10:908. doi: 10.3390/plants10050908

Shibata, M., Katoh, H., Sonoda, M., Ohkawa, H., Shimoyama, M., Fukuzawa, H., et al. (2002). Genes essential to sodium-dependent bicarbonate transport in cyanobacteria: function and phylogenetic analysis. *J. Biol. Chem.* 277, 18658–18664. doi: 10.1074/jbc.M112468200

Singhal, R., and Fernandez, D. E. (2017). Sorting of SEC translocase SCY components to different membranes in chloroplasts. *J. Exp. Bot.* 68, 5029–5043. doi: 10.1093/jxb/erx318

Smeekens, S., De Groot, M., Van Binsbergen, J., and Weisbeek, P. (1985). Sequence of the precursor of the chloroplast thylakoid lumen protein plastocyanin. *Nature* 317, 456–458. doi: 10.1038/317456a0

South, P. F., Cavanagh, A. P., Liu, H. W., and Ort, D. R. (2019). Synthetic glycolate metabolism pathways stimulate crop growth and productivity in the field. *Science* 363:eaat9077. doi: 10.1126/science.aat9077

Spalding, M. H. (2008). Microalgal carbon-dioxide-concentrating mechanisms: *Chlamydomonas* inorganic carbon transporters. *J. Exp. Bot.* 59, 1463–1473. doi: 10.1093/jxb/erm128

Sui, N., Huang, F., and Liu, L. N. (2020). Photosynthesis in phytoplankton: insights from the newly discovered biological inorganic carbon pumps. *Mol. Plant* 13, 949–951. doi: 10.1016/j.molp.2020.05.003

Sültemeyer, D., Klughammer, B., Badger, M. R., and Price, G. D. (1998). Fast induction of high-affinity HCO_3^- transport in cyanobacteria. *Plant Physiol.* 116, 183–192. doi: 10.1104/pp.116.1.183

Tester, M., and Davenport, R. (2003). Na^+ tolerance and Na^+ transport in higher plants. *Ann. Bot.* 91, 503–527. doi: 10.1093/aob/mcg058

Tolleter, D., Chochois, V., Poiré, R., Price, G. D., and Badger, M. R. (2017). Measuring CO_2 and HCO_3^- permeabilities of isolated chloroplasts using a MIMS-^{18}O approach. *J. Exp. Bot.* 68, 3915–3924. doi: 10.1093/jxb/erx188

Torrecilla, I., Leganés, F., Bonilla, I., and Fernández-Piñas, F. (2004). Light-to-dark transitions trigger a transient increase in intracellular Ca^{2+} modulated by the redox state of the photosynthetic electron transport chain in the cyanobacterium *anabaena* sp. PCC7120. *Plant Cell Environ.* 27, 810–819. doi: 10.1111/j.1365-3040.2004.01187.x

Tsujii, M., Tanudjaja, E., and Uozumi, N. (2020). Diverse physiological functions of cation proton antiporters across bacteria and plant cells. *Int. J. Mol. Sci.* 21:4566. doi: 10.3390/ijms21124566

Uehara, S., Adachi, F., Ito-Inaba, Y., and Inaba, T. (2016). Specific and efficient targeting of cyanobacterial bicarbonate transporters to the inner envelope membrane of chloroplasts in *Arabidopsis*. *Front. Plant Sci.* 7:16. doi: 10.3389/fpls.2016.00016

Uehara, S., Sei, A., Sada, M., Ito-Inaba, Y., and Inaba, T. (2020). Installation of authentic BicA and SbtA proteins to the chloroplast envelope membrane is achieved by the proteolytic cleavage of chimeric proteins in *Arabidopsis*. *Sci. Rep.* 10:2353. doi: 10.1038/s41598-020-59190-1

Uehlein, N., Sperling, H., Heckwolf, M., and Kaldenhoff, R. (2012). The *Arabidopsis* aquaporin PIP1;2 rules cellular CO_2 uptake. *Plant Cell Environ.* 35, 1077–1083. doi: 10.1111/j.1365-3040.2011.02473.x

Viana, A. A. B., Li, M., and Schnell, D. J. (2010). Determinants for stop-transfer and post-import pathways for protein targeting to the chloroplast inner envelope membrane. *J. Biol. Chem.* 285, 12948–12960. doi: 10.1074/jbc.M110.109744

Vojta, L., Soll, J., and Bölter, B. (2007). Protein transport in chloroplasts—targeting to the intermembrane space. *FEBS J.* 274, 5043–5054. doi: 10.1111/j.1742-4658.2007.06023.x

von Heijne, G. (1986). The distribution of positively charged residues in bacterial inner membrane proteins correlates with the trans-membrane topology. *EMBO J.* 5, 3021–3027. doi: 10.1002/j.1460-2075.1986.tb04601.x

Wang, Y., Duanmu, D., and Spalding, M. H. (2011). Carbon dioxide concentrating mechanism in *Chlamydomonas reinhardtii*: inorganic carbon transport and CO_2 recapture. *Photosynth. Res.* 109, 115–122. doi: 10.1007/s11120-011-9643-3

Wang, Y., Stessman, D. J., and Spalding, M. H. (2015). The CO_2 concentrating mechanism and photosynthetic carbon assimilation in limiting CO_2: how *Chlamydomonas* works against the gradient. *Plant J.* 82, 429–448. doi: 10.1111/tpj.12829

Wang, C., Sun, B., Zhang, X., Huang, X., Zhang, M., Guo, H., et al. (2019). Structural mechanism of the active bicarbonate transporter from cyanobacteria. *Nat. Plants* 5, 1184–1193. doi: 10.1038/s41477-019-0538-1

Wickell, D. A., and Li, F. W. (2020). On the evolutionary significance of horizontal gene transfers in plants. *New Phytol.* 225, 113–117. doi: 10.1111/nph.16022

Wojcik, S., and Kriechbaumer, V. (2021). Go your own way: membrane-targeting sequences. *Plant Physiol.* 185, 608–618. doi: 10.1093/plphys/kiaa058

Woodger, F. J., Badger, M. R., and Price, G. D. (2005). Sensing of inorganic carbon limitation in *Synechococcus* PCC7942 is correlated with the size of the internal inorganic carbon pool and involves oxygen. *Plant Physiol.* 139, 1959–1969. doi: 10.1104/pp.105.069146

Xu, X., Ouyang, M., Lu, D., Zheng, C., and Zhang, L. (2020). Protein sorting within chloroplasts. *Trends Cell Biol.* 31, 9–16. doi: 10.1016/j.tcb.2020.09.011

Yao, Z., Shen, B., Yang, X., and Long, M. (2020). The chloroplast localization of protease mediated by the potato rbcS signal peptide and its improvement for construction of photorespiratory bypasses. *Not. Bot. Horti Agrobot. Cluj-Napoca* 48, 14–23. doi: 10.15835/NBHA48111762

Conflict of Interest: The authors declare that the research was conducted in the absence of any commercial or financial relationships that could be construed as a potential conflict of interest.

Publisher's Note: All claims expressed in this article are solely those of the authors and do not necessarily represent those of their affiliated organizations, or those of the publisher, the editors and the reviewers. Any product that may be evaluated in this article, or claim that may be made by its manufacturer, is not guaranteed or endorsed by the publisher.

frontiers in Plant Science

REVIEW
published: 24 September 2021
doi: 10.3389/fpls.2021.708370

The Algal Chloroplast as a Testbed for Synthetic Biology Designs Aimed at Radically Rewiring Plant Metabolism

Harry O. Jackson[1], *Henry N. Taunt*[1], *Pawel M. Mordaka*[2], *Alison G. Smith*[2] *and Saul Purton*[1]*

[1] *Department of Structural and Molecular Biology, University College London, London, United Kingdom,* [2] *Department of Plant Sciences, University of Cambridge, Cambridge, United Kingdom*

Sustainable and economically viable support for an ever-increasing global population requires a paradigm shift in agricultural productivity, including the application of biotechnology to generate future crop plants. Current genetic engineering approaches aimed at enhancing the photosynthetic efficiency or composition of the harvested tissues involve relatively simple manipulations of endogenous metabolism. However, radical rewiring of central metabolism using new-to-nature pathways, so-called "synthetic metabolism", may be needed to really bring about significant step changes. In many cases, this will require re-programming the metabolism of the chloroplast, or other plastids in non-green tissues, through a combination of chloroplast and nuclear engineering. However, current technologies for sophisticated chloroplast engineering ("transplastomics") of plants are limited to just a handful of species. Moreover, the testing of metabolic rewiring in the chloroplast of plant models is often impractical given their obligate phototrophy, the extended time needed to create stable non-chimeric transplastomic lines, and the technical challenges associated with regeneration of whole plants. In contrast, the unicellular green alga, *Chlamydomonas reinhardtii* is a facultative heterotroph that allows for extensive modification of chloroplast function, including non-photosynthetic designs. Moreover, chloroplast engineering in *C. reinhardtii* is facile, with the ability to generate novel lines in a matter of weeks, and a well-defined molecular toolbox allows for rapid iterations of the "Design-Build-Test-Learn" (DBTL) cycle of modern synthetic biology approaches. The recent development of combinatorial DNA assembly pipelines for designing and building transgene clusters, simple methods for marker-free delivery of these clusters into the chloroplast genome, and the pre-existing wealth of knowledge regarding chloroplast gene expression and regulation in *C. reinhardtii* further adds to the versatility of transplastomics using this organism. Herein, we review the inherent advantages of the algal chloroplast as a simple and tractable testbed for metabolic engineering designs, which could then be implemented in higher plants.

Keywords: crop improvement, chloroplast, synthetic biology, transplastomics, *Chlamydomonas reinhardtii*

OPEN ACCESS

Edited by:
Patricia León,
National Autonomous University of Mexico, Mexico

Reviewed by:
Jianhua Fan,
East China University of Science and Technology, China
Sangram Keshari Lenka,
TERI Deakin Nanobiotechnology Centre, India

***Correspondence:**
Saul Purton
s.purton@ucl.ac.uk

Specialty section:
This article was submitted to Plant Biotechnology, a section of the journal Frontiers in Plant Science

Received: *11 May 2021*
Accepted: *10 August 2021*
Published: *24 September 2021*

Citation:
Jackson HO, Taunt HN, Mordaka PM, Smith AG and Purton S (2021) The Algal Chloroplast as a Testbed for Synthetic Biology Designs Aimed at Radically Rewiring Plant Metabolism. Front. Plant Sci. 12:708370. doi: 10.3389/fpls.2021.708370

INTRODUCTION

The latter half of the 20th century witnessed what is widely referred to as the "Green Revolution". By implementing agricultural technologies such as novel high-yielding varieties of cereal crops in combination with the adoption of synthetic fertilisers, new crop protection technologies, and intensive irrigation regimes, it is estimated that global food production tripled between the 1960's and early 2000's (Pingali, 2012). However, the returns from such technologies are plateauing for all major crops, particularly for the cereals (Grassini et al., 2013), and it is recognised that more radical changes to the phenotypes of crop species will be needed in order to significantly increase their productivity and improve their nutritional content. Changes that are essential to meet the challenges of dramatic climatic changes and an ever-increasing global population (Bailey-Serres et al., 2019). Carefully managed commercial production of transgenic crops with resistance to herbicides (Duke, 2015) and insect pests (Tabashnik et al., 2013) has already become a reality and has shown promise for future undertakings. One can imagine further desirable improvements, such as tolerance to weather extremes (Bailey-Serres et al., 2019), more efficient light harvesting and energy conversion through manipulations of the photosynthetic apparatus (Perera-Castro and Flexas, 2020), "upgrading" the carbon-fixation pathway (Simkin et al., 2015, 2017; Ding et al., 2016) and even the elimination of the ubiquitous but inefficient Rubisco enzyme (Sharwood, 2017; Cummins et al., 2018). Further radical engineering might include the introduction of nitrogen fixation into the plant tissue (Liu et al., 2018) or new anabolic pathways for key nutrients currently lacking in plants, such as vitamin B_{12} (Smith et al., 2007) and long-chain polyunsaturated fatty acids (Venegas-Calerón et al., 2010). Clearly, realising such goals will require approaches beyond conventional breeding and selection, namely sophisticated genetic engineering tools combined with synthetic biology and systems biology technologies for the major crop species, together with a simple model chassis that can serve as a tractable and malleable testbed for exploring these radical ideas.

For many of the desired improvements, the plastid is a key player since it is the site of photosynthesis within green tissue, as well as the site of major metabolic pathways, such as starch, haem, and fatty acid biosynthesis (Neuhaus and Emes, 2000), and a proposed location for nitrogen fixation (Liu et al., 2018). Since plastids contain their own small genome (termed, the plastome) and a genetic system derived from their prokaryotic ancestry (Green, 2011), this represents an attractive target for genetic engineering compared to the nuclear genome. Here, novel enzymes or structural proteins would be synthesised *in situ* in the plastid rather than requiring import from the cytosol, and the physical separation of the plastome from the nuclear genome may allow for more radical modifications, such as genetic recoding for biocontainment of the transgenes (Clark and Maselko, 2020). Genetic engineering of the plastome (transplastomics) is well-established in *Nicotiana tabacum* and is feasible for approximately 20 other plant species (Bock, 2015; Yu et al., 2020), and we are now seeing the development of synthetic biology (SynBio) assembly methods and libraries of validated DNAs that will allow for the rapid design and construction of different transgene assemblies (Occhialini et al., 2019). Ideally, these should be tested via multiple cycles of Design-Build-Test-Learn (DBTL; **Figure 1**) to explore the engineering space. However, implementation is challenging, not least because the obligate phototrophy of these plants makes manipulations of photosynthetic function problematic, and their macroscopic size and the many months needed to generate mature transgenic plants limit the scale and speed of DBTL cycles (Schindel et al., 2018). In contrast, the unicellular microalga, *Chlamydomonas reinhardtii* (hereafter *Chlamydomonas*) is able to dispense completely with photosynthesis and possesses a single chloroplast that is readily transformable (Boynton et al., 1988; Chen, 1996; Wannathong et al., 2016). Transplastomic lines can be generated in only a few weeks, and the microbial nature of *Chlamydomonas* means it is amenable to high-throughput analysis, either as colonies on agar plates (Shao and Bock, 2008; Ferenczi et al., 2017; Nouemssi et al., 2020), liquid cultures arrayed in microtiter plates (Haire et al., 2018), or as single cells sorted using flow cytometry or microdroplet technology (Pan et al., 2011; Velmurugan et al., 2013; Kim et al., 2017; Yu et al., 2021).

Since the first demonstration of chloroplast transformation of *Chlamydomonas* in 1988 (Boynton et al., 1988), the molecular tools and the know-how for manipulating the plastome have steadily improved, and we are now seeing the emergence of SynBio technologies that allow for the reduction and refactoring of the plastome, the standardised assembly and targeted insertion of multiple transgenes, and the analysis and regulation of these genes (Gimpel et al., 2016; Larrea-Alvarez and Purton, 2020). Importantly, algal transplastomics is now spreading beyond this model species with a flurry of reports of chloroplast transformation in other microalgae, including commercially-important species that are gaining traction as future sources of food and feed (Georgianna et al., 2013; Cui et al., 2014; Gan et al., 2018). If these results can be reproduced and implemented, improving the productivity and nutrition of these species will provide at least a partial solution to feeding the world.

In this review, we discuss the evolution and tractability of the chloroplast genetic system, recent advances in genetic engineering technologies for the algal chloroplast, the emergence of SynBio approaches, and the potential for the application of DBTL in the context of the algal chloroplast. We summarise examples of projects for which there is great potential for the algal chloroplast as a SynBio testbed for the kind of advanced, step-change modifications needed to power the Green Revolution 2.0.

EVOLUTION AND TRACTABILITY OF THE CHLOROPLAST GENETIC SYSTEM

The chloroplasts of plants and algae evolved from a single endosymbiotic event ∼1.5 billion years ago when a cyanobacterial ancestor was engulfed by a heterotrophic eukaryote (Green, 2011). The evolution of the chloroplast

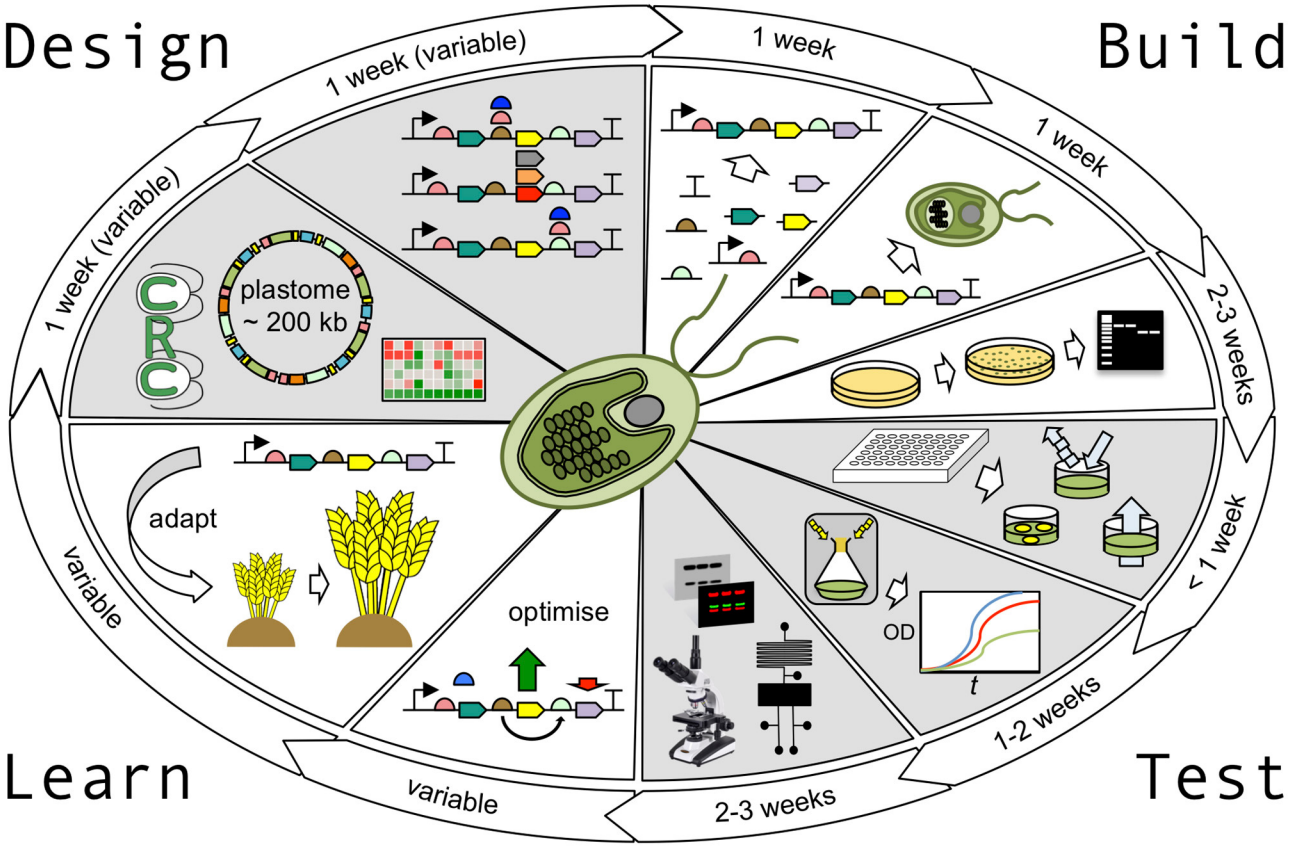

FIGURE 1 | The *Chlamydomonas* plastid testbed. The design stage of the Design-Build-Test-Learn (DBTL) cycle is supported by the availability of accurately detailed genomic and transcriptomic information and a vast library of parental mutant strains, readily available from the *Chlamydomonas* Resource Center. Golden Gate cloning strategies can be used to design parallel builds of multiple construct variants with ease. In the build phase, these constructs can then be assembled in one-pot cloning reactions to generate validated plasmids in less than a week. The chloroplast transformation procedure takes ∼1 week, including culturing time, with colonies taking ∼1 week to appear and a further ∼3 weeks to generate homoplasmic transgenic cell lines. In the test phase, rapid absorbance, fluorescence, and luminescence assays can be carried out in <1 week to screen cell lines before more robust growth analysis (1–2 weeks), and sophisticated physiological analysis is performed (2–3 weeks). Depending on the output of the test phase, designs can either be optimised further or adapted for use in higher plants. The entire DBTL cycle can be as short as 10–13 weeks.

involved multiple gene losses and extensive transfer of genes to the host-cell nucleus. Consequently, the plastome has undergone a dramatic reduction in size and complexity compared to the original cyanobacterial genome, with ∼90% of chloroplast proteins now being encoded by the nucleus and imported into the organelle. Most of the hundred-or-so genes that have been retained on the plastome encode core components of the photosynthetic apparatus or the transcription–translation machinery of the organelle. The plastid can therefore be viewed as a naturally evolved minimal cell, containing a streamlined genome and genetic system that retains many prokaryotic features (Scharff and Bock, 2014). The nucleus controls much of the genetic function of the chloroplast, encoding many of the ribosomal proteins and other housekeeping components, as well as specificity factors for RNA transcription, processing, stability, and translation. At the same time, retrograde signalling from the organelle regulates nucleus-encoded photosynthetic genes in response to the physiological status of the chloroplast (Chan et al., 2016).

Whilst targeting of foreign genes into the plastome has been reported for various higher plants and algae, it is most established for tobacco and *Chlamydomonas* (Purton et al., 2013; Yu et al., 2020). Transformation of the *Chlamydomonas* chloroplast genome was first demonstrated over 30 years ago, with DNA delivered into the organelle by the bombardment of lawn of cells with DNA-coated microparticles (Boynton et al., 1988). This "biolistics" method is highly effective with initial transformant colonies recovered after ∼7 days (Purton, 2007) and has been routinely adopted in many labs around the world. Alternatively, a simpler, although less efficient, method for the transformation of the *Chlamydomonas* chloroplast involves vortexing a cell suspension with glass beads and DNA (Larrea-Alvarez et al., 2021). DNA insertion into the plastome occurs exclusively *via* homologous recombination, allowing for precise and predictable integration of transgenes (Bock, 2015). However, there are between ∼40 and ∼100 copies of the plastome in each chloroplast, depending on the physiological state of the cell (Lau et al., 2000), and only a few copies initially acquire the foreign

DNA (so-called heteroplasmy). It is, therefore, necessary to drive the transformant lines to homoplasmy by single colony isolation on selective media; this process takes a further 2–3 weeks for *Chlamydomonas*, whereas for plants that possess multiple chloroplasts per cell (so as many as 10,000 plastome copies per cell) this can require multiple rounds of plant regeneration from leaf tissue and can take several months (Bock, 2015).

The DNA sequence of the 205 kb circular plastome of *Chlamydomonas* was first assembled in 2002, revealing a typical chloroplast DNA structure of two single-copy regions separated by two large inverted repeats (Maul et al., 2002). The presence of many short-dispersed repeats (SDRs) was observed as a major contributor to the high repetitive sequence content of the plastome (∼20%). An improved plastome sequence, derived from a single strain (CC-503) was produced in 2009 (Smith and Lee, 2009), before a *de novo* sequence of the complete plastome was generated by shotgun sequencing in 2018 and complemented with RNA-Seq-guided gene annotations, amending several discrepancies in previous versions (Gallaher et al., 2018). The *Chlamydomonas* plastome encodes 108 genes (including duplicates) (Gallaher et al., 2018): 8 rRNA genes, 29 tRNAs, and 71 protein-coding genes (**Figure 2**), a typical gene content for chloroplast genomes (Green, 2011).

Gene expression in the *Chlamydomonas* chloroplast is simpler than that in higher plant plastids. Transcription involves a single eubacterial type of RNA polymerase and promoter recognition mediated by a single sigma^{70}-like factor (Smith and Purton, 2002). This contrasts with plant plastids that possess two or more RNA polymerases and multiple sigma factors with distinct promoter preferences (Puthiyaveetil et al., 2021). All of the transcription start sites on the *Chlamydomonas* plastome have recently been mapped, together with most of the RNA processing sites (Cavaiuolo et al., 2017). Only three gene transcripts (those for *psaA*, *psbA,* and *rrnL*) undergo RNA splicing, and unlike in higher plants (Rodrigues et al., 2017), there is no RNA editing. Post-transcriptional steps of transcript processing, stabilisation, and translation initiation are mediated by nuclear-encoded factors, most of which are pentatricopeptide repeat (PPR), tetratricopeptide repeat (TPR), or octatricopeptide repeat (OPR) proteins (Gorchs-Rovira and Smith, 2019). Many of the *cis* elements on chloroplast transcripts that are the binding targets for these factors have been mapped (Cavaiuolo et al., 2017), and an increasing number of the factors themselves have been characterised in *Chlamydomonas*, including identification of their target genes (Johnson et al., 2010; Jalal et al., 2015; Marx et al., 2015; Cline et al., 2017; Viola et al., 2019; Ozawa et al., 2020).

The study of photosynthesis-related genes in *Chlamydomonas* has been greatly aided by its facultative heterotrophy. When provided with acetate as a source of fixed carbon, *Chlamydomonas* is able to dispense completely with photosynthesis and grow as a heterotroph. This key feature has enabled researchers not only to knock out most of the 37 photosynthetic genes, thus experimentally validating their dispensability (Rochaix, 2002) but also to generate mutations in hundreds of photosynthesis genes carried by the haploid nuclear genome. The functions of several *ycf* genes (hypothetical chloroplast open reading *f*rame), conserved in the plastomes of algae and in higher and lower plants, have also been elucidated through the analysis of *Chlamydomonas* knockout mutants (Boudreau et al., 1997). As a consequence, a vast array of mutants have been isolated that are defective in key photosynthetic processes, such as light capture, electron transfer, carbon fixation, and pigment biosynthesis (Harris, 2009; Dent et al., 2015). The availability of such mutants, together with a simple sexual cycle, and the ability to genetically engineer both the nuclear and chloroplast genomes has resulted in *Chlamydomonas* becoming an important reference organism for molecular-genetic research into photosynthesis and chloroplast biology (Salomé and Merchant, 2019).

EMERGING SYNBIO TOOLS FOR ENGINEERING THE *CHLAMYDOMONAS* PLASTOME

Early interest in *Chlamydomonas* was centred on basic research, but in the last two decades, interest has grown in the use of this algal species as a production platform. This has mainly focused on the light-driven synthesis of high-value therapeutic proteins and metabolites (Gimpel et al., 2015; Dyo and Purton, 2018; Taunt et al., 2018; Lauersen, 2019); however, with the increasing availability of SynBio tools, such as interchangeable parts and high throughput assembly tools, the goals of such applied projects have become more ambitious. This section describes the progress made in the development of SynBio in the algal chloroplast.

Gene Regulation Tools

Successful therapeutic protein production platforms are heavily reliant upon the ability to achieve high levels of transgene expression, and even for metabolic engineering sufficient levels of heterologous enzyme expression are required to ensure adequate substrate capture from endogenous metabolism and sufficient production rates for downstream steps. Moreover, the ability to precisely regulate gene expression to fine-tune metabolic pathways is important for optimal yields. For high constitutive expression of transgenes, endogenous chloroplast 5′-untranslated regions (5′-UTRs) of photosynthetic genes, such as that of the *psbA* and *psaA* genes, have typically been used in combination with the strong 16S ribosomal RNA promoter (Rasala et al., 2011; Bertalan et al., 2015). The expression strength of these endogenous 5′-UTR sequences is often limited by negative feedback regulation that would prevent the over-accumulation of photosynthetic subunits in the native context of the corresponding genes (Choquet and Wollman, 2002). Consequently, the 5′-UTR is often the limiting factor for transgene expression (Coragliotti et al., 2011). A promising strategy to mitigate this is the use of synthetic 5′-UTR variants that are not subject to these feedback mechanisms. Such variants have already been generated and used to improve the transgene expression (Specht and Mayfield, 2013).

Enabling advancements have recently been made in the development of tools for regulating gene expression in the *Chlamydomonas* chloroplast. One such system uses a modified version of a synthetic tRNA gene (*trnW$_{UCA}$*), which encodes a

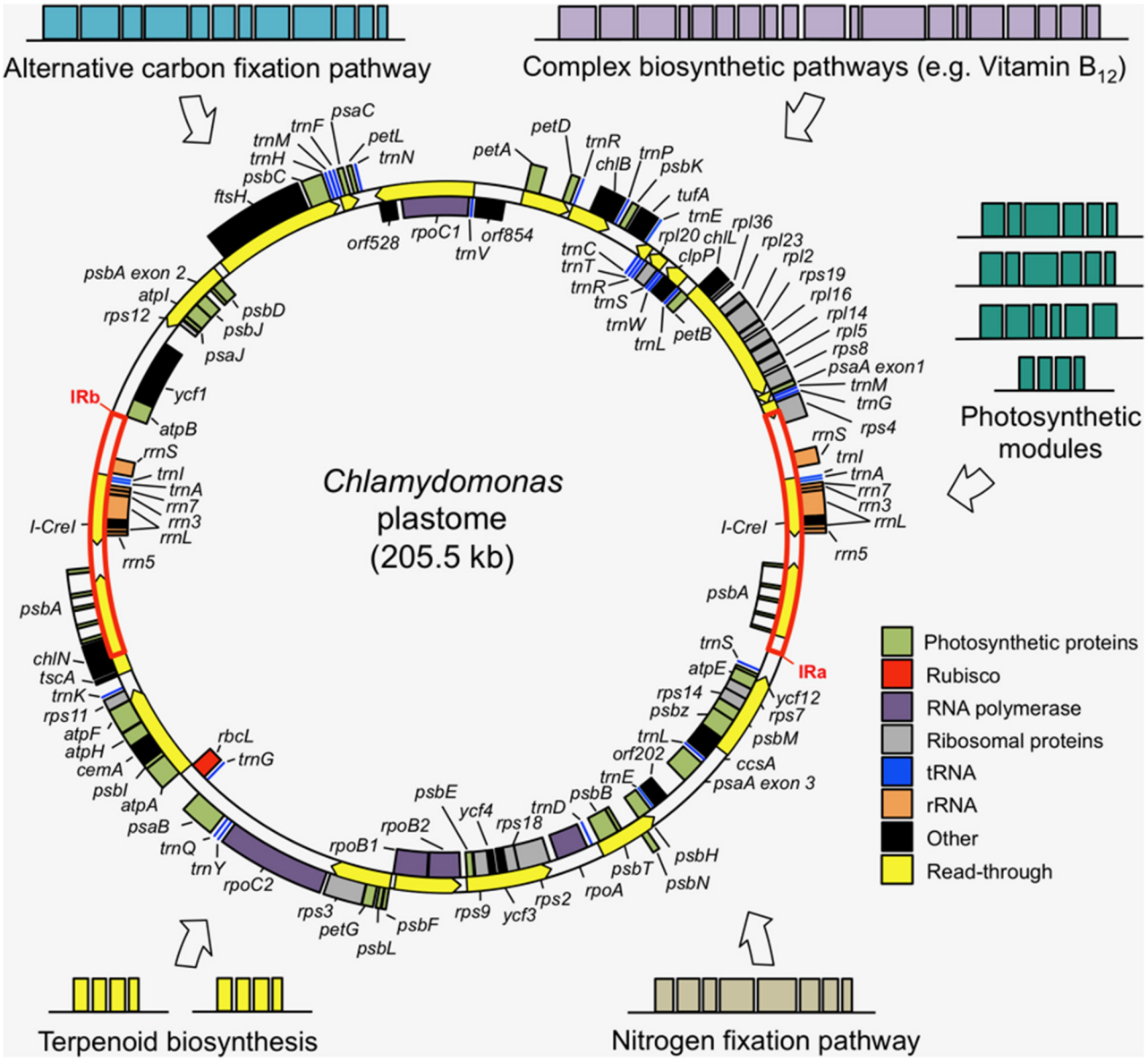

FIGURE 2 | Examples of transgene modules that could be added to the *Chlamydomonas* plastome to introduce novel metabolisms into the chloroplast. The wild-type plastome is composed of two single copy regions separated by two inverted repeats (IRa and IRb), with most genes encoding key subunits of the photosynthetic complexes and the transcription and translation machinery. The simplicity and tractability of the plastome make it a well-suited genetic system for complex metabolic engineering efforts. The plastome map was produced using the Cpv4 genomic data (Gallaher et al., 2018) with transcriptional read-through annotations (yellow arrows) from Cavaiuolo et al. (2017).

temperature-sensitive tRNA that allows for the translation of an unused stop codon (TGA) in the *Chlamydomonas* chloroplast as a tryptophan codon. The translation of transgenes that have been modified to contain one or more internal TGA codons can then be tuned by shifting the culture temperature from 35°C (translation stalls at the internal stop codons) to 18°C (translational read-through occurs). The induction behaviour can be further tailored by changing the number of TGA codons incorporated within the transgene (Young and Purton, 2016, 2018).

Many nuclear-encoded factors have been shown to regulate the expression of specific chloroplast genes at the posttranscriptional level, often by binding to target sites located in the 5′-UTR of the mRNA (Barkan and Goldschmidt-Clermont, 2000). Knowledge of such factors has been exploited to establish chloroplast repressible systems (Rochaix et al., 2014). For example, the nuclear-encoded NAC2 protein stabilises the *psbD* mRNA encoding the D2 protein of photosystem II by binding to the 5′-UTR of the transcript (Nickelsen et al., 1994). Fusion of

the *NAC2* gene to the inducible promoter of the *CYC6* gene, which is tightly repressed when copper is present in the growth medium and strongly expressed under copper deprivation or in the presence of nickel (Quinn et al., 2002), and introduction of this chimeric gene into the nuclear genome of a *nac2* mutant, has been shown to permit the regulation of the chloroplast, *psbD* 5′-UTR by changing the copper/nickel content of the growth medium (Surzycki et al., 2007; Rochaix et al., 2014). This repressible system can be applied to any chloroplast gene of interest by switching its 5′-UTR to that of *psbD,* with the option of preserving photosystem II expression and assembly under repression conditions by introducing a version of the *psbD* gene under the control of a 5′-UTR that is not responsive to NAC2 (Surzycki et al., 2007). Similarly, thiamine-based nuclear regulation of chloroplast transgenes has been established by the use of a TPP-responsive riboswitch in the *THI4* gene (Croft et al., 2007). Inclusion of the thiamine riboswitch in the NAC2 construct allows for its expression to be repressed in the presence of thiamine (Ramundo and Rochaix, 2015). Another recently established nuclear inducible chloroplast regulation system uses the C-terminus of the nuclear-encoded factor, TDA1 (cTDA1) that regulates the stability and translation of *atpA* transcripts through interactions with its 5′-UTR. The cTDA1, under the control of the chimeric promoter, *HSP70A-RBCS2*, was introduced into the nucleus of a chloroplast transformant expressing green fluorescent protein (GFP) under the control of the *atpA* 5′-UTR, enabling the control of GFP levels by light and heat-shock treatments (Carrera-Pacheco et al., 2020).

Multigenic Expression

To date, there have been reports of over 100 different foreign proteins produced in the *Chlamydomonas* chloroplast (Larrea-Alvarez and Purton, 2020) Whilst these studies have typically involved the introduction of a single transgene and selection marker into the plastome, reports of multigenic genetic engineering approaches involving up to six transgenes are now appearing (Gimpel et al., 2016; Macedo-Osorio et al., 2018; Larrea-Alvarez and Purton, 2020). Multiple genes can be integrated as discrete transcriptional units, each under the control of a dedicated promoter, and 5′- and 3′-UTRs. However, the use of the same *cis* element in more than one transcription unit needs to be avoided to prevent unwanted recombination events between direct repeats leading to transgene instability (Gimpel et al., 2016; Larrea-Alvarez and Purton, 2020). An alternative strategy to creating separate transcriptional units is to express multiple transgenes as a single synthetic operon (Bock, 2013; Macedo-Osorio et al., 2018; Hsu et al., 2019). Many endogenous genes in the chloroplast are co-expressed from a single promoter as polycistronic transcripts separated by "intercistronic expression elements" (IEEs). The IEEs facilitate the processing of the primary transcript to yield translatable monocistronic mRNAs (Bock, 2013). These IEEs are useful tools for stacking genes in synthetic operons for chloroplast metabolic engineering in both *Chlamydomonas* and tobacco. For example, three key genes involved in the tocochromanol (Vitamin E) pathway were assembled into a synthetic operon in tobacco, resulting in a 10-fold increase in tocochromanol accumulation compared to the expression without the use of the IEEs (Lu et al., 2013).

The Arrival of Standardised Modular Cloning Platforms, Such as Golden Gate

The rate at which complex DNA constructs can be designed and assembled has historically been a bottleneck for basic molecular research. However, the implementation of rapid and standardised assembly methods, such as Golden Gate, Gibson Assembly, and ligase cycling reaction (Casini et al., 2015) have led to a paradigm shift in the capabilities for genetic engineering, facilitating the application of the SynBio DBTL approach. Golden Gate methods are particularly well-suited for the hierarchical, high-throughput assembly of the multiple constructs needed to explore the design space. Briefly, these technologies use a single Type IIS restriction enzyme for the cutting and joining of all DNA parts, thereby eliminating the context-specific nature that is true of traditional cloning methods. Golden Gate relies on a specific and universal "syntax" (i.e., the sequence of a single-stranded overhang generated by digestion with the type IIS enzyme) for each fundamental DNA "part" or "level 0" (these include coding sequences, promoters, UTRs, IEEs, terminators, etc.) (Weber et al., 2011). Individual transcriptional units ("level 1") are then assembled from the chosen level 0 parts in a single digestion/ligation reaction with the syntax ensuring the joining of parts in the correct order and orientation within the designed construct. The constructs of Level 1 are then similarly assembled into higher level constructs containing one or more transcription units, a selectable marker, and other elements required in the final transformation plasmid. These approaches have given rise to modular cloning (MoClo) kits for nuclear transformation of a range of organisms including yeast (Lee et al., 2015), plants (Noor-Mohammadi et al., 2012; Engler et al., 2014), and animal cells (Vasudevan et al., 2019), and are now being employed for the *Chlamydomonas* nucleus (Crozet et al., 2018) and chloroplast (Noor-Mohammadi et al., 2012; Oey et al., 2014; Bertalan et al., 2015). A recent adaptation of the Golden Gate method, known as "Start-Stop Assembly," has been developed for bacteria (Taylor et al., 2019), and is also particularly applicable to chloroplast engineering. Central to the method is a 3-base syntax, with the DNA joinings at either end of the coding sequence part corresponding to the start and stop codons (ATG and TAA, respectively), which allows for completely scar-free assembly of coding sequences into the expression units. The further development and adoption of this technology will significantly advance chloroplast SynBio research by reducing the time and effort needed to complete each DBTL cycle, increasing the number of different plasmid designs that can be assembled in parallel and fed into each cycle, and by reducing the duplication of efforts and inconsistencies between research groups with a library of standardised and validated parts that can be readily shared.

Whole Plastome Engineering

The design of a highly reduced synthetic genome, or "minimal genome" in which all non-essential genes are removed, and its successful transplantation into a recipient cell or organelle is widely regarded as one of the next great challenges for SynBio (Lachance et al., 2019). Such systems not only provide a bottom-up approach to exploring fundamental molecular processes within a simplified cell or organelle but also provide a naïve chassis onto which can be bolted new desirable traits or a drastically restructured metabolism. In the case of a minimal synthetic plastome (Scharff and Bock, 2014), this could allow for the remodelling of large elements of the photosynthetic apparatus without interference from the native system, for example, introducing entire photosystems from other organisms and evaluating their performance. The *Chlamydomonas* plastome is particularly well-suited for such an undertaking given the non-essential nature of all the photosynthetic genes, the detailed knowledge of its transcriptome, and the SynBio resources available for subsequent genetic engineering of the minimal plastome. In a first exploration of this, O'Neill et al. (2012) assembled a variant of the entire *Chlamydomonas* plastome in yeast and introduced it into the chloroplast. However, this resulted in the formation of chimeric forms of the plastome due to unwanted DNA recombination between the native and introduced versions. This illustrates a major challenge that must be overcome for a clean plastome transplantation: namely, the need to develop a method for selective elimination of the native DNA either prior to or immediately following transformation. Nevertheless, a simple *in silico* analysis of all the non-essential regions of the *Chlamydomonas* plastome (i.e., all the photosynthetic genes, one copy of the large inverted repeat, the short-dispersed repeats, and the *rrnL* intron) leads to a design that is ∼96 kb in size and possesses just 57 RNA and protein genes. This minimal synthetic plastome could be easily assembled and propagated in yeast prior to transplantation into the algal chloroplast. In addition to minimisation, another improvement that could be made to generate a powerful SynBio chassis strain is the re-factoring of genes into functionally defined clusters on the synthetic plastome, as has been done for six genes encoding Photosystem II subunits (Gimpel et al., 2016). Extension of this more broadly would allow for a modular approach to plastome engineering in which whole sets of genes can be easily replaced or additional gene modules bolted on during the design/build stage without requiring *de novo* synthesis of the whole plastome.

DESIGN-BUILD-TEST-LEARN STRATEGIES

The Design-Build-Test-Learn cycle (**Figure 1**) is a systematic and iterative approach in SynBio and strain development that is being widely adopted in metabolic engineering to obtain a design that satisfies a given specification (Pouvreau et al., 2018; Opgenorth et al., 2019). The critical feature is that rather than one design, researchers explore parameter space to find an optimal engineered solution to the problem. With the currently available genomic/transcriptomic resources for *Chlamydomonas* and the efficient DNA assembly methods, the Design and Build stages of the DBTL cycle can be performed in a matter of days. Indeed, high-throughput parallel assemblies of multiple DNA constructs for chloroplast engineering are possible in less than a week once all parts are available, either as pre-existing parts within a library or by the generation of new parts through PCR amplification of genomic DNA/cDNA or gene synthesis (Noor-Mohammadi et al., 2012; Oey et al., 2014; Bertalan et al., 2015; Crozet et al., 2018; Gallaher et al., 2018; Occhialini et al., 2019).

In order to test the efficacy of engineering efforts, precise techniques for monitoring basic physiology, protein expression levels, and genomic stability are of vital importance. Growth analysis of *Chlamydomonas* can be performed easily and robustly at a range of scales, either in microplate format (Haire et al., 2018), at flask-scale using lab-scale photobioreactors that offer precision control of environmental conditions, or in mid-scale commercial bioreactors (Changko et al., 2020). Amongst the DNA parts available are an array of fluorescent and luminescent reporter genes for studying nuclear and chloroplast gene expression *in vivo* in *Chlamydomonas* (Rasala et al., 2013; Lauersen et al., 2015; Esland et al., 2018). These reporters provide a rapid and high-throughput method to assess gene expression and can be made quantitative through the use of recombinant standards. Alternatively, quantitative measurements of recombinant proteins can be achieved *via* Western blot by incorporating an epitope tag into the design of the protein (Stoffels et al., 2017; Larrea-Alvarez and Purton, 2020).

Imaging techniques for *Chlamydomonas* have also undergone significant improvement in recent years and will serve as powerful diagnostics tools for chloroplast engineering. Confocal microscopy is routinely used to visualise whole cell architecture *via* bright-field, or for fluorescence analysis and visualisation of endogenous or recombinant fluorescent proteins (Rasala et al., 2013). Live imaging of nucleoids (the DNA–protein conglomerates within chloroplasts that contain multiple copies of the plastome) within single cells has been performed using strains expressing a YFP-tagged histone-like DNA binding protein, as was deployed in conjunction with microfluidic technology to reveal the dynamic nature of nucleoid networks over the course of cellular division (Kamimura et al., 2018). *In situ* cryo-electron tomography has now made it possible to visualise individual Photosystem I and Photosystem II (PSI & PSII) complexes within the thylakoid membrane with stunning detail, laying the foundation for the use of this technology to observe photosynthetic regulation at the level of single-protein complexes (Wietrzynski et al., 2020).

Together, these technologies for engineering and analysing the *Chlamydomonas* plastid enable DBTL to be carried out in very short order, in turn accelerating the rate of progress of basic and applied SynBio studies. This knowledge could then be adapted for more complex multicellular systems, such as higher plants, to realise the ambitious metabolic redesign goals for these species on a more relevant time scale.

PRIORITY PROJECTS FOR THE TESTBED

There are many potential trait adjustments to plant crops that could help them cope with the increasing production demands and potentially extreme environmental challenges of the future. Of the many SynBio projects that could be envisaged, some priority projects that lend themselves well to the algal chloroplast testbed are briefly discussed in this section and illustrated in **Figure 2**.

Improving Photosynthesis

The microalgal chloroplast has been used extensively for the study of photosynthesis and more recently as a target for improving the efficiency of photosynthesis and the overall productivity of light-driven production systems. Among the proposed strategies that are applicable to higher plants is the expansion of the spectral band used for photosynthesis by the introduction of additional light-harvesting pigments (Blankenship and Chen, 2013; Trinugroho et al., 2020), enhancing photoprotective mechanisms (Leister, 2019), and even the introduction of recombinant photosystems (Gimpel et al., 2016).

The high degree of evolutionary constraint on the essential photosynthetic complexes, PSI & PSII and the cytochrome b_6f complex, has resulted in the so-called "frozen metabolic state" (Gimpel et al., 2016). Modification to these complexes is made challenging by the strong conservation of the structural components and the need for simultaneous modification of multiple protein subunits, often encoded in both the nucleus and the chloroplast genomes (Leister, 2019). Re-factoring of the six-gene PSII core in the chloroplast of *Chlamydomonas* illustrated that there were additional limiting interactions beyond the core subunits that reduced the overall quantum yield of recombinant variants (Gimpel et al., 2016). The use of 'synthetic photosynthetic modules' that contain a sufficient number of the necessary proteins, genetic elements, and auxiliary factors for the proper functioning of a given complex has thus been highlighted as an important consideration for these SynBio approaches (Leister, 2019).

An alternative to engineering the highly intricate photosynthetic machinery is to introduce a heterologous electron sink that can harvest the reducing power from photosynthesis and use it to power unrelated metabolic processes (Mellor et al., 2017). This concept holds promise as it is not reliant on modifying the photosynthetic machinery but rather harvesting the excess reducing power that would otherwise be dissipated to prevent photodamage. Pioneering studies in cyanobacteria and plant plastids have shown that reducing equivalents from PSI can be redirected to cytochrome P450 enzymes and, due to the extreme versatility of this enzyme family, coupled to a wide variety of metabolic processes (Lassen et al., 2014a,b; Berepiki et al., 2016; Nielsen et al., 2016). The chloroplast of *Chlamydomonas* would be an ideal platform to develop these strategies due to the ease and speed of genetic engineering as well as the ability to grow the cell mixotrophically in the presence of acetate, thus enabling more reducing power to be harvested from photosynthesis without perturbing cell fitness and growth. A gene (*CYP79A1*) encoding a cytochrome P450 from *Sorghum bicolor* has already been introduced into the *Chlamydomonas* chloroplast, resulting in the stable expression of the P450 and its targeting to the chloroplast membrane. The heterologous P450 was shown to catalyse the first reaction (conversion of tyrosine to p-hydroxyphenylacetaldoxime) of the biosynthesis pathway of dhurrin, a plant defence compound (Gangl et al., 2015). This work provides a proof of concept for the light-driven production of complex plant metabolites in the algal chloroplast using cytochrome P450s.

Carbon Fixation

Improving the efficiency with which plant crops convert CO_2 into biomass will be key to meeting the agricultural yield requirements of an ever-growing global population. Accordingly, improving the rate of carbon fixation in plants has been a target for metabolic engineering (Kubis and Bar-Even, 2019). Proposed strategies for boosting carbon fixation include engineering a more efficient Rubisco (Loganathan et al., 2016; Sharwood, 2017), optimisation of the expression levels of Calvin cycle enzymes (Simkin et al., 2015), design and integration of alternative computationally derived synthetic pathways for carbon fixation (Siegel et al., 2015), and introduction of algal carbon-concentrating mechanisms (Long et al., 2016; Rae et al., 2017; Mackinder, 2018). Critical to the success of such efforts is the ability to regulate and tune the expression of genes of a synthetic pathway within the complex biological context of the host organism (Kubis and Bar-Even, 2019). As such, the algal plastid could provide a suitable platform to carry out basic research given the on-going development of engineering tools for the regulation of gene expression and the relative simplicity of the plastid genetic system, as discussed in the previous sections.

For example, a long-standing goal in carbon assimilation research has been to address the limitations of the carbon-fixation enzyme, Rubisco (Sharwood, 2017). In theory, it should be possible to use a rational design approach to improve the rate of catalysis of the enzyme, and its relative affinity for CO_2 over the competing substrate O_2. This could then pave the way for plant varieties in which the abundance of Rubisco in green tissue is significantly reduced whilst rates of carbon-fixation are increased. Early efforts to produce a functional recombinant Rubisco in *Escherichia coli* for such design studies were unsuccessful because of the lack of native chaperones required for the folding and assembling of the large (L) and small (S) subunits into the L_8S_8 structure. More recently, this issue has been addressed through the co-expression in *E. coli* of multiple chloroplast chaperones from *Arabidopsis* together with the large and small subunits (Aigner et al., 2017). Using this *E. coli* system to explore the design space now allows for the discovery of superior L- and S-subunit variants that can then be tested by introduction into plant models. However, replacement of the endogenous plant genes is complicated by their separate genomic locations, with the L-subunit gene (*rbcL*) located in the plastome and the S-subunit gene family (*RBCS*) in the nuclear genome. Researchers have sought to address this using

RNA interference-mediated gene silencing to generate master-lines of *Nicotiana tabacum* in which the nuclear *RBCS* gene is suppressed, enabling the production of Rubisco variants by the transformation of the chloroplast with an *rbcL-rbcS* operon (Martin-Avila et al., 2020). Placing the S-subunit gene in the plastome simplifies comparative studies since both genes can be targeted to a specific locus in a single transformation step. However, the use of *N. tabacum* to test the initial designs is not ideal, given its obligate phototrophy and the limitations for rapid DBTL cycling. *Chlamydomonas* represents an attractive intermediate model since a nuclear mutant is already available in which both members of the *RBCS* gene family are deleted (Khrebtukova and Spreitzer, 1996), and deletion of *rbcL* in the plastome is straightforward (Newman et al., 1991). A double mutant could therefore serve as the recipient for chloroplast transformation using an *rbcS-rbcL* operon. This would allow a rapid assessment of the findings from the *E. coli* studies whereby different combinations of protein engineering within the L- and S-subunits are screened: initially for function by direct selection for restored phototropic growth, and then through biochemical analysis of Rubisco accumulation and catalytic activity. The best designs could then be carried forward for testing in a higher plant such as *N. tabacum*.

Nitrogen Fixation

Whilst plants are capable of assimilating carbon directly from the atmosphere through photosynthesis, they are not able to directly fix atmospheric nitrogen. Plants are therefore reliant on diazotrophic bacteria and archaea that possess the nitrogen-fixing enzyme, nitrogenase, and are thus able to supply bioavailable forms of this essential element. The Green Revolution was driven in large part by the development of an alternative, chemical method for fixing nitrogen (the Haber–Bosch process) allowing for the production of huge quantities of cheap agricultural fertilisers (Rogers and Oldroyd, 2014). However, there is increasing recognition of the deleterious environmental consequences of our heavy reliance on these chemical fertilisers. These consequences include the consumption of vast amounts of fossil fuels and associated release of CO_2 during fertiliser production, the release into the atmosphere of large amounts of nitrous oxides following application on the field, and the eutrophication of aquatic ecosystems owing to run-off of excess dissolved nitrates (Sutton et al., 2011). This has incentivised several avenues of research seeking to introduce the capacity for biological nitrogen fixation into crop species (Rosenblueth et al., 2018). One approach is the genetic engineering of cereal crops to improve their association with nitrogen-fixing bacteria that colonise plant roots, with the ultimate goal of reproducing the bacteria-containing root nodules of legumes in the engineered plants (Rogers and Oldroyd, 2014). An alternative approach would be the introduction of the bacterial nitrogenase enzyme into the cells of crop plants such that they are able to directly fix atmospheric nitrogen (Hardy and Havelka, 1975; Rosenblueth et al., 2018). Attempts to engineer plant genomes with the bacterial *nif* genes required for nitrogenase biosynthesis are made challenging by the complexity of the biosynthesis pathway, with as many as 16 gene products required for the functional assembly of the molybdenum-containing metalloenzyme (Curatti and Rubio, 2014). Furthermore, the enzyme is highly oxygen-sensitive, and has a high energy demand with 16 ATP molecules required to convert one N_2 molecule to NH_3. However, chloroplasts and mitochondria have sufficient energy reserves to carry out nitrogen fixation and have long been discussed as possible subcellular locations for nitrogenase fixation (Merrick and Dixon, 1984; Beatty and Good, 2011). Recent SynBio efforts involve nuclear engineering of yeast and tobacco such that the *nif* gene products are targeted to the mitochondrion or the chloroplast, respectively, show promising results but also highlight the significant technical challenges of producing a functional nitrogenase enzyme in a eukaryotic organelle (López-Torrejón et al., 2016; Eseverri et al., 2020; Xiang et al., 2020). Furthermore, synthesis of a functional nitrogenase in the chloroplast would require separation from the oxygen evolved by photosynthesis, either temporally, by inducing *nif* gene expression only at night, or spatially, by selectively expressing the *nif* genes in non-photosynthetic tissue (Rosenblueth et al., 2018). *Chlamydomonas* lends itself well to such complex design studies since multiple *nif* genes could be expressed directly in the chloroplast, and the oxygen issue can be circumvented either by using a photosynthetic mutant incapable of oxygen evolution or by culturing the cells in the dark. The capabilities and reduced timescale of the DBTL cycle for chloroplast engineering in this alga could contribute significantly to an iterative effort aimed at solving the many design challenges prior to transferring the technology into crop plants.

Engineering Crop Plants for the Production of Novel Metabolites

Chloroplast metabolic engineering offers many opportunities for exploiting plants as low-cost and scalable factories for the production of pharmaceutical compounds (so-called plant molecular farming: Obembe et al., 2011), or for developing biofortified crop varieties with high levels of beneficial nutrients such as vitamins, antioxidants, essential amino acids, and minerals (Díaz-Gómez et al., 2017). Whilst some pioneering progress has been made in chloroplast metabolic engineering using plant models, such as tobacco and tomato (Fuentes et al., 2018), it is by its very nature a challenging endeavour since the engineering inevitably perturbs the metabolism of the chloroplast. Multiple cycles of DBTL are therefore necessary to tune the metabolic flux to the novel product and minimise the accumulation of undesirable intermediates. Here, we consider two examples where engineering the *Chlamydomonas* chloroplast can serve as a simple testbed for such studies, namely the synthesis of commercially-important terpenoid compounds and biofortification of crops with vitamin B_{12}.

Terpenes are complex linear or cyclic hydrocarbons produced by plants and microorganisms, and are synthesised from multiple units of a 5-carbon branched precursor. Terpenoids are then derived from terpenes through the functionalisation of the hydrocarbon skeleton with oxygen-containing groups, such as hydroxyl, ketone, aldehyde, carbonyl, and peroxide groups, giving rise to a huge diversity of natural compounds (Breitmaier,

2006). Many of these have commercial applications including as pharmaceutical and nutraceutical bioactives, fragrances in cosmetics and cleaning agents, flavourings in food and drinks, and natural insecticides. However, the chiral complexity of terpenoids often precludes their chemical synthesis, and whilst they can be derived from natural plant or microbial sources, the levels are typically very low or present only in specialised organs making the extraction expensive (Vavitsas et al., 2018). Transfer of the biosynthetic pathways into platform species is therefore desirable, and much work has focussed on the biosynthesis of medicinal terpenoids in *E. coli* and yeast, including precursors of the anti-malarial drug, artemisinin and the anti-cancer therapeutic, paclitaxel (Ajikumar et al., 2010; Paddon et al., 2013). Although these two microorganisms are highly advanced platforms for metabolic engineering, the use of plants and algae as alternative platforms offers a number of potential advantages when considering terpenoid biosynthesis (Vavitsas et al., 2018). Specifically, photosynthetic organisms naturally produce a wide variety of terpenoids and devote significant metabolic resources to their biosynthesis. The necessary metabolic infrastructure and high flux potential are therefore already established in these hosts, unlike the situation in *E. coli* and yeast. Furthermore, terpenoid biosynthesis in the chloroplast can be directly linked to photosynthesis *via* electron transfer proteins, thereby providing the reductant necessary for the biosynthesis of terpene skeletons and their functionalisation by heterologous cytochrome P450s (Mellor et al., 2017). Once again, *Chlamydomonas* offers an attractive intermediary production platform to optimise production, with the modular characteristics of terpenoid biosynthesis making it well-suited for systems biology and SynBio approaches to plastid and nuclear genome engineering (Wichmann et al., 2020). Indeed, synthesis of heterologous diterpenoid products, such as casbene, taxadiene, and 13R(+) manoyl oxide has already been demonstrated in the chloroplast of *Chlamydomonas* (Lauersen et al., 2018; Mehrshahi et al., 2020). Diterpenoids produced in the organelle are released from the cell and can be easily captured in dodecane culture overlays for analysis by gas chromatography mass spectrometry, providing a powerful platform for the study of phototrophic heterologous terpenoid production (Lauersen, 2019).

Vitamin B_{12} (B_{12}, hereafter) is widely known to be the only vitamin that cannot be acquired directly from plant-derived foods since it is synthesised solely by a subset of prokaryotes (Warren et al., 2002). B_{12} is also by far the most chemically complex of the vitamins with an elaborate 63-carbon tetrapyrrole structure. Fortification of foods with B_{12} or production of B_{12} supplements is therefore dependent on industrial fermentation of bacterial species that natively produce the vitamin (Balabanova et al., 2021). Heterologous biosynthesis of B_{12} has also been achieved by engineering the non-producing bacterium, *E. coli*. This was successful despite the genetic complexity of the biosynthetic pathway, with 28 transgenes from five different bacterial species required for *de novo* synthesis in *E. coli* (Fang et al., 2018). The study serves as a primer for the more challenging but more economic strategy of introducing a B_{12} biosynthetic pathway directly into plant plastids to produce biofortified food crops. To this end, the algal plastid could serve as a useful platform to define the minimum number of enzymes required (given that all the enzymes for the early part of the pathway leading to the synthesis of the related tetrapyrroles, haem and chlorophyll are already located in the chloroplast; Oborník and Green, 2005), and to optimise B_{12} yield through iterative testing of different gene sets and expression levels.

CONCLUDING REMARKS

SynBio research will play a vital role in securing a productive and sustainable future for plant-based agriculture. Among the ambitious improvements proposed for plant crops are the introduction of novel nitrogen/carbon fixation pathways to boost overall biomass production, fortification against environmental threats and extreme weather conditions, and the integration of complex multigene pathways for the production of novel bio-products.

Similar to traditional engineering disciplines, the SynBio approach uses abstraction, decoupling, and standardisation to make the design of complex biological systems more manageable and efficient (Boehm and Bock, 2019). This is illustrated in the systematic characterisation of DNA parts as modular units with a predictable function, which can be organised into genetic systems (or levels) with hierarchical complexity that can be optimised through successive rounds of DBTL (**Figure 1**).

Synbio research in plant species is still in its infancy and is in need of advancements to the available genetic tools and a deeper understanding of the metabolic systems that are being targeted. As is the case for all host organisms, the time requirement associated with generating transgenic crop plants limits the rate at which the SynBio method of DBTL can be carried out. Furthermore, the space requirement for plant growth also limits the number of different design permutations that can be tested in parallel within a single cycle of DBTL. Clearly, the reduced DBTL timescale and greater numerical capacity of microbial platforms offer significant advantages when exploring the genetic engineering landscape using an iterative approach.

Major breakthroughs using microbial model organisms, such as the re-programming of *E. coli* with a novel synthetic genome (Fredens et al., 2019) and the functional integration of complex metabolic pathways into *E. coli* and yeast (e.g., Paddon et al., 2013; Fang et al., 2018) demonstrate the promise of SynBio. We are now seeing the early stages of the application of SynBio in chloroplast biotechnology (Scharff and Bock, 2014; Schindel et al., 2018; Occhialini et al., 2019), thus opening the possibility of similar breakthroughs in higher plants. Chloroplast SynBio research using single-cell models such as *Chlamydomonas* provides a good starting point and attractive testbed for such ambitious metabolic engineering efforts prior to their exportation to higher plants.

However, the limitations and differences inherent in any model must also be appreciated. *Chlamydomonas* is an aquatic single cell adapted to a mixotrophic lifestyle in freshwater and soil where light, oxygen, and nutrient availability are often limited (Sasso et al., 2018). Its environment is therefore

significantly different from that of crop plants, and to consider it a "unicellular plant" is naïve, especially given that chlorophyte algae and land plants diverged from a common ancestor over 800 million years ago (Donoghue and Paps, 2020). *Chlamydomonas* possesses only a single chloroplast per cell compared to the 50–100 chloroplasts typically found in a plant mesophyll cell. Furthermore, plants contain different plastid types depending on the tissue, and the plastids are able to undergo differentiation into different types (Choi et al., 2021). In contrast, the algal chloroplast does not undergo differentiation, and indeed is able to form a fully functional chloroplast when grown in complete darkness, unlike angiosperms (Reinbothe et al., 2010). There are also distinct differences in the finer details of chloroplast gene expression. In *Chlamydomonas,* all chloroplast genes are transcribed by a single eubacterial-type RNA polymerase using a single sigma factor, whereas, in plants, the transcription is shared between eubacterial and bacteriophage-type polymerases with the former employing multiple sigma factors (Puthiyaveetil et al., 2021). Optimisation of parameters for the transcription of transgene clusters using the algal model will not, therefore, be directly transferable to the plant chloroplast. Similarly, RNA editing is a feature of plant chloroplasts that is not seen in *Chlamydomonas* (Small et al., 2020), and might need to be taken into account when sharing DNA parts between the two systems. Finally, differences in the control mechanisms underlying post-transcriptional steps (RNA processing, RNA stability, and translation initiation), as well as codon preference and protein stability, are all likely to affect the expected recombinant protein levels when transferring from algal to plant model (Faè et al., 2017). Nonetheless, despite these caveats, the many advantages of engineering the *Chlamydomonas* chloroplast mean that it has much to offer as a simple and tractable testbed for radical re-engineering of crop species for the 21st century.

AUTHOR CONTRIBUTIONS

HJ researched and wrote the review with support from HT and PM who provided valuable feedback and contributions to the text. SP and AS supervised the work and provided critical discussion, feedback, and comments on the manuscript. All authors have approved the submitted version.

FUNDING

Chloroplast SynBio research of the authors was funded by the grants BB/R016534/1 and BB/R01860X/1 from the Biotechnology and Biological Sciences Research Council of the United Kingdom.

REFERENCES

Aigner, H., Wilson, R. H., Bracher, A., Calisse, L., Bhat, J. Y., Hartl, F. U., et al. (2017). Plant RuBisCo assembly in *E. coli* with five chloroplast chaperones including BSD2. *Science* 358, 1272–1278. doi: 10.1126/science.aap9221

Ajikumar, P. K., Xiao, W. H., Tyo, K. E. J., Wang, Y., Simeon, F., Leonard, E., et al. (2010). Isoprenoid pathway optimization for Taxol precursor overproduction in *Escherichia coli*. *Science* 330, 70–74. doi: 10.1126/science.1191652

Bailey-Serres, J., Parker, J. E., Ainsworth, E. A., Oldroyd, G. E. D., and Schroeder, J. I. (2019). Genetic strategies for improving crop yields. *Nature* 575, 109–118. doi: 10.1038/s41586-019-1679-0

Balabanova, L., Averianova, L., Marchenok, M., Son, O., and Tekutyeva, L. (2021). Microbial and genetic resources for cobalamin (Vitamin b12) biosynthesis: from ecosystems to industrial biotechnology. *Int. J. Mol. Sci.* 22:4522. doi: 10.3390/ijms22094522

Barkan, A., and Goldschmidt-Clermont, M. (2000). Participation of nuclear genes in chloroplast gene expression. *Biochimie* 82, 559–572. doi: 10.1016/S0300-9084(00)00602-7

Beatty, P. H., and Good, A. G. (2011). Future prospects for cereals that fix nitrogen. *Science* 333, 416–417. doi: 10.1126/science.1209467

Berepiki, A., Hitchcock, A., Moore, C. M., and Bibby, T. S. (2016). Tapping the unused potential of photosynthesis with a heterologous electron sink. *ACS Synth. Biol.* 5, 1369–1375. doi: 10.1021/acssynbio.6b00100

Bertalan, I., Munder, M. C., Weiß, C., Kopf, J., Fischer, D., and Johanningmeier, U. (2015). A rapid, modular and marker-free chloroplast expression system for the green alga *Chlamydomonas reinhardtii*. *J. Biotechnol.* 195, 60–66. doi: 10.1016/j.jbiotec.2014.12.017

Blankenship, R. E., and Chen, M. (2013). Spectral expansion and antenna reduction can enhance photosynthesis for energy production. *Curr. Opin. Chem. Biol.* 17, 457–461. doi: 10.1016/j.cbpa.2013.03.031

Bock, R. (2013). Strategies for metabolic pathway engineering with multiple transgenes. *Plant Mol. Biol.* 83, 21–31. doi: 10.1007/s11103-013-0045-0

Bock, R. (2015). Engineering plastid genomes: Methods, tools, and applications in basic research and biotechnology. *Annu. Rev. Plant Biol.* 66, 211–241. doi: 10.1146/annurev-arplant-050213-040212

Boehm, C. R., and Bock, R. (2019). Recent advances and current challenges in synthetic biology of the plastid genetic system and metabolism. *Plant Physiol.* 179, 794–802. doi: 10.1104/pp.18.00767

Boudreau, E., Takahashi, Y., Lemieux, C., Turmel, M., and Rochaix, J. D. (1997). The chloroplast *ycf3* and *ycf4* open reading frames of *Chlamydomonas reinhardtii* are required for the accumulation of the photosystem I complex. *EMBO J.* 16, 6095–6104. doi: 10.1093/emboj/16.20.6095

Boynton, J. E., Gillham, N. W., Harris, E. H., Hosler, J. P., Johnson, A. M., Jones, A. R., et al. (1988). Chloroplast transformation in *Chlamydomonas* with high velocity microprojectiles. *Science* 240, 1534–1538. doi: 10.1126/science.2897716

Breitmaier, E. (2006). *Terpenes: Importance, General Structure, and Biosynthesis*. Terpenes: Flavors, Fragrances, Pharmaca, Pheromones.

Carrera-Pacheco, S. E., Hankamer, B., and Oey, M. (2020). Light and heat-shock mediated TDA1 overexpression as a tool for controlled high-yield recombinant protein production in *Chlamydomonas reinhardtii* chloroplasts. *Algal Res.* 48:101921. doi: 10.1016/j.algal.2020.101921

Casini, A., Storch, M., Baldwin, G. S., and Ellis, T. (2015). Bricks and blueprints: Methods and standards for DNA assembly. *Nat. Rev. Mol. Cell Biol.* 16, 568–576. doi: 10.1038/nrm4014

Cavaiuolo, M., Kuras, R., Wollman, F. A., Choquet, Y., and Vallon, O. (2017). Small RNA profiling in *Chlamydomonas*: Insights into chloroplast RNA metabolism. *Nucleic Acids Res.* 45, 10783–10799. doi: 10.1093/nar/gkx668

Chan, K. X., Phua, S. Y., Crisp, P., McQuinn, R., and Pogson, B. J. (2016). Learning the languages of the chloroplast: Retrograde signaling and beyond. *Annu. Rev. Plant Biol.* 67, 25–53. doi: 10.1146/annurev-arplant-043015-111854

Changko, S., Rajakumar, P. D., Young, R. E. B., and Purton, S. (2020). The phosphite oxidoreductase gene, *ptxD*, as a bio-contained chloroplast marker and crop-protection tool for algal biotechnology using *Chlamydomonas*. *Appl. Microbiol. Biotechnol.* 104, 675–686. doi: 10.1007/s00253-019-10258-7

Chen, F. (1996). High cell density culture of microalgae in heterotrophic growth. *Trends Biotechnol.* 14, 421–426. doi: 10.1016/0167-7799(96)10060-3

Choi, H., Yi, T., and Ha, S.-H. (2021). Diversity of plastid types and their interconversions. *Front. Plant Sci.* 12, 1–14. doi: 10.3389/fpls.2021.692024

Choquet, Y., and Wollman, F. A. (2002). Translational regulations as specific traits of chloroplast gene expression. *FEBS Lett.* 529, 39–42. doi: 10.1016/S0014-5793(02)03260-X

Clark, M., and Maselko, M. (2020). Transgene biocontainment strategies for molecular farming. *Front. Plant Sci.* 11:210. doi: 10.3389/fpls.2020.00210

Cline, S. G., Laughbaum, I. A., and Hamel, P. P. (2017). CCS2, an octatricopeptide-repeat protein, is required for plastid cytochrome *c* assembly in the green alga *Chlamydomonas reinhardtii*. *Front. Plant Sci.* 8:1306. doi: 10.3389/fpls.2017.01306

Coragliotti, A. T., Beligni, M. V., Franklin, S. E., and Mayfield, S. P. (2011). Molecular factors affecting the accumulation of recombinant proteins in the *Chlamydomonas reinhardtii*. *Mol. Biotechnol.* 48, 60–75. doi: 10.1007/s12033-010-9348-4

Croft, M. T., Moulin, M., Webb, M. E., and Smith, A. G. (2007). Thiamine biosynthesis in algae is regulated by riboswitches. *Proc. Natl. Acad. Sci USA,* 104, 20770–20775. doi: 10.1073/pnas.0705786105

Crozet, P., Navarro, F. J., Willmund, F., Mehrshahi, P., Bakowski, K., Lauersen, K. J., et al. (2018). Birth of a photosynthetic chassis: aMoClo toolkit enabling synthetic biology in the microalga *Chlamydomonas reinhardtii*. *ACS Synth. Biol.* 7, 2074–2086. doi: 10.1021/acssynbio.8b00251

Cui, Y., Qin, S., and Jiang, P. (2014). Chloroplast transformation of *Platymonas (Tetraselmis) subcordiformis* with the *bar* gene as selectable marker. *PLoS ONE* 9:e98607. doi: 10.1371/journal.pone.0098607

Cummins, P. L., Kannappan, B., and Gready, J. E. (2018). Directions for optimization of photosynthetic carbon fixation: Rubisco's efficiency may not be so constrained after all. *Front. Plant Sci.* 9:183. doi: 10.3389/fpls.2018.00183

Curatti, L., and Rubio, L. M. (2014). Challenges to develop nitrogen-fixing cereals by direct *nif*-gene transfer. *Plant Sci.* 225, 130–137. doi: 10.1016/j.plantsci.2014.06.003

Dent, R. M., Sharifi, M. N., Malno,ë, A., Haglund, C., Calderon, R. H., Wakao, S., et al. (2015). Large-scale insertional mutagenesis of *Chlamydomonas* supports phylogenomic functional prediction of photosynthetic genes and analysis of classical acetate-requiring mutants. *Plant J.* 82, 337–351. doi: 10.1111/tpj.12806

Díaz-Gómez, J., Twyman, R. M., Zhu, C., Farr,é, G., Serrano, J. C., Portero-Otin, M., et al. (2017). Biofortification of crops with nutrients: factors affecting utilization and storage. *Curr. Opin. Biotechnol.* 44, 115–123. doi: 10.1016/j.copbio.2016.12.002

Ding, F., Wang, M., Zhang, S., and Ai, X. (2016). Changes in SBPase activity influence photosynthetic capacity, growth, and tolerance to chilling stress in transgenic tomato plants. *Sci. Rep.* 6, 1–14. doi: 10.1038/srep32741

Donoghue, P., and Paps, J. (2020). Plant evolution: assembling land plants. *Curr. Biol.* 30, R81–R83. doi: 10.1016/j.cub.2019.11.084

Duke, S. O. (2015). Perspectives on transgenic, herbicide-resistant crops in the United States almost 20 years after introduction. *Pest Manag. Sci.* 71, 652–657. doi: 10.1002/ps.3863

Dyo, Y. M., and Purton, S. (2018). The algal chloroplast as a synthetic biology platform for production of therapeutic proteins. *Microbiol* 164, 113–121. doi: 10.1099/mic.0.000599

Engler, C., Youles, M., Gruetzner, R., Ehnert, T. M., Werner, S., Jones, J. D. G., et al. (2014). A Golden Gate modular cloning toolbox for plants. *ACS Synth. Biol.* 3, 839–843. doi: 10.1021/sb4001504

Eseverri, Á., López-Torrejón, G., Jiang, X., Burén, S., Rubio, L. M., and Caro, E. (2020). Use of synthetic biology tools to optimize the production of active nitrogenase Fe protein in chloroplasts of tobacco leaf cells. *Plant Biotechnol. J.* 18, 1882–1896. doi: 10.1111/pbi.13347

Esland, L., Larrea-Alvarez, M., and Purton, S. (2018). Selectable markers and reporter genes for engineering the chloroplast of *Chlamydomonas reinhardtii*. *Biology* 7:46. doi: 10.3390/biology7040046

Faè, M., Accossato, S., Cella, R., Fontana, F., Goldschmidt-Clermont, M., Leelavathi, S., et al. (2017). Comparison of transplastomic *Chlamydomonas reinhardtii* and *Nicotiana tabacum* expression system for the production of a bacterial endoglucanase. *Appl. Microbiol. Biotechnol.* 101, 4085–4092. doi: 10.1007/s00253-017-8164-1

Fang, H., Li, D., Kang, J., Jiang, P., Sun, J., and Zhang, D. (2018). Metabolic engineering of *Escherichia coli* for *de novo* biosynthesis of vitamin B_{12}. *Nat. Commun.* 9, 1–12. doi: 10.1038/s41467-018-07412-6

Ferenczi, A., Pyott, D. E., Xipnitou, A., Molnar, A., and Merchant, S. S. (2017). Efficient targeted DNA editing and replacement in *Chlamydomonas reinhardtii* using Cpf1 ribonucleoproteins and single-stranded DNA. *Proc. Natl. Acad. Sci. U.S.A.* 114, 13567–13572. doi: 10.1073/pnas.1710597114

Fredens, J., Wang, K., de la Torre, D., Funke, L. F. H., Robertson, W. E., Christova, Y., et al. (2019). Total synthesis of *Escherichia coli* with a recoded genome. *Nature* 569, 514–518. doi: 10.1038/s41586-019-1192-5

Fuentes, P., Armarego-Marriott, T., and Bock, R. (2018). Plastid transformation and its application in metabolic engineering. *Curr. Opin. Biotechnol.* 49, 10–15. doi: 10.1016/j.copbio.2017.07.004

Gallaher, S. D., Fitz-Gibbon, S. T., Strenkert, D., Purvine, S. O., Pellegrini, M., and Merchant, S. S. (2018). High-throughput sequencing of the chloroplast and mitochondrion of *Chlamydomonas reinhardtii* to generate improved *de novo* assemblies, analyze expression patterns and transcript speciation, and evaluate diversity among laboratory strains and wild isolates. *Plant J.* 93, 545–565. doi: 10.1111/tpj.13788

Gan, Q., Jiang, J., Han, X., Wang, S., and Lu, Y. (2018). Engineering the chloroplast genome of oleaginous marine microalga *Nannochloropsis oceanica*. *Front. Plant Sci.* 9:439. doi: 10.3389/fpls.2018.00439

Gangl, D., Zedler, J. A. Z., Włodarczyk, A., Jensen, P. E., Purton, S., and Robinson, C. (2015). Expression and membrane-targeting of an active plant cytochrome P450 in the chloroplast of the green alga *Chlamydomonas reinhardtii*. *Phytochemistry* 110, 22–28. doi: 10.1016/j.phytochem.2014.12.006

Georgianna, D. R., Hannon, M. J., Marcuschi, M., Wu, S., Botsch, K., Lewis, A. J., et al. (2013). Production of recombinant enzymes in the marine alga *Dunaliella tertiolecta*. *Algal Res.* 2, 2–9. doi: 10.1016/j.algal.2012.10.004

Gimpel, J. A., Henríquez, V., and Mayfield, S. P. (2015). In metabolic engineering of eukaryotic microalgae: Potential and challenges come with great diversity. *Front. Microbiol.* 6:1376. doi: 10.3389/fmicb.2015.01376

Gimpel, J. A., Nour-Eldin, H. H., Scranton, M. A., Li, D., and Mayfield, S. P. (2016). Refactoring the six-gene photosystem II core in the chloroplast of the green algae *Chlamydomonas reinhardtii*. *ACS Synth. Biol.* 5, 589–596. doi: 10.1021/acssynbio.5b00076

Gorchs-Rovira, A., and Smith, A. G. (2019). PPR proteins – orchestrators of organelle RNA metabolism. *Physiol. Plant.* 166, 451–459. doi: 10.1111/ppl.12950

Grassini, P., Eskridge, K. M., and Cassman, K. G. (2013). Distinguishing between yield advances and yield plateaus in historical crop production trends. *Nat. Commun.* 4, 1–11. doi: 10.1038/ncomms3918

Green, B. R. (2011). Chloroplast genomes of photosynthetic eukaryotes. *Plant J.* 66, 34–44. doi: 10.1111/j.1365-313X.2011.04541.x

Haire, T. C., Bell, C., Cutshaw, K., Swiger, B., Winkelmann, K., and Palmer, A. G. (2018). Robust microplate-based methods for culturing and *in vivo* phenotypic screening of *Chlamydomonas reinhardtii*. *Front. Plant Sci.* 9:235. doi: 10.3389/fpls.2018.00235

Hardy, R. W. F., and Havelka, U. D. (1975). Nitrogen fixation research: A key to world food? *Science* 188, 633–643. doi: 10.1126/science.188.4188.633

Harris, E. H. (2009). *The Chlamydomonas Sourcebook: Introduction to Chlamydomonas and Its Laboratory Use*. San Diego, CA: Academic Press.

Hsu, S. C., Browne, D. R., Tatli, M., Devarenne, T. P., and Stern, D. B. (2019). N-terminal sequences affect expression of triterpene biosynthesis enzymes in *Chlamydomonas* chloroplasts. *Algal Res.* 44:101662. doi: 10.1016/j.algal.2019.101662

Jalal, A., Schwarz, C., Schmitz-Linneweber, C., Vallon, O., Nickelsen, J., and Bohne, A. V. (2015). A small multifunctional pentatricopeptide repeat protein in the chloroplast of *Chlamydomonas reinhardtii*. *Mol. Plant* 8, 412–426. doi: 10.1016/j.molp.2014.11.019

Johnson, X., Wostrikoff, K., Finazzi, G., Kuras, R., Schwarz, C., Bujaldon, S., et al. (2010). MRL1, a conserved pentatricopeptide repeat protein, is required for stabilization of *rbcL* mRNA in *Chlamydomonas* and *Arabidopsis*. *Plant Cell* 22, 234–248. doi: 10.1105/tpc.109.066266

Kamimura, Y., Tanaka, H., Kobayashi, Y., Shikanai, T., and Nishimura, Y. (2018). Chloroplast nucleoids as a transformable network revealed by live imaging with a microfluidic device. *Commun. Biol.* 1, 1–7. doi: 10.1038/s42003-018-0055-1

Khrebtukova, I., and Spreitzer, R. J. (1996). Elimination of the *Chlamydomonas* gene family that encodes the small subunit of ribulose-1,5-bisphosphate carboxylase/oxygenase. *Proc. Natl. Acad. Sci. U.S.A.* 93, 13689–13693. doi: 10.1073/pnas.93.24.13689

Kim, H. S., Hsu, S. C., Han, S. I., Thapa, H. R., Guzman, A. R., Browne, D. R., et al. (2017). High-throughput droplet microfluidics screening platform for selecting fast-growing and high lipid-producing microalgae from a mutant library. *Plant Direct* 1:e00011. doi: 10.1002/pld3.11

Kubis, A., and Bar-Even, A. (2019). Synthetic biology approaches for improving photosynthesis. *J. Exp. Bot.* 70, 1425–1433. doi: 10.1093/jxb/erz029

Lachance, J.-C., Rodrigue, S., and Palsson, B. O. (2019). Synthetic biology: minimal cells, maximal knowledge. *Elife* 8, 1–4. doi: 10.7554/eLife.45379

Larrea-Alvarez, M., and Purton, S. (2020). Multigenic engineering of the chloroplast genome in the green alga *Chlamydomonas reinhardtii*. *Microbiol* 166, 510–515. doi: 10.1099/mic.0.000910

Larrea-Alvarez, M., Young, R., and Purton, S. (2021). A simple technology for generating marker-free chloroplast transformants of the green alga *Chlamydomonas reinhardtii*. *Methods Mol. Biol.* 2317, 293–304. doi: 10.1007/978-1-0716-1472-3_17

Lassen, L. M., Nielsen, A. Z., Olsen, C. E., Bialek, W., Jensen, K., Møller, B. L., et al. (2014a). Anchoring a plant cytochrome P450 via PsaM to the thylakoids in *Synechococcus* sp. PCC 7002: Evidence for light-driven biosynthesis. *PLoS ONE* 9:e102184. doi: 10.1371/journal.pone.0102184

Lassen, L. M., Nielsen, A. Z., Ziersen, B., Gnanasekaran, T., Møller, B. L., and Jensen, P. E. (2014b). Redirecting photosynthetic electron flow into light-driven synthesis of alternative products including high-value bioactive natural compounds. *ACS Synth. Biol.* 3, 1–12. doi: 10.1021/sb400136f

Lau, K. W. K., Ren, J., and Wu, M. (2000). Redox modulation of chloroplast DNA replication in *Chlamydomonas reinhardtii*. *Antioxidants Redox Signal.* 2, 529–535. doi: 10.1089/15230860050192305

Lauersen, K. J. (2019). Eukaryotic microalgae as hosts for light-driven heterologous isoprenoid production. *Planta* 249, 155–180. doi: 10.1007/s00425-018-3048-x

Lauersen, K. J., Kruse, O., and Mussgnug, J. H. (2015). Targeted expression of nuclear transgenes in *Chlamydomonas reinhardtii* with a versatile, modular vector toolkit. *Appl. Microbiol. Biotechnol.* 99, 3491–3503. doi: 10.1007/s00253-014-6354-7

Lauersen, K. J., Wichmann, J., Baier, T., Kampranis, S. C., Pateraki, I., Møller, B. L., et al. (2018). Phototrophic production of heterologous diterpenoids and a hydroxy-functionalized derivative from *Chlamydomonas reinhardtii*. *Metab. Eng.* 49, 116–127. doi: 10.1016/j.ymben.2018.07.005

Lee, M. E., DeLoache, W. C., Cervantes, B., and Dueber, J. E. (2015). A highly characterized yeast toolkit for modular, multipart assembly. *ACS Synth. Biol.* 4, 975–986. doi: 10.1021/sb500366v

Leister, D. (2019). Genetic engineering, synthetic biology and the light reactions of photosynthesis. *Plant Physiol.* 179, 778–793. doi: 10.1104/pp.18.00360

Liu, D., Liberton, M., Yu, J., Pakrasi, H. B., and Bhattacharyya-Pakrasi, M. (2018). Engineering nitrogen fixation activity in an oxygenic phototroph. *MBio* 9:18. doi: 10.1128/mBio.01029-18

Loganathan, N., Tsai, Y. C. C., and Mueller-Cajar, O. (2016). Characterization of the heterooligomeric red-type rubisco activase from red algae. *Proc. Natl. Acad. Sci. U.S.A.* 113, 14019–14024. doi: 10.1073/pnas.1610758113

Long, B. M., Rae, B. D., Rolland, V., Förster, B., and Price, G. D. (2016). Cyanobacterial CO_2-concentrating mechanism components: Function and prospects for plant metabolic engineering. *Curr. Opin. Plant Biol.* 31, 1–8. doi: 10.1016/j.pbi.2016.03.002

López-Torrejón, G., Jiménez-Vicente, E., Buesa, J. M., Hernandez, J. A., Verma, H. K., and Rubio, L. M. (2016). Expression of a functional oxygen-labile nitrogenase component in the mitochondrial matrix of aerobically grown yeast. *Nat. Commun.* 7, 1–6. doi: 10.1038/ncomms11426

Lu, Y., Rijzaani, H., Karcher, D., Ruf, S., and Bock, R. (2013). Efficient metabolic pathway engineering in transgenic tobacco and tomato plastids with synthetic multigene operons. *Proc. Natl. Acad. Sci. U.S.A.* 110, E623–E632. doi: 10.1073/pnas.1216898110

Macedo-Osorio, K. S., Pérez-España, V. H., Garibay-Orijel, C., Guzmán-Zapata, D., Durán-Figueroa, N. V., and Badillo-Corona, J. A. (2018). Intercistronic expression elements (IEE) from the chloroplast of *Chlamydomonas reinhardtii* can be used for the expression of foreign genes in synthetic operons. *Plant Mol. Biol.* 98, 303–317. doi: 10.1007/s11103-018-0776-z

Mackinder, L. C. M. (2018). The *Chlamydomonas* CO_2-concentrating mechanism and its potential for engineering photosynthesis in plants. *New Phytol.* 217, 54–61. doi: 10.1111/nph.14749

Martin-Avila, E., Lim, Y. L., Birch, R., Dirk, L. M. A., Buck, S., Rhodes, T., et al. (2020). Modifying plant photosynthesis and growth via simultaneous chloroplast transformation of rubisco large and small subunits. *Plant Cell* 32, 2898–2916. doi: 10.1105/TPC.20.00288

Marx, C., Wünsch, C., and Kück, U. (2015). The octatricopeptide repeat protein RAA8 is required for chloroplast *trans* splicing. *Eukaryot. Cell* 14, 998–1005. doi: 10.1128/EC.00096-15

Maul, J. E., Lilly, J. W., Cui, L., DePamphilis, C. W., Miller, W., Harris, E. H., et al. (2002). The *Chlamydomonas reinhardtii* plastid chromosome: Islands of genes in a sea of repeats. *Plant Cell* 14, 2659–2679. doi: 10.1105/tpc.006155

Mehrshahi, P., Nguyen, G. T. D. T., Gorchs-Rovira, A., Sayer, A., Llavero-Pasquina, M., Lim Huei Sin, M., et al. (2020). Development of novel riboswitches for synthetic biology in the green alga *Chlamydomonas*. *ACS Synth. Biol.* 9, 1406–1417. doi: 10.1021/acssynbio.0c00082

Mellor, S. B., Vavitsas, K., Nielsen, A. Z., and Jensen, P. E. (2017). Photosynthetic fuel for heterologous enzymes: the role of electron carrier proteins. *Photosynth. Res.* 134, 329–342. doi: 10.1007/s11120-017-0364-0

Merrick, M., and Dixon, R. (1984). Why don't plants fix nitrogen? *Trends Biotechnol.* 2, 162–166. doi: 10.1016/0167-7799(84)90034-9

Neuhaus, H. E., and Emes, M. J. (2000). Non-photosynthetic metabolism in plastids. *Annu. Rev. Plant Physiol.* 51, 111–134. doi: 10.1146/annurev.arplant.51.1.111

Newman, S. M., Gillham, N. W., Harris, E. H., Johnson, A. M., and Boynton, J. E. (1991). Targeted disruption of chloroplast genes in *Chlamydomonas reinhardtii*. *Mol. Gen. Genet.* 230, 65–74. doi: 10.1007/BF00290652

Nickelsen, J., Van Dillewijn, J., Rahire, M., and Rochaix, J. D. (1994). Determinants for stability of the chloroplast *psbD* RNA are located within its short leader region in *Chlamydomonas reinhardtii*. *EMBO J.* 13, 3182–3191. doi: 10.1002/j.1460-2075.1994.tb06617.x

Nielsen, A. Z., Mellor, S. B., Vavitsas, K., Wlodarczyk, A. J., Gnanasekaran, T., Perestrello Ramos H de Jesus, M., et al. (2016). Extending the biosynthetic repertoires of cyanobacteria and chloroplasts. *Plant J.* 87, 87–102. doi: 10.1111/tpj.13173

Noor-Mohammadi, S., Pourmir, A., and Johannes, T. W. (2012). Method to assemble and integrate biochemical pathways into the chloroplast genome of *Chlamydomonas reinhardtii*. *Biotechnol. Bioeng.* 109, 2896–2903. doi: 10.1002/bit.24569

Nouemssi, S. B., Ghribi, M., Beauchemin, R., Meddeb-Mouelhi, F., Germain, H., and Desgagné-Penix, I. (2020). Rapid and efficient colony-PCR for high throughput screening of genetically transformed *Chlamydomonas reinhardtii*. *Life* 10, 1–13. doi: 10.3390/life10090186

Obembe, O. O., Popoola, J. O., Leelavathi, S., and Reddy, S. V. (2011). Advances in plant molecular farming. *Biotechnol. Adv.* 29, 210–222. doi: 10.1016/j.biotechadv.2010.11.004

Oborník, M., and Green, B. R. (2005). Mosaic origin of the heme biosynthesis pathway in photosynthetic eukaryotes. *Mol. Biol. Evol.* 22, 2343–2353. doi: 10.1093/molbev/msi230

Occhialini, A., Piatek, A. A., Pfotenhauer, A. C., Frazier, T. P., Stewart, C. N., and Lenaghan, S. C. (2019). MoChlo: A versatile, modular cloning toolbox for chloroplast biotechnology. *Plant Physiol.* 179, 943–957. doi: 10.1104/pp.18.01220

Oey, M., Ross, I. L., and Hankamer, B. (2014). Gateway-assisted vector construction to facilitate expression of foreign proteins in the chloroplast of single celled algae. *PLoS ONE* 9:e86841. doi: 10.1371/journal.pone.0086841

O'Neill, B. M., Mikkelson, K. L., Gutierrez, N. M., Cunningham, J. L., Wolff, K. L., Szyjka, S. J., et al. (2012). An exogenous chloroplast genome for complex sequence manipulation in algae. *Nucleic Acids Res.* 40, 2782–2792. doi: 10.1093/nar/gkr1008

Opgenorth, P., Costello, Z., Okada, T., Goyal, G., Chen, Y., Gin, J., et al. (2019). Lessons from two design-build-test-learn cycles of dodecanol production in *Escherichia coli* aided by machine learning. *ACS Synth. Biol.* 8, 1337–1351. doi: 10.1021/acssynbio.9b00020

Ozawa, S. I., Cavaiuolo, M., Jarrige, D., Kuras, R., Rutgers, M., Eberhard, S., et al. (2020). The OPR protein MTHI1 controls the expression of two different subunits of ATP synthase CFo in *Chlamydomonas reinhardtii*. *Plant Cell* 32, 1179–1203. doi: 10.1105/TPC.19.00770

Paddon, C. J., Westfall, P. J., Pitera, D. J., Benjamin, K., Fisher, K., McPhee, D., et al. (2013). High-level semi-synthetic production of the potent antimalarial artemisinin. *Nature* 496, 528–532. doi: 10.1038/nature12051

Pan, J., Stephenson, A. L., Kazamia, E., Huck, W. T. S., Dennis, J. S., Smith, A. G., et al. (2011). Quantitative tracking of the growth of individual algal cells in microdroplet compartments. *Integr. Biol.* 3, 1043–1051. doi: 10.1039/c1ib00033k

Perera-Castro, A. V., and Flexas, J. (2020). Recent advances in understanding and improving photosynthesis. *Fac. Rev.* 9:5. doi: 10.12703/b/9-5

Pingali, P. L. (2012). Green revolution: Impacts, limits, andthe path ahead. *Proc. Natl. Acad. Sci. U.S.A.* 109, 12302–12308. doi: 10.1073/pnas.0912953109

Pouvreau, B., Vanhercke, T., and Singh, S. (2018). From plant metabolic engineering to plant synthetic biology: The evolution of the design/build/test/learn cycle. *Plant Sci.* 273, 3–12. doi: 10.1016/j.plantsci.2018.03.035

Purton, S. (2007). Tools and techniques for chloroplast transformation of *Chlamydomonas*. *Adv. Exp. Med. Biol.* 616, 34–45. doi: 10.1007/978-0-387-75532-8_4

Purton, S., Szaub, J. B., Wannathong, T., Young, R., and Economou, C. K. (2013). Genetic engineering of algal chloroplasts: progress and prospects. *Russ. J. Plant Physiol.* 60, 491–499. doi: 10.1134/S1021443713040146

Puthiyaveetil, S., McKenzie, S. D., Kayanja, G. E., and Ibrahim, I. M. (2021). Transcription initiation as a control point in plastid gene expression. *Biochim. Biophys. Acta - Gene Regul. Mech.* 1864:194689. doi: 10.1016/j.bbagrm.2021.194689

Quinn, J. M., Eriksson, M., Moseley, J. L., and Merchant, S. (2002). Oxygen deficiency responsive gene expression in *Chlamydomonas reinhardtii* through a copper-sensing signal transduction pathway. *Plant Physiol.* 128, 463–471. doi: 10.1104/pp.010694

Rae, B. D., Long, B. M., Förster, B., Nguyen, N. D., Velanis, C. N., Atkinson, N., et al. (2017). Progress and challenges of engineering a biophysical CO_2-concentrating mechanism into higher plants. *J. Exp. Bot.* 68, 3717–3737. doi: 10.1093/jxb/erx133

Ramundo, S., and Rochaix, J. D. (2015). Controlling expression of genes in the unicellular alga *Chlamydomonas reinhardtii* with a vitamin-repressible riboswitch. *Methods Enzymol.*, 550, 267–281. doi: 10.1016/bs.mie.2014.10.035

Rasala, B. A., Barrera, D. J., Ng, J., Plucinak, T. M., Rosenberg, J. N., Weeks, D. P., et al. (2013). Expanding the spectral palette of fluorescent proteins for the green microalga *Chlamydomonas reinhardtii*. *Plant J.* 74, 545–556. doi: 10.1111/tpj.12165

Rasala, B. A., Muto, M., Sullivan, J., and Mayfield, S. P. (2011). Improved heterologous protein expression in the chloroplast of *Chlamydomonas reinhardtii* through promoter and 5' untranslated region optimization. *Plant Biotechnol. J.* 9, 674–683. doi: 10.1111/j.1467-7652.2011.00620.x

Reinbothe, C., Bakkouri, M., El Buhr, F., Muraki, N., Nomata, J., Kurisu, G., et al. (2010). Chlorophyll biosynthesis: Spotlight on protochlorophyllide reduction. *Trends Plant Sci.* 15, 614–624. doi: 10.1016/j.tplants.2010.07.002

Rochaix, J. D. (2002). *Chlamydomonas*, a model system for studying the assembly and dynamics of photosynthetic complexes. *FEBS Lett.* 529, 34–38. doi: 10.1016/S0014-5793(02)03181-2

Rochaix, J. D., Surzycki, R., and Ramundo, S. (2014). Tools for regulated gene expression in the chloroplast of *Chlamydomonas*. *Methods Mol. Biol.* 1132, 413–424. doi: 10.1007/978-1-62703-995-6_28

Rodrigues, N. F., Christoff, A. P., da Fonseca, G. C., Kulcheski, F. R., and Margis, R. (2017). Unveiling chloroplast RNA editing events using next generation small RNA sequencing data. *Front. Plant Sci.* 8:1686. doi: 10.3389/fpls.2017.01686

Rogers, C., and Oldroyd, G. E. D. (2014). Synthetic biology approaches to engineering the nitrogen symbiosis in cereals. *J. Exp. Bot.* 65, 1939–1946. doi: 10.1093/jxb/eru098

Rosenblueth, M., Ormeño-Orrillo, E., López-López, A., Rogel, M. A., Reyes-Hernández, B. J., Martínez-Romero, J. C., et al. (2018). Nitrogen fixation in cereals. *Front. Microbiol.* 9:1794. doi: 10.3389/fmicb.2018.01794

Salomé, P. A., and Merchant, S. S. (2019). A series of fortunate events: Introducing *Chlamydomonas* as a reference organism. *Plant Cell* 31, 1682–1707. doi: 10.1105/tpc.18.00952

Sasso, S., Stibor, H., Mittag, M., and Grossman, A. R. (2018). The natural history of model organisms from molecular manipulation of domesticated *Chlamydomonas reinhardtii* to survival in nature. *Elife* 7, 1–14. doi: 10.7554/eLife.39233

Scharff, L. B., and Bock, R. (2014). Synthetic biology in plastids. *Plant J.* 78, 783–798. doi: 10.1111/tpj.12356

Schindel, H. S., Piatek, A. A., Stewart, C. N., and Lenaghan, S. C. (2018). The plastid genome as a chassis for synthetic biology-enabled metabolic engineering: players in gene expression. *Plant Cell Rep.* 37, 1419–1429. doi: 10.1007/s00299-018-2323-4

Shao, N., and Bock, R. (2008). A codon-optimized luciferase from *Gaussia princeps* facilitates the *in vivo* monitoring of gene expression in the model alga *Chlamydomonas reinhardtii*. *Curr. Genet.* 53, 381–388. doi: 10.1007/s00294-008-0189-7

Sharwood, R. E. (2017). Engineering chloroplasts to improve Rubisco catalysis: prospects for translating improvements into food and fiber crops. *New Phytol.* 213, 494–510. doi: 10.1111/nph.14351

Siegel, J. B., Smith, A. L., Poust, S., Wargacki, A. J., Bar-Even, A., Louw, C., et al. (2015). Computational protein design enables a novel one-carbon assimilation pathway. *Proc. Natl. Acad. Sci. U.S.A.* 112, 3704–3709. doi: 10.1073/pnas.1500545112

Simkin, A. J., Lopez-Calcagno, P. E., Davey, P. A., Headland, L. R., Lawson, T., Timm, S., et al. (2017). Simultaneous stimulation of sedoheptulose 1,7-bisphosphatase, fructose 1,6-bisphophate aldolase and the photorespiratory glycine decarboxylase-H protein increases CO_2 assimilation, vegetative biomass and seed yield in Arabidopsis. *Plant Biotechnol. J.* 15, 805–816. doi: 10.1111/pbi.12676

Simkin, A. J., McAusland, L., Headland, L. R., Lawson, T., and Raines, C. A. (2015). Multigene manipulation of photosynthetic carbon assimilation increases CO_2 fixation and biomass yield in tobacco. *J. Exp. Bot.* 66, 4075–4090. doi: 10.1093/jxb/erv204

Small, I. D., Schallenberg-Rüdinger, M., Takenaka, M., Mireau, H., and Ostersetzer-Biran, O. (2020). Plant organellar RNA editing: what 30 years of research has revealed. *Plant J.* 101, 1040–1056. doi: 10.1111/tpj.14578

Smith, A. C., and Purton, S. (2002). The transcriptional apparatus of algal plastids. *Eur. J. Phycol.* 37, 301–311. doi: 10.1017/S0967026202003694

Smith, A. G., Croft, M. T., Moulin, M., and Webb, M. E. (2007). Plants need their vitamins too. *Curr. Opin. Plant Biol.* 10, 266–275. doi: 10.1016/j.pbi.2007.04.009

Smith, D. R., and Lee, R. W. (2009). Nucleotide diversity of the *Chlamydomonas reinhardtii* plastid genome: addressing the mutational-hazard hypothesis. *BMC Evol. Biol.* 9, 1–9. doi: 10.1186/1471-2148-9-120

Specht, E. A., and Mayfield, S. P. (2013). Synthetic oligonucleotide libraries reveal novel regulatory elements in *Chlamydomonas* chloroplast mRNAs. *ACS Synth. Biol.* 2, 34–46. doi: 10.1021/sb300069k

Stoffels, L., Taunt, H. N., Charalambous, B., and Purton, S. (2017). Synthesis of bacteriophage lytic proteins against *Streptococcus pneumoniae* in the chloroplast of *Chlamydomonas reinhardtii*. *Plant Biotechnol. J.* 15, 1130–1140. doi: 10.1111/pbi.12703

Surzycki, R., Cournac, L., Peltier, G., and Rochaix, J. D. (2007). Potential for hydrogen production with inducible chloroplast gene expression in *Chlamydomonas*. *Proc. Natl. Acad. Sci. U.S.A.* 104, 17548–17553. doi: 10.1073/pnas.0704205104

Sutton, M. A., Oenema, O., Erisman, J. W., Leip, A., Van Grinsven, H., and Winiwarter, W. (2011). Too much of a good thing. *Nature* 472, 159–161. doi: 10.1038/472159a

Tabashnik, B. E., Brévault, T., and Carrière, Y. (2013). Insect resistance to Bt crops: Lessons from the first billion acres. *Nat. Biotechnol.* 31, 510–521. doi: 10.1038/nbt.2597

Taunt, H. N., Stoffels, L., and Purton, S. (2018). Green biologics: The algal chloroplast as a platform for making biopharmaceuticals. *Bioengineered* 9, 48–54. doi: 10.1080/21655979.2017.1377867

Taylor, G. M., Mordaka, P. M., and Heap, J. T. (2019). Start-Stop Assembly: A functionally scarless DNA assembly system optimized for metabolic engineering. *Nucleic Acids Res.* 47:e17. doi: 10.1093/nar/gky1182

Trinugroho, J. P., Bečkov,á, M., Shao, S., Yu, J., Zhao, Z., Murray, J. W., et al. (2020). Chlorophyll *f* synthesis by a super-rogue photosystem II complex. *Nat. Plants* 6, 238–244. doi: 10.1038/s41477-020-0616-4

Vasudevan, R., Gale, G. A. R., Schiavon, A. A., Puzorjov, A., Malin, J., Gillespie, M. D., et al. (2019). Cyanogate: A modular cloning suite for engineering

cyanobacteria based on the plant moclo syntax. *Plant Physiol.* 180, 39–55. doi: 10.1104/pp.18.01401

Vavitsas, K., Fabris, M., and Vickers, C. E. (2018). Terpenoid metabolic engineering in photosynthetic microorganisms. *Genes* 9:520. doi: 10.3390/genes9110520

Velmurugan, N., Sung, M., Yim, S. S., Park, M. S., Yang, J. W., and Jeong, K. J. (2013). Evaluation of intracellular lipid bodies in *Chlamydomonas reinhardtii* strains by flow cytometry. *Bioresour. Technol.* 138, 30–37. doi: 10.1016/j.biortech.2013.03.078

Venegas-Calerón, M., Sayanova, O., and Napier, J. A. (2010). An alternative to fish oils: Metabolic engineering of oil-seed crops to produce omega-3 long chain polyunsaturated fatty acids. *Prog. Lipid Res.* 49, 108–119. doi: 10.1016/j.plipres.2009.10.001

Viola, S., Cavaiuolo, M., Drapier, D., Eberhard, S., Vallon, O., Wollman, F. A., et al. (2019). MDA1, a nucleus-encoded factor involved in the stabilization and processing of the atpA transcript in the chloroplast of *Chlamydomonas*. *Plant J.* 98, 1033–1047. doi: 10.1111/tpj.14300

Wannathong, T., Waterhouse, J. C., Young, R. E. B., Economou, C. K., and Purton, S. (2016). New tools for chloroplast genetic engineering allow the synthesis of human growth hormone in the green alga *Chlamydomonas reinhardtii*. *Appl. Microbiol. Biotechnol.* 100, 5467–5477. doi: 10.1007/s00253-016-7354-6

Warren, M. J., Raux, E., Schubert, H. L., and Escalante-Semerena, J. C. (2002). The biosynthesis of adenosylcobalamin (vitamin B_{12}). *Nat. Prod. Rep.* 19, 390–412. doi: 10.1039/b108967f

Weber, E., Engler, C., Gruetzner, R., Werner, S., and Marillonnet, S. (2011). A modular cloning system for standardized assembly of multigene constructs. *PLoS ONE* 6:e16765. doi: 10.1371/journal.pone.0016765

Wichmann, J., Lauersen, K. J., and Kruse, O. (2020). Green algal hydrocarbon metabolism is an exceptional source of sustainable chemicals. *Curr. Opin. Biotechnol.* 61, 28–37. doi: 10.1016/j.copbio.2019.09.019

Wietrzynski, W., Schaffer, M., Tegunov, D., Albert, S., Kanazawa, A., Plitzko, J. M., et al. (2020). Charting the native architecture of *Chlamydomonas* thylakoid membranes with single-molecule precision. *Elife* 9, 1–19. doi: 10.7554/eLife.53740

Xiang, N., Guo, C., Liu, J., Xu, H., Dixon, R., Yang, J., et al. (2020). Using synthetic biology to overcome barriers to stable expression of nitrogenase in eukaryotic organelles. *Proc. Natl. Acad. Sci. U.S.A.* 117, 16537–16545. doi: 10.1073/pnas.2002307117

Young, R., and Purton, S. (2018). CITRIC: Cold-inducible translational readthrough in the chloroplast of *Chlamydomonas reinhardtii* using a novel temperature-sensitive transfer RNA. *Microb. Cell Fact.* 17:186. doi: 10.1186/s12934-018-1033-5

Young, R. E. B., and Purton, S. (2016). Codon reassignment to facilitate genetic engineering and biocontainment in the chloroplast of *Chlamydomonas reinhardtii*. *Plant Biotechnol. J.* 14, 1251–1260. doi: 10.1111/pbi.12490

Yu, Y., Yu, P. C., Chang, W. J., Yu, K., and Lin, C. S. (2020). Plastid transformation: How does it work? Can it be applied to crops? what can it offer? *Int. J. Mol. Sci.* 21, 1–21. doi: 10.3390/ijms21144854

Yu, Z., Geisler, K., Leontidou, T., Young, R., Vonlanthen, S., Purton, S., et al. (2021). Droplet-based microfluidic screening and sorting of microalgal populations for strain engineering applications. *Algal Res.* 56:102293. doi: 10.1016/j.algal.2021.102293

Conflict of Interest: The authors declare that the research was conducted in the absence of any commercial or financial relationships that could be construed as a potential conflict of interest.

Publisher's Note: All claims expressed in this article are solely those of the authors and do not necessarily represent those of their affiliated organizations, or those of the publisher, the editors and the reviewers. Any product that may be evaluated in this article, or claim that may be made by its manufacturer, is not guaranteed or endorsed by the publisher.

frontiers in Plant Science

ORIGINAL RESEARCH
published: 25 November 2021
doi: 10.3389/fpls.2021.758290

Complete Chloroplast Genome Sequence of *Erigeron breviscapus* and Characterization of Chloroplast Regulatory Elements

Yifan Yu[1,2], Zhen Ouyang[1], Juan Guo[2], Wen Zeng[2], Yujun Zhao[2] and Luqi Huang[1,2]**

[1]School of Food and Biological Engineering, Jiangsu University, Zhenjiang, China, [2]State Key Laboratory Breeding Base of Dao-di Herbs, National Resource Center for Chinese Materia Medica, China Academy of Chinese Medical Sciences, Beijing, China

Erigeron breviscapus is a famous medicinal plant. However, the limited chloroplast genome information of *E. breviscapus*, especially for the chloroplast DNA sequence resources, has hindered the study of *E. breviscapus* chloroplast genome transformation. Here, the complete chloroplast (cp) genome of *E. breviscapus* was reported. This genome was 152,164 bp in length, included 37.2% GC content and was structurally arranged into two 24,699 bp inverted repeats (IRs) and two single-copy areas. The sizes of the large single-copy region and the small single-copy region were 84,657 and 18,109 bp, respectively. The *E. breviscapus* cp genome consisted of 127 coding genes, including 83 protein coding genes, 36 transfer RNA (tRNA) genes, and eight ribosomal RNA (rRNA) genes. For those genes, 95 genes were single copy genes and 16 genes were duplicated in two inverted regions with seven tRNAs, four rRNAs, and five protein coding genes. Then, genomic DNA of *E. breviscapus* was used as a template, and the endogenous 5' and 3' flanking sequences of the *trnI* gene and *trnA* gene were selected as homologous recombinant fragments in vector construction and cloned through PCR. The endogenous 5' flanking sequences of the *psbA* gene and *rrn16S* gene, the endogenous 3' flanking sequences of the *psbA* gene, *rbcL* gene, and *rps16* gene and one sequence element from the psbN-psbH chloroplast operon were cloned, and certain chloroplast regulatory elements were identified. Two homologous recombination fragments and all of these elements were constructed into the cloning vector pBluescript SK (+) to yield a series of chloroplast expression vectors, which harbored the reporter gene *EGFP* and the selectable marker *aadA* gene. After identification, the chloroplast expression vectors were transformed into *Escherichia coli* and the function of predicted regulatory elements was confirmed by a spectinomycin resistance test and fluorescence intensity measurement. The results indicated that *aadA* gene and *EGFP* gene were efficiently expressed under the regulation of predicted regulatory elements and the chloroplast expression vector had been successfully constructed, thereby providing a solid foundation for establishing subsequent *E. breviscapus* chloroplast transformation system and genetic improvement of *E. breviscapus*.

Keywords: *Erigeron breviscapus*, chloroplast genome sequencing, chloroplast regulatory elements, gene assembly, prokaryotic expression

OPEN ACCESS

Edited by:
Thomas D. Sharkey, Michigan State University, United States

Reviewed by:
Jitesh Kumar, University of Minnesota Twin Cities, United States
Yongbo Duan, Huaibei Normal University, China

****Correspondence:***
Yujun Zhao
zhaoyj@nrc.ac.cn
Luqi Huang
huangluqi01@126.com

Specialty section:
This article was submitted to Plant Biotechnology, a section of the journal Frontiers in Plant Science

Received: *13 August 2021*
Accepted: *20 October 2021*
Published: *25 November 2021*

Citation:
Yu Y, Ouyang Z, Guo J, Zeng W, Zhao Y and Huang L (2021) Complete Chloroplast Genome Sequence of Erigeron breviscapus and Characterization of Chloroplast Regulatory Elements. Front. Plant Sci. 12:758290. doi: 10.3389/fpls.2021.758290

INTRODUCTION

Erigeron breviscapus (Vant.) Hand-Mazz. is a well-known medicinal plant that belongs to the family Asteraceae, and it is distributed in the southwestern region of China, mainly in Yunnan, Sichuan, Guizhou, and Guangxi Provinces (Li et al., 2013). This herb is commonly used for treating occlusive cerebrovascular disease and sequelae of cerebral hemorrhage and for improving microcirculation, reducing blood viscosity, and preventing platelet aggregation (Li et al., 1998; Sheng et al., 1999; Liu et al., 2010). In addition, *E. breviscapus* has the characteristics of a short growth period, strong vitality, an efficient tissue culture system (Chen et al., 2018), and available genomic information (Jiang et al., 2014; Yang et al., 2017).

However, with the in-depth study of *E. breviscapus* chloroplasts, the current research on the genetic background of this species mainly focuses on the use of the chloroplast genome of *E. breviscapus* for phylogenetic research and germplasm resource protection (Li et al., 2019; Meng et al., 2019), Meng et al. (2019) used the Illumina sequencing platform to obtain a chloroplast genome with a size of 152,183 bp, but the article only briefly mentioned the basic structural information of the species's chloroplast genome and the type and number of genes, and the phylogenetic position of *E. breviscapus* was determined. Li et al. (2019) used the Illumina sequencing platform to obtain a chloroplast genome with a size of 152,367 bp, and only briefly introduced the basic structural information of the species's chloroplast genome and the type and number of genes in the article, and the phylogenetic analysis was conducted to infer phylogenetic position of *E. breviscapus* and *Erigeron multiradiatus* within the family of Asteraceae, the above two reports did not mention the test data and its quality control. Both of the above mentioned studies lacked systematic prediction of the gene structure of the chloroplast genome of *E. breviscapus* and bioinformatics analysis such as codon usage bias analysis and simple sequence repeat (SSR) analysis. In addition, the relevant regulatory elements of the chloroplasts of this species have not been identified. Therefore, for follow-up research on the establishment of the chloroplast genetic transformation system of *E. breviscapus*, it is necessary to obtain a complete *E. breviscapus* cp genome and screen out highly efficient genetic regulatory elements.

Previous studies have reported some chloroplast regulatory elements and proved that these elements play an important role in the level of gene expression. Native genes *trnA/trnI* are located at transcriptionally active spacer regions. After an herbicide resistance gene was integrated into the transcriptionally active spacer region for the first time (Daniell et al., 1998), most subsequent studies preferentially used this site of integration. Compared with the transcriptional silencing spacer (rbcl/accD), the integration of the transgene into the transcriptionally active spacer (trnl/trnA) resulted in 25-fold higher expression of transgenes (Krichevsky et al., 2010) and the *trnA* gene intron included the chloroplast origin of replication and generated more copies of the template (chloroplast vector) to integrate the transgene cassette (Daniell et al., 1990). In addition to the integration site, regulatory sequences located upstream (promoter, 5'UTR) and downstream (3'UTR) of the transgene play a major role in determining its expression level. The most commonly used promoters are photosystem II reaction center promoter PpsbA and *rrn16S* gene promoter Prrn; moreover, the psbA regulatory region, which was first used almost 30 years ago (Daniell et al., 1990), still appears to be the best option for use in an expression cassette because the *psbA* gene mediates light-induced activation of translation (Ruhlman et al., 2010) and it also encodes the most highly translated protein in the chloroplast (Klein and Mullet, 1987). In a pioneering work, Fei et al. (2007) studied the *psbB* operon from tobacco chloroplasts and identified a small cistronic element called IEE, which was included in the synthetic structure to drive the expression of *nptII* and *yfp* and proved to be sufficient for mediating polycistronic expression. The polycistronic transcript has been processed into stable and translatable monocistronic mRNA, and this function has been used to express transgenic polycistronic mRNA from a single promoter in a single transformation event (Lu et al., 2013; Bock, 2014; Fuentes et al., 2016). Therefore, for the in-depth study of chloroplast transformation in medicinal plants, it is necessary to further develop and explore the endogenous regulatory elements and establish a more efficient chloroplast transformation system. In this work, we combined second-generation and third-generation sequencing technologies to obtain more completely and accurate *E. breviscapus* cp genome sequence information and performed detailed bioinformatics analysis, including gene annotation, structural statistics, SSR analysis, and codon usage bias analysis. Then, a series of chloroplast regulatory elements were cloned from *E. breviscapus*, and the corresponding chloroplast expression vectors of *E. breviscapus* were constructed and the biological functions of these chloroplast regulatory elements were verified through *in vitro* experiments, thus providing a foundation for the establishment of the subsequent chloroplast genetic transformation system and research on the biology and evolution of *E. breviscapus*.

MATERIALS AND METHODS

Materials and Reagents

Soaked the seeds in deionized water for 3–4 h, then placed the seeds at room temperature to fully dry them for 3–4 h, soaked the seeds in 1% NaClO solution for 10 min in the Vertical Flow Clean Bench, and then washed them with sterile water three times. About 20–30 sterilized seeds were inoculated per petri dish in MS solid medium (Murashige and Skoog, 1962) for germination and then maintained in a culture room under white fluorescent lamps (1,900 lux), with a 16 h light/8 h dark cycle at 25°C for 4–7 days. Individual germinated seedlings were transferred to a sterile tissue culture bottle containing MS medium supplemented with 30 g/L sucrose and kept in a culture room under white fluorescent lamps (1,900 lux), with a 16 h light/8 h dark cycle at 26°C for 4–7 weeks.

Total DNA Extraction and Sequencing

Total genomic DNA was used to build sequence libraries (Illumina Inc., San Diego, CA, United States), and it was extracted from leaves using the cetyltrimethylammonium bromide (CTAB) method. The experimental procedures were performed in accordance with the standard protocol provided by Illumina, and sequence libraries were prepared with the NEB Next Ultra DNA Library Prep Kit. An Illumina NovaSeq sequencer was used to sequence paired-end (PE) sequencing libraries with an average 350 bp insert length at the Wuhan Benagen Tech Solutions Company Limited. From these data, over 20 million clean reads with a 150 bp read length were passed through quality control. Then, we performed nanopore sequencing to facilitate the connection of high-quality contigs into longer complete sequences in subsequent genome assembly.

Chloroplast Genome Assembly

Since the original sequencing data may contain low-quality sequences, adaptor sequences, etc. (Ewing and Green, 1998), to ensure the reliability of the information analysis results, the original sequencing data need to be filtered to obtain clean reads, which are stored in FASTQ format (Cock et al., 2009). This project used the filtering software SOAPnuke (version: 1.3.0) to remove reads with an N base content of more than 5%, low-quality (quality value less than or equal to 5) reads with a base number of 50%, and reads with adapter contamination.

UniCycler (0.4.8) software was used to assemble the filtered reads (Wick et al., 2017). First, high-accuracy Illumina data (Q30 > 85%) were assembled to obtain a high-quality cp genome skeleton (contig), and then nanopore data were used to connect the high-quality contig into a longer complete sequence. The accuracy of the cp genome assembled by this strategy is determined by the accuracy of the Illumina data, and it can effectively avoid the sequence contamination introduced by the error of nanopore data splitting. Finally, Pilon software was used to further correct the Illumina data for errors in the assembled genome, resulting in a genome with higher final accuracy.

Unicycler software was aligned with the close reference genome (NC_043882.1) by blastn (version: BLAST 2.2.30+; parameter: -evalue 1e-5), and the best candidate sequence was selected based on the alignment. The chloroplast genome connection relationship was determined based on the sequence sequencing depth and read alignment and by comparison with closely related species. The connection relationship and whether it forms a loop need to be further experimentally verified.

Gene Structure Prediction

Chloroplast genome function annotation includes coding gene prediction and noncoding RNA annotation [ribosomal RNA (rRNA) and transfer RNA (tRNA) annotation]. CPGAVAS2[1] was used for gene annotation and drawn based on the results of the cp genome annotation (Shi et al., 2019).

Codon Usage Bias Analysis

CodonW (Version: 1.4.4) was used to analyze codon usage bias and statistically estimate the frequency of relative synonymous codon usage (RSCU). Codons with RSCU values >1 were defined as high-frequency codons. We conducted a codon usage bias analysis using the following gene sequences: "ATG", "TTG", "CTG", "ATT", "ATC", "GTG", and "ATA", which were used as start codons; and "TGA", "TAG", and "TAA", which were used as stop codons; in addition, protein-coding genes shorter than 300 bp in length were excluded from the base composition analysis to avoid sampling bias (Wright, 1990).

Simple Sequence Repeat and Long Repetitive Sequences Analysis

MISA (Sebastian et al., 2017) was used to perform a SSR analysis of the *E. breviscapus* chloroplast [version: 1.0; default parameters: the corresponding minimum number of repetitions of each repeating unit (unit size) are: 1–8, 2–4, 3–4, 4–3, 5–3, and 6–3, with 1–8 meaning that when a single nucleotide is used as the repeat unit, the number of repeats must be at least 8 to be detected; see http://pgrc.ipk-gatersleben.de/misa/misa.html for details].

The software vmatch[2] was used to find scattered long repetitive sequences in the *E. breviscapus* cp genome (Jean-Simon et al., 2010). The long repeat sequences included three types: forward (F), palindrome (P), and tandem (T) repeats.

Chloroplast Genome Extraction and PCR Cloning

There is no report on the extraction method of chloroplast of *E. breviscapus* before, therefore, we have developed a method suitable for extracting chloroplast DNA of *E. breviscapus*, which is based on the modified high – salt low – pH method (Shi et al., 2012). Borax was not used in this method, which greatly guaranteed the safety of the operators. In addition, we removed the step of "add 1.5 ml of 5 mol/L KAc (PH 5.2) and continue freezing for 30 min. Then centrifuge at 10,000 *g* for 15 min, and discard the precipitate", this saved extraction time and effectively simplified the extraction step. After extracting high-quality chloroplast genomic DNA of *E. breviscapus*, regular PCR was performed as follows: a 30 s initial denaturation step at 98°C, followed by 35 cycles of denaturation for 10 s at 98°C, annealing for 30 s at 55–63°C, extension for 30 s per kbp sequence length at 72°C, and a final 7 min extension step at 72°C. Phusion High-Fidelity DNA Polymerase (New England Biolabs, China) and 2 × EasyTaq PCR SuperMix (+dye; TransGen Biotech, China) were utilized for DNA cloning and PCR analysis, respectively. The sequence information of the primers for amplification was provided in **Supplementary Table S1**. The pEASY-Blunt Zero Cloning Kit (TransGen Biotech, China) was utilized for seamless cloning of the selected amplified fragments.

[1]http://47.96.249.172:16019/analyzer/annotate

[2]http://www.vmatch.de/

Construction of Transforming Vectors

The synthetic operon constructs for chloroplast transformation (pBtEa1t, pBtEa2t, pBtEat3, and pBtEIat) were based on the empty vector pBluescript SK (+). They were all constructed using the pEASY-Uni Seamless Cloning and Assembly Kit (TransGene Biotech, China), which can be used to recombine the vector linearized by any method and the PCR fragment with 15–25 bp overlapping region with both ends of the linearized vector. All the fragments needed for chloroplast expression vector construction were then assembled into synthetic operons as follows:

For the first round (Round I) of gene assembly, The empty vector pBluescript SK (+) was digested with Not I and Hind III, and then Eb-PpsbA, *aadA* gene and Eb-TpsbA were cloned into linearized vector and generating construct pBa1, Eb-Prrn, *aadA* gene, and Eb-TrbcL were cloned into linearized vector and generating construct pBa2, Eb-Prrn, *aadA* gene, and Eb-Trps16 were cloned into linearized vector and generating construct pBa3, all the recombinant vectors were verified by Sanger sequencing for the next round of gene assembly.

For the second round (Round II) of gene assembly, the vectors pBa1, pBa2, pBa3, and pBluescript SK (+) were digested with Sal I, and then Eb-PpsbA, *EGFP* gene, and Eb-TpsbA were cloned into linearized vector pBa1 and generating construct pBEa1, Eb-Prrn, *EGFP* gene, and Eb-TrbcL were cloned into linearized vector pBa2 and generating construct pBEa2, Eb-Prrn, *EGFP* gene, and Eb-Trps16 were cloned into linearized vector pBa3 and generating construct pBEa3, Eb-Prrn, *EGFP* gene, Eb-IEE, *aadA* gene, and Eb-Trps16 were cloned into linearized vector pBluescript SK (+) and generating construct pBEIa, all the recombinant vectors were verified by Sanger sequencing for the next round of gene assembly.

For the third round (Round III) of gene assembly, the vectors pBEa1, pBEa2, pBEa3, and pBEIa were digested with Kpn I, and then the homologous recombination fragment Eb-trnI was cloned into linearized vectors and generating construct pBtEa1, pBtEa2, pBtEa3, and pBtEIa, respectively and verified by Sanger sequencing. Finally, the vectors pBtEa1, pBtEa2, pBtEa3, and pBtEIa were digested with Sac I, and then the homologous recombination fragment Eb-trnA was cloned into linearized vectors and generating construct pBtEat1, pBtEat2, pBtEat3, and pBtEIat (**Supplementary Figure S1**) and verified by Sanger sequencing.

Analysis of *aadA* Gene Expression in *E. coli*

After PCR identification and Sanger sequencing, four verified vectors (pBtEat1, pBtEat2, pBtEat3, and pBtEIat) and the empty vector pBluescript SK (+) were transformed into the *E. coli* expression strain Transetta (DE3). Then, the transformed *E. coli* strains were grown in Luria-Bertani (LB) medium at 37°C unless otherwise indicated. Spectinomycin and ampicillin were used for selection at appropriate concentration.

Gene Expression Analysis of *EGFP*

After culturing in 20 ml of LB medium for 14–16 h at 16°C (150–180 rpm), *EGFP* gene expression in transformed *E. coli* strains was examined using a Thermo Scientific Varioskan LUX Multimode Microplate Reader (Thermo Fisher Scientific, MA, United States). The loading volume was 200 µl, and the "Fluorescence" protocol was executed in Skanlt Software 6.1 RE, which included an excitation wavelength at 485 nm and an emission wavelength at 520 nm. Subsequently, the fluorescence intensity of *E. coli* strains containing different vectors was counted. Each sample was repeated for three times to ensure the credibility of the data, in order to compare the effects of different combinations of chloroplast regulatory elements on the expression level of green fluorescent protein in *E. coli*, the expression level of fluorescent protein in each sample was compared by unpaired *t*-test ($p < 0.05$), the results are represented as a bar graph.

Statistical Analysis

The statistical evaluation was performed using SPSS 19.0 software (IBM Corp., United States). All data were presented as the means ± SE of at least three replicates. ANOVA was followed by a *t*-test. Mean values were considered significantly different at $p < 0.05$.

RESULTS

Chloroplast Assembly and Genome Features

This project adopted the whole genome shotgun strategy to construct a 350 bp library from the DNA samples of *E. breviscapus* and then used the Illumina NovaSeq sequencer to perform PE sequencing on this library, and the reads were 150 bp in length. In this sequencing, the raw data sequencing volume of the *E. breviscapus* sample was 4.2 Gbp. After data filtering, the clean data volume of the sample was 4.1 Gbp (**Table 1**). The original sequencing statistics of the third-generation nanopore sequencing were shown in **Supplementary Table S2**.

The *E. breviscapus* cp genome was completely assembled into a single molecule of 152,164 bp, the assembly result of the cp genome of *E. breviscapus* contained 0 Gap, the GC content was 37.20, the assembly coverage was 332.55X, and the sequencing quality value (Phred) was above 30 (**Figure 1**), indicating that the sequencing quality was high.

The conserved size and quadripartite structure of the complete *E. breviscapus* cp genome was similar to the cp genomes of previously published data. These genomes were usually 152 kb in size and included two inverted repeat regions (IRs) and two single-copy regions, namely, a large single copy and small single copy (LSC and SSC, respectively) region.

The cp genome of *E. breviscapus* consisted of two single-copy regions isolated by two identical IR regions of 24,699 bp each, one LSC region of 84,657 bp and one SSC region of 18,109 bp. The proportions of LSC, SSC, and IR sizes in the entire cp genome were 55.6, 11.9, and 32.5%, respectively

TABLE 1 | Sequencing data volume information statistics.

Sample name	Length (bp)	Raw reads	Raw bases (bp)	Clean reads	Clean bases (bp)	GC (%)	Q20 (%)	Q30 (%)
Erigeron breviscapus	150	27,679,808	4,151,971,200	27,467,550	4,120,132,500	37.73	98.55	95.37

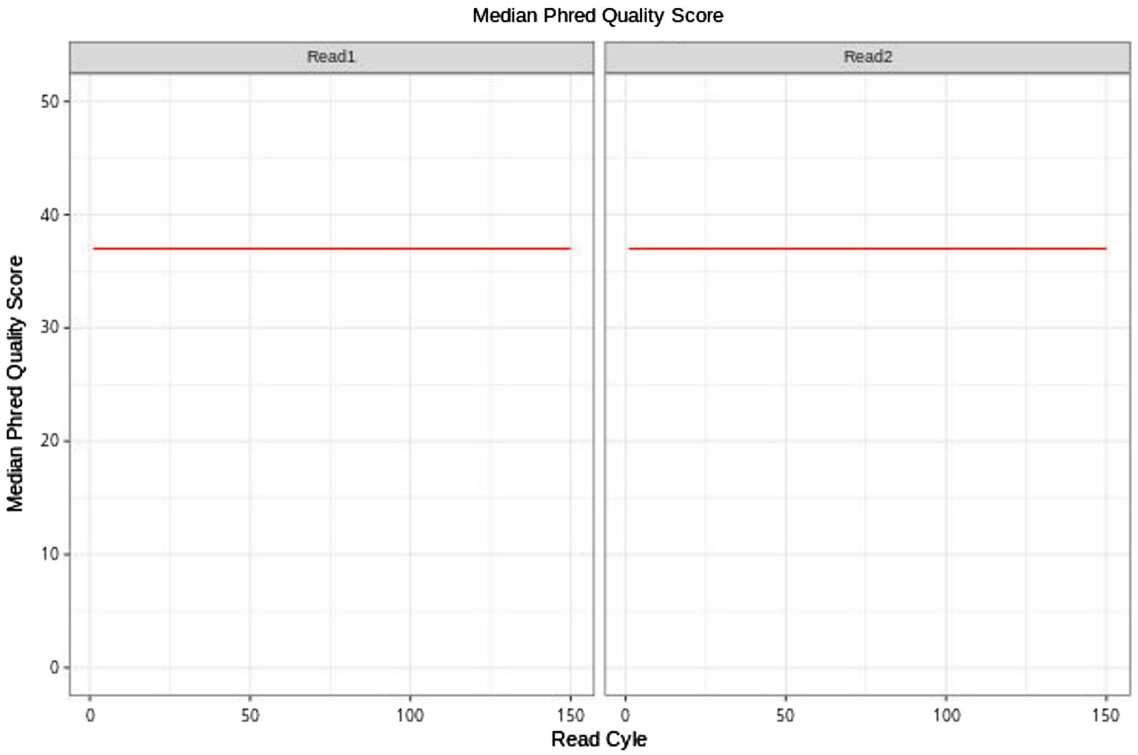

FIGURE 1 | Base quality value distribution graph of *E. breviscapus* sample. The graph reflects the average sequencing quality (Y-axis) of read 1 and read 2 along the Read Cycle (X-axis).

(**Figure 2**; **Table 2**). The GC contents of the LSC, SSC, and IR and whole cp genome were 35.06, 31.00, 43.13, and 37.20%, respectively, which were consistent with the published *E. breviscapus* cp genomes (**Supplementary Table S3**). The cp genome of *E. breviscapus* was compared to previously published data, no structural differences were found among all compared data, it demonstrated that gene order, gene content, and entire genome structure were conserved in *E. breviscapus* cp genome.

Gene Content and Structure

The cp genome of *E. breviscapus* consisted of 127 coding regions made up of 83 protein-coding genes, 36 tRNAs, and eight rRNAs, of which 95 genes were unique and 16 genes were repeated in two inverted regions consisting of five protein coding genes, seven tRNAs, and four rRNAs (**Figure 2**; **Table 3**). Among these 95 unique genes, one gene crossed different cp genome boundaries: *rps12* crossed two IR regions, the LSC region and the SSC region (two 3′ end exons repeated in IRs and 5′ end exon situated in LSC; **Figure 2**). Of the remaining 94 genes, 82 were situated in the LSC, including 61 protein-coding genes and 21 tRNAs, and 12 were situated in the SSC, including 11 protein-coding genes and one tRNA.

The *E. breviscapus* cp genome was composed of protein coding genes, tRNAs, rRNAs, and intronic and intergenic regions. Noncoding DNA accounted for 68,539 bp (45.0%) of the whole *E. breviscapus* cp genome, protein-coding genes accounted for 71,850 bp (47.2%), tRNA accounted for 2,725 bp (1.8%), and rRNA accounted for 9,050 bp (6.0%).

Most of the protein-coding genes contained only one exon, while 13 genes contained at least one intron, of which eight genes were distributed in the LSC, one was distributed in the SSC and four were distributed in both IRs (**Supplementary Table S4**). Among them, three genes (*rps12*, *clpP*, and *ycf3*) contained two introns, while 10 genes (*trnA-UGC*, *trnE-UUC*, *trnL-UAA*, *rpl2*, *ndhA*, *ndhB*, *petB*, *atpF*, *rpoC1*, and *trnK-UUU*) contained one intron. The longest intron of *trnK-UUU* was 2,543 bp, and it included the 1,515 bp encoding the *matK* gene (Gu et al., 2016). The *rps12* gene was predicted to be trans-spliced with a repeated 3′ end duplicated in the two IRs and a single 5′ end exon in the LSC (Redwan et al., 2015).

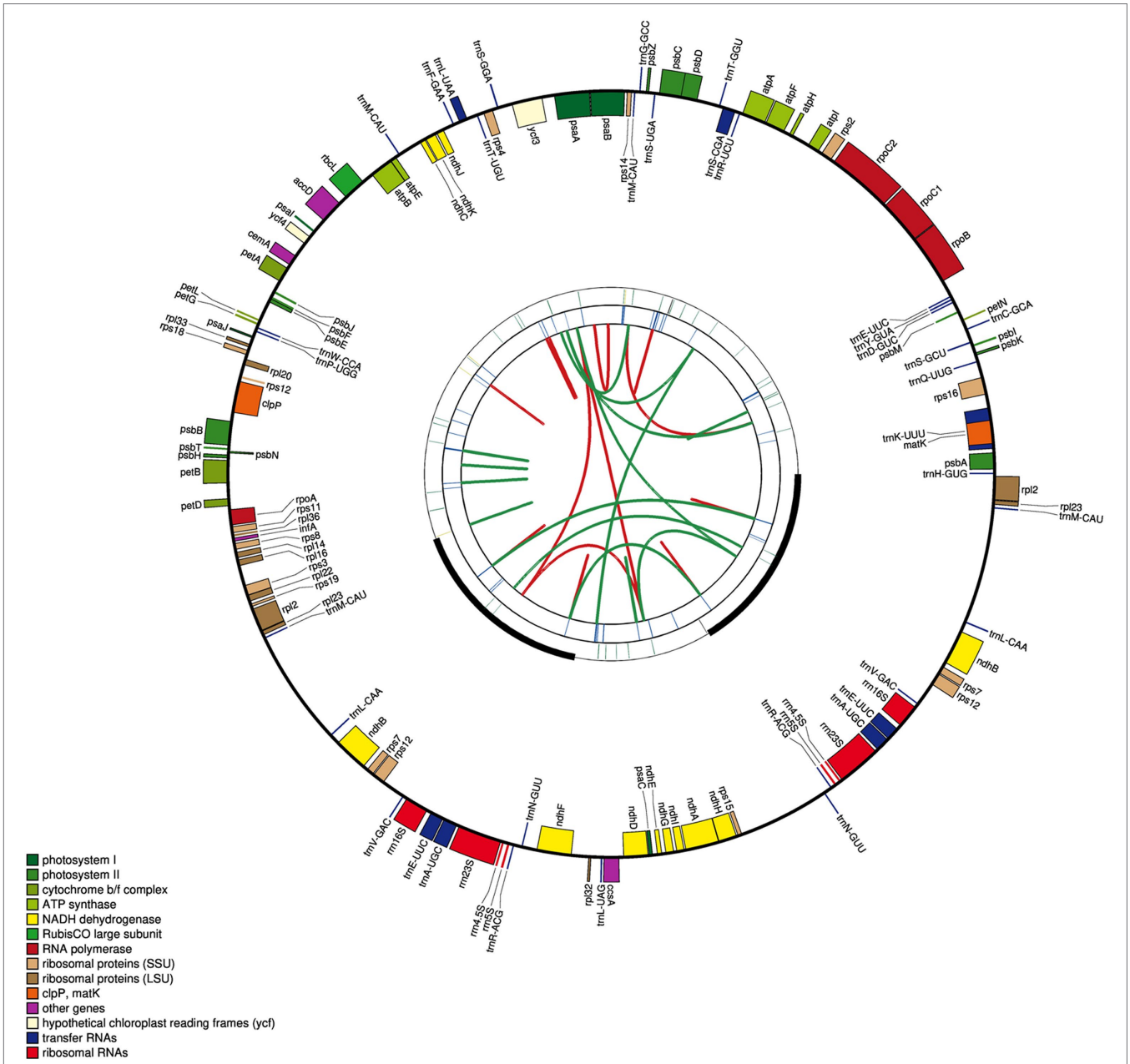

FIGURE 2 | Circular map of the *E. breviscapus* cp genome. There are four rings on the cp genome map. From the center to the outside, the first circle shows the forward and reverse repetitions connected by the red arc and the green arc respectively; The second circle shows the tandem repeat marked with a short bar; The third circle is the microsatellite sequence identified by MISA; the fourth circle was drawn with genemap to show the gene structure on the plastids, Genes shown outside and inside of the fourth circle are transcribed counterclockwise and clockwise, respectively; the colors of genes are distinguished according to their functional classification.

Statistics of Codon Usage Bias

Relative synonymous codon usage is an assessment of synonymous codon usage bias. This value is equal to the ratio of the actual observed value of synonymous codons to the expected value of the average use of synonymous codons. If there is no bias for codon usage, then the RSCU value will be 1; if the codon is used more frequently than other synonymous codons, then its RSCU value will be greater than 1; otherwise, the RSCU value will be less than 1 (Nie et al., 2012; Liu et al., 2020).

The results of the RSCU value analysis (**Supplementary Table S5**) of various amino acids showed that there were 31 codons with RSCU $\geq$ 1, of which 12 codons, such as UUA, AGA, CAA, and GGA, end in A; 16 codons, such as UCU, GCU, ACU, and UAU, end in U; and the only ones ending with G are UUG, UGG, and AUG. These findings

TABLE 2 | Chloroplast structure statistics of *Erigeron breviscapus* samples.

Region	Start	End	Length	A (%)	T (%)	C (%)	G (%)	AT (%)	GC (%)
Total genome	1	152,164	152,164	31.36	31.45	18.54	18.65	62.80	37.20
LSC	1	84,657	84,657	32.29	32.65	17.25	17.80	64.94	35.06
IRA	84,658	109,356	24,699	28.37	28.50	20.73	22.40	56.87	43.13
SSC	109,357	127,465	18,109	34.97	34.03	16.33	14.67	69.00	31.00
IRB	127,466	152,164	24,699	28.50	28.37	22.40	20.73	56.87	43.13

TABLE 3 | List of genes in the *E. breviscapus* cp genome.

Gene group	Gene name
NADH dehydrogenase	*ndh*, *ndhI*, *ndhJ*, *ndhK*, *ndhA*, *ndhH*, *ndhD*, *ndhC*, *ndhB*, *ndhG*, and *ndhE*
Other genes	*ccsA*, *cemA*, and *accD*
RNA polymerase	*rpoC2*, *rpoA*, *rpoB*, and *rpoC1*
Transfer RNAs	*trnS-GCU*, *trnD-GUC*, *trnH-GUG*, *trnM-CAU*, *trnR-ACG*, *trnF-GAA*, *trnY-GUA*, *trnP-UGG*, *trnT-GGU*, *trnS-GGA*, *trnL-UAA*, *trnC-GCA*, *trnV-GAC*, *trnG-GCC*, *trnL-CAA*, *trnS-UGA*, *trnQ-UUG*, *trnR-UCU*, *trnS-CGA*, *trnA-UGC*, *trnL-UAG*, *trnT-UGU*, *trnE-UUC*, *trnN-GUU*, *trnK-UUU*, and *trnW-CCA*
Ribosomal proteins (SSU)	*rps18*, *rps19*, *rps2*, *rps7*, *rps16*, *rps15*, *rps8*, *rps11*, *rps12*, *rps4*, *rps3*, and *rps14*
Maturase	*matK*
Cytochrome b/f complex	*petA*, *petL*, *petG*, *petB*, *petD*, and *petN*
Photosystem II	*psbK*, *psbT*, *psbB*, *psbH*, *psbD*, *psbF*, *psbZ*, *psbC*, *psbM*, *psbA*, *psbN*, *psbJ*, *psbI*, and *psbE*
ATP synthase	*atpI*, *atpA*, *atpE*, *atpF*, *atpB*, and *atpH*
Photosystem I	*psaJ*, *psaC*, *psaB*, *psaA*, and *psaI*
RubisCO large subunit	*rbcL*
Ribosomal proteins (LSU)	*rpl20*, *rpl32*, *rpl23*, *rpl33*, *rpl16*, *rpl2*, *rpl14*, *rpl36*, and *rpl22*
Translational initiation factor	*infA*
Ribosomal RNAs	*rrn23S*, *rrn16S*, *rrn5S*, and *rrn4.5S*
Protease	*clpP*
Hypothetical chloroplast reading frames (ycf)	*ycf2*, *ycf3*, and *ycf4*

indicated that the codons ending with A and U in the chloroplast genome of *E. breviscapus* appeared more frequently and are preferred codons, while the codons ending with C and G were non-preferred codons.

Chloroplast Genome Simple Sequence Repeats

Simple sequence repeats are sequences with motifs from 1 to 6 bp in length repeated multiple times (see section "Materials and Methods" for cutoff criteria), and they are distributed throughout the cp genome and often used as markers for breeding studies, population genetics, and genetic linkage mapping (Grassi et al., 2002; Timme et al., 2007).

A total of 223 SSRs were found in the *E. breviscapus* cp genome (**Figure 3**; **Supplementary Table S6**). These SSRs included 142 complex repeat-type SSRs (63%), 50 dinucleotide SSRs (22%), 12 trinucleotide SSRs (5%), 14 tetranucleotide (6%), four pentanucleotide SSRs (1%), and one hexanucleotide SSR (0.003%; **Figure 3A**; **Supplementary Table S6**). Among the 223 SSRs, 87% of SSRs (195) were the AT type, with copy numbers from 8 to 23 (**Supplementary Table S6**). Forty-eight SSRs were detected in protein-coding genes, 19 SSRs were detected in introns, and 156 were detected in intergenic regions (**Figure 3C**). In relation to the quadripartite, 151 SSRs were situated in the LSC, while 32 and 40 were identified in the IR and SSC, respectively (**Figure 3B**).

Identification of Long Repetitive Sequences

Long repetitive sequences may promote the rearrangement of the cp genome and increase population genetic diversity (Cavalier-Smith, 2002). A total of three unique repeats were found in the *E. breviscapus* cp genome, the size of two palindromic repeats were 48 bp and 24,699 bp, and the forward repeat was 39 bp in size. The palindromic repeat which was 48 bp in size had two same starting sites in the chloroplast genome sequence, these two starting sites were located at 74,576 bp, another palindromic repeat's two starting site were located at 84,657 and 127,465 bp respectively, the first starting site of the forward repeat located at 43,603 bp and the second starting site located at 119,435 bp. In addition, forward repeats are usually caused by transposon activity (Gemayel et al., 2012), which will increase under cell stress (Voronova et al., 2014). However, the origin and production mechanism of long repetitive sequences are not yet fully understood. Previous studies have shown that slipped-strand mispairing and inapposite recombination of repetitive sequences may lead to genome rearrangement (Timme et al., 2007). Moreover, forward repeats can cause changes in genome structure; therefore, they can be used as markers in phylogenetic studies.

Cloning of Chloroplast Regulatory Elements of *E. breviscapus*

Before cloning the target sequence, we first obtained the specific sequence information of the target sequence through previous research, and this information included the sequence length, putative transcriptional elements, and secondary structure. Then, through a sequence alignment, secondary structure analysis, etc., the specific information of these target sequences was initially obtained from the cp genome of *E. breviscapus* (**Table 4**).

Using *E. breviscapus* genomic DNA as a template, the target gene fragment was amplified with the primers shown in **Supplementary Table S1**. As shown in **Figure 4**, all amplified bands were the same size as the target gene fragment. Eb-Prrn was a fragment containing the rRNA operon promoter from *E. breviscapus* which was PCR amplified with a Shine-Dalgarno (SD) sequence derived from the chloroplast *rbcL* gene, Eb-psbA was a fragment containing the *E. breviscapus* psbA promoter

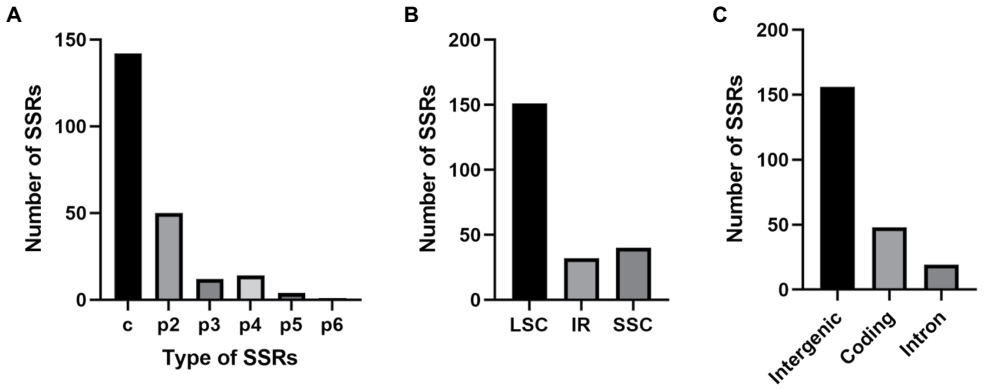

FIGURE 3 | The type, distribution, and presence of simple sequence repeats (SSRs) in *E. breviscapus* cp genome. **(A)** Number of different SSR types detected in *E. breviscapus* cp genome. **(B)** Frequency of SSRs in the large single copy (LSC), small single copy (SSC), and inverted repeat (IR) regions. **(C)** Frequency of SSRs in the protein-coding regions, intergenic spacers, and intron.

TABLE 4 | Regulatory elements of *E. breviscapus* cp genome.

Feature	Type	Size (bp)	Transcriptional elements	
Eb-trnI	Site of integration	1,322	-	
Eb-trnA	Site of integration	936	-	
Eb-Prrn	Promoter+rbcL5'UTR	135	−10 consensus sequence	TATATT
			−35 consensus sequence	TTGACG
			GAA-box	GAA
			SD-like sequence	GGAGG
Eb-PpsbA	Promoter+psbA5'UTR	244	−10 consensus sequence	TATACT
			−35 consensus sequence	TTGACA
			Ribosome binding site 1	AAG
			Ribosome binding site 2	TGATAAT
			AU-box	TAAATAAA
Eb-TpsbA	3'UTR	138	Stem-loop	
Eb-TrbcL	3'UTR	309	Stem-loop	
Eb-Trps16	3'UTR	303	Stem-loop	
			Stem-loop	-
Eb-IEE	IEE+rbcL5'UTR	67	S-box	AAGTCAA
			SD-like sequence	GGAGG

and the *E. breviscapus* psbA leader. Eb-TpsbA, Eb-TrbcL, and Eb-Trps16 were the terminator of *psbA*, *rbcL* and *rps16* gene, respectively. Eb-IEE was an intercistronic expression element conferring intercistronic RNA processing and, in this way, enhancing expression of downstream cistrons of the operon. Eb-trnI was a fragment containing the *trnI* gene and part of the flanking sequence of this gene and Eb-trnA was a fragment containing the *trnA* gene and part of the flanking sequence of this gene. The cloned chloroplast regulatory element sequence can be used for subsequent vector construction.

Analysis of *aadA* Gene Expression in *E. coli*

The verified vectors pBtEat1, pBtEat2, pBtEat3, and pBtEIat were transformed into the *E. coli* expression strain Transetta (DE3). As shown in **Figure 5**, after incubation, *E. coli* containing the empty vector could not grow on LB medium containing ampicillin and spectinomycin (**Figure 5A**). However, *E. coli* containing the recombinant vector could be grown on LB medium containing ampicillin and spectinomycin (**Figures 5B–E**), indicating that the selected regulatory elements had prokaryotic characteristics and could mediate the correct expression of foreign genes.

Detection of *EGFP* Expression

As shown in **Figure 6**, the fluorescence intensity of the *E. coli* expression strain containing the recombinant vector was higher than that of the control test group. Among them, the expression strain containing the recombinant vector pBtEat3 (containing the Prrn-EGFP-Trps16 expression cassette) had the highest fluorescence intensity, which showed that the promoters Prrn and 3′ UTR Trps16 could mediate the high-efficiency expression of foreign genes in *E. coli*. In this study, the *EGFP* gene was efficiently expressed in *E. coli* transformed with the *E. breviscapus* chloroplast expression vector, suggesting that the *EGFP* gene may also be highly expressed in *E. breviscapus* chloroplasts.

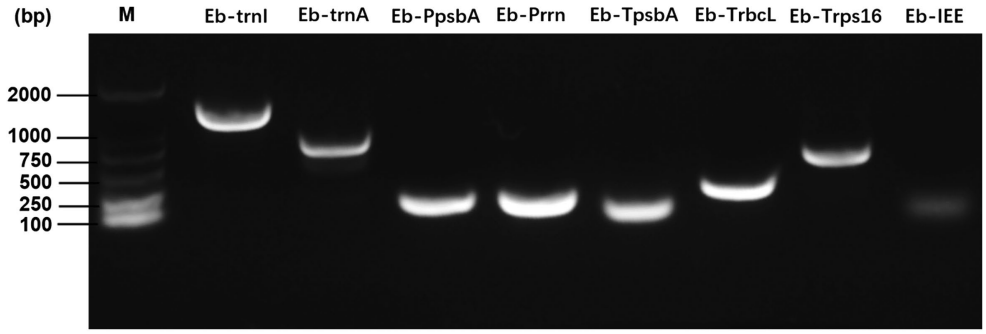

FIGURE 4 | PCR amplification of chloroplast regulatory elements of *E. breviscapus*.

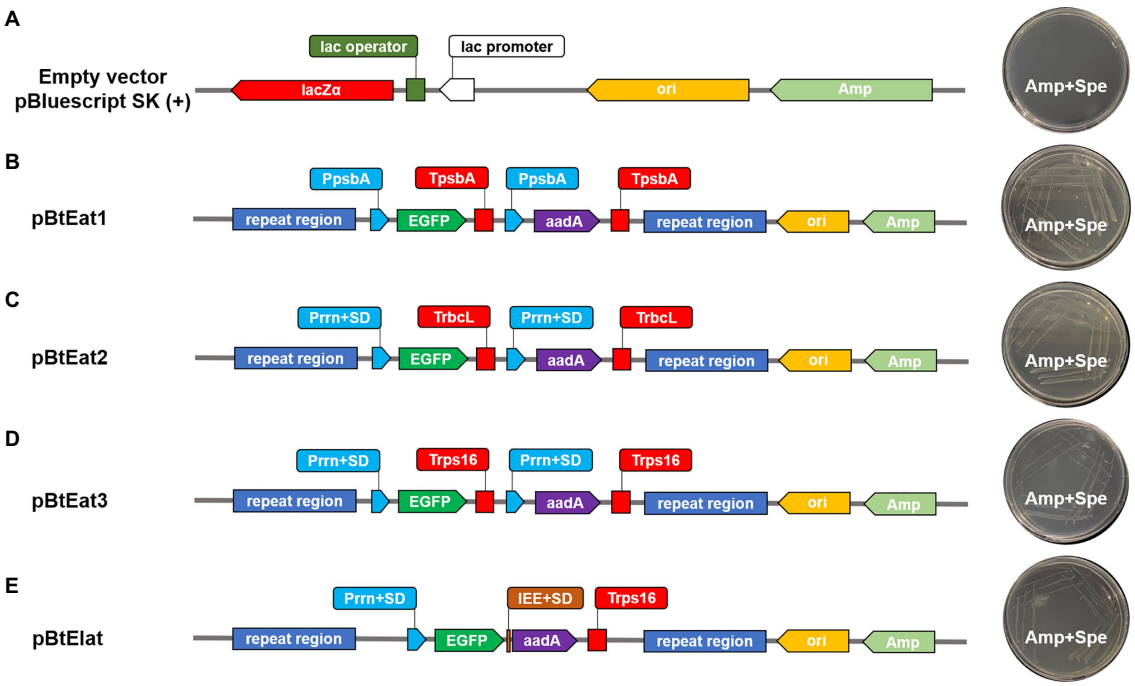

FIGURE 5 | The expression of *aadA* gene in *Escherichia coli*. **(A)**: *Escherichia coli* containing empty vector, **(B–E)**: *Escherichia coli* containing recombinant vector.

DISCUSSION

The present work was to use high-throughput sequencing technology to systematically and comprehensively analyze the chloroplast genome of *E. breviscapus*. On this basis, we used the prokaryotic expression system to screen out high-efficiency chloroplast regulatory elements, which laid the foundation for the subsequent establishment of the chloroplast genetic transformation system of *E. breviscapus*.

Although, there have been reported on the chloroplast genome of *E. breviscapus*, since the *E. breviscapus* used in this study is cultivated species, It is difficult to rule out differences in genetic background between cultivated species and other varieties. In order to have a clearer understanding of the genetic background of the chloroplast of *E. breviscapus* used in this article, as well as to provide an accurate reference for the selection of chloroplast regulatory elements and the efficient expression of foreign genes for chloroplast transformation, we combined second-generation and third-generation sequencing technologies, the advantage of this method is the long read lengths (Eid et al., 2009), which facilitate *de novo* genome assembly, particularly in the four chloroplast junctions between the single-copy regions and IR regions. At the same time, using the Illumina short read length can also improve the low accuracy of the long reads generated by the nanopore platform (~85% of the raw data; Redwan et al., 2015). The chloroplast genome assembly statistics and bioinformatics analysis data in this article were compared with the previously published data. It was obviously that the chloroplast genome of *E. breviscapus* reported in the three

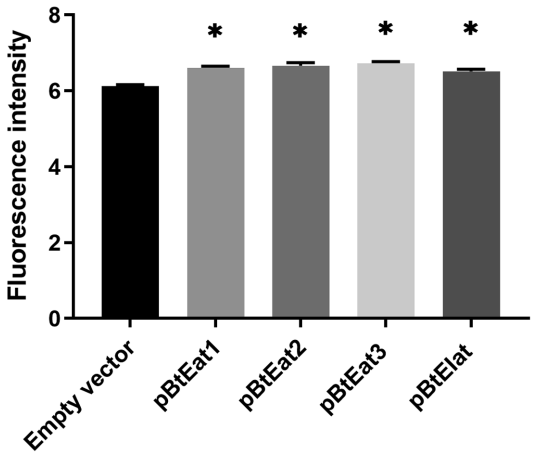

FIGURE 6 | The expression level of *EGFP* gene in *E. coli*. Data are presented as mean ± SE ($n = 3$). The asterisk represents a significant difference ($^*p < 0.05$).

articles were conserved in gene order, gene content, and entire genome structure, but previous reports only provided a little bit of genome information and have not provided a more systematic and comprehensive bioinformatics analysis of the chloroplast genome of *E. breviscapus*. Therefore, we conducted an in-depth analysis of chloroplast genome data of *E. breviscapus*, including a systematic classification of chloroplast genes, SSR analysis, codon usage bias analysis, long repetitive sequences analysis, and this process allowed us to further understand the genomic structure and genetic background of the chloroplast of *E. breviscapus*. On this basis, we successfully screened the target chloroplast regulatory elements from the cp genome of *E. breviscapus* through an extensive literature research and accurate bioinformatics analysis. Active promoters with suitable 5′ UTR and 3′ UTR are important constitutions of efficient transformation and expression vectors. It is generally thought that the use of these endogenous genes can greatly promote the integration and expression of foreign genes in the host genome (Radakovits et al., 2010). In this work, two homologous recombinant fragments, two high-efficiency promoters, three 3′ UTR sequences, one SD sequence and one intercistronic expression element were identified from the chloroplasts of *E. breviscapus*.

Sequence analysis was performed on the chloroplast regulatory elements for prediction of its potential cis-acting elements involved with transcription initiation, regulation, or termination. In the Eb-PpsbA and Eb-Prrn sequence, −10 consensus sequence, and -35 consensus sequence were detected. The −10 consensus sequence is located at the core promoter region and involved with accurate transcription initiation. The −35 consensus sequence commonly exists in many prokaryotic promoters, which acts as an enhancer region. Translation initiation occurs on a specific sequence called the ribosome binding site, this is a short base sequence located in front of the coding region. This site can be complementary to the 3′ end of the ribosomal 16S rRNA, which promotes the binding of the ribosome to the mRNA and facilitates the initiation of translation. Two ribosome binding sites were identified from Eb-PpsbA, since Eb-Prrn lacks a ribosome binding site, we added a ribosome site from the *rbcL* gene of *E. breviscapus* chloroplast at the 3′ end of Eb-Prrn by PCR amplification to ensure that the sequence can have transcription and translation initiation function. The 3′ UTR sequence of the prokaryotic expression system can ensure the stability of mRNA and facilitate the accumulation of protein level, these 3′ UTR sequences usually contain a stable stem-loop structure (Monde et al., 2000). Through, the RNA secondary structure prediction analysis of Eb-TpsbA, Eb-TrbcL, and Eb-Trps16, we found that they all have a stable stem-loop structure. Before this report, IEE for the stacking and expression of foreign genes in the chloroplast of *E. breviscapus* had not been identified. Therefore, we preliminarily screened out the endogenous IEE sequence of *E. breviscapus* through sequence comparison and applied it to the construction of the polycistronic expression cassette of the vector.

To ensure that the selected regulatory elements have the correct biological functions, we have further identified these chloroplast regulatory elements through the prokaryotic expression system. The most effective selectable marker used in chloroplast transformation is the *aadA* gene, which confers resistance to streptomycin and spectinomycin. In this study, the transformed *E. coli* can grow on LB medium containing spectinomycin. The result indicated that these regulatory elements could regulate gene expression in *E. coli* and had the correct prokaryotic expression characteristics. Finally, we used a microplate reader to determine the accumulation level of green fluorescent protein *in vitro*, and compared the expression efficiency of different combinations of regulatory elements by fluorescence intensity. Compared with the empty vector, all the transformed *E. coli* exhibited extremely high fluorescence intensity, suggesting that Eb-Prrn and Eb-PpsbA had priming activity, which ensured the efficient transcription of the *EGFP* gene. In addition, the 5′ UTR regions and ribosome binding sites contained in these two sequences also promote the translation of green fluorescent protein in *E. coli*; Eb-TpsbA, Eb-TrbcL, and Eb-Trps16 can also promote the accumulation of green fluorescent protein. Comparing the fluorescence intensity of pBtEat2 and pBtEat3 strains, we found that different 3′ UTR sequences (Eb-TrbcL and Eb-Trps16) could cause different accumulation level of green fluorescent protein when *EGFP* gene was driven by Eb-Prrn. The pBtEIat strain could be grown on LB medium with spectinomycin and could be detected with green fluorescence. These results indicated that Eb-IEE could active the expression of *EGFP* gene and *aadA* gene as well as polycistronic expression. Notably, the pBtEat3 strain had the highest fluorescence intensity, which indicated that the combination of Eb-Prrn and Eb-Trps16 had higher transcription and translation efficiency. This combination could be used for subsequent chloroplast transformation system, which is the preferred choice for vector construction.

In conclusion, this study provided complete information on the cp genome of *E. breviscapus* and identified a series of

chloroplast expression elements with prokaryotic expression characteristics, and these findings can provide a foundation for the establishment of a chloroplast genetic transformation system of *E. breviscapus*.

DATA AVAILABILITY STATEMENT

The data presented in the study are deposited in the GenBank repository, accession number: OK524211 (Eb-trnI), OK524212 (Eb-trnA), OK524213 (Eb-Prrn), OK524214 (Eb-PpsbA), OK524215 (Eb-Trps16), OK524216 (Eb-TpsbA), OK524217 (Eb-TrbcL), and OK524218 (Eb-IEE).

AUTHOR CONTRIBUTIONS

YY and YZ wrote the manuscript. YY, YZ, ZO, JG, and WZ performed the experiments. LH and YZ supervised the research. All authors contributed to the article and approved the submitted version.

FUNDING

This work was supported by the National Key R&D Program of China (2020YFA0908000), the National Natural Science Foundation of China (81891013), and the Key Project at Central Government Level: The ability establishment of sustainable use for valuable Chinese Medicine Resources (2060302) to LH, and the Fundamental Research Funds for the Central public welfare research institutes (ZZXT202103) to YZ.

SUPPLEMENTARY MATERIAL

The Supplementary Material for this article can be found online at: https://www.frontiersin.org/articles/10.3389/fpls.2021.758290/full#supplementary-material

REFERENCES

Bock, R. (2014). Genetic engineering of the chloroplast: novel tools and new applications. *Curr. Opin. Biotechnol.* 26, 7–13. doi: 10.1016/j.copbio.2013.06.004

Cavalier-Smith, T. (2002). Chloroplast evolution: secondary symbiogenesis and multiple losses. *Curr. Biol.* 12, R62–R64. doi: 10.1016/S0960-9822(01)00675-3

Chen, R., Chen, X., Zhu, T., Liu, J., Xiang, X., Jian, Y., et al. (2018). Integrated transcript and metabolite profiles reveal that EbCHI plays an important role in scutellarin accumulation in *Erigeron breviscapus* hairy roots. *Front. Plant Sci.* 9:789. doi: 10.3389/fpls.2018.00789

Cock, P., Fields, C. J., Naohisa, G., Heuer, M. L., and Rice, P. M. (2009). The sanger FASTQ file format for sequences with quality scores, and the solexa/Illumina FASTQ variants. *Nucleic Acids Res.* 38, 1767–1771. doi: 10.1093/nar/gkp1137

Daniell, H., Datta, R., Varma, S., Gray, S., and Lee, S. B. (1998). Containment of herbicide resistance through genetic engineering of the chloroplast genome. *Nat. Biotechnol.* 16, 345–348. doi: 10.1038/nbt0498-345

Daniell, H., Vivekananda, J., Nielsen, B. L., Ye, G. N., Tewari, K. K., and Sanford, J. C. (1990). Transient foreign gene expression in chloroplasts of cultured tobacco cells after biolistic delivery of chloroplast vectors. *Proc. Natl. Acad. Sci. U. S. A.* 87, 88–92. doi: 10.1073/pnas.87.1.88

Eid, J., Fehr, A., Gray, J., Luong, K., Lyle, J., Otto, G., et al. (2009). Real-time DNA sequencing from single polymerase molecules. *Science* 323, 133–138. doi: 10.1126/science.1162986

Ewing, B., and Green, P. (1998). Base-calling of automated sequencer traces using Phred. II. Error probabilities. *Genome Res.* 8, 186–194. doi: 10.1101/gr.8.3.186

Fei, Z., Karcher, D., and Bock, R. (2007). Identification of a plastid intercistronic expression element (IEE) facilitating the expression of stable translatable monocistronic mRNAs from operons. *Plant J.* 52, 961–972. doi: 10.1111/j.1365-313X.2007.03261.x

Fuentes, P., Zhou, F., Erban, A., Karcher, D., Kopka, J., and Bock, R. (2016). A new synthetic biology approach allows transfer of an entire metabolic pathway from a medicinal plant to a biomass crop. *Elife* 5:e13664. doi: 10.7554/eLife.13664

Gemayel, R., Cho, J., Boeynaems, S., and Verstrepen, K. J. (2012). Beyond junk-variable tandem repeats as facilitators of rapid evolution of regulatory and coding sequences. *Genes* 3, 461–480. doi: 10.3390/genes3030461

Grassi, F., Labra, M., Scienza, A., and Imazio, S. (2002). Chloroplast SSR markers to assess DNA diversity in wild and cultivated grapevines. *Vitis-Geilweilerhof* 41, 157–158. doi: 10.1023/A:1017573817633

Gu, C., Tembrock, L. R., Johnson, N. G., Simmons, M. P., and Wu, Z. (2016). The complete plastid genome of lagerstroemia fauriei and loss of rpl2 intron from lagerstroemia (Lythraceae). *PLoS One* 11:e0150752. doi: 10.1371/journal.pone.0150752

Jean-Simon, B., Christian, O., Claude, L., and Monique, T. (2010). The exceptionally large chloroplast genome of the green alga floydiella terrestris illuminates the evolutionary history of the chlorophyceae. *Genome Biol. Evol.* 2, 240–256. doi: 10.1093/gbe/evq014

Jiang, N. H., Zhang, G. H., Zhang, J. J., Shu, L. P., Wei, Z., Long, G. Q., et al. (2014). Analysis of the transcriptome of *Erigeron breviscapus* uncovers putative scutellarin and chlorogenic acids biosynthetic genes and genetic markers. *PLoS One* 9:e100357. doi: 10.1371/journal.pone.0100357

Klein, R. R., and Mullet, J. E. (1987). Control of gene expression during higher plant chloroplast biogenesis. Protein synthesis and transcript levels of psbA, psaA-psaB, and rbcL in dark-grown and illuminated barley seedlings. *J. Biol. Chem.* 262, 4341–4348. doi: 10.1016/S0021-9258(18)61353-5

Krichevsky, A., Meyers, B., Vainstein, A., Maliga, P., Citovsky, V., and Uversky, V. N. (2010). Autoluminescent plants. *PLoS One* 5:e15461. doi: 10.1371/journal.pone.0015461

Li, N. G., Liang, F. Z., Zhang, J. R., Xu, S. X., and Li, X. H. (1998). Effect of *Erigeron breviscapus* hand on hemorheology and microcirculation of acute cerebral infarction. *Chinese J. Hemorheol.* 42–44.

Li, Z. J., Liu, Y. Y., Yang, C. W., Qian, Z. G., and Li, G. D. (2019). The complete chloroplast genome sequence of *Erigeron breviscapus* and *Erigeron multiradiatus* (Asteraceae). *Mitochondrial DNA B Resour.* 4, 3826–3827. doi: 10.1080/23802359.2019.1683478

Li, X., Zhang, S., Yang, Z., Song, K., and Yi, T. (2013). Conservation genetics and population diversity of *Erigeron breviscapus* (Asteraceae), an important Chinese herb. *Biochem. Syst. Ecol.* 49, 156–166. doi: 10.1016/j.bse.2013.03.009

Liu, H., Lu, Y., Lan, B., and Xu, J. (2020). Codon usage by chloroplast gene is bias in *Hemiptelea davidii*. *J. Genet.* 99:8. doi: 10.1007/s12041-019-1167-1

Liu, H., Xiao-Qiao, T., Wang, Y., Tang, R., Xiang-Lian, Y., Xu-Dong, F. U., et al. (2010). Effects of scutellarin on rat cerebral blood flow determined by laser speckle imagine system. *Chinese J. Hosp. Pharm.* 30, 719–722.

Lu, Y., Rijzaani, H., Karcher, D., Ruf, S., and Bock, R. (2013). Efficient metabolic pathway engineering in transgenic tobacco and tomato plastids with synthetic multigene operons. *Proc. Natl. Acad. Sci. U. S. A.* 110, E623–E632. doi: 10.1073/pnas.1216898110

Meng, J., Zhang, L., Dong, Z., and He, J. (2019). Complete plastid genome sequence of *Erigeron breviscapus* (Asteraceae), an endemic traditional Chinese herbal medicine. *Mitochondrial DNA B Resour.* 4, 4077–4078. doi: 10.1080/23802359.2019.1605854

Monde, R. A., Greene, J. C., and Stern, D. B. (2000). The sequence and secondary structure of the 3'-UTR affect 3'-end maturation, RNA accumulation, and translation in tobacco chloroplasts. *Plant Mol. Biol.* 44, 529–542. doi: 10.1023/A:1026540310934

Murashige, T., and Skoog, F. (1962). A revised medium for rapid growth and bio assays with tobacco tissue cultures. *Physiol. Plant.* 15, 473–497. doi: 10.1111/j.1399-3054.1962.tb08052.x

Nie, X., Lv, S., Zhang, Y., Du, X., Wang, L., Biradar, S. S., et al. (2012). Complete chloroplast genome sequence of a major invasive species, Crofton weed (Ageratina adenophora). *PLoS One* 7:e36869. doi: 10.1371/journal.pone.0036869

Radakovits, R., Jinkerson, R. E., Darzins, A., and Posewitz, M. C. (2010). Genetic engineering of algae for enhanced biofuel production. *Eukaryot. Cell* 9, 486–501. doi: 10.1128/EC.00364-09

Redwan, R. M., Saidin, A., and Kumar, S. V. (2015). Complete chloroplast genome sequence of MD-2 pineapple and its comparative analysis among nine other plants from the subclass *Commelinidae*. *BMC Plant Biol.* 15:196. doi: 10.1186/s12870-015-0587-1

Ruhlman, T., Verma, D., Samson, N., and Daniell, H. (2010). The role of heterologous chloroplast sequence elements in transgene integration and expression. *Plant Physiol.* 152, 2088–2104. doi: 10.1104/pp.109.152017

Sebastian, B., Thomas, T., Thomas, M., Uwe, S., and Martin, M. (2017). MISA-web: a web server for microsatellite prediction. *Bioinformatics* 33, 2583–2585. doi: 10.1093/bioinformatics/btx198

Sheng, J., Zhao, P., and Huang, Z. (1999). Influence of Deng Zhan xi Xin (*Erigeron breviscapus*) on thrombolytic treatment during acute coronary thrombosis by affecting function of blood platelet and coagulation. *Chinese J. Cardiol.* 27, 115–117.

Shi, L., Chen, H., Jiang, M., Wang, L., Wu, X., Huang, L., et al. (2019). CPGAVAS2, an integrated plastome sequence annotator and analyzer. *Nuclc Acids Res.* 47, W65–W73. doi: 10.1093/nar/gkz345

Shi, C., Hu, N., Huang, H., Gao, J., Zhao, Y. J., and Gao, L. Z. (2012). An improved chloroplast DNA extraction procedure for whole plastid genome sequencing. *PLoS One* 7:e31468. doi: 10.1371/journal.pone.0031468

Timme, R. E., Kuehl, J. V., Boore, J. L., and Jansen, R. K. (2007). A comparative analysis of the Lactuca and Helianthus (Asteraceae) plastid genomes: identification of divergent regions and categorization of shared repeats. *Am. J. Bot.* 94, 302–312. doi: 10.3732/ajb.94.3.302

Voronova, A., Belevich, V., Jansons, A., and Rungis, D. (2014). Stress-induced transcriptional activation of retrotransposon-like sequences in the scots pine (Pinus sylvestris L.) genome. *Tree Genet. Genomes* 10, 937–951. doi: 10.1007/s11295-014-0733-1

Wick, R. R., Judd, L. M., Gorrie, C. L., and Holt, K. E. (2017). Unicycler: resolving bacterial genome assemblies from short and long sequencing reads. *PLoS Comput. Biol.* 13:e1005595. doi: 10.1371/journal.pcbi.1005595

Wright, F. (1990). The 'effective number of codons' used in a gene. *Gene* 87, 23–29. doi: 10.1016/0378-1119(90)90491-9

Yang, J., Zhang, G., Zhang, J., Liu, H., Chen, W., Wang, X., et al. (2017). Hybrid de novo genome assembly of the Chinese herbal fleabane *Erigeron breviscapus*. *GigaScience* 6, 1–7. doi: 10.1093/gigascience/gix028

Conflict of Interest: The authors declare that the research was conducted in the absence of any commercial or financial relationships that could be construed as a potential conflict of interest.

Publisher's Note: All claims expressed in this article are solely those of the authors and do not necessarily represent those of their affiliated organizations, or those of the publisher, the editors and the reviewers. Any product that may be evaluated in this article, or claim that may be made by its manufacturer, is not guaranteed or endorsed by the publisher.

Advantages of publishing in Frontiers

OPEN ACCESS
Articles are free to read for greatest visibility and readership

FAST PUBLICATION
Around 90 days from submission to decision

HIGH QUALITY PEER-REVIEW
Rigorous, collaborative, and constructive peer-review

TRANSPARENT PEER-REVIEW
Editors and reviewers acknowledged by name on published articles

Frontiers
Avenue du Tribunal-Fédéral 34
1005 Lausanne | Switzerland

Visit us: www.frontiersin.org
Contact us: frontiersin.org/about/contact

REPRODUCIBILITY OF RESEARCH
Support open data and methods to enhance research reproducibility

DIGITAL PUBLISHING
Articles designed for optimal readership across devices

FOLLOW US
@frontiersin

IMPACT METRICS
Advanced article metrics track visibility across digital media

EXTENSIVE PROMOTION
Marketing and promotion of impactful research

LOOP RESEARCH NETWORK
Our network increases your article's readership